

**REPORT DOCUMENTATION PAGE**

Form Approved OMB No. 0704-0188

Public reporting burden for this collection of information is estimated to average 1 hour per response, including the time for reviewing instructions, searching existing data sources, gathering and maintaining the data needed, and completing and reviewing the collection of information. Send comments regarding this burden estimate or any other aspect of this collection of information, including suggestions for reducing this burden to Washington Headquarters Services, Directorate for Information Operations and Reports, 1215 Jefferson Davis Highway, Suite 1204, Arlington, VA 22202-4302, and to the Office of Management and Budget, Paperwork Reduction Project (0704-0188), Washington, DC 20503.

1. AGENCY USE ONLY (Leave blank)		2. REPORT DATE  30 July 1998	3. REPORT TYPE AND DATES COVERED  Conference Proceedings	
4. TITLE AND SUBTITLE  21st International Symposium on Rarefied Gas Dynamics			5. FUNDING NUMBERS  F6170898W0021	
6. AUTHOR(S)  Conference Committee				
7. PERFORMING ORGANIZATION NAME(S) AND ADDRESS(ES)  I.U.S.T.I. Technopole de Chateau-Gombert; 5 Rue Enrico Fermi Marseille 13453 France			8. PERFORMING ORGANIZATION REPORT NUMBER  N/A	
9. SPONSORING/MONITORING AGENCY NAME(S) AND ADDRESS(ES)  EOARD PSC 802 BOX 14 FPO 09499-0200			10. SPONSORING/MONITORING AGENCY REPORT NUMBER  CSP 98-1024	
11. SUPPLEMENTARY NOTES  3 Volumes - Oral sessions, Poster sessions, and Special Session				
12a. DISTRIBUTION/AVAILABILITY STATEMENT  Approved for public release; distribution is unlimited.			12b. DISTRIBUTION CODE  A	
13. ABSTRACT (Maximum 200 words)  The Final Proceedings for 21st International Symposium on Rarefied Gas Dynamics, 26 July 1998 - 31 July 1998  This is an interdisciplinary conference. Topics include Boltzman equation and kinetic theory; Mathematical methods and models; Flow in transitional and rarefied regimes; Numerical simulations of RGD flows; Instrumentation and diagnostics in RGD flows; Free jets and molecular beams; Elementary collisional processes; Transport and relaxation phenomena; Chemical processes; Shock waves; Low density plasmas and ionized gases; Gas-surface interactions; Molecular beams; Clusters; Aerosols; Phase change; Aerodynamics and aerothermochemistry of space vehicles; Industrial applications I (vacuum technology, thin film, microengines...); Industrial applications II (beams, jets, lasers, reactors...); Astrophysics; Environmental aspects.				
14. SUBJECT TERMS  EOARD, Rarefied Gas Dynamics, Low Density Plasma			15. NUMBER OF PAGES  875	
			16. PRICE CODE N/A	
17. SECURITY CLASSIFICATION OF REPORT  UNCLASSIFIED	18. SECURITY CLASSIFICATION OF THIS PAGE  UNCLASSIFIED	19. SECURITY CLASSIFICATION OF ABSTRACT  UNCLASSIFIED	20. LIMITATION OF ABSTRACT  UL	

NSN 7540-01-280-5500

Standard Form 298 (Rev. 2-89)  
Prescribed by ANSI Std. Z39-18  
298-102



21st International  
Symposium on

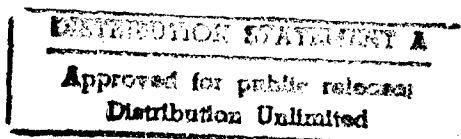
Rarefied Gas  
Dynamics

Marseille (France)  
26-31 July 1998



## Book of Abstracts Volume II

### Poster Sessions



19990115 046

AQF99-04-0640

KINETIC THEORY AND MODELS - KTM P

TUESDAY, JULY 28, 1998

16:15

# Sensitivity of Transport Coefficients to Intermolecular Potential. Application to a High Temperature Air Flow. \*

J.P. Dudon<sup>1</sup>, A. Chikhaoui<sup>1</sup>, M. Dudeck<sup>2</sup>

<sup>1</sup>IUSTI, Marseille, France

<sup>2</sup>Laboratoire d'Aérodynamique, Meudon, France.

This contribution deals with transport properties prediction in thermochemical nonequilibrium reacting gas flows. The derivation of transport terms in such a mixture considering different levels of vibrational and chemical nonequilibrium has been carried out in ref. [1]. It is well known that the probability of chemical reactions in gases increase with temperature so that the modeling of high enthalpy gas flows such as hypersonic flows around a body (for example during its earth - or else - atmospheric reentry), should take into account the reactivity of the mixture. In this case the understanding of the dissipative processes is fundamental in order to evaluate the heat shield of the space vehicle. Moreover an adequate macroscopic description of the flow requires the evaluation of transport terms such as thermal conductivity, viscosity, multicomponent and thermal diffusion coefficients.

Most of the fluid dynamic computations have been carried out using empirical formulae for the transport properties without any discussion about  $\Omega$ -integrals. The aim of this paper is to evaluate the sensitivity of high temperature air mixture transport coefficients corresponding to the parameters of the attractive-repulsive intermolecular potential, and particularly in relation to the collision diameters which can be considered as the molecular 'size'. Here we consider a polyatomic gas mixture in strong chemical nonequilibrium and weak vibrational nonequilibrium. In the generalized Chapman-Enskog formalism, based on the resolution of the Boltzmann equation following an asymptotic method in which the small parameter is the ratio of the rapid processes characteristic time to the slow processes one, these conditions correspond to the so-called one-temperature approach [1, 2].

It is well known that the multicomponent transport coefficients can be finally expressed under the form of the ratio of two determinants including elastic

and inelastic bracket integrals. If we develop these integrals considering the commonly used Mason and Monchick approximations [3], they can be finally expressed as a function of internal mode relaxation times, corresponding to inelastic energy exchanges, and of collision integrals  $\Omega_{\alpha\beta}^{(l,s)}$  which are related to the elastic collision cross sections.

It is important to notice that the above integrals appear in the commonly used approximate formulae for transport coefficients, like Wilke [4] formula for shear viscosity or Mason & Saxena [5] one for heat conductivity.

In the frame of Mason & Monchick approximations, these  $\Omega_{\alpha\beta}^{(l,s)}$  integrals can be calculated in the same way than in the case of a mixture of monoatomic gases [6], [7]. It is well known that for realistic potential  $\Omega_{\alpha\beta}^{(l,s)}$  cannot be evaluated analytically due to the complicated dependance of the scattering angle  $\chi$  on the relative velocity  $g$  and the impact parameter  $b$ . The *hard sphere* model is the simplest one which allow to compute these integrals.

Moreover this potential is useful to give rapid approximate evaluation for transport properties or for testing approximation method as the Sonine polynomial expansion method, is also used to define *reduced  $\Omega$  - integrals* under the following form :

$$\Omega_{\alpha\beta}^{(l,s)*} = \Omega_{\alpha\beta}^{(l,s)} / [\Omega_{\alpha\beta}^{(l,s)}]_{h.s.}$$

As it is shown in ref. [6], these reduced  $\Omega$ -integrals have the advantage of being closer to unity and of being more smoothly varying functions of temperature than unnormalized ones. There exist many models for attractive-repulsive potential, all characterized by the two fundamental parameters  $d_{\alpha\beta}$  and  $\varepsilon_{\alpha\beta}$ . In this work we choose the well-known (6 - 12) *Lennard - Jones* intermolecular potential which gives the best agreement with experimental results for many gases, in particular for  $O_2$ ,  $N_2$ ,  $NO$ ,  $O$  and  $N$  species which constitute the air mixture considered here. This potential corresponds to the relation :  $\phi(r) = 4\varepsilon_{\alpha\beta}[(\frac{d_{\alpha\beta}}{r})^{12} - (\frac{d_{\alpha\beta}}{r})^6]$ .

\*Abstract 1536 submitted to the 21st International Symposium on Rarefied Gas Dynamics, Marseille, France, July 26-31, 1998



In this contribution, we give the results about the sensitivity of a high temperature air mixture transport coefficients, first in relation to the model potential (*hard sphere* or *Lennard – Jones*), then in relation to the collision diameter  $d_{\alpha\beta}$  and the minimal energy  $\varepsilon_{\alpha\beta}$  of the Lennard-Jones potential. In this way, we computed the different transport coefficients in a temperature range from 1000 K to 10 000 K, using successively the values of  $d_{\alpha\beta}$  and  $\varepsilon_{\alpha\beta}$  for the five air species from the references [8, 9, 10, 11]. The numerical results presented show that the fact of using chemical data from two different sources can lead to significant effects on the final results. The order of magnitude of the observed discrepancy lies between 5% and 100% depending on the considered coefficient and it increases more or less rapidly with the temperature. For example one can observe on figure 1 that for shear viscosity the results obtained with the collision diameters from Glotz [9] are 35% greater than those from Moss [10] for 10 000K. The difference between the two other curves is less because Anderson [8] and Chemkin [11] give approximately the same diameters for atoms O and N which constitute the dominant species of the air mixture at high temperature. For thermal diffusion coefficients, the difference is even more.

## References

- [1] A. Chikhaoui, J. P. Dudon, E. Kustova, E. Nagnibeda. *Transport properties in reacting mixture of polyatomic gases*. Physica A, déc. 1997.
- [2] A.Chikhaoui, J.P. Dudon, S. Genieys, E.V. Kustova and E. A. Nagnibeda. *Multi-temperature kinetic model for heat transfer in reacting gas mixture flows..* Phys. of Fluids (in revision).
- [3] L. Monchick, A.N.G. Pereira and E.A. Mason *Heat conductivity of Polyatomic and polar gases and gas mixtures. Journ. of Chem. Phys.*, 42, 9, 1965.
- [4] C. R. Wilke, *A viscosity equation for gas mixtures*, Jour. Chem. Physics, vol. 18, n4, (1949).
- [5] E. A. Mason, S. C. Saxena. *Approximate formula for the thermal conductivity of gas mixtures*, Phys. Fluids, 1, no. 5, (1958).
- [6] J.H. Ferziger, H.G. Kaper. *Mathematical theory of transport processes in gases*, North Holland Publishing Company, London, 1972.

- [7] Hirshfelder J., Curtiss Ch., Bird R., *Molecular theory of gases and liquids*, Wiley and Sons, New York, 1954.
- [8] J.D. Anderson, *Hypersonic and High temperature kinetic model for ionizing air*, AIAA paper 87-1574, 1987.
- [9] G. Glotz, W. Schönauer, *Einfluß des chemiemodells und der randbedingungen auf die hyperschallgrenzschicht bei luft*, Universität Karlsruhe-Rechenzentrum Interner Bericht no.12/77.
- [10] J.N. Moss, *Reacting viscous-Shock layer solution with multicomponent diffusion and mass injection*, NASA TR-R-411, june 1974.
- [11] R. J. Kee, J. A. Miller, T. H. Jefferson, *CHEMKIN: A general-purpose, problem independent, transportable, fortran chemical kinetics code package*, SNL Liv., Mars 1980.

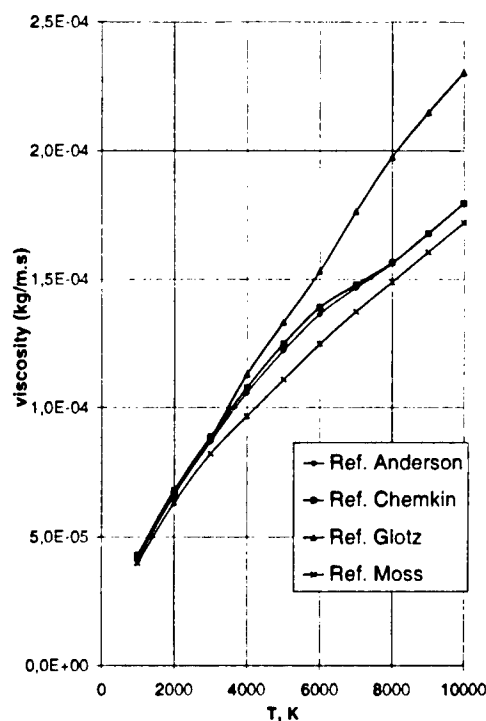


Figure 1: Shear viscosity of air : Influence of collision diameters.

# The Mathematical Modelling of Rarefied Gas Flows in Cavity \*

Alexeev B.V., Mikhailov V.V.

Physics Dpt., Moscow Fine Chemical Technology Institute, Moscow, Russia

The lid-driven flow in cavity has become a widely used vehicle for testing different numerical schemes and flow models. The main result of the comparison between mathematical modelling based on the Navier-Stokes equation (NSE) and experimental data can be formulated by the following way [1]: the measured mean velocity profiles are significantly different from those produced by a numerical simulation at both  $Re = 3200$  and  $Re = 10000$ . One might expect that a two-dimensional simulation would compare favorable to data from symmetry plane, [1].

We consider a two-dimensional rectangular cavity with lid under uniform translation to the right as shown in Fig.1. The generalized hydrodynamic equations (GHE) [2-4] written in the generalized Euler approximation are applied for the two-dimensional mathematical simulation of this flow :

$$\begin{aligned}
 & \frac{\partial}{\partial t} \left\{ \rho - \tau \left[ \frac{\partial \rho}{\partial t} + \frac{\partial (\rho u)}{\partial x} + \frac{\partial (\rho v)}{\partial y} \right] \right\} + \frac{\partial}{\partial x} \cdot \left\{ \rho u - \tau \left[ \frac{\partial (\rho u)}{\partial t} + \frac{\partial (\rho u^2)}{\partial x} + \frac{\partial (\rho uv)}{\partial y} + \frac{\partial P}{\partial x} \right] \right\} + \\
 & + \frac{\partial}{\partial y} \left\{ \rho v - \tau \left[ \frac{\partial (\rho v)}{\partial t} + \frac{\partial (\rho vu)}{\partial x} + \frac{\partial (\rho v^2)}{\partial y} + \frac{\partial P}{\partial y} \right] \right\} = 0, \\
 & \frac{\partial}{\partial t} \left\{ \rho u - \tau \left[ \frac{\partial (\rho u)}{\partial t} + \frac{\partial (\rho u^2)}{\partial x} + \frac{\partial (\rho uv)}{\partial y} + \frac{\partial P}{\partial x} \right] \right\} + \\
 & + \frac{\partial}{\partial x} \left\{ P + \rho u^2 - \tau \left[ \frac{\partial (P + \rho u^2)}{\partial t} + \frac{\partial}{\partial x} (3Pu + \rho u^3) + \frac{\partial}{\partial y} (\rho u^2 v + 2Pu) \right] \right\} + \\
 & + \frac{\partial}{\partial y} \left\{ \rho uv - \tau \left[ \frac{\partial (\rho uv)}{\partial t} + \frac{\partial}{\partial x} (\rho u^2 v) + \frac{\partial}{\partial y} (Pu + \rho uv^2) \right] \right\} = 0, \\
 & \frac{\partial}{\partial t} \left\{ \rho v - \tau \left[ \frac{\partial (\rho v)}{\partial t} + \frac{\partial (\rho v^2)}{\partial y} + \frac{\partial (\rho uv)}{\partial x} + \frac{\partial P}{\partial y} \right] \right\} + \\
 & + \frac{\partial}{\partial y} \left\{ P + \rho v^2 - \tau \left[ \frac{\partial (P + \rho v^2)}{\partial t} + \frac{\partial}{\partial y} (3Pv + \rho v^3) + \frac{\partial}{\partial x} (\rho v^2 u + 2Pu) \right] \right\} + \\
 & + \frac{\partial}{\partial x} \left\{ \rho uv - \tau \left[ \frac{\partial (\rho uv)}{\partial t} + \frac{\partial}{\partial y} (\rho uv^2) + \frac{\partial}{\partial x} (Pv + \rho u^2 v) \right] \right\} = 0, \\
 & \frac{\partial}{\partial t} \left\{ \rho v_0^2 + 3P - \tau \left[ \frac{\partial (\rho v_0^2 + 3P)}{\partial t} + \frac{\partial}{\partial x} (u (\rho v_0^2 + 5P)) + \frac{\partial}{\partial y} (v (\rho v_0^2 + 5P)) \right] \right\} +
 \end{aligned}$$

\*Abstract 1918 submitted to the 21st International Symposium on Rarefied Gas Dynamics, Marseille, France, July 26-31, 1998

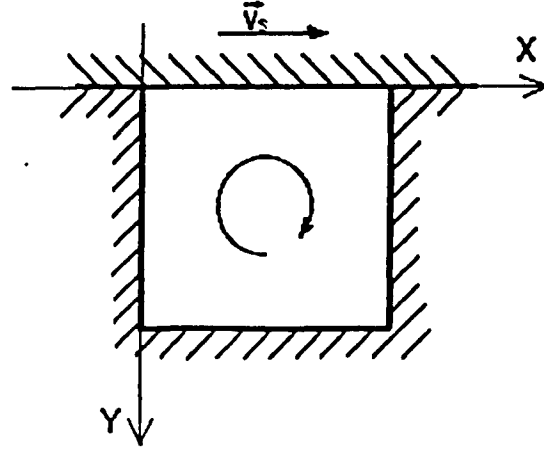


Figure 1:

$$\begin{aligned}
 & + \frac{\partial}{\partial x} \left\{ u(\rho v_0^2 + 5P) - \tau \left[ \frac{\partial}{\partial t} (u(\rho v_0^2 + 5P)) + \frac{\partial}{\partial x} (u^2 \rho v_0^2 + P v_0^2 + 7P u^2 + 5 \frac{P^2}{\rho}) \right. \right. \\
 & \quad \left. \left. + \frac{\partial}{\partial y} (u v \rho v_0^2 + 7P u v) \right] \right\} + \\
 & + \frac{\partial}{\partial y} \left\{ v(\rho v_0^2 + 5P) - \tau \left[ \frac{\partial}{\partial t} (v(\rho v_0^2 + 5P)) + \frac{\partial}{\partial x} (u v \rho v_0^2 + 7P u v) + \right. \right. \\
 & \quad \left. \left. + \frac{\partial}{\partial y} (v^2 \rho v_0^2 + P v_0^2 + 7P v^2 + 5 \frac{P^2}{\rho}) \right] \right\} = 0,
 \end{aligned}$$

where  $v_0^2 = u^2 + v^2$ ;  $u, v$  - components of the hydrodynamic velocity  $\vec{v}_0$  in the  $x, y$  - directions,  $\tau$  - mean free time between collisions which in hydrodynamic regime can be written as  $\tau = \Pi \mu / P$ ;  $\mu$  - dynamical viscosity,  $P$  - static pressure, parameter  $\Pi$  depends on the model of the particles interaction.

Initial conditions :

$(t = 0) \rho = \rho_\infty, P = P_\infty, u = 0, v = 0.$

Boundary conditions:

$(t > 0) u(x, 0) = V_s, v(x, 0) = 0, u(x, L) = 0, v(x, L) = 0$  for  $x \in [0, L]$ ;

$u(0, y) = 0, v(0, y) = 0, u(L, y) = 0, v(L, y) = 0$  for  $y \in [0, L]$ ;

$\left[ \frac{\partial \rho}{\partial x} \right]_{x=0} = 0, \left[ \frac{\partial \rho}{\partial x} \right]_{x=L} = 0$ , for  $y = [0, L]$ ;  $\left[ \frac{\partial \rho}{\partial y} \right]_{y=0} = 0, \left[ \frac{\partial \rho}{\partial y} \right]_{y=L} = 0$ , for  $x = [0, L]$ ;

$\left[ \frac{\partial P}{\partial x} \right]_{x=0} = 0, \left[ \frac{\partial P}{\partial x} \right]_{x=L} = 0$ , for  $y = [0, L]$ ;  $\left[ \frac{\partial P}{\partial y} \right]_{y=0} = 0, \left[ \frac{\partial P}{\partial y} \right]_{y=L} = 0$ , for  $x = [0, L]$ ;

The terms in square brackets, which are proportional to  $\tau$ , correspond to Kolmogorov statistical fluctuations. The system of Eqs. (1)-(4) written in dimensionless form was numerically solved in the vast area of the  $Re, Eu$  alteration,  $6.2 \leq Re \leq 10000$ . Typical flow portraits for the same time moments are different for GHE and NSE simulation.

## References

- [1] Koseff J.R., Street R.L., *Transactions of the ASME*, V.106, pp. 390-398 (1984).
- [2] Alexeev B.V., *Phil. Trans. Roy. Soc., London A*. 349, pp. 417 - 443 (1994).
- [3] Alexeev B.V., *The Generalized Boltzmann Physical Kinetics* (two volumes, in Russian) Publ. Center of the Moscow Fine Chemical Tech.Inst.(1997).

# Numerical Study of Shock Wave Structure Based on Quasigasdynamic Equations with Rotational Nonequilibrium. \*

I. A. Chirokov<sup>1</sup>, T. G. Elizarova<sup>1</sup>, J. C. Lengrand<sup>2</sup>

<sup>1</sup> Institute of Mathematical Modeling, Russian Academy of Sciences, Moscow, Russia

<sup>2</sup> Lab. d'Aérodynamique du CNRS, Meudon, France

## 1 Introduction

The quasigasdynamic (QGD) equation system, obtained in the late 80's, is a model for the description of viscous gas flows. Computer modeling and theoretical investigations showed the validity of this system of equations to describe viscous heat-conductive flows and confirmed also some advantages of it compared with the Navier-Stokes system [1].

This work presents the generalization of the QGD system to flows of non-monoatomic gases with a difference between translational and rotational temperatures. This new system is referred to as QGDR.

## 2 System of equations

A molecule is considered as a rigid rotator, possessing only kinetic energy. We start from the Boltzmann equation, use the Maxwell and Hinshelwood distribution functions for translational and rotational energies, respectively. We use the same procedure as described in [4] and we obtain the QGDR system. The form of this system depends on the number of degrees of freedom of the molecule. The systems for three and two rotational degrees of freedom were obtained in arbitrary 3-dimensional space coordinates.

For the 1D plane flow of molecules, possessing two rotational degrees of freedom, this system has the following form:

$$\begin{aligned} \frac{\partial}{\partial t} \rho + \frac{\partial}{\partial x} \rho u &= \frac{\partial}{\partial x} \tau \frac{\partial}{\partial x} (\rho u^2 + p_T), \\ \frac{\partial}{\partial t} \rho u + \frac{\partial}{\partial x} (\rho u^2 + p_T) &= \frac{\partial}{\partial x} \tau \frac{\partial}{\partial x} (\rho u^3 + 3p_T u_x), \end{aligned}$$

$$\begin{aligned} \frac{\partial}{\partial t} E_T + \frac{\partial}{\partial x} u (E_T + p_T) &= \frac{\partial}{\partial x} \tau \frac{\partial}{\partial x} (E_T + \frac{5}{2} p_T) u^2 \\ &+ \frac{5}{2} \frac{\partial}{\partial x} \tau \frac{p_T}{\rho} \frac{\partial}{\partial x} p_T + \frac{5}{2} \frac{\partial}{\partial x} \tau \frac{p_T}{\rho} \frac{\partial}{\partial x} p_T + S_T, \end{aligned}$$

$$\begin{aligned} \frac{\partial}{\partial t} E_r + \frac{\partial}{\partial x} u E_r &= \frac{\partial}{\partial x} \tau \frac{\partial}{\partial x} E_r u^2 \\ &+ \frac{\partial}{\partial x} \tau \frac{p_r}{\rho} \frac{\partial}{\partial x} p_T + Pr^{-1} \frac{\partial}{\partial x} \tau p_T \frac{\partial}{\partial x} \frac{p_r}{\rho} + S_r. \end{aligned}$$

Here  $p_T$ ,  $E_T$ ,  $p_r$ ,  $E_r$  pressures and energies associated to translation and rotation and defined as

$$\begin{aligned} E_T &= \frac{\rho u^2}{2} + \frac{3p_T}{2} \quad \text{with} \quad p_T = \rho (\mathcal{R}/\mathcal{M}) T_T, \\ E_r &= p_r \quad \text{with} \quad p_r = \rho (\mathcal{R}/\mathcal{M}) T_r, \end{aligned}$$

where  $\mathcal{M}$  is the molar mass and  $\mathcal{R}$  is the universal gas constant. Average pressure and temperature are defined as

$$p_{av} = (3p_T + 2p_r)/5 = \rho (\mathcal{R}/\mathcal{M}) T_{av}.$$

The Prandtl number is taken from Eucken's approximation:  $\gamma = (5 + \zeta)/(3 + \zeta)$ , where  $\gamma$  is the specific heat ratio and  $\zeta$  is the number of internal degrees of freedom of the molecule. For the present work, we had  $\zeta = 2$ ,  $\gamma = 7/5$ ,  $Pr = 14/19$ . The parameter  $\tau$  is the Maxwellian relaxation time  $\tau = \mu/p_{av}$ , where  $\mu$  is the viscosity. The latter is estimated as  $\mu \propto T_{av}^\omega$ , consistent with the model of Variable Hard Sphere molecules.

To calculate exchange terms in energy equations the relaxation model for the collision integral was used and resulted in

$$S_T = \frac{3}{5\tau_r} (p_r - p_T); \quad S_r = -S_T,$$

where  $\tau_r$  can be interpreted as the rotational relaxation time. The equation for rotational energy  $E_r$  can be simplified and approximated as

\*Abstract 2056 submitted to the 21st International Symposium on Rarefied Gas Dynamics, Marseille, France, July 26-31, 1998

$$\frac{\partial}{\partial t} T_r + u \frac{\partial}{\partial x} T_r = (T_{av} - T_r) / \tau_r.$$

Similar equations are often used in the investigations of relaxation processes (see [2], p. 117).

In the case of temperature equilibrium ( $p_T = p_r = p_{av} = p$ ), the QGDR system turns into the one-temperature QGD system with the adequate value of  $\gamma$  for non-monoatomic gas. The equation for energy (for 1D plane flow) writes then

$$\begin{aligned} \frac{\partial}{\partial t} E + \frac{\partial}{\partial x} u(E + p) &= \frac{\partial}{\partial x} \tau \frac{\partial}{\partial x} (E + \frac{5}{2} p) u^2 + \\ &+ \frac{\gamma}{\gamma - 1} \frac{\partial}{\partial x} \frac{\tau p}{\rho} \frac{\partial}{\partial x} p + Pr^{-1} \frac{\gamma}{\gamma - 1} \frac{\partial}{\partial x} \tau p \frac{\partial}{\partial x} \frac{p}{\rho}. \end{aligned}$$

### 3 Results

The present QGDR model can be applied to 3D RGD flows. In this work, however, it was used to investigate the 1D rotational relaxation in a shock wave. The rotational relaxation time was estimated as  $\tau_r = 5\tau$ , although more complicated models, including temperature-dependent ones could be introduced.

An explicit finite-difference method was used. Calculations were carried out for shock waves in a gas of hard-sphere molecules ( $\omega = 1/2$ ) at Mach numbers in the range 2–13. The profiles obtained are shown in Figs.1 and 2, where  $x$  is reduced by the upstream mean free path. Ordinates are reduced as usual based on the Rankine-Hugoniot values upstream and downstream of the shock wave. One can note the similarity between these curves and results presented by Bird [2], p. 298, and by Koura [3]. Detailed comparisons will be presented in the final paper.

The calculation confirmed the stability properties of the QGD system with its associated computational algorithm.

### 4 Conclusion

A continuum model (QGDR) for the description of RGD flows has been developed. It includes the treatment of nonequilibrium between translational and rotational temperatures. Results were obtained based on QGDR equations for the shock wave problem in a wide range of Mach numbers. They show that these equations can be used in addition to approaches based on kinetic theory or DSMC method.

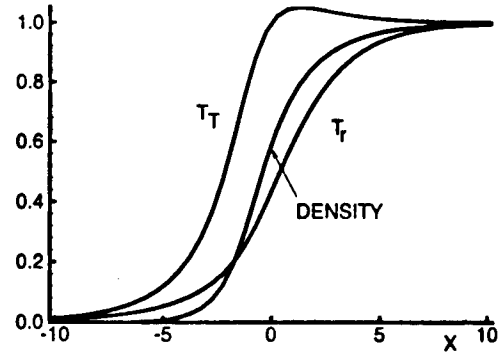


Figure 1: Profiles of reduced temperatures and density for  $Ma = 2$

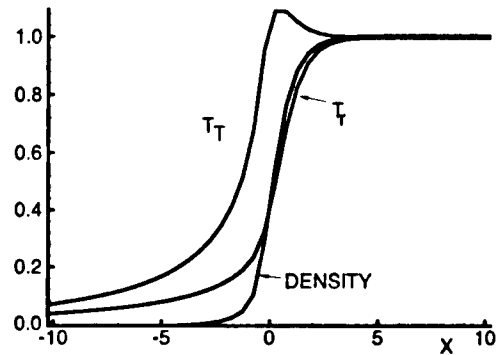


Figure 2: Profiles of reduced temperatures and density for  $Ma = 12.9$

### References

- [1] Elizarova T.G., Graur I.A., Lengrand J.C., Chpoun A., *Rarefied Gas Flow Simulation Based on Quasigasdynamic Equations*, AIAA Journal, 1995, V.33, No.12, pp.2316–2324.
- [2] Bird G.A., *Molecular Gas Dynamics and the Direct Simulation of Gas Flows*, Clarendon press, Oxford, 1994.
- [3] Koura K., *Monte Carlo Direct Simulation of Rotational Relaxation of Diatomic Molecules Using Classical Trajectory Calculations: Nitrogen Shock Wave*, Phys. Fluids, 1997, V.9, No.11, pp. 3543–3549.
- [4] Elizarova T.G., Lengrand J.C., Graur I.A., *Gradient Expansions for Distribution Functions and Derivation of Moment Equations*, this symposium.

# Two-point Kinetic Theory and Two-point Hydrodynamics \*

M. Grmela<sup>1</sup>, G. Lebon<sup>2</sup>

<sup>1</sup> Ecole Polytechnique de Montréal, Canada

<sup>2</sup> Université de Liège, Belgique

The Boltzmann kinetic equation can be cast into the form[1]

$$\frac{dx}{dt} = L(x) \frac{\partial E(x)}{\partial x} - \frac{\partial \Psi}{\partial \left( \frac{\partial S(x)}{\partial x} \right)} \quad (1)$$

where  $x \equiv f_1(1)$  is the one-point distribution function,  $1 \equiv (\mathbf{r}_1, \mathbf{v}_1)$  denoting the position vector and velocity,  $E(x)$  is the energy,  $S(x)$  the entropy,  $L(x)$  the Poisson operator expressing the kinematics of  $x$  and  $\Psi \left( \frac{\partial S(x)}{\partial x} \right)$  is the dissipation potential arising for instance in the Guldberg-Waage dynamics (collisions are regarded as binary chemical reactions, the velocity  $\mathbf{v}$  parametrizes the species).

Also the Navier-Stokes-Fourier hydrodynamic equations can be cast into the form (1). In this case  $x$  represents the five hydrodynamic fields while  $E$ ,  $S$ ,  $L$  and  $\Psi$  have the same physical meaning as for the Boltzmann equation. The passage from the Boltzmann equation to the Navier-Stokes-Fourier equations is thus a reduction preserving the structure (1). It can be shown that the structure (1) guarantees that solutions of any time evolution equation possessing it, agree with the experimentally observed approach to thermodynamic equilibrium.

In this paper we formulate a two-point extension of the Boltzmann equation[2] as another realization of (1) with  $x \equiv (f_2(1), f_2(1,2))$  where  $f_2(1,2)$  is the two-point distribution function. The most interesting new feature of this extension is the collision term. As in the original Boltzmann equation, it is the term that introduces dissipation and time irreversibility into the dynamics. It is however different from the Boltzmann collision term. In the present description collisions redistributing the velocities of the interacting particles are replaced by "precollisions" in which only the identities of the interacting particles are redistributed but their velocities remain unchanged.

In the passage from the two-point kinetic theory to hydrodynamics, we follow two routes. The first one consists of the passage from the two-point kinetic theory to the one-point kinetic theory followed by the passage to hydrodynamics (both passages are, of course, required to preserve the structure (1)). This route is appropriate if the correlations (both the one existing at equilibrium and the one created in the flow) decay faster than the higher moments (in the velocity) of the distribution functions. If the opposite is true, we follow the second route where we pass from two-point kinetic theory first to two-point hydrodynamics and afterwards from the two-point hydrodynamics to classical hydrodynamics. Again, both passages are required to preserve the structure (1). The two-point hydrodynamics obtained in this way represents a new extension of classical hydrodynamics.

## References

- [1] M. Grmela and H.C. Ottinger, Phys.Rev. E56 (1997).
- [2] M.Grmela et al., J.Math.Phys. 34 (1993) 2290

\*Abstract 2651 submitted to the 21st International Symposium on Rarefied Gas Dynamics, Marseille, France, July 26-31, 1998

# Onsager-Casimir Reciprocity Relations in Rotating Gaseous Systems \*

F.M. Sharipov

Departamento de Física, Universidade Federal do Paraná  
81531-990, Curitiba, Brazil

Recently, transport phenomena in rotating systems have attracted an attention of many researchers, see e.g. the papers [1, 2]. The rotation creates an anisotropy in gases and qualitatively changes the transfer of mass, heat and momentum. Moreover, new phenomena appear in rotating gas, which cannot exist in systems at rest.

The aim of the present paper is to obtain the Onsager-Casimir reciprocity relations [3, 4] for rotating gaseous systems basing on the Boltzmann equation and on the boundary condition for the distribution function.

The main idea of the reciprocity relations is as follows: Consider a system rotating with an angular velocity  $\Omega$ . In weak non-equilibrium state all irreversible phenomena arising in the system can be described in the following linear form:

$$J_k = \sum_{n=1}^N \Lambda_{kn}(\Omega) X_n, \quad (1)$$

where  $X_k$  are thermodynamic forces,  $J_k$  are conjugated thermodynamic fluxes and  $\Lambda_{kn}(\Omega)$  are kinetic coefficients, which depend on the angular velocity  $\Omega$ . If the thermodynamic forces and fluxes are chosen so as the entropy production has the form of the sum

$$\sigma = \sum_{k=1}^N J_k X_k, \quad (2)$$

the kinetic coefficients  $\Lambda_{kn}(\Omega)$  are coupled by the Onsager-Casimir reciprocity relations as

$$\Lambda_{kn}(\Omega) = \pm \Lambda_{nk}(-\Omega), \quad (3)$$

The sign is "plus" if both thermodynamic forces  $X_k$  and  $X_n$  have the same parity with respect to the time reversal. If the forces have the different parity, the sign is "minus".

\*Abstract 2686 submitted to the 21st International Symposium on Rarefied Gas Dynamics, Marseille, France, July 26-31, 1998

To prove the relations (3) we start from the stationary Boltzmann equation, which in the rotating reference frame reads

$$\mathbf{v} \cdot \frac{\partial f}{\partial \mathbf{r}} + \mathbf{a} \cdot \frac{\partial f}{\partial \mathbf{v}} = Q(ff_*), \quad (4)$$

$$\mathbf{a} = 2[\mathbf{v} \times \Omega] + [\Omega \times [\mathbf{r} \times \Omega]],$$

where  $Q(ff_*)$  is the collision integral.

We apply the boundary condition regarding the processes of evaporation and condensation on the surface

$$|v_n| f^+(\mathbf{r}, \mathbf{v}) = |v_n| [1 - \alpha(\mathbf{r}, -\mathbf{v})] f_w(\mathbf{r}, \mathbf{v}) + \int_{v'_n < 0} |v'_n| R(\mathbf{r}, \mathbf{v}' \rightarrow \mathbf{v}) f^-(\mathbf{r}, \mathbf{v}') d\mathbf{v}', \quad (5)$$

where  $f^+$  is the distribution function of particles leaving the surface,  $f^-$  is the distribution function of incident particles,  $v_n$  is the normal velocity component,  $f_w$  is the surface Maxwellian. The scattering kernel  $R(\mathbf{r}, \mathbf{v}' \rightarrow \mathbf{v})$  satisfies the normalizations condition

$$\int_{v_n > 0} R(\mathbf{r}, \mathbf{v}' \rightarrow \mathbf{v}) d\mathbf{v} = \alpha(\mathbf{r}, \mathbf{v}'),$$

where

$$0 \leq \alpha(\mathbf{r}, \mathbf{v}') \leq 1,$$

and the reciprocity condition

$$|v'_n| f'_w R(\mathbf{v}' \rightarrow \mathbf{v}) = |v_n| f_w R(-\mathbf{v} \rightarrow -\mathbf{v}'). \quad (6)$$

In the equilibrium state the Maxwellian distribution function is established

$$f_0 = n_0(\mathbf{r}) \left( \frac{m}{2\pi k T_0} \right)^{3/2} \exp \left( -\frac{mv^2}{2kT_0} \right),$$

where  $T_0$  is the equilibrium temperature, which is constant over the whole region occupied by the gas. The number density  $n_0(\mathbf{r})$  has a non-uniform distribution, which can be obtained from the static

equilibrium between the centrifugal force and the gas pressure.

In case of weak non-equilibrium state the linearization of the distribution function is performed near the Maxwellian  $f_0$ , i.e.

$$f(\mathbf{r}, \mathbf{v}) = f_0 [1 + h(\mathbf{r}, \mathbf{v})], \quad |h| \ll 1. \quad (7)$$

Substituting (7) into (4) one obtains the linearized Boltzmann equation

$$\hat{D}(\Omega)h - \hat{L}h = 0, \quad (8)$$

where  $\hat{D}$  is the differential operator containing  $\Omega$  via the acceleration  $\mathbf{a}$

$$\hat{D}(\Omega) = \mathbf{v} \cdot \frac{\partial}{\partial \mathbf{r}} + \mathbf{a} \cdot \frac{\partial}{\partial \mathbf{v}},$$

and  $\hat{L}$  is the linear collision operator.

The linearized boundary condition (5) takes the form

$$h^+ = \hat{A}h^- + h_w - \hat{A}h_w,$$

where  $\hat{A}$  is the gas-surface interaction operator and  $h_w$  is the perturbation of the surface Maxwellian

$$f_w = f_0(1 + h_w).$$

Let us introduce the following scalar products

$$(\phi, \psi) = \int f_0 \phi(\mathbf{r}, \mathbf{v}) \psi(\mathbf{r}, \mathbf{v}) d\mathbf{v},$$

$$((\phi, \psi)) = \int_{\mathcal{R}} (\phi, \psi) d\mathbf{r},$$

where  $\mathcal{R}$  is the region occupied by the gas, and the operator of the time reversal

$$\hat{T}\phi(\mathbf{r}, \mathbf{v}) = \phi(\mathbf{r}, -\mathbf{v}).$$

The linear collision operator  $\hat{L}$  satisfies the well-known relation

$$((\hat{T}\hat{L}\phi, \psi)) = ((\hat{T}\hat{L}\psi, \phi)). \quad (9)$$

With the help of (6) it can be proved that

$$\begin{aligned} & ((\hat{T}\hat{D}(\Omega)\phi, \psi)) + \int_{\partial\mathcal{R}} (\hat{T}v_n\phi_w, \psi) \\ &= ((\hat{T}\hat{D}(-\Omega)\psi, \phi)) + \int_{\partial\mathcal{R}} (\hat{T}v_n\psi_w, \phi). \end{aligned} \quad (10)$$

If a set of the small parameters  $X_k$  are used for the linearization, the perturbation of the surface Maxwellian  $h_w$  and the solution  $h$  of Eq.(8) can be decomposed as

$$h_w(\mathbf{r}, \mathbf{v}) = \sum_k h_w^{(k)}(\mathbf{r}, \mathbf{v}) X_k, \quad (11)$$

$$h(\mathbf{r}, \mathbf{v}) = \sum_k h^{(k)}(\mathbf{r}, \mathbf{v}) X_k. \quad (12)$$

In the present work it is proved that the entropy production in the system has the following expression

$$\sigma = \int_{\partial\mathcal{R}} (v_n h_w, h) dS. \quad (13)$$

Substituting (11) into (13) one can see that to satisfy Eq.(2) the thermodynamic fluxes must be defined as

$$J_k = \int_{\partial\mathcal{R}} (v_n h_w^{(k)}, h) dS, \quad (14)$$

if  $X_k$  are assumed to be thermodynamic forces. Substituting (12) into (14) and comparing it with (1) we conclude that the kinetic coefficients have the form

$$\Lambda_{kn}(\Omega) = \int_{\partial\mathcal{R}} (v_n h_w^{(k)}, h^{(n)}) dS. \quad (15)$$

In the report the relations (3) for the kinetic coefficients (15) are proved basing on the relations (9) and (10). Some examples of the application of the present theory are given. New cross effects arising only in rotating systems are indicated.

## References

- [1] F.M. Sharipov and G.M. Kremer, *Eur. J. Mech. B/Fluids* **15**, 493 (1996).
- [2] P. Biscari and C. Cercignani, *Continuum Mech. Thermodyn.* **9**, 1 (1997).
- [3] L. Onsager, *Phys. Rev.* **37**, 405 (1931); **38** 2265 (1931).
- [4] H.B.G. Casimir, *Rev. Mod. Phys.* **17** 343 (1945).



# Discrete kinetic models for the Boltzmann equation and applications to evaporation and condensation problems \*

I. Nicodin, P. Duruisseau, R. Gatignol

Laboratoire de Modélisation en Mécanique, Université Pierre et Marie Curie et CNRS,  
Paris, France

In discrete kinetic theory, the choice of the discrete molecular models is very important. To introduce the temperature, which is a fundamental quantity in the problems of evaporation and condensation, the models must include velocities with at least two different moduli. Owing to the discretisation the definition of temperature given by the classical kinetic theory is no longer valid, so, here we use the "kinetic" temperature [2]. We present in this paper a class of discrete plane models with binary collisions and we analyze the evaporation condensation problem.

## 1 Two dimensional plane models

For a gas with identical particles we introduce two dimensional models related to the square. The velocities of a model are  $\vec{u}_i = a_k \vec{i} + b_k \vec{j}$ , in an orthonormal system of coordinates ( $Oxy$ ), with:  $-(2l-1) \leq a_k \leq 2l-1$ ;  $-(2l-1) \leq b_k \leq 2l-1$ ;  $a_k, b_k \in \mathbb{Z}$ ,  $l \in \mathbb{N}^*$ . This is the model "l". The velocities are symmetrically with respect to the coordinates axis, then the determinations of the binary collisions are easily made by computer. By mathematical proof, we show that there are only physical linearly independent summational invariants (mass, momentum, energy).

## 2 Boundary conditions

As usual we denote by  $N_j$  the number density of particles  $\vec{u}_j$ ,  $N_{jw}$  the Maxwellian density of particles  $\vec{u}_j$ , the index  $w$  referring the particles on respect to the boundary. We suppose that we don't have parallel velocities to the interface boundary and the velocity set is symmetrical with respect to this interface. The indices  $i, r$  are referring at impinging and reflected particles on respect to the boundary. Here we take models having velocities symmetrical with respect to the interface.

For vacuum evaporation  $N_r = n_{sat} N_{rw}$ . For evaporation condensation at equilibrium the fluxes of evaporating and condensing molecules counterbalance each other. We have  $n_r = \frac{n_{sat}}{2}$ . With  $n_{sat}$  is the saturation density and  $n_r = \sum N_r$  the total density for the reflected particles. In the general case, we make the assumption that the number of emitted particles is the same in equilibrium as in non-equilibrium. So we put  $N_r = n_{sat} N_{rw}$ .

## 3 Evaporation condensation problem

*Evaporation condensation between two interfaces.* In the orthonormal system of coordinates ( $Oxy$ ), we consider two condensed phases limited by two plane parallel surfaces located at  $y = 0$  and  $y = L$ . The two condensed phases are kept at constant different temperatures. The geometric modification brought by the evaporation or the condensation are assumed negligible. So we can suppose that the motion of the gas is stationary and the microscopic quantities (and the macroscopic also) depend on only one space variable, the distance in the direction orthogonal to the interfaces. The boundary condition on  $y = 0$  are given only for the microscopic densities of emerging particles and on  $y = L$  only the others densities.

*The half space problem.* We analyze the steady behavior of the gas from the plane  $y = 0$  to the infinity. The boundary conditions on  $y = 0$  are given as the previous problem and at infinity, the gas is uniform and has a normal velocity to the condensed phase, and thus its molecular distribution is Maxwellian with the temperature  $T_\infty$ , the numerical density  $n_\infty$  and the velocity component  $v_\infty$ . The problem can be solved when some relations

\* Abstract 3001 submitted to the 21st International Symposium on Rarefied Gas Dynamics, Marseille, France, July 26-31, 1998

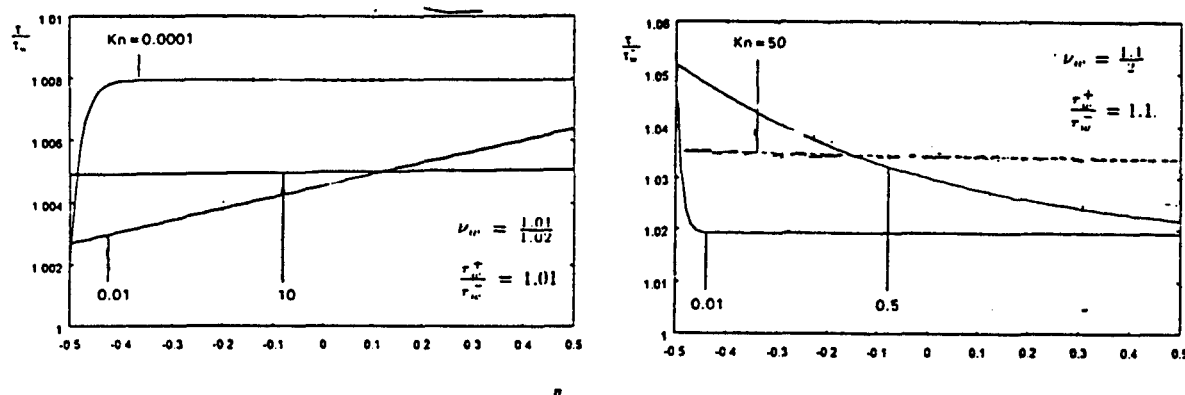
between the macroscopic variables of the condensed phase at  $y = 0$  and the macroscopic variables at infinity are satisfied .

We solve two problems numerically by a Runge-Kuta method, for the several models "I" , for a large number of parameters.

## 4 Results

For the evaporation condensation problem between two surfaces we analyze the profile of the kinetic temperature and the profile of the other macroscopic quantities also . We observe here the jumps of the kinetic temperature on the interfaces. With adequate choice of the parameters the kinetic temperature suffers a jump at the hotter interface , remains almost constant until the flux coming from the hotter interface meets the flux coming from the cooler one . With other choices of the flow parameters, we are a monotonically increasing or decreasing profile with a maximum of the kinetic temperature. At last we can also observe the "famous" inverted profile of the kinetic temperature. These results are in good agreement with the results obtained by Aoki and Masukawa [4].

We realize this study for a several models "I" . We observe that the profiles for the different "I" are comparable.



For the half space evaporation problem, the kinetic temperature profile is monotonically increasing.

## 5 Conclusions

The aim of this work has been to obtain a kinetic temperature profile for the evaporation condensation problems, by using discrete simple models. We show that, we do not have to take a large number of velocities to obtain similar results to those already establish with other methods of resolution of the Boltzmann equation.

To look to the future, the case under consideration is to study the same problem by using three dimensional models, and also to compare with a Monte Carlo solution.

## References

- [1] A. d'Almeida - *These de Doctorat de l'Université Paris 6* , 53-68 86-99,1995
- [2] A.d'Almeida , R. Gatignol - *Eur. J Math. Fluids*,116, 401-428, 1997
- [3] K. Aoki, Y. Sone, T. Yamada -*Phys. Fluids,A*, Vol 2,1867-1878,1990.
- [4] K. Aoki and N. Masukawa *Phys. Fluids*, Vol 6,1378-1395, 1994

# Numerical Experiments and Modelling of Non-Equilibrium Effects in Dilute Granular Flows \*

M. Sakiz<sup>1</sup>, O. Simonin<sup>1, 2</sup>

<sup>1</sup> Laboratoire National d'Hydraulique / EDF, Chatou, France

<sup>2</sup> Institut de Mecanique des Fluides / INPT, Toulouse, France

## 1 Introduction

Continuum theories of highly agitated granular flows have recently been developed in the frame of the kinetic theory of gases, with the mean kinetic energy of the particle velocity fluctuations corresponding to the temperature of the gas. This approach has originally been applied to dense systems of identical, smooth, nearly elastic spheres. For these flows, the main difference between kinetic theory for gas and granular materials is due to the inelasticity of the grains which induces a loss of kinetic energy in collisions between pairs of particles. So, the practical closure laws for the momentum flux, energy flux and rate of dissipation due to collision can be derived by presuming a velocity distribution close to equilibrium maxwellian function. Extension towards dilute flows involves the determination of the influence of the surrounding fluid, which can induce dissipation or production of particle kinetic energy, and of non-equilibrium effects due to the low collision frequency. This paper concerns numerical simulation and continuum modelling of particles suspended in a turbulent gas vertical channel flow. Comparisons are made between the results obtained with a discrete particle simulation method (the so-called numerical experiment) and those obtained using a continuum approach derived in the frame of Grad's theory. The influence of the fluid turbulence on the particles and the influence of the particles on the fluid (two-way coupling) are not included in the computations, in order to focus on the effect of inter-particle and wall-particle collisions on the particle statistics. In the discrete particle simulations, particle movement is only governed by drag, gravity and inter-particle collisions. Wall-particle interaction treatment allows to account for frictional inelastic bouncing. Periodic boundary conditions are used in the streamwise and spanwise directions.

The computational domain for the discrete particle simulations is a rectangular box, 240mm long and 40mm wide, with periodic boundary conditions in the streamwise and spanwise directions. The stationary state for the mean particle properties is usually reached after about 10 times the fluid/particle interaction characteristic time and 100 times the collisional characteristic time. Afterwards, statistics are calculated over 50000 to 100000 time steps in order to get more than  $3.10^6$  particle velocity measurements in each averaging cell.

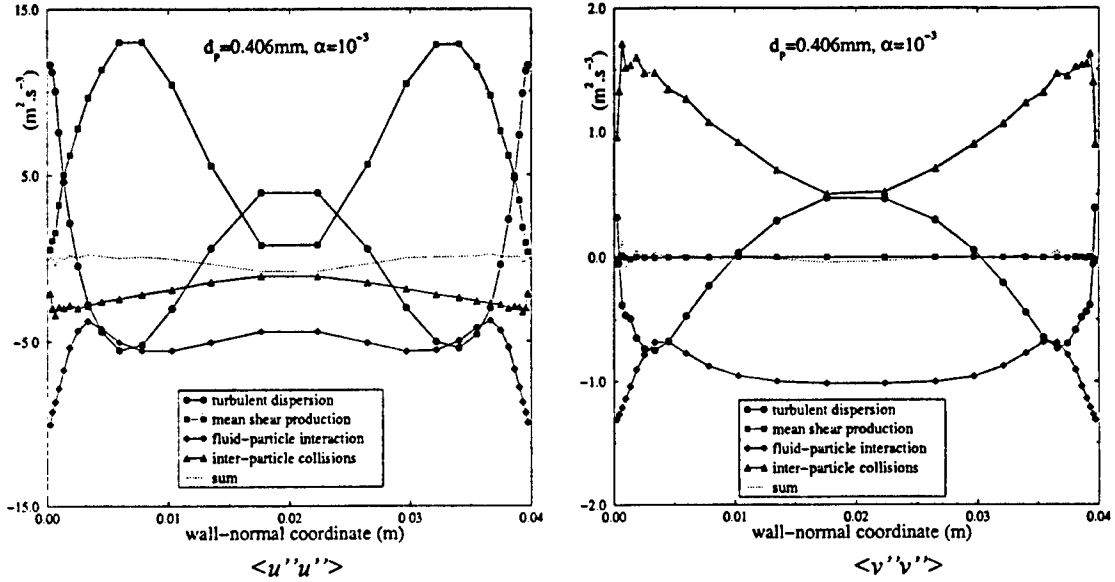
The continuum approach is based on the calculation of separate transport equations for the first three velocity moments of the particle distribution function: number density, mean velocity and kinetic stress tensor components. A Boussinesq approximation is used to model the third order moments. Discrete particle simulation results are presented and discussed for two different particle diameters and various concentrations. Budget graphs are drawn to show the main production, transport and destruction mechanisms up to the third order velocity moments. Comparisons between measured velocity distribution from simulations and presumed maxwellian or Grad distributions are performed, focussing on the very near-wall region.

## References

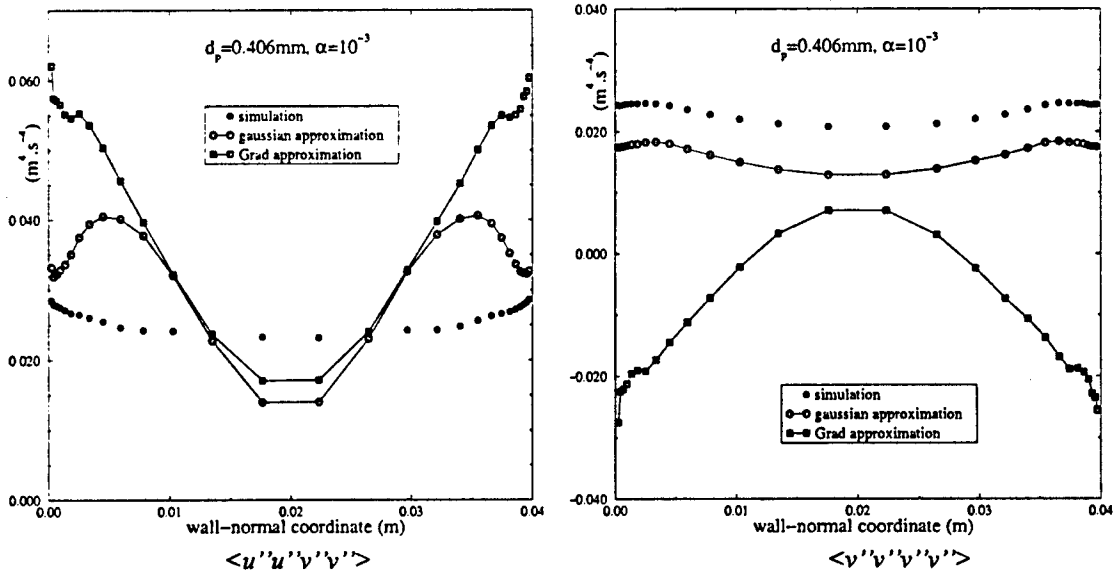
- [1] Grad H., *On the Kinetic Theory of Rarefied Gases*, Comm. Pure and Appl. Math., Vol. 2, pp. 331-407, 1949.
- [2] He J., Simonin O., *Non-Equilibrium Prediction of the Particle-Phase Stress Tensor in Vertical Pneumatic Conveying*, Gas-Solid Flows, ASME FED, Vol. 166, pp. 253-263, 1993.
- [3] Jenkins J.T., Richmann M.W., *Grad's 13-Moments System for a Dense Gas of Inelastic Spheres*, Arch. Ration. Mech. Anal., Vol. 87, pp. 355-377, 1985.

\*Abstract 3003 submitted to the 21st International Symposium on Rarefied Gas Dynamics, Marseille, France, July 26-31, 1998

- [4] Simonin O., *Continuum Modelling of Dispersed Two-Phase Flows*, in *Combustion and Turbulence in Two-Phase Flows*, 1995-1996 Lectures Series Programme, von Karman Institute, Belgium, 1996.



Profiles of the budget of the second-order velocity correlation equations computed from discrete particle simulation results in a vertical gas-solid channel flow : particle diameter  $d_p = 406 \mu\text{m}$ , particle density  $\rho_p = 1038 \text{ kg m}^{-3}$ , particle volumetric fraction  $\alpha = 10^{-3}$  ( $u''$  and  $v''$  are the streamwise and wall-normal turbulent particle velocity components, respectively).



Comparison between discrete particle simulation results and continuum model predictions for the fourth-order particle velocity correlations.

# Some Properties of a Gas with an Ellipsoidal Velocity Distribution Function \*

T.G. Elizarova<sup>1</sup>, J.C. Lengrand<sup>2</sup>

<sup>1</sup> Institute for Mathematical Modeling, Russian Acad. Sci., Moscow, Russia

<sup>2</sup> Laboratoire d'Aérodynamique du CNRS, Meudon, France

A number of properties of a gas with an ellipsoidal distribution function  $f_e$  are examined. The purpose of this work is to express the translational relaxation time in terms of direction-dependent temperatures  $T_x, T_y, T_z$ , rather than in terms of a unique temperature  $T$ .

After transformation we get

$$\langle c \rangle = \text{Int}(A, B, C) / [2\sqrt{\pi^3}].$$

Thus ratio between the mean relative velocity and the mean thermal velocity is equal to

$$\langle c_r \rangle / \langle c \rangle = \sqrt{2},$$

as in an equilibrium gas. This conclusion is interesting in itself and moreover it has a consequence on the mean free path  $\lambda$  in a hard-sphere gas of total collisional cross-section  $\sigma_0$  and number density  $n$ :

$$\lambda = \frac{\langle c \rangle}{\langle c_r \rangle} \times \frac{1}{n\sigma_0} = \frac{1}{\sqrt{2}n\sigma_0}$$

both for Maxwellian and ellipsoidal distribution functions.

## Three-temperature gas

The mean relative velocity of gas molecules (1) and (2) is calculated as

$$\begin{aligned} \langle c_r \rangle &= \frac{1}{\rho^2} \iint |\vec{c}_1 - \vec{c}_2| f_e(\vec{c}_1) f_e(\vec{c}_2) d\vec{c}_1 d\vec{c}_2 = \\ &= \frac{1}{\pi^3} \iint \sqrt{(c_{x1} - c_{x2})^2 + (c_{y1} - c_{y2})^2 + (c_{z1} - c_{z2})^2} \\ &\times \exp\left(-\frac{c_{x1}^2 + c_{x2}^2}{2RT_x}\right) \exp\left(-\frac{c_{y1}^2 + c_{y2}^2}{2RT_y}\right) \exp\left(-\frac{c_{z1}^2 + c_{z2}^2}{2RT_z}\right) \\ &\times \frac{dc_{x1}}{\sqrt{2RT_x}} \frac{dc_{x2}}{\sqrt{2RT_x}} \frac{dc_{y1}}{\sqrt{2RT_y}} \frac{dc_{y2}}{\sqrt{2RT_y}} \frac{dc_{z1}}{\sqrt{2RT_z}} \frac{dc_{z2}}{\sqrt{2RT_z}} \end{aligned}$$

where  $R$  is the perfect-gas constant and  $\rho$  is the density. After transformation, we get

$$\langle c_r \rangle = \text{Int}(A, B, C) / \sqrt{2\pi^3},$$

where

$$A = 2RT_x, \quad B = 2RT_y, \quad C = 2RT_z \quad \text{and}$$

$$\text{Int}(A, B, C) = \int_0^\pi \sin \theta \times \int_0^{2\pi} \sqrt{A \sin^2 \theta \cos^2 \phi + B \sin^2 \theta \sin^2 \phi + C \cos^2 \theta} d\phi \times d\theta.$$

Similarly we calculate the mean thermal velocity:

$$\begin{aligned} \langle c \rangle &= \frac{1}{\rho} \int c f_e d\vec{c} = \frac{1}{\sqrt{\pi^3}} \int \sqrt{c_x^2 + c_y^2 + c_z^2} \\ &\times \exp\left(-\frac{c_x^2}{2RT_x}\right) \exp\left(-\frac{c_y^2}{2RT_y}\right) \exp\left(-\frac{c_z^2}{2RT_z}\right) \\ &\times \frac{dc_x}{\sqrt{2RT_x}} \frac{dc_y}{\sqrt{2RT_y}} \frac{dc_z}{\sqrt{2RT_z}} \end{aligned}$$

\*Abstract 3237 submitted to the 21st International Symposium on Rarefied Gas Dynamics, Marseille, France, July 26-31, 1998

## Two-temperature gas

We consider the (extreme) particular nonequilibrium case, with  $A = B \neq C$ , which corresponds to  $T_x = T_y \neq T_z$ . Such a situation is encountered, e.g., in the problem of shock wave structure, in the 1D relaxation problem, in the 1D gas expansion problem and in a number of other situations where the flow velocity is directed along the  $z$ -axis. The integral  $\text{Int}(A, B, C)$  can be found explicitly as

$$\text{Int}(A, C) = 2\pi \int_0^\pi \sin \theta \sqrt{A \sin^2 \theta + C \cos^2 \theta} d\theta.$$

For  $A < C$  or  $T_x = T_y < T_z$ , we find

$$\begin{aligned} \text{Int}(A, C) &= \\ &= 2\pi\sqrt{C} \left( 1 + \frac{A}{2\sqrt{C(C-A)}} \ln \frac{\sqrt{C} + \sqrt{C-A}}{\sqrt{C} - \sqrt{C-A}} \right). \end{aligned}$$

For  $A > C$  or  $T_x = T_y > T_z$ , we find

$$\text{Int}(A, C) = 2\pi\sqrt{C} \left( 1 + \frac{A}{\sqrt{C(A-C)}} \arcsin \frac{\sqrt{A-C}}{A} \right).$$

In both cases, the resulting expression of  $\langle c_r \rangle$  is

$$\langle c_r \rangle = 2\sqrt{\frac{RT_z}{\pi}} (1 + \mathcal{A}(T_z, T_x)),$$

where  $\mathcal{A}(T_z, T_x) =$

$$\left\{ \begin{array}{l} = \frac{T_x}{2\sqrt{T_z(T_z - T_x)}} \times \ln \frac{\sqrt{T_z} + \sqrt{T_z - T_x}}{\sqrt{T_z} - \sqrt{T_z - T_x}} \\ \quad \text{if } T_x < T_z \\ \\ = \frac{T_x}{\sqrt{T_z(T_x - T_z)}} \times \arcsin \sqrt{\frac{T_x - T_z}{T_x}} \\ \quad \text{if } T_x > T_z \end{array} \right.$$

When  $T_x \rightarrow T_z$ , both expressions result in  $\mathcal{A} \rightarrow 1$ , and  $\langle c_r \rangle \rightarrow 4\sqrt{RT/\pi}$  which is the mean relative velocity in an equilibrium gas.

The mean collisional time  $\tau_c$  and the mean collision frequency  $\nu$  are given by

$$\tau_c = 1/\nu = 1/(\langle \sigma c_r \rangle n)$$

where  $\sigma$  is the total collisional cross-section.

For the limiting case of **hard-sphere molecules** ( $\sigma = \sigma_0 = \text{cste}$ )

$$\langle \sigma c_r \rangle = \sigma_0 \langle c_r \rangle \quad \text{and}$$

$$\tau_c = 1/(n \sigma_0 \langle c_r \rangle).$$

We calculate the ratio of the collisional times  $\tau_{c,e}$  and  $\tau_{c,0}$  in gases with ellipsoidal distribution function (temperatures  $T_x, T_y, T_z$ ) and with maxwellian distribution function (temperature  $T = (1/3)(T_z + 2T_x)$ ), respectively.

$$\frac{\tau_{c,e}}{\tau_{c,0}} = \frac{2\sqrt{T}}{\sqrt{T_z}(1 + \mathcal{A}(T_z, T_x))}.$$

The variation of  $\tau_{c,e}/\tau_{c,0}$  against  $\Delta T/T$  is plotted in Fig.1, where  $\Delta T = T_z - T_x$  ( $T_x = T - \Delta T/3$ ,  $T_z = T + 2\Delta T/3$ ).

For  $\Delta T = 0$ ,  $T_x = T_z = T$ ,  $\mathcal{A} = 1$  and  $\tau_{c,e} = \tau_{c,0}$ .

When  $\Delta T$  increases ( $T_z > T_x$ ), the value of  $\tau_{c,e}$  increases monotonically and reaches a maximum value equal to  $1.15 \tau_{c,0}$  for  $\Delta T = 3T$ , which corresponds to  $T_x = 0$ ,  $T_z = 3T$ .

When  $\Delta T$  decreases ( $T_z < T_x$ ), the value of  $\tau_{c,e}$  increases monotonically again and reaches a maximum value equal to  $1.04 \tau_{c,0}$  for  $\Delta T = -(3/2)T$ , which corresponds to  $T_z = 0$ ,  $T_x = (3/2)T$ .

In the limiting case of **hard-sphere molecules** with an ellipsoidal distribution function,  $\tau_{c,e} \geq \tau_{c,0}$  and differs by at most 15 % from an equilibrium gas estimation based on the average temperature  $T$ .

In the other limiting case of **Maxwell molecules**,  $\sigma$  is proportional to  $c_r^{-1}$  and  $\tau_c$  does not depend on molecular velocities. We have always  $\tau_{c,e} = \tau_{c,0}$ .

Thus for realistic gases the mean collisional time always surpasses the equilibrium one and can be estimated from the mean temperature with an accuracy better than 15%.

The quasigasdynamic (QGD) equations [1] introduce a translational relaxation time  $\tau = \mu/p$  where  $\mu$  is the viscosity coefficient and  $p$  the pressure. For **VHS molecules** characterized by  $\mu \propto T^\omega$ , intermediate between hard-sphere ( $\omega = 1/2$ ) and Maxwell ( $\omega = 1$ ) molecules, the ratio  $\tau/\tau_c$  is a function of  $\omega$  only. Thus the above conclusion for  $\tau_c$  holds also for  $\tau$ . When solving QGD equations in their three-temperature formulation, results are nearly indistinguishable whether the expression for  $\tau$  accounts for anisotropy or not.

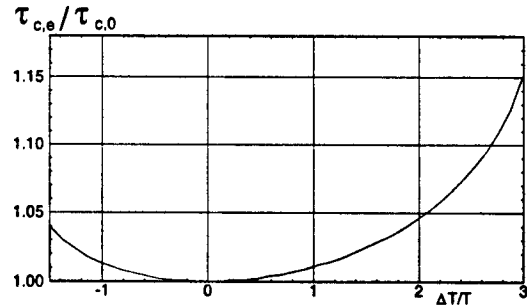


Figure 1: Variation of collisional time with translational nonequilibrium (hard-sphere molecules)

## References

- [1] Elizarova T.G., Lengrand J.C., Graur I.A., *Gradient Expansions for Distribution Functions and Derivation of Moment Equations*, this symposium.

# Transport phenomena in magnetized plasmas \*

B. Lucquin-Desreux

Lab. d'Analyse Numérique, Univ. P. et M. Curie, France

## 1 Introduction

We here look for the macroscopic behaviour of a mixture composed of electrons and of one species of ions. The starting point of the study is the coupled system formed by the kinetic equations associated with each of the two species of the mixture: these are Vlasov equations with source terms of Fokker-Planck type which model either the intra-species collisions or the collisions with the particles of the other species. This study which started in [1] in the homogeneous case, was then extended to the inhomogeneous case in [2] and [3]. The present case is more general, since it includes the presence of a magnetic field. We also give a mathematical frame in order to justify the asymptotic expansions used to derive the limit fluid model.

## 2 The scaled kinetic equations

We introduce a small parameter  $\varepsilon$  which represents the square root of the mass ratio between the two species (the index  $L$  is related to the light species, i.e. the electrons, and the index  $H$  represents the ions):  $\varepsilon = \sqrt{m^L/m^H}$ ,  $m^L \ll m^H$ . The distribution function  $f^\alpha = f^\alpha(t, x, v)$  of the  $\alpha$  species ( $\alpha$  and  $\beta$  denote each one of the indices  $L$  or  $H$ ) satisfies the following Vlasov-Fokker-Planck equation

$$\begin{aligned} \frac{\partial f^\alpha}{\partial t} + v \cdot \nabla_x f^\alpha + \frac{F^\alpha}{m^\alpha} \cdot \nabla_v f^\alpha \\ = Q^{\alpha\alpha}(f^\alpha, f^\alpha) + Q^{\alpha\beta}(f^\alpha, f^\beta), \quad \beta \neq \alpha, \end{aligned}$$

where  $F^\alpha = F^\alpha(t, x, v) = q^\alpha [E(t, x) + v \wedge B(t, x)]$  denotes the Lorentz force. The Fokker-Planck operators  $Q^{\alpha\alpha}$  and  $Q^{\alpha\beta}$  represent all the collisions of a  $\alpha$  particle with the particles of the same species or of the other species respectively. We suppose the two following hypothesis:

- the interacting potentials between the different species are all of the same order of magnitude,

so that the scattering cross-sections only differ through the masses

- the two species have temperatures and densities of the same order of magnitude; we denote them respectively by  $n_0$  and  $T_0$ .

We deduce that the thermal velocities defined by  $V^\alpha = \sqrt{k_B T_0 / m^\alpha}$ ,  $k_B$  being the Boltzmann constant, satisfy  $V^H = \varepsilon V^L$ . We then have a "double scaling"

$$m^L = \varepsilon^2 m^H, \quad V^H = \varepsilon V^L,$$

concerning the masses and the velocities.

Choosing a set of some relevant characteristic physical sizes, we scale the above kinetic equations. This puts in evidence the order of magnitude of the different collision operators as well as that of the transport terms. More precisely, let us denote by  $t_0$  the characteristic collision time of the light species (note that  $t_0/\varepsilon$  is the characteristic collision time of the heavy particles) and by  $L_0$  the common mean free path of the two species. Let us choose an electric field unit  $E_0$  and a magnetic field one  $B_0$  such that  $E_0 L_0 = k_B T_0$  and  $V^L B_0 = E_0$ . At the kinetic scale  $(t_0, L_0, E_0, B_0)$  of the light species, the equations write (the intra-species collision operators still depend on  $\varepsilon$ )

$$\begin{aligned} \frac{\partial f^L}{\partial t} + v^L \cdot \nabla_x f^L + F^L \cdot \nabla_{v^L} f^L \\ = Q^{LL}(f^L, f^L) + Q^{LH,\varepsilon}(f^L, f^H), \\ \frac{\partial f^H}{\partial t} + \varepsilon [v^H \cdot \nabla_x f^H + F^H \cdot \nabla_{v^H} f^H] \\ = \varepsilon [Q^{HL,\varepsilon}(f^H, f^L) + Q^{HH}(f^H, f^H)], \end{aligned}$$

with  $F^L = E + v^L \wedge B$  and  $F^H = E + \varepsilon v^H \wedge B$ .

## 3 Hilbert and Chapman-Enskog expansions

We describe the evolution of the mixture, by considering "expanded" time-space and force scales. The most interesting scale is  $(t_0/\varepsilon^2, L_0/\varepsilon, \varepsilon E_0, B_0)$ :

\* Abstract 3257 submitted to the 21st International Symposium on Rarefied Gas Dynamics, Marseille, France, July 26-31, 1998

it is in fact an hydrodynamic scale for the heavy species and a diffusive one for the light particles. Although these results exactly correspond to the classical mono-species theory applied to any of the two species, let us note that we do not need here any additional condition, like incompressibility: in fact, the very rapid relaxation towards 0 of the mean velocity of the light species, makes that the convection terms of the light species are of order 1 instead of being of order  $1/\varepsilon$ .

By an Hilbert expansion, we obtain at this scale a coupled system made of classical Euler compressible equations for the density, mean velocity and temperature of the heavy species, coupled with diffusion equations for the density and temperature of the light particles. The coupling appears on one hand through reacting terms in the right hand side of the equations, which represent the transfers of impulse and energy between the two species; on the other hand, through various transport coefficients. A Chapman-Enskog expansion allows to compute corrective terms, of order  $\varepsilon$ , in the gas dynamic equations for the heavy species; the expression of the viscous and thermal diffusion terms are exactly the same as in the mono-species theory. A similar Chapman-Enskog expansion for the light species does not give any supplementary term.

Finally, we can write this model in a conservative form. We then obtain a coupled system of compressible Navier-Stokes equations in which the inertial and viscosity terms of the light species have been neglected. Concerning the heavy particles, the viscous strain tensor and the heat flux are both of order  $\varepsilon$ .

## 4 Mathematical justification

In order to justify the previous Hilbert expansion, we study the linearized operator  $\Gamma^L$  associated with the light species. This operator is the sum of three operators: a classical mono-species Fokker-Planck operator, an operator of diffusion type which is connected to the heavy species only through its density, and finally an antisymmetric operator due to the magnetic field.

We first study the solvability properties of equations of the type  $\Gamma^L \varphi = \psi$ . The main difficulties are to show that the operator  $\Gamma^L$  is closed and of closed range. The presence of an antisymmetric operator does not allow to use classical perturbation techniques; we thus decide to work in terms of maximal accretive operators. The analysis is completely carried out in the case of hard potentials. It is done in the frame of  $L^2$  type spaces which are weighted

by a centered Maxwellian  $M^L$  (i.e. of zero mean velocity), namely in  $\{\varphi, \int_{\mathbb{R}^3} \varphi M^L dv < +\infty\}$ .

We give necessary and sufficient conditions for the solvability of equations  $\Gamma^L \varphi = \psi$ . We also show two types of regularity results for the eventual solutions  $\varphi$ . All the results we obtain are also valid for the linearized operator associated with the heavy species, since this one is the classical mono-species Fokker-Planck linearized operator. These properties allow to completely justify the Hilbert expansion; we can also justify the Champan-Enskog expansion for the heavy species.

## References

- [1] P. Degond, B. Lucquin-Desreux, *The asymptotics of collision operators for two species of particles of disparate masses*, Math. Models and Methods in the Appl. Sciences, vol.6, No 3, 1996, pp 405-436.
- [2] P. Degond, B. Lucquin-Desreux, *Comportement hydrodynamique d'un mélange gazeux formé de deux espèces de particules de masses très différentes*, C. R. Acad. Sci. Paris, t. 322, Série I, p. 405-410, 1996.
- [3] P. Degond, B. Lucquin-Desreux, *Transport coefficients of plasmas and disparate mass binary gases*, Transp. Theory in Stat. Phys., Vol 25, n° 6, pp. 595-633, 1996.
- [4] B. Lucquin-Desreux, *Fluid limit for magnetized plasmas*, Publication du Labo. d'Analyse Numérique de Paris 6 n° 97019, 1997 ; submitted.



# Solutions to Steady Detonation and Linear Stability in Discrete Kinetic Theory 21st International Symposium on Rarefied Gas Dynamics \*

M. Pandolfi Bianchi<sup>1</sup>, A. J. Soares<sup>2</sup>

<sup>1</sup>Dipartimento di Matematica, Politecnico di Torino, Italy

<sup>2</sup>Departamento de Matemática, Universidade de Coimbra, Portugal

## 1 Introduction

The detonation is usually studied as a shock driven by the energy release of an exothermic chemical reaction in a high speed compressible flow. The governing equations describing the system are the hyperbolic Euler equations of inviscid compressible flow with chemical reaction added. In the literature, detonation models so far available are the earliest due to Chapman-Jouguet, for instantaneous irreversible reaction, and the one due to Zeldovich, von Neumann and Doering (ZND), for non-instantaneous irreversible reaction. Extensions of ZND model to more complicated reacting processes can be found in the book [1] by Davis and Fickett. Within discrete kinetic theory extended to chemically reacting gases, a general mathematical procedure has been proposed in order to solve detonation problems within discrete velocity models for chemically reacting gases. Steady detonation waves have been characterized for gases undergoing to one reversible reaction of bimolecular type [2] or autocatalytic type [3]. Moreover, in paper [3], the sonic properties of the flow in thermodynamical equilibrium conditions have been studied. In a more recent paper (in progress), the one-dimensional stability has been formulated in discrete kinetic theory, with the aim of investigating the stability of the detonation solutions obtained in [2, 3]. At this end, the approach to linear stability due to Lee and Stewart has been followed [4]. Discrete models allow to study the detonation at a microscopic level and recover, at a macroscopic scale, the main results obtained for classical detonation models. At the same time, they have a rather simple mathematical structure so that their equations can be numerically solved in order to evaluate some relevant physical

quantities in such phenomenology.

In this work some detonation results are presented for either bimolecular and autocatalytic reactions, providing the characterization of the complete, as well as the wave thickness for different detonation velocities and the speeds of sound.

### Euler equations of the model

After determining the collision invariants of the discrete velocity model and defining the progress variable  $\lambda$ , which specifies the chemical composition of the system, the kinetic equations lead to the rate and conservation equations of the model. The definition of the collision invariants allows also to deduce the chemical equilibrium condition, as well as to characterize the states of Maxwellian (mechanical) equilibrium and complete thermodynamical equilibrium, crucial for the detonation problem. Conservation and rate equations, when referred to the Maxwellian equilibrium, constitute the closed set of reactive Euler equations of the model. They govern, at microscopic level, the reacting gas in Maxwellian equilibrium and chemical disequilibrium conditions. At last, the kinetic formulation of the governing equations allows to study the detonation at a microscopic scale and comparisons with results known from experimental works are possible once the macroscopic variables are evaluated.

## 2 Steady Detonation Waves

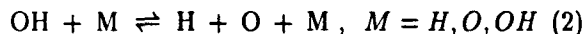
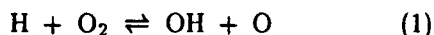
According to the ZND description of a steady detonation, a planar shock wave propagates with constant velocity  $\tilde{D}$  into an unreacted gas. The incoming wave raises the pressure and density of the initial state  $I$  to very high values, triggering an exothermic chemical reaction which proceeds in the reaction zone following the wave. The reacting gas evolves from the von Neumann state  $N$ , where the reaction starts, to the final state  $F$ , where the che-

\* Abstract 4146 submitted to the 21st International Symposium on Rarefied Gas Dynamics, Marseille, France, July 26-31, 1998

mical reaction reaches the equilibrium conditions. The different domains correspond to different discrete velocity models. The detonation problem consists first, in characterizing the relevant states  $N$ ,  $F$ , and intermediate  $R$ , for given detonation velocity  $\mathcal{D}$  and initial state, and finally, in determining the following flow connecting the final state to the assigned rear boundary [2, 3]. The solution to the first part is obtained from the Rankine-Hugoniot conditions and rate equation. The sonic properties of the flow at the final state are crucial to solve the second part [3]. The Hugoniot diagram of the model can be constructed for given state  $I$  and  $\mathcal{D}$  belonging to the admissible computed range [2, 3]. The detonation wave thickness is computed as the width of the reaction zone, integrating the rate equation with suitable initial data.

### 3 Numerical Results

The reacting Hydrogen-Oxygen system is considered, with reference to the elementary reactions



which occur in the branching chain reactions of  $\text{H}_2$ - $\text{O}_2$  system. From the experiments (see, for instance, Ref. [1], it is well known that (1) is an important reaction of the  $\text{H}_2$ - $\text{O}_2$  system, through which the radicals  $\text{OH}$  and  $\text{O}$  are formed from a stable species  $\text{O}_2$  and a radical  $\text{H}$ . This reaction occurs in the thermally neutral induction stage of the  $\text{H}_2$ - $\text{O}_2$  combustion and proceeds very quickly; the corresponding equilibrium final state is reached in few time and a small wave thickness is observed. On the other hand, reaction (2) occurs in the second stage of the  $\text{H}_2$ - $\text{O}_2$  combustion, which involves slower exothermic autocatalytic reactions. The pressure and density reach very high values and an extensive reaction zone is found.

Table 1 shows the jumps of specific volume and pressure, and table 2 shows the detonation wave thickness  $\Omega$  for different values of  $\mathcal{D}$ . The jumps on pressure and density  $\rho = 1/v$  are greater for the autocatalytic reaction (2), and the length of the reaction zone is smaller for the bimolecular reaction (1). The numerical results of the proposed kinetic approach satisfactorily agree with the behaviour predicted by the classical theory and experimental works [1].

Table 1: Von Neumann and final states

Bimolecular Reaction				
von Neumann state			Final state	
$\mathcal{D}$	$v_N/v_0$	$p_N/p_0$	$v_F/v_0$	$p_F/p_0$
0.4450	0.9171	5.4105	0.9658	3.3520
0.5200	0.9000	7.8736	0.9286	5.8132
0.6400	0.8635	13.5389	0.8995	8.9675
0.7200	0.8266	19.4421	0.8759	12.0557
0.8000	0.7685	28.8529	0.8402	17.0956
Autocatalytic Reaction				
von Neumann state			Final state	
$\mathcal{D}$	$v_N/v_0$	$p_N/p_0$	$v_F/v_0$	$p_F/p_0$
0.7761	0.8161	35.3517	0.8827	28.9505
0.7800	0.8122	36.1514	0.8696	31.8312
0.7850	0.8083	37.2105	0.8596	34.1613
0.7900	0.8042	38.3112	0.8512	36.1557
0.8050	0.7910	41.8768	0.8295	41.5785

Table 2: Wave thickness

Bimolecular Reaction				
$\mathcal{D}$	0.4450	0.5200	0.6400	0.7200
$\Omega$	26.8296	8.7660	6.2156	4.5500
Autocatalytic Reaction				
$\mathcal{D}$	0.7761	0.7800	0.7850	0.7900
$\Omega$	35.0547	25.7889	22.5999	20.3111

### References

- [1] W. Fickett and W. C. Davis, *Detonation*, University of California Press, 1979.
- [2] R. Monaco, M. Pandolfi Bianchi and A. J. Soares, "Steady Detonation Waves in Classical and Discrete Kinetic Theory", *Comm. on Appl. Nonlinear An.*, vol.3, No.3, 1996.
- [3] M. Pandolfi Bianchi and A. J. Soares, "A Kinetic Model for a Reacting Gas Flow: Steady Detonation and Speeds of Sound", *Phys. Fluids*, vol. 8, p. 3423, 1996.
- [4] H. I. Lee and D. S. Stewart, "Calculation of Linear Detonation Instability: One Dimensional Instability of Plane Detonation", *J. Fluid Mech.*, vol. 216, p. 103, 1990.

# Contingency Stochastic Probability in Free Molecular Flows Inside Vessel \*

R.N.Miroshin, V.N.Petrova  
St.-Petersburg State University, St.-Petersburg, Russia

## 1 Introduction

The initiation of stochastics in flows of liquid, i.e. their turbulencing is explicable on the basis of the existence of so-called strange attractors at dissipative deterministic systems [1]. The strange attractor is understood as set in a phase space of the system, having complex structure, as a rule, of fractional Hausdorff's dimension to which the trajectories of the system are attracted in the course of time. The behaviour of the system on this set has casual unpredictable character, described by probabilistic functions of distribution. In the report is considered perhaps the simplest example of flow chaotisation - free molecular flow of gas in a vessel.

## 2 Reduction to iteration scheme

Given the reflecting properties of walls of a vessel, i.e. the factors of an exchange by normal  $\rho$  and tangent  $\tau$  pulses, one can construct the simple model of reflection (ray model of reflection), which is a generalization for the specular reflection one. Namely, incident and reflex rays lay in the same plain with normal to wall in a point of collision of gas atom with wall as well as the angles of incidence  $\vartheta'$  and reflection  $\vartheta$  are related by the dependence [2]

$$\tan \vartheta = (2 \sin \vartheta' \cos \vartheta' - \tau) / (\rho - 2 \cos^2 \vartheta')$$

Here  $\rho$  and  $\tau$  are the functions of  $\vartheta'$ . There are for them the simple semi-empirical formulas type of modified Newton's formula or approximations of the theory of local interaction [3], so that the right part can be represented by a function of the form  $f(\tan \vartheta')$ .

Elementary geometrical reasons for specific forms of vessels permit to express  $\tan \vartheta'_i$  through  $\tan \vartheta_{i-1}$ :  $\tan \vartheta_i = \varphi(\tan \vartheta_{i-1})$ , where the bottom index

marks serial number of atom collisions with the surface of a vessel. Finally, angle of reflection at collision with number  $i$  is connected to angle of incidence at previous collision as

$$\tan \vartheta_i = f(\varphi(\tan \vartheta_{i-1})) \equiv F(\tan \vartheta_{i-1})$$

The problem has been reduced to iteration scheme, hence it can be decided by methods of non-linear dynamics (theory of attractors) [1].

## 3 Numerical calculations

In particular, given free molecular flows in a plane tunnel there is  $\varphi(x) = x$ , given some into a wedge with angle of solution  $\beta$  there is  $\vartheta' = \vartheta - \beta$  i. e.  $\varphi(x) = (x - \tan \beta) / (1 + x \cdot \tan \beta)$  etc. We have used of the three-parametrical approximation of local interaction theory to obtain  $\rho$  and  $\tau$  [3]. For the flow in a plane tunnel we have obtained to exist with according to the relationship among approximation parameters both the usual (deterministic) attractors of various periods on  $i$  and the chaotic attractors with fractional dimension turned by cascade of Feigenbaum's bifurcations [4], [5]. Thus, the situation is essentially equivalent that observed in iterations of logistic equation. After running up to the chaotic attractor, an initial flow of atoms moving with identical velocities give the probabilistic distribution of atom velocity on the exit from enough long tunnel, i.e. a laminar flow is turbulented. This effect is caused by nonlinear law of atom interactions with a wall and sufficient tunnel length. The latter needs to be run up to the attractor an iteration scheme, i.e. the atoms are to be reflected from walls sufficient times.

A similar pattern is observed in a flow into a wedge but the tunnel blocking effect is replaced by the dynamic adsorption one when with parameters of the flow, after scattering from walls times out of number the atom tends to the vertex of a wedge.

\* Abstract 5062 submitted to the 21st International Symposium on Rarefied Gas Dynamics, Marseille, France, July 26-31, 1998

## References

- [1] Schuster G., *Deterministic Chaos*, Weinheim, 1994.
- [2] Barantsev R.G. *Interaction of rarefied gases with streamline surfaces*, M., 1975. (in Russian)
- [3] Miroshin R.N., Khalidov I.A. *Theory of local interaction*, L., 1991. (in Russian)
- [4] Miroshin R.N. *On the nonlinear dynamics methods of some interior problems of rarefied gas dynamics*, Vestnik SPbGU. Ser.1. 1993. Iss.2. P.94-98. (in Russian)
- [5] Miroshin R.N. *On velocity bifurcations of the rarefied gas flow into plane tunnel*, Vestnik SPbGU. Ser.1. 1994. Iss.4. P.63-65. (in Russian)

# Modification of Burnett Equations \*

O.G. Buzykin, V.S. Galkin, V.I. Nosik

Dep. of Fundamental Research, Central Aerohydrodynamic Institute, Zhukovsky, Russia

## 1 Introduction

Interest to Burnett equations has much grown at last time. The cause is that the accuracy of Burnett equations for a number of problems has turned out to be well above, than the accuracy of Navier-Stokes equations. It was demonstrated, in particular, for problems of sound propagation and when investigating the structure of a strong shock wave.

However, full Burnett equation system has some inherent lacks. It needs for the additional boundary conditions owing to the increase of a system order, but strict enough theory for obtaining of such conditions is not developed. Also, the full equation system is unstable for short-wave perturbations. To suppress these perturbations the additional damping terms was included, aggravating the problem of boundary conditions.

The modification of the Chapman-Enskog method was proposed by Grad to get out of this crisis. The re-expansion of the Chapman-Enskog method equations chain about the Navier-Stokes equations with respect to Knudsen number  $Kn \ll 1$  was suggested. As a result the differential operator of the derived equation system is the same as the steady Navier-Stokes operator, and the order of a system is not increased. However, the accuracy of such a procedure is doubtful for problems, in which Navier-Stokes equations have low accuracy.

The analysis of some modifications of Burnett equations is given in present report. Modifications were carried out by means of selection of suitable basis, which was used to built a perturbation method. The obtained non-uniform equation systems are stable for short-wave perturbations and have accuracy not worse, than the full Burnett equation system. The order of these system equations is not higher than that of Navier-Stokes equations, so no additional boundary conditions are necessary.

## 2 Method

Instead of Burnett equations a system of following equations can be used

$$L_1(\Sigma) + L_2^{(1)}(\Sigma) + L_2^{(2)}(\Sigma_0) = 0$$

Where  $L_1(\Sigma)$ - Navier-Stokes equations,  $L_2(\Sigma)$ - Burnett equations. Gasdynamic variables are designated as  $\Sigma$ .  $\Sigma_0$  is the solution of uniform equations

$$L_1(\Sigma_0) + L_2^{(1)}(\Sigma_0) = 0,$$

$L_2^{(2)}$  contains the terms of  $p_{ij}^{(2)}$  and  $q_i^{(2)}$  with all the second derivatives and with some of binary products of the first derivatives.  $L_2^{(1)}$  includes the rest of Burnett terms. Thus, the basis is not the Navier-Stokes system  $L_1$ , but the truncated Burnett equation system  $L_1 + L_1^{(2)}$ . As it is shown below, such a system gives practically the same results for a number of problems, as the full Burnett equation system.

## 3 Comparison of Different Perturbation Methods

To demonstrate the features of various perturbation methods of the Boltzman equation solution, the comparison of results given by these methods with the experimental data for a problem of sound propagation is done. Especial attention was paid to the Chapman-Enskog method. The dispersion relations are obtained by all the methods.

For the sound mode, investigated experimentally, the Chapman-Enskog method gives approximations of wave number  $k(Kn)$ , containing out of the order of Knudsen number terms. This results in that the Navier-Stokes approximation has rather wide area of applicability. The Burnett approximation expands the domain of macroscopic description with respect to the Navier-Stokes equations. However, owing to increase of a dispersion equation order, this approximation gives an extra mode, the status of which is not defined, and the statement of boundary conditions is not clear.

\*Abstract 5087 submitted to the 21st International Symposium on Rarefied Gas Dynamics, Marseille, France, July 26-31, 1998

Gilbert method gives a chain of non-uniform Euler equations, that after transformations coincides with the solution of Chapman-Enskog method, if in this method the out of order terms of the expansion of  $k(Kn)$  in a series on  $Kn$  powers are neglected. However, the segment of this series corresponding to the Burnett approximation has much smaller applicability range of  $Kn$  than the Burnett approximation and even Navier-Stokes approximation.

Modification of Chapman-Enskog method is considered, in which instead of Burnett equations the non-uniform Navier-Stokes equations are solved. The results obtained are close to the Burnett where the Burnett equations are in good agreement with experimental data. The number of modes is the same, as in Navier-Stokes approximation. The accuracy of such modification is close to accuracy of the solution of Burnett equations in the total area of their applicability.

#### 4 Numerical Results: Strong Shock Wave Structure

The accuracy of our modifications is also examined by the problem on a strong shock wave structure as an example. The results of calculations were compared with well known results of the solution of Navier-Stokes equations, Burnett equations and solution of Boltzmann equation by method of direct simulation (Monte Carlo). It is shown, that a system of non-uniform truncated Burnett equations satisfies to the requirements specified above. Such a system is obtained from the full Burnett equation system, in which senior derivatives and the that terms of  $p_{ij}^{(2)}$  which are proportional to the square of temperature gradient, are included in a non-uniform part, computed by the solution of a uniform truncated system (Burnett equations without the specified terms).

This system gives practically the same results for the strong shock waves structure as is given by the full Burnett system in the range of Max number  $M = 1.5 - 50$ . The maximum error takes place in forward wing of a temperature profile, as well as it is for a full Burnett equation system.

Also, the other more exact macroscopic model is proposed, giving for structures of a strong shock wave practically the same results in the range  $M = 5 - 50$ , as compared with the direct simulation method. It is derived by adding the certain super-Burnett terms, by discarding some Burnett members and by varying of coefficients of the retained terms. The equations of the model developed are

much simplest then the Burnett and the super-Burnett equations, and are very exact. The aspects of hypersonic stabilization of shock waves are also considered.

Some results of calculations for maxwellian molecules and the molecules - hard spheres at  $M = 11$  are shown in Figs.1 and 2 respectively as the dependencies of normalized temperature and density on the ratio of distance to the mean free path in front of the shock wave. The curves 1 denotes the Navier-Stokes solution, 2 - Burnett solution, 3 - our modification of Burnett equation, 4 - our macroscopic model, open circles 5 - direct simulation method.

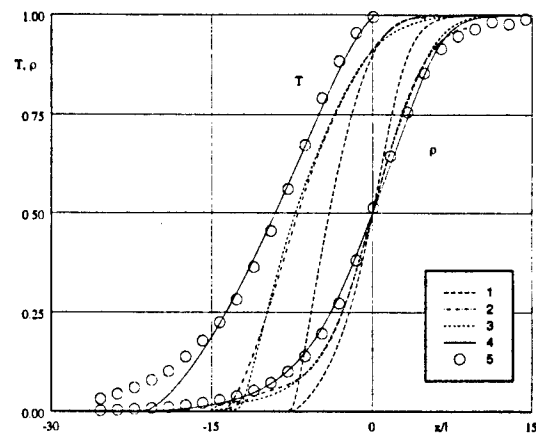


Figure 1: Shock structure for maxwellian molecules

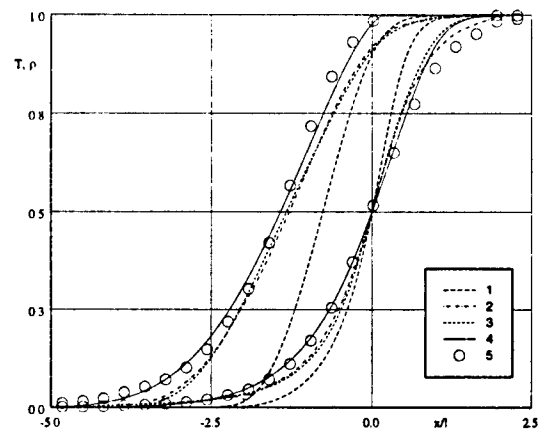


Figure 2: Shock structure for hard spheres

This work was supported by the Russian Foundation for Basic Research (Grant 96-01-01244 and State Program for Leading Research Groups Grant 96-15-9603).

# The Interaction Potential of Carrier Rarefied Gas Molecules with Dispersed Particle \*

V.Ya. Rudyak, S.L. Krasnolutski

Novosibirsk State University of Civil Engineering, Novosibirsk, Russia

## 1 Introduction

The potentials of the interparticles interaction are the basis of the many particles statistical mechanics and kinetic theory in particular. There are no such potentials for heterogeneous medium. In particular, the potentials of carrier medium (gas, liquid or plasma) molecules with dispersed particles have not been constructed yet. The object of the present paper is the derivation of the interaction potential of a hard dispersed particle with an isolated carrier gas molecule. Thus it is supposed that required potential is a pair one. It is true certainly on condition a carrier gas is rarefied enough. In addition it is supposed that the molecule charge was uniformly distributed over whole volume of the particle. Such assumption had been usually made when molecule - hard surface potential was simulated (see for example [1]).

## 2 Interaction potential of molecule with dispersed particles

In a general case the molecule interaction with the dispersed particle is a very complicated process. It is necessary to solve respective quantum mechanics problem for derivation of formulae describing such interaction. However the molecule-particle interaction can be described classically by means of a model potential function in a wide region of variation parameters of two-phase fluid. Namely such an approach will be used in the present paper. The similar models are successfully used in different aerospace applications and in certain technological spheres. The simulation idea is very simple that it is one of the most important advantage of given approach. It is supposed that the interaction potential of a gas molecule and a hard surface is

summed of the interaction of this molecule with all atoms of crystal lattice of surface. We shall realize similar approach in this paper for simulation of the molecule-dispersed particle interaction potential. Let us considering the dispersed particle to be homogeneous and spherical and  $R$  is the radius of this particle. The interaction of a molecule with a certain atom  $i$  of the considered hard surface is described by the pair potential  $\Phi_i(|\vec{r} - \vec{r}_i|)$ , where  $\vec{r}$  and  $\vec{r}_i$  are the radius-vectors of molecule and particle respectively. If we suppose the molecule interaction with the particle atoms is additive then the molecule interaction potential with this particle has the form

$$\Phi_i(\vec{r}) = \sum_i \Phi_i(|\vec{r} - \vec{r}_i|). \quad (1)$$

Here summation is carried out over all atoms (or molecules) of the particle. We will assume that the interaction of the molecule with an individual atom of a particle is central and it is described by the Lennard-Jones 12-6 type potential.

$$\Phi_i(|\vec{r}|) = 4\epsilon \left[ \left( \frac{\sigma}{r} \right)^{12} - \left( \frac{\sigma}{r} \right)^6 \right]. \quad (2)$$

We shall use another form of this potential too

$$\Phi_i(|\vec{r}|) = \frac{C_{12}}{r^{12}} - \frac{C_6}{r^6} = \sum_{m=6,12} \frac{C_m}{r^m}. \quad (3)$$

In a general case we can not find the sum of the series (1) therefore the summation in formula (1) is usually replaced by the integration. Physically it is meant that the considered hard particle is simulated by the continuum model. As a result it can be shown that the effective potential of a gas molecule with hard dispersed particle is described by the following formula

$$\Phi_{ball}(r) = \Phi_9(r) - \Phi_3(r), \quad (4)$$

where

$$\Phi_9(r) = \frac{\pi C_{12}}{45S\sigma} \left\{ \left( \frac{1}{(r-R)^9} - \frac{1}{(r+R)^9} \right) \right\}$$

\*Abstract 5138 submitted to the 21st International Symposium on Rarefied Gas Dynamics, Marseille, France, July 26-31, 1998

$$\Phi_3(r) = -\frac{9}{8r} \left( \frac{1}{(r-R)^8} - \frac{1}{(r+R)^8} \right) - \frac{\pi C_6}{6S\sigma} \left\{ \left( \frac{1}{(r-R)^3} - \frac{1}{(r+R)^3} \right) - \frac{3}{2r} \left( \frac{1}{(r-R)^2} - \frac{1}{(r+R)^2} \right) \right\}.$$

### 3 Combining rules

To use the formula obtained in the previous section for the calculation of the interaction potentials of the carrier gas molecules and the dispersed particles it is necessary to know the parameters of the interaction pair potential of this molecules with an atom (molecule) of the particle. In particular, it is the Lennard-Jones potential used here. Obviously the parameters in intermolecular potential function are determined by the experimental data of the transport or virial coefficient measurements. It is possible to do it with good accuracy and methodically strictly for the molecules of the same matter. Usually the combining rules are used to calculate the potential parameters of the unlike molecules. These rules permit to determine the interaction potential parameters of the unlike molecules if the same parameters of the like molecules are known. Naturally we can determine such rules when the same potential model is used for each component molecules and for the unlike ones. In present section the known combining rules and the original ones are discussed. It was shown that from practical point of view the following combining rules

$$\sigma_{ij} = \sqrt{\sigma_i \sigma_j}, \quad \epsilon_{ij} \sigma_{ij}^6 = \sqrt{\epsilon_{ii} \epsilon_{jj} \sigma_{ii}^3 \sigma_{jj}^3}.$$

and

$$\sigma_{ij} = \frac{1}{2}(\sigma_i + \sigma_j), \quad \epsilon_{ij} = \sqrt{\epsilon_{ii} \epsilon_{jj}}.$$

$$\sigma_{ij} = \sqrt{\sigma_i \sigma_j}, \quad \epsilon_{ij} = \sqrt{\epsilon_{ii} \epsilon_{jj}}.$$

are the most convenient ones. The testing of these and certain other combining rules with the use of the known experimental data of diffusion coefficients was carried out.

### 4 Discussion and conclusion

In conclusion the applicability region of the constructed model is discussed. The tables of the interaction molecule-particle potentials for different carrier gas molecules and material of the particles are given. The dispersed particles the molecules of

which consist of metal atoms and gas ones were considered. In particular, we consider certain type of molecule clusters in condensing flows as dispersed particles. Then using the constructed interaction potential between the hard particle and the carrier gas molecules we calculate the aerodynamic drag of a small particle in a free molecule flow. We consider the different sizes of particles (from  $10^{-7}$  cm to  $10^{-4}$  cm). The obtained results are compared with the known experimental data.

### References

- [1] Goodman F.O., Wachman H.Y., *Dynamics of Gas-Surface Scattering*, Academic Press, 1976.
- [2] Rudyak V.Ya., Krasnolutskii S.L. *Nonequilibrium statistical mechanics of heterogeneous medium. V. Potential of molecule-particle interaction*, Preprint NSUACE, No.1(11)-98, Novosibirsk, 1998.



## Translational Relaxation in a Gas Composed of Non- Spherical Molecules \*

J. Stark

Department of Engineering, Queen Mary & Westfield College University of London

It is well known that analytical solutions to the Boltzmann equation are limited, although the case of equilibrium has been extensively studied. The equilibrium solution resulting in the classical Maxwell-Boltzmann distribution requires certain constraints, such as molecular chaos (see for example[1,2]). One particular mathematical limitation on solutions, which is frequently overlooked, is that the molecular potential (required within the collision integral to yield the Maxwellian) should be spherically symmetric. Mathematical complexity introduced by aspherical forces leads to substantial difficulties even in the case of the equilibrium state. It is therefore surprising since the widespread adoption of the Direct Simulation Monte Carlo method for finding numerical solutions to engineering problems describable by the Boltzmann equation, that little attention has been given to molecular models other than those containing spherical symmetry. Most polyatomic molecules are generally not spherical and it may be assumed that the nature of asphericity contributes to the way in which energy may be transferred between translational, rotational and vibrational modes.

The general justification for the adoption of spherical models, from the simplest rigid sphere to those which are phenomenologically based and more able to describe flows, such as the VHS or VSS models, derives from a variety of factors. Such models lead to computational simplicity; detailed physical description (e.g. via quantum mechanics), within flow situations is beyond the capabilities of existing computers; the vast numbers of collisions which take place in a flow results in orientation averaging, thus masking aspheric effects[3]. It is further stated that if appropriate disposable parameters (such as temperature exponents) are assumed, then these simple models can generally represent experimentally determined properties over a range of temperatures and other conditions reasonably well. The very nature of the VHS type model is derived not from physics, but from a phenomenological approach. Further phenomenological methodologies, again avoiding detailed physics, are additionally used to incorporate the way in which energy can be transferred between modes of excitation, the most frequently adopted being the Borgnakke-Larsen model. Thus the overall methodology underpinning the DSMC approach to solving the collision integral, appearing in the Boltzmann equation, therefore essentially follows the same line of attack as that adopted earlier, when mathematical

---

\*Abstract 5731 submitted to the 21st International Symposium on Rarefied Gas Dynamics, Marseille, France, July 26-31, 1998

problems were encountered when trying to solve the Boltzmann equation analytically, namely two types of state transformation processes are possible: the elastic and inelastic collision. The former of these affects only translational energy, whilst the latter is concerned with 'internal' energy modes. Clearly, from a physical viewpoint (and as shown from molecular dynamics computations) it is the detailed nature of the collision process and in particular the molecular orientation during the interaction, which will result in the transfer of energy between the various degrees of freedom.

Most experimental data relates to conditions not far displaced from equilibrium, other than data obtained within the structure of shock waves (wherein experimental measurements are difficult to gain which unambiguously separate out the effects of molecular properties from the gas dynamics). Since the molecular properties (e.g. reference cross sections at certain temperatures, and exponents such as  $\omega$ : the temperature exponent of the coefficient of viscosity) are mainly based on near-equilibrium measurements, the ability of these near-equilibrium properties to depict far from equilibrium conditions, should be considered with some caution. Indeed since the way in which most DSMC codes commence calculation from an equilibrium distribution function for the single particle velocity distribution, adopting a spherical molecular potential, a solution which arrives at near equilibrium conditions is hardly surprising.

In this paper two themes relating to the above discussion are developed. These two themes are the influence of the molecular properties on translational relaxation and the way in which the initial conditions influence relaxation, when initiation is far from equilibrium. There have been few reported simulations of relaxation processes which start from a highly non-equilibrium state. However it would be anticipated that for system states which are near to equilibrium, discrepancies between existing molecular models and those which adopt aspheric effects would be small. The influence of asphericity upon relaxation is more likely in the far from equilibrium state, and hence the need to consider far from equilibrium initial states. DSMC simulations have therefore been performed enabling an investigation of the influence of molecular properties upon relaxation processes. In this paper results are reported on the relaxation (rate and the velocity distribution function) as a function of both molecular asphericity and the degree to which the initial conditions reflect a non-equilibrium state. The intention in this work is not to establish new, more realistic molecular models (with their added computational overhead), rather it is to consider how robust the DSMC procedure is in predicting properties far from equilibrium.

## References

- [1] Vincenti WG and CH Kruger 'Physical Gas Dynamics', pb. Krieger, 1982.
- [2] Chapman S and TG Cowling 'The Mathematical Theory of Non-Uniform Gases' pb. Cambridge University Press, 1970.
- [3] Bird GA, 'Molecular Gas Dynamics and the Direct Simulation of Gas Flows' pb. Oxford Scientific Publications 1994.

# Discrete Dynamical Systems in Solving Chandrasekhar H-equations \*

W. Greenberg, J. Chen, R.L. Bowden

Center for Transport Theory & Mathem. Physics, Virginia Tech, Blacksburg, U.S.A.

Three discrete dynamical models are used to solve the Chandrasekhar H-equations

$$H(\mu) = 1 + \mu H(\mu) \int_0^1 \frac{\psi(\nu)}{\mu + \nu} H(\nu) d\nu$$

with positive and negative characteristic functions  $\psi$ . An iteration model of the  $n$ th approximation for the H-equation is discussed:

$$h_{n+1}(\mu_i) = 1 + \mu_i h_n(\mu_i) \sum_{j=1}^n \frac{a_j \psi(\mu_i)}{\mu_i + \mu_j} h_n(\mu_j)$$

This is a nonlinear  $n$ -dimensional dynamical system.

We study the solutions of the  $n$ th approximation and the mathematical structure and behavior of the orbits with respect to the characteristic function. The stability of fixed points and stable and unstable manifolds passing through them are explored, as well as the behavior of attractors and bounded orbit regions. Bifurcation phenomena are described.

---

\*Abstract 5866 submitted to the 21st International Symposium on Rarefied Gas Dynamics, Marseille, France, July 26-31, 1998

# Discrete Velocity Models as Approximation of the Boltzmann Equation: Numerical Issues and Improvements \*

J. Schneider

ISITV, Université de Toulon et du Var, France

In the past few years several numerical approaches were proposed to solve the Boltzmann equation in the frame of Discrete Velocity Models [5, 11, 2, 9, 10]. Let us recall that such models were widely studied and developped in the 70 – 80\* aiming for modelling complex systems (see for example [3, 4]). More recently one has studied their mathematical link with the Boltzmann equation itself [11, 6, 7, 9] so that the question of approximation of solutions of the Boltzmann equation by DVM is now quite well understood. We want therefore to focus more here on numerical issues. We are in particular concerned with computational cost provided solving real rarefied gas problems is extensively CPU time and memory consuming.

A typical DVM computational effort in its deterministic version is of order  $O(N^2 \log N)$  while DSMC only needs  $O(N)$  where  $N$  is the number of velocity points. It is therefore crucial to look for techniques that can reduce that cost of computation without damaging its quality. A technique which is now widely used consists in introducing some “stochasticity” in the computation of discrete collision terms (see [5, 2, 1, 10]) without modifying the structure of DVM (fixed grid of velocity points in the whole physical space). Other approaches such as finite element methods or spectral methods may be also studied...

We shall make in the present talk a state-of-the-art on DVM focusing on numerical issues with a particular stress on acceleration techniques.

## References

- [1] Y. Bahi (1997): *Contribution à la simulation numérique des écoulements de gaz raréfiés*, PhD thesis, University Pierre et Marie Curie, Paris 6, April 1997.
- [2] C. Buet (1996): *A Discrete Velocity Scheme for the Boltzmann Operator of Rarefied Gas Dynamics*, Transp. Theory and Statist. Phys., Vol. 25, pp. 33- 60.

---

\*Abstract 6801 submitted to the 21st International Symposium on Rarefied Gas Dynamics, Marseille, France, July 26-31, 1998

- [3] H. Cabannes (1980): *The Discrete Boltzmann Equation (Theory and application)*, Lectures notes, University of California, Berkeley.
- [4] R. Gatignol (1975): *Théorie Cinétique des gaz à répartition discrète des vitesses*, Lecture Notes in Physics , Springer Verlag, 36.
- [5] D. Goldstein and B. Sturtevant and J. E. Broadwell (1989): *Investigations of the Motion of Discrete-Velocity Gases*, Rarefied Gas Dynamics: Theoretical and Computational Techniques, Ed. E. P. Muntz, 118, In Proceedings of 16th International Symposium on Rarefied Gas Dynamics, Pasadena, CA (1988), Progress in Aeronautics and Astronautics, pp. 100- 117.
- [6] S. Mischler (1996): *Convergence of discrete velocity schemes for the Boltzmann equation*, to appear in Arch. Rat. Mech. Anal.
- [7] A. Palczewski, J. Schneider and A.V. Bobylev (1997): *A consistency result for a discrete velocity model of the Boltzmann equation*, SIAM J. for Numer. Anal., Vol. 34, No. 5, pp. 1865- 1883, October 1997.
- [8] A. Palczewski and J. Schneider (1997): *Existence, stability and convergence of solutions of discrete velocity models to the Boltzmann equation*, preprint.
- [9] V. Panferov (1997): *Convergence of Discrete-Velocity Models to the Boltzmann Equation*, Research report No 1997-22/ISSN 0347-2809, Chalmers University of Technology and Göteborg University, Sweden.
- [10] P. Kowalczyk, T. Platkowski, W. Walus (1997): *Numerical Analysis of Shock Wave Focussing*, Workshop on Numerical Methods for Kinetic Equations, Berlin, September 01-05, 1997.
- [11] F. Rogier and J. Schneider (1994): *A Direct Method for Solving the Boltzmann Equation*, Special issue devoted to the proceedings of the Colloquium Euromech n0287 Discrete Models in Fluid Dynamics, Transport Theory and Statistical Physics, Vol. 23, numbers 1-3.

# Bobylev-Krook-Wu-modes: Explicit Form and Applications for Modeling \*

Yu.N.Grigoryev

Inst. Computational Technologies SB RAS, Novosibirsk, Russia

## Introduction

About two decades ago Bobylev [1] and, independently, Krook and Wu [2] obtained the exact solution of Boltzmann kinetic equation (BE) now is commonly known as BKW-mode. This solution was used by the numerous authors for illustration of some peculiarities of the relaxation processes in one-component gas. From this point of view the analogous solutions for  $N$ -component gas mixture could be of even greater interest. However, the generalization of BKW-mode to binary gas mixture presented by authors [2] in [3] look incomplete even for such a simple case. Recently, in [4] BKW- modes were obtained for a binary gas mixture but only in the asymptotic limit when the ratio of species masses tends to zero. In this case the authors of [4] have practically dealt with a single BE as in [1].

In this paper we present the comprehensive results on BKW- modes for an arbitrary  $N$ -component mixture of monatomic gases. They are based on the rigorous calculation of the widest Lie group of the transformations admissible by the system of BE [5].

## BKW-modes for $N$ -component mixture

We study the system of BE with Maxwell molecular interaction model. The system in terms of the Fourier transformation of the velocity distribution functions (DF)  $\varphi_\alpha(\mathbf{k}_\alpha, t) = \int d\mathbf{v}_\alpha e^{i\mathbf{k}_\alpha \cdot \mathbf{v}_\alpha} f_\alpha(\mathbf{v}_\alpha, t)$ , isotropic in the velocity space are presented as follows

$$\frac{\partial \varphi_\alpha(x_\alpha, t)}{\partial t} = \sum_{\beta=1}^N \int_0^1 ds \rho_{\alpha\beta}(s) [\varphi_\alpha(x_\alpha(1 - \varepsilon_{\alpha\beta}s)) \times \varphi_\beta(x_\alpha \varepsilon_{\alpha\beta}s) - \varphi_\alpha(x_\alpha) \varphi_\beta(0)], \alpha \in [1, N]. \quad (1)$$

Making use of our approach [5] to the group analysis of the integral-differential equations we calculated the widest Lie group  $G^4$  of the transformation admissible by the system Eq.1. The basis of group  $G^4$  consists of the infinitesimal generators

$$X_1 = \partial_t, \quad X_2 = \sum_{\alpha=1}^N x_\alpha \varphi_\alpha \partial_{\varphi_\alpha}, \\ X_3 = \sum_{\alpha=1}^N x_\alpha \partial_{x_\alpha}, \quad X_4 = \sum_{\alpha=1}^N \varphi_\alpha \partial_{\varphi_\alpha} - t \partial_t.$$

The class of invariant BKW-solutions is determined by the generator  $X = X_2 - X_3 + c^{-1} X_1$  depended on the unique constant  $c$ . This allows us after some calculations to obtain the BKW-modes

$$f_\alpha(v_\alpha, t) = \frac{n_\alpha}{[2\pi T(t)]^{3/2}} \left[ 1 - a_1^{(\alpha)} \frac{1 - T(t)}{T(t)} \times \left( \frac{v_\alpha^2}{2T(t)} - \frac{3}{2} \right) \right] \exp\left(-\frac{v_\alpha^2}{2T(t)}\right), \quad \alpha \in [1, N] \quad (2)$$

where  $T(t) = 1 - \theta_0 e^{ct}$ , the constant  $\theta_0$  is determined by the arbitrary choice of time origin. It is essential to emphasize that here in contradiction to [3] the identical temperature functions  $T(t)$  for all the species are not postulated, but are the consequence of the strict calculation of the BKW-class generator. There are two alternative sets of the conditions when BKW-modes Eq.2 exist. The first one-to choose

$$c = -\left[ n_\alpha \int_0^1 ds \rho_{\alpha\alpha}(s) s(1-s) + \sum_{(\beta)}' n_\beta \varepsilon_{\alpha\beta} \times \int_0^1 ds \rho_{\alpha\beta}(s) (1 - \varepsilon_{\alpha\beta} s) \right], \quad \alpha \in [1, N]. \quad (3)$$

Then  $a_1^{(\alpha)} = -1, \alpha \in [1, N]$  and DF are nonnegative for  $v_\alpha \in [0, \infty), t > 0, \theta_0 \in [0, 2/5]$ . As can be seen this is a direct generalization of obtaining BKW-mode in one-component gas [1].

The second one is the following choice.

$$c = -\int_0^1 ds \rho_{\alpha\beta}(s) s \varepsilon_{\alpha\beta}, \quad \alpha < \beta, \alpha \in [1, r], \beta \in [2, N].$$

\*Abstract 6631 submitted to the 21st International Symposium on Rarefied Gas Dynamics, Marseille, France, July 26-31, 1998

$$c = -[n_\alpha a_1^{(\alpha)} \int_0^1 ds \rho_{\alpha\alpha}(s) s(1-s) + \sum_{(\beta)}' n_\beta a_1^{(\beta)} \varepsilon_{\alpha\beta} \times \int_0^1 \rho_{\alpha\beta}(s) (1 - \varepsilon_{\alpha\beta} s) ds], \quad \alpha \in [1, N]. \quad (4)$$

Here the coefficients  $a_1^{(\alpha)} = -a^{(\alpha)}$ ,  $\alpha \in [1, r]$ ; can be arbitrarily chosen,  $a_1^{(\alpha)} = -(1 - \sum_{\alpha=1}^r n_\alpha a^{(\alpha)}) / \sum_{\alpha=r+1}^N n_\alpha$ ,  $\alpha \geq r$ .

In this case the BKW-modes will be nonnegative if all the  $a^{(\alpha)} \geq 0$ ,  $\alpha \in [1, r]$ ;  $\sum_{\alpha=1}^r a^{(\alpha)} n_\alpha < 1$ ;  $0 \leq \theta_0 \leq \min[\theta_{01}, \theta_{02}]$ , where  $\theta_{01} = 2/(2 + 3a_M)$ ,  $a_M = \max_{(\alpha)} a^{(\alpha)}$ ;  $\theta_{02} = 2/[2 + 3(1 - \sum_{\alpha=1}^r a^{(\alpha)} n_\alpha) / \sum_{\alpha=r+1}^N n_\alpha]$ . The choice of some  $a^{(\alpha)} = 0$  means that the corresponding BKW-modes are transformed into unsteady Maxwell DF with the temperature  $T(t)$ . The restrictions Eq.3 and Eq.4, as well as the dependence on the unique constant  $c$  (universal temperature function  $T(t)$ ) for presented BKW-solutions Eq.2, have the meaning of necessary and sufficient conditions, which cannot be weakened.

## Applications for modeling

Presented BKW-modes we used to model in explicit form some physically interesting kinetic processes that were before available just through the very precise numerical computing of BE. For binary gas mixture we investigate in particular:

- relaxation in mixtures with disparate species masses (Lorentz gas, Rayleigh gas, etc.);
- relaxation nonequilibrium impurity in Maxwell bath (Maxwell impurity on the nonequilibrium background);
- unsteady overpopulation of the far tail of DF;
- operating high energy threshold kinetic process.

## Conclusion

- Exact invariant solutions of spatially uniform Boltzmann equations, so-called BKW-modes, are presented in the explicit form for arbitrary N-species gas mixture. The corresponding necessary and sufficient conditions imposed on the molecular parameters are formulated. The completeness of the results obtained is supported by the rigorous group analysis of Boltzmann equations.
- BKW-modes obtained can be used for modeling some kinetic processes of physical interest.

## References

- [1] Bobylev A.V. *On exact solutions of Boltzmann Equation*, Dokl. Ak. Nauk SSSR, Vol.225, No.5, pp.1296-1299, 1975. (in Russian).
- [2] Krook M., Wu T.T. *Formation of Maxwellian tails*, Phys. Rev. Lett., Vol.36, No 19, pp.1107-1109, 1976.
- [3] Krook M., Wu T.T. *Exact solution of Boltzmann equations for multicomponent systems*, Phys. Rev. Lett., Vol.38, No 18, pp.991-993, 1977.
- [4] Bobylev A.V. and Spiga G. *On the relaxation processes in a mixture of Maxwell gases*, Riv. Mat. Univ. Parma, Vol.1, No 5, pp.255-264, 1992.
- [5] Grigoryev Yu.N. and Meleshko S.V. *The full Lie group and invariant solutions of the system of Boltzmann equations of a multicomponent gas mixture*, Siberian Mathem. J., Vol.38, No 3, pp.434-448, 1997.

# Group Theory Description of Temperature and Mass Dependence of Linear Boltzman Collision Operator. \*

V.L. Saveliev

Institute of Ionosphere, Almaty, Kazakstan

## 1 Introduction

Last year's steady interest remains in studying groups of symmetry of the mathematical physics equations. It is so especially in the case where the transformations taken into consideration affect the parameters of an equation as well as its variables, that is, the basis of the renormgroup ideology. In the last decades the traditional theory of symmetry as an application for group analyses of differential equations was actively developed by classic investigations of Ovsianikov, Ibragimov, Olver, et. al. The report is a principally new example of broadening of the field of application of traditional theory of symmetry to the equations that contain integral operators. The Lie group of the transformations affecting the parameters of the linear Boltzmann collision operator such as temperature of background gas and ratio of masses of colliding particles and molecules is discovered. The group also describes the conservation laws for collisions and main symmetries of the collision operator. New algebraic properties of the collision operator are derived. Transformations acting on the variables and parameters and leaving the linear Boltzmann kinetic equation invariant are found. For the constant collision frequency the integral representation of solutions for nonuniform case in terms of the distribution function of particles drifting in a gas with zero temperature is deduced. The new exact relaxation solutions are obtained too.

## 2 Temperature and Mass Dependence

The evolution due to collisions of the distribution function  $f(v)$  of particles having mass  $m_1$  (for example, ions) with particles of mass  $m_2$  (molecules), distributed on speed according to the distribution

function  $\Psi(u)$  is defined by the operator of collisions:

$$[\hat{I}f](v) = \int \nu(v) \chi(\mu, v) [f(v')\Psi(u') - f(v)\Psi(u)] d\Omega_{v'} du,$$

We will assume that distribution of scattering centers (molecules) is the Maxwellian distribution with temperature  $T$ . By differentiating the collision operator on  $T$ ,

$$\frac{\partial}{\partial T} \hat{I} = \frac{k}{2m_2} \nabla * \nabla * \hat{I}, \quad \text{where } \nabla = \frac{\partial}{\partial v},$$

we will have an expression for the generator of the temperature transformations' semigroup. An action of the generator on the operator  $\hat{I}$  is expressed through the double commutator. We will denote by the operator belonging to some algebra  $K$  marked from the right side with the sign  $*$  (i.d.  $\hat{a}*, \hat{a} \in K$ ) the linear map  $\hat{a}*: K \rightarrow \hat{a}*K$  of the algebra  $K$  into itself:

$$\hat{a}*\hat{b} \equiv \hat{a}\hat{b} - \hat{b}\hat{a} \equiv [\hat{a}, \hat{b}], \quad \hat{a}, \hat{b} \in K$$

Taking into account that definitions, we can express the collision operator in terms of the collision operator of the scattering on molecules at rest before the collision with the help of the transformation  $F_T$ :

$$\hat{I} = e^{\frac{kT}{2m_2} \nabla * \nabla *} \hat{J}$$

Differentiating the collision operator with respect to mass variable  $\xi = \ln(1+m)$ , where  $m = \frac{m_1}{m_2}$  one get:

$$\frac{\partial}{\partial \xi} \hat{I} = \nabla v * \hat{I}$$

Thus, semigroup of the transformations,  $e^{\xi \nabla v *}$ ,  $\infty > \xi \geq 0$ ; describes the mass dependence of the collision operator and together with the transformation  $F_T$  allows to express the operator  $\hat{I}$  in terms of the operator  $\hat{\chi}$  that describes a process of scattering on the infinitely heavy ( $m = 0$ ) centers being

\*Abstract 6761 submitted to the 21st International Symposium on Rarefied Gas Dynamics, Marseille, France, July 26-31, 1998



at rest. The operator  $\hat{\chi}$  is the simplest collision operator. So, we have:

$$\hat{I} = e^{\frac{kT}{m_2} \nabla \cdot \nabla + \ln(1+m) \nabla \cdot \nabla} \hat{\chi},$$

$$[\hat{\chi}f](v) = \int \nu(v) \chi(\mu, v) [f(v') - f(v)] d\Omega_{v'},$$

here  $v'^2 = v^2 = v^2$ ,  $\hat{\chi} = \hat{\chi}$ .

$$\hat{I} = e^{\frac{kT}{m_2} \nabla \cdot \nabla + \ln(1+m) (\nabla \cdot \nabla + \nabla \cdot \nabla)} \hat{\chi}.$$

### 3 Energy Conservation Law

The energy conservation law for scattering on infinitely heavy center being at rest is reduced to the fact that the squares of velocities before and after collision remain equal, or another words:  $v^2 \hat{\chi} = 0$ , and the operator  $\hat{\chi}$  is a stationary object with respect to the group of transformations defined by generator  $v^2 \hat{\chi}$ :

$$e^{\alpha v^2 \hat{\chi}} \hat{\chi} = \hat{\chi}.$$

One more property of symmetry is added in the case of the constant collision frequency ( $\nu = \text{const}$ , so called Maxwell's particles):  $\nabla^2 \hat{\chi} = 0$ .

### 4 Lie Algebra and Group

To create from the set of generators  $\nabla \cdot \nabla$ ,  $\nabla v$ ,  $v^2$ ,  $\nabla^2$ , the basis of Lie algebra, one need to add to it three more elements:  $\nabla \cdot v$ ,  $v \cdot v$ ,  $(v \nabla) \cdot$ . This seven-dimensional Lie algebra is determined by commutative relations that look most simply in the bases:

$$P_1 = \frac{1}{\sqrt{8}} \nabla \cdot \nabla, \quad P_2 = \frac{1}{2} \nabla \cdot v, \quad P_3 = \frac{1}{\sqrt{8}} v \cdot v,$$

$$Q_1 = \frac{1}{\sqrt{8}} \nabla^2, \quad Q_2 = \frac{1}{2} (v \nabla) \cdot, \quad Q_3 = \frac{1}{\sqrt{8}} v^2,$$

$$S = M - Q_2 - P_2; \quad \text{where } M = \nabla v,$$

and can be represented in the form:

$$[P_i, P_k] = 0,$$

$$[Q_i, P_k] = e_{ikl} b_{lm} P_m, \quad [Q_i, Q_k] = e_{ikl} b_{lm} Q_m,$$

$$[S, P_k] = P_k, \quad [S, Q_k] = 0,$$

where  $e_{ikl}$  is the antisymmetric Levi-Civita tensor,  $b_{lm}$  is an antidiagonal matrix ( $b_{13} = b_{31} = -b_{22} = 1$ ).

We will call as extended collision operator the following operator:

$$\hat{I}_g(p, q, s) = e^{p \cdot P} e^{s \cdot S} e^{q_1 Q_1} e^{q_2 Q_2} e^{q_3 Q_3} \hat{\chi}$$

that one can obtain acting by a transformation from the group  $GPQS$  on the simplest collision operator  $\hat{\chi}$  for collisions with infinitely heavy centers being at rest.

We consider a linear Boltzmann kinetic equation with the extended collision operator:

$$\frac{\partial f}{\partial t} + v \nabla f + (w + v \times \Omega) \nabla f = \hat{I}_g(p, q, s) f,$$

where  $w = \frac{eE}{m}$ ;  $\Omega = \frac{eB}{mc}$ ;  $\nabla = \frac{\partial}{\partial r}$ ;  $\nabla = \frac{\partial}{\partial r}$ ;

The distribution function  $f(v, r, t)$  of charged particles that not uniformly drift through the gas of heated molecules in the electric and magnetic fields. satisfies the equation with the extended operator parameters having values:  $p_1 = \sqrt{2}kT/m_2$ ,  $p_2 = m$ ,  $p_3 = 0$ ;  $q_1 = 0$ ,  $q_2 = \ln(1+m)$ ,  $q_3 = 0$ ,  $s = \ln(1+m)$ . The kinetic equation is invariant regarding a transformations with parameters  $\bar{q}_1, \bar{q}_2, \bar{q}_3$ :

$$q'_1 = q_1 + \frac{\bar{q}_1}{1 - q_3 \bar{q}_1 / 2} e^{-q_2},$$

$$q'_2 = (q_2 + \bar{q}_2) \ln(1 - q_3 \bar{q}_1 / 2)^2,$$

$$q'_3 = \bar{q}_3 + \frac{q_3}{1 - q_3 \bar{q}_1 / 2} e^{-\bar{q}_2},$$

$$f'(v, r, t; w, p', q', s') = e^{\frac{q'_1}{2} (\nabla^2 - 2 \nabla \cdot \nabla)} e^{\frac{q'_2}{2} (\nabla + \nabla + \nabla)} e^{\frac{q'_3}{2} (v^2 - 2)} f(v, r, t; w, p, q, s).$$

Where  $\bar{T}_{ik}(q)$  is a matrix of the conjugated representation of subgroup  $GQ$ ,  $G(q)Q_k G^{-1}(q) = Q_i \bar{T}_{ik}(q)$ . In the case of the constant collision frequency, it is possible to express the distribution function of charged particles drifting in a heated gas ( $T \neq 0$ ) in terms of the distribution function of charged particles drifting in a cold gas ( $T = 0$ ):

$$f'(v, r, t; w, T) = e^{\frac{q'_1}{2} (\nabla^2 - 2 \nabla \cdot \nabla)} f(v, r, t; w, T = 0)$$

### References

- [1] Shirkov D.V., *Bogolubov renormgroup*. Uspehi matem. nauk, 49, No.5, 147 (1994), (in Russian)
- [2] Saveliev V.L., *Temperature and mass dependence of the Boltzmann linear collision operator from the group theory point of view*. Journal of Mathematical Physics Vol.37, No.12, pp.6139-51, 1996.

# Singular Perturbations Problems for the Euler-Poisson System \*

A. Ambroso<sup>1</sup>, F. Méhats<sup>1</sup>, P. A. Raviart<sup>1</sup>

<sup>1</sup> Centre de Mathématiques Appliquées, Ecole Polytechnique, Palaiseau, France

## 1 Introduction

The system we consider is formed by a plasma of a single species of ions, enclosed between two infinite plane electrodes, one at the same potential than the plasma  $\phi = 0$  and the other at a fixed negative potential  $-\phi_c$ . This problem has been studied when the applied potential is such that  $e\phi_c$  is much bigger of the electron thermal energy and it has been shown that the asymptotic solution is given by Child-Langmuir law (cf. [1]).

We consider here the case in which  $e\phi_c$  is of the same order of magnitude of the electron thermal energy. We start presenting the fluid model of this problem and we show that it leads to the resolution of a singular perturbation non-linear Poisson problem for the electric potential. By the introduction of the Sagdeev potential function, we prove the existence of solutions of this problem and we show that, in the quasi-neutral limit, that is to say when the observation scale is much bigger than the Debye length in the plasma, the limit of these solutions depends only on the shape of the Sagdeev potential in the neighborhood of its minima.

## 2 Mathematical Model

We consider a one dimensional stationary system formed by a plasma that occupies a bounded region of space  $[0, L]$ .

We use a fluid description for ions

$$\begin{aligned} \frac{d}{dx}(nu) &= 0, \\ m_i \frac{d}{dx}(nu^2) + \frac{dp_i}{dx} &= -en \frac{d\phi}{dx}, \end{aligned}$$

where  $n$  and  $u$  are ion density and speed respectively,  $\phi$  is the electric potential,  $m_i$  is ion mass,  $e$  is the fundamental charge and  $p_i$ , the ion pressure, is such that  $p_i = nkT_i$ , where  $k$  is the Boltzmann constant and  $T_i$  the ionic temperature.

The hydrodynamic equations are closed by the equation of state

$$p_i = nkT_i = C n^\gamma, \quad C = \text{constant}, \quad \gamma \geq 1.$$

We assume that electron density follows a Maxwell-Boltzmann distribution law

$$n_e = n_p \exp\left(\frac{e\phi}{kT_e}\right),$$

where  $T_e$  is the given electronic temperature and  $n_p$  is the electron density when  $\phi = 0$ .

The electric potential and electron and ion densities are linked by Poisson equation

$$-\frac{d^2\phi}{dx^2} = \frac{e}{\epsilon_0}(n - n_e),$$

where  $\epsilon_0$  is the vacuum dielectric constant.

We assume plasma neutrality in  $x = 0$ . The boundary conditions are

$$\begin{aligned} n_e(0) &= n(0) = n_0, \\ u(0) &= u_0, \\ T_i(0) &= T_0, \\ \phi(0) &= 0, \quad \phi(L) = -\phi_c < 0. \end{aligned}$$

We perform a scaling of the system on the basis of physical considerations, we set

$$\begin{aligned} x &= Lx', \quad n_e = n_0 n'_e, \quad \phi = -\frac{kT_e}{e}\phi', \\ n &= n_0 n', \quad u = \sqrt{\frac{kT_e}{m_i}} u', \quad T_i = T_0 T'_i. \end{aligned}$$

With a little algebra and after suppression of the primes for the dimensionless variables, the model, in the case  $\gamma > 1$ , can be written as

$$n_e = \exp(-\phi)$$

$$nu = u_0, \quad (1)$$

$$\frac{1}{2}u^2 + \frac{\gamma}{\gamma-1} \frac{T_0}{T_e} T_i - \phi = \frac{1}{2}u_0^2 + \frac{\gamma}{\gamma-1} \frac{T_0}{T_e}, \quad (2)$$

$$n^{1-\gamma} T_i = 1, \quad (3)$$

$$n(0) = 1, u(0) = u_0, T_i(0) = 1. \quad (4)$$

\*Abstract 6776 submitted to the 21st International Symposium on Rarefied Gas Dynamics, Marseille, France, July 26-31, 1998

$$\left(\frac{\lambda_D}{L}\right)^2 \frac{d^2\phi}{dx^2} = n - n_e ,$$

$$\phi(0) = 0 , \quad \phi(1) = \phi_c ,$$

where we used the Debye length

$$\lambda_D = \sqrt{(\epsilon_0 k T_e)/(n_0 e^2)} .$$

### 3 Non-Linear Poisson Problem

Equations (1), (2), (3) and (4) allow the computation of the ion density as a function of the electric potential, i.e.  $n = \mathcal{N}_i(\phi)$ .

Setting

$$\mathcal{N}(\phi) = \mathcal{N}_i(\phi) - \exp(-\phi) ,$$

the whole model can be written as a non-linear Poisson problem

$$\left(\frac{\lambda_D}{L}\right)^2 \frac{d^2\phi}{dx^2} = \mathcal{N}(\phi) ,$$

$$\phi(0) = 0 , \quad \phi(1) = \phi_c > 0 .$$
(5)

The function  $\mathcal{N}$  has been analyzed in [2] and we find that it strongly depends on the difference between the ion injection speed and the ion-acoustic speed:

$$c_S^2 \stackrel{\text{def}}{=} (T_e + \gamma T_0)/T_e .$$

Setting

$$\varepsilon \stackrel{\text{def}}{=} \lambda_D/L ,$$

and noting that, in most cases,  $\varepsilon \ll 1$ , we see that the system (5) is a singular perturbation problem. We begin to analyze (5) considering  $\varepsilon$  as a positive parameter and we study the existence and multiplicity of its solutions.

We define the Sagdeev potential function as

$$V(\phi) \stackrel{\text{def}}{=} \int_0^\phi \mathcal{N}(\psi) d\psi .$$

In all the possible cases that arise from the resolution of the Euler system, the Sagdeev potential presents a unique point  $\phi_m$ , such that

$$V'(\phi_m) = 0 , \quad V''(\phi_m) \geq 0$$

and, for  $\phi \geq \phi_m$ , the Sagdeev potential is strictly increasing.

From the non-linear Poisson equation we have the first integral

$$\left|\frac{d\phi}{dx}(x)\right|^2 = \left|\frac{d\phi}{dx}(0)\right|^2 + \frac{2}{\varepsilon^2} V(\phi) .$$

Analyzing the problem with  $\varepsilon$  fixed we can prove the existence and unicity of monotone increasing solutions of the problem (5), when  $\phi_c > \phi_m$  and under a supplementary hypothesis that relies on the shape of the Sagdeev potential, we show the existence of non-monotone solutions of the same problem, for  $\varepsilon$  small enough.

### 4 Quasi-Neutral Limit

In plasma physics, when the scale of the observation is very large compared to the Debye length  $\lambda_D$ , the studied system is said to be at the quasi-neutral limit. Mathematically this leads to the study of the limit  $\varepsilon \rightarrow 0$  of the solutions  $\phi_\varepsilon$  of the non-linear Poisson problem (5). We show that these solutions always converge to  $\phi_m$ , with the exclusion of some boundary layers or some free layers which depend only on the shape of the Sagdeev potential in a neighborhood of  $\phi_m$ . We find that in the case  $u_0 < c_S$  there is a unique limit potential profile which presents two exponential boundary layers in  $x = 0$  and  $x = 1$  and between them the potential is constant and equal to the value  $\phi_m > 0$ , for which  $n = n_e$ .

In the case  $u_0 = c_S$ , again the limit of solutions of the non-linear Poisson problem is unique and it is constant and equal to  $\phi_m = 0$  in all the domain but in a neighborhood of  $x = 1$ , where a parabolic boundary layer is present.

In the supersonic case the situation is more complicated, for all  $u_0 > c_S$  there is a limit solution similar to the sonic one with the exception of the boundary layer that now is exponential, but, if  $c_S < u_0 < K c_S$  ( $K > 1$ ), there is a second limit solution that presents the same features than the first one, but, in  $x = 1/3$ , it takes a negative value  $\phi_3$  and in a neighborhood of this point has a double exponential free layer.

### References

- [1] Ben Abdallah N., Mas-Gallic S., Raviart P.A., *A Mathematical Analysis of Electric Probe Models*, Transp. Theo. Stat. Phys. vol.25, 3-5, 263-281 (1996).
- [2] Ambroso A., Gosset J., Méhats F., Raviart P.A. *On singular perturbation problems for the nonlinear Poisson equation*, course for the GdR SPARCH summer school in Oleron 15-20 September '97.

# A Comparison of Kinetic Theory and Molecular Dynamics in the Context of Granular Flows\*

L. Popken

University of Kaiserslautern, Germany

## 1 Introduction

Flows of granular materials are widely met in our environment, be it in natural phenomena like avalanches or sand storms, or in industrial and technological processes where bulk materials like grains or coal are transported, screened or crushed.

Different approaches to the dynamics of granular flow lead to a hierarchy of different levels of description, namely molecular dynamics, kinetic theory and macroscopic equations. This work is concerned with the comparison of two such levels, namely soft-sphere molecular dynamics (MD) and the kinetic level.

### 1.1 The Kinetic Scheme

A kinetic description of granular flow (see e.g. [1]) is given by a modification of the Enskog equation for moderately dense gases. Let  $v$  denote the velocity and  $\omega$  the spin of spheres with diameter  $a$  and mass  $m$ , then the evolution of the density in phase space,  $f$ , is given by

$$\frac{\partial f}{\partial t} + v \cdot \nabla_x f = J(f, f), \quad (1)$$

where for the collision operator  $J$  see Figure 1 on the next page.

In a granular regime, the velocity transformation  $T_\eta$  is energy dissipating.  $T_\eta$  is usually a hard sphere model, see e.g. [2].

One method of solving Eq. (1) is based on a finite pointset method similar to the solving of the Boltzmann equation, see [3]. The code considers 6 degrees of freedom (3 translational and 3 rotational).

### 1.2 The Microscopic Model

To model inelastic collisions in molecular dynamics one requires at least two terms, namely repulsion

\*Abstract 7101 submitted to the 21st International Symposium on Rarefied Gas Dynamics, Marseille, France, July 26-31, 1998

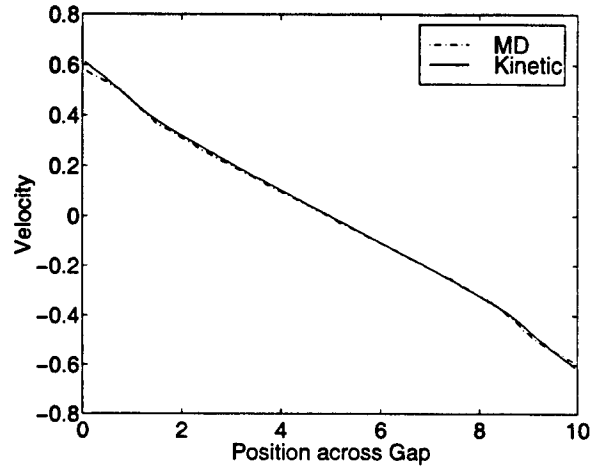


Figure 2: Velocity profile

and some sort of energy dissipation. The simplest force with the desired properties is the damped harmonic oscillator force

$$F_n = -c_n v_n - k_n x, \quad (2)$$

$$F_t = \min\{-c_t v_t - k_t \int v_t dt, -\mu F_n\}, \quad (3)$$

with  $c_n, c_t$  the damping coefficients and  $k_n, k_t$  the spring constants for the normal force  $F_n$  and the tangential force  $F_t$ , respectively.  $v_n, v_t$  denote the relative velocity at contact point in normal and tangential direction. The tangential force is limited by the friction  $\mu F_n$ . The coefficient of normal restitution  $e$  is defined as the ratio  $e = -v_n''/v_n'$ .

The present work refers to the code developed at CSIRO, Australia, see [4], and is restricted to three degrees of freedom (two translational, one rotational).

## 2 Test Case and Results

As a test case a 1d Couette flow is considered. The binary collisions of both models are as given by Eqs. (2) and (3). The parameters are a constant

$$\begin{aligned}
 J(f, f) &= \int_{\mathcal{R}^6} \int_{S^2} k(v_{21}'' \cdot \eta) Y(n(t, x - \frac{a}{2}\eta)) f(t, x, w'') f(t, x - a\eta, w_*'') d\eta dw_*'' \\
 &\quad - \int_{\mathcal{R}^6} \int_{S^2} k(v_{21} \cdot \eta) Y(n(t, x - \frac{a}{2}\eta)) f(t, x, w) f(t, x - a\eta, w_*) d\eta dw_*,
 \end{aligned}$$

Figure 1: Collision operator for a granular flow. The double primed variables denote the precollisional velocities  $w'' = (v'', \omega'')$  such that the binary collision of a particle with velocity  $w''$  and a second particle with  $w_*''$  changes its velocities according to the transformation  $T$  with  $(w, w_*) = T_\eta(w'', w_*'')$ . The unprimed variables are the postcollisional ones. The hard sphere collision kernel  $k(\cdot)$  depends on the relative velocity  $v_{21} = v_* - v$ . The pair correlation function at contact,  $Y(n)$ , is taken from Standard Enskog Theory, see e.g. [3]. The number density is denoted by  $n$ , the collision direction by  $\eta \in S^2$ .

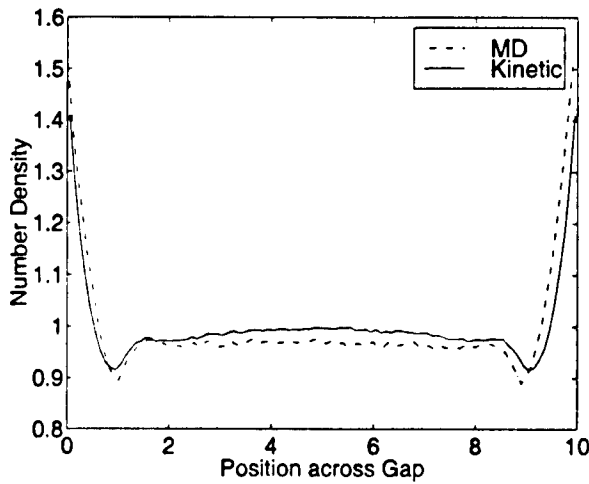


Figure 3: Density profile

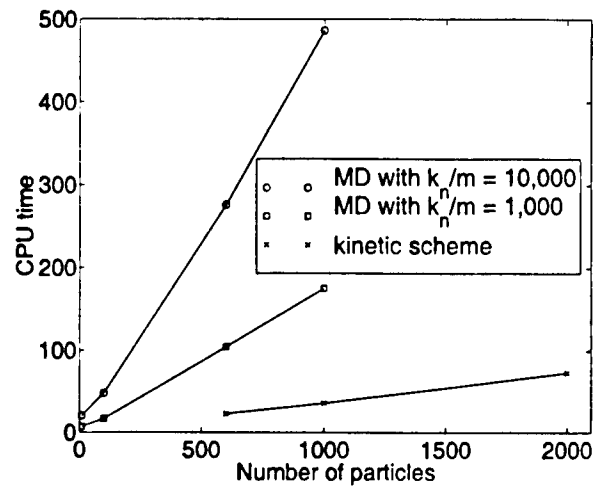


Figure 4: CPU time per 100 sec simulation time

$\epsilon = 0.95$ , a ratio  $k_t/k_n = 0.3$ ,  $k_n/m = 10,000$  and  $\mu = 1,000$ . The initial solid fraction in the kinetic model is  $\nu = 0.1$ , in the molecular dynamics accordingly, such that the mean free paths are equal. The shear velocity of each wall is normalized to one, the distance between the walls is 10 mean free paths. Molecular dynamics calculations base on 100 particles, the kinetic ones on 10,000. The stationary velocity profile is shown in Figure 2. The density profile (normalized to the initial density) is shown in Figure 3. Both profiles show a good agreement if one keeps in mind the completely different origin of both methods.

### 3 Conclusions

In the regime of moderately dense granular flow the kinetic scheme and molecular dynamics render comparable results. For reasonable spring constants the kinetic scheme is 5 to 12 times faster than the

molecular dynamics, see Figure 4.

### References

- [1] Goldshtein A., Shapiro M., *Mechanics of collisional motion of granular materials. Part 1. General hydrodynamic equations*, J. Fluid Mech. Vol. 282, pp. 75–114, 1995.
- [2] Lun C.K., Savage S.B., *A simple kinetic theory for granular flow of rough, inelastic, spherical particles*, ASME: J. Appl. Mech., Vol. 54, pp. 47–53, 1987.
- [3] Popken, L., *Grid-free particle method for the inhomogeneous Enskog equation and its application to a Riemann-problem*, Eur. J. Mech. B/Fluids, Vol. 17, No. 2, pp. 255–265, 1998.
- [4] Cleary, P., *A report on postdoctoral fellowship work in granular flows*, First Annual report for CSIRO postdoctoral fellowship, 1990.

**GAS-SURFACE INTERACTION - GS P**

**TUESDAY, JULY 28, 1998**

**16:15**

## Study of the Catalycity of SiC at High Temperatures \*

P. Rousseau, S. Cavadias, J. Amouroux  
Laboratoire de Chimie Appliquée et Génie des Procédés Industriels  
ENSCP, Paris, France

The heat transfer due to the recombination of atoms on space vehicles during the re-entry phase in the earth can lead to the damage of the protective materials. By measurements of recombination and accommodation coefficient ( $\gamma$  and  $\beta$ ) of oxygen atoms and by the determination of a specific surface heating rate (kw: that represents the total energy transferred), the surface chemistry (catalycity) of the materials can be evaluated.

In order to quantify the energy transfer due to the recombination of oxygen atoms in the silicon carbide (SiC), the recombination and accommodation coefficient have been measured independently in a large domain of temperatures from room temperature to 1100 K. The recombination coefficient is evaluated by a spectroscopic method of actinometry leading to the determination of oxygen atoms profile concentrations versus the distance from a surface at stagnation point configuration assuming a diffusion regime.

The determination of the accommodation coefficient is performed by a calorimetric method based on the determination of the energy released from the atomic recombination in the sample.

The main experimental results show an increase of the SiC catalycity with the surface temperature: the recombination coefficient varies from  $4.0 \times 10^{-3}$  at 298 K and  $4.1 \times 10^{-2}$  at 1123 K while the accommodation coefficient goes up to 0.26 until 0.71 at 523 K.

---

\*Abstract 1106 submitted to the 21st International Symposium on Rarefied Gas Dynamics, Marseille, France, July 26-31, 1998

# Molecular Dynamics Simulation of Energy Accommodation at Gas-Surface Interfaces \*

J. Blömer, A.E. Beylich  
Rheinisch-Westfälische Technische Hochschule,  
52056 Aachen, Germany

## 1 Introduction

When leaving the limit of continuum mechanics, in the regime of rarefied gas dynamics, the interactions between gas flows and condensed matter surfaces influence the properties of the flowfield. Nowadays flows of rarefied gases can be calculated for example by DSMC methods, although the formulation of boundary conditions is not always clear. To reach a better understanding of gas-surface-interactions the exchange of energy and momentum during the collision of diatomic gas molecules with internal degrees of freedom and condensed matter surfaces are studied by classical trajectory calculations.

The calculations which are presented here are performed for Nitrogen molecules colliding with a Platinum  $\langle 111 \rangle$  surface.

## 2 Model

The gas molecule is simulated by a rigid rotator with two internal degrees of freedom according to classical mechanics. For the collision energies which are used in this work (max 1000K) vibrational degrees of freedom are not taken into account. For the simulation of gas-surface-interaction an efficient model of the surface is essential because most of the computational work is needed to calculate the mutual interaction of the surface atoms. In this work only a small part of the surface is simulated in detail on a molecular level: three layers of the lattice, each containing 37 atoms which are arranged in a shape of a hexagon according to the  $\langle 111 \rangle$  surface of a cubic face centered lattice. The influence of the lattice atoms outside of the primary simulation area is considered by a temperature bath which is realised by the *Langevin* differential equation following ideas introduced to gas-surface-interaction

by *Tully* [3]. Details and basic properties of the model have been shown in a previous paper [1].

## 3 Calculations

The interaction between gas molecules and condensed matter surfaces can roughly be divided into two different channels: Molecules are following either the direct scattering mechanism or the adsorption-desorption mechanism. For directly scattered molecules it seems obvious that they usually do not reach equilibrium with the surface because of the short interaction time: Besides the mass of the molecule, the mass of the surface atom and the interaction potentials which are constant for one combination of species, the exiting state is determined by the initial properties of the molecule and the temperature of the surface. Adsorbed molecules lose all their information about the initial properties and during the long interaction time they are able to reach equilibrium with the surface atoms. But experimental [2] studies and molecular dynamic studies show that for higher surface temperatures ( $T > 400K$ ) the rotational temperature of desorbing molecules is significantly lower than the temperature of the surface.

This phenomenon can be understood by taking the opposite process into account, i.e. looking at the probability of gas molecules to be trapped during the collision. For example trajectories are calculated for gas molecules taken from their equilibrium distributions with the same temperature as the surface ( $T_{rot} = T_{kin} = T_{solid} = 800K$ ). The other parameters like angle of incidence, rotational orientation etc., are randomly taken from the corresponding distributions.

The figures show the distributions of rotational and kinetic energy for the incoming molecules. The total distributions, which are following the *Maxwell* and the *Boltzmann* distribution, respectively, are split into two parts: One part belongs to molecules

\* Abstract 1627 submitted to the 21st International Symposium on Rarefied Gas Dynamics, Marseille, France, July 26-31, 1998



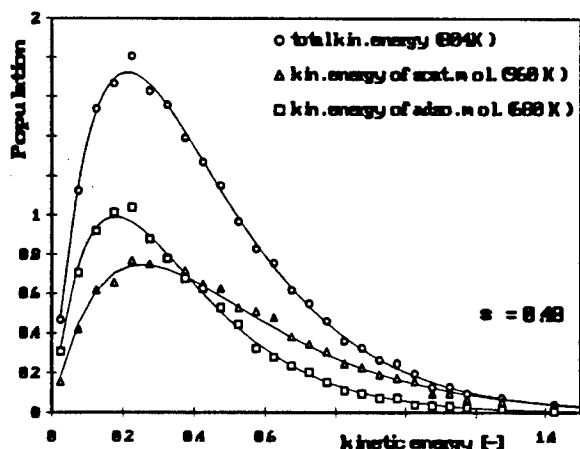


Figure 1: Translational energy distributions of incoming molecules

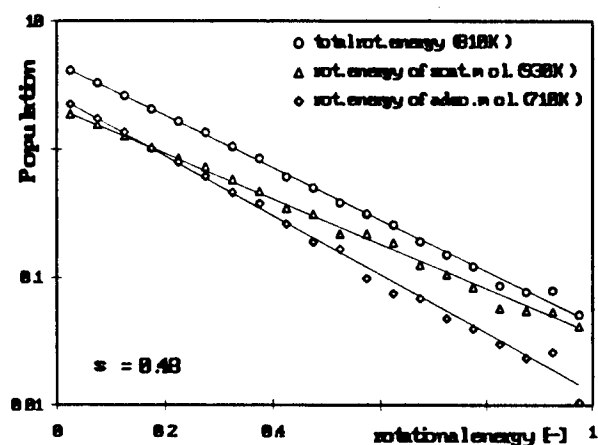


Figure 2: Rotational energy of incoming molecules

which will be scattered and the other part belongs to molecules which will be adsorbed. (All distributions are normalized to the total amount of incoming molecules, i.e. the distributions of the adsorbed molecules are scaled with the average sticking coefficient  $\sigma$  and the distributions of scattered molecules are scaled with  $(1-\sigma)$ . The partial distributions have a similar shape as the complete ones. Although this is only an approximation, the temperatures of these distributions are used to determine the average energy of the distributions: The rotational and translational temperatures of the molecules which will be scattered are higher than the temperatures of molecules which will be adsorbed. The local sticking coefficient as a function of the incident energy can be calculated by the relation of the distributions of the adsorbed molecules to the total distribution: As expected, at lower energies the sticking coefficient increases,

although there are still molecules which are able to escape from the surface. By arguments of detailed balancing this means that the distributions of the desorbing molecules are shifted towards lower temperatures. Calculations of trajectories of desorbing molecules for the same configuration yielded  $T_{kin} = 530K$  and  $T_{rot} = 590K$ .

Similar calculations for other temperatures and cases when the gas has a different temperature than the surface were also performed.

## References

- [1] Blömer, J.; Beylich, A.E.: *MD-Simulation of inelastic Molecular Collisions with Condensed Matter Surfaces*, RGD 20 (1997)
- [2] Mödl, A.; Robota, H.; Segner, J.; Vielhaber, W.; Lin, M.C.; Ertl, G.: *Rotational state distributions of NO molecules after interaction with germanium surfaces*; J. Chem. Phys. Vol. 83 pp. 4800 (1985)
- [3] Tully, J.C.: *Dynamics of gas-surface interactions: 3D generalized Langevin model applied to fcc and bcc surfaces*, J. Chem. Phys. Vol. 73 pp. 1975 (1980)

# On Normalization of Scattering Function on a Rough Surface \*

M.V.Anolik<sup>1</sup>, V.D.Khabalov<sup>2</sup>, I.A.Khalidov<sup>1</sup>

<sup>1</sup> St.Petersburg State University, St.Petersburg, 198904, Russia

<sup>2</sup> North-Ossetic State University, Vladikavkaz, 362031, Russia

Aerodynamical characteristics for single and for both single and twofold reflections from a rough surface are compared. Unlike [1], the case of specular reflection from a small area is considered. The scattering function on a rough surface  $V(\vec{u}_1|\vec{u})$  depending on the impinging  $\vec{u}_1$  and on the emerging  $\vec{u}$  gas atom velocities is expanded into a series

$$V = \sum_{m=1}^{\infty} V_m, \quad N_m = \int \int \int_{u_z > 0} V_m(\vec{u}|\vec{u}_1) d\vec{u},$$

$$\sum_{m=1}^{\infty} N_m = 1, \quad (1)$$

where  $V_m$  is the scattering function of the  $m$ -fold reflection, and  $N_m$  is the  $m$ -fold reflection probability.

In the same way as in [1], we calculated aerodynamical characteristics in the following four approximations for  $V$

$$V_c^{(1)} = V_1, \quad V_c^{(1,2)} = V_1 + V_2,$$

$$V_n^{(1)} = \frac{V_1}{N_1}, \quad V_n^{(1,2)} = \frac{V_1 + V_2}{N_1 + N_2}. \quad (2)$$

The inadequacy of  $V_c^{(1)}$  and  $V_c^{(1,2)}$  is that normalizing condition Eq.1 is not valid for them. To eliminate this defect, we propose the following new four approximations for  $V$

$$V_s^{(1)} = V_1 + (1 - N_1)V_{0s},$$

$$V_s^{(1,2)} = V_1 + V_2 + (1 - N_1 - N_2)V_{0s},$$

$$V_d^{(1)} = V_1 + (1 - N_1)V_{0d},$$

$$V_d^{(1,2)} = V_1 + V_2 + (1 - N_1 - N_2)V_{0d}. \quad (3)$$

where  $V_{0s} = \delta(\vec{u} - \vec{u}_1 + 2\vec{u}_{1n})$  is the specular scattering function on smooth surface with the same normal  $\vec{n}$  as the normal to the mean level of a rough surface,  $V_{0d} = 2h^2\pi^{-1}u \cos\theta \exp\{-hu^2\}$  is the diffuse

one with parameter  $h = 2u_1^{-2}$  which corresponds to the energy exchange coefficient  $q = 0$  ( $\theta$  is the reflection angle). The corrected momentum  $p$ ,  $\tau$  exchange coefficients (at  $\lambda = u_1\sqrt{h} = \sqrt{2}$ ) are

$$p_s^{(1)} = p_c^{(1)} + 2(1 - N_1)\cos^2\theta_1,$$

$$p_s^{(1,2)} = p_c^{(1,2)} + 2(1 - N_1 - N_2)\cos^2\theta_1,$$

$$\tau_s^{(1)} = \tau_c^{(1)} - (1 - N_1)\sin 2\theta_1,$$

$$\tau_s^{(1,2)} = \tau_c^{(1,2)} - (1 - N_1 - N_2)\sin 2\theta_1,$$

$$p_d^{(1)} = p_c^{(1)} + \frac{\sqrt{\pi}}{\lambda}(1 - N_1)\cos\theta_1,$$

$$p_d^{(1,2)} = p_c^{(1,2)} + \frac{\sqrt{\pi}}{\lambda}(1 - N_1 - N_2)\cos\theta_1,$$

$$\tau_d^{(1)} = \tau_c^{(1)}, \quad \tau_d^{(1,2)} = \tau_c^{(1,2)}.$$

The dependence of  $N_1$  and  $N_2$  on the incidence angle  $\theta_1$  and on the roughness parameter  $\sigma_1$  is shown in Fig.1 and Fig.5, respectively. One can see that  $N_1 + N_2 > 1$  at large values of  $\sigma_1$  and  $\theta_1$ . The failure of normalizing condition Eq.1 is explained by the error of our method of computation: it is too large at large values of  $\sigma_1$  and  $\theta_1$  (cf. [1]). Figs 2,6,3,7 show the dependence of  $p_c^{(1)}$ ,  $p_n^{(1,2)}$ ,  $\tau_c^{(1)}$ ,  $\tau_n^{(1,2)}$  on  $\theta_1$  and on  $\sigma_1$ . The dependence of the aerodynamical resistance coefficient  $c_x$  on  $\sigma_1$  in a free molecular flow is shown in Fig.4 for sphere and in Fig.8 for cylinder in cross flow for all eight approximations given in Eq.2 and Eq.3 ( $\sigma_1$  is plotted at the logarithmic scale).

## References

- [1] Anolik M.V., Khabalov V.D., Khalidov I.A., *Twofold Reflections of Rarefied Gas Atoms from a Rough Surface*, In: Ching Shen Ed. *Rarefied Gas Dynamics*, pp.422-427. Peking: University Press, 1997.

\*Abstract 1921 submitted to the 21st International Symposium on Rarefied Gas Dynamics, Marseille, France, July 26-31, 1998

# GAS - SURFACE INTERACTION - GS P

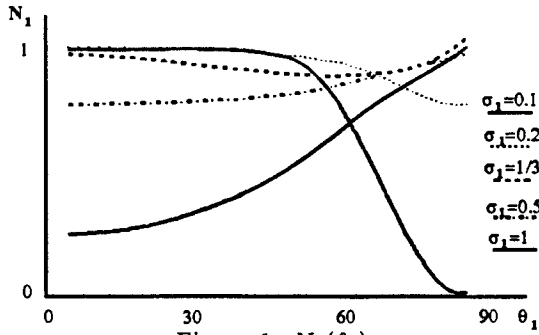


Figure 1:  $N_1(\theta_1)$

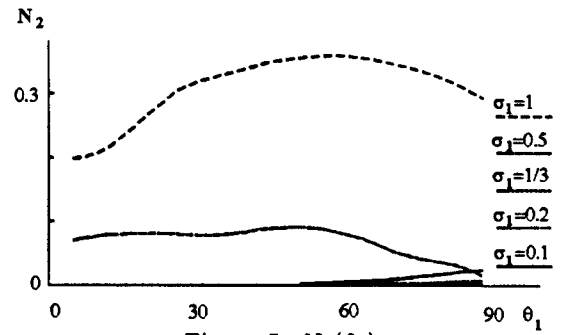


Figure 5:  $N_2(\theta_1)$

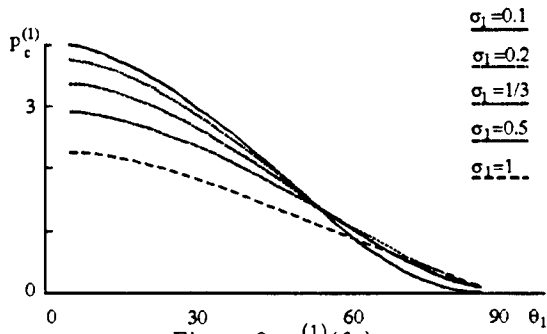


Figure 2:  $p_c^{(1)}(\theta_1)$

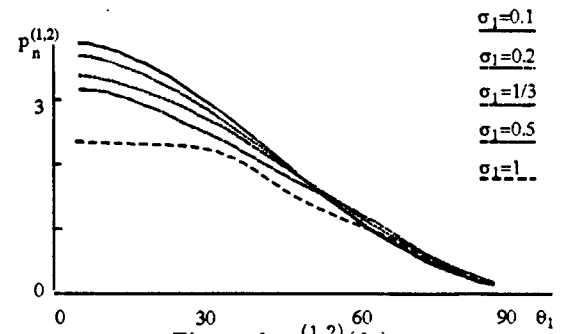


Figure 6:  $p_n^{(1,2)}(\theta_1)$

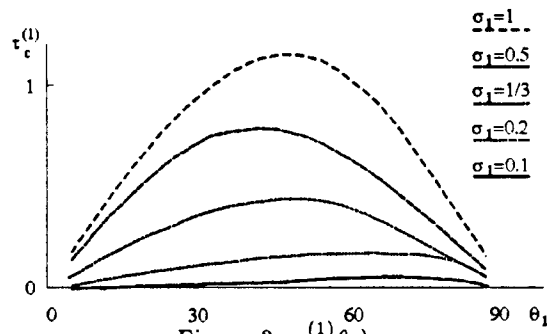


Figure 3:  $\tau_c^{(1)}(\theta_1)$

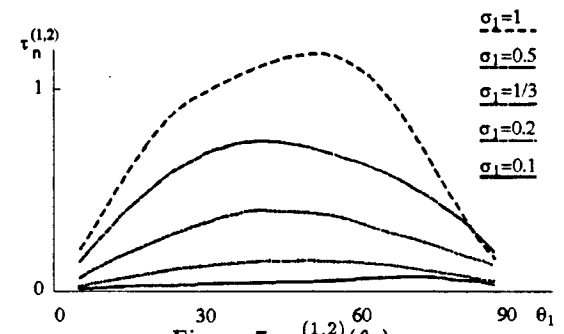


Figure 7:  $\tau_n^{(1,2)}(\theta_1)$

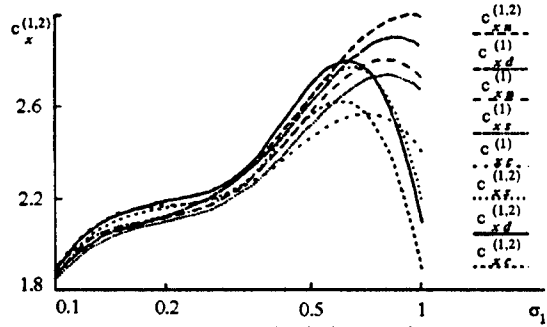


Figure 4:  $c_x(\sigma_1)$  (sphere)

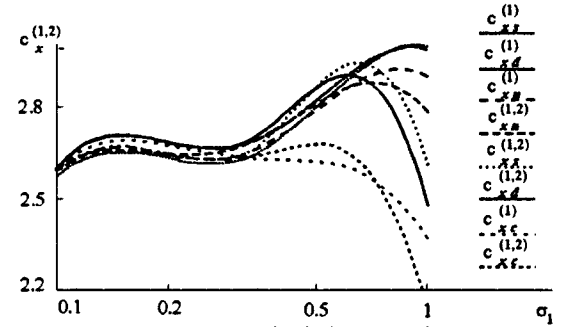


Figure 8:  $c_x(\sigma_1)$  (cylinder)

# Laboratory and Flight Results of Accommodation Coefficients Measurements \*

O.G. Friedlander<sup>1</sup>, A.P. Nikiforov<sup>1</sup>, V.P. Bass<sup>2</sup>, A.N. Aksyutenko<sup>2</sup>,  
V.S. Yurasov<sup>3</sup>, A.I. Nazarenko<sup>4</sup>, V.N. Shakhmistov<sup>5</sup>

<sup>1</sup>Central Aerohydrodynamics Institute (TsAGI), Zhukovsky, Russia

<sup>2</sup>Applied Mechanics Institute, Dnepropetrovsk, Ukraina

<sup>3</sup>Scientific Research Center "Kosmos", Moscow, Russia

<sup>4</sup>Programmes Research Center RAN, Moscow, Russia

<sup>5</sup>AeroSpace University, Samara, Russia

## 1 Introduction

The force interaction of Space Objects (SO) with the upper atmosphere varies not only with the density, SO trajectory and orientation but also depends on the molecule interaction with surface of SO (accommodation coefficients). Its value may be determined to considerable extent on the basis of laboratory experiments. This approach is limited by the capabilities of the simulation facility. On the other hand, the difference in simulation capabilities hampers the correlation of data obtained by various groups of investigators. It's very difficult also to conduct even single flight experiment (the example - a number of papers by Blanchard et al.).

## 2 Short description of experiments

Therefore the experiments were conducted in two different vacuum facilities [1- 3] with different parameters of molecular beams. The accommodation coefficients of various materials were measured with the same samples of external SO surface. The test experimental data were compared also with the results of flight experiments PION [4-5].

The main distinction of test facility of TsAGI [1,2] and ITM [3] consist in different energy of molecular beam and different gas pressure in the work chamber. It leads to distinction in characteristics of adsorbed layers on the samples surfaces.

The flight experiment consists in observation of the two passive standard satellites which were sepa-

rated from the spacecraft RESURS at the one day interval. The diameters and masses of these satellites were almost equal, but the materials of external surface were different with different accommodation coefficients (enamel, ceramics, aluminum). By the monitoring of this pair of SO the relation of drag coefficients were determined with small errors. The flight experimental data confirm the main results of test experiments.

## Acknowledgements

Completion of these investigation were partly supported by Russian Foundation for Basic Research (grant 96-01-01805) and State Program for Leading Research Groups Support (grant 96-15-96063).

## References

- [1] Musanov S.V., Nikiforov A.P., Omelik A.I., Friedlander O.G., *Experimental determination of momentum transfer coefficients in hypersonic free molecular flow and distribution function recovery of reflected molecules*, Rarefied Gas Dynamics. Proc. 13-th Symp. v.1, Novosibirsk, 1982,p.669-676.
- [2] Friedlander O.G., Nikiforov A.P. *Modeling aerodynamic atmospheric effects on the space vehicle surface based on test data*, Proc. 2-nd Symp.Environmental Testing for Space Programmes ESTEC/ESA, 1993, p. 307-312.
- [3] Abramovskaya M.G., Bass V.P., Petrov O.V., Stasenko S.T., Tokovoi S.V. *Some features of aerodynamic drag in upper atmosphere. Observation of artificial space objects*, Astronomy

\*Abstract 2069 submitted to the 21st International Symposium on Rarefied Gas Dynamics, Marseille, France, July 26-31, 1998

## GAS - SURFACE INTERACTION - GS P

Council of AN USSR, M.1988, N.84, part 1, p.5-16 (in Russian).

- [4] Batyr G., Bratchikov V., Kravchenko S., Nazarenko A., Veniaminov S., Yurasov V. *Upper atmosphere density variation based on Russian space surveillance system data*, Proc. 1-st European Conf.on Space Debris. Darmstadt, 1993, 367-372.
- [5] Anisimov V.D. Bass V.P., Komissarov I.N., Kravchenko S.N., Nazarenko A.I., Piatnitsky Yu. S., Rychkov A.P., Sych V.I., Tarasov Yu.L., Friedlander O.G., Shakhmistov V.M., Yurasov V.S. *The results of aerodynamic drag investigation and upper atmosphere density measurements by the passive satellites PION. Observation of artificial space objects*, Astronomy Council of AN USSR. M. 1990, N86, part 1, p.19-29 (in Russian).

# Modeling adsorption-desorption processes in rarefied flows: determination of surface coverage rate \*

S. Oualid, J.C. Lengrand  
Lab. d'Aérodynamique du CNRS, Meudon, France

## 1. Introduction

Modelling surface coverage is essential to understand and describe chemistry at the gas-wall interface. This study focusses on modeling adsorption-desorption processes. Most previous works on this subject considered the macroscopic level<sup>1</sup> although some of them considered the microscopic level<sup>2,3</sup>. The aim of this study is to propose a model of adsorption-desorption processes at the microscopic scale and to incorporate it into a DSMC code.

## 2. Modeling adsorption - desorption processes

Let us consider an infinite crystalline surface, i.e. a three-dimensional lattice of atoms regularly arranged. The characteristic dimensions of this lattice are denoted  $a$  and  $b$  in the tangential direction and  $c$  in the direction normal to the surface. The wall atoms are supposed to be at rest. We first calculate the interaction force induced by the wall and deduce from it a condition of adsorption of the incident gas atom.

The interaction force  $\vec{F}(O_{i,j}, M)$  between one surface atom, located in  $O_{i,j}$  and an incident gas atom, located in  $M$  can be given by the Lennard-Jones expression

$$\vec{F}(O_{i,j}, M) = \frac{4\epsilon}{\sigma} \left[ 12 \left( \frac{\sigma}{O_{i,j}M} \right)^{13} - 6 \left( \frac{\sigma}{O_{i,j}M} \right)^7 \right] \frac{\vec{O}_{i,j}M}{O_{i,j}M}$$

where  $\epsilon$  is the depth of the potential energy well and  $\sigma$  is the distance at which the potential is zero. The incident gas atom interacts with each surface atom. The interaction force  $\vec{F}_T(h)$  is obtained by summation over all the atoms constituting the wall. Approximating the discrete summations by integrals results in<sup>4</sup>

$$\vec{F}_T(h) = \left( 0, 0, \frac{4\pi\sigma^2\epsilon}{abc} \left[ \frac{1}{5} \left( \frac{\sigma}{h} \right)^{10} - \frac{1}{2} \left( \frac{\sigma}{h} \right)^4 \right] \right)$$

where  $h$  is the distance of the gas atom above the surface. The resultant force is normal to the wall.

This is consistent with the results of Arumainayagam<sup>5</sup> who calculated numerically the potential induced by a surface composed of 108 atoms and concluded that it was nearly independent of the tangential directions.

The equilibrium height of the incident atoms is denoted  $r_0$ . A critical velocity  $V_C$ , is defined as follows : when a gas atom located at height  $r_0$ , has a normal velocity component directed away from the wall and larger than  $V_C$ , it escapes from the wall attraction. These quantities are calculated as<sup>4</sup>

$$r_0 = \left( \frac{2}{5} \right)^{1/6} \sigma \quad \text{and} \quad V_C = \sqrt{\frac{4\sqrt{10}\pi}{9} \cdot \frac{\epsilon\sigma^3}{mabc}}$$

where  $m$  is the mass of the gas atom. In the present model, a gas atom is assumed to oscillate around the distance  $r_0$ , and to be released after a so-called *lifetime*. The part of the atom trajectory above  $r_0$ , is treated by classical mechanics, based on the above equations, without any influence of wall temperature. The part of the trajectory below  $r_0$ , is not treated. We assume that the atom crosses the equilibrium plane  $r_0$ , away from the surface with a random velocity that corresponds to a gas in equilibrium at surface temperature  $T_w$ . In the Maxwell gas-surface interaction model, a similar condition is used, but applied to the velocity of the molecule *at infinity* rather than at distance  $r_0$ .

The gas atom oscillates until it receives a normal velocity larger than  $V_C$ . The higher  $T_w$ , the shorter the *lifetime*. The atom experiences a number of oscillations denoted  $N_{osc}$ , and the lifetime is the sum of the durations of these  $N_{osc}$  oscillations. After calculations, we find<sup>4</sup> an average lifetime  $t_{life}$ .

\* Abstract 3238 submitted to the 21st International Symposium on Rarefied Gas Dynamics, Marseille, France, July 26-31, 1998

$$t_{life} = [t_{evol}(\bar{v}_r) + t_{evol}(-\bar{v}_r)] \cdot \exp\left(\frac{mV_c^2}{2kT_w}\right)$$

where  $t_{evol}(v)$  is the duration of half an oscillation for an atom crossing the equilibrium plane with a normal velocity  $v$ .  $\bar{v}_r$  is the average value of  $v$ .

$$\bar{v}_r = \sqrt{\frac{2kT_w}{m}}, \quad t_{evol}(v) = 1,2783 \sqrt{\frac{mabc}{5\pi\epsilon r_0}} \left(\frac{v_c}{v_c - v}\right)^{0,87}$$

The lifetime is found with an Arrhenius-type form, like the empirical expressions generally used by other authors. But because of the lack of precision of our expression for the potential well and because of the effects of the exponential factor, some of our results differ from those results one can find in the literature.

### 3. Coverage rate

We estimated the coverage rate (i.e. the fraction of total available monolayer surface sites occupied by adsorbates) for a surface with  $s_0$  adsorption sites per unit area. All sites are assumed to be free at time  $t=0$ . We neglect recombination. The number of atoms impinging the surface per unit time and area is denoted  $N$ . All atoms that impinge the wall on a free site are adsorbed during a constant time  $t_{life}$ . Then, they are released. Atoms that impinge on an occupied site are immediately released. The temporal evolution of the coverage rate  $\theta(t)$  is found to be

$$\theta(t) = \sum_{j=0}^K \frac{1}{j!} \left[ \frac{N}{s_0} \left( t - jt_{life} \right) \right]^j \exp \left[ -\frac{N}{s_0} \left( t - jt_{life} \right) \right]$$

if  $t \in [Kt_{life}, (K+1)t_{life}]$

and the value of this rate at equilibrium  $\theta_{final}$

$$\theta_{final} = \frac{N \cdot t_{life}}{s_0 + N \cdot t_{life}}$$

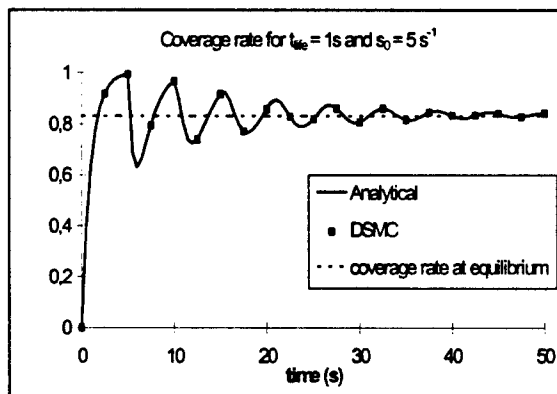


Fig.1 Temporal evolution of coverage rate

This model was incorporated into the DSMC code developed at the Laboratoire d'Aérothermique and the same problem was simulated. The results obtained by both methods is identical (Fig.1). Results obtained with recombination have also be obtained.

### 4. Conclusion

We developed a model of adsorption and desorption at the molecular scale that results in an Arrhenius-type form for the average lifetime of an atom adsorbed at the wall. This form is consistent with experimental results found in the literature. This model could be easily incorporated in a DSMC code, while being less expensive, for example, than Matsumoto's one<sup>2</sup>.

This model has been used to find the temporal evolution of the coverage rate of the surface and the value of this rate at equilibrium. Identical results were obtained both analytically and by DSMC for a wall with all sites free at initial time.

Other calculations that account for recombination have also been carried out.

### References

- [1] Bergemann F., "A detailed surface chemistry model for the DSMC method", 19th International Symposium on Rarefied Gas Dynamics, Oxford, 1994.
- [2] Matsumoto Y. and Matsui J., "Numerical analysis of gas-surface interaction by the molecular dynamics method", 17th International Symposium on Rarefied Gas Dynamics, pp. 889-896, 1990.
- [3] Simmons R.S. and Lord R.G., "DSMC simulation of hypersonic metal catalysis in a rarefied hypersonic nitrogen/oxygen flow", 20th International Symposium on Rarefied Gas Dynamics, 1996.
- [4] Oualid S., "Simulation numérique d'écoulements raréfiés à haute température: modélisation de l'interaction gaz-surface", Thèse de Doctorat de l'Université Pierre et Marie Curie, 1997.
- [5] Arumainayagam C.R., Madix R.J., McMaster M.C., Suzawa V.M. and Tully J.C., "Trapping dynamics of Xenon on Pt(111)", Surface Science, Vol 226, pp. 180-190, 1990.

# Numerical Study of Molecular Scattering on the Surface with Adsorbate Molecules \*

J. Matsui <sup>1</sup>, M. Nakakita <sup>1</sup>, Y. Matsumoto <sup>2</sup>

<sup>1</sup> Dept. of Mechanical Eng., Yokohama National University, Japan

<sup>2</sup> Dept. of Mechanical Eng., University of Tokyo, Japan

## 1 Introduction

Recently, microscopic understanding of scattering process of gas molecule on clean surface has been progressed very much by accurate experiments and numerical simulations. However, on the practical surface, adsorbate molecules usually exist and they may have strong effect on the scattering process. Though some experimental and numerical studies have been made, much more understanding is required. Here, using the classical molecular-dynamics method, the scattering process of a gas molecule on the crystal molecules with some adsorbate molecules is simulated and analyzed. The effect of parameters such as the coefficient of the molecular potential, incident energy of gas molecule, surface temperature, and number of adsorbate molecules is studied.

## 2 Assumptions and Numerical Method

adsorbate molecules, and crystal molecules are simulated with classical molecular-dynamics method. Each molecular motion is calculated under the assumptions that the motion is governed by Newton's equation. This equation is integrated numerically by the Runge-Kutta-Fehlberg scheme, that sets the adequate time step automatically.

Here we assume that the gas molecule and adsorbate molecules are same sort. Also, we calculate 2 dimensional system for the first step of study. Of course the 2 dimensional result such as the distribution of scattering angle is largely different from the realistic 3 dimensional result, but we confirm that the result about energy transferring is quantitatively same.

The Lennard-Jones inverse 6-12 power poten-

tial is used for the interaction potential between molecules, as

$$\phi(r) = 4\epsilon\{(R/r)^{12} - (R/r)^6\}.$$

Here  $\epsilon$  and  $R$  are potential parameters. These parameters between crystal molecules,  $\epsilon_{C-C}$  and  $R_{C-C}$ , are set to reproduce the potential between Platinum molecules. Between gas and crystal molecule, potential parameters are defined as,  $\epsilon_{G-C} = \gamma\epsilon_{C-C}$ , and  $R_{G-C} = \rho R_{C-C}$ . When gas molecule is Xenon and crystal molecule is Platinum,  $\gamma = 0.0846$  and  $\rho = 1.11$ . We set the parameters between gas molecules from the empirical relations, as

$\epsilon_{G-G} = \sqrt{\epsilon_{G-C}\epsilon_{C-C}}$ ,  $R_{G-G} = \frac{1}{2}(R_{G-C} + R_{C-C})$ . In this study  $\gamma$  is varied from 0.02 to 0.127, and  $\rho$  is from 0.89 to 1.33. The mass of gas molecule is fixed to  $0.673 m_C$ , where  $m_C$  is the mass of crystal molecule.

At first, the equilibrium state of both crystal molecules and adsorbates are calculated for the surface temperature,  $T_S$ . The crystal molecules are placed in 8 layers of 2 dimensional face-centered-cubic lattice, where each layer contains 12 molecules. And some gas molecules are put over the surface as adsorbates. A periodical boundary condition is applied to the tangential direction of surface. We give some kinetic energy to all these molecules, and calculate the trajectory for a certain period, keeping the temperature of the system to a certain value,  $T_S$ .

Next, a gas molecule collides on this prepared surface. The first position of this colliding molecule is chosen randomly. This calculation is continued until the gas molecule leaves about 11.3 angstrom from the surface plane, or until the calculation reaches to 10000 steps. After one calculation, all molecules are set back to the state of thermal equilibrium, Then the next gas molecule starts colliding from another position. In this study the incident angle is 0 degree, that is, the gas molecule falls down from the normal direction of the surface plane. The incident

\*Abstract 3861 submitted to the 21st International Symposium on Rarefied Gas Dynamics, Marseille, France, July 26-31, 1998



energy of gas molecule varies from 0.155 [eV] to 0.435 [eV]. The number of adsorbates over the surface,  $N$ , varies from 2 to 6. The temperature of the surface,  $T_S$  is 40 [K] or 300 [K]. More than 300 of colliding molecules are simulated for each condition.

### 3 Results

From the observation of trajectory and of energy transferring pattern of gas molecule, we put the gas molecules into three groups. The first group, "group A", is the case when the gas molecule collides to the adsorbate molecule. After the collision it flies away from the surface or it comes back to collide again. The second group, "group B" is the case when the gas molecule collides mainly to the crystal molecule. When the gas molecule collides slightly to the adsorbate and, just after that, collides to crystal molecule, we put the case into "group B' ". molecule to other molecules,  $\Delta E$ , is defined by the difference of the total energy of gas molecule during the first bounding. The distribution of  $\Delta E$  of group B' becomes almost same as that of group B, even when the molecular potential and the incident energy are changed. So here we put the group B' into group B in the discussion about the energy transferring.

The distribution of  $\Delta E$  of group B is recognized as the normal distribution, and its average and deviation are almost same as the case of scattering on the clean surface. Figure 1 shows this relation between the average of  $\Delta E$  and the potential parameter  $\epsilon$ , when incident energy is 0.256 [eV] and  $\rho = 1.11$ . The Average of  $\Delta E$  of group B varies according to the potential coefficient and incident energy of gas molecule.

The average and deviation of  $\Delta E$  of the group A are very different from the case of clean surface. Also, the average of transferred energy depends only on the incident energy. When the potential coefficient is changed, the average of  $\Delta E$  is almost constant. We can see such relation in figure 1. We think that the difference of process of energy transferring is one of the reason of this phenomenon. In the case of group B, the gas molecule gives much energy to the crystal molecules once, and then gets back some part of it. In the case of group A, the adsorbate molecule which gets energy from the gas molecule moves largely during the collision process, therefore the gas molecule can not get back its energy again. When the number of adsorbate molecule is changed, the average of the  $\Delta E$  is also different. But the average of each group is almost independent on the number of adsorbates. Here we define the represen-

tative ratio of group A, as  $\eta = \frac{N_A/N_T}{(2R_{G-G})n_G}$ . Here  $N_A$  is the number of molecules of group A,  $N_T$  is total number of gas molecule which collides on surface, and  $n_G$  is the number density of adsorbate molecules per unit area. This value  $\eta$  shows the ratio of group A to the all molecules, normalized by the  $n_G$ . This  $\eta$  is always about 0.4 when the potential parameters, incident energy, surface temperature, and the number of adsorbates are varied. We can easily estimate the ratio of  $N_A/N_T$  from this relation, and total average of  $\Delta E$ .

### 4 Concluding Remarks

The scattering process of gas molecule on the adsorbed surface is simulated in the 2 dimensional system.

- The gas molecule which makes collision on the surface can be put into two groups from its pattern of energy transfer.
- One group whose molecule collide to crystal molecules shows same scattering results as that on clean surface.
- The average of transferred energy of the other group, whose molecule collide to the adsorbate molecule, is only depends on the incident energy, not on the potential parameters.
- The ratio of these two groups can be estimated by some simple formula.

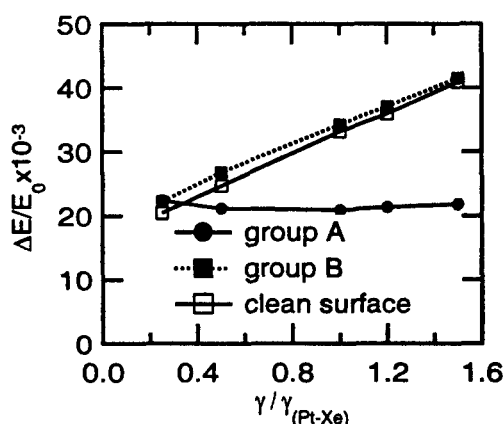


Figure 1: Average of transferred energy of each group

# The Multi- Stage Reflection Model for DSMC Calculations \*

N. Yamanishi and Y. Matsumoto

Department of Mechanical Engineering, University of Tokyo, Japan

## 1. Introduction

Proper boundary conditions must be set to obtain reliable results from numerical analysis of rarefied gas flows. Recent models for gas-surface interaction are based on knowledge from molecular beam experiments, which give limited information. Other models are either unrealistic or too complicated for DSMC calculations. Molecular Dynamics studies are able to give quantitative agreement with experimental data, and the method is an important tool for the understanding of the dynamics for any scattering system. In this paper, based on the large body of data obtained from molecular dynamics simulations<sup>[1],[2]</sup>, we present the Multi-stage model for gas molecules scattering from solid surfaces.

## 2. The Multi-Stage Model

The present version of the Multi-stage model is for the Ar or O<sub>2</sub>/Graphite system (Fig.1). Since our molecular dynamics calculations were performed at the energy range of 500 ~ 2000K, the model belongs to the thermal scattering regime. The basic idea of the model is to separate the collision into different stages. At each stage, the energy loss, the scattering direction and the trapping probability of the gas molecule will be determined by a simple model equation. All coefficients used in the equations were obtained from the large set of data of molecular dynamics simulations.

**Stage 1** The energy transfer stage determines the translational energy loss  $\Delta E_{tr}$  and rotational energy  $\Delta E_{rot}$  after each collision. Each energy has a correlation with the initial condition of the gas molecule,  $E_{tr}$ ,  $E_{rot}$  and  $\theta_{in}$ . The mean translational energy loss  $\langle \Delta E_{tr} \rangle$  is as follows.

$$\langle \Delta E_{tr} \rangle = c_n E_{tr} \cos^2 \theta_{in} + c_t E_{tr} \sin^2 \theta_{in} + c_r E_{rot} - c_s E_s \quad (1)$$

The constants  $c_n \sim c_s$  are determined from MD results. The standard deviation  $\sigma$  of  $\Delta E_{tr}$  also can be expressed by the same formula. Finally, the translational energy loss of the gas molecule can be determined from eq.(2), where  $f_N(m, s^2)$  gives a random gaussian distribution with  $m$  and  $s^2$  as the mean and variance.

$$\Delta E_{tr} = f_N(\langle \Delta E_{tr} \rangle, \sigma(\Delta E_{tr})^2) \quad (2)$$

Next,  $E_{rot,f}$  follows a similar procedure except that two different distributions are given depending on incident rotational energy  $E_{rot}$ . If  $E_{rot} \leq 100K$ , a combination of the Boltzmann and the non-Boltzmann distribution is given<sup>[3]</sup>. If  $E_{rot} \geq 100K$ , only the non-Boltzmann distribution is given.

\*Abstract 4431 submitted to the 21st International Symposium on Rarefied Gas Dynamics, Marseille, France, July 26-31, 1998

**Stage 2** Next, at the reflection stage, the gas molecule reflects from the potential energy surface  $\phi$ . Here we have specular reflection, where the molecular velocity component parallel to the potential energy surface conserved and the normal component reversed. We have simplified  $\phi$  with  $z = \Lambda(x, y)$  using the cosine function as in eq.(3).

$$\Lambda(x, y) = \frac{a_1}{2} \left\{ \cos\left(\frac{2\pi}{\sqrt{3}L}y\right) - 1 \right\} + \frac{a_2}{2} \left\{ 1 - \cos\left(\frac{2\pi}{L}x\right) \right\} + a_3 \quad (3)$$

The constants  $a_1 \sim a_3$  are set to fit the actual potential energy surface, but has a gaussian distribution since the potential energy surface trembles with the vibrational motion of the solid molecule.

**Stage 3** Finally, the gas molecule scatters, reenters or is trapped to the surface. The gas molecule scatters if it has enough  $E_{tr,n}$  and reenters if not so. After 15 collisions or if it is trapped, the diffuse model is applied.

Figure 2 is a comparison with molecular beam experiments for the  $O_2$ /Graphite system. The initial condition is set to  $\langle E_{tr} \rangle = 746K$ ,  $T_{rot} = 50K$  and  $\theta_{in} = 35, 60^\circ$  (case 1,2). The solid line is the velocity distribution of scattered molecules obtained from experiments and the open symbols are results from the present model. Both results show good agreement. Such agreement with molecular beam experiments shows the superiority of the present model.

### References

- [1] Matsumoto, Y., Yamanishi, N. and Shobatake, K., *Proc. 19th Int. Symp. on Rarefied Gas Dynamics*, pp.995-1001.
- [2] N. Yamanishi and Matsumoto, Y., *Proc. 20th Int. Symp. on Rarefied Gas Dynamics*, pp.381-386.
- [3] Danckert, A., *Proc. 20th Int. Symp. on Rarefied Gas Dynamics*, pp.404-409.

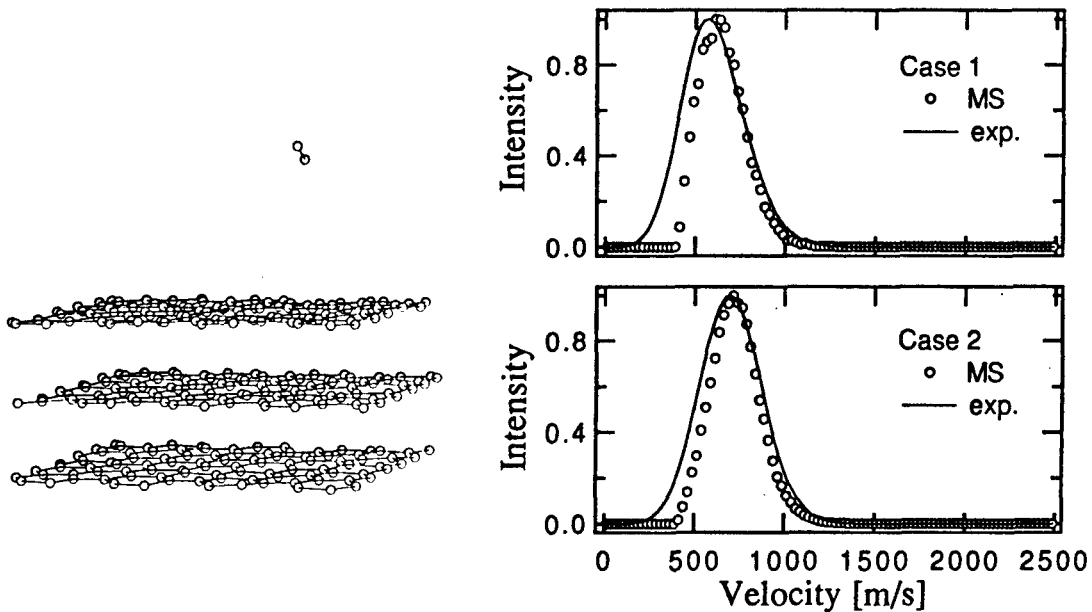


Fig. 1  $O_2$ /Graphite system

Fig. 2 Comparison of velocity distribution

# Influence of Surface Diffusion and Adsorbate Interaction on Heterogeneous Catalysis \*

Yu. G. Markoff

Institute for Mathematics and Mechanics Saint- Petersburg State University  
St- Petersburg, RUSSIA

In the present report the influence of surface diffusion and lateral interactions of reactants on heterogeneous catalytic reactions are investigated. The kinetics of adatoms are described in the frame of so called generalized kinetic BET - model (GKBET - model) [1,2]. I choose circular active sites of radius  $r_a$  and consider the reaction to occur only on the perimeter. According to assumptions of GKBET - model the reaction on an active site is described by the equation

$$\partial_t \theta(\vec{r}, t) = \lambda \partial_{\vec{r}} \{ D(\theta) q^2(\theta) \partial_{\vec{r}} B^D(\theta) \} + q(\theta) [b_* - B^a(\theta)], \quad (1)$$

$$B^{D,a}(\theta) = \frac{\theta}{1-\theta} \exp\{-\phi\theta\} \exp\{-\beta \epsilon^{D,a}\},$$

$$b_* = \frac{j\sigma}{\nu} \exp\{\beta \epsilon_*^a\}.$$

with the boundary conditions  $\theta(r_a) = 0$ ,  $\theta(r) \rightarrow \theta_s$  if  $r \rightarrow \infty$ . In this equation  $\epsilon^{D,a}$  are the diffusion and adsorption potentials, respectively;  $\theta(\vec{r}, t)$  is the coverage;  $q(\theta) = 1 - \theta$ ;  $\lambda = (\omega_*/a_*) \exp\{\beta(\epsilon_*^a - \epsilon_*^D)\}$ ;  $\omega_*, a_*$  are the average probabilities of diffusion jumps and desorption;  $\epsilon_*^{D,a}$  are the average diffusion and adsorption potentials;  $j$  is the density flux of gaseous atoms;  $\sigma$  is the area of a cell;  $\nu$  is the attempt frequency of adatoms;  $T$  is the temperature;  $b_* = (j\sigma/\nu)$ ;  $\phi = \beta z \epsilon_{nn}$ ,  $\beta = (kT)^{-1}$ ,  $z$  is the coordination number of adsorbate,  $\epsilon_{nn}$  is the energy of lateral interactions of adatoms,  $\theta_s$  is the equilibrium solution of Eq.(1). In the Eq.(1) the operators  $B^{D,a}$  are written in the form of mean field approximation. Other types of adsorbate interaction approximations are considered also. It is the peculiarity of the GKBET - model that in this model the chosen approximation of adsorbate interactions determines the form of the diffusion and

adsorption - desorption operators. So it is necessarily to consider unified diffusion - adsorption - desorption process in the general case. In the case of quasistationary solutions of Eq.(1) the equation for chemical potential of adsorbate is obtained without any apriori assumptions about the type of adsorbate interactions. In the report the criteria of Langmuir - Hinshelwood and Eley - Rideal reaction kinetics in the dependence on the  $\phi, b_*, T$  are established. There are done the expressions of reaction rates. Also the comparison of results obtained in the frame of GKBET - model with experimental data and the results of other authors are carried out using the singular spectrum analysis. References

1. Dubrovskiy G.V. (1994): Realistic kinetic boundary conditions on surfaces. *Proceedings of RGD18 Symposium*, **158**, 554 - 561. Vancouver, Canada.
2. Dubrovskiy G.V., Kuzmenko A.V., Markoff Yu.G. (1995): A three - dimensional lattice gas approximation for multilayer adsorption. *Theoretical and Mathematical Physics*, **105**, 1291 - 1306.

\* Abstract 5046 submitted to the 21st International Symposium on Rarefied Gas Dynamics, Marseille, France, July 26-31, 1998

# Numerical Analysis of Two-Dimensional Sink Flow of Rarefied Gas to Absorbing Part of Plane Boundary \*

E.M. Shakhov, V.A. Titarev  
Moscow State Technical University, Moscow, Russia

The paper deals with two-dimensional steady flow of rarefied monoatomic gas which is at rest at infinity and involved into motion because of absolute absorption at a part of plane boundary. The flow may be treated as a model for flow to cryogenic panel at the bounding surface or a sink flow through a slit. The problem is investigated by numerical integration of the kinetic model equation. As boundary conditions out of the absorbing part of the bounding plane wall the specular reflection or completely diffuse scattering of molecules is assigned.

Far from absorbing surface a radial flow is formed that is in correspondence with the subsonic branch of gasdynamical solution for cylindrical sink. Near absorbing part of the boundary the flow is essentially non-radial one. Under boundary condition of specular reflection at the plane wall out of the sink and for small Knudsen number the effect of rarefaction appears mainly near absorbing part of the plane. However, under diffuse molecular scattering a boundary layer at the surface is formed in addition. This layer is of unusual structure because its thickness first increases in sink direction from zero at infinity to a maximum and then decreases to zero again in close nearby of the sink. These understandable qualitative features of the flow are confirmed by numerical studies.

The main computed integral flow characteristic of principal interest is the mass flux through the absorbing part of the boundary as a function of Knudsen number. This relation is presented for both specular and diffuse boundary condition.

The solution is compared with that obtained for radial flow to absolutely absorbing cylinder.

---

\* Abstract 5172 submitted to the 21st International Symposium on Rarefied Gas Dynamics, Marseille, France, July 26-31, 1998

## Low Temperature Oxidation of Semiconductor Surfaces with Fast Atomic Oxygen \*

J. C. Gregory<sup>1</sup>, S. Cook<sup>2</sup>, M. A. George<sup>1</sup>, M. A. Hoffbauer<sup>2</sup>, and T. H. Prettyman<sup>2</sup>

<sup>1</sup> University of Alabama in Huntsville

<sup>2</sup> Los Alamos National Laboratory

In a series of space flight experiments and laboratory simulations of the hyperthermal atomic oxygen environment of space we have investigated the oxidation of semiconductor surfaces at temperatures from ambient to a few hundred degrees Centigrade. We typically observe accelerated reaction rates far greater than those observed at the same temperatures with molecular or thermal atomic oxygen. There are several applications of this discovery, one being the ability of growing passivation oxide layers on compound semiconductors at temperatures below which they decompose or otherwise are modified causing degradation of their beneficial electrical properties. The oxidation of a Ge surface by orbital atomic oxygen is described and that of a cadmium zinc telluride gamma-ray detector crystal. The latter produced a notable fall in surface leakage current and improvement in gamma-ray line resolution.

### Germanium

Thin films of Ge on one-inch-diameter fused silica optical flats were exposed to 5 eV atomic oxygen on the Long Duration Exposure Facility (LDEF) (Gregory and Peters, 1984). The films were RF-sputter deposited and of thicknesses 22 and 67 nm. The films were characterized by optical transmission, stylus profilometry using a Taylor-Hobson Talystep, x-ray photoelectron spectroscopy (XPS) and thin film x-ray diffractometry (XRD). The films were exposed to a total fluence of  $9 \times 10^{21}$  oxygen atoms  $\text{cm}^{-2}$  at a substrate temperature of about 290 K. Half of each film was covered by a mask during the flight exposure, and served as a reference or control sample.

After flight, the Ge films were much more optically transmissive in the area exposed to fast oxygen and in the case of the 22 nm film, were almost invisible

to the eye. Stylus profilometry measurements however showed that the oxidized film was still present, with a measured thickness of about 40 nm. XPS measurements showed the exposed area of both films to be covered with a C,O and Si-containing layer of contamination about 10 nm thick. XRD results (Figure 1, Gregory et al., 1995) obtained with a Rigaku D Max 3BX Thin Film Diffractometer on the thin Ge film showed only  $\text{GeO}_2$ . A 22 nm thick Ge film totally converted to theoretical

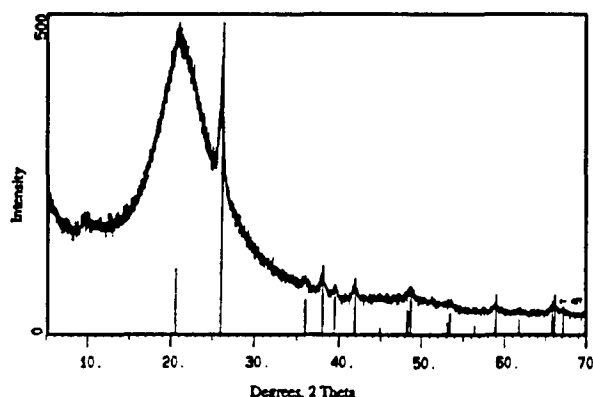


Figure 1: X-ray diffraction pattern obtained from the oxidized 22 nm Ge film exposed on LDEF experiment A0114. Vertical lines correspond to File 4-497 ( $\text{GeO}_2$ ) from the Powder Diffraction File. Diffraction lines from Fe are not observable.

density  $\text{GeO}_2$  would have a thickness of 28 nm. Together with 10 nm of amorphous contamination this yields a total thickness consistent with that measured with the stylus. XRD was not performed on the thicker film, but from its partial optical transmissivity and measured film thickness of 104 nm, it was indicated that some 50 nm of Ge had been converted to oxide with about 20 nm of elemental Ge remaining.

In summary, we noted that Ge surfaces were converted at ambient temperature to stoichiometric  $\text{GeO}_2$  of sufficient crystallinity and thickness to

\*Abstract 5876 submitted to the 21st International Symposium on Rarefied Gas Dynamics, Marseille, France, July 26-31, 1998

yield strong x-ray diffraction patterns. Up to 50 nm of Ge were converted to oxide under these conditions. The flight experiment did not allow determination of the temperature response of the reaction but yielded the idea that oxide layers of useful thickness might be grown on other semiconductor surfaces of importance at temperatures far below those required for normal oxidation.

## Cadmium Zinc Telluride, $\text{Cd}_{1-x}\text{Zn}_x\text{Te}$

Cadmium zinc telluride (CZT) is a ternary compound, wide band-gap, semiconductor with attractive potential for room-temperature gamma-ray spectroscopy. Until recently, its utility has been limited by the experimental difficulty of making high resistivity crystals with uniform electrical properties over the required detector volumes (several  $\text{cm}^3$ ).

The performance of CZT detectors is also influenced by surface and contact effects. Surface leakage increases the dark current, especially in gridded or pixellated devices. As the quality of the bulk material improves, the noise contribution from surface leakage becomes much more important and may become the dominant factor.

A number of passivation methods have been studied to reduce surface leakage. These include the use of passivating paint, and oxidation by aqueous hydrogen peroxide (Chen et al. 1997). More recently it has been found that atomic oxygen may produce the best passivation to date (Chen et al, 1998).

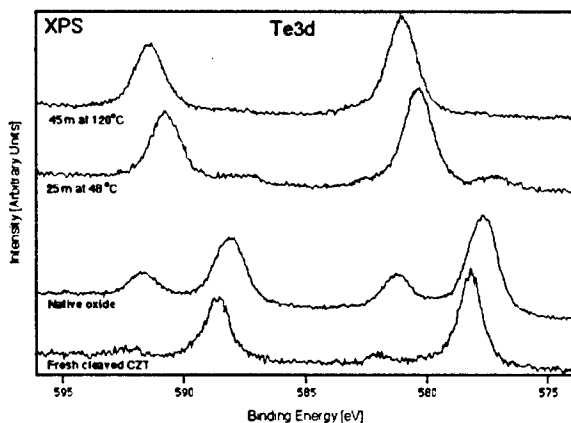


Figure 2: XPS Spectra of CZT samples.

Detector-grade crystals of CZT were exposed at several temperatures to the fast atomic oxygen beam at Los Alamos National Laboratory. The surface

oxide phases produced were characterized in the Laboratory for Materials and Surface Science at the University of Alabama in Huntsville using XPS, sputter-depth profiling, thin-film x-ray diffraction and atomic force microscopy. Figure 2 shows the Te 3d line spectra for a freshly cleaved surface, one covered with very thin native oxide, and two other surfaces exposed to the fast O beam. These results and others clearly show that stoichiometric layers of  $\text{TeO}_2$  are formed on the surface with film thicknesses depending on substrate temperature and exposure time. AFM results show a more homogeneous surface after exposure. Electronic characterization and gamma-ray resolution measurements made at the 662 keV line of  $^{137}\text{Cs}$  showed marked improvement in performance of the detectors. These results are discussed in detail.

## References

- [1] H. Chen, K. Chattopadhyay, K-T. Chen, A. Burger, M. A. George, J. C. Gregory, P. K. Nag, J. J. Weimer and R. B. James, *Passivation of CdZnTe Surfaces by Oxidation in Low Energy Atomic Oxygen*, accepted for publication in J. Vac. Sci. Technol., 1998.
- [2] K-T. Chen, D. T. Shi, H. Chen, B. Granderson, M. A. George, W. E. Collins, A. Burger and R. B. James, *Study of Oxidized Cadmium Zinc Telluride Surfaces*, J. Vac. Sci. Technol. B, 15(3)(1997)1.
- [3] J.C. Gregory and P.N. Peters, *The Interaction of Oxygen Atoms with Solid Surfaces at Orbital Altitudes, in The Long Duration Exposure Facility (LDEF): Mission 1 Experiments*, L. G. Clark, W. H. Kinard Editors, NASA Langley Research Center, NASA SP- 473:14, (1984).
- [4] J. C. Gregory, G. N. Raikar, J. B. Cross, M. A. Hoffbauer and P. N. Peters, *Surface Processing of Semiconductors with Atomic Oxygen*, AIP Conference Proceedings No 325, Eds M.S. AlGenk and R.P. Whitten, American Institute of Physics, New York, (1995).

## Kinetic Model of Gas-Surface Interaction \*

V.D. Seleznev<sup>1</sup>, I.P. Alexandrychev<sup>2</sup><sup>1</sup> Ural State Technical University, Ekaterinburg, Russia<sup>2</sup> Industrial Ecology Institute of RAS, Ekaterinburg, Russia

As well as the majority of real physical-chemical phenomena observed in heterogeneous systems, the scattering of gas molecules from surface represents an extremely complicated scientific problem. Certainly, it is stipulated by a large number of the interacting objects and various factors influencing to its character. For this reason the exact solution of the given problem is hardly possible in general and all theoretical approaches to analysis based on "first principles" can serve faster only as a good basis for the further inevitable approximations. Even the simplest case of the scattering of an unstructured gas particle from the surface of ideal single crystal has not received the full and final theoretical interpretation up to the present moment.

Fortunately, there is no need of clearing up of all details of the happening by scattering in the overwhelming majority cases of practical application of such solution, and some averaged outcome data are enough. From this point of view the use of the possibilities of statistical physics is rather perspective. However, the combined application of achievements of the common scattering theory and advantages of the statistical analysis of systems with large number of particles are even more successful. One of alternative modes of the realization of such approach to interpretation of phase-boundary interaction in gas-solid system is presented below. The scattering kernel taking into account such important surface processes as adsorption and desorption was constructed with its help.

The basis of this approach is a representation of gas-surface interaction potential  $U(\vec{r})$  as a superposition of the weak attraction and intensive repulsion, which are concentrated in different spatial areas. The distinction in the character of phase-boundary interaction in the gas-solid systems, when the distance of molecules from surface are reduced, results in the essential difference of the gas evolution process in two corresponding areas of surface layer. In the area of attraction the relaxation is stipulated by interaction molecules with low-energy lattice phonons, therefore it proceeds slowly. Opposite in repulsion region one or several high-energy phonons may be born and destroyed by each collision of gas molecules with solid atoms and the condition of gas may change dramatically. In addition to that, the size of attraction area and weakness of interaction of the gas particles, which are here, with the fluctuating potential field of crystal leads very often to the situation, when the statistical analysis of this subsystem becomes useful. Taking also into account the fact, that it is enough to describe the evolution of gas in this area of surface layer quasiclassically in the wide range of the scattering conditions, there is the natural desire to use existing possibilities to simplify of the common formalism.

For reaching of this purpose and for constructing the kinetic approach to the interaction between phases of the gas-solid systems the attempt of the separate analysis of the inelastic processes in both surface areas of the gas phase was undertaken. Thus the mathematical interpretation of scattering can be given on the basis of two operators  $\hat{G}$  and  $\hat{H}$ . The first operator characterizes slow evolution of the density matrix of gas particles in attraction layer  $\rho(t)$ ; and it exhibits quantum properties very rarely. The second operator gives the result of scattering of molecules from the repulsion region. This part of the solution comprises exactly almost all quantum peculiarities of gas-solid systems observed in experiments (e.g. "rainbow scattering", diffraction etc.).

Since the process of scattering is usually a sequence of oscillations of gas molecule in the surface potential field, frequently called "hops", it is possible to present the connection between the density matrix of the incident on the surface particles of gas  $\rho^-(t)$  and the density matrix of the scattering from surface molecules  $\rho^+(t)$  as the infinite series

\*Abstract 6527 submitted to the 21st International Symposium on Rarefied Gas Dynamics, Marseille, France, July 26-31, 1998



$$\rho^+(t) = \hat{G}^+ \sum_{k=0}^{\infty} (\hat{H} \hat{G}^-)^k \rho^-(t) = \hat{R} \rho^-(t) \quad (1)$$

where  $\hat{G}^+ \rho(t) = \hat{G} \rho(t) |_{r \in \Omega_S}$ ,  $\hat{G}^- \rho(t) = \hat{G} \rho(t) |_{r \in \Omega_R}$ ,  $\Omega_S$  and  $\Omega_R$  is accordingly the external and internal boundary of attraction layer.

From equation (1) it is obvious, that the solution of scattering problem is reduced to the definition of the concrete appearance of operators  $\hat{G}$  and  $\hat{H}$ . Certainly, in the common case, such variant of the analysis has no advantages before the traditional approaches. However, if the one-particle and moreover, quasiclassical statistical interpretation of gas behaviour in the attraction region is possible, the scattering problem becomes essentially simpler. In this case, operator  $\hat{G}$  and the derivative of it operators  $\hat{G}^+$  and  $\hat{G}^-$  are determined by a solution of the appropriate kinetic equation (frequently this is a Fokker-Plank equation) and the operator  $\hat{H}$  represents the scattering function of gas particles from repulsion potential, which can be obtained on a basis of common quantum mechanical approaches with a consequent average on quantum states. Then the boundary condition connecting the quasiclassical one-partial distribution function of the incident molecules,  $f^-(\vec{r}, \vec{v}, t)$ , and the similar distribution function of molecules scattered from surface,  $f^+(\vec{r}, \vec{v}, t)$ , is as follows

$$|v_z| f^+(\vec{r}, \vec{v}, t) = \left[ \hat{G}_S^+ + \hat{G}_R^+ \sum_{k=1}^{\infty} (\hat{H} \hat{G}_R^-)^k \hat{H} \hat{G}_S^- \right] |v_z| f^-(\vec{r}, \vec{v}, t) \quad (2)$$

where  $\hat{G}_S^-$  and  $\hat{G}_S^+$  determine the leaving gas streams on the boundaries  $\Omega_S$  and  $\Omega_R$  with the given entering stream on the boundary  $\Omega_S$ . Operators  $\hat{G}_R^-$  and  $\hat{G}_R^+$  define the same, but with entering stream on the surface  $\Omega_R$ . The expression (1) can be transformed to its usual form of the integrated boundary condition with the scattering kernel. Then, for example, in stationary case it will look like (here  $\vec{\phi} = \{\vec{r}, \vec{v}\}$ )

$$\begin{aligned} |v_z| f^+(\vec{\phi}) &= \int_{\Omega_S} d\vec{r}' \int_{v'_z < 0} d\vec{v}' |v'_z| f^+(\vec{\phi}') R(\vec{\phi}' \rightarrow \vec{\phi}) \quad , \\ R(\vec{\phi}' \rightarrow \vec{\phi}) &= G_S^+(\vec{\phi}' \rightarrow \vec{\phi}) + \sum_{k=1}^{\infty} \int_{\Omega_R} d\vec{r}'' \int_{v''_z > 0} d\vec{v}'' G_R^+(\vec{\phi}'' \rightarrow \vec{\phi}) W_k(\vec{\phi}' \rightarrow \vec{\phi}'') \quad , \\ W_1(\vec{\phi}' \rightarrow \vec{\phi}) &= \int_{\Omega_R} d\vec{r}_1 \int_{v_{1z} < 0} d\vec{v}_1 H(\vec{\phi}_1 \rightarrow \vec{\phi}) G_S^-(\vec{\phi}' \rightarrow \vec{\phi}_1) \quad , \\ W_k(\vec{\phi}' \rightarrow \vec{\phi}) &= \int_{\Omega_R} d\vec{r}_2 \int_{v_{2z} < 0} d\vec{v}_2 H(\vec{\phi}_2 \rightarrow \vec{\phi}) \int_{\Omega_R} d\vec{r}_1 \int_{v_{1z} > 0} d\vec{v}_1 G_R^-(\vec{\phi}_1 \rightarrow \vec{\phi}_2) W_{k-1}(\vec{\phi}' \rightarrow \vec{\phi}_1) \quad . \end{aligned}$$

Such a look of the scattering kernel except its relative simplicity also has one more very important advantage: with its help it is possible not only to describe the result of scattering, but also to analyze the behaviour of gas particles in area of the phase-boundary interaction (Here it means the trapping of them by physical-adsorption potential hole of the surface, the gradual thermalization and consequent desorption). Besides that, the possible multi-phonons interaction is already considered in the structure of scattering kernel and is described in the most natural way. It is necessary to tell, that besides the regime of "thermal scattering", for which the validity of the given approach is proved strictly the expression (3) should also remain quite efficient in the condition of "structural scattering" at high energies of incident gas particles, as in this case the result of scattering is almost completely determined by processes happening in the repulsion region, but exactly this part of the common task is offered to have a strict consideration within the framework of the common scattering theory.

With practical application of expression (3) for the analysis of the "thermal scattering" regime we approximated the attractive potential by right-angled step, and for the determination of functions  $\hat{G}_S^-$ ,  $\hat{G}_S^+$ ,  $\hat{G}_R^-$  and  $\hat{G}_R^+$  we used the known variant of the scattering interpretation by Cercignani and Lampis. Finally we could construct a very simple scattering kernel, which has allowed us not only to describe large number of the known experimental facts, but also has obtained a very interesting information about processes of the interaction between phases of gas-solid systems.

# Sticking, Thermalization and Accommodation by Scattering Gas Atoms from Surface \*

V.D. Seleznev<sup>1</sup>, I.P. Alexandrychev<sup>2</sup>

<sup>1</sup> Urals State Technical University, Ekaterinburg, Russia

<sup>2</sup> Industrial Ecology Institute of RAS, Ekaterinburg, Russia

Processes of sticking, thermalization and accommodation do not take the last place in the problem of gas atoms scattering from surface. However, despite of the steadfast and productive attention to these processes from measurements the theoretical investigations has appeared not up to the mark, and there are some moments requiring the serious analysis and explanation now. So, for example, the principle of detailed balance for sticking-desorption processes, which is used rather frequently for determination of differential sticking coefficient  $S$  and differential desorption probability  $D$

$$S(v, \theta, T_s) f_M(v, T_s) \cos \theta = D(v, \theta, T_s) f_M(v, T_s) \quad (1)$$

(here  $f_M$  is a Maxwell distribution and  $\theta$  is the deviation from the surface normal) includes, in particular, the assumption that the distribution of gas trapped in physisorption potential hole is Maxwellian. However the given fact is not distinct at all since only the distribution of all particles should be Maxwellian in thermal equilibrium system, but any part of scattering stream may have not this property. In addition to that, the equation (1) supposes, that all gas molecules, which were transferred in the bound state, are equilibrium with the surface (therefore they are completely thermalized), but it does not correspond to the reality frequently. Moreover, in such notation the fully valid assumption about the non-equilibrium of the desorption stream is not accompanied even by hints on the reasons of violation of the thermal equilibrium in desorption.

One more problem arises after familiarity with the definition of accommodation coefficients, especially differential ones, in case, when the incident stream

is monoenergetic beam

$$\alpha(g) = \frac{g(\vec{v}) - \int_{v_z > 0} g(\vec{v}) R(\vec{v} \rightarrow \vec{v}) d\vec{v}}{g(\vec{v}) - J_M \int_{v_z > 0} g(\vec{v}) |v_z| f_M(\vec{v}) d\vec{v}} \quad (2)$$

where  $g(\vec{v})$  is the molecular indicator and  $J_M = 2(\pi/2RT_s)^{1/2}$ . It is not easy to see, that the denominator of this expression can be converted to zero. Then for the continuity of functions  $\alpha(g)$  it is necessary, at least, that numerator (2) was also equal to zero. It would mean the unique character of scattering of the gas stream possessing an equilibrium value of any molecular indication  $g(\vec{v})$ . It should happen without the variation  $g(\vec{v})$ . However, taking into account the sufficient effectiveness of exchange processes by scattering, such preservation of equilibrium values of the macroscopic characteristics without delay is more surprising, than it is expected. Furthermore the expression (2) also includes the assumption about the fact that the gas distribution after full accommodation is Maxwellian, which remains by a peculiar axiom till now.

First of all, to understand the expressed doubts it is necessary to analyse the trapping of gas particles by surface and their behaviour in the bound state, including processes of thermalization and desorption. We make it in terms of scattering kernel. It is supposed to inform about details of construction of this scattering kernel in other report on the same symposium. It is known, that the scattering process represents a series of oscillations of molecules in the fluctuating potential field of solid. For the purpose of creation of the gas-solid interaction model the rather productive possibility of separate consistent describing of each oscillation is used, due to which the obtained scattering kernel has the ability not only to calculate the final result of scattering, but also to characterize gradual evolution of gas in surface region including thermalization.

Coming back to the problems considered here, it is possible to tell, that the approach to the prob-

\* Abstract 6528 submitted to the 21st International Symposium on Rarefied Gas Dynamics, Marseille, France, July 26-31, 1998

lem of gas-solid interaction realized here allows us to divide the reflected stream into three components rather easily: direct scattering, trapping-desorption and adsorption-desorption. The first channel contains particles which have made the unique oscillation in surface region and the distinction between two last scattering channels consists in the different degree of thermalization of particles belonging to it. So, the trapping-desorption scattering process is carried out without a full equilibration of molecules with crystal, and the adsorption-desorption channel corresponds to a full thermalization.

Without doubts, the most important moment of the conducted analysis is the conclusion that the velocity distribution of gas after full thermalization never coincides with Maxwellian. The distinctions are increased with surface temperature, however simultaneously the weight of the adsorption-desorption channel decreases. The greatest deviations are observed for large normal velocities  $v_z$  though they are quite appreciable and for  $v_z \sim 0$ . It is fully natural, since the molecules have normal velocity more than critical value  $v_*$ , when leaving the adsorption layer, while it receives the particles with  $v_z < v_*$ . Thus, the thermalized distribution takes place of Maxwellian distribution during analysis of gas evolution in surface region. As well as Maxwellian function, this distribution depends on temperature of the system, but besides this it is influenced by such parameters as the height of adsorption barrier and the speed of relaxation of gas during its interaction between phases of gas-solid system.

The distribution function of the full thermalized molecules is as follows:

$$f_t(\vec{v}) = f_M(v, T_s) \exp\left(\frac{U_0}{k_B T_s}\right) B_N(v_z) \quad , \quad (3)$$

where

$$B_k(v_z) = \int_{-v_*}^0 dv'_z W_{1z}(-v_z \rightarrow -v'_z)$$

$$B_{k-1}(-v'_z) \quad , \quad B_1(v_z) = 1 \quad ,$$

and  $N$  is the number of oscillation after which it is possible to consider, that the molecules stayed in the surface region have completely lost the "memory" on the condition up to the incident. As well as it was necessary to expect that this number is limited by the velocity of gas relaxation on tangential directions, since it is well known, that this velocity is essentially less than the relaxation rates on normal direction. So, for example, for a system Ar/Pt

at surface temperature  $T_s = 200$  K the normal component of velocity distribution is gained its stable form after 20 oscillations, whereas already 100 hops are needed for the full thermalization of the tangential part. By this approximately 25% of the incident molecules remain in the surface layer. The function  $W_1$  representing the scattering kernel for one separate oscillation is determined by concrete solutions of both the gas evolutionary equation in the attraction region and reflection problem of gas particles from repulsion potential.

During the analysis of the continuity of accommodation coefficient given by equation (2), the flux mean kinetic energy and flux mean normal kinetic energy were considered by scattering of monoenergetic collimating beam from surface. Although, when the beam mean kinetic energies had the equilibrium values, small deviations (about 10%) of the scattered flux mean kinetic energies from the equilibrium values were observed, it is too early to make an univalent conclusion about continuously and discontinuously of the functions (2). Firstly, the deviation can be connected with the shortage of information about the velocity of relaxational processes during gas-solid interaction. Secondly, it can be influenced by the nonadequation of the definition (2), since the gas has not Maxwellian velocities distribution frequently, when it was desorbed from surface after full accommodation. Undoubtedly to clear up the given situation, the experimental research of this problem can help greatly.

## Normal Momentum Transfer in Gas Mixture-Surface Interaction \*

Ph.J.Polykarpov, S.F.Borisov

Physics Dept., Ural State University, Ekaterinburg, Russia

## 1 Introduction

The measurement of a normal momentum transfer characteristics of gas-surface interaction is of importance, relating to the aeronautics and vacuum sciences and technologies. Besides the such kind information is useful for adequate process simulations. For this measurement the dynamical method has been suggested earlier [1].

Experimental study of normal momentum transfer in gas-solid body system by dynamical technique has some advantages

- i) simplicity of the measuring technique;
- ii) integral character of the result data;
- iii) low non-equilibrium conditions of gas-solid body system.

The absolute gas pressure must be known to determine some characteristics of normal momentum transfer in the rarefied gas - surface system by this technique. The problem of measurement the gas absolute pressure at  $10^{-1}$  Pa and less is well known [2]. The second problem is connected with one mentioned above is creation of the accurate value of gas pressure at this range. Actually in real situation the residual gas and outgassing process form the gas phase in gas - solid body system.

The general purpose of the present investigation is to develop an experimental technique based on low non-equilibrium conditions for measuring the normal momentum transfer between different gas mixtures and single crystal silicon surface under low gas pressure.

## 2 Experimental background

The experimental apparatus has been described in details elsewhere [3]. The main elements of the experimental set-up are L-C oscillator, frequency-sensitive detector, amplifier, computer. The gas mixture composition is controlled by monopole mass spectrometer at  $10^{-3}$  Pa and less. The single

Mass, Amu	2	4	18	28	40
Regime1				96	4
Regime2	62	13	11.6	12.2	1.2

Table 1: Composition of vacuum chamber outgassing gas mixtures at two measurement regimes, p.c.

crystal silicon plate has been prepared by chemical etching with square dimension (5x5)mm. The plate resonance oscillation frequency is 1250 Hz.

An essential stage of the experimental procedure is damping coefficient measurement for free linear oscillations of the plate at fixed gas pressures. The relative pressure variations are measured by mass spectrometer.

Free molecular gas flow conditions are supplied by low pressure and small amplitude of the plate oscillations.

It should be emphasized that no special cleaning operations are performed, meaning that the surface is contaminated with various oxides, vapors, and adsorbed gases.

The gas mixtures in vacuum chamber are formed by the outgassing process from different elements of the vacuum system. The chemical composition of the mixture corresponding to measured damping coefficient is presented in Table 1.

## 3 Results

The results of damping coefficient as pressures ratio  $\frac{P}{P_0}$  are presented in graphical form in Fig. 1.  $P_0$  is some initial pressure.

Observing the data permits to make the following conclusions.

- The damping coefficient is linear in the pressure.
- The experimental results clear indicate an increase in damping coefficient with increasing of effective mass of the gas mixture. The results for two gas mixtures exhibit considerable

\*Abstract 6736 submitted to the 21st International Symposium on Rarefied Gas Dynamics, Marseille, France, July 26-31, 1998

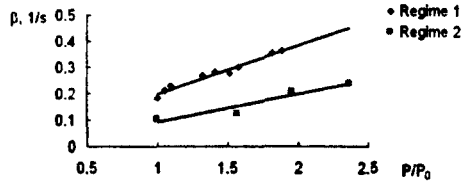


Figure 1: Experimental results for two regimes of outgassing

difference in the slopes. This difference is believed to be due to variations as well in effective mass of gas mixture as in normal momentum accommodation coefficient (NMAC). According to the expression for  $\beta$ , concluded earlier [3], the damping coefficient for gas mixture may be expressed as

$$\beta = \frac{2 - \alpha_n}{\rho h} P \sqrt{\frac{2m_{eff}}{\pi k T}}, \quad (1)$$

where  $\alpha_n$  is traditional Knudsen's definition NMAC;  $\rho$  is density of the plate material;  $h$  is thickness of the plate;  $P$  is total pressure of gas mixture;  $m_{eff}$  is effective molecular mass of gas mixture;  $k$  is the Boltzman's constant;  $T$  is temperature.

According to Dalton's law and additivity of a normal force an effective mass of a gas mixture may be defined as

$$m_{eff} = \left( \sum_i (x_i \sqrt{m_i})^2 \right), \quad (2)$$

where  $x_i$  is molar percentage of respective element;  $m_i$  is molecular mass of respective element of a gas mixture.

- To determine the NMAC from this equation the absolute gas pressure must be known. Unfortunately the absolute gas pressure can not be measured or determined accurate enough in this experiment.
- From Eq.1 a variation range of the ratio for NMACs is expressed as

$$\frac{1}{2} < \frac{2 - \alpha_n^1}{2 - \alpha_n^2} < 2, \quad (3)$$

where  $\alpha_n^1$  and  $\alpha_n^2$  are NMACs for two respective regimes.

In present study

$$\frac{2 - \alpha_n^1}{2 - \alpha_n^2} = 0.78. \quad (4)$$

This result confirms our background modeling assumptions that were made earlier[3].

- It is difficult to compare the values presently obtained from Eq.4 with ones obtained by others since present experiment is done at low non-equilibrium conditions with Maxwellian incident gas.

The only comparison can be made for the relative variations of NMAC (Eq.4) with different parameters of gas - surface system.

## 4 Acknowledgements

The authors is indebted to Dr.N.Ph.Balakhonov, Mr.P.I.Bogdanov for their contribution in this paper.

## References

- [1] Balakhonov N.Ph. et.al., *Normal Momentum Transfer in Low Non-Equilibrium Gas - Solid Body System*, Rarefied Gas Dynamics, Ed. by M.N.Kogan, MEI, Moscow. 1991.P.57-63. (In Russian).
- [2] Dushman S., *Scientific foundations of vacuum technique*, John Wiley & Sons, Inc. New York - London. 1962.
- [3] Borisov S.F., Polyckarpov Ph.J., *An Experimental Study of Momentum Accommodation in Gas-Solid Body System* Rarefied Gas Dynamics, Proc. of the 20-th Int.Symp. 19-23, August, 1996 Beijing, China. Ed.by Ching Shen. Peking University Press, Beijing, China. 1997.P.387-391.

# Tangential Momentum Accommodation on Atomic Clean and Contaminated Surface \*

S.F. Borisov, O.V. Sazhin, Ph.J. Polyckarpov, I.A. Grachyov  
Physics Dept., Ural State University, Ekaterinburg, Russia.

A study of molecular beam scattering on a clean surface [1] as well as rarefied gas flow experiments in a tube with a metal sprayed walls [2] show a great influence of the surface chemical composition and a gas nature on momentum accommodation coefficients. At the same time in flow experiments for contaminated surfaces both for metal [2, 3] and glass [4] channels the difference in accommodation coefficients is not essential even for light gases.

However a detailed analysis shows that results both for metal and glass channels with the surface without special pretreatment are similar but not the same. It looks like a long distance influence of the layers under adsorbed coat on a gas molecule scattering takes place. For example, tangential momentum accommodation coefficient for glass and metal (Ti or Mo) reaches 0,93 and 0,98 for He, respectively. A similar long distance effect one can find in other experiments devoted to surface quality influence on Knudsen flow [5].

The other conclusion that can be made is the metal drilled channels [3] as well as channels with metal sprayed surface [2] are not so long as glass capillaries. So, as a result the gas-surface interaction contribution in a gas flow for short channels is smaller than for infinite ones.

In this paper the results for tangential momentum accommodation coefficient measurement using lately described multifunctional ultrahigh vacuum system with surface controlled condition [6] are obtained for different gas-sprayed metal surface systems. An influence of the surface chemical composition for Pt, W and Mo sprayed channels on tangential momentum accommodation coefficient is studied. To estimate a contribution of gas-surface interaction in an internal rarefied gas flow for short channels the numerical study of the problem has been made using DSMC method.

The modern review of the experimental results regarding an influence of surface chemical composition on accommodation coefficients is presented too.

## References

- [1] Steinheil E., Scherber W., Seide M., Rieger H., *Investigation on the interaction of gases and well-defined solid surfaces with respect to possibilities for reduction of aerodynamic friction and aerothermal heating*, Rarefied Gas Dynamics. Ed. by Potter J.L. Academic Press. New York. 1977. P.589-602.
- [2] Nakarjakov A.V., Borisov S.F., Sharipov F.M., Suetin P.E., *The effect of the surface composition on a free molecular gas flow in a cylindrical channel*, Proc. 19-th Int.Symp.Rarefied Gas Dynamics.Vol.2.Oxford University Press. 1995. P.954-959.
- [3] Lund L.M., Berman A.S., *Flow and self-diffusion of gases in capillaries*, Appl. Phys.-1966.-v.37, p.2489-2508.
- [4] Porodnov B.T., Suetin P.E., Borisov S.F., Akinshin V.D., *Experimental investigation of rarified gas flow in different channels*, J.Fluid mech.-1974.-V.64.-P.417-437.
- [5] Hermans L.J.F., Horne R., Kuscer I., *Influence of surface quality on Knudsen flow of rotating molecules as measured by the field effect*, Proc. 17-th Int.Symp.Rarefied Gas Dynamics, July 8-14, 1990, Aachen, Germany/ ed. by Alfred E. Beylich.-Weinheim; New York; Basel; Cambridge: VCH,1991.- P.1318-1324.
- [6] Borisov S.F., *A study of gas molecules energy and momentum accommodation on a controlled surface*, Proc. 17-th Int.Symp.Rarefied Gas Dynamics. July 8-14, 1990, Aachen,Germany/ ed. by Alfred E. Beylich.-Weinheim; New York; Basel; Cambridge: VCH,1991.- P.1412-1418.

\*Abstract 6737 submitted to the 21st International Symposium on Rarefied Gas Dynamics, Marseille, France, July 26-31, 1998

NUMERICAL SIMULATION - NS P

TUESDAY, JULY 28, 1998

16:15

# Numerical Modules for Solving the Boltzmann Equation in the Transition Regime \*

Alfred E. Beylich

Technische Hochschule Aachen, 52062 Aachen, Germany

## Abstract

In some flow problems, typically with large variations or gradients of the moments, there exist regimes where, when coming from the low density side, numerical molecular flight path/collision calculations (MD, DSMC) or distribution-function-based calculations (discrete ordinate methods, etc.) may become inefficient when cell-Knudsen numbers  $Kn_c$  are small or cell sizes have to be reduced; when coming from the high density side, on the other hand, perturbation methods which reduce information to a small set of conservation equations for a few observables (Navier-Stokes eqs.) are no longer applicable as soon as the perturbation  $\epsilon$  in the Navier-Stokesian  $f_{NS\epsilon} = f_M(1 + \epsilon)$  is not small.

We are interested in the development of modules for the numerical calculation of elements of the kinetic equation that can help to bridge the gap between small and large cell-Knudsen numbers, and that should become complementary or competitive to the usual flight path calculations. For this aim, we start on the configuration-averaged level. Using modern high speed, high capacity (small) computers, we develop modules that can quickly be composed and be used in any program; and we make use of pre-calculation whenever it is possible and saves computing time.

Starting with the Boltzmann equation for the distribution function  $f(\mathbf{r}, \mathbf{c}, t)$ ,

$$Df \equiv \frac{\partial f}{\partial t} + \mathbf{c} \cdot \nabla f = \nu(G/\nu - f), \quad (1)$$

and its integrated form (for a trajectory along  $\mathbf{c}$ )

$$f = f_0 \exp\left[-\int_0^t \nu dt'\right] \quad (2)$$

$$+ \int_0^t \exp\left[-\int_{t'}^t \nu dt''\right] G dt', \quad (3)$$

we have studied the limitations and severe consequences due to the introduction of functions  $f_{\mathbf{r},\mathbf{c},t}$  which are discrete and finite in physical ( $\mathbf{r}$ ) and in velocity ( $\mathbf{c}$ ) space. By Eq.2 one is reminded of the fact that the zone of influence is limited to a length of the order of a mean free path,  $\lambda$ , and in a discretized physical space, for small  $Kn_c$ -numbers, it becomes necessary to subscale in order to avoid distortions of  $f$  and artificial dissipation. Thus, we try to introduce interpolated  $f$  which, however, can only be determined up to the conservation of a limited number of moments. If we use Eq.1 (D-module) in our scheme, the 2-Scale Module (2S) becomes active whenever  $Kn_c < O(1)$ . Alternatively, a two-point integral (2PI-module) scheme was developed starting from Eq.2.

For the collision term, different modules are used: For development work and as a starter for a relaxation towards a steady state, the very simple and rapid BGK-model is used, i.e.  $G/\nu = f_M$ . A next step is to use in the calculation of  $G, \nu$  a set of 8 points (8P-module) being strictly conservative on an equally spaced cartesian grid in  $\mathbf{c}$ -space. In general, fundamental problems exist in such a grid due to the fact that scattered points fall outside the lattice and, as a consequence, problems of conservation of moments arise. This would make such a lattice which, on the other hand, has great advantages in the numerical treatment inferior to the old discrete ordinate methods and their prescribed collision quadruples; however, as has been discussed by Tcheremissine [1], it is feasible to redistribute to neighbour lattice points in such a manner that some of the lower moments are conserved. In a third step, we have developed a module for the calculation of  $G, \nu$  where the lower moments are conserved ( $G\nu$ -module). The calculation is accelerated by pre-calculation of all scattering data, which is possible for an equally spaced lattice. Furthermore, for steady state problems, we use a thinning and refreshing technique in the calculation of  $G, \nu$  for the relaxation towards the steady state. For a thinning factor  $\Delta$  we refresh the elements  $(G, \nu)_{\kappa, \xi, m}$ , with

\* Abstract 1626 submitted to the 21st International Symposium on Rarefied Gas Dynamics, Marseille, France, July 26-31, 1998



$\kappa = (i, j, k)$  in c-space,  $m$  = indices in r-space, and  $\xi = \Delta_{i,j,k}$ , and where  $\Delta_l$  are random initial points for a 3-dimensional  $\Delta$ -spaced rake.

The limitations of Eq.1 on a grid with  $Kn_c \ll 1$  makes it attractive to introduce a 2-Level Module (2L): From the equation of transfer we obtain a set of equations for the summational invariants. This set of upper-level equations is interlaced with Eq.1. For a first study, we used the BGK-model. Thus, for a time step, we determine the first five moments from the upper-level set and introduce them into  $f_M$  at the lower-level, and we calculate the remaining eight moments at the lower-level and introduce them into the upper-level equations. Consequently, we make use of the ability of the upper-level set to transport information in the form of waves, and of the property of the lower-level set to create deformations of the distribution function due to the drifting of molecules. Some calculations using a 2S-2L-Module have shown that it is possible to penetrate the  $Kn_c < 1$ -region to values at least an order of magnitude smaller in  $Kn_c$  than if only the 2S-Module had been used. The interlacing has also been extended to the general case where  $G, \nu$  is not simplified.

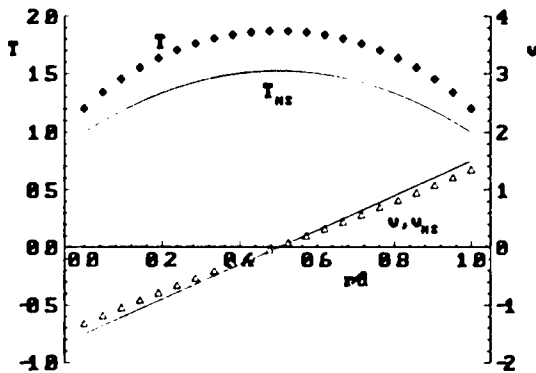


Figure 1: Temperature and velocity profiles.  $T$  and  $v$  are calculated with a D-2S-BGK-module,  $T_{NS}$  and  $v_{NS}$  are the Navier-Stokes profiles. Xe-gas,  $Kn_0 = 0.067$ ,  $Kn_c \sim 1$ ,  $Mach_w = 1.5$ ,  $T_w = 250K$ ,  $p_w = 0.06mbar$ .

The development and the numerical experiments were performed using the planar Couette flow being of the most simple one-dimensional problems. The limits  $Kn_0 \rightarrow \infty$  and  $Kn_0 \rightarrow 0$  are well known, and it is convenient to study the effects of the different modules on the flow properties in the transition regime, particularly the subtle interaction of

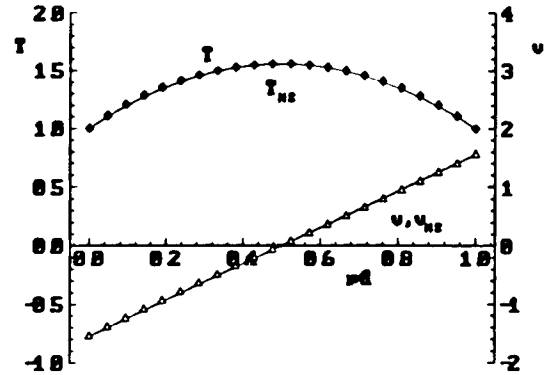


Figure 2: Temperature and velocity profiles, the same as in Fig.1 but using a 2TPI-2S-2L-module, and with  $Kn_0 = 0.002$ ,  $Kn_c \sim 0.05$ ,  $p_w = 2.0mbar$ .

the shearing tensor and the heat flux vector. Some sample calculations are given here: In Fig.1 a D-2S-BGK-module is used for a case with wall Mach number  $Mach_w = 1.5$  and  $Kn_0 = \lambda_w/d = 0.067$ . In Fig.2, for higher densities, some results using a 2PI-2S-2L-module show good agreement with the N-St profiles.

## References

- [1] Tcheremissine F.G., *Conservative discrete ordinate method for solving the Boltzmann kinetic equation*, In: Communications of Applied Mathematics, Computing Center of the Russian Academy of Sciences, Moscow 1996.

# Effect of the Centrifugal Forces on a Gas between Rotating Cylinders \*

L.M.de Socio<sup>1</sup>, N.Ianiro<sup>2</sup>, L.Marino<sup>2</sup>

<sup>1</sup> Dip. Meccanica e Aeronautica, Università "La Sapienza", Roma, Italy

<sup>2</sup> Dip. MeMoMat, Università "La Sapienza", Roma, Italy

## 1 Abstract

We consider the one-dimensional problem of a gas contained between two infinite, isothermal, concentric cylinders which rotate at very close and steady angular velocities.

The work consists of two parts. The first one deals with the case where the two walls have the same angular velocity  $\Omega$ . It shows that the tangential velocity and the macroscopic state parameters distributions along the radius can be evaluated either by the free molecular flow approximation or by the Navier-Stokes model, no matter what the mean Knudsen number is.

A direct simulation by means of a Montecarlo method was also carried out which confirmed the analytical results. In all treated cases the walls were assumed diffusive and such that the distribution function of the re-emitted molecules is Maxwellian.

The second part of the paper concerns the situation where the angular velocities of the two walls are only slightly different.

This problem is solved by linearization around the solution obtained in the first part and by adopting the BGK model. Again the results are compared with those provided by a direct simulation.

The effects of the centrifugal forces on the characteristics of a gas between rotating cylinders have been investigated by several authors either by analytical and numerical methods, whereas the available experimental data are very scarce for relatively high Knudsen numbers  $Kn$ .

In the references listed in the bibliography we provide, without discussion in this abstract, some of the more significant contributions.

The dimensionless products governing the problem are the ratio of the gap between the walls  $\Delta R$  to the radius of the inner cylinder  $R_1$ , the ratio of specific

heats  $\gamma$ , the mach number of the two peripheral tangential velocities  $Ma_1$ ,  $Ma_2$ , the mean Knudsen number  $Kn_m$ .

In the first part of the work we started from the Boltzmann equation in cylindrical coordinates

$$v_r \frac{\partial f}{\partial r} + v_\varphi \frac{\partial f}{\partial \varphi} + v_z \frac{\partial f}{\partial z} + \frac{v_\varphi^2}{r} \frac{\partial f}{\partial v_r} - \frac{v_\varphi v_r}{r} \frac{\partial f}{\partial v_\varphi} = J(f, f)$$

for which, in the one dimensional case, we determined the hydrodynamic limit corresponding to the Navier-Stokes equation in the Couette simplification. On the other hand the solution of the Vlasov approximation provided the free molecular flow characteristics. As we said, when the wall Mach numbers  $Ma_1 = \frac{R_1 \Omega}{c}$  and  $Ma_2 = \frac{R_2 \Omega}{c}$  are such that  $\frac{Ma_1}{Ma_2} = \frac{R_1}{R_2}$  then we have proved that the radial distributions of the macroscopic quantities are the same by using either the Navier-Stokes equation or the free molecular solution.

Fig 1(a,b) shows the velocity and the local Knudsen number distributions as functions of the radial distance, as obtained via the different models and by direct simulation in the case  $\frac{\Delta R}{R_1} = 0.1$ ,  $\gamma = 1.66$ ,  $Ma_2 = 4$ ,  $Kn_m = 0.1$ .

The comparisons are excellent.

In the sequel the Mach number at the external wall was perturbed so that  $\epsilon = \frac{\Delta Ma_2}{Ma_2}$  was adopted as a small parameter for a linearization procedure of the BGK model of the Boltzmann equation. The zeroth order approximation corresponds to the free molecular case. The first order approximation corresponds to a set of linear ordinary differential equations whose unknowns are the coefficients of a series expansions of the distribution function.

Fig.2(a,b) shows the values of the macroscopic quantities as a function of the radial co-ordinate for  $\epsilon = 0.5$  whereas all the other dimensionless products are those of the case of Fig. 1.

It is evident the possibility of distinguishing two different adjacent domains such that a transition from the continuous model to the free molecular regime takes place.

\* Abstract 1766 submitted to the 21st International Symposium on Rarefied Gas Dynamics, Marseille, France, July 26-31, 1998

This fact offers the opportunity of further research developments where different procedures can be applied for determining the flow characteristics in situation more complex than those which were treated here.

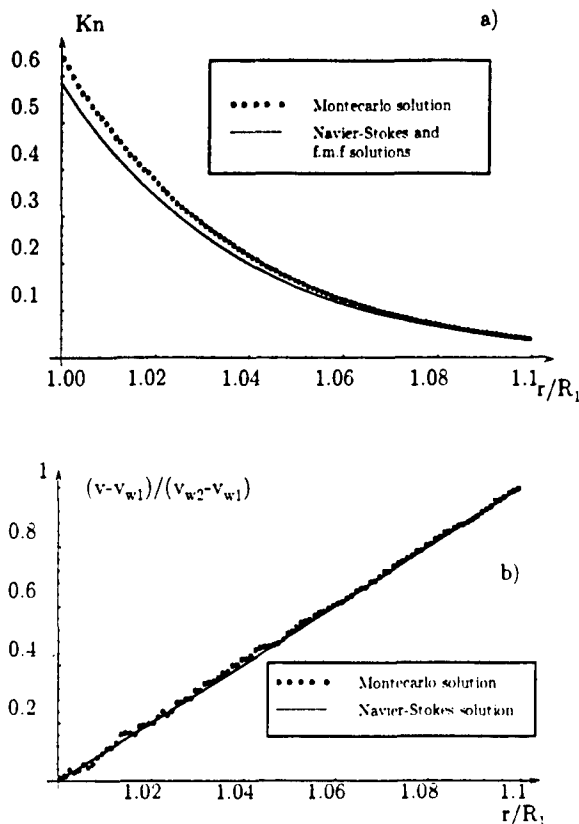


Figure 1: Analysis for  $\frac{Ma_1}{Ma_2} = \frac{R_1}{R_2}$ . Comparison of the Knudsen number (a) and peripheral velocity (b) distributions as obtained by direct simulation and Navier-Stokes and free molecular flow models.

## 2 Acknowledgments

This work was partially supported by ASI and by CNR-GNFM.

## References

- [1] Cercignani C., Sernagiotto F. *Cylindrical Couette Flow of a Rarefied Gas*, The Physics of Fluids, Vol. 10, No. 6, pp.1200-1204, 1967.
- [2] Alofs D.J., Springer R.W. *Cylindrical Couette Flow Experiments in the Transition Regime*, The Physics of Fluids, Vol. 14, No. 2, pp.298-305, 1971.
- [3] Johnson E.A., *Shear Flow in the Presence of 'strong rotation': I. Exact free-molecular solu-*

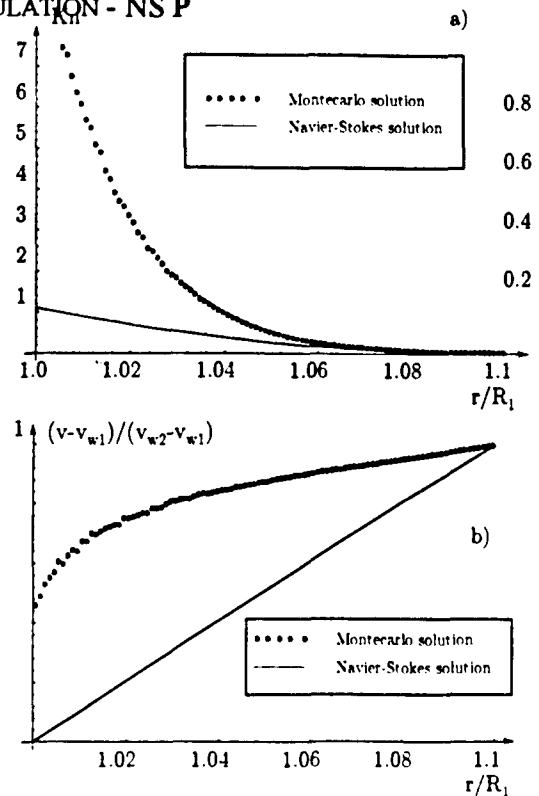


Figure 2: Analysis for  $\frac{Ma_1}{Ma_2} \neq \frac{R_1}{R_2}$ . Comparison of the Knudsen number (a) and peripheral velocity (b) distributions as obtained by direct simulation and Navier-Stokes models.

tion, J. Phys. D: Appl. Phys., Vol. 16, pp.1201-1206, 1983.

- [4] Johnson E.A., Stopford P.J. *Shear Flow in the Presence of 'strong rotation': II. Approximation for continuum-plus-rarefied flow*, J. Phys. D: Appl. Phys., Vol. 16, pp.1207-1215, 1983.
- [5] Cassel J.S., Williams M.R.M. *An integral equation arising in the theory of the gas centrifuge*, J. Phys. D: Appl. Phys., Vol. 16, pp.1391-1406, 1983.
- [6] Nanbu K. *Analysis of cylindrical Couette flows by use of the direct simulation method*, Phys. Fluids, Vol. 27, No. 11, pp.2632-2635, 1984.
- [7] Cercignani C., Lampis M., *Variational approach to rarefied gas flows in an external force field with an application to the gas centrifuge*, Proceedings of the 14th International Congress on RGD, Japan pp.89-98, 1984.
- [8] Sharipov F.M., Kremer G.M. *Nonlinear Couette Flow Between Two Rotating Cylinders*, Transport Theory Stat. Phys., Vol. 25, No. 2, pp.217-229, 1996.

# Perturbation of the Linearized Boltzmann Equation and the Monte Carlo Collision Method \*

S. Longo

Dipartimento di Chimica and Centro di Studio per la Chimica dei Plasmi del CNR  
Bari University, Italy

In this paper it will be shown that when linear perturbation techniques similar to the one applied to the field equations in the Many-Body Theory[1] are applied to the Green function formulation of the linearized Boltzmann equation, the Monte Carlo Collision method [2, 3] can be retrieved. This way of deriving the method is straightforward and shows direct connection to the transport equation. As a result, the *quasi particle* nature of the objects computer simulated in the Monte Carlo Collision method is better understood, and also this method is opened to modifications and optimizations keeping its real mathematical content. Our starting point is the linearized Boltzmann equation, describing the evolution of the velocity distribution function including volume forces and space non uniformities, as well as a source/sink term  $S(r, v, t)$ :

$$\left( \frac{\partial}{\partial t} + v \frac{\partial}{\partial r} + \frac{F(r, v, t)}{m} \frac{\partial}{\partial v} \right) f(r, v, t) = \int \int \int dv' dV dV' \left[ \sigma(v', V, v, V') |v' - V| f(v') f'(V) - \sigma(v, V, v', V') |v - V| f'(V) f(v) \right] + S(r, v, t) \quad (1)$$

Here,  $f(r, v, t)$  is the particle distribution, normalized according to:

$$\int dv f(r, v, t) = n(r, t) \quad (2)$$

and  $n(r, t)$  is the particle number density,  $\sigma(v, V, v, v')$  is the cross section for a binary particle collision process leading to the final velocities  $v$  and  $v'$  for the collision partners at the pre-collision velocities  $v$  and  $V$ ,  $f'$  the velocity distribution of background gas particles,  $F(r, v, t)$  is the volume force field,  $m$  the particle mass.

The equation above can be written in a shorter form by introducing the transition probabilities per unit time given by

$$p_{v \rightarrow v'}(r, t) = \int dV \int dV' |v - V| \sigma(v, V, v', V') f'(r, V, t) \quad (3)$$

and also by introducing the *convective* time derivative

$$\frac{d}{dt} = \frac{\partial}{\partial t} + v \frac{\partial}{\partial r} + \frac{F(r, v, t)}{m} \frac{\partial}{\partial v} \quad (4)$$

Our goal is to calculate the Green function  $G(r, r_0, v, v_0, t, t_0)$  of the equation. Let us split the collision operator on the right hand side in two parts,  $T$  and  $W$ , whose effect on an arbitrary function  $f$  is given by

$$Tf = -\nu(r, v, t) f(r, v, t) \quad (5)$$

with

$$\nu(r, v, t) = \int dv' p_{v \rightarrow v'}(r, t) \quad (6)$$

and

$$Wf = \int dv' f(r, v', t) p_{v' \rightarrow v}(r, t) \quad (7)$$

The operator  $T$  describes the loss of probability for a given state due to transitions to any other state, while the operator  $W$  describes the gain due to transitions. Now let us consider the simplified equation:

$$\frac{df(r, v, t)}{dt} = Tf(r, v, t) \quad (8)$$

as a starting point. The Green function of the equation above can be calculated simply starting from the Dirac function initial condition, and it is given by

$$g(r, r_0, v, v_0, t, t_0) = \delta(r - r(t)) \delta(v - v(t)) H(t - t_0) \exp\left(-\int_{t_0}^t dt' \nu(r(t'), v(t'), t')\right) \quad (9)$$

\* Abstract 1802 submitted to the 21st International Symposium on Rarefied Gas Dynamics, Marseille, France, July 26-31, 1998

where  $r(t)$  and  $v(t)$  are calculated by tracking a particle from the initial point  $r_0, t_0$  under the effect of the volume force field.

Now can calculate the Green function of the full equation (or exact Green function)  $G$ , i.e. the solution of

$$\left(\frac{d}{dt} - T\right)G(r, r_0, v, v_0, t, t_0) = \delta(r - r_0)\delta(v - v_0)\delta(t - t_0) + WG(r, r_0, v, v_0, t, t_0) \quad (10)$$

by a linear perturbation technique, considering the  $W$  operator as a perturbation.

Let us write  $G$  in terms of the unperturbed Green function, considering the whole right-hand side of the equation above as a source. In this way the Dyson-like equation [1]

$$G(r, r_0, v, v_0, t, t_0) = g(r, r_0, v, v_0, t, t_0) + \int \int \int dr_1 dv_1 dv_2 \int_{t_0}^t dt_1 g(r, r_1, v, v_2, t, t_1) p_{v_1 \rightarrow v_2}(r_1, t_1) G(r_1, r_0, v_1, v_0, t_1, t_0) \quad (11)$$

is obtained.

By inserting iteratively the right-hand side of the Dyson equation in place of the exact Green function  $G$  on the right hand side itself one obtains the Born expansion [4] for  $G$ . Some of the integrations need not actually be performed because of the delta functions in the expressions of  $W$  and  $g$ , nevertheless the task is quite heavy, and becomes heavier for higher order terms. It is very natural to apply to this task the classical Monte Carlo method for multidimensional integration, based on an estimation of the mean value of the integral over an (iper)volume  $R$  in the independent variable space. The Monte Carlo estimate of the integral is obtained as usual by selecting random values for the integration variables in the proper range, and applying the theorem of the mean value to the integral. The result is an ensemble of Monte Carlo Collision trajectories.

To summarize: particles involved in the Monte Carlo Collision method represent the Green function of the linearized Boltzmann equation, and any of them can be assigned to a given term of the Born series resulting in turn by considering the  $W$  part of the collision operator as a perturbation.

The application of the perturbation method can be visualized as usual by the diagram technique [1], any diagram corresponding to a multidimensional integral.

This derivation of the Monte Carlo Collision Method directly from the Boltzmann Equation suggests many possible modifications of the model that can be useful in specific cases.

## References

- [1] Richard D. Mattuk, A Guide to Feynmann Diagrams in the Many-Body Problem, Dover N.Y. (1992)
- [2] S.L.Lin and J.N.Bardley, J.Chem.Phys. 66, 435 (1977)
- [3] R.W.Hockney and J.W.Eastwood, Computer Simulation Using Particles, Adam Hilger (1991)
- [4] P. Schattschneider, Fundamentals of inelastic electron scattering, Springer-Verlag Wien (1986)

# Combination of Asymptotics in the Knudsen Layer.

## II. Testing \*

M.V. Anolik, R.G. Barantsev

St. Petersburg State University, St. Petersburg, 198904, Russia

### 1 Introduction

The Knudsen layer is considered as a transitional layer separating domains of comparatively simple asymptotics. In [1] we suggested the method for combining such asymptotics via two-point Padé-approximants. Here this method is tested in case when the distribution function  $f(y, \vec{u})$  is represented by the main moments.

### 2 Kinetic Equation

The exact solution is first found in the next statement

$$\begin{aligned} n(y) &= \int f(y, \vec{u}) d\vec{u}, \\ U_x(y) &= \frac{1}{n(y)} \int u_x f(y, \vec{u}) d\vec{u}, \\ U_y(y) &= \frac{1}{n(y)} \int u_y f(y, \vec{u}) d\vec{u}, \\ h(y) &= \frac{3}{2} n(y) \left\{ \int [\vec{u} - \vec{U}(y)]^2 f(y, \vec{u}) d\vec{u} \right\}^{-1}, \\ f(y, \vec{u}) &= \begin{cases} f_M(0, \vec{u}) \exp(-\frac{y}{u_y}) + \\ \int_0^{\frac{y}{u_y}} f_M(y - tu_y, \vec{u}) e^{-t} dt, & u_y \geq 0, \\ f_M(y_m, \vec{u}) \exp(\frac{y_m - y}{u_y}) + \\ \int_0^{\frac{y_m - y}{u_y}} f_M(y - tu_y, \vec{u}) e^{-t} dt, & u_y < 0, \end{cases} \\ f_M(y, \vec{u}) &= n(y) \left[ \frac{h(y)}{\pi} \right]^{3/2} e^{-h(y)[\vec{u} - \vec{U}(y)]^2}, \end{aligned}$$

$$\vec{U} = \{U_x, U_y, 0\}, \quad y_m \gg 1.$$

The iteration method is used starting from

$$n_0(y) = \frac{T_s^{-1} + (1 + y_m - T_s^{-1})y/y_m}{1 + y},$$

$$U_{x0}(y) = \frac{(1 + y_m)y/y_m}{1 + y},$$

$$U_{y0}(y) = 0, \quad h_0(y) = s^2 n_0(y),$$

where  $s = \sqrt{\frac{5}{6}} M$ ,  $M$  is the Mach number,  $T_s$  is the surface temperature. The dimensionless variables are chosen so that  $n = 1, U_x = 1, h = s^2$  as  $y \rightarrow +\infty$ .

### 3 Numerical Method

Instead of the distribution function  $f(y, \vec{u})$ , we introduce the function  $\varphi(y, \vec{u}) = f(y, \vec{u})/f_M(y, \vec{u})$ , where the Maxwellian distribution function is used as a weight function in  $k$ -th iteration for evaluation of integrals with respect to  $\vec{u}$  using the Gauss-Hermite quadrature formulas with 10 points along  $u_y$  and 6 ones along  $u_x$  and  $u_z$ . The main moments are calculated in terms of  $\varphi(y, \vec{u})$  on a mesh with width  $h_y = 0.05$  or  $0.02$  at  $0 \leq y \leq y_m$  ( $y_m = 20, 30, 40$ ). After the substitution  $\eta = y - tu_y$  the integrals with respect to  $\eta$  are computed by the trapezoid rule with integrating width  $h_\eta = h_y$  which enables us to avoid interpolation in the tables of moments. To improve the convergence of the iteration method a linear correction of boundary conditions is made. Fig.1 shows the speed of convergence of value  $n(0)$  at  $s = 2$  for  $T_s = 2, 3$  and 4 ( $k$  is the iteration number).

### 4 Padé-approximation

If only the limit terms of asymptotics are taken into account, then the Padé-approximants may be chosen in the form

$$n = \frac{n_s + y}{1 + y}, \quad U_x = \frac{y}{1 + y}, \quad h = \frac{s^2(1 + T_s y)}{T_s(1 + y)}$$

with only free parameter  $n_s$ . In this test we have obtained exact solution  $n_e(y)$  so that  $n_s$  is easily

\* Abstract 1922 submitted to the 21st International Symposium on Rarefied Gas Dynamics, Marseille, France, July 26-31, 1998

found by the method of least squares. By minimizing the functional

$$J(n_s) = \int_0^{y_m} \left( \frac{n_s + y}{1+y} - n_e(y) \right)^2 dy,$$

we obtain

$$n_s = \frac{1+y_m}{y_m} \int_0^{y_m} \left( n_e(y) - \frac{y}{1+y} \right) \frac{dy}{1+y}.$$

The comparison of exact solutions  $n_e(y)$ ,  $U_{xe}(y)$ ,  $h_e(y)$  (grey symbols) and Padé-approximants  $n_a(y)$ ,  $U_{xa}(y)$ ,  $h_a(y)$  (black symbols) at  $s = 2$  for  $T_s = 2, 3$  and 4 is given in Figs 2–4, respectively. It is clear that the next terms of asymptotics are needed for better exactness. In the paper we consider some other approximants and values of parameters as well.

## References

- [1] Barantsev R.G., *Combination of Asymptotics in the Knudsen Layer. I. Method*, In: Ching Shen Ed. *Rarefied Gas Dynamics*, pp.345–347. Peking: University Press, 1997.

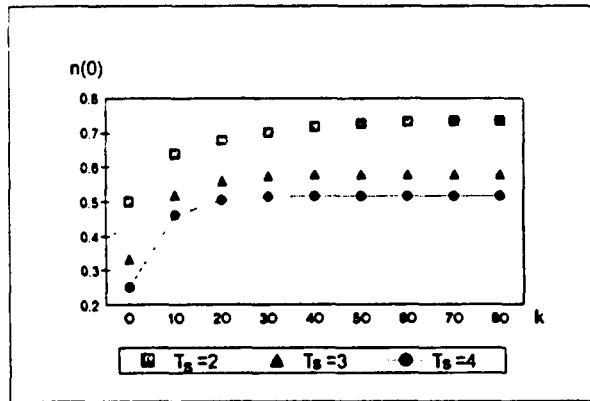


Figure 1: Speed of convergence

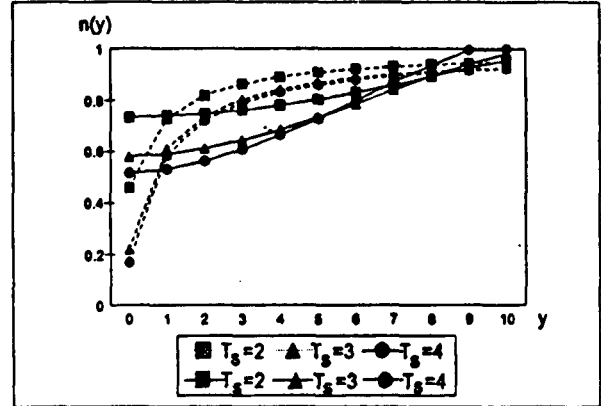


Figure 2:  $n_e(y)$  and  $n_a(y)$

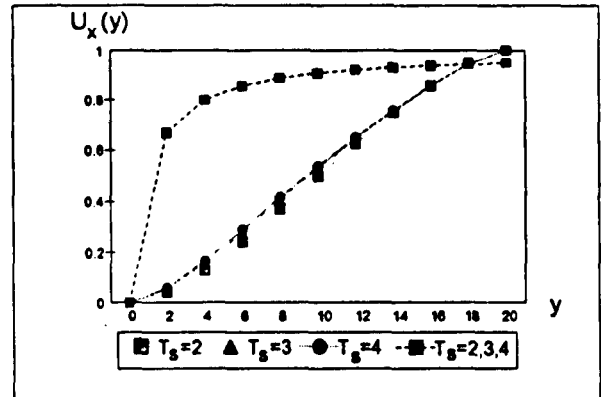


Figure 3:  $U_{xe}(y)$  and  $U_{xa}(y)$

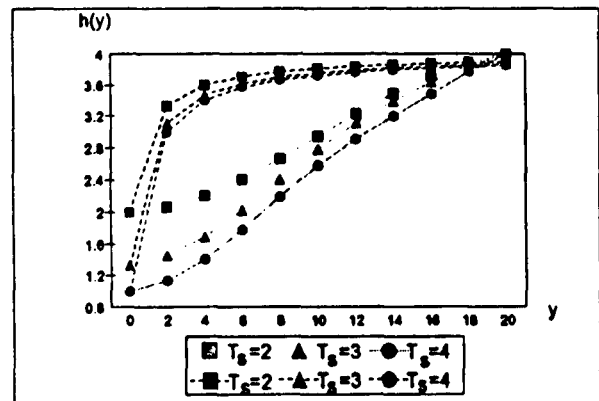


Figure 4:  $h_e(y)$  and  $h_a(y)$

# Study of Unstable Numerical Solutions of the Boltzmann Equation and Description of Turbulence \*

V.V. Aristov

Computing Center of the Russian Academy of Sciences, Moscow, Russia

The aim of the present paper is to determine the possible connection between the instabilities in numerical solutions at small Knudsen numbers and the appropriate theoretical notions concerning description of turbulence in a gas on the basis of the kinetic equation. The supersonic underexpanded free jets, where the instabilities originated in a mixing layer (see [1,2]), is the intriguing subject for numerical study owing to the absence of solid boundaries, the strong changes of parameters on a scale of the initial stage of a jet, not very high Mach numbers and so on. The first solutions for a free jets contained some chaotic features have been noted in [3], in [4] nonstationary solutions with large scale oscillations having the steady properties in the character of fluctuations have been observed.

The approach on the basis of the Boltzmann equation differs from some kinetic approaches, (see, e.g. [5,6]) where the molecular chaos hypothesis is discarded and turbulence is related to correlations on the molecular description level (the two-particle distribution function is considered). From our point of view the Boltzmann equation (of course, including the molecular chaos concept) is the adequate apparatus for this problem. The correlations in a turbulent flow would be described by means of the nonequilibrium distribution functions.

The kinetic description by the distribution function has the peculiarities in comparison with the macroscopic description. The dissipative values (the stress tensor components, the heat flux) are computed as the integrals over velocity space not as the derivatives as in the macroscopical description. So the computations in the velocity space could be more important task and the unstable solutions and expected nonequilibrium distributions at these regimes could determine the growth of dissipation in turbulent flows. The calculations in the physical space as supposed could be made with not such high accuracy as in the analogous problems for

the Navier-Stokes equations.

We search for the bifurcations in the solutions of the Boltzmann equation when the outer parameter (Knudsen number) tends to the zero. The critical numerical Knudsen number is determined and influence of parameters of the numerical scheme on the transition is studied as well. In fact the real disturbances in a flow are simulated by the numerical disturbances of the scheme.

The conservative splitting method (CSM) is used with the implicit schemes in the right-hand side of the Boltzmann equation (see [3,4]). Monte Carlo procedure to evaluate the collision integrals is applied. The computations on a large time scale are made to analyse spectral characteristic of oscillations and to separate the "background" numerical fluctuations.

In the pictures of dependence of the amplitude of oscillations on the frequency (for example for the heat flux) the features of chaotic flow can be noted. Namely, the spectrum is the continuum one and the amplitude is significantly more than the amplitude of pulsations at large Knudsen numbers. It can be treated as the manifestation of the growth of a dissipation in unstable regims.

The numerical results in [4] have been obtained on the crude meshes and some more accurate computations are made now. The steps in the physical space was smaller than in [4]. Especially it is important in the radial direction of a jet. The numerical solutions demonstrated the similar character pulsations. The distributions of macroparameters in the transversal direction of a jet are considered to compare results with the axial intability and so-called petal structure from [7]. The non-axisymmetric character of the boundary of a jet is observed in the computations. The roughness of the orifice, which is one of a source of instabilities in a jet, is modelled by the rectangular cells approximating the circle orifice.

The growth of the oscillation amplitudes of moments dependent upon the increase of the characteristic Reynolds number is noted. This growth is

\*Abstract 1932 submitted to the 21st International Symposium on Rarefied Gas Dynamics, Marseille, France, July 26-31, 1998



in the same range as for the experiment in [2] (the characteristic Reynolds number is between  $10^3$  and  $10^4$  when the transition to unstable flows in the mixing layer is observed). The magnitude of density pulsations increases in the mentioned range of the Reynolds numbers and then tends to the limiting value of the amplitude.

## References

- [1] Kutateladze S.S., Novopashin S.A., Perepelkin A.L., Yarygin V.N., *Thin structure of the flow of a supersonic underexpanded jet*, Dokl. Acad. Nauk SSSR., Vol.295, No.3, pp.556-558, 1987.
- [2] Novopasin S.A., Perepelkin A.L., Yarygin V.N., *The use of pulse lasers for flow visualisation and local density measurements in free jets*, Proc. 15th Intern. Symp. on Raref. Gas Dynam. B.G. Teubner Stuttgart. : V. Boffi, C. Cercignani, eds., Vol. II, pp. 623-632, 1986.
- [3] Aristov V.V., *Numerical analysis of free jets at small Knudsen numbers*, Proc. 19th Intern. Symp. on Raref. Gas Dynam., Oxford Univ. Press, Vol. 2, pp.1225-1231, 1995.
- [4] Aristov V.V., *Instabilities in jets at small Knudsen numbers*, Proc. 20th Intern. Symp. on Rarefied Gas Dynamics. : Peking Univ. Press, C. Shen ed., pp.315-320, 1997.
- [5] Tsuge S., *Kinetic theory and turbulence*, Proc. 13th Intern. Symp. on Raref. Gas Dynam., Plenum Press, Vol. 1, pp.1225-1231, 1995.
- [6] Zhigulev V.N., *Equations for turbulent motion of a gas*, Dokl. Acad. Nauk SSSR., Vol.10, No.3, pp.1003-1005, 1966.
- [7] Novopasin S.A., Perepelkin A.L., *Axial symmetry loss of a supersonic preturbulent jet*, Phys. Lett. A., Vol. 135, No.4, pp. 623-632, 1989.

# A Quasi-Monte Carlo Simulation of the Boltzmann Equation \*

Christian Lécot

Laboratoire de Mathématiques, Université de Savoie  
73376 Le Bourget-du-Lac cedex, France

## 1 Introduction

Monte Carlo simulations are used for solving various equations of statistical physics. Particles are sampled from some known initial distribution and then move and interact according to the dynamics described in the equation. Pseudo-random numbers are used to decide which particles collide and the results of the collision. Examples of this are the Direct Simulation Monte Carlo (DSMC) schemes of Bird [1] and Nanbu [2] for the Boltzmann equation. Quasi-random sequences are a deterministic alternative to pseudo-random sequences for use in Monte Carlo methods. Quasi-Monte Carlo methods are particularly powerful in the area of multidimensional integration [3], but the scope of these methods was widened in recent years [4]. In this paper we propose a quasi-Monte Carlo (QMC) simulation of the spatially homogeneous Boltzmann equation. We derive the method as the natural extension of quasi-Monte Carlo simulations of the Kac model [5] and of the linear Boltzmann equation [6].

## 2 Quasi-Monte Carlo scheme

We consider the Boltzmann equation with isotropic scattering

$$\begin{aligned} \frac{\partial f}{\partial t}(\mathbf{v}, t) &= \frac{1}{4\pi} \int_{\mathbb{R}^3 \times S^2} (f(\mathbf{v}', t)f(\mathbf{w}', t) \\ &\quad - f(\mathbf{v}, t)f(\mathbf{w}, t))\gamma(|\mathbf{v} - \mathbf{w}|)d\mathbf{w}d\mathbf{n}, \quad (1) \\ f(\mathbf{v}, 0) &= f_0(\mathbf{v}), \quad (2) \end{aligned}$$

where  $\mathbf{v} \in \mathbb{R}^3$ ,  $t > 0$ ,

$$\mathbf{v}' = \frac{1}{2}(\mathbf{v} + \mathbf{w} + |\mathbf{v} - \mathbf{w}|\mathbf{n}),$$

$$\mathbf{w}' = \frac{1}{2}(\mathbf{v} + \mathbf{w} - |\mathbf{v} - \mathbf{w}|\mathbf{n}),$$

$$0 \leq \gamma(x) \leq \gamma^* < +\infty \quad \text{and} \quad \int_{\mathbb{R}^3} f_0(\mathbf{v})d\mathbf{v} = 1.$$

We use the following weak formulation

$$\begin{aligned} \frac{d}{dt} \int_{\mathbb{R}^3} \varphi(\mathbf{v})f(\mathbf{v}, t)d\mathbf{v} = \\ \frac{1}{4\pi} \int_{\mathbb{R}^3 \times S^2} (\varphi(\mathbf{v}') - \varphi(\mathbf{v}))\gamma(|\mathbf{v} - \mathbf{w}|) \\ \cdot f(\mathbf{v}, t)f(\mathbf{w}, t)d\mathbf{v}d\mathbf{w}d\mathbf{n}, \quad (3) \end{aligned}$$

for any regular function  $\varphi$  on  $\mathbb{R}^3$ . Let  $c \geq 2$  and  $m \geq 0$  be integers. We put  $N = 2c^m$ . Let  $d_1, d_2, d_3$  be integers with  $d_1 + d_2 + d_3 = m$ . For integers  $0 \leq a_1 < c^{d_1}, 0 \leq a_2 < c^{d_2}, 0 \leq a_3 < 2c^{d_3}$ , let  $\mathbf{a} = (a_1, a_2, a_3)$ . We choose a set  $V^{(0)}$  with  $N$  points  $\mathbf{v}_a^{(0)}$  in  $\mathbb{R}^3$  sampled from the initial distribution  $f_0(\mathbf{v})$ . Let  $\Delta t$  be a time step, with  $\Delta t\gamma^* < 1$ . We introduce discrete times  $t_n = n\Delta t$  and we put  $f_n(\mathbf{v}) = f(\mathbf{v}, t_n)$ . We need a quasi-random sequence  $\mathbf{y}_0, \mathbf{y}_1, \dots$  in  $I^9 = [0, 1]^9$ . Point sets  $V^{(n)}$  of  $N$  points  $\mathbf{v}_a^{(n)}$  in  $\mathbb{R}^3$  are computed by a step-by-step procedure.

- The points of  $V^{(n)}$  are reordered so that

$$1. a_1 < b_1 \Rightarrow v_{a,1}^{(n)} \leq v_{b,1}^{(n)},$$

$$2. a_1 = b_1, a_2 < b_2 \Rightarrow v_{a,2}^{(n)} \leq v_{b,2}^{(n)},$$

$$3. a_1 = b_1, a_2 = b_2, a_3 < b_3 \Rightarrow v_{a,3}^{(n)} \leq v_{b,3}^{(n)}.$$

This technique improves the efficiency of the quasi-Monte Carlo approximation (see [5, 6]).

- Let  $[x]$  denote the greatest integer  $\leq x$ . For  $0 \leq j < N$ , let

$$\begin{aligned} a^{(n)}(j) &= ([c^{d_1}y_{nN+j,1}], [c^{d_2}y_{nN+j,2}], [2c^{d_3}y_{nN+j,3}]), \\ b^{(n)}(j) &= ([c^{d_1}y_{nN+j,4}], [c^{d_2}y_{nN+j,5}], [2c^{d_3}y_{nN+j,6}]), \\ \mathbf{n}(j) &= (1, 2y_{nN+j,8} - 1, 2\pi y_{nN+j,9}), \\ &\quad \text{in spherical polar coordinates.} \end{aligned}$$

Then

$$\mathbf{v}_{a^{(n)}(j)}^{(n+1)} = \mathbf{v}_{a^{(n)}(j)}^{(n)},$$

\*Abstract 2381 submitted to the 21st International Symposium on Rarefied Gas Dynamics, Marseille, France, July 26-31, 1998

$$\begin{aligned} & \text{if } y_{nN+j,7} \geq \Delta t \gamma (|\mathbf{v}_{a^{(n)}(j)}^{(n)} - \mathbf{v}_{b^{(n)}(j)}^{(n)}|), \\ & \mathbf{v}_{a^{(n)}(j)}^{(n+1)} = \frac{1}{2} \left( \mathbf{v}_{a^{(n)}(j)}^{(n)} + \mathbf{v}_{b^{(n)}(j)}^{(n)} \right. \\ & \left. + |\mathbf{v}_{a^{(n)}(j)}^{(n)} - \mathbf{v}_{b^{(n)}(j)}^{(n)}| \mathbf{n}(j) \right), \quad \text{otherwise.} \end{aligned}$$

Momentum, kinetic energy are conserved and small errors in quasi-Monte Carlo approximations are guaranteed if  $Y$  is constructed by duplicating a  $(0, 9)$ -sequence in base  $c$  (see [3, 5]).

### 3 Numerical experiments

We solve the model problem of Krook and Wu [7], for which an exact solution is known. The problem is implemented using three particle simulations: the DSMC methods of Bird and Nanbu and the QMC scheme. We choose  $c = 11$  and a time step  $\Delta t = 0.01$ . The error is defined by

$$\begin{aligned} D_N^*(V^{(n)}, f_n) = \sup_{r>0} & \left| \frac{1}{N} \# \{a : |\mathbf{v}_a^{(n)}| < r\} \right. \\ & \left. - \int_{[0,r] \times S^2} f(\mathbf{v}, t_n) d\mathbf{v} \right|. \end{aligned}$$

In Figures 1, 2 and 3 we plot the errors of the schemes versus the time. Dashed lines correspond to the DSMC method of Bird and thin lines correspond to the DSMC method of Nanbu. Thick lines correspond to the QMC scheme. In general, the results show that quasi-random simulation is superior to standard pseudo-random simulations, although not to as large an extent as in 1-D case [5] or in 3-D linear case [6].

### References

- [1] Bird G.A., *Molecular Gas Dynamics and the Direct Simulation of Gas Flows*, Clarendon Press, Oxford, 1994.
- [2] Nanbu K., *Direct simulation scheme derived from the Boltzmann equation. I. Monocomponent gases*, J. Phys. Soc. Japan, Vol.49, No.5, pp.2042–2049, 1980.
- [3] Niederreiter H., *Random Number Generation and Quasi-Monte Carlo Methods*, Society for Industrial and Applied Mathematics, Philadelphia, 1992.
- [4] Niederreiter H., Hellekalek P., Larcher G., and Zinterhof P., Eds, *Monte Carlo and Quasi-Monte Carlo Methods 1996*, Springer, New York, 1997.
- [5] Coulibaly I. and Lécot C., *Particle simulations of the Kac model of the Boltzmann equation*, J. Comput. Appl. Math., Vol.87, No.1, pp.169–193, 1997.
- [6] Lécot C. and Coulibaly I., *A quasi-Monte Carlo scheme using nets for a linear Boltzmann equation*, SIAM J. Numer. Anal., Vol.35, No.1, 1998.
- [7] Krook M. and Wu T.T., *Exact solutions of the Boltzmann equation*, Phys. Fluids, Vol.20, No.10, pp.1589–1595, 1977.

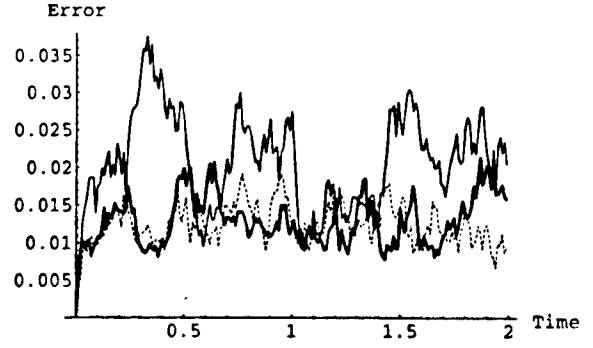


Figure 1: Simulations with  $N = 2,662$

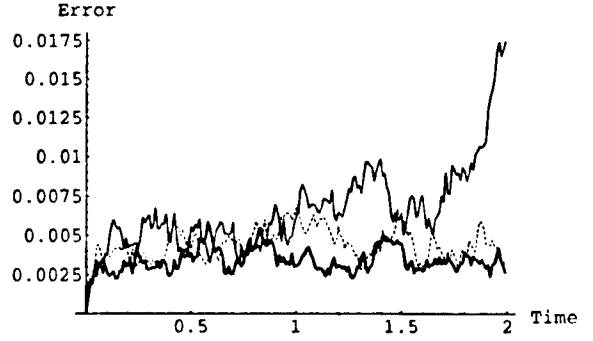


Figure 2: Simulations with  $N = 29,282$

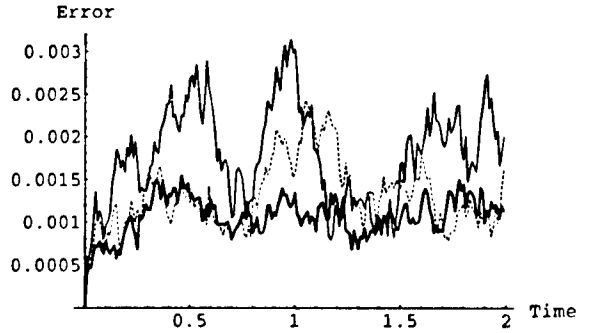


Figure 3: Simulations with  $N = 322,102$

# Heat, Mass and Momentum Transfer through a Rotating Rarefied Gas \*

Gilberto M. Kremer<sup>1</sup>, Felix M. Sharipov<sup>1</sup>, Liliana M. G. Cumin<sup>2</sup>

<sup>1</sup> Departamento de Física,

<sup>2</sup> Departamento de Matemática,

Universidade Federal do Paraná, Curitiba, Brazil

Linearized transport phenomena of a rarefied gas confined between two rotating cylinders were analyzed recently by Sharipov and Kremer [1, 2] and by Cumin, Sharipov and Kremer [3]. In these works heat [1], momentum [2] and mass transfer [3] were considered separately. Here we shall treat all these three phenomena jointly.

We consider a rarefied gas confined between two coaxial cylinders with radii  $R_0$  and  $R_1$  ( $R_0 > R_1$ ), the axes of the cylinders coinciding with the  $z$ -axis. The cylinders are assumed to be so long that the end effects can be neglected, i.e. the solution does not depend on the  $z$ -coordinate. It is assumed also that both cylinders may rotate around the  $z$ -axis.

The cylinders adsorb all incident particles and evaporate the particles according to a Maxwellian.

If both cylinders rotate with the same angular velocity  $\Omega_0$ , if they have the same temperature  $T_0$  and if each of them evaporates the same number of molecules that condensates, then the velocity distribution function is a Maxwellian.

The number density has the following distribution between the cylinders

$$n_0(r') = C \exp[\beta(\Omega_0 r')^2],$$

$$\beta = \frac{m}{2kT_0}$$

where  $C$  is a constant,  $m$  is the mass of a gas molecule and  $k$  is the Boltzmann constant.

We consider the situation when the equilibrium state is weakly disturbed by three factors:

- The pressure of evaporated particles from the inner cylinder  $P_1$  slightly differs from the equilibrium pressure at its surface, i.e.

$$P_1 = P_0(R_1) + \Delta P,$$

$$\frac{|\Delta P|}{P_0(R_1)} \ll 1,$$

while the outer cylinder evaporates the particles with the equilibrium pressure  $P_0(R_0)$ . Here

$$P(r') = n_0(r')kT_0.$$

- The angular velocity of the inner cylinder  $\Omega_1$  slightly differs from  $\Omega_0$ , i.e.

$$\Omega_1 = \Omega_0 + \Delta\Omega,$$

$$\frac{|\Delta\Omega|}{\Omega_0} \ll 1$$

while the outer cylinders has the angular velocity  $\Omega_0$ ;

- The temperature of the inner cylinder  $T_1$  slightly differs from the equilibrium temperature  $T_0$ , i.e.

$$T_1 = T_0 + \Delta T,$$

$$\frac{|\Delta T|}{T_0} \ll 1$$

while the outer cylinder has the temperature  $T_0$ .

The aim of this paper is to calculate the fields of the density, temperature, bulk velocity, heat flux vector and stress tensor between the cylinders as a function of the parameters: Knudsen number and angular velocity of the cylinders.

\*Abstract 2676 submitted to the 21st International Symposium on Rarefied Gas Dynamics, Marseille, France, July 26-31, 1998

We apply the S-model of the Boltzmann equation [4] as the basic equation for the distribution function  $f(\mathbf{r}', \mathbf{v})$ , which for a stationary gas flow reads

$$\mathbf{v} \cdot \frac{\partial f}{\partial \mathbf{r}} = \frac{P}{\mu} \left\{ f^M \left[ 1 + \frac{8\beta^2}{15nm} \mathbf{q}' \cdot \mathbf{V} \left( \beta V^2 - \frac{5}{2} \right) \right] - f(\mathbf{r}', \mathbf{v}) \right\},$$

where  $\mathbf{v}$  is the molecular velocity,  $\mu$  is the shear viscosity,  $n$  is the number density,  $f^M$  is the local Maxwellian,  $\mathbf{q}'$  is the heat flux vector.  $\mathbf{V} = \mathbf{v} - \mathbf{u}'$  with  $\mathbf{u}'$  denoting the bulk velocity.

The kinetic equation has been solved by the discrete velocity method and the discontinuity of the distribution function [5] is also taken into account.

The calculations have been carried out for the radius ratio  $R_1/R_0=0.5$  in the range of inverse Knudsen number from 0.01 to 40. Five values of the dimensionless angular velocity have been considered: 0, 0.25, 0.5, 0.75, and 1.

To estimate the numerical accuracy test calculations have been carried out for inverse Knudsen number  $\delta = 0.1; 1; 10$ ; and 40 with doubling of every grid parameter. An analysis of the test calculations showed that the distribution function moments change within 0.5%. This value can be considered as the calculation precision

To gain more precision criteria the fulfillment of the mass, momentum and energy conservation laws were verified as well as the Onsager-Casimir reciprocity relations [6].

In the main text the fields of density, velocity, temperature, heat flux vector and stress tensor are presented for a wide range of the Knudsen number. An analysis of the influence of the rotation of the cylinders on the fields is also given.

## References

- [1] Sharipov, F. M.; Kremer, G. M., *Heat Conduction through a Rarefied Gas between two Rotating Cylinders at Small Temperature Difference*, ZAMP, Vol. 46, pp. 680-692, 1995.
- [2] Sharipov, F. M.; Kremer, G. M., *Linear Couette Flow between two Rotating Cylinders*, Eur. J. Mech., B/Fluids, Vol.15, pp.493-505, 1996.
- [3] Cumin, L. M. G.; Sharipov, F. M.; Kremer, G. M., *Rarefied Gas Flow between two Cylinders*

*caused by the Evaporation and Condensation on their Surfaces*, submitted for publication, 1997.

- [4] Shakhov, E. M., *Generalization of the Krook Kinetic Equation*, Fluid Dynamics, Vol.3, pp.95-99, 1968.
- [5] Sugimoto, H.; Sone, Y., *Numerical Analysis of Steady Flows of a Gas Evaporating from its Cylindrical Condensed Phase on the Basis of Kinetic Theory*, Phys. Fluids, Vol A4, pp 419-440, 1992.
- [6] Sharipov, F. M., *Onsager-Casimir Reciprocity Relations in Rotating Gaseous Systems*, abstract 2686 in Rarefied Gas Dynamics, 21 Int. Symp., Book of Abstracts.

# Rarefied Gas Flow through a Channel with Rectangular Cross Section \*

F.M. Sharipov

Departamento de Física, Universidade Federal do Paraná, Curitiba, Brazil

The rarefied gas flow between two parallel infinite plates caused by a longitudinal pressure gradient is a classical problem of the rarefied gas dynamics, see e.g. the papers [1, 2]. Because of simplicity of such type of the flow this problem was solved by many methods applying many kinetic model equations and the Boltzmann equation itself. Today this solution can serve as a test for new numerical methods and new kinetic models. Moreover, since the rarefied gas flow through a channel is sensitive to the gas-surface interaction law, it can serve as an indirect measurement of the accommodation coefficients.

But the solution of this problem has a peculiarity: the mass flow rate through a cross section of the channel tends to infinity in the free-molecular regime flow. This unphysical behavior of the flow rate is explained by the fact that we deal with the degenerated geometry: the channel has the infinite length and the infinite width.

In practice this degenerated geometry does not exist: a real channel has a finite length and a finite width and, hence the real flow rate has always a finite value in the free-molecular regime flow [3]. To perform a correct comparison of theoretical results with experimental data one must know the conditions when the end effects (i.e. the finiteness of the channel length) and the influence of the lateral wall of the channel can be neglected. To obtain these conditions we have to calculate the flow rate through a channel having the finite length and/or the finite width.

The gas flow through a channel with the finite length was considered in the works [4, 5] where a finite value of the flow rate in the free-molecular regime was obtained. It was given a condition when the end effects can be neglected.

The aim of the present work is to calculate the flow rate through a long channel having a restricted

width, i.e. the channel cross section has a rectangular form. Some results on the gas flow through a rectangular channel are available in the paper by Loyalka et al. [6]. But since a range of the channel width was small, it was not given the condition when the effect of the lateral walls can be neglected. To indicate this condition here we consider a large range of the channel width.

Consider a channel created by two parallel plates fixed at  $y' = \pm a/2$  and two more parallel plates placed at  $z' = \pm b/2$ . In the  $x$ -direction the channel is so long that the end effects can be neglected. The channel is occupied by a single monatomic gas, which has a small longitudinal gradient of the pressure

$$\nu = \frac{a}{P} \frac{dP}{dx'}, \quad |\nu| \ll 1,$$

while the temperature of the gas is constant and equal to  $T$ . We are going to calculate the flow rate as a function of the rarefaction parameter

$$\delta = \frac{\sqrt{\pi}}{2} \frac{a}{\lambda},$$

and of the height-to-width ratio  $a/b$  of the channel. Here,  $\lambda$  is the mean free path.

We apply the BGK model as an input equation. To linearize it the distribution function is represented as

$$f(\mathbf{r}', \mathbf{v}) = f^M \left[ 1 + \nu \left( \frac{x'}{a} + h(y', z', \mathbf{v}) \right) \right],$$

where  $\mathbf{r}'$  is the position vector,  $\mathbf{v}$  is the molecular velocity,  $f^M$  is the Maxwellian

$$f^M = n \left( \frac{m}{2\pi kT} \right)^{3/2} \exp \left( -\frac{mv^2}{2kT} \right).$$

Then the linearized BGK equation for the perturbation function  $h$  in the dimensionless form reads

$$c_y \frac{\partial h}{\partial y} + c_z \frac{\partial h}{\partial z} = \delta(2c_x u - h) - c_x, \quad (1)$$

\* Abstract 2687 submitted to the 21st International Symposium on Rarefied Gas Dynamics, Marseille, France, July 26-31, 1998

$\delta$	$G$			
	$a/b=1.$	0.1	0.01	0 work [1]
0.01	0.8069	1.873	2.713	3.0489
0.1	0.7846	1.654	1.975	2.0314
1.0	0.7594	1.413	1.513	1.5389
5.0	0.9668	1.836	1.922	1.9883

 Table 1: Flow rate  $G$  vs  $\delta$  and  $a/b$ 

$a/b$	1.	0.1	0.01	0
$G/\delta$	0.0703	0.1562	0.1656	0.1667

 Table 2: Flow rate  $G$  vs  $a/b$  at  $\delta \rightarrow \infty$ 

where

$$\mathbf{r} = \frac{\mathbf{r}'}{a}, \quad \mathbf{c} = \sqrt{\frac{m}{2kT}} \mathbf{v},$$

and  $u$  is the dimensionless bulk velocity

$$u(y, z) = \frac{1}{\pi^{3/2}} \int \exp(-c^2) h(y, z, c) c_x dc.$$

The reduced flow rate is defined as

$$G = 2 \frac{a}{b} \int_{-b/2a}^{b/2a} \int_{-1/2}^{1/2} u(y, z) dy dz.$$

The kinetic equation (1) was solved by the discrete velocity method. Some preliminary results on the flow rate  $G$  are presented in Table 1. In the fifth column the results by Cercignani and Pagani [1] for the infinite plates are given.

It would be seemed that the ratio  $a/b$  could serve as a criterion of the influence of the lateral walls on the flow rate. However, from Table 1 one can see that near the free molecular regime flow ( $\delta = 0.01$ ) the lateral wall influence reaches 10% at  $a/b=0.01$ .

In the hydrodynamic regime flow ( $\delta \rightarrow \infty$ ) the Stokes equation was solved numerically. The results of the calculations are given in Table 2. One can see that in this regime flow the influence of the lateral wall on the flow rate is the least in comparison with the transition and near free-molecular regimes.

In the report the velocity profile and the flow rate will be presented for the wide ranges of the rarefaction parameter  $\delta$  and of the height-to-width ratio  $a/b$ . The criterion of the influence of the lateral wall on the flow rate will be given for the whole range of  $\delta$ .

## References

- [1] Cercignani C. and Pagani C.D, *Variational Approach to Boundary-Value Problems in Kinetic Theory*, Physics of Fluids, Vol.9, No.6, pp.1167-1173, 1966.
- [2] Hickey K.A. and Loyalka S.K., *Plane Poiseuille Flow: Rigid Sphere Gas*, J. Vac. Sci. Technol. A, Vol.8, No.2, pp.957-960, 1990.
- [3] Porodnov B.T., Suetin P.E., Borisov S.F., and Akinshin V.D. *Experimental Investigation of Rarefied Gas Flow in Different Channels*, J. Fluids Mech., Vol.64, pp.417-437, 1974.
- [4] Akinshin V.D., Makarov A.M., Seleznev V.D., and Sharipov F.M. *Rarefied Gas Flow through a Short Channel over the Whole Range of the Knudsen Number*, Zhurnal Prikladnoi Mekhaniki i Tekhnicheskoi Fiziki, No.5, pp.48-53, 1989.
- [5] Sharipov F.M. and Seleznev V.D., *Rarefied Gas Flows through Short Channels under Pressure and Temperature Drops*, in Rarefied Gas Dynamics, Proc. 17th Int. Symp., ed. by A.E. Beylich (Germany, 1990).
- [6] Loyalka S.K., Storvik T.S., and Park H.S., *Poiseuille Flow and Thermal Creep Flow in Long. Rectangular Channels in the Molecular and Transition Flow Regimes*, J. Vac. Sci. Technol., Vol.16, No.6, pp.1188-1192, 1976.

# Large Program Marking of Surface Elements and the Determination of Large Molecular Surface Reflection in Position Element Algorithm of DSMC \*

Jing Fan<sup>1</sup>, Shiliu Peng<sup>1</sup>, Ching Shen<sup>1</sup>, Liming Chen<sup>2</sup>

<sup>1</sup>Institute of Mechanics, CAS, Beijing, China

<sup>2</sup>Engineering Mechanics Department, Qinghua University, Beijing, China

Two innovations concerning the improvement of our position element version<sup>[1]</sup> in the calculation of the three-dimensional transitional flow by the DSMC method (cf. [2],[3]) are elucidated in this paper.

The marking of the surface elements for each case of presentation of the body configurations is a heavy burden in the position element algorithm of the DSMC method. This difficulty is resolved in the present work by compiling a dedicated program capable of handling various cases of presentation of the configuration. Any initial presentation of the configuration is rearranged in such a way that the modified presentation is composed of strips distributed alongside the flow direction, each strip being composed of small plane triangles, represented by their three apices. Then the intersection of the arrise of the element-cube with the body surface is determined easily in general case as the intersection of a straight line with such triangle. After the surface elements being marked the related necessary geometric parameters of the surface elements (areas, 'external volumes' and direction cosines of the normals) are calculated in the similar way as in [1]. Example calculations have shown the quickness and effectiveness of this program of marking the surface elements in various configuration presentations (sphere, Hermes type of space vehicle, projectile body of revolution and etching cavity etc.).

The probability criterion of molecule reflection on the surface used in [1] is replaced by a deterministic criterion in this paper. This is a natural approach, as in our position element version the locations of molecules are recorded as real numbers, i.e., are given exactly. When a molecule has intersected with a certain surface of a position element cube, the point of intersection  $(x_s, y_s, z_s)$ , the velocity of it  $(u, v, w)$  and the remainder time  $\Delta t_r$  in the current

time step are recorded. From  $(x_s, y_s, z_s), (u, v, w)$  and the geometric parameters of the body surface plane it is easy to calculate the times  $\Delta t_x, \Delta t_y, \Delta t_z$  and  $\Delta t_w$  for the molecule to reach the element surfaces in the x,y,z directions and the body surface plane respectively. Denoting the smallest of  $\Delta t_x, \Delta t_y$  and  $\Delta t_z$  as  $\Delta t_s$ , the criterion of reflection of the molecule is: when and only when

$$\Delta t_w \leq \Delta t_s, \quad \Delta t_w \leq \Delta t_r$$

the molecule reflects from this surface element. This criterion is tested again in the simulation of heat flux and pressure distribution on a sphere in the case of free molecule flow. Excellent agreement of the simulation result and exact solution is obtained. This criterion is used in the example calculations.

## References

- [1] C. Shen, J. Fan, Z. Hu, X. Xu, *A new version of position element algorithm of DSMC in calculation of 3-D transitional flows*, in *Rarefied Gas Dynamics 20*, ed. by C. Shen, Peking Univ. Press, pp.162-167 (1997).
- [2] G.A. Bird, *Molecular Gas Dynamics and Direct Simulation of Gas Flows*, Oxford, Clarendon Press(1994).
- [3] G.A. Bird, *Application of the DSMC method to the full shuttle geometry*, AIAA paper 90-1692(1990).

\*Abstract 2846 submitted to the 21st International Symposium on Rarefied Gas Dynamics, Marseille, France, July 26-31, 1998



# Application of the $\delta f$ Discretization Scheme to the Numerical Resolution of the Boltzmann Equation \*

R. Zorat, M. Tessarotto

Department of Mathematical Sciences, University of Trieste, Trieste, ITALY

## 1 Introduction

The  $\delta f$  discretization scheme, was originally developed in the field of numerical simulation of magnetoplasma dynamics [1], [2], [3], for reducing the simulation noise in the study of non linear phenomena of magnetoplasmas, such as transport caused by plasma microinstabilities. The aim of this work is to apply the  $\delta f$  discretization scheme to the resolution of the Boltzmann equation. The problem can be, in principle, of interest for a wide variety of systems, varying from dense plasmas to non neutral electron plasmas and partially ionized gases in which atomic processes are relevant.

The  $\delta f$  discretization scheme is a low noise algorithm, which permits to describe the non linear dynamics of a mechanical system, composed by a very high number of particles interacting each other, by evolving *only* the perturbation  $\delta f$  of the distribution function  $f = f_0 + \delta f$ . The distribution function  $f$ , satisfying a suitable kinetic equation (for example the Vlasov equation or the Boltzmann equation), is supposed to be suitably close to the analytically known equilibrium function  $f_0$ , so the error on the calculation of the moments of  $f$ , due to the use of a limited number of test particles in the simulation, is highly reduced, because only  $\delta f$  (and not  $f_0$ ) produces noise.

Collisions can be consistently included in the simulation scheme, only provided the adopted collision operators satisfy the basic collision conservation laws (particle density, linear momentum and total energy). In this work are described the treatments used for resolving first the Landau-Fokker-Planck (LFP) equation and then the Boltzmann equation.

## 2 The $\delta f$ discretization scheme

A short explanation of the  $\delta f$  discretization scheme, which we adopt [4], is below given, together with the main differences respect to discretization schemes used in conventional particle simulations. We assume that the distribution function  $f$ , describing one of the particle species of the system obeys the Vlasov equation  $\frac{d}{dt}f = 0$ , which is valid for Hamiltonian particle dynamics, not necessarily expressed by Hamiltonian variables. Then we assume  $f = f_0 + \delta f$ , where  $f_0$  is an analytically known distribution function and  $\delta f$  is its perturbation. During its evolution,  $f$  is supposed to stay suitably close to  $f_0$ , which can be considered an equilibrium distribution function. In a conventional particle simulation scheme, the  $N_T$  test particles and its phase space variables  $\mathbf{x}_i(t)$  are used to discretize completely  $f$ ,  $f^{(D)}(\mathbf{x}, t) = c \sum_{i=1}^{N_T} \delta(\mathbf{x} - \mathbf{x}_i(t)) k_i f(\mathbf{x}, t)$ , where  $k_i$  and  $c$  are suitable quantities, and this expression is used to calculate approximately suitable velocity space integrals of  $f$ , necessary for subsequent calculation in the simulation cycle. Instead, in a  $\delta f$  scheme these integrals are divided in integrals of  $f_0$ , not possessing noise, because are calculated using the analytically known expression of  $f_0$ , and in integrals of  $\delta f$ , that are the only contribution to the noise, due to the limited number of test particles. So, in a  $\delta f$  scheme, using the same number of test particles, the noise is enormously reduced respect to conventional particle simulation schemes.

## 3 Treatment of the Landau-Fokker-Planck equation

The  $\delta f$  scheme above described for the Vlasov equation can be suitably extended for treating the LFP equation [4], in order to consider the Coulombic collision in a magnetoplasma. For this purpose Monte Carlo operators are used, which approximate the linearized LFP collision operator and which sat-

\* Abstract 4241 submitted to the 21st International Symposium on Rarefied Gas Dynamics, Marseille, France, July 26-31, 1998

isfy its fundamental conservation laws [5]. The LFP equation is replaced by a stochastic Liouville equation  $\mathcal{L}\delta f_s = -S_1 f_{0,s}$ , which contains on the right term a stochastic force, which describes the effect of the diffusion on the velocity space. For the considered gyrokinetic variables, a set of finite difference stochastic equations are constructed, which are deterministic *between* the considered collision instants, but not *at* the collision instants, when the stochastic effects of collisional diffusion are included. At these instants we must impose  $(\delta f_s)_- = (\delta f_s)_+$  and  $(f_{0,s})_- = (f_{0,s})_+$  as continuity conditions.

## 4 Treatment of the Boltzmann equation

The previously described  $\delta f$  discretization scheme is applied to treat particle systems described by Boltzmann type collision operators. This involves both charged and neutral species. In the case of neutrals we adopt a point of view analogous of [6], [7], namely we shall deal with only one population of neutral particles, those in the fundamental levels and use its standard approximations for the Boltzmann equation of the neutral component. The Boltzmann equation to be solved is

$$\frac{\partial}{\partial t} f_n(\mathbf{r}, \mathbf{v}) + \mathbf{v} \cdot \frac{\partial}{\partial \mathbf{r}} f_n(\mathbf{r}, \mathbf{v}) = S_t(f_n)$$

where the Boltzmann collision operator  $S_t(f_n)$  is

$$S_t(f_n) = f_D(n_n \langle \sigma_{ex} v \rangle + n_D \langle \sigma_r v \rangle) - (1) \\ - f_n(n_D \langle \sigma_{ex} v \rangle + n_D \langle \sigma_{ion} v \rangle),$$

where  $f_D$  is the ion distribution function of the plasma background. Here  $\langle \sigma_{ex} v \rangle$ ,  $\langle \sigma_{ion} v \rangle$  and  $\langle \sigma_r v \rangle$  are the charge exchange, the ionization and the radiative recombination rate coefficients. The Boltzmann equation is solved either in a half-space or in a symmetric plane slab with symmetric boundary conditions [8], assuming for the background plasma a translational symmetry.

## 5 Conclusion

- Application of the  $\delta f$  discretization scheme to algorithms for resolving particular types of the Boltzmann equation.

## References

- [1] Tajima T., Perkins F. 1983 *International Sherwood Fusion Theory Conference*.
- [2] Kotschenreuther M., *Bull. Am. Phys. Soc.* **34**, 2107 (1988).
- [3] Parker S.E., Lee W.W., *Phys. Fluids B* **5**, 77 (1993).
- [4] Zorat R., Tessarotto M., proceedings of the 7<sup>th</sup> *European Fusion Theory Conference*, Juelich - Germany, October 8-10, 1997.
- [5] Tessarotto M., White R.B., Zheng L.-J., *Phys. Plasmas* **1**, 951 (1994).
- [6] Rehker S., Wobig H., *Plasma Phys.* **15**, 1083 (1973).
- [7] Hackmann J., Kim Y.C., Souw E.K., Uhlenbusch J., *Plasma Phys.* **20**, 309 (1978).
- [8] Cercignani C., *Mathematical methods in kinetic theory* Plenum Press, New York (1969)

# Molecular Dynamics Simulations of Shock Wave Propagations \*

T. Saito<sup>1</sup>, K. Takayama<sup>2</sup>

<sup>1</sup> Nihon SiliconGraphics-Cray K.K.

<sup>2</sup> Shock Wave Research Center, Institute of Fluid Science, Tohoku Univ., Japan

## 1 Introduction

Recent progresses in shock-wave studies are significant [1, 2]. Shock waves now are the objects not only in the basic research but also for useful applications in several important areas such as medical treatment. In the medical applications, specifically, it is necessary to discuss shock interactions with matters in a very small scale [3, 4]. Our objectives is to develop means to investigate shock wave phenomena in microscopic scales by using the method of molecular dynamics. This report presents the current progress in this activity at the Shock Wave Research Center, Institute of Fluid Science, Tohoku University.

Generations of shock waves by a moving piston in argon is simulated and the propagations and reflections of shock waves are investigated. Although the resolutions are not high enough in the current simulations, it is shown that the molecular dynamics method is useful for investigating the shock wave phenomena.

## 2 Numerical Method

In the present study, a soft-core molecular dynamics method is used [5]. Shock waves are generated in argon by moving a piston with a constant speed along a tube with rectangular cross section. The domain of molecular dynamics simulations is a rectangular box as shown in Fig.1(a). It has a cross section of  $100\text{\AA} \times 100\text{\AA}$  and is  $3000\text{\AA}$  long in the direction of shock wave propagation. The domain is further divided into cells of  $10\text{\AA}$  thick in order to calculate local gasdynamic parameters such as pressures, densities and temperatures at each cell location. Mirror reflections of argon atoms are used at the right wall and the moving left wall as boundary conditions. Periodic boundary conditions are used

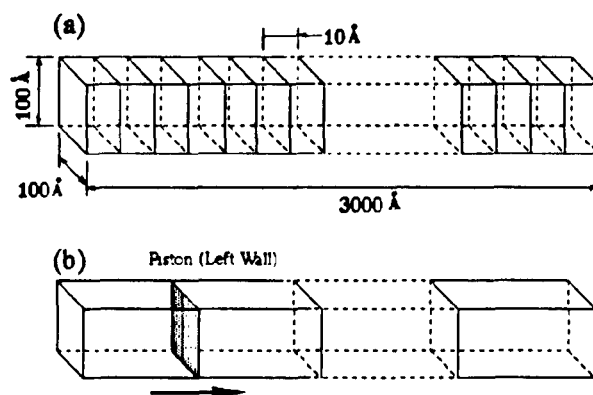


Figure 1: Numerical Domain

in other directions. Initially argon atoms are distributed at random around the body-centered lattice locations by using random numbers. The velocities of atoms are so assigned that the velocity distribution matches the Maxwell-Boltzmann's distribution of a specified temperature. A shock wave is initiated by moving the left solid wall as a moving piston as in Fig.1(b) with a specified constant speed as a moving piston. Calculations are carried out for ten thousands time steps before starting to move the left wall (piston) as a preparation run in order to obtain better distributions of both atom locations and their velocities. The velocity adjustment is also done so that the global translational energy becomes zero during the preparation run. Lennard-Jones potential and exp-6 potential [6] are used in the current study. Although the exp-6 potential usually give better results in higher pressures, both potentials give similar results for the pressure of 10 atmosphere in the current study. The time integration is done by Verlet's method and the time step of 2fs is used in the simulation.

## 3 Results and Discussions

Figure 2 shows the x-t diagram constructed from the pressure distributions. The number of argon

\*Abstract 4551 submitted to the 21st International Symposium on Rarefied Gas Dynamics, Marseille, France, July 26-31, 1998

atom is 7680. The piston speed and the initial density are 200m/s and 16.99Kg/m<sup>3</sup>, respectively. It is obtained from the figure that the speed of the incident shock wave is 492 m/s and agrees with the expected value of 483 m/s with the error of 1.8 %. It is interesting to note that the propagations of characteristic lines with appropriate speed is observed as streak lines in the x-t diagram. The incident shock wave is reflected at the right wall and propagates to the left. The reflected shock wave is again reflected at the moving wall. All these wave movements are clearly seen in the figure.

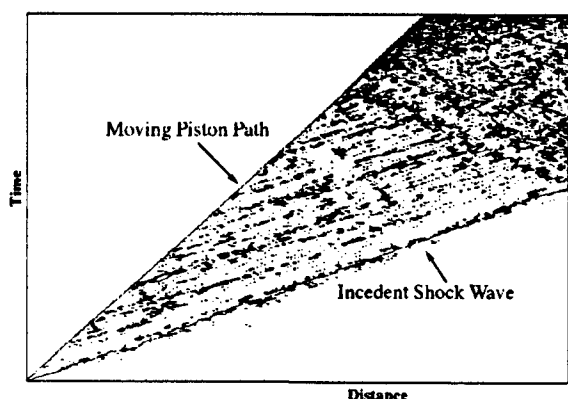


Figure 2: x-t diagram

Figure 3 shows the pressure distribution at 0.32 ns after the wall starts to move. The pressure behind the wall is arbitrarily set to zero since there is no particle there. The shock wave is recognized as the rapid increase in pressure in the plot but the values at 10Å width cells fluctuate rather significantly with the number of particle used in the current simulation.

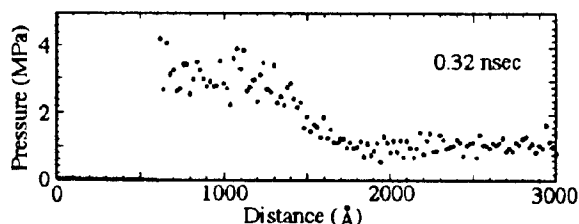


Figure 3: Pressure distribution

In the case of constant piston speed as in the present study, an averaged shock pressure distribution can be obtained. Fig.4 is the pressure distribution averaged over 20 distributions at different moments. The ratios of pressure, density and temperature across the incident shock wave are also obtained. It

is found that those values agree with the expected values from the Rankine-Hugoniot's relation within 10 %.

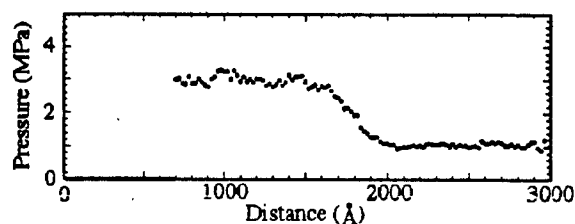


Figure 4: Averaged pressure distribution

## 4 Conclusion

A shock wave generation and its propagation are properly simulated with the molecular dynamics method. The shock wave structure is obtained by averaging distributions of parameters such as pressure. The characteristics are also visible in the x-t diagram. Current work continues and more results will be presented at the conference.

## References

- [1] Watanabe M., Abe A., Casey R.T and Takayama K., *Holographic interferometric observation of shock wave phenomena*, SPIE, Vol.1553, 1991.
- [2] Takayama K., *A Holographic Interferometric Study of Shock Wave Phenomena*, SPIE, Vol.1801, 1992.
- [3] Kuwahara A., Kambe K., Kurosu S., Orikasa S. and Takayama K., *Extracorporeal Stone Disintegration Using Chemical Explosive Pellets as an Energy Source of Underwater Shock Waves*, J. of Urology, Vol.135, 1986.
- [4] Takayama K., *Application of Underwater Shock wave Focusing to the Development of Extracorporeal Shock Wave Lithotripsy*, Jpn. J. Appl. Phys., Vol.32, 1993, pp2192o2198.
- [5] Ueda A., *Computer Simulation*, Asakura Shoten, 1990.
- [6] Ree F.H., *Simple mixing rule for mixtures with exp-6 interactions*, J. Chem. Phys., Vol.78, 1983, p.409.

# Flow of Rarefied Gas in a Channel with Flat Walls at Different Temperatures \*

M. Tomoeda

Kumamoto Institute of Technology,  
Department of Structural Engineering, Kumamoto, Japan

An analytical study is performed to investigate the slow flow of slightly rarefied gas in a channel with flat walls at temperatures different from the flow temperature. This is a fundamental problem, but particularly interesting from fluid dynamics point of view. The BGKW [1], [2] model of the Boltzmann equation is used to analyze the flow. Figure 1 shows a geometry of the flow in a channel with flat walls at different wall temperatures.

We assume that the speed ratio  $S$  and the Knudsen number  $K$  are so small that the BGKW model equation may be linearized and written in terms of the nondimensional distribution function  $\Phi$  [3], [4], as follows

$$KX \frac{\partial}{\partial \bar{X}} \Phi + \Phi = 2X_1 U + N + \left( X^2 - \frac{3}{2} \right) \Theta, \\ X^2 = X_1^2 + X_2^2 + X_3^2, \quad (1)$$

where  $U(U, 0, 0)$  and  $X(X_1, X_2, X_3)$  are the nondimensional flow velocity and molecular velocity respectively. The quantities  $N$  and  $\Theta$  are the perturbed nondimensional number density and temperature, respectively. The boundary conditions to Eq.1 are prescribed at the wall surfaces as follows:

1. The gas molecules are assumed to reflect perfectly diffusely with the temperatures equal to the the wall temperatures,  $T_{w1}$  and  $T_{w2}$ , respectively, which may be described by the Maxwellian distribution function,
2. It is assumed that there is no condensation or evaporation of the gas, i.e. no net mass flux.

The flow region may be effectively divided into the asymptotic flow region and the Knudsen layer region.

\*Abstract 4656 submitted to the 21st International Symposium on Rarefied Gas Dynamics, Marseille, France, July 26-31, 1998

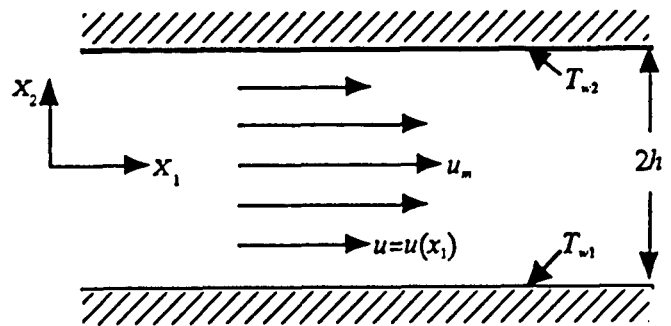


Figure 1: Flow in a channel with flat walls

In the asymptotic flow region which is far from the walls in terms of the molecular mean free path  $l$  the flow properties vary gradually with respect to  $l$  and Eq.1 leads to the conventional fluid dynamic equations. In order to analyze the Knudsen layer region where the flow properties vary significantly within a few mean free paths from the walls, Eq.1 has to be solved together with the boundary conditions 1) and 2). The solution will be expanded up to the second order of the Knudsen number  $K$ . The solution thus obtained in the Knudsen layer region will be matched asymptotically with that of the asymptotic flow region. As a final solution, the flow velocity and temperature profiles including the velocity slip and the temperature jump at the wall surfaces are calculated for various combinations of the wall temperatures.

## References

- [1] Bhatnagar P.L., Gross E.P., and Krook, M., *A Model for Collision Processes in Charged and Neutral One-Component Systems*, Physical Review, Vol.94, No.3, 1954, pp.511-525.
- [2] Welander P., *On the Temperature Jump in a Rarefied Gas*, Arkiv for Physik, Vol.7, No.44,

1954, pp.507-553.

- [3] Tomoeda M., *A Theoretical and Experimental Study on the Flow of Rarefied Gas past a Sphere*, University of Toronto, Institute for Aerospace Studies (UTIAS) Report No.216, 1977.
- [4] Tomoeda M., *Flow of Slightly Rarefied Gas Past a Liquid Sphere*, *Rarefied Gas Dynamics* 19, Vol.1, 1995, pp.93-99.

# Analysis of the Use of Weighting Factors in the DSMC Method \*

A.A. Morozov, M.Yu. Plotnikov  
Institute of Thermophysics, 630090 Novosibirsk, Russia

## 1 Introduction

One of the methods to increase the efficiency in DSMC axially symmetric flowfield calculation is the weighting factor (WF) [1]. The use of WFs is a complicated and scantily explored issue. The objective of this work was to investigate possibilities of various WFs and to make a comparative analysis of their efficiency.

## 2 Correctness of WFs

To estimate the correctness of the use of WFs, there were calculated the normalized collision number  $\Theta$  and the ratio of the number of duplicate molecules to the total number of the molecules  $\Omega = \sum (m - 1) / \sum m$  ( $m$  is the number of identical particles in the cell) for cells located at different distances from the axis. Numerical experiments were performed for subsonic and supersonic flows.

As an example of a subsonic flow, there was considered a flow with the Mach number  $M \approx 0.01$ . As units of measure, there were used the mean free path  $\lambda_0$  and the most probable molecular thermal speed. The comparison of efficiency of various WFs was performed for the obtained flowfield at the cylinder length  $10\lambda_0$  and its diameter  $8\lambda_0$ . The total number of cells in the flowfield is  $640(40 \times 16)$  with equal spacing  $0.25\lambda_0$  in each direction. The total number of particles without WFs is 40,000. The hard sphere model was employed for the description of intermolecular collisions.

WFs may be introduced by setting a maximum value  $W_{max}$  of the WF. The limiting cases of these WFs for the used net are  $W_{max} = 31$ , which corresponds to WFs proportionate to cell volumes and  $W_{max} = 1$ , which corresponds to computation without WFs.

\*Abstract 5067 submitted to the 21st International Symposium on Rarefied Gas Dynamics, Marseille, France, July 26-31, 1998

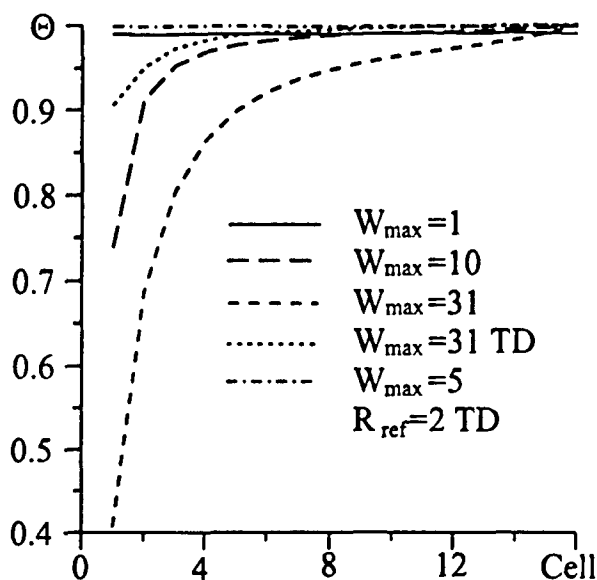


Figure 1: The normalized collision number for various WFs. TD corresponds to the time delay.

For  $W_{max} = 31$  the total number of molecules averages 2,500. In this case considerable variations of the density in the range 50 - 150 % are observed in the process of computation, whereas computing without WFs, the density deviation does not exceed 1 %. Besides, a decrease of the collision number  $\Theta$  near the axis by 60 % is observed (fig.1). That may be believed to be the consequence of a large number of duplicate molecules (fig.2). More satisfactory results have been obtained for lesser WF ( $W_{max} = 10$ ), but the small collision number near the axis does not allow to use even this WF (fig.1). To decrease the number of duplicate molecules near the axis, the case was considered when WFs were introduced from some reference radius  $R_{ref}$ . As an example, there was chosen  $R_{ref} = 2$ . The maximum value  $W_{max}$  was taken equal to 5. The obtained collision number is close enough to the correct value, but despite the large number of simulated molecules ( $\approx 19,800$ ), density fluctuations remain at the range from 80 to 120 %.

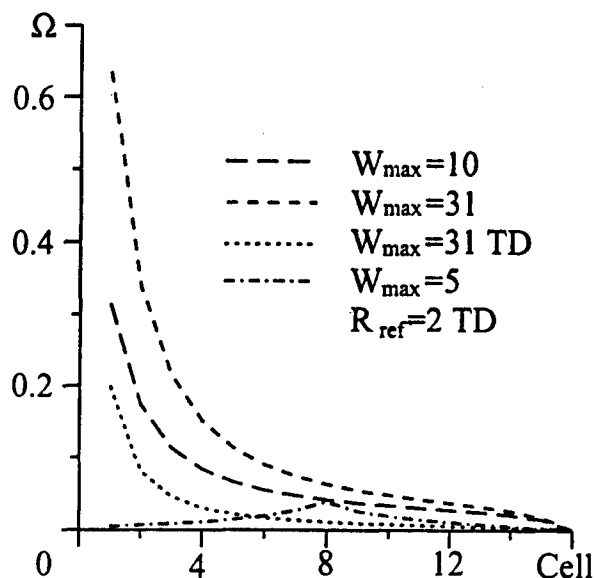


Figure 2: The ratio of the number of duplicate molecules to the total number of molecules for various WFs. TD corresponds to the time delay.

The undesirable impact of the molecule duplication may be lessened in a steady flow by the imposition of a time delay on the appearance of the duplicate molecule [1]. The use of such a delay for  $R_{ref} = 2$  and  $W_{max} = 5$  has admitted to obtain the right collision rate (fig.1) and the minimum number of duplicate molecules (fig.2). But even in this case the density deviation during the computation reaches 20 %, and this does not permit to calculate the density accurately using these WFs.

When simulating a supersonic flow with a Mach number of 2 with WFs proportional to cell volumes, a significant decrease of density variations during the computation has been obtained — the maximum deviation has not exceeded 10 %. The behaviour of other calculated values is analogous to one for the subsonic flow.

### 3 Comparison of efficiency

To compare the efficiency, there were calculated the dispersion of the density and the computational costs during its calculation. By the computational cost is meant a value  $S = t \cdot D\xi / n$ , which is generally taken in the Monte Carlo method for the estimation of the algorithm quality [2]. Here  $t$  is the total computer time spent on the simulation,  $n$  is the number of events for counting the dispersion  $D\xi$ . The obtained computational costs are presented in fig.3.

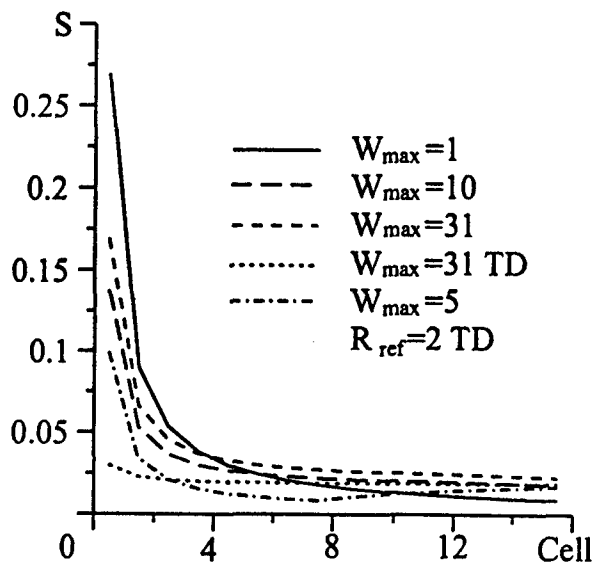


Figure 3: The computational cost at the calculation of the density for various WFs. TD corresponds to the time delay.

### 4 Conclusions

The performed investigation has shown that we may decrease the computational cost on retention of the correct collision rate by the selection of proper WFs. But simulating a subsonic flow in which the motion of the molecules towards the axis is expressed significantly, for any WFs large density variations are observed during the computation. So, for such subsonic flows it is not recommended to use WFs.

These density fluctuations become minor when modelling supersonic flow. It may be deduced that WFs with proper selected  $W_{max}$ ,  $R_{ref}$ , and the time delay may be sufficiently profitably used for the simulation of steady supersonic flows.

This work was supported by the Russian Foundation for Basic Research through Grant 97-01-00878.

### References

- [1] Bird G.A., *Molecular Gas Dynamics and the Direct Simulation of Gas Flows*, Clarendon Press, Oxford, 1994.
- [2] Mikhailov G.A., *Minimization of computational cost of nonanalogue Monte Carlo methods*, World Scientific, Singapore-New Jersey-London-Hong Kong, 1991.



# DSMC Calculation on Natural Convection of Rarefied Gas between Two Coaxial Cylinders \*

M. Usami, T. Nishide  
Mie University, Tsu, Japan

The heat transfer in rarefied gas between coaxial cylinders is investigated by the DSMC calculation paying special attention to the beginning of natural convection. In the free molecular regime, heat transfer except radiation is due to free motion of molecules and a rate of heat transfer is proportional to the number density. At intermediate pressure the motion of molecules is restricted by other molecules so that the heat transfer does not increase so much as an increase of density. In the continuum regime since the increase of density balances to the restriction of molecular motion, the heat transfer is not affected by circumference pressure. As the pressure increases furthermore, however, the gravity induces natural convection due to buoyancy and the heat transfer increases dramatically. Although the natural convection is one of the most interesting target that should be analyzed by molecular simulation of DSMC, the convection is a phenomenon occurring at full continuum regime and it is difficult to calculate it even if using the newest system of computer. Nevertheless in the present paper the natural convection is managed to be reproduced using the DSMC method by imposing an unrealistic large value of imaginary gravity on gases between two coaxial cylinders.

The flowfield between coaxial cylinders is shown in Fig.1. The radius of an inner cylinder  $R_i$  is 2.5mm and that of an outer cylinder  $R_o$  is 35mm, and temperature of the inner cylinder is  $T_i = 400\text{K}$  and that of the outer cylinder is  $T_o = 300\text{K}$ , which is selected according to the experiment already carried out. The conditions of calculation are;  $1/Kn=1, 10, 100$  and  $1000$ , where  $Kn$  is the Knudsen number based on the mean free path  $\lambda$  of the undisturbed gas whose temperature is  $300\text{K}$  and the difference between radii of two cylinders  $L = R_o - R_i$ . The VHS molecular model for argon and the null-collision scheme for intermolecular collisions are adopted. The diffuse reflection is assumed on the

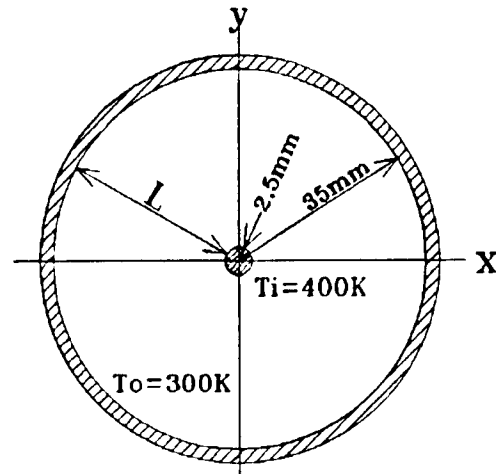


Figure 1: Simulated region

surfaces of the cylinders.

Figure 2 indicates temperature of the flowfield without gravity at  $1/Kn=100$ . Temperature is normalized by the temperature of the outer cylinder  $T_o$  so that the temperature of the inner cylinder is 1.333. There is almost no temperature jump near the surfaces of the cylinders at  $1/Kn=100$ . Figure 3 is density profile at  $1/Kn=100$  with imaginary large gravity (about  $10^5$  times actual gravity). The imaginary gravity act on gas molecules in  $-y$  direction. Density is normalized by the density of the undisturbed gas whose temperature is  $300\text{K}$ . Normalized density at various pressures has very similar profile such as indicated in Fig.3. Velocity vectors of gas flow with the gravity are shown in Fig.4 ( $1/Kn=10$ ), Fig.5 ( $1/Kn=100$ ) and Fig.6 ( $1/Kn=1000$ ). Although the magnitude of flow velocity at  $1/Kn=100$  is larger than that at  $1/Kn=10$ , it is not small in comparison with that at  $1/Kn=1000$ . Figure 7 is temperature profile at  $1/Kn=100$  with the gravity. Because of the gas flow by the convection, the temperature variation is relatively small except near the surfaces of the cylinders. Since the density at upper side ( $y > 0$ ) of the flowfield becomes very low due to the gravity, the temperature jump appears there.

\*Abstract 4673 submitted to the 21st International Symposium on Rarefied Gas Dynamics, Marseille, France, July 26-31, 1998

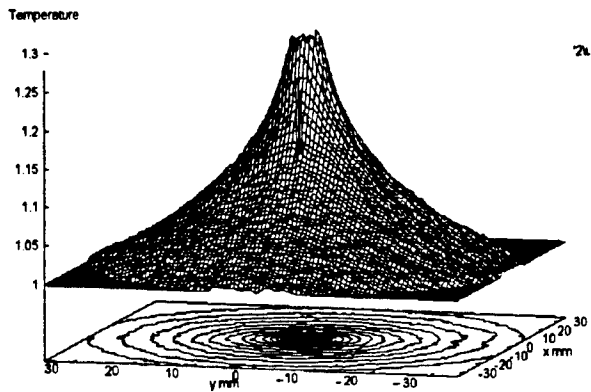


Figure 2: Temperature without gravity ( $1/Kn=100$ )

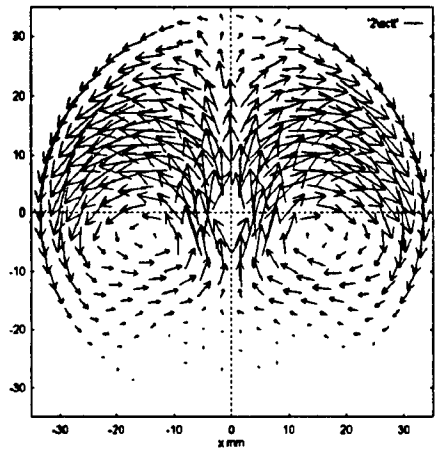


Figure 5: Flow pattern ( $1/Kn=100$ )

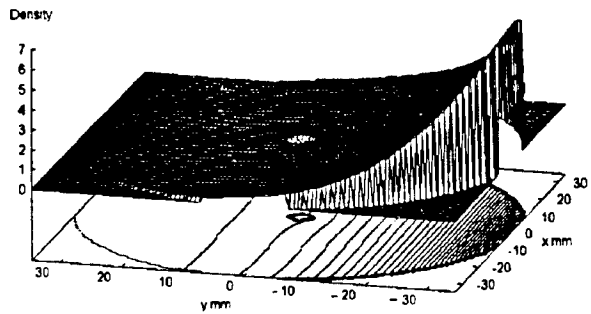


Figure 3: Density with gravity ( $1/Kn=100$ )

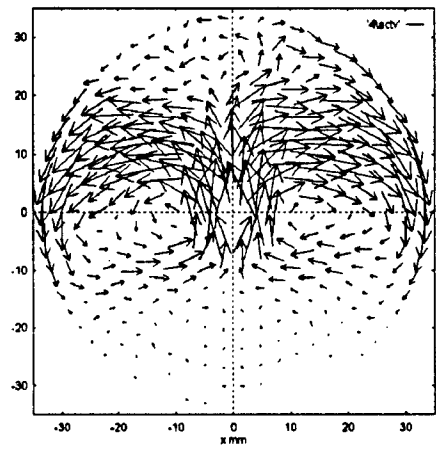


Figure 6: Flow pattern ( $1/Kn=1000$ )

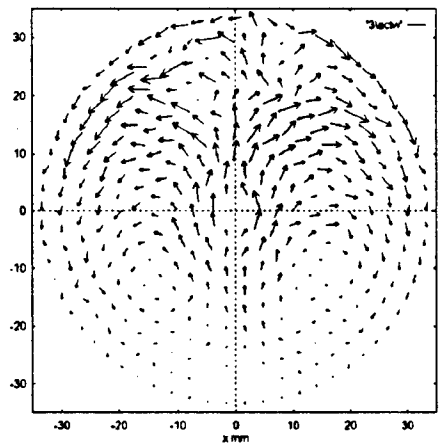


Figure 4: Flow pattern ( $1/Kn=10$ )

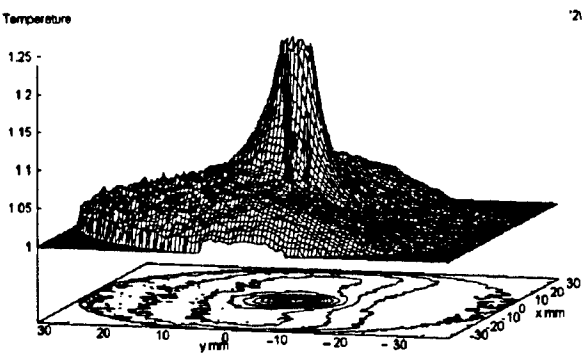


Figure 7: Temperature with gravity ( $1/Kn=100$ )

# Numerical Study of Pressure and Temperature Amplification in Shock Wave Focusing \*

P. Kowalczyk, T. Płatkowski, W. Waluś  
Institute of Applied Mathematics and Mechanics  
Department of Mathematics, Informatics and Mechanics  
Warsaw University, Poland

The process of focusing of a shock wave by a concave surface (reflector) in a rarefied noble gas is investigated by a numerical solution of the corresponding two dimensional initial-boundary value problem for the Boltzmann equation.

The numerical method is based on the splitting algorithm, which decouples the Boltzmann equation on each time step into two equations: the free flow (i.e. collisionless transport) equation solved numerically using the second order finite volume scheme, and the spatially homogeneous Boltzmann equation with the collision operator evaluated by the Monte Carlo quadrature formula (see [1]). The interaction of the gas with the reflecting surface is modeled by the Maxwell boundary conditions.

We analyze influence of various factors, involved in the mathematical model of the problem, on the process of focusing. In particular, we investigate the pressure amplification factor – the ratio of the maximum value of the pressure to its reference value – and study its dependence on the strength of the shock, the accommodation coefficient appearing in the Maxwell boundary conditions, and on the shape of the reflector. We observe the saturation of the pressure amplification for increasing Mach number. To illustrate the dependence of the phenomena on the shape of the reflector we compare the results for various shapes: a parabola, a semisphere and an angle.

We also compare the reflected shock trajectory with the trajectories obtained from the experiment and Monte Carlo simulations of Walenta [2].

Moreover, we study macroscopic effects related to the variation of temperature of the reflector. In particular, we analyze the temperature amplification factor, including the case in which the reflector temperature is different from that of the gas. We also

study the dependence of the pressure and temperature amplification factors on the temperature of the reflector in the case of the Maxwell boundary conditions with nonzero diffusive accommodation coefficient.

Below we present a sample graph showing the isobars of the shock wave which focuses after being reflected from the parabolic surface.

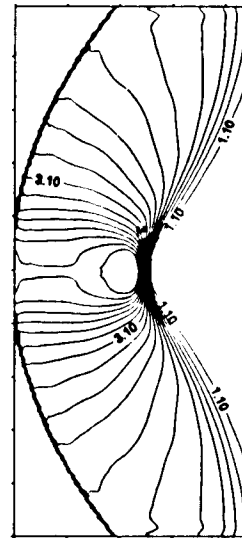


Figure 1: The isobars for  $M = 1.6$

## References

- [1] Aristov V.V., Tcheremissine F.G., *Direct numerical solutions of the kinetic Boltzmann equation*, Computing Center of Russian Academy of Sciences, Moscow, 1992 (in Russian).
- [2] Walenta Z., *Focusing a shock wave: Microscopic structure of the phenomenon*, – preprint 1997.

\*Abstract 4741 submitted to the 21st International Symposium on Rarefied Gas Dynamics, Marseille, France, July 26-31, 1998

# Rarefied Gas Flow from a Spherical Sink and Source \*

V.N. Gusev, V.I. Vlasov  
Central Aerohydrodynamic Institute (TsAGI)  
1, Zhukovsky str., 140160 Zhukovsky, Russia

The class of exact solutions of the one-dimensional Navier-Stokes equations which corresponds to the gas flows from a spherical sink and source was investigated analytically and numerically. In addition to the interest itself these investigations were undertaken with the purpose to understand the reason of obtained unexpected results : the tendency of the gas velocity to approach zero when the gas issues into vacuum [1], the absence of limit transition to an inviscid flow for a sink and an increase of mass flow as compared to a limit inviscid value [2]. The analysis has shown that the searching of unknown solutions of the Navier-Stokes equations essentially depends on a choice of the boundary conditions in an infinitely remote point. For example, a sought solution for sink can be obtained for a class of solutions with a finite value of heat flux in an infinitely remote point. For viscous and heat conductive gas critical values of a velocity and temperature on a sound sink line appear less and the density and pressure are greater than respective values for an ideal gas. In this case an increase of gas density becomes especially noticeable. At low Reynolds number it results in an increase of mass flow in the sink as compared to its limiting value for an ideal gas.

However the limited applicability of the Navier-Stokes equations with increase of the Knudsen number does not allow to describe a full flow pattern in a sink and source from the continuum to free molecule regimes. Therefore below this problem is investigated numerically by Monte Carlo method.

A spherical flow from infinity to a specularly reflecting sphere (a sink) with following expansion of gas in vacuum from this sphere (a source) is considered. The interaction of these two flows is the result of the only specular reflection of molecules on sphere. The method of trial molecules Monte Carlo [3] was used at a numerical solution of this problem. The flow parameters in a spherical sink and source were defined at various values of the Reynolds number. The

maximum value of mass flow was calculated. The results are compared with data, obtained by means of the Navier-Stokes equations [2] and experiment [4].

## Acknowledgment

The work was carried out at support of the Russian Foundation for Basic Research (Grant 97-01-00577) and State Program for Leading Research Groups Support (Grant 96-15-96063)

## References

- [1] Gusev V.N., Zhabkova A.V., *Features of spherical expansion of viscous gas into a constant-pressure medium*, Uchenye Zapiski TsAGI, v.7, no.4, 1976 (in Russian).
- [2] Gusev V.N., Khmel'nitskaja E.V., *On a maximum value of mass gas flow through an orifice* Proc. 17th RGD Intern. Symp., Aachen, Germany, pp.612-617, 1991.
- [3] Vlasov V.I., *Conservative variant of a method of trial molecules (Monte Carlo)* Trans. of 8th All-Union conference on RGD, M., 1986 (in Russian).
- [4] Liepmann H.W., *Gaskinetics and gasdynamics of orifice flow* Journal of Fluid Mechanics, v.10, p.1, 1961.

\*Abstract 4873 submitted to the 21st International Symposium on Rarefied Gas Dynamics, Marseille, France, July 26-31, 1998

# On the Costs of Continuous Time Monte Carlo Algorithms for the Boltzmann Equation of Rarefied Gases \*

A.I. Khisamutdinov, L.L. Sidorenko

Sobolev Institute of Mathematics, Russian Academy of Sciences, Novosibirsk, Russia

In papers [1]-[8] the constructive continuous time Monte Carlo (CTMC) methods  $(\mathcal{P}_0, \theta_0)$  for the spatially inhomogeneous smoothed Boltzmann equation were introduced and developed. Here  $\mathcal{P}_0$  denotes a Markov random process with jumps,  $\theta_0(\cdot, t^*)$  is an estimator (a function of the trajectory),  $t^*$  is a given time instant. These methods are different from well known direct simulation Monte Carlo (DSMC) methods; and the latter ones may be obtained from CTMC methods by dividing the time variable into  $\Delta t$  steps and splitting the operator of master equations.

According to the terminology used we distinguish the notions of Monte Carlo method and a Monte Carlo algorithm: the latter includes, additionally to Monte Carlo method, the specific structure of the simulation of distributions and the concrete forms of implementation of random estimators. A method can be implemented through different algorithms. We constructed the following algorithms: the "algorithm with different time coordinates", the "algorithm with additional jumps" and the "algorithm with generalized null-collision technique" (GNCT) ([4]-[8]).

We mean the cost of algorithm  $A$  as the product  $Cost(A) = \mathcal{D}_{\mathcal{P}_0}(\theta_0) \cdot \bar{t}$ . Here  $\mathcal{D}_{\mathcal{P}_0}(\cdot)$  is the variance of the method  $(\mathcal{P}_0, \theta_0)$ ,  $\bar{t}$  is the mean time needed to model one trajectory. We assume that the main contributions into  $\bar{t}$  on the trajectories  $A$  are resulted from quantities  $\nu_t, \nu_s$ , which are mean numbers of operations (per second) needed to simulate the intersections of the boundaries and the collisions between the particles, respectively.

Some whole picture of relation of costs of different simulation algorithms of CTMC methods may be obtained on the base of comparison of asymptotical costs, which are asymptotical on 3 parameters:  $N_1$ ,  $\mathcal{K}$  and  $\Delta t$ , where  $N_1 \equiv \bar{n}_0 V_0$ ,  $\mathcal{K} \equiv (Kn)^{-1}$ ,  $\bar{n}_0$  is the mean initial density of gas in the whole volume ( $V$ ),  $V_0$  is the volume of interaction,  $Kn$  is

the Knudsen's number,  $\Delta t$  is the step of splitting in DSMC methods. The costs of the best algorithms of CTMC methods are linear on  $N_1$  and square on  $\mathcal{K}$ ; the costs of the best algorithms of DSMC methods are linear on  $\mathcal{K}$  and  $(1/\Delta t)$  and mostly linear on  $N_1$ . The GNCT is used in the best algorithms of CTMC methods. In contrast to null-collision technique from [9] here one more constant is used; i.e., the upper bound of the number of interacting pairs. In this paper, first, the asymptotical costs of the algorithms  $A_{01}$ ,  $A_{00}$  for the one-dimensional problem are given. In  $A_{01}$  the traditional for DSMC methods model of interactions is used: two particles  $l$  and  $m$  interact if and only if when they are in the same subvolume ("cell"). In  $A_{00}$  they interact, when the distance between them does not exceed  $\rho$ ,  $|r^l - r^m| \leq \rho$  (see, for example[4]).

Second and third, in this paper two new approaches to the construction of CTMC methods algorithms are considered which allow to construct:

- a) the algorithms (C1) of CTMC methods, whose costs have the dependence on  $N_1$  as  $(N_1)^\alpha$ ,  $0 < \alpha < 1$ ,
- b) the algorithms (C2) of CTMC methods with costs linear on  $\mathcal{K}$  and on  $(\Delta t)^{-1}$ .

In (C1) we use hierarchical numbering of particles. The algorithms (C2) are approximate, they are based on a scheme of splitting, which is different from the scheme in DSMC methods; it is characteristic for our algorithms that restrictions on the size of subvolume ("cell") are absent.

A lot of numerical experiments connected with comparison of different algorithms and with confirmation of asymptotic estimations is presented in this paper.

This work is supported with grant 97-01-00776 of Russian Foundation of Basic Research.

## References

- [1] Khisamutdinov A.I., *On a simulation Monte Carlo method for modeling of dynamics of rar-*

\*Abstract 4917 submitted to the 21st International Symposium on Rarefied Gas Dynamics, Marseille, France, July 26-31, 1998

- efied gases* , Preprint No 599, Vychisl. Tsentr Sibirsk. Otdel. Akad. Nauk SSSR, Novosibirsk, 1985. (in Russian)
- [2] Khisamutdinov A.I. , *Simulation statistical modeling of the kinetic equation of rarefied gases*, Dokl. Akad. Nauk SSSR, Vol. 302, No. 1, pp. 75-79, 1988, (in Russian); Engl. transl. in Soviet Phys. Dokl., Vol. 33, (1988).
  - [3] Khisamutdinov A.I. , *Different time coordinate algorithms of Monte Carlo methods for nonlinear "smoothed" Boltzmann equation* ,Dokl. Akad. Nauk SSSR, Vol. 316, No. 4, pp. 829-833, 1991, (in Russian); Engl. transl. in Soviet Math. Dokl., Vol. 43, (1991).
  - [4] Khisamutdinov A.I. , *On a simulation method of statistical modeling of rarefied gases*,Dokl. Akad. Nauk SSSR, Vol. 291, No. 6, pp. 1300-1304, 1986; Engl. transl. in Soviet Math. Dokl., Vol. 34, (1987).
  - [5] Khisamutdinov A.I. , *The null collisions algorithms of the continued time Monte Carlo methods for the Boltzmann equation* ,Ross. Akad. Nauk Dokl., Vol. 328, No. 6, pp. 662-665, 1993, (in Russian); Engl. transl. in Russian Acad. Sci. Dokl. Math., Vol. 47, (1993).
  - [6] Khisamutdinov A.I., Sidorenko L.L., *The continuous time Monte Carlo methods and algorithms for the Boltzmann equation of rarefied gases*,Book of Abstracts.19th Int. Symp. Raref. Gas Dynam. Oxford, p. 78, 1994.
  - [7] Khisamutdinov A.I., Sidorenko L.L., *Monte Carlo fictitious collision algorithms for nonlinear Boltzmann equation* ,Monte Carlo Methods and Applications, VSP, Utrecht, The Netherlands, Tokyo, Japan, Vol. 1, No 3, pp. 221-240, 1995.
  - [8] Khisamutdinov A.I., Sidorenko L.L., *The algorithms of the continuous time Monte Carlo methods for kinetic equation of rarefied gases*,Mat. Modelirovanie, Vol. 6, No 2, pp. 47-60, 1994. (in Russian)
  - [9] Koura K., *Null-collision technique in the direct simulation Monte Carlo method*, Phys. Fluids. Vol. 29, No 11, pp. 3509-3511, 1986.

# Dynamics of Instabilities in Rarefied Gas Flow \*

I.N. Larina, V.A. Rykov  
Computing Center of RAS, Moscow, Russia

Numerical analysis of rarefied gas flows allows to study the evolution of instabilities that arise in flows at small Knudsen numbers. This direction of rarefied gas investigation was started in papers [1-5] when considering shear Taylor-Couette flow. In these papers the direct simulation Monte Carlo method of the first order accuracy was applied for numerical solution of the problem. The main difficulty that arises takes place upon calculating rarefied gas flow with the use of the first order difference schemes is the scheme viscosity that may be competitive with physical one at the small Knudsen numbers. To avoid this effect in calculations it is necessary that time and space step sizes were less than the Knudsen number.

In this paper the model kinetic Krook equation is used for describing a gas flow. Its solution is carried out by a regular numerical method that is specially adapted to the calculation of a gas flow at small Knudsen number [6]. The method is conservative, of the second order accuracy with respect to time and space and has no scheme viscosity in the sense that the second space derivatives corresponding to the scheme viscosity are not present in the difference approximations of the numerical scheme.

This method is used for studying the axially symmetric gas flow between two coaxial infinitely-long circular cylinders that are rotating with different velocities. First of all, Taylor vortexes have been reproduced, that are generating as a result of flow instability with decreasing the Knudsen number. This case has been considered before in [1-5].

We consider a new case of instability generation when both cylinders are rotating around the axis as a solid body with a constant angular acceleration. In the gap between the cylinders due to the inertia force a closed one-dimensional flow of the Poiseuille type is generated. As the Knudsen number decreases the loss of the flow stability occurs and there appear non-stationary vortex structures periodically located along the axis.

This problem has analogy for viscous incompress-

ible fluid. With time in the reference linked with the solid body a stationary one-dimensional flow is stated. For this flow an exact solution of Navier-Stokes equations is found and its stability is investigated numerically. The result is very useful for comparison with rarefied gas flow as well as the Taylor result for incompressible fluid [7]. For rarefied gas flows and for incompressible fluid the values of rotation momentum acting on each of cylinders with time are calculated. Presented numerical results show the instability evolution in gases on the basis of the kinetic approach.

## References

- [1] Stefanov S., Cercignani C., *Monte Carlo simulation of the Taylor-Couette flow of a rarefied gas*, J. Fluid Mech., Vol.256, pp.199-213, 1993.
- [2] Riechermann D., Nandu K., *Monte Carlo direct simulation of the Taylor instability in rarefied gas*, Phys. Fluids, A5(11),Nov., pp.2585-2587, 1993.
- [3] Usami M., *Direct simulation Monte Carlo on Taylor vortex flow*, Proc. 19th Inter. Symp. Rarefied Gas Dynamics, Oxford Univ. Press, vol.1, pp.389-395, 1995.
- [4] Riechermann D., Nandu K., *Three-dimensional simulation of wavy vortex flow by direct simulation Monte Carlo method*, Phys. Fluids, 9(4),Apr., pp.811-813, 1997.
- [5] Bird G.A., *The initiation of centrifugal instabilities in an axially symmetric flow*, Proc.of the 20th Inter. Symp. Rarefied Gas Dynamics, Peking Univ.Press, pp.149-154, 1997.
- [6] Larina I.N., Rykov V.A., *Numerical analysis of rarefied gas flows in long channels at small Knudsen numbers*, Proc.of the 20th Inter. Symp. Rarefied Gas Dynamics, Peking Univ.Press, pp.149-154, 1997.
- [7] Taylor G.I., *Stability of a viscous liquid contained between two rotating cylinders*,Philos. Trans. R. Soc. London, Ser. A233, pp.289-343, 1923.

\*Abstract 5016 submitted to the 21st International Symposium on Rarefied Gas Dynamics, Marseille, France, July 26-31, 1998

# Solution of Boltzmann and BGK Equations for High-Velocity Tails of Distribution Functions.\*

A.A.Abramov<sup>1</sup>, S.F.Gimelshain<sup>2</sup>, M.S.Ivanov<sup>2</sup>, N.K.Makashev<sup>1</sup>

<sup>1</sup> Central Aerohydrodynamic Institute, Zhukovsky, Moscow Region, 140160, Russia

<sup>2</sup> Institute of Theoretical and Applied Mechanics, Novosibirsk, 630090, Russia

## 1 Introduction

Calculations of macroscopic rates of chemical reactions and thermal relaxation processes can be performed with specified values of corresponding collision cross-sections and distribution functions of reacting molecules. In case of high energy threshold of chemical reaction, high-velocity (or energy) tails of molecular distribution functions have to be known for these calculations. An accurate determination of these tails for spatially nonuniform rarefied flows is rather complicated due to the complex nature of the Boltzmann equation. Therefore, first numerical results were obtained for BGK model equation [1, 2]. As for the Boltzmann equation, only a general qualitative analysis was performed in [3, 4].

As a result, a number of properties of distribution function tails was obtained for BGK model equation only. At present, there is no direct evidence of correspondence between the solutions of the Boltzmann equation for distribution function tails and those for BGK model. Such an evidence is needed to confirm the basic principles of the asymptotic theory of distribution function tails. This is also useful for effective calculation of macroscopic rates of high-threshold reactions. The main objective of this paper is the study of high-velocity tails of distribution functions by the direct simulation Monte Carlo (DSMC) method.

The DSMC solutions of the Boltzmann equation will be presented for the problem considered in [1, 2], namely, the determination of distribution function tails for one-dimensional problem of heat transfer and for Couette flow. The high-velocity tails of distribution functions were computed with acceptable accuracy with two different numerical schemes of the DSMC method, [5, 6] and [7]. The calculations were performed for two molecular collision models, hard spheres and pseudo-maxwellian

molecules. Results of computations were compared with known solutions of BGK equation [1, 2].

## 2 State of the art

The following statements come from [1, 2, 3, 4]:

1. At small Knudsen number,  $Kn$ , a strong perturbation of local-equilibrium Maxwellian distribution  $f_0$  arises at molecular velocities whose value is of the order of  $C_T(Kn)^{-1/3}$  in case of Maxwellian molecules and  $C_T(Kn)^{-1/2}$  for hard spheres. Here  $C_T = \sqrt{2RT}$  is the most probable molecular thermal speed,  $Kn = l/L$  is the local Knudsen number,  $l$  is the molecular mean free path, and  $L = |\nabla \ln T|^{-1}$  is the local value of flow space scale.
2. From item 1 follows, in particular, that for the problem of heat transfer, the perturbation of local Maxwellian distribution is stronger and occurs at smaller molecular velocities if we consider gas near the cold wall. The reason for this is the increase of the local Knudsen number near this wall.
3. The tails of distribution functions may have local and non-local properties at  $Kn \ll 1$ . The local solution comes from molecules moving in the direction of temperature increasing. The solution becomes non-local for large molecular velocities of opposite direction. This is because of extremely large number of fast molecules in high-temperature regions.
4. In agreement with these results, the usually calculated normalized distribution function  $F_1 = f_1(V_X)/f_{01}(V_X)$  has strongly deviates from unity at large positive  $V_X$  where  $F_1 < 1$ , and at large negative  $V_X$  where  $F_1 \gg 1$ . In the second case the solution may have non-local properties [1, 2, 3, 4]. Here,  $X$ -axis is normal to the walls and directed to the hot one. The function  $f_{01}(V_X)$  is the one-component Maxwellian distribution. The value of dimensionless molecular velocity is  $V = C/C_T$ .

\*Abstract 5039 submitted to the 21st International Symposium on Rarefied Gas Dynamics, Marseille, France, July 26-31, 1998



### 3 Numerical results

The calculations of profiles of macroparametes (density, velocity and temperature) and gas transport properties does not make a problem from computational point of view for one-dimensional flows. However, obtaining high-velocity tails of the distribution functions by the DSMC method with acceptable accuracy (better than 5%) require a huge amount of CPU time even for 1D case. This is because of an extremely low population of high-velocity tails. In order to provide an acceptable accuracy for distribution function in a wide range of velocities, the total sampling size was about  $10^6$  timesteps, and the number of collisions with a cold wall was about  $1.5 \cdot 10^8$ .

The study of statistical dependence between model molecules has also been conducted. It was found that corresponding errors caused by statistical dependence of molecules did not exceed 0.5%.

The computations of normalized distribution function tails showed that the data taken from BGK solutions are in reasonable qualitative agreement with the DSMC results.

### 4 Acknowledgments

This work was supported by Russian Foundation for Basic Research (Project No. 96-01-00573 and Grant No. 96-15-9603). This support is gratefully acknowledged.

### References

- [1] Abramov A.A., Makashev N.K., *Perturbation of equilibrium kinetics of high threshold reactions in flows with spatially variable temperature of gas*, Dokl. AN SSSR, 1982, Vol. 263, No 5, 1083-1087.
- [2] Vermel A.V., Makashev N.K., *Peculiarities of non-equilibrium high velocity tails of molecular distribution function in Couette flow of compressible gas*, Izv. RAN, Mech. Zhidkosti i Gasa. 1998, No 2. In press.
- [3] Makashev N.K., *Properties of Boltzman equation solution at high energies of translational motion of the molecules and their consequences*, Dokl. AN SSSR, 1981, Vol. 258, No 1, 52-56.
- [4] Abramov A.A., Asmolov E.S., Makashev N.K., *High energy molecules in gas dynamics*, Proc. of 13-th Symp. on RGD. Novosibirsk, 1982. Ed. by O.M. Belotserkovskii et al.. Plenum Press, N.Y. 1985, Vol.1, 177-184.
- [5] Ivanov M.S., Rogasinsky S.V., *Theoretical analysis of traditional and modern schemes of the DSMC method*, Proc. of 17-th Symp. on RGD, Aachen, Germany, 1990, 629-642.
- [6] Ivanov M.S., Rogasinski S.V., *Analysis of numerical techniques of the direct simulation Monte-Carlo method in rarefied gas dynamics*, Sov.J. Numer. Anal. Math. Modeling. 1988, Vol.2, No 6, 453-465.
- [7] Belotserkovskii O.M., Yanitskii V.E., *Statistical method of „particles in cells,, for the solving of the problems of rarefied gas dynamics. Parts I and II*, Zhurn. vychislit. matematiki i matem. fiziki. 1975, Vol.15, No 5, 1195-1208, and No. 6, 1553-1567.

# Comparative Analysis of Efficiency of Various Estimations for the DSMC Method \*

A.A. Morozov, M.Yu. Plotnikov  
Institute of Thermophysics, 630090 Novosibirsk, Russia

## 1 Introduction

One of the leading instruments for the numerical solution of applied problems of rarefied gas dynamics is the direct simulation Monte Carlo (DSMC) method [1]. There may be used distinct estimations for calculations of macroscopic properties of the gas flow in this method.

The commonly employed estimation of parameters in a cell is performed by a "photograph" of the state of the molecules on each time step with equal contribution of each molecule [1]. Further this estimation will be referred to as the "photograph" estimation.

When using the "intersection" estimation [2], the summation of data required for the calculation of gas properties occurs during the motion of the molecules, and the necessary values are determined at preset planes. As soon as a molecule crosses such a plane, the summation of the information with a weight  $1/v_x$  happens ( here  $v_x$  is the velocity of the molecule in the direction perpendicular to the plane).

For the "time" estimation the information is summed to cells that molecules passed through, and the contribution of a molecule is proportional to the time that the molecule stays in the cell.

The objective of this work was comparison of efficiency of these estimations for the simulation of one-dimensional flows. For this purpose there were calculated computational costs during the calculation of various macroscopic properties. By the computational cost is meant a value  $S = t \cdot D\xi/n$ , which is generally taken in the Monte Carlo method for the estimation of the algorithm quality [3]. Here  $t$  is the total computer time spent on the simulation,  $n$  is the number of events for counting the dispersion  $D\xi$ .

\* Abstract 5102 submitted to the 21st International Symposium on Rarefied Gas Dynamics, Marseille, France, July 26-31, 1998

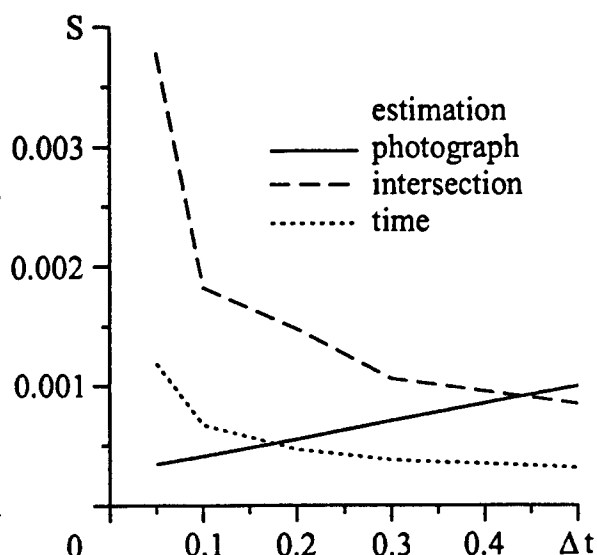


Figure 1: The time step dependence of the computational cost at the temperature calculation for the fixed cell number  $N = 10$ .

## 2 Calculations

The analysis was performed for the problem of heat transfer between parallel plates enclosing rarefied gas for the Knudsen number  $Kn = 1$ . The hard sphere model was employed for the description of intermolecular collisions. As units of measure, there were used the mean free path  $\lambda_0$  and the most probable molecular thermal speed. To avoid influence of gradients of macroscopic properties, the case of equal temperatures of the plates was considered ( $T_1/T_0 = 1$ ). During the investigation there were varied the time step for the fixed cell number  $N = 10$  and the cell number for the fixed time step  $\Delta t = 0.1$ . The density, the temperature, the heat flux, and the computational costs at the calculation of the considered quantities were calculated.

The obtained relationships between the computational cost at the temperature calculation and the time step  $\Delta t$  (fig.1) and the number of cells  $N$  (fig.2) are presented. Similar results are obtained for cal-

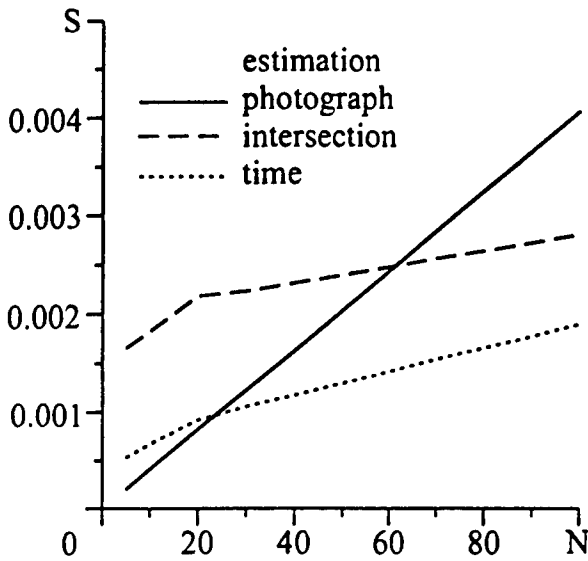


Figure 2: The cell number dependence of the computational cost at the temperature calculation for the fixed time step  $\Delta t = 0.1$ .

culations of the density and the heat flux, with the "time" estimation being more efficient in comparison with the "photograph" estimation for the heat flux and less efficient for the density.

It should be pointed out that the "time" estimation produces more correct results in the calculation of the highest moments of the distribution function for sufficiently large time steps in comparison with the "photograph" estimation. To demonstrate this fact, computations of the heat flux were performed for various time steps for the Knudsen number  $Kn = 1$  and for the temperature ratio  $T_1/T_0 = 4$ .

The solution obtained by the simulation using the "time" estimation with the time step of 0.01 was considered standard. Beginning with the  $\Delta t \leq 0.1$  results for this estimation practically coincide with the standard solution (fig.3). For the "photograph" estimation, although a much smaller time step was used, even for  $\Delta t = 0.005$  the obtained profile distinctly differs from the correct one. So the "time" estimation allows to use much larger time steps than the "photograph" estimation, with more accurate results being obtained.

### 3 Conclusions and discussion

From the performed investigation, the following deductions may be made:

1) The traditional sampling procedure [1] seems to be the most natural, can be readily realized, but is

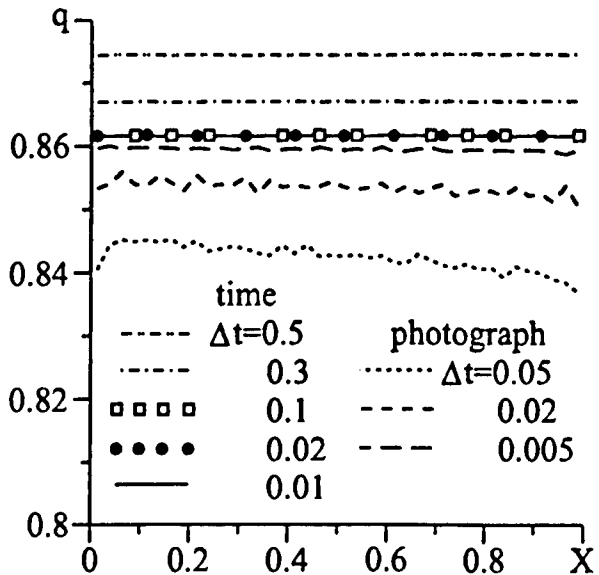


Figure 3: The heat flux profiles for various time steps for the "time" and "photograph" estimations when solving the heat transfer problem for the temperature ratio  $T_1/T_0 = 4$ .

not effective or even incorrect for calculations of the highest moments of the distribution function.

2) The advantage of the "intersection" estimation is the opportunity of calculation of the boundary conditions. Its shortcoming is a large dispersion.

3) The "time" estimation is recommended to use for the highest moment computations, with its efficiency increasing with the rise of the number of cells passed through by a molecule at the time step. But this procedure is hardly applicable for the simulation of not one-dimensional flows.

### References

- [1] Bird G.A., *Molecular Gas Dynamics and the Direct Simulation of Gas Flows*, Clarendon Press, Oxford, 1994.
- [2] Perlmutter M., *Analysis of Couette flow and heat transfer between parallel plates enclosing rarefied gas by Monte Carlo*, Proceedings of the Fifth Int. Symp. on Rarefied Gas Dynamics, Vol.1, pp.455-480, 1967.
- [3] Mikhailov G.A., *Minimization of computational cost of nonanalogue Monte Carlo methods*, World Scientific, Singapore-New Jersey-London-Hong Kong, 1991.

# C - Approach to Optimization of Solving Nonlinear Integral Equation by the Monte Carlo Method. \*

E.V.Shkarupa  
Computing Center SD RAS, Novosibirsk, Russia

Replacing the initial problem by a sequence of linear problems is one of the most-used approaches of solving nonlinear problems by the Monte Carlo method. In the present work this approach is considered on a basis of solving initial nonlinear equation by the simple iteration method. Therewith linear integral equation is solved by the Monte Carlo method with the use of the frequency polygon method (estimation solution in grid nodes with following multilinear approximation).

Let us consider the nonlinear integral equation  $\varphi = G(\varphi)$ . We assume that the solution  $\varphi^*(.)$  of this equation can be found by the iteration method, starting with some approximation  $\varphi_0(.)$  and holds

$$\|G(\varphi_n) - \varphi^*\| \leq q \|\varphi_n - \varphi^*\|, \quad q < 1.$$

The symbol  $\varphi_n(.)$  ( $\tilde{\varphi}_n(.)$ ) denotes exact solution (stochastic estimation by the Monte Carlo method) of  $n$ -th iteration provided that the value of the  $(n-1)$ -th iteration is fixed and coincides with approximation of the frequency polygon method  $L_{(M)}\tilde{\varphi}_{n-1}(x)$ . This means, in particular, that the relation  $\varphi_n(x) = G(L_{(M)}\tilde{\varphi}_{n-1}(x))$  is valid. We interest the total error on  $n$ -th iteration

$$\delta_n = \rho(L_{(M)}\tilde{\varphi}_n(x) - \varphi^*(x)).$$

The symbols  $M_i, N_i$  denote number of grid nodes and number of path of the frequency polygon method used for solving linear integral equation on  $i$ -th iteration. The theory of the Monte Carlo method widely uses the concept of computational cost [1]. The problem of choice of optimal relation between the number of path  $N_i$  and the number of grid nodes  $M_i$  for the linear and nonlinear integral equation was solved in  $L_2$ -metric [1]. Analogical problem in  $C$ -metric was solved for the "free-path" estimation [2].

In this work we consider  $C$ -approach [3] in which the metric of the function space  $C(D)$  is used as

$\rho(.)$  and

$$\delta_n = \sup_{x \in D} |L_{(M)}\tilde{\varphi}_n(x) - \varphi^*(x)|.$$

Relation of the form

$$P(\delta_n < T(n, M_1, \dots, M_n, N_1, \dots, N_n)) > 1 - \varepsilon, \quad (1)$$

where  $T(n, M_1, \dots, M_n, N_1, \dots, N_n) \rightarrow 0$

for  $M_i, N_i \rightarrow +\infty, \quad i = 1, \dots, n$

and for a small positive  $\varepsilon$  are obtained. From (1) follows the approach to choosing of the optimal parameters  $M_i, N_i, i = 1, \dots, n$  for fixed  $n$ . This approach consist of solving the minimization problem [1]:

$$\min_{M_i, N_i} S(M_i, N_i) \quad (2)$$

when  $T(n, M_1, \dots, M_n, N_1, \dots, N_n) = \alpha$

for the fixed level of possible error  $\alpha > 0$ . Here  $S(.)$  is the computational cost.

Let us assume that the kernel of linear integral equation on  $i$ -th iteration satisfy the condition  $k_i(y, x) \in C_y(D) \times C_x^p(D)$ . We consider two cases:  $p = 1$  and  $p = 2$ . If some additional assumptions are valid [3], then we obtain the following form for  $T$ :

$$\hat{T}(n, M_1, \dots, M_n, N_1, \dots, N_n) = C_{1,p} \sum_{i=1}^n \frac{q^{n-i}}{M_i^{p/l}} + \mu C_2 \sum_{i=1}^n \frac{q^{n-i} \sqrt{M_i}}{\sqrt{N_i}}.$$

Here  $l$  is the dimensionality of the space. Constants  $C_{1,p}$  and  $C_2$  are estimated the basis of the preliminary calculations by a maximum of the variance and the upper bound of the  $p$ -order derivatives correspondingly.

The computational cost of considered method is proportional to the value

$$S(n, M_1, \dots, M_n, N_1, \dots, N_n) = t \cdot \sum_{i=1}^n N_i,$$

\*Abstract 5191 submitted to the 21st International Symposium on Rarefied Gas Dynamics, Marseille, France, July 26-31, 1998

where  $t$  designate the average cost of computing the path. Solving problem (2), we obtain the following optimal relations:

$$\begin{aligned} M_n &= \left( \frac{C_{1,p}(2p+l)(1+Q)}{l} \right)^{1/p} \alpha^{-1/p}, \\ N_n &= \frac{\mu^2 C_2^2 l^2}{4p^2 C_{1,p}^2} M_n^{(l+2p)/l}, \\ M_i &= M_n \cdot q^{\frac{(n-i)l}{l+3p}}, \\ N_i &= N_n \cdot q^{\frac{(n-i)(l+2p)}{l+3p}}, \quad i = 1, \dots, n-1, \\ Q &= \sum_{i=1}^{n-1} q^{\frac{(n-i)(l+2p)}{l+3p}}. \end{aligned} \quad (3)$$

Thus, the value  $M_i$  and  $N_i$  are connected by the following relation:

$$N_i M_i^{-(l+2p)/l} = \frac{\mu^2 C_2^2 l^2}{4p^2 C_{1,p}^2}.$$

Here  $\mu$  has a form:

$$\begin{aligned} \mu^2 &= 2 \ln \left( \frac{M_n}{1 - q^{\frac{l+3p}{l+3p}}} \right) - \ln \ln \left( \frac{M_n}{1 - q^{\frac{l+3p}{l+3p}}} \right) - \\ &\quad - 2 \left( \ln \left( (-\ln(1-\epsilon)/2) \right) - \frac{\ln 4\pi}{2} \right). \end{aligned}$$

Then we obtain the following minimal value of computational cost:

$$S_* \sim \alpha^{\frac{(l+2p)}{p}} \ln \alpha^{-1/p}.$$

The optimal relations (2) are tested for the model kinetic equation (BGK) for a classical problem on heat transfer between two infinite plane. The computational experiments with the optimal relations (3) show that obtained error does not exceed the fixed level of possible error  $\alpha$ .

## References

- [1] Mikhailov G.A., *New Monte Carlo methods with estimating derivatives*. Utrecht: VSP, 1995.
- [2] Plotnikov M.Yu., *Using the weighted Monte Carlo method for solving nonlinear integral equations.* // Rus.J.Numer.Anal.Math Modelling, 9, N 2, 1994, p.121-147
- [3] Shkarupa E.V., Voytishek A.V., *Optimization of discrete-stochastic procedures in estimating globally the solution of an integral equation of the second kind.* // Rus.J.Numer.Anal.Math Modelling, 12, N 6, 1997, p.1-21

# Angular Momentum Conservative Algorithm of Collisional Process in DSMC Method \*

P.A. Skovorodko

Institute of Thermophysics SB RAS, Novosibirsk, Russia

## 1 Introduction

The traditional algorithm of collisional process in DSMC method, used for calculation of velocities of molecules after collision, is based on the conservation laws for linear momentum and total energy [1]. This algorithm does not provide conservation of angular momentum with respect to some axis, but for non-rotating flow this circumstance is insignificant, since the mean value of angular momentum of such kind of flow is equal to zero.

The situation changes for axisymmetric flow with rotation. In this case the traditional procedure leads to some internal source or sink of angular momentum that may distort the flowfield.

In this paper the investigation of the above effect is made. The angular momentum conservative (AMC) algorithm of collisional process is proposed.

## 2 Problem Formulation

The investigations were made for one-dimensional axisymmetric flow of monoatomic gas in the tube with specular wall. The evolution of initially swirling flow during the time was studied. The gas in the tube with uniform initial density  $n_0$  and temperature  $T_0$  and equilibrium distribution function was assumed to start rotating as a solid body, the initial tangential speed on the wall being equal to  $v_w$ . For given molecular model the problem contains two governing parameters: the Knudsen number  $Kn$ , defined by the ratio of the mean free path in the gas at  $t = 0$  to the radius of the tube  $r_t$ , and the speed ratio  $S_w = v_w / \sqrt{2RT_0}$ . For any values of  $Kn$  and  $S_w$  there should be no temporal dependence of total energy  $E$  and total angular momentum  $I$  of the gas. The computations show that this condition is satisfied only for  $E$ .

Fig.1 illustrates the dependencies of  $I/I_0$  on the time for some of considered variants for  $S_w = 1$ . The time is normalized by the value of  $t_0 = 2\pi r_t / v_w$ , so  $t/t_0$  represents the number of revolutions of solid body with  $v(r_t) = v_w$ .

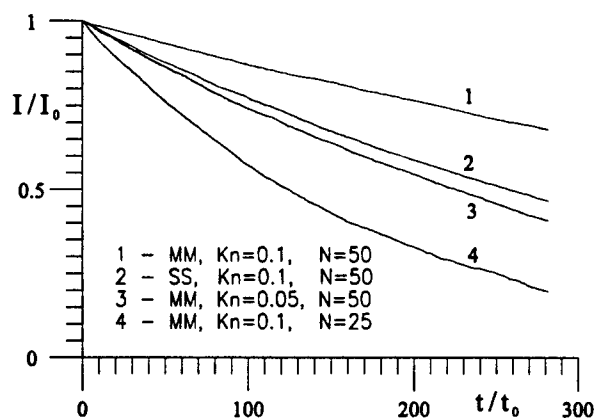


Figure 1: Temporal dependence of total angular momentum

As can be seen from Fig.1, for all of the variants the decreasing of  $I/I_0$  with increasing of  $t/t_0$  is observed. For given  $Kn$  the effect is more pronounced for solid sphere molecules (SS) in comparison with VSS molecular model for Maxwell molecules (MM). The effect depends on the Knudsen number: the less  $Kn$  the more the effect. But the highest sensitivity of the effect is observed to the grid size: changing the number  $N$  of cells from 50 to 25 causes the same effect as the decrease of the Knudsen number approximately by 4 times.

Due to the dependence of  $I(t)$  it is difficult to obtain steady solution of the problem except terminal one, when at  $t \rightarrow \infty$  the gas will stop with uniform density  $n_0$  and temperature  $T = 2E/3R$ .

## 3 AMC Algorithm

The reason of temporal dependence of total angular momentum is quite clear: the colliding molecules

\*Abstract 5217 submitted to the 21st International Symposium on Rarefied Gas Dynamics, Marseille, France, July 26-31, 1998

have different radial coordinates  $r_1, r_2$ , that leads to the difference in angular momentum  $m_1 v_1 r_1 + m_2 v_2 r_2$  of these molecules before and after collision ( $v$  denotes the tangential component of velocity of the molecule). To provide the conservation of angular momentum the algorithm of collisional process should be changed. One possible variant of AMC algorithm is as follows.

Let us denote by  $u$  the vector containing axial and radial components of velocity of molecule. The post-collision velocities calculated by traditional procedure will be denoted by symbol  $*$ , while the symbol  $'$  will be used for these velocities in the proposed algorithm.

The algorithm is based on conservation law of angular momentum  $m v r$  for tangential component of velocity instead of linear momentum  $m v$ . That is why the post-collision tangential velocities are calculated by usual relations [1], with the value of  $m_i$  being replaced by the product  $m_i r_i$ . The obtained velocities  $v'_1, v'_2$  provide precise conservation of angular momentum, but the post-collision energy of molecules differs from the pre-collision one. To provide energy conservation the correction of velocities  $u'_1$  and  $u'_2$  is needed. To do this correction the analysis of energy defects  $dE_i = m_i (v_i'^2 - v_i^2)$  is made. Three possible relations between energy defects  $dE_i$  and velocities  $u_i^*$  are as follows.

1. If  $m_1 u_1^{*2} > dE_1$  and  $m_2 u_2^{*2} > dE_2$ , both components of vectors  $u_i^*$  are corrected by the factor  $\sqrt{1 - dE_i / m_i u_i^{*2}}$ .
2. If  $m_1 u_1^{*2} + m_2 u_2^{*2} > dE_1 + dE_2$ , the correction factor for components of both velocities  $u_i^*$  is the same and equal to  $\sqrt{1 - (dE_1 + dE_2) / (m_1 u_1^{*2} + m_2 u_2^{*2})}$ .
3. If none of the above conditions is satisfied, the collision is considered to be "bad" and is not performed, i. e. the molecules conserve their pre-collision velocities.

The computations show that the relative number of collisions of types 1 and 2 is about 99% and 1%, respectively. The relative number of "bad" collisions never exceeds  $10^{-4}$ , so the effect caused by the neglecting of these collisions is small.

The described algorithm provides precise conservation of angular momentum and energy. All the curves, presented in Fig.1 transform into straight line  $I/I_0 = 1$ , if this algorithm is applied.

The proposed algorithm enables to obtain the steady solution of the considered problem. This solution proves to be the same, as the prediction of Navier-Stokes theory and has the following features.

1. The flow is isothermal.
2. The gas rotates as a solid body ( $v = v_w r / r_t$ ).
3. The radial distribution of density is described by the relation  $n(r) = n(0) \exp(v^2 / 2RT)$ .
4. The solution is completely determined by the values of  $n_0, E, I$  and does not depend on the way of initial swirling.
5. The solution does not depend either on the molecular model or on the Knudsen number.

These features of the considered flow are important for understanding the nature of the Ranque effect [2, 3].

## 4 Conclusion

The proposed algorithm provides precise conservation of angular momentum and energy and may be used for simulation of flows with rotation.

It should be noted, however, that the improvement of the results, obtained by this algorithm may be important only for the problems without external source or sink of angular momentum. If solid surface with diffuse reflection is in the flowfield, the changes in angular momentum, caused by this surface will be much greater than those, caused by nonconservative nature of traditional algorithm of collisional process. For such kind of flows there is no need to use the proposed algorithm, especially taking into account that it takes 10% – 15% more CPU time.

Nevertheless, for some problems the application of proposed algorithm is advisable. An example of such kind of problem is the Ranque effect [2], which nature is determined by conservation of angular momentum of the gas flow in the vortex tube [3].

## References

- [1] Bird G.A., *Molecular Gas Dynamics and Direct Simulation of Gas Flows*, Oxford, Clarendon, 1994.
- [2] Ranque G.J., *Experiences sur la Detente Giratoire avec Productions Simultanees d'un Enchappement d'Air Chaud et d'un Enchappement d'Air Froid*, J. Phys. Radium, 4, pp. 112 - 114, 1933.
- [3] Rebrov A.K., Skovorodko P.A., *The Ranque Effect in Rarefied Gas*, Abstract 5218 submitted to the 21st International Symposium on Rarefied Gas Dynamics, Marseille, France, July 26-31, 1998.

# The Ranque Effect in Rarefied Gas \*

A.K. Rebrov, P.A. Skovorodko  
Institute of Thermophysics SB RAS, Novosibirsk, Russia

## 1 Introduction

The effect of separation of air flow into hot and cold flows in a vortex tube was discovered in 1933 by Ranque [1] and has been the subject of many studies. In spite of its widely use for cooling applications, till now the nature of the effect has not been completely understood.

In this paper the simulation of the flow in the vortex tube is made in order to study, whether the Ranque effect is observed in rarefied gas.

## 2 Flow in the Vortex Tube

The length of studied vortex tube was 10 times its radius  $r_t$ . The radius of orifice for cold flow, that is placed on the left end of the tube, was chosen to be  $r_c/r_t = 0.5$ . On the right end of the tube the ring-shaped orifice for hot flow, formed by the tube wall and the disc with radius  $r_h$  is placed. The injection of molecules into the tube was organized from the rotating band of evaporating surface with saturation pressure  $p_0$  and temperature  $T_0$ . The band of width of  $\delta$  was placed on the tube wall, the distance from the left end of the tube to the middle of the band being equal to  $r_t$ . The linear velocity of rotation of band is  $v_\varphi$ . The full absorption of incident molecules on the band surface and specular reflection on other solid surfaces of the tube were assumed. The gas outside the tube was assumed to be equilibrium with pressure  $p_e$  and temperature  $T_e$ .

The flow of monoatomic gas in the tube was simulated by DSMC method with angular momentum conservative algorithm of collisional process [2]. For given molecular model, geometry of the tube and temperature ratio  $T_0/T_e$  the problem contains three governing parameters: the Knudsen number  $Kn$ , defined by the ratio of the mean free path in the gas outside the tube to the radius of the tube, the speed ratio  $S_\varphi = v_\varphi/\sqrt{2RT_0}$  and the pressure

ratio  $p_0/p_e$ . Most simulations were performed for  $T_0 = T_e$ ,  $Kn = 0.2$  and  $S_\varphi = 1$  for VSS molecular model for Maxwell molecules. Uniform grid containing  $20 \times 50$  cells was used.

The fluxes of mass ( $M$ ), energy ( $E$ ) and angular momentum ( $I$ ) on three control surfaces (band, cold and hot outlet orifices) were stored during the simulation. The inlet and outlet fluxes through each control surface will be denoted by upper symbol  $+$  and  $-$ , respectively, while lower symbols  $b$ ,  $c$  and  $h$  will be used to denote the corresponding control surfaces. On the steady stage the condition  $M_b^+ + M_c^+ + M_h^+ = M_b^- + M_c^- + M_h^-$  and similar conditions for fluxes  $E$  and  $I$  should be satisfied.

Let us denote by  $q$  the fraction of total mass flux that is issued out through the cold outlet orifice  $q = (M_c^- - M_c^+)/((M_b^+ - M_b^-))$ , and by  $\bar{E}_i$  the mean specific energy of gas flow through the corresponding surface. Since the mean specific energy of molecules injected from the band is equal to  $RT_0(2 + S_\varphi^2)$ , it is advisable to introduce specific heat capacity  $C_p = R(2 + S_\varphi^2)$  and transform the values of  $\bar{E}_i$  into stagnation temperatures  $\bar{T}_i$  using the relation  $\bar{T}_i = \bar{E}_i/C_p$ . The Ranque effect consists of the inequality  $\bar{T}_c < \bar{T}_b < \bar{T}_h$ .

Fig.1 illustrates the streamline picture in the vortex tube flowfield for  $\delta/r_t = 0.1$ ,  $p_0/p_e = 6$  and  $r_h/r_t = 0.98$ , the value of  $q$  at these conditions being equal to 0.62. As can be seen from this picture, the flow is of complex character with secondary vortex in meridional plane.

The results for cooling effect  $\Delta\bar{T}_c = \bar{T}_b - \bar{T}_c$  dependence on cold mass flux fraction  $q$  for  $T_0 = 300K$  are shown in Fig.2 by symbols for three values of ratio  $p_0/p_e$  and  $\delta/r_t = 0.06$ . The results for  $p_0/p_e = \infty$ , corresponding to the case of expansion into vacuum, were obtained for  $p_0/p_e = 6$  by neglecting the inlet fluxes through cold and hot orifices. The studied range of  $q$  corresponds to the range of  $0.9 \div 1$  for  $r_h/r_t$ .

The shown results illustrate that the Ranque effect not only takes place in rarefied gas, but has the values, close to those in continuum flow. It should be noted, that traditional collisional procedure, that

\*Abstract 5218 submitted to the 21st International Symposium on Rarefied Gas Dynamics, Marseille, France, July 26-31, 1998



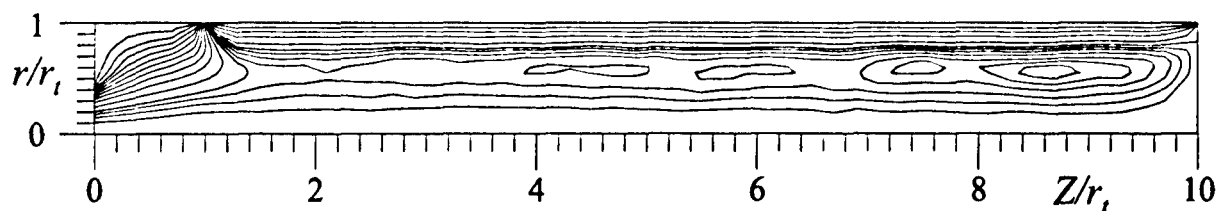
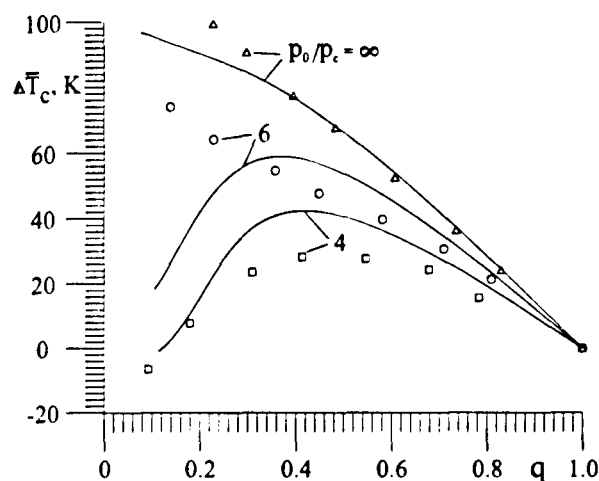


Figure 1: Streamline picture of the flow in the vortex tube

does not provide conservation of angular momentum [2], distorts the flowfield in the vortex tube and reduces the cooling effect by 10 – 20 K for middle values of  $q$ .


 Figure 2: The dependence of cooling effect on the cold mass flux fraction  $q$ 

### 3 One-Dimensional Model

The main features of the flowfield in the vortex tube, obtained by the simulation are small gradients of temperature and linear dependence of tangential velocity on the radius. Based on these results and on the features of steady swirling flow in the tube with specular wall [2], the following one-dimensional model of the Ranque effect was developed.

The radial distribution of parameters of isothermal steady flow in the vortex tube is determined by three values: temperature  $T$ , density on the axis  $n(0)$  and the tangential velocity on the tube wall  $v_w$ . The radial distributions of tangential velocity and the density are described by the relations  $v = v_w r/r_i$ ,  $n(r) = n(0) \exp(v^2/2RT)$  [2].

Based on these distributions and on tube geometry, the fluxes  $M_i^{+-}$ ,  $E_i^{+-}$  and  $I_i^{+-}$  may be determined. The conservation conditions for these fluxes

will give three relations, that allow one to find the unknown values of  $T$ ,  $n(0)$  and  $v_w$ .

The results for cooling effect obtained by this model are shown in Fig.2 by solid lines. As can be seen, these results are in good agreement with the DSMC ones. Some difference is observed for small values of  $q$ , when the two-dimensional effects became more important.

### 4 Conclusion

The Ranque effect is observed in rarefied gas and has the values, close to those in continuum flow.

The one-dimensional model of the Ranque effect provides good description of the results of numerical experiments. Similar model for continuum flow may be used for optimizing the real device.

The steady flow in the vortex tube is formed in the way providing the balance between inlet and outlet fluxes of mass, energy and angular momentum. The latter requirement is the most severe: for  $q \rightarrow 1$ , when the cooling effect is small, the mean angular momentum of the flow in the tube is several times more than the injected one  $\bar{I}_b$ . This circumstance gives the key for understanding the nature of the effect: the difference in stagnation temperatures  $\bar{T}_c$  and  $\bar{T}_h$  is mainly determined by the difference in angular momentum of corresponding fluxes.

### References

- [1] Ranque G.J., *Experiences sur la Detente Girationnelle avec Productions Simultanees d'un Enchappement d'Air Chaud et d'un Enchappement d'Air Froid*, J. Phys. Radium, 4, pp. 112 – 114, 1933.
- [2] Skovorodko P.A., *Angular Momentum Conservative Algorithm of Collisional Process in DSMC Method*, Abstract 5217 submitted to the 21st International Symposium on Rarefied Gas Dynamics, Marseille, France, July 26-31, 1998.

# Solution of Boltzmann Equation for Arbitrary Molecular Potentials \*

F.G.Tcheremissine  
Computing Center of RAS, Moscow, Russia

Conservative Discrete Ordinates Method (CDOM) previously used for a gas of hard sphere molecules [1] is applied for a general form of central-symmetric molecular potential. This extension of the method permits more adequate modeling of flows of real gases.

The CDOM requires the evaluation of "post-collision" velocity vectors  $\xi'$  and  $\xi'_1$  for a pair of velocity nodes  $\xi$  and  $\xi_1$  entering in the formulae of numerical evaluation of the 8-dimension  $Q$ -integral which projections into velocity space nodes give conservative estimates of Boltzmann collision integrals. For hard sphere molecules the vectors  $\xi'$  and  $\xi'_1$  are evaluated analytically, but for a general case the solution of a well-known integral equation [2] which determines the deflection angle for given collision parameters is needed. Such subroutine is included in a general program. Before the main computation begins it precalculates all needed for numerical integration velocity vectors (more precisely, the numbers which corresponds to these vectors in arrays of the distribution function) and then the computed values are used in a number of space nodes and at different iterative steps. Consequently, the computational time don't exceeds much that for hard sphere molecules.

The method was tested on a problem of a steady shock wave structure in a mono atomic gas. The following molecular potentials were used: hard sphere molecules; inverse power potential with different exponent; Lennard-Jones (6,12) potential; Shtockmeier potential  $\phi(r) = 4\epsilon[(\sigma/r)^{12} - (\sigma/r)^6 - \delta(\sigma/r)^3]$ , in which the last term presents the effect of interaction of polarized molecules; Coulomb potential. The computations for Coulomb potential were made under the assumption of binary interactions of a finite range [2]. For all considered potentials convergent solutions of Boltzmann equation were obtained and shock wave structure plots compared. Namely, the comparison of graphics for

Lennard-Jones and Shtockmeier potential for about the same parameters  $\epsilon$  and  $\sigma$  (Argon and Water vapor taken at different temperature were considered) has shown the influence of the polarization force. The comparison of calculated profiles for Argon with experimental data [3] has shown a good agreement.

The constructed module of collision integral evaluation is universal and can be used for solving two- and three-dimensional problems as well.

## References

- [1] Tcheremissine F.G., *Conservative Discrete Ordinates Method for solving of Boltzmann kinetic equation*, Proceedings of 20-th Internat.Symp.on RGD, Ching Shen ed., Peking Univ.Press, Beijing, China, pp.297-302, 1997.
- [2] Chapman S. and Cowling T., *The mathematical theory of non-uniform gases*, Cambridge University Press, 1952.
- [3] Schmidt B., *Electron beam density measurements in shock waves in Argon*, J.Fluid Mech., Vol.39, N 2, pp.361-373, 1969.

\*Abstract 5247 submitted to the 21st International Symposium on Rarefied Gas Dynamics, Marseille, France, July 26-31, 1998

# Direct Simulation Monte-Carlo of Inviscid Flows Method and Examples \*

I.V. Voronich, M.M. Moiseev, V.V. Popov, Yu.I. Khlopkov  
Moscow Institute of Physics & Technology Russia

## 1. Introduction

On the basis of the approach adopted in Direct Simulation Methods (the splitting scheme, the ensemble of modeling particles) the analysis of possibility of calculations of inviscid flows using local-equilibrium function  $f_0$  is performed. Using well-known results in this field and calculation algorithms [1,2,3] the approximation characteristics of the method are obtained.

## 2. Algorithm description

The main features of the method are following. In accordance with [3] the particles are uniformly distributed across the cell at each time step before the stage of transition, the ensemble of the velocities is simulated according to [3,4] as

$$\xi_{x_i} = \sqrt{2RT} \sqrt{-\ln \alpha_1} \cdot \sin(2\pi\alpha_2),$$

where  $\alpha_1, \alpha_2$  are uniformly distributed on (0,1) random values. The correction of the velocities ensemble is performed for the energy and impulse conservation. The size of the cells is chosen in accordance with the condition of small changes of macroparameters across the size of the cell, that is as in continuum mechanics. Boundary conditions are the mirror reflection of the particles from the body and the conditions on the outer boundaries are as in RGD. The analysis of the approximation features shows that the algorithm under the given conditions simulates inviscid flows with the first order of accuracy for the time and space variables. The time of calculations by means of this method proves to be less than that in calculations of rarefied gas flows because the coordinates and velocities of the particles are not stored, but they are calculated at each time step. If it is necessary to restrict the time of calculation, weighting factors are used [5] so that the level of statistics is

limited. Inner degrees of freedom are taken into account by simple distribution of mean internal energy of particle in equilibrium state.

The following problems were taken as the calculated examples:

- a) the piston problem (examination of validation of the Rankine - Gugeniot conditions);
- b) the Riemann problem (standard test in gas dynamics, practical examination of monotony);
- c) supersonic flows past a wedge and a cone (examinations of the attached shock waves positions);
- d) supersonic flows past wedge- and cone-shaped bodies at the separated shock wave regimes [6] (sufficiently complicated problem in gas dynamics);
- e) supersonic flow past a flat-nosed body (one of the typical problems that are used in spatial examinations of calculation methods [7]),
- f) supersonic flow past a flat-nosed body with heater in the flow in front of the body (the test for the possibilities of the method and examination of the decrease of  $C_x$  for blunt-nosed bodies).

The features of the numerical data obtained will be discussed in the report. Some results are shown on Fig. 1,2 (the cone, the wedge with separated shock wave).

The questions of the statistical fluctuations influence on the results (especially in unsteady flows) and more thorough consideration of inner degrees of freedom are to be examined in the future.

\* Abstract 5292 submitted to the 21st International Symposium on Rarefied Gas Dynamics, Marseille, France, July 26-31, 1998

### 3. Conclusions

The method discussed proved to be well adapted to flows with complicated geometry; there is an opportunity to use triangle cells which was made in calculations of flows past sharp-nosed bodies. Also there is an opportunity to take into account chemical processes [8] and various physical fields. Besides on the basis of this method it is possible to build finite-difference schemes for gas dynamics both the first and the second degree of accuracy in the space, which possess monotony and compact template, that will be shown in the second report (some work in this field is discussed in [9]).

This work is supported by Russian Fund of Fundamental Research grant 96-15-96063.

### References

- [1] M.N. Kogan, A.S. Kravchuk, Yu.I. Khlopkov. 'Relaxation-transition' method for calculation of flows in wide diapason of rarefaction. TsAGI Scientific Notes, Vol.XIX, No.2, pp.106, 1988 (in Russian).
- [2] D.I. Pullin. Direct Simulation Methods for Compressible Inviscid Ideal-Gas Flow. J. Comput. Phys., Vol.34, No.2, pp. 231, 1980.
- [3] Yu.I. Khlopkov, A.S. Kravchuk. Direct statistic simulation methods of three - dimensional flow over bodies by inviscid gas. Book of abstracts of 17th Symposium on Rarefied Gas Dynamics, Aachen, pp.584, 1990.
- [4] A.A.Abramov, A.S. Kravchuk, V.V.Podlubny. Statistical simulation of gas surface injection in moving flow. J. of Comput. Math. and Math. Phys., Vol.31, No.12, pp.1849, 1991 (in Russian).
- [5] G.A. Bird. Molecular Gas Dynamics and Direct Simulation of Gas Flows.-Oxford: Oxford Univ. Press, 1994.
- [6] S.V.Mikhailov, N.S. Yatskevich. Calculation of space flows over sharp bodies in regimes with separated shock wave. TsAGI Scientific Notes, Vol. XXII, No.6, pp.27, 1991 (in Russian).
- [7] O.M. Belotzerkovsky. Numerical simulation in continuum mechanics. Moscow: Science, 1994 (in Russian).
- [8] A.A. Abramov, A.S. Kravchuk. Action of heat pulse on the surface in tangential flow. Transactions of USSR Academy of Sciences. Mechanics of Fluid and Gas, No.1, pp.139, 1994 (in Russian).
- [9] T.G. Elizarova, I.A. Graur, A. Chpoun, J.C. Lengrand. Comparison of Continuum and Molecular Approaches. Proc. of 19th Symposium

on Rarefied Gas Dynamics, Vol.2, pp.780, Oxford, 1995.

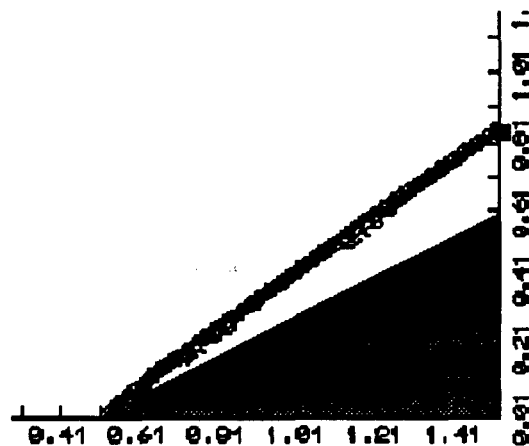


Figure1. Conic supersonic flow.

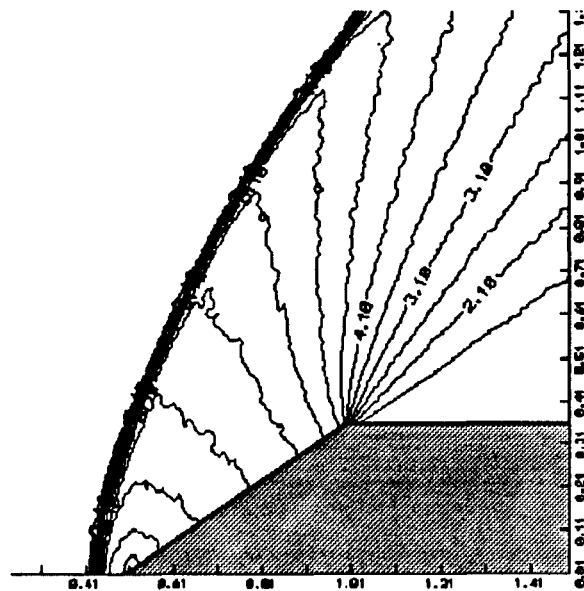


Figure2. Wedge supersonic flow with separated shock.

# Monte-Carlo Network Machine Its application in problems of direct numerical modeling (aerodynamic problems)\*

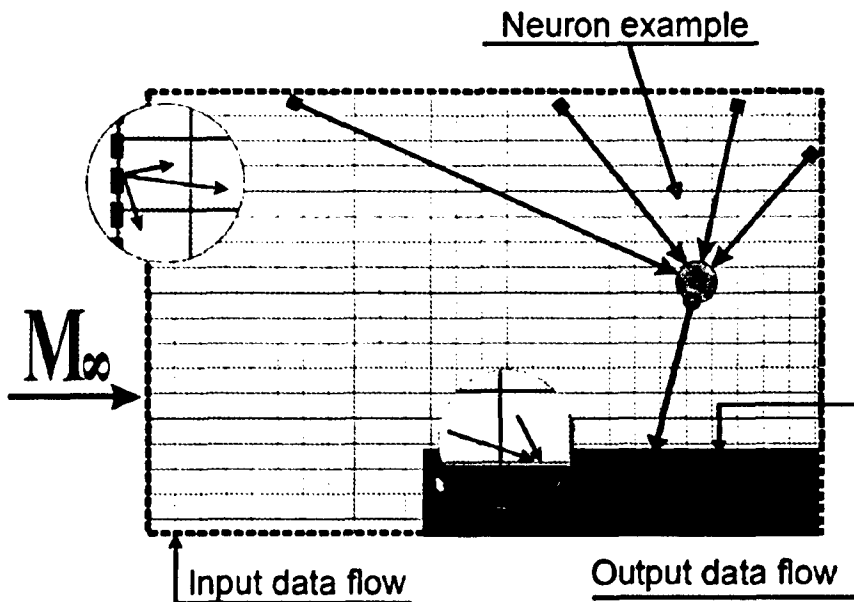
Khlopkov Yu., Kuzyakin D.  
Moscow Institute of Physics and Technology

Method of the neural networks construction based on a stochastic neuron design and trainee on problems of direct numerical modeling is offered in work.

Main idea of Monte-Carlo network machine construction is weight factors replacement in neuron gear functions and selection criterion which based on analysis of entropy signals distribution arriving from acson of each neuron during network training. The considering machine is single-level neural network. Each neuron presents elementary perseptron. The resulting signal from acson of each neuron

participates in formation total output flow of a training network. The signals gear functions factors in each of synapses are determined equiprobably in a specified interval (as a rule from 0 up to 1).

As a given network application example a problem of flow modeling around end face cylinder by a supersonic flow is considered. Neural network training data (input data) are initials parameters of molecules inleting in a cylinder zone flow. Output data are, accordingly, distribution of pressure on a cylinder surface.

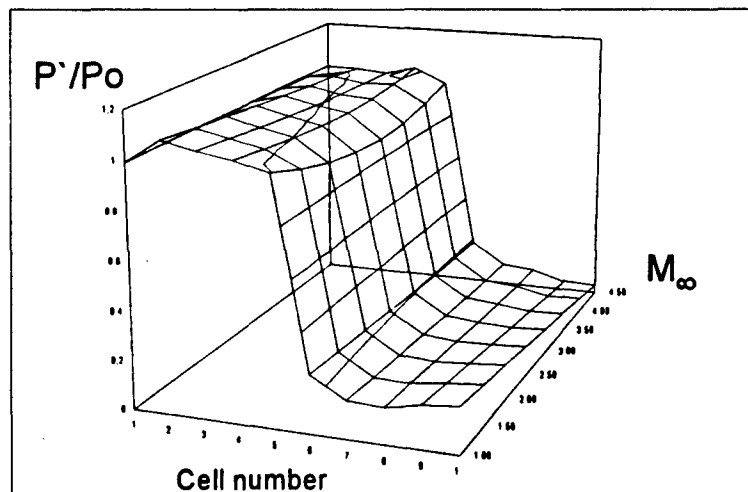
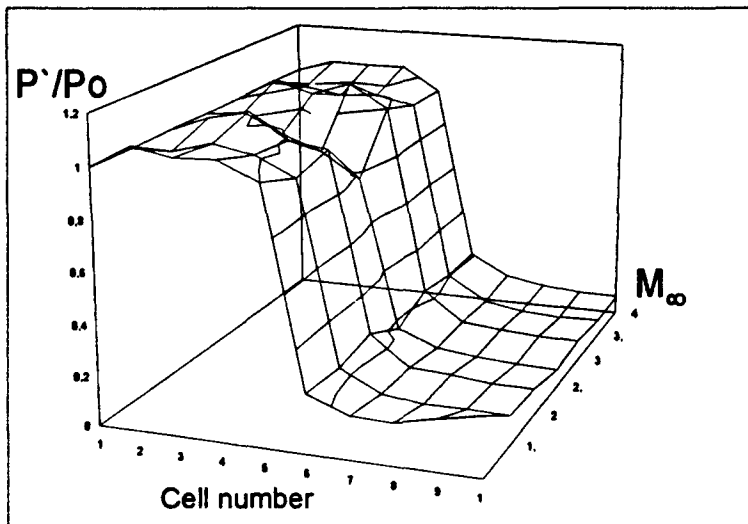


\* Abstract 5294 submitted to the 21st International Symposium on Rarefied Gas Dynamics, Marseille, France, July 26-31, 1998

## NUMERICAL SIMULATION - NS P

Trained network should predict behavior of pressure distribution on a cylinder for conditions not participating in training. Below shown two histograms. First is distribution of pressure to a cylinder surface depending on Mach number of acting flow. This data received by the direct numerical

modeling program are represented. On second data processing through neural network are presented. Besides it on second histogram we can to see extrapolation of distribution for Mach numbers not participating in training.



This work is supported by Russian Fund of Fundamental Research grant 96-01-00715 and state program for leading research groups support (96-15-96063).

# Effects of Species Weighting Factors On Intermolecular Collisions in the DSMC Method \*

Jeff C. Taylor

The Johns Hopkins University Applied Physics Laboratory, Laurel, Maryland USA

## 1 Introduction

The use of weighting factors is an integral part of the Direct Simulation Monte Carlo (DSMC) method.<sup>1,2</sup> The primary weighting factor used in the DSMC method, generally termed *Fnum*, allows one to simulate flows with a representative sample of the actual number of real molecules. This feature alone allows the DSMC method to be applied to most rarefied problems of interest. Without this feature, the applicability of the method would be critically lessened.

Other types of weighting factors can also be employed in the DSMC method. One weighting factor, generally termed the radial weighting factor, can be employed to aid in maintaining a uniform distribution of simulated particles in axisymmetric simulations. However, certain studies<sup>2,3</sup> have illustrated possible undesirable effects under certain conditions and guidelines have been established<sup>2</sup> for minimizing these so-called random walk effects.

The weighting factors of interest in this study are the species weighting factors used to overcome the large statistical fluctuations associated with minor species properties. Many problems involving combustion exhaust, optical signatures, spacecraft contamination and many others can be driven by effects from species which exist in orders of magnitude lower amounts than the other species. A few examples of these types of problems where the DSMC method using species weighting factor models have been developed and/or employed are the representation of species separation in rarefied nozzle back-flow regions,<sup>4</sup> optical signatures from contaminants and plumes,<sup>5</sup> expansion flows involving large species concentration variations,<sup>6</sup> and spacecraft glow<sup>7</sup> to name a few.

Many of these studies use species weighting factors, but do not present effects of the species weighting

factors on the conservation laws during collision selection, collision energy and momentum exchange, and reactions. Though earlier the use of species weighting factors was introduced and supported by Bird,<sup>1</sup> the new investigations presented in his latest book<sup>2</sup> recommend against their use. More recently, researchers have presented studies examining the impact of species weighting factors for some specific cases.<sup>8,9</sup> Additionally, a conservative weighting factor scheme has been proposed by Boyd<sup>9</sup> which quantitatively addressed weighting factors and how to implement them for their problem of interest.

Most of the species weighting factor models are based on the same basic concept which allows for energy and momentum exchange in collisions to occur only part of the time. The probability for this exchange is the ratio of the weighting factors of the two colliding species. For the case of a single collision in which the energy and momentum are not exchanged, conservation of momentum and energy are not conserved. The species weighting scheme proposed by Boyd<sup>9</sup> adds the ability to monitor this deviation from total momentum and energy conservation and periodically corrects the loss in each computational cell. Thus, the new method still does not conserve momentum and energy at the microscopic levels, but only conserves them on average.

The goal of the paper is to quantitatively study the effects of several different species weighting factor models for a variety of cases in an attempt to quantify at least one aspect of the problem. That is, the conservation, or lack thereof, of total momentum and energy in the system as a function of the number of collisions for a variety of weighting factor ranges.

## 2 Approach

A 0-D DSMC code will be employed with several different weighting factor approaches to look at

\*Abstract 6406 submitted to the 21st International Symposium on Rarefied Gas Dynamics, Marseille, France, July 26-31, 1998

the time dependent variation in total energy and momentum of an isolated system as functions of weighting factor for a two species gas.

For this problem, the exact solution for a method which conserves momentum and energy explicitly at the microscopic level during collisions is simple: Total momentum and energy of the system will remain constant. Thus, this is an ideal problem to examine the effects and rates of any conservation losses due to non-conservative methods.

Since it is during intermolecular collisions between the differently weighted species that conservation is questioned, any conservation losses can be expected to be functions of the collision frequency between the different species and of the ratio of the different species weighting factors. For those methods that do not conserve momentum and energy, the percent loss as a function of weighting factor and collision frequency will be determined. For those that do not microscopically conserve momentum and energy, discussion will be presented to address the flow times required for conserving on average.

The above study addresses only the conservation of momentum and energy. Since reactions are not considered, mass is explicitly conserved. However, for subsequent studies involving understanding the effects of species weighting factors during the reaction process, mass conservation effects will need to be addressed.

## References

- [1] Bird, G. A., *Molecular Gas Dynamics*, Oxford University Press, London, 1976.
- [2] Bird, G. A., *Molecular Gas Dynamics and the Direct Simulation of Gas Flows*, Oxford University Press, New York, 1994.
- [3] Deng, H., Stark, J., and Liddell, H., "An Investigation Into the Effect of Weighting Factor on Computational Performance in 2D Axisymmetric Flow Past a Flat-nosed Cylinder", *Rarefied Gas Dynamics 20*, edited by C. Shen, Peking University Press, Beijing, 1997, pp. 155-161.
- [4] Chung, C. H., DeWitt, K. J., Jeng, D. R., and Penko, P. F., "DSMC Analysis of Species Separation in Rarefied Nozzle Flows", AIAA Paper 92-2859, July, 1992.
- [5] Elgin, J. and Bernstein, L. S., *The Theory Behind the SOCRATES Code*, Phillips Laboratory Report PL-TR-92-2207, August, 1992.
- [6] Bartel, T. J. and Justiz, C. R., "DSMC Simulation of Ionized Rarefied Flows", AIAA 93-3095, July, 1993.
- [7] Collins, R. J., Dogra, V. K., and Levin, D. A., "Modeling of High Altitude Spacecraft Environments", AIAA Paper 97-0987, January, 1997.
- [8] Wysong, I. J. and Campbell, D. H., "Comparison of DSMC Predictions with Temporally Resolved Vibrational State Measurements in NO", *Rarefied Gas Dynamics 19*, edited by J. Harvey and G. Lord, Vol. 1, Oxford University Press, New York, 1995, pp. 592-598.
- [9] Boyd, I. D., "Conservative Species Weighting Scheme for the Direct Simulation Monte Carlo Method", *Journal of Thermophysics and Heat Transfer*, Vol. 10, No. 4, Oct.-Dec., 1996, pp. 579-585.



# Rarefied Aerothermodynamic Predictions for Mars Global Surveyor \*

R. G. Wilmoth<sup>1</sup>, D. F. G. Rault<sup>1</sup>, R. W. Shane<sup>2</sup>, R. H. Tolson<sup>2</sup>

<sup>1</sup> NASA Langley Research Center, Hampton, VA, USA

<sup>2</sup> George Washington University, Hampton, VA, USA

## Abstract

Mars Global Surveyor (MGS) is the first planetary mission designed to use aerobraking as a primary means of customizing its orbit in order to achieve its mission objectives [1]. The aerobraking requirements together with post-launch anomalies [2] have presented a unique challenge to provide accurate predictions of the aerothermodynamic environment of the spacecraft in the rarefied transitional flow regime. A variety of three-dimensional Direct Simulation Monte Carlo (DSMC) and free-molecular techniques have been used to satisfy the prediction requirements, and this is the first major planetary mission in which rarefied-flow predictions have played such a critical role all the way through the design, mission planning, and operational phases. The purpose of this paper is to discuss these requirements, describe the particular three-dimensional DSMC and free-molecular tools used, and present selected results from the computational studies.

The studies performed include pre-launch aerodynamic and heating predictions that were used (1) in the design of the solar panel arrays which are the principal drag-producing components, (2) in the mission planning for selecting specific aerobraking parameters, e.g., altitude, attitude limits, and panel sweep angles and (3) to investigate specific issues such as aerodynamic interactions caused by reaction control jet firings [3]. Incomplete deployment of one of the solar arrays shortly after launch produced additional analysis requirements: (1) to devise an alternate aerobraking configuration and confirm its aerodynamic characteristics, (2) to investigate specific aerodynamic heating issues arising for this modified configuration, and (3) to re-define the aerodynamic databases needed for atmospheric density reconstruction from on-board ac-

celerometer measurements. Finally, anomalous deflections of the partially-deployed solar panel that occurred in the early drag passes required extensive analyses to determine the aerodynamic stability of alternate configurations that might reduce these deflections[4].

The analyses were carried out using three-dimensional DSMC and free-molecular codes that have been developed in recent years for analyzing complex geometries. The NASA LaRC 3D DSMC code (denoted DSMC1 herein) uses an unstructured grid where each computational cell is composed of one or more elements from an underlying uniform Cartesian mesh which may be made finer near the body[5]. The body geometry is described as a discrete set of small Cartesian elements but the code retains information on local surface normals from a more exact geometry definition and allows the inclusion of a body-fitted grid region near the wall to capture Knudsen layers. The DAC (DSMC Analysis Code) code (denoted DSMC2 herein) uses a two-level Cartesian grid, where the first level is a uniform structured mesh and the second level consists of a locally refined Cartesian mesh within each first-level cell[6]. The body geometry is described as an unstructured triangular grid which clips the local Cartesian grid. Each code has certain unique advantages but both codes use similar DSMC procedures and physical models and both are capable of handling the complex geometry of the MGS spacecraft. The DSMC codes are complemented by several 3D free-molecular codes each of which uses analytical free-molecular analysis and line-of-sight shadowing techniques to model the flow about complex geometries.

Analysis of MGS aerodynamics and heating was performed primarily using DSMC1 in the design phase and in the early post-launch, pre-aerobraking phase[7], while DSMC2 was used primarily in the later post-launch, pre-aerobraking phase and in the early operational phase of aerobraking. Calculations were performed for a variety of solar panel po-

\*Abstract 6466 submitted to the 21st International Symposium on Rarefied Gas Dynamics, Marseille, France, July 26-31, 1998

sitions and spacecraft attitudes and for atmospheric densities ranging from free-molecular to transitional flow (Knudsen numbers less than 0.1). A typical geometry model used in computations with DSMC1 is shown in Fig. 1. This model was constructed from a highly detailed thermal analysis model and contains considerable details of the spacecraft bus assembly. A somewhat simplified model (not shown) was used by DSMC2. The simplified model has a similar definition of the solar panels but a simpler description of the spacecraft bus constructed from a free-molecular geometry model used for much of the mission analysis. Results obtained with each model and code demonstrate that both approaches give quite similar aerodynamic predictions in the free-molecular and transitional flow regimes. A sample comparison of drag coefficients computed for various geometry models is shown in Fig. 2 as a function of atmospheric density. The final paper will include selected results that illustrate the computational capabilities in providing the needed predictions, comparisons of the aerodynamic predictions between the various DSMC and free-molecular codes, and results that demonstrate the significant transitional flow effects on both the heating and aerodynamic behavior of MGS. Emphasis will be given to more recent results that address specific post-launch rarefied aerothermodynamic issues.

## References

- [1] Dallas, S. Sam, *Mars Global Surveyor Mission*, Proceedings of IEEE Aerospace Conference, Vol. 4, Snowmass at Aspen, CO, Feb. 1-8, 1997, pp. 173-189.
- [2] Lyons, Daniel T., *Mars Global Surveyor: Aerobraking with a Broken Wing*, AAS Paper 97-618.
- [3] Rault, D. F. G., *RCS Plume Effect on Spacecraft Aerodynamics*, 20th Rarefied Gas Dynamics Symposium, Beijing, China, August, 1996.
- [4] Wilmoth, R. G., Cheatwood, F. M., Engelund, W. C., Qualls, G. D., and Shane, R. W., *Rarefied Aerodynamics of Mars Global Surveyor Aerobraking Configurations*, Submitted to Journal of Spacecraft and Rockets.
- [5] Rault, D. F. G., *Towards an Efficient Three-Dimensional DSMC code for Complex Geometry Problems*, 18th Rarefied Gas Dynamics Symposium, Vancouver, British Columbia, July 1992
- [6] Wilmoth, R. G., LeBeau, G. J.; and Carlson, A. B., *DSMC Grid Methodologies for Computing Low-Density, Hypersonic Flows About Reusable Launch Vehicles*, AIAA Paper 96-1812, June 1996.
- [7] Shane, R. W., Rault, D. F. G., and Tolson, R. H., *Mars Global Surveyor Aerodynamics for Maneuvers in Martian Atmosphere*, AIAA Paper 97-2509, June 1997.

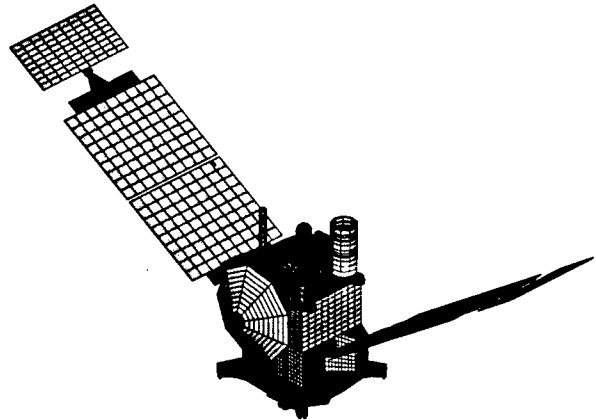


Figure 1: Detailed Pre-Launch MGS Geometry Model. (Actual surface resolution used was higher for some elements. Resolution reduced for illustration purposes only.)

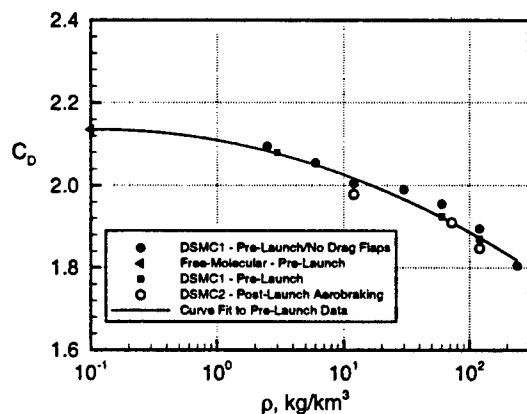


Figure 2: Comparison of Drag Predictions for Various Geometry Models and DSMC Codes.

# Calculation of Gas Flow Field in Fast Rotating Cylinder \*

V.I.Tokmantsev, A.G.Ivanov, B.T.Porodnov, V.D.Seleznev, F.Shvedov  
Ural State Technical University, Ekaterinburg, Russia

As the characteristic length of gas macroparameters change turns out to be comparable with the mean free path of molecules then the simplified hydrodynamic gas model fails and more accurate kinetic approach have to be used.

The practical aspects of conformation of kinetic results with main hydrodynamic solutions arise when investigating rarefied flow near solid surface and gas effusion into vacuum, shock wave structure studies and other applications of gas dynamics.

Optimising calculations of greatly nonhomogeneous internal flows are more difficult. In the present paper the gas flow in fast rotating cylinder for isotope volatile compounds mixture separation is described. It is known that separation effect increases in the field of countercurrent which is slow circular viscous flow relative to fast rotating cylinder walls at the condition of great radial density gradient. The Knudsen number  $Kn = \lambda/a$  ( $\lambda$  is the local mean free path of gas molecules,  $a$  is the cylinder radius) changes from  $Kn \gg 1$  at the cylinder axis, where gas inlet is usually located, to  $Kn \ll 1$  in the continual flow region near cylinder side wall. Light component outlet is usually located in the intermediate region  $Kn \sim 1$ .

Those are the peculiarities of the system under consideration that the diffusion process takes place in fast rotating mixture, the main dense flow inside is bounded by the rarefied gas, there is a transition of mass, momentum and energy through this conditional boundary, and the distribution function in molecules co-ordinates and velocities can essentially nonequilibrium in the intermediate region. On one hand, to calculate the flow in both rarefied and intermediate regions at a given input distribution function the Monte-Carlo direct simulation method is used. On the other hand, the quantitative description of steady viscous compressible flow is carried out by means of Navier-Stokes equations numerical solution at given conditions on the dense region boundaries.

However, though one can use the standard condi-

tions of nonpermeability and sticking on the cylinder solid walls, but correct flow parameters on the inside continuum boundary at  $r = r_i$  ( $Kn(r_i) \sim 0.01$ ) can be determined from the kinetic solution only.

The following iterative procedure can be used to conform the solutions for rarefied and dense regions on the boundary  $r = r_i$ . As a first approximation  $f^{(1)}(\mathbf{v}, \mathbf{r})$  to exact distribution function  $f(\mathbf{v}, \mathbf{r})$  in rarefied region one can use MCDS solution taking into account the molecules effused from specified axial feed inlet, but not those from unknown continuum boundary. Then the mass, momentum and energy rarefied flow densities obtained from kinetic calculation are enough to determine the boundary conditions first approximation for hydrodynamic problem. It latter can be numerically solved and now the local equilibrium distribution function for molecules effused from continuum boundary can be specified. The kinetic problem solution taking into account the collisions with those molecules gives the second approximation  $f^{(2)}(\mathbf{v}, \mathbf{r})$  for rarefied distribution function. The latter gives an opportunity to specify the boundary conditions for hydrodynamic problem again and so on. This procedure results in the accurately conformed flow field inside the cylinder.

Besides, the kinetic consideration allows to find fictitious conditions for macroparameters on the surface  $r = r_i^* < r_i$  deep in the intermediate region ( $Kn \geq 1$ ) providing good Navier-Stokes approximation in the dense region  $r > r_i$ . The difference between accurate and approximate solutions represents the local error of hydrodynamic gas model. This relative error in macroparameters was shown to be very small in dense region, but it increases to the value of  $Kn \geq 1$  in the intermediate region  $r_i^* < r < r_i$ . Therefore to obtain very close approximation to the accurate flow field in cylinder dense region  $r > r_i$ , the Navier-Stokes equations can be solved in extended region  $r > r_i^*$ . Due to constriction of kinetic region the time taken for conformed calculation in this case decreases.

\*Abstract 6529 submitted to the 21st International Symposium on Rarefied Gas Dynamics, Marseille, France, July 26-31, 1998

# Application of a New DSMC Analysis Code to a Variety of Three-Dimensional Rarefied Gas Dynamics Problems \*

G.J. LeBeau<sup>1</sup>, R.G. Wilmoth<sup>2</sup>

<sup>1</sup> NASA Johnson Space Center, Houston, Texas, USA

<sup>2</sup> NASA Langley Research Center, Hampton, Virginia, USA

## Introduction

The Direct Simulation Monte-Carlo (DSMC) methodology of Bird [1] is a well established technique for the modeling of low density fluid flows. While many have contributed to the development of DSMC implementations with the ability to simulate three-dimensional problems, there now exists a need for enhanced capabilities. This is driven by the desire to handle a wide variety of applications in a consistent manner, and the ever present challenge to reduce the time-to-solution for a given problem. To address these issues, a development initiative was undertaken within the NASA DSMC community. The product of that effort was the DAC Series of DSMC software, which first appeared in Ref. [2].

Through an integrated implementation of successful schemes found in previous DSMC codes, combined with additional innovative strategies, it is felt that this new software successfully addresses the development objectives. Most notable of DAC's features are the decoupling of the surface and flow field discretizations and the ability to harness the scalable power of parallel computing. The decoupling of the two grid systems allows the software to deal with the creation of an appropriately discretized flow field grid. The user is provided the simpler task of generating the surface representation, which is facilitated through the use of well established grid generation software.

Confidence in the implementation of the DAC software has been gained through comparisons to other well established DSMC codes [3] and applicable flight data [4]. In this paper, the capabilities of DAC are demonstrated by spotlighting the variety of problems for which it has been utilized. A condensed list of examples would include the plume flow field and plume impingement issues as

described in Ref. [5], to which refined solutions have been produced and shown in Figs. 1 and 2. There have also been a number of studies performed [6, 7, 8] where the DAC software has been used in the analysis of atmospheric re-entry simulations. A notable example is work that was done on the Mars Global Surveyor vehicle, shown in Fig. 3. The software has also been used to investigate the high altitude aerodynamic characteristics of NASA's X-38 vehicle (Fig. 4). Worth noting is that each of these applications can be executed utilizing the scalable parallelism of the DAC software, which is illustrated in Fig. 5.

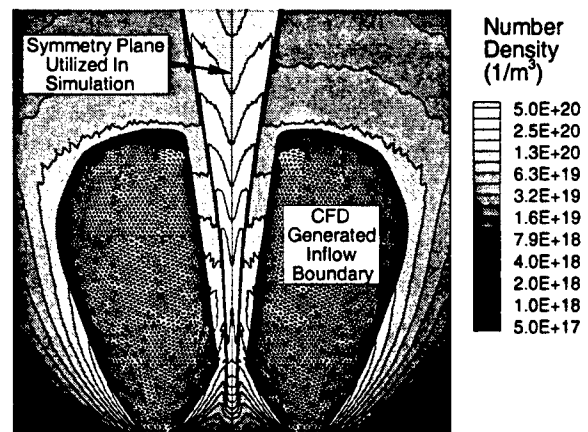


Figure 1: Dual Jet PRCS Interaction

## References

- [1] Bird G.A., *Molecular Gas Dynamics and the Direct Simulation of Gas Flows*, Clarendon Press, Oxford, 1994.
- [2] Wilmoth R.G., LeBeau G.J., and Carlson A.B., *Aerodynamics of the Shuttle Orbiter at High Altitudes*, AIAA Paper 96-1812, June 1996.

\* Abstract 6730 submitted to the 21st International Symposium on Rarefied Gas Dynamics, Marseille, France, July 26-31, 1998

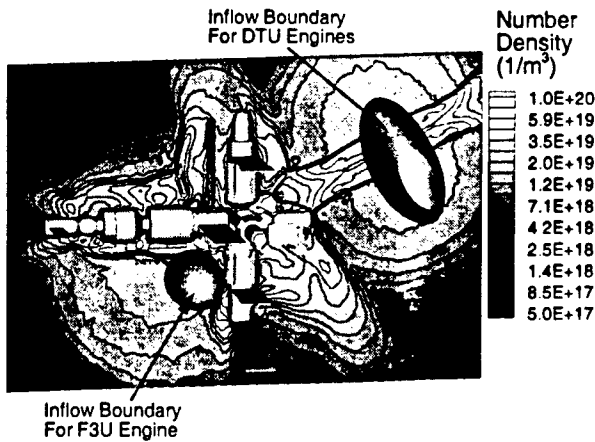


Figure 2: Norm-Z PRCS Impingement on Mir

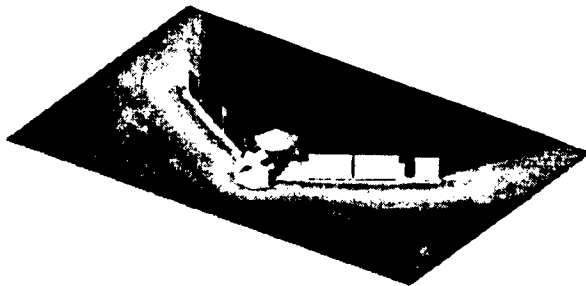


Figure 3: Mars Global Surveyor

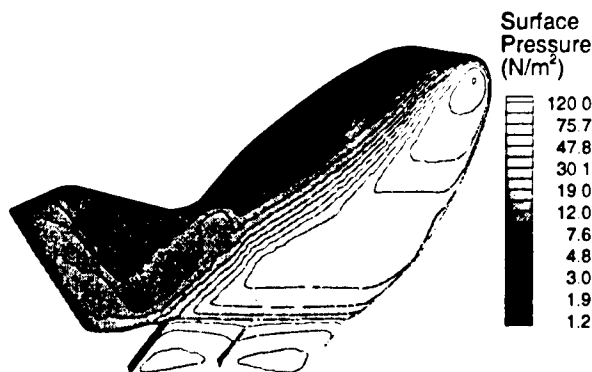


Figure 4: NASA X-38 Crew Return Vehicle

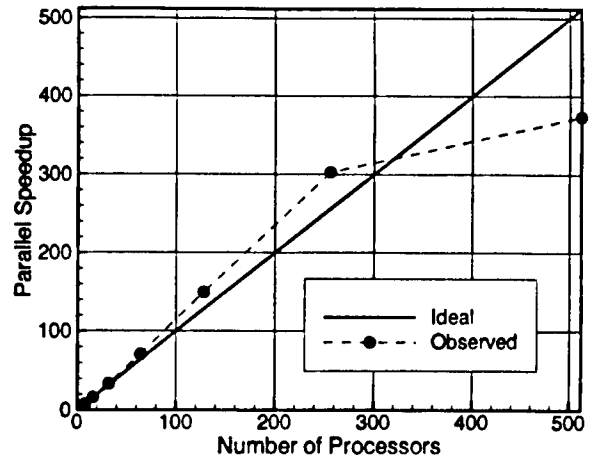


Figure 5: Representative Scalability of DAC DSMC Software on Cray T3E

*biter Aerodynamic Acceleration Flight Measurements*, Journal of Spacecraft and Rockets, Vol. 34, No. 1, pp. 8-15, 1997.

- [5] Lumpkin F.E., Stuart P.C., and LeBeau G.J., *Enhanced Analyses of Plume Impingement During Shuttle-Mir Docking Using a Combined CFD and DSMC Methodology*, AIAA Paper 96-1812, June 1996.
- [6] Moss J.N., Wilmoth R.G., and Price J.M., *DSMC Simulations of Blunt Body Flows for Mars Entries: Mars Pathfinder and Mars Microprobe Capsules*, AIAA Paper 97-2508, June 1997.
- [7] Wilmoth R.G., Mitcheltree R.A., and Moss J.N., *Low-Density Aerodynamics of the Stardust Sample Return Capsule*, AIAA Paper 97-2510, June 1997.
- [8] Wilmoth R.G., Rault D.F.G., Shane R.W., and Tolson R.H., *Rarefied Aerothermodynamic Predictions for Mars Global Surveyor*, to be submitted to the 21st International Symposium on Rarefied Gas Dynamics, Marseille, France, July 26-31, 1998.

- [3] Moss J.N., LeBeau G.J., Blanchard R.C., and Price J.M., *Rarefaction Effects on Galileo Probe Aerodynamics*, 20th International Symposium of Rarefied Gas Dynamics, Beijing, China, August 1996.
- [4] Blanchard R.C., Wilmoth R.G., and LeBeau G.J., *Rarefied-Flow Transition Regime Or-*

# Numerical Simulation of Shock Waves Propagation in Shock Tube and Supersonic Nozzle Flows \*

A. Hadjadj, D. Vandromme  
LMFN, CORIA, CNRS  
St Etienne du Rouvray, France

The aerothermodynamics phenomena in shock tube and nozzle flows transients, like in start-up or shut-down processes are a challenging problem in aerospace application. Indeed, during the engine start-up or shut-down phases of space vehicles at low altitude flight, asymmetric lateral loads may occur on the diverging part of the nozzle structure. These strains are prejudicial to the mechanical behaviour of the nozzle and can possibly cause damages. According to different numerical and experimental investigations [1], [2], [4], [6], [7], [8], the shock propagation induced boundary layer separation is the principal cause of this phenomenon. Indeed, the overexpanded character of the nozzle exhaust flow leads to an unsteady flow separation; shock waves and vortex rings occur in the diverging part of the nozzle and their interactions with the boundary layer give rise to the flow separation.

During the last thirty years experimental set-ups combining a shock tube and a nozzle block have been widely used to simulate gasdynamics and chemical relaxation processes occurring in supersonic flows. Shock tube applications use the region between the reflected shock and the end wall because, ideally, this is a region of uniform flow. In practice, when a reflected shock interacts with the boundary layer, in certain case, the shock bifurcates near the wall and the properties of the gas are no longer guaranteed to be uniform in this region [7], [8]. Nevertheless, the shock wave propagation mechanism is quite complex and not yet clearly understood. Indeed, much of the prediction theories of shock wave/vortex and shock wave/boundary layer interactions rely largely on experimental data and fundamental knowledge of the transient flow physic is still needed.

The aim of this study is to understand the mechanisms of the unsteady flow separation phenomenon in shock tubes and supersonic exhaust nozzles.

The flow field is studied numerically by solving unsteady axisymmetric and two-dimensional Navier-Stokes equations for turbulent compressible flows [4]. The equations are solved by an explicit time-dependent finite volume technique on a structured mesh including robust shock capturing (TVD scheme with flux-splitting formulation).

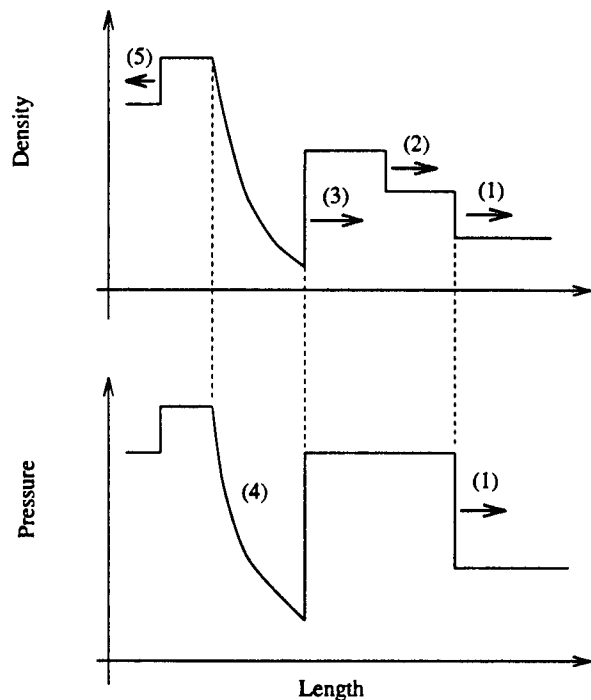


Figure 1: Nozzle start-up process

- (1) : Incident shock
- (2) : Contact discontinuity
- (3) : Recompression shock
- (4) : Expansion fan
- (5) : Reflected shock

The Vulcain nozzle has been used as model and impulsive start-up processes have been analyzed, in which two quiescent gases, in the nozzle with temperature  $T = 300 K$ , and in the shock tube a

\*Abstract 6856 submitted to the 21st International Symposium on Rarefied Gas Dynamics, Marseille, France, July 26-31, 1998

temperature  $T_c = 3000\text{ K}$ , are separated by a diaphragm located at the inlet section of the nozzle. The flow transient starts as the diaphragm is removed. The discontinuity of the fluid dynamic values yields an expansion fan, that is assumed to occur downstream the throat section, two strong shocks (incident and recompression), which move fast towards the exit, and a contact discontinuity, due to the different entropy level between the gas in the chamber and in the nozzle, which follows the incident shock (see figures 1 and 2).

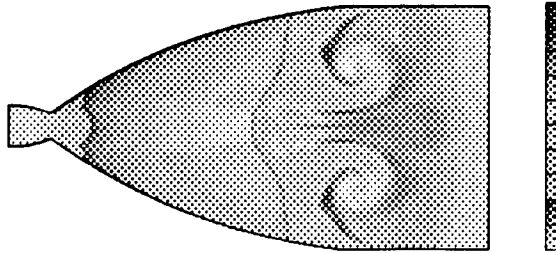


Figure 2: Development of vortex structures downstream of the recompression shock in unsteady nozzle flow (impulsive start-up process). Temperature field visualization, ( $\min=300\text{ K}$ ,  $\max=1000\text{ K}$ )

Figure 2 shows a flow field picture of the unsteady nozzle jet at an instant 50 ms after the start of the incident shock. We notice that the start-up process occurring in a supersonic nozzle is characterized by the formation of shock waves and vortex rings. A shock wave structure develops within the nozzle with a starting shock ahead of the outflowing gas.

Particular attention has been devoted to understand the influence of different parameters such as pressure and temperature ratios, on the transient evolution and the relevant flow structures (vortex ring, reflected shock, recompression shock...). The obtained results will be presented in more detail in the full-length paper.

## References

- [1] Chen C.L., Chakravarthy, S.R., Hung, C.M., *Numerical investigation of separated nozzle flow*, AIAA Journal, Vol. 32, No. 9, 1994
- [2] Glass I.I., Shiun Liu W., Takayama K., Brimelow P.I., *Interactions of shock structure with shock-induced quasi-steady laminar side-wall and flat-plate boundary-layer flows in ionizing argon*, in Proceedings of the 12th Interna-

tional Symposium on Shock Tubes and Waves, 1979.

- [3] Golub V.V., *Development of shock wave and vortex structures in unsteady jets*, Shock Waves (1994) 3:279-285.
- [4] Hadjadj A., *Analyse physique et simulation numérique des écoulements compressibles, application aux tuyères de propulseurs*, Thèse de Doctorat, Université de Rouen, 1997.
- [5] Hadjadj A., Kudryavtsev A.N., Ivanov M.S., Vandromme D., *Numerical investigation of hysteresis effect and slip surface instability in the steady Mach reflection*, 21st International Symposium on Shock Waves, Queensland - Australia, July 20-25, 1997
- [6] Nasuti, F., Onofri, M., *Transient flow analysis of nozzle start-up by a shock fitting technique*, in Proceedings of Unsteady Flows in Aeropropulsion (Ed. Wing Ng et al.), ASME-AD, Vol. 40, 1994.
- [7] Taylor J.R., Hornung H.G., *Real gas and roughness effects on the bifurcation of the shock reflected from the end wall of a tube*, in Proceedings of the 13th International Symposium on Shock Tubes and Waves, edited by C. E. Treanor and J. G. Hall (State University of New York Press, Albany, NY 1981), p. 262.
- [8] Weber Y.S., Oran E.S., Boris J.P., Anderson J. D., *The numerical simulation of shock bifurcation near the end wall of a shock tube*, Phys. Fluids 7(10), October 1995.

# Numerical Algorithms for the Homogeneous Fokker-Planck-Landau Equation \*

M. Lemou

Lab. Mathématiques pour l'Industrie et la Physique.  
UMR 5640 du CNRS, Université Paul Sabatier, UFR MIG, Toulouse. France

## 1 Introduction

The Fokker-Planck-Landau (FPL) equation is used to describe the binary collisions between charged particles, for which the interaction potential is the long-range Coulomb interaction. If  $f(t, v)$  is the distribution function of particles (assumed to be spatially homogeneous), then the homogeneous FPL equation is

$$\frac{\partial f}{\partial t} = Q(f, f) = \nabla_v \cdot \int_{\mathbb{R}^3} \Phi(v - v') (f(v') \nabla f(v) - f(v) \nabla f(v')) dv' \quad (1.1)$$

$Q(f, f)$  is the FPL collision operator.  $\Phi(v)$  is the  $3 \times 3$  matrix

$$\Phi(v) = |v|^{\gamma+2} S(v) = |v|^\gamma (|v|^2 I_3 - v \otimes v) \quad (1.2)$$

$S(v)$  is the orthogonal projector onto the plane orthogonal to  $v$  and  $\gamma > -5$ . The FPL operator can be written in a weak formulation as follows

$$\begin{aligned} & \int_{\mathbb{R}^3} Q(f, f)(v) \psi(v) dv \\ &= -\frac{1}{2} \int \int_{\mathbb{R}^3 \times \mathbb{R}^3} f(v) f(v') (\nabla \psi(v) - \nabla \psi(v'))^T \\ & \quad \Phi(v - v') (\nabla(\log f)(v) - \nabla(\log f)(v')) dv dv' \end{aligned} \quad (1.3)$$

for any smooth test function  $\psi$ . From this duality relation, we check (at least formally) that the only functions  $\psi$  such that for all  $f$ ,  $\int Q(f, f) \psi dv = 0$ , are linear combinations of  $1$ ,  $v$  and  $|v|^2$  (conservation of mass, momentum and energy). Furthermore, letting  $\psi = \log(f)$  in 1.3 leads to the entropy inequality (H-theorem). Here we are concerned with numerical discretizations of the homogeneous FPL equation that respects discrete analogous

properties (conservation and entropy). We first analyse the case of three dimensional velocity space and show how the use of fast algorithms (namely the Fast Multipole Method) improves the computational complexity, preserving simultaneously the above properties. The second numerical analysis deals with the expression of the FPL operator in a cylindrical geometry (in the velocity space). Additional problems arise in this geometry (weak formulation, discretization near the axis, conservation and entropy, etc.) and a numerical discretization satisfying all the above physical properties is presented.

## 2 Fast algorithms in three dimensions

Let us consider a regular discretization of  $\mathbb{R}^3$ ,  $v_i = i \Delta v$ ,  $i = (i^1, i^2, i^3) \in \mathbb{Z}^3$ , and denote by  $\bar{f}_i$  an approximation of  $f(v_i)$ . Let  $D$  be a finite-difference operator that approximates the usual gradient operator  $\nabla$  at least up to the first order, and let  $D^*$  be its formal adjoint. we recall that a basic conservative and entropy discretization is given by the following weak-form [1]:

$$\sum_{i \in \mathbb{Z}^3} \bar{Q}(\bar{f}, \bar{f})_i \psi_i = -\frac{1}{2} \sum_{i, j \in \mathbb{Z}^3 \times \mathbb{Z}^3} \bar{f}_i \bar{f}_j ((D\bar{\psi})_i - (D\bar{\psi})_j)^T \Phi(v_i - v_j) ((D(\log \bar{f}))_i - (D(\log \bar{f}))_j) \Delta v^3 \quad (2.4)$$

where  $\bar{Q}(\bar{f}, \bar{f})_i$  approximates  $Q(f, f)(v_i)$  and  $\bar{\psi}$  is a test sequence. Scheme (2.4) (with a suitable choice of  $D$ ) satisfies all the above physical properties of conservation and entropy (at the discrete level). Unfortunately, direct numerical evaluations of the discrete FPL operator via the weak formulation (2.4) are very expensive (of the order  $N^2$  where  $N$  is the total number of points in the velocity grid). This will be prohibitive when one wants to solve the inhomogeneous case (with the transport term).

\* Abstract 6926 submitted to the 21st International Symposium on Rarefied Gas Dynamics, Marseille, France, July 26-31, 1998



Thus, the use of fast algorithms is necessary. We first use a multigrid hierarchy:

We split the domain of integration  $C_0$  (assumed to be a cube of length 1) in several parts according to the following hierarchy: At *Level one*, we split  $C_0$  into 8 equal cubes (called its children)  $C_1^i$  ( $i = 1..8$ ) and  $C_0$  is called their father. At *Level two*, we split each  $C_1^i$  into 8 equal cubes (its children), and obtain 64 cubes  $C_2^j$  etc. The center of a cube  $C_k^i$  (of level  $k$ ) is denoted by  $r_k^i$ . We iterate this process until the finest mesh level  $ng$ . Let  $C_k^i$  and  $C_k^j$  be two cubes of level  $k$ . We say that  $C_k^i$  and  $C_k^j$  are *well-separated* if they are separated at least by one cube of the same level, else we say that they are *neighbors*. We also define and denote by  $Int(C_k^i)$  the *interaction list* of a given cube  $C_k^i$  of level  $k$ , as the set of cubes  $C_k^j$  of the same level  $k$ , which are well-separated, and whose fathers are neighbors. Thus following this process, the weak formulation may be written as

$$\int_{C_0} Q(f, f)(v) \psi(v) dv = -\frac{1}{2} \sum_{k=1}^{+\infty} \sum_{i,j/C_k^i \in Int(C_k^j)} \int_{C_k^i \times C_k^j} f(v) f(v') (\nabla \psi(v) - \nabla \psi(v'))^T \Phi(v - v') (\nabla(\log f)(v) - \nabla(\log f)(v')) dv dv' \quad (2.5)$$

Two approaches have been performed to discretize this formulation:

- **Monte Carlo integration [2]:** It consists in approximating the integrals on  $C_k^i \times C_k^j$  by a Monte Carlo quadrature formula. This method leads to a total complexity of the order  $N \log N$ .
- **Multipole expansion [3]:** The main observation is that the velocities  $v$  and  $v'$ , in (2.5), are only coupled through the factor  $|v - v'|^\gamma$  coming from the expression of the matrix  $\Phi(v - v')$ , otherwise the two variables would be uncoupled and the complexity would simply be of the order  $N$ . To uncouple  $v$  and  $v'$ , we replace the terms  $|v - v'|^\gamma$  under the integrals on  $C_k^i \times C_k^j$  by their expansions around  $|r_k^i - r_k^j|^\gamma$ . This is valid because the cubes  $C_k^i$  and  $C_k^j$  are well separated. The order of these expansions govern the total error of the approximation. This strategy leads to a complexity of the order  $N$ .

### 3 Axisymmetric case

In this section we suppose that the distribution function  $f$  presents a cylindrical symmetry, i.e depends only on two variables  $v_\parallel \in \mathbb{R}$  and  $v_\perp \in \mathbb{R}_+$

(we say also that  $f$  is axisymmetric), and we establish a simplified expression of the FPL operator in this geometry. If we set  $V = (v_\parallel, v_\perp)$  and  $V' = (v'_\parallel, v'_\perp)$ , then we prove that there is still a weak formulation similar to (1.3) according to

$$\int_{\mathbb{R} \times \mathbb{R}_+} Q(f, f)(V) \psi(V) v_\perp dV = -\frac{1}{2} \int_{(\mathbb{R} \times \mathbb{R}_+)^2} f(V) f(V') \begin{pmatrix} \partial_\parallel \psi(V) - \partial_\parallel \psi(V') \\ \partial_\perp \psi(V) \\ \partial_\perp \psi(V') \end{pmatrix}^T \Omega(V, V') \begin{pmatrix} \partial_\parallel (\ln f)(V) - \partial_\parallel (\ln f)(V') \\ \partial_\perp (\ln f)(V) \\ \partial_\perp (\ln f)(V') \end{pmatrix} v_\perp v'_\perp dV dV' \quad (3.6)$$

for any smooth test function  $\psi$ .  $\Omega(V, V')$  is a  $3 \times 3$  positive semi-definite matrix. Its nullspace is the one dimensional space spanned by  $(v_\parallel - v'_\parallel, v_\perp, v'_\perp)$  (when this vector is not 0). Using this weak formulation, we check that the only functions  $\psi$  for which  $\int_{\mathbb{R} \times \mathbb{R}_+} Q(f, f)(V) \psi(V) v_\perp dV = 0$  for all  $f$  are linear combinations of  $1, v_\parallel, v_\parallel^2 + v_\perp^2$ .

Because of the axis and in order to preserve all the above properties at the discrete level, we first perform a symmetrization of the continuous formulation with respect to the axis ( $v_\perp = 0$ ). To do so, the functions  $f$  and  $\psi$  are extended to  $\mathbb{R} \times \mathbb{R}$  to even functions with respect to  $v_\perp$ , and the matrix  $\Omega$  is suitably modified so as the weak formulation remains valid when the integration is taken on  $\mathbb{R} \times \mathbb{R}$  instead of  $\mathbb{R} \times \mathbb{R}_+$ . The discretization of the new obtained formulation leads to a completely conservative and entropy scheme.

### References

- [1] P. DEGOND AND B. LUCQUIN-DESREUX. An entropy scheme for the Fokker-Planck collision operator of plasma kinetic theory. *Numerische Mathematik*. vol. 68, pp 239-262, (1994).
- [2] C. BUET, S. CORDIER, P. DEGOND AND M. LEMOU, Fast algorithms for numerical, conservative and entropy approximations of the Fokker-Planck-Landau equation. *J. comput. Phys.* **133**, p. 310-322, 1997.
- [3] M. LEMOU, Multipole expansions for the Fokker-Planck-Landau equation. To appear in *Numerische Mathematik* 1998.

**TWO-PHASE FLOWS - TP P**

**TUESDAY, JULY 28, 1998**

**16:15**

# Transfer Processes in Vapor- Gas Mixture and Generalized Theory of Nucleation Kinetics\*

S.P. Fisenko

A.V. Luikov Heat & Mass Transfer Institute, Minsk, Belarus

Classical theory of the nucleation kinetics considers the phase transition at isothermal approximation when the temperatures of new phase cluster and vapor-gas mixture are the same. Recently some works have been done in order investigate non-isothermal nucleation kinetics [1,2,3]. The temperature difference arises as the result of release of the latent heat of phase transition. The discrepancy of theoretical predictions of the nucleation rate and experimental results is about 1-3 order of value. In order to overcome this discrepancy it's necessary to increase the accuracy as experimental investigations as the theoretical ones. The most promising way for theory is to use more detailed description of new phase cluster.

The new kinetic equation for the distribution function  $f(g, E)$  was derived, where  $g$  is the number of molecules (cluster size) and  $E$  is the cluster energy. For derivation this new kinetic equation for cluster distribution function the methods of non-equilibrium statistical thermodynamics have been used [4]. This kinetic equation is two-dimensional Fokker-Plank equation. All kinetic coefficients, obtained as Green-Kubo formulas, are calculated at the free molecular approximation.

The results of theoretical and numerical investigation of the two-dimensional kinetic equation are presented. The boundary conditions are the generalization of the standard for nucleation kinetics boundary conditions. Galerkin's method is used for numerical investigation. The Zeldovich's solution was used as basic function for approximation of distribution function. The limits of isothermal nucleation kinetics is discussed versus carrier gas concentration, value of latent heat and specific heat capacity.

For big concentration of carrier gas the tail of energy transfer processes manifest itself as fluctuation of nucleation rate. The calculation of fluctuation nucleation rate is presented [5]. Its shown that the

renormalisation effect of a nucleation rate arises. The observable nucleation rate  $\langle I \rangle$  can be written as

$$\langle I \rangle = I_z (1 - 2/g^*)$$

where  $I_z$  is Zeldovich nucleation rate and  $g^*$  is the number of molecules at critical cluster.

## References

- [1] Bashkirov A.G. and Fisenko S. P., J. of Theoretical and Mathematical Physics, v. 48, No1, 1981.
- [2] Fisenko S. P., Proc.19 Intern. Symposium on Rarefied Gas Dynamics, Oxford, Oxford, 1995
- [3] Ford I. J., J. Aerosol Science, v.23, p.447, 1992
- [4] Zubarev D.N., Non-equilibrium Statistical Thermodynamics, Consultants Bureau, New York, 1974.
- [5] Fisenko S. P., in Nucleation and Atmospheric Aerosols, ed. M. Kulmala and P.E. Wagner, Pergamon Press, 1996

---

\* Abstract 2621 submitted to the 21st International Symposium on Rarefied Gas Dynamics, Marseille, France, July 26-31, 1998

## Ion-Induced Nucleation on Well Defined Ions\*

D.B.Kane, S.P.Fisenko, M.S.El-Shall

Chemistry Department, Virginia Commonwealth University, Richmond, USA

Ion-induced nucleation of supersaturated vapors, as mechanism for new particle formation in plasmas and interstellar space, remains poorly understood phenomena. The use of resonance multi-photon ionization in a diffusion cloud chamber (DCC) provides the opportunity to investigate nucleation of supersaturated vapors on well defined ions [1]. In particular, positive ions of benzene, styrene p-xylene and toluene have been generated. The ion -induced nucleation of methanol and nonane vapor on these ions has been investigated. It was shown that there are two fast and two slow processes which are important for understanding our experiments; correspondingly, laser ionization (characteristic time  $\sim 10^{-8}$  s ) and nucleation (characteristic time  $\sim 10^{-6}$  s ) from one side and ion motion (characteristic time  $\sim 10^{-2}$  s ) and droplet growth and motion (characteristic time  $\sim 10^{-1}$  s ) [2].

The nucleation rate as function of time has been measured by light scattering from droplets resulting from nucleation. These experimental results are presented. The mathematical models have been developed to describe the relatively slow processes involved in ion-induced nucleation at DCC [3]. The problem of distinguishing ion-induced nucleation rate from effects of droplets growth are discussed. During the experiments the Knudsen number for droplet changes in very broad range. A comparison of the numerical simulation results and experimental ones is presented. The influence of the depletion effect, related with spatial ion distribution, on macroscopic results of an ion-induced nucleation is discussed. In particularly, it was shown by solving inverse problem that Thompson's model of the free energy cluster formation predicts the position of maximum of nucleation rate in non-uniform conditions of DCC very well.

Experimental measurements of the ion-induce nucleation rate as function of applied electric field show that there is an "ion sign effect". This effect is a preference for the nucleation of the vapor on ions either positive or negative sign. The effects of ion

cluster mobility and other factors which may influence this effect have been determined. After discriminating these effects the influence of the ion sign on the free energy barrier to nucleation remains. Correlations between the vapor properties and "sign effect" are under investigation.

### References

- [1] Kane, D. and El-Shall, M. S.: *Nucleation and Atmospheric Aerosols*, ed. M.Kulmala and P.E.Wagner, Elsevier Science Publishing, p.46, 1996.
- [2] Kane, D, Fisenko S. P. and El-Shall, M. S, *Chemical Physics Letters*, v.277, No 1, pp.6-12, 1997.
- [3] Kane, D, Fisenko S. P. and El-Shall, M. S., *Chemical Physics Letters*, v.277, No 1, pp.13-19, 1997.

---

\* Abstract 2622 submitted to the 21st International Symposium on Rarefied Gas Dynamics, Marseille, France, July 26-31, 1998

# Transient Evaporation Phenomena Induced by Impingement of Second Sound on a Superfluid Helium-Vapor Interphase \*

T. Furukawa, M. Murakami

Inst. of Engineering Mechanics, Univ. of Tsukuba, Tsukuba, Japan

## 1 Introduction

Transient evaporation phenomena in a superfluid helium(He II)-helium vapor system were studied experimentally, in which a practically pure liquid-vapor system is available due to an absolutely low temperature environment, lower than 2.17 K. At these temperatures, all gases except helium are in frozen state. So it may be considered as a practically pure liquid-vapor system. In He II, there exists a thermal wave called a second sound wave. A finite amplitude second sound non-linearly develops into a thermal pulse having a temperature discontinuity. A sharp rise and fall, and well defined value of the heat flux are characteristic features of heating by impingement of a thermal pulse on He II-helium vapor free surface. A thermal pulse can provide approximately stepwise heating of a liquid-vapor free surface.

## 2 Experimental Set-up

A cryostat with optical windows is used for the visualization study. The test section immersed in He II in the cryostat has a rectangular cross section (10 mm  $\times$  60 mm  $\times$  37 mm) as shown in Figure 1. It is enclosed by two side walls of Bakelite and two glass plates for windows. A planar Ni/Cr thin film heater vacuum-deposited on a quartz glass substrate is installed at the bottom of the test section to generate a thermal pulse. Electric current in a trapezoidal form varying in time for several hundred  $\mu$ s is applied to generate a thermal pulse. The density variation in the vapor phase due to evaporation is visualized in the form of interference fringes by applying a laser holographic interferometer. The pressure in the evaporation wave is measured by a pressure transducer. The temperature in a free surface region and in vapor phase is measured by a supercon-

ductive temperature sensor[2], of which sensing element is gold-tin superconductive thin film vacuum-deposited on the outer surface of quartz glass fiber with a length of 2 mm and a diameter of 40  $\mu$ m.

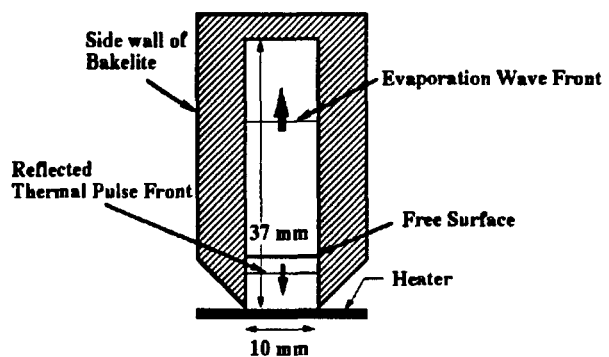


Figure 1: Cross-sectional view of test section

## 3 Results and Discussion

In the experiment a thermal pulse emitted from the heater propagates upward through He II at the speed of second sound. It causes evaporation upon the impingement on the free surface. An evaporation wave is formed and propagates through the vapor phase. At the same time, some portion of the incident thermal pulse is reflected from the free surface. The reflected thermal pulse propagates downward. The formation of an evaporation wave front is clearly seen in Figure 2. The interferogram is taken by finite-fringe method. Wave feature of evaporated vapor front clearly seen because it propagates in pure vapor without non-condensable gas effects, and because the free surface is stepwise heated by a thermal pulse impingement. The propagation speed of the evaporation wave front is nearly equal to the speed of sound. It is seen in the interferogram the sign of reflected thermal pulse is not reversed and the reflected and incident thermal pulses overlap. This indicates that the pulse amplitude of the reflected portion has to be taken into consideration to

\*Abstract 4266 submitted to the 21st International Symposium on Rarefied Gas Dynamics, Marseille, France, July 26-31, 1998

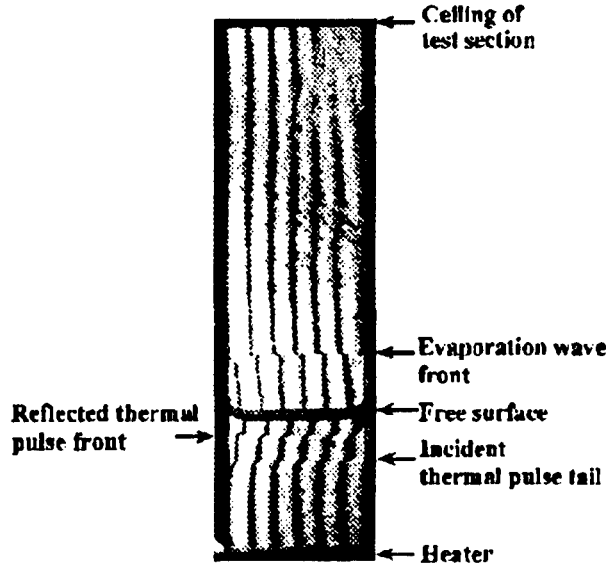


Figure 2: Finite-fringe interferogram showing wave fronts of evaporation wave reflected thermal pulse, and wave tail of incident thermal pulse. Initial bath temperature  $T_I=1.74\text{K}$ , heater applied heat flux  $q=25\text{ W/cm}^2$ , heating time  $t_H=200\text{ }\mu\text{s}$ .

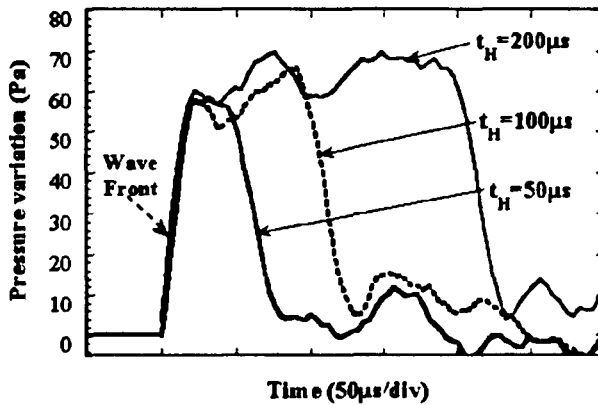


Figure 3: Time variation of the pressure in evaporated vapor for three heating times  $t_H=50, 100, 200\text{ }\mu\text{s}$  measured at 10 mm above the free surface. Initial bath temperature  $T_I=1.74\text{ K}$ , heater applied heat flux  $q=15\text{ W/cm}^2$ .

evaluate the temperature of a free surface,  $T_W$ .

The time variation of the pressure in evaporated vapor is shown for three heating times in Figure 3. It is seen that the interval when the pressure rises almost coincides with the heating time.

The pressure of evaporated vapor is plotted against the normalized temperature of free surface in Figure 4. The temperature difference,  $T_W-T_I$ , is, in fact, found to be approximately twice the amplitude of an incident thermal pulse. The pressure condition

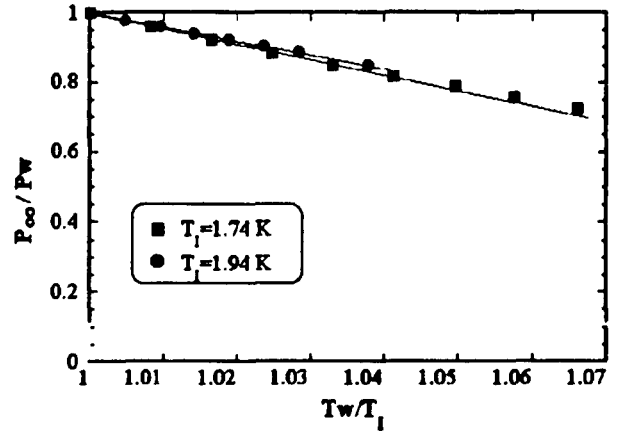


Figure 4: The pressure of evaporation wave plotted against the normalized temperature of the free surface. Initial bath temperatures  $T_I=1.74$  and  $1.94\text{ K}$ .

is given as a function of particle velocity outside the knudsen layer,  $V_\infty$ , as follows[1],

$$\frac{P_\infty}{P_W} = h_1(Mn_\infty), \quad Mn_\infty = \frac{V_\infty}{\sqrt{\frac{5}{3}RT_\infty}}. \quad (1)$$

Here  $T_\infty$  and  $P_\infty$  are the temperature and the pressure of the vapor outside of the knudsen layer, and  $P_W$  is the saturated vapor pressure at the temperature of He II free surface,  $T_W$ . We now conduct experiments to measure  $V_\infty$ [3].

## References

- [1] Sone Y., Aoki K., *Molecule Gas Dynamics (in Japanese)*, Asakura Pub., 1994.
- [2] Borner H., *Experimental Investigation on Fast Gold-Tin Metal Film Second-Sound Detector and Their Application*, J. of Low-Temp. Phys., Vol.50, Nos.5/6, pp.405-426, 1983.
- [3] Casting B., *Hot wire anemometer operating at cryogenic temperature*, American Inst. of Phys., Vol.63, No.9, pp.4167-4173, 1992.

# Motions of a Vapor between the Spherical Condensed Phases – Formation of Standing Shock Waves – \*

Y. Onishi, T. Doi, Ooshida T.

Department of Applied Mathematics and Physics, Tottori University, Japan

## 1 Introduction

Transient motions of a vapor associated with strong evaporation and condensation processes between the coaxial spherical condensed phases are considered here. Wave propagations and the possible formation of a standing shock wave in the flow field caused by the phase change processes occurring at the concentric spherical condensed phases are the main subject of this study. The investigation of such transient motions of the vapor is of fundamental importance in gas dynamics in the sense that one can understand how the waves (shock waves, contact regions and sometimes expansion waves involved) caused by these processes bring the flow fields to their final states. Continuous interaction of the various waves with themselves and with the boundaries and their propagation through nonuniform flow fields are also of theoretical interest. Flow fields of this kind have already been studied for the case of strong and not so strong phase change processes between the plane condensed phases placed in parallel ([1], [2], [3]), where the transition process of the flow fields to their final states has been clarified in terms of the propagation and interaction of the various waves involved. The present spherical problem, however, which may differ in many respects from dimensionally degenerate problems such as already treated in [1]–[3], may be expected to involve virtually adiabatic and strong initial expansion of the flow field near the inner condensed phase where evaporation is taking place because of the 3-dimensional expanse of region involved. The expansion, when it is strong, may lead the flow to supersonic one near the inner condensed phase and eventually lead to the formation of a standing shock wave within the flow region to connect the supersonic flow and the subsonic one prevailing near the outer condensed phase.

## 2 Setting of Problem

Consider a vapor between the concentric spherical condensed phases with the inner and outer radii  $r_1$  and  $r_2$ , respectively. Initially, the gas phase and its inner and outer condensed phases are in complete equilibrium at a temperature  $T_0$ , the pressure and number density of the gas at this state being  $P_0$  and  $N_0$ , respectively. Suppose that, at time  $t = 0$ , the temperature of the inner condensed phase is suddenly changed from  $T_0$  to  $T_1$ , the temperature of the outer condensed phase being unchanged and kept at  $T_0$ . The saturated vapor pressure and number density at this temperature  $T_1$  is denoted by  $P_1$  and  $N_1$ , respectively. With a difference scheme applied, the Boltzmann equation of BGK type [4] are solved numerically for this problem under the condition of diffusive reflection at the interface between the condensed phase and the gas phase.

## 3 Results

The calculations have been carried out for a number of sets of the parameters governing the motions of the vapor, i.e.,

$$\frac{r_2}{r_1}, \quad Kn = \frac{l_0}{r_1}, \quad \frac{T_1}{T_0}, \quad \Gamma = \frac{h_L}{RT_0}$$

where  $R$  is the gas constant and  $h_L$  is the latent heat of vaporization per unit mass of the vapor.  $l_0$  is the mean free path at the initial reference state defined by  $l_0 = (8RT_0/\pi)^{1/2}/(N_0\nu_c)$ ,  $N_0\nu_c$  being the collision frequency at the reference state. The distributions of various fluid dynamic quantities including the mass and energy flows for the transient and final steady states have been obtained together with the distribution function for molecules.

A sample of the results is shown in Figs.1–3, which shows the transition process of a flow field to its final state due to the evaporation process taking place at the inner condensed phase. It can be seen that a shock wave is produced followed by a contact region with strong incipient flow expansion near the

\*Abstract 4541 submitted to the 21st International Symposium on Rarefied Gas Dynamics, Marseille, France, July 26-31, 1998

evaporation surface. This expansion drives the part of the flow to supersonic, leading to the gradual formation of a standing shock wave in the flow field to connect the supersonic flow region and the subsonic one within a short distance.

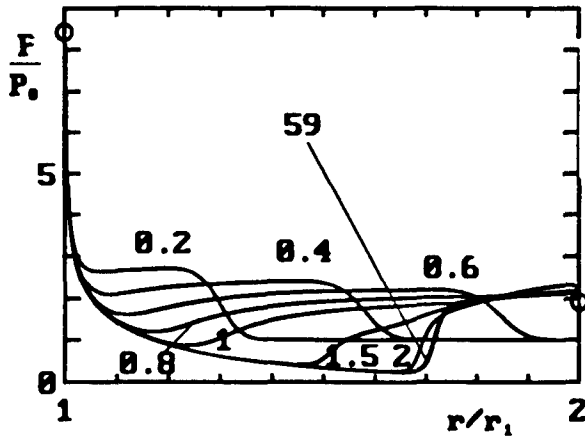


Figure 1: Transient pressure distributions  $P/P_0$  for  $r_2/r_1 = 2.0$ ,  $Kn = 0.01$ ,  $T_1/T_0 = 1.3$ ,  $\Gamma = 11$  (or  $P_1/P_0 = 12.66$ ,  $N_1/N_0 = 9.74$ ). The numbers in the graphs indicate the values of time  $t/\tau_0$ , where  $\tau_0 = r_1/(2RT_0)^{1/2}$ .  $\circ$  indicates the virtually final values (at  $t/\tau_0 = 9.0$ ) of the quantity at  $r = r_1$  and  $r = r_2$ .

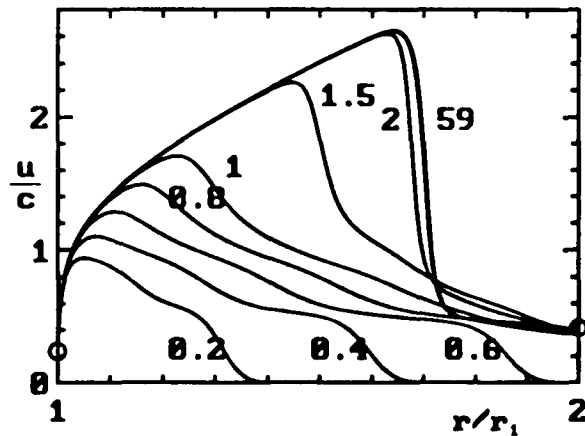


Figure 2: Transient local Mach number distributions  $u/c$  for  $r_2/r_1 = 2.0$ ,  $Kn = 0.01$ ,  $T_1/T_0 = 1.3$ ,  $\Gamma = 11$  (or  $P_1/P_0 = 12.66$ ,  $N_1/N_0 = 9.74$ ).  $c = (5RT/3)^{1/2}$  is a local sound speed. The numbers in the graphs indicate the values of time  $t/\tau_0$ , where  $\tau_0 = r_1/(2RT_0)^{1/2}$ .  $\circ$  indicates the virtually final values (at  $t/\tau_0 = 9.0$ ) of the quantity at  $r = r_1$  and  $r = r_2$ .

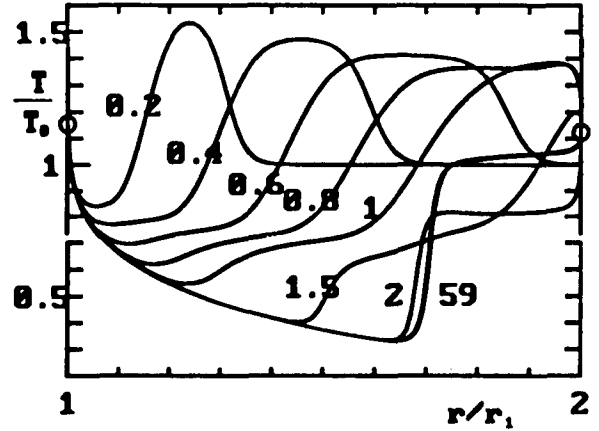


Figure 3: Transient temperature distributions  $T/T_0$  for  $r_2/r_1 = 2.0$ ,  $Kn = 0.01$ ,  $T_1/T_0 = 1.3$ ,  $\Gamma = 11$  (or  $P_1/P_0 = 12.66$ ,  $N_1/N_0 = 9.74$ ). The numbers in the graphs indicate the values of time  $t/\tau_0$ , where  $\tau_0 = r_1/(2RT_0)^{1/2}$ .  $\circ$  indicates the virtually final values (at  $t/\tau_0 = 9.0$ ) of the quantity at  $r = r_1$  and  $r = r_2$ .

## References

- [1] Onishi, Y., Shoji T. and Tsuji, H., *Interactions of shock and expansion waves caused in a vapor between the two plane condensed phases*, Proceedings of the International Symposium on Aerospace and Fluid Science, edited by S. Kamiyama, Institute of Fluid Science, Tohoku University, pp.517-524, 1993.
- [2] Onishi, Y. and Tsuji, H., *Transient behavior of a vapor due to evaporation and condensation between the plane condensed phases*, Rarefied Gas Dynamics 19, edited by John Harvey and Gordon Lord, Oxford University Press, Oxford, pp.284-290, 1995.
- [3] Onishi, Y., *Propagation of waves in a vapor due to strong evaporation and condensation*, Proceedings of the 21th International Symposium on Shock Waves (held in Australia, July 20-25, 1997), to be published.
- [4] Bhatnager, P.L., Gross, E.P. and Krook, M., *A model for collision processes in gases*, Phys. Rev. Vol.94, 511-525, 1954.



# New Kinetic Model of Diffusion-Limited Nucleation at Low Concentrations of the Condensible Vapor \*

A.L. Itkin

Inst. High-Performance Compt. and Data Bases, Moscow Branch, Russia &  
Inst. Problems of the Asteroid Hazard, Moscow, Russia

In the existing theories of homogeneous nucleation it is accustomed to consider that a concentration of a noncondensable (carrier) gas does not affect the rate of nucleation. Moreover, it is supposed that the higher the gas concentration, the closer the nucleation process is to the isothermal one for which classical nucleation theory (CNT) was originally built. However, in paper [1] and many others on the basis of the experimental data on homogeneous condensation of  $H_2O$ ,  $D_2O$  and some alcohols in an inert gaseous atmosphere it was discovered that the critical supersaturation linearly increases with the increase of the carrier gas pressure  $P_0$ . Besides, with the temperature decrease a slope of isotherms  $S_*(P_0)$  becomes more abrupt.

That is why the aim of this work was to consider in more detail the kinetic processes in DCC using some ideas specific for the kinetics of chemical reactions. Here we propose a model of the nucleation process under conditions when a transport of condensing molecules to the cluster surface is determined by their diffusion through a carrier gas. The main physical idea exploited within our approach is the following. If a certain cluster transits to another sort by attaching a monomer the rate of this process in the usual nucleation theory is proportional to a free-molecular flux of monomers on the surface of this cluster and this flux is determined by the volume concentration of monomers. Under the conditions of DCC this assumption stops to be valid because the real concentration of monomers at the external boundary of the Knudsen layer over the cluster surface differs from the concentration  $n_1$  determined far from the cluster in view of the presence of a carrier gas. It is caused by the existence of a concentration jump in the vicinity of the cluster surface and the value of this jump becomes considerable when the mean free path of the condensing molecules in the carrier gas is of order of the cluster

radius.

Further we use a special mathematical formalism which is strongly based on the microscopic theory of nucleation [3] put forward by the author and allows one to obtain an analytical representation of the cluster's concentrations through supersaturation, the gas temperature and, that is quite new, the carrier gas pressure. It is shown that the usual conditions of experiments in diffusion cloud chambers where the concentration of the vapor is small, meet the requirements of the model validity that means this model can be adopted to explain a mechanism of the carrier gas pressure influence on the nucleation kinetics [4] observed in experiments [1]. In particular, as follows from our analysis instead of a usual supersaturation  $S$  all expressions of the theory contain a product  $S\Theta$  where  $\Theta \propto 1/P_0$  and depends upon the cross-section of the carrier gas and condensing molecules.

The main conclusion which can be made based on the above results is that at certain values of the temperature and, that is more important, pressure of a carrier gas a special regime of nucleation may establish. As follows from the presented analysis this case is realized at high pressures of the carrier gas, a large effective diameter (or cross-section) of the condensing molecules, comparatively low temperatures. We call this regime "diffusion-limited nucleation", but such processes are well known and even rather wide occur in chemical kinetics [2]. However, for nucleation this effect here is considered for the first time.

From the results obtained it follows that in addition at the diffusion-limited nucleation the quasisteady concentrations of clusters as well as the rate of the evolution of the monomer's mass fraction  $\alpha_1$  become no longer be a function of two parameters —  $T$  and  $S$ , but three because now in addition they depend on the carrier gas pressure as well as on the nature of both the carrier gas and the condensing vapor. This dependence appears through the values

\*Abstract 4881 submitted to the 21st International Symposium on Rarefied Gas Dynamics, Marseille, France, July 26-31, 1998

of the collision cross-section and the mean free path of the vapor molecules through the carrier gas, and it must be taken into account when treating and comparing the experimental results with the others and with a theoretical prediction.

This result in some degree explains why in some experiments in expansion chambers the dependence of the nucleation rate on the carrier gas pressure have not been detected at all or was comparatively slight [5] while in experiments [1] it was pronounced. On the other hand a slight effect of the carrier gas pressure in nozzles and jets [6] (see also a more extent description of this problem in [3]) has to be associated with the dependence of the parameter  $r$  — the main parameter of MNT — on  $P_0$ . The reason is that under the conditions of these experiments  $P_0 \sim P_1$  - the vapor pressure - and thus for small clusters their intracluster vibrations are nonequilibrium because of the limited number of collisions with both the carrier gas and vapor molecules. Thus, another kinetic theory is needed to describe this situation, for instance, MNT in its original treatment [3].

Finally, analytical dependencies of critical supersaturation  $S_*$  and  $\partial S_*/\partial P$  on a carrier gas pressure  $P_0$  and temperature  $T$  in a diffusion cloud chamber (DCC) are derived on the basis of the above approach. These dependencies qualitatively reproduce the available experimental data. In addition the influence of the nature of both the carrier gas and condensing vapor on the observed phenomenon is discussed. The conclusion is made that the effect of the carrier gas in the experiments in DCC has no connection to the real rate of chemical reactions of clusterization and at other conditions (for instance, in expansion chambers) may not occur. Nevertheless an existence of the carrier gas influence on the total nucleation rate can be of great importance for the control of nucleation.

## References

- [1] Bertelsmann A., Stuczynski R., and Heist R., *Effects of background gases on the homogeneous nucleation of vapors. 3.*, J. Phys. Chem., Vol.100, p.9762, 1996.
- [2] Frank-Kamenetskii D.A., *Diffusion and heat transfer in chemical kinetics*, Acad. Sci. USSR, Moscow & Leningrad, 1947.
- [3] Itkin A.L., and Kolesnichenko E.G., *Microscopic theory of condensation in gases and*

*plasma*, World Scientific, New York, London, HongKong, 1997.

- [4] Itkin A.L., *Nucleation in a diffusion chamber. I. Kinetic model of diffusion-limited nucleation*, subm. J. Aerosol Sci., 1997.
- [5] Wagner P., and Strey R., *Homogeneous nucleation rates of water vapor measured in a two piston expansion chamber*, J. Phys. Chem., Vol.85, p.2694, 1981.
- [6] Wyslouzil B., Wilemski G., Beals M., and Frish M., *Effect of carrier gas pressure on condensation in a supersonic nozzle*, Physics of Fluids, Vol.6, p.2845, 1994.

## Acknowledgments

This work was supported in part by the Russian Ministry of Science and Technology and by the Russian Foundation for Basic Researches, Grant N 97-03-32434.

# Photophoresis in a Rarefied Gas: Influence of Particle Optical Properties \*

A. Starinov, S. Beresnev, P. Suetin

Department of Molecular Physics, Ural State University, Ekaterinburg, Russia

## 1 Introduction

In this study we continuous to investigate theoretically and experimentally photophoresis phenomena in rarefied gas ( the movement of aerosol particle on the influence of light beam [1,2] ). The radiometric nature of photophoresis binds with the appearance of the force that exerts on the non-uniformly heated by light particle in the rarefied gas. The problem of photophoresis is known to have a complex character: it is necessary to solve electrodynamic and kinetic parts for the calculations of values of photophoresis force and velocity. The heat sources of electromagnetic nature into the particle volume are known to be calculated according to Lorentz-Mie theory concerning homogeneous spherical particle assumption [3] (electrodynamic part). Processes of the heat and momentum transfer to the suspended in gas particle are believed to be calculated according to the principles of kinetic theory. Furthermore, electrodynamic part can be investigated independently from kinetic part due to the linear problem statement.

## 2 Basic equations and results

We have used this problem property and analyzed force and velocity dependence on Knudsen number, thermophysical and accommodation particle properties in [1] in detail. In particular, the solution of the kinetic equation is obtained by using integral-moments method for the whole Knudsen numbers range and the expression for photophoretic force can be written in form:

$$\vec{F}_{ph} = -\frac{2\pi}{3} \sqrt{\frac{\pi M}{8RT_0}} \vec{T}_0 J_1 R_0^2 \times \frac{\alpha_E \psi_1}{\alpha_E + \frac{15}{4} \Lambda K n (1 - \alpha_E) + \alpha_E \Lambda \psi_2}, \quad (1)$$

\*Abstract 4901 submitted to the 21st International Symposium on Rarefied Gas Dynamics, Marseille, France, July 26-31, 1998

where  $\vec{T}$  is light intensity;  $\Lambda = \lambda_p/\lambda_g$  is the ratio of particle and gas thermal conductivities;  $R_0$  is the particle radius; and functions  $\psi_1$  and  $\psi_2$  depend on  $Kn$  numbers and accommodation coefficients of normal ( $\alpha_n$ ) and tangential momentum ( $\alpha_\tau$ ) of gas molecules on the particle surface;  $\alpha_E$  is the energy accommodation coefficient;  $J_1$  is the asymmetry factor of particle surface temperature. It is defined as

$$J_1(m, \rho) = \frac{3n\kappa}{\rho^3} \int_0^\rho \tilde{\rho}^3 \int_{-1}^1 P_1^0(\mu) B(\tilde{\rho}, \mu) d\mu d\tilde{\rho} \quad (2)$$

where  $m = n + i\kappa$  is a complex refractive index of particle substance;  $\rho = 2\pi R/\lambda$  is radiative size parameter (the diffraction parameter);  $P_1^0(\mu)$  is Legendre polinomial;  $B(x, \theta_0)$  is so-called source function;  $\mu = \cos \theta_0$ , and  $\theta_0$  is polar angle on the particle surface [1]. The direction of particle photophoretic movement is defined completely with the sign of  $J_1$  factor and no variations of accommodation coefficients can change the force sign as recent analysis of equation (1) showed. In addition, it turns out that  $J_1$  factor essentially defines the order of photophoretic force magnitudes. So, it is clear, to calculate and analyze photophoretic complex problem we ought to give attention to the precision of this electrodynamical parameter. No systematic analysis of asymmetry factor values for the real atmospheric aerosols seemed to have been elaborated. Thus, the aim of this investigation is the evaluation of  $J_1$  factor for the basic group of atmospheric aerosols; the analysis of the typical features of  $J_1$  behavior as function of  $m$  and diffraction parameter  $\rho$ ; the estimation of photophoretic force magnitudes taking in consideration the complete solution of this complex problem. So, it is necessary to calculate  $J_1$  as exactly as possible, but excellent precision requires too much evaluation time. Our algorithm allows to get 18 decimal digits and guaranteed correct values for the whole range of diffraction parameter and complex refractive index. Precision of

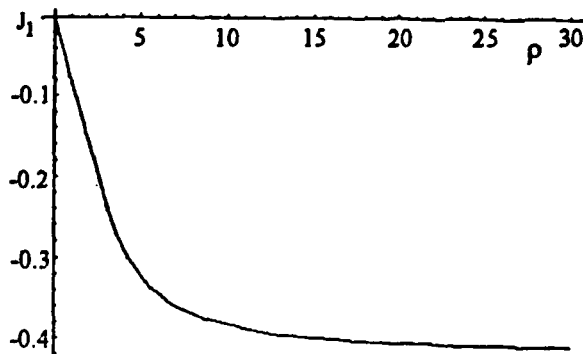


Figure 1: Dependence of  $J_1$  factor on diffraction parameter  $\rho$  for soot particle; the light wavelength is  $\lambda = 0.5 \mu\text{m}$ ;  $m = 1.82 + 0.74i$  [4]

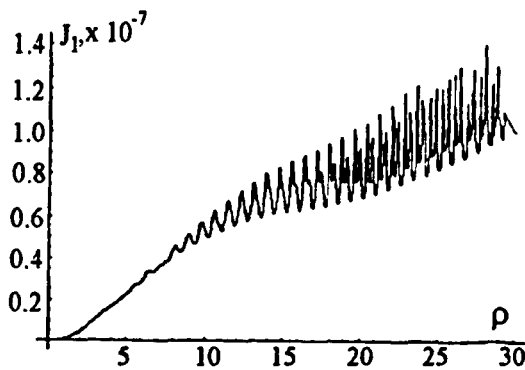


Figure 2: Dependence of  $J_1$  factor on diffraction parameter  $\rho$  for water droplet; the light wavelength is  $\lambda = 0.525 \mu\text{m}$ ;  $m = 1.334 + 1.32 \cdot 10^{-9}i$  [5]

used method is approached by combination of the best sides of Lenz, Mackowski and Bohren-Huffmen algorithms. Logarithmic derivation and the complex mathematical functions were calculated with continued fraction method, besides the criterion of the number items in Mie series was modified too. There are dependencies  $J_1$  on  $\rho$  for soot spherical particles and water drops as typical samples of real atmospheric aerosols, which have the essential difference of optical properties on Fig. 1 and 2. It is known [6] that photophoresis causes the aerosol particles levitation at upper stratosphere. Fig. 3 illustrates the competition of photophoretic force with the gravitational force for upper stratosphere. Further environmental applications in detail can be expound in full presentation version.

This work was partially supported by the Grant for Scientific Research (No. 96-01-00756) from the Russian Foundation for Basic Research (RFFI).

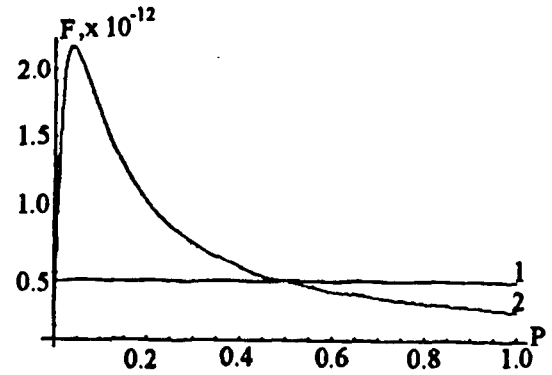


Figure 3: Dependences gravitational (1) and photophoretic (2) forces on pressure  $P$  (in atmospheric pressure units) for soot particle.  $R_0 = 4 \mu\text{m}$ ;  $\Lambda = 4.91$  and particle density  $165 \frac{\text{kg}}{\text{m}^3}$  [7];  $I = 1368 \frac{\text{W}}{\text{m}^2}$  [4];  $T_0 = 255\text{K}$ ;  $\lambda = 0.525 \mu\text{m}$

## References

- [1] Beresnev S., Chernyak V., Fomyagin G., *Photophoresis of a spherical particle in rarefied gas*, Phys. Fluids A., Vol.5, No.8, pp.2043-2052, 1993.
- [2] Beresnev S.A., Bogolepov A.I., Suetin P.E., *Theoretical and experimental study of macroscopic particle photophoresis at arbitrary Knudsen numbers*, Proceeding of the 20th International Symposium on Rarefied Gas Dynamics, pp.918-923, Peking University Press, Beijing, China, 1997.
- [3] Bohren C.F. and Huffmen D.R., *Absorption and scattering of light by small particles*, Wiley Pub, New York, 1983.
- [4] Zuev V.E., Krekov G.M., *Optical atmosphere models / The modern problems of atmosphere optics. Vol.2*, Gidrometeoizdat, Leningrad, 1986 (in Russian).
- [5] Hale G.M., Querry M.R., *Optical constants of water in the 200-nm to 200- $\mu\text{m}$  wavelength region*, Applied Optics, Vol.12, No.3, pp.556-558, 1973.
- [6] Rohatschek H., *Levitation of mesospheric and stratospheric aerosols by gravito-photophoresis*, J. Aerosol Sci., Vol.27, No.3, pp.467-471, 1996.
- [7] Chyrkin V.S. *Thermophysics properties of the nuclear thechnics substances*, Atomizdat, Moscow, 1968 (in Russian).

# Diffusiophoresis of a Spherical Particle at Arbitrary Knudsen Numbers \*

S.A.Beresnev, V.G.Chernyak, S.A.Starikov

Department of Molecular Physics, Ural State University, Ekaterinburg, Russia

## 1 Introduction

Concentration gradients of the chemical species in a gas mixture are known to cause movement of aerosol particles. The particle motion is commonly termed "diffusiophoresis", and the force producing this motion is known as "diffusion force". This phenomenon, which cannot be described within the ordinary continuum theory, may find various technological applications, one of which will be the separation and collection of small particles (micron- and submicron-sized). The theory of diffusiophoresis has been developed previously only for particles whose radius was either much smaller or much larger than the mean-free path of the gas molecules [1]. The analysis covering the regime of an intermediate Knudsen number, i.e., the transition regime, is an important but difficult problem in aerosol microphysics. Various technological applications require reliable theoretical predictions for the diffusiophoretic force and velocity over the wide range of Knudsen numbers, covering the range from the slip flow to the free-molecular flow. A few studies have been made in the transition regime based on various approximations of the Boltzmann equation solutions or on numerical calculations for the gas-kinetic model equations. Among semi-empirical theories giving a satisfactory description of the diffusion force and velocity over a wide range of Knudsen numbers are the works by Annis et al. (the "giant molecules" method) [2]. This theoretical model treats the aerosol particles as one component of the multicomponent gas mixture. This method, however, is not free from certain physical contradictions and includes a great number of adjustable parameters. A strict approach to this problem should be based on solving the kinetic equation with corresponding boundary conditions. The complexity of the collision integral in the Boltzmann equation has led to the use of gas-kinetic model equations. A

simple method of construction of the linearized kinetic models for gaseous mixtures was proposed by McCormack [3]. In this study the diffusiophoresis problem was solved on the basis of the linearized McCormack kinetic equation [3] with diffuse type boundary conditions on the particle surface. Thus, the aim of this work is the elaboration of a consistent gas-kinetic theory for the diffusion force, friction force, diffusiophoretic velocity and the study of their dependencies on the properties of an aerosol particle and binary gas mixture.

## 2 Statement of the problem

Consider a spherical particle of radius  $R_0$  suspended in an infinite expanse of binary gas mixture with a low concentration gradient  $|\nabla x_1|$  (far from the particle) along OZ axis. The particle surface temperature and the temperature of a gas mixture are the same (and constant). The total gas pressure is constant and equals  $p_0$ . As the concentration gradients are small, the velocity distribution functions for the species 1 and 2 can be linearized. This allows to split the problem (the diffusion force problem and the friction force problem). Here we devote the main attention to the first aspect; the second has been considered in detail in [4], and these results can be used here to calculate the diffusiophoretic velocity. The origin of the spherical coordinates  $(r, \theta, \varphi)$  is at the center of the particle. Axial symmetry applies here, i.e., the macroscopic parameters characterizing the states of particle and gas are dependent only on the radial coordinate  $r$  and polar angle  $\theta$ . Then the state of the gas can be described by a molecular velocity functions that are slightly different from the Maxwellian distributions:

$$f_1 = f_{10} \left[ \frac{1 + \frac{|\nabla x_1|}{x_1} z}{+2C_{1z}(U_{1\infty} + V_{1\infty}) + h_1} \right], \quad (1)$$

$$f_2 = f_{20} \left[ \frac{1 - \frac{|\nabla x_1|}{1-x_1} z}{+2C_{2z}(U_{2\infty} + V_{2\infty}) + h_2} \right], \quad (2)$$

\*Abstract 4902 submitted to the 21st International Symposium on Rarefied Gas Dynamics, Marseille, France, July 26-31, 1998

where  $f_{\alpha 0}$  are the Maxwellian distributions with parameters  $T, n_{\alpha 0}$  (at  $r \rightarrow \infty, \theta = \pm \frac{\pi}{2}$ );  $C_{\alpha z}(\vec{U}_{\alpha \infty}, \vec{V}_{\alpha \infty}) = V_{\alpha z}(\vec{U}_{\alpha \infty}, \vec{V}_{\alpha \infty})$ ; where  $V_{\alpha}$  is the molecular velocity of species  $\alpha$ ,  $\vec{U}_{\alpha \infty}$  is the mean velocity of species  $\alpha$ , and  $\vec{V}_{\infty}$  is the mass average velocity of the gas mixture.

The problem is solved in a steady-state formulation on the basis of linearized McCormack kinetic equation of second order [3]:

$$\vec{C}_1 \frac{\partial}{\partial \vec{r}_1} h_{1D} = -h_{1D} + \nu_1 + 2(1 - \varphi_{12}^{(1)}) \times (C_{1r}U_{1r} + C_{1\theta}U_{1\theta}), \quad (3)$$

$$\vec{C}_2 \frac{\partial}{\partial \vec{r}_2} h_{2D} = -h_{1D} + \nu_2 + 2(C_{2r}U_{2r} + C_{2\theta}U_{2\theta}), \quad (4)$$

where  $\vec{r}_\alpha = \vec{r} \gamma_{\alpha 2} \sqrt{\frac{m_\alpha}{2kT}}$ ,  $\varphi_{12}^{(1)} = \frac{\nu_{12}^{(1)}}{\gamma_{12}}$ , and the collision frequencies  $\gamma_{\alpha\beta}, \nu_{\alpha\beta}^{(i)}$  are defined in [3]. Consider a special cases for gaseous mixture approximations (so-called the Lorentz's and the Rayleigh's (quasi-Lorentz's) mixture. In the first case  $n_1/n_2 \ll 1, m_1/m_2 \ll 1$ ; in the second case  $n_1/n_2 \ll 1, m_1/m_2 \gg 1$ .

At these assumptions from Eqs.(3)-(4) we obtain the simplified kinetic equations for species 1 and 2.

### 3 Basic equations and the method of solution

The kinetic equations (3)-(4) at approximation  $x_1 \ll 1$  are formally integrated along the characteristics and transformed into the systems of integral equations for the number density and macroscopic velocity of species 1 and 2. The resulting system closes with integral relations obtained from balance equations on the particle surface. The integral equations included into the system being the non-uniform Fredholm equations. The Bubnov-Galerkin method can be used for their solution. The trial functions for macroparameters are chosen so as to obtain the correct hydrodynamic solution [1]. The exact free molecular values for macroparameters are contained in the absolute terms of the system. Further solution of the problem is reduced to the numerical calculation of Galerkin integral coefficients, determination of the constants in trial functions, and, ultimately, to the calculation of the diffusion force as a function of Knudsen number. The particle moving in non-uniform gaseous mixture is also affected by viscous drag [4]. In this case, the velocity of the unfixed particle in a concentration gra-

dient field (the diffusiophoretic velocity) is determined from condition

$$\vec{F}_D + \vec{F}_U = 0 \quad (5)$$

### 4 The results

In the slip-flow regime ( $Kn \ll 1$ ) and in the free-molecular limit ( $Kn \rightarrow \infty$ ) for the case of complete accommodation we obtain following asymptotic expressions:

$$F_D (\text{Lorentz}) = -\frac{6\pi}{\sqrt{2}} \eta_2 \sqrt{\frac{m_1}{m_2}} \times \times R_0 D_{12} \frac{d_2^2}{d_{12}^2} |\nabla x_1|, \quad (6)$$

$$d_{12} = \frac{d_1 + d_2}{2},$$

$$F_D (\text{Releigh}) = 6\pi \eta_2 \frac{m_1}{m_2} \times \times R_0 D_{12} |\nabla x_1|, \quad (7)$$

$$F_D (\text{Lorentz}) = -\frac{8}{3} R_0^2 n_{20} \times \times \sqrt{2\pi kT} |\nabla x_1| \times \times \sqrt{m_1} D_{12} \left(1 + \frac{\pi}{8}\right) \quad (8)$$

$$F_D (\text{Releigh}) = \frac{8}{3} R_0^2 n_{20} \times \times \sqrt{2\pi kT} |\nabla x_1| \times \times \frac{m_1}{\sqrt{m_1}} D_{12} \left(1 + \frac{\pi}{8}\right). \quad (9)$$

Numerical calculations were carried out at intermediate Kn numbers in the case  $x_1 \ll 1$ . The comparison of the presented theory with available experimental data represents a great interest. Among not numerous experimental data which satisfy to the assumption  $x_1 \ll 1$ , it is necessary to mark out the results [5-6] (stationary diffusion of water vapour through stagnant air [5] and nitrogen [6]; so-called diffusion of species 1 through stagnant species 2, SD-scheme [1]). It is seen that the predicted diffusiophoretic velocity is the same in the slip-flow regime as in the transition regime [2].

This work was supported by the Grant for Scientific Research (No. 96-01-00756) from the Russian Foundation for Basic Research.

### References

- [1] Hidy G.M., Brock J.R. *The dynamics of aerosol colloidal systems*. Pergamon Press, 1970.

- [2] Mason E.A., Malinauskas A.P. *Gas transport in porous media: The dusty-gas model*. Elsevier, 1983.
- [3] McCormack F.J. *Construction of linearized kinetic models for gaseous mixtures and molecular gases*. Physics of Fluids, 1973, Vol.16, No.12, p.2095-2105.
- [4] Beresnev S.A., Chernyak V.G., Fomyagin G.A. *Motion of a spherical particle in a rarefied gas. Part 2. Drag and thermal polarization*. J.Fluid Mechanics, 1990, Vol.219, p.405-421.
- [5] Derjaguin B.V., Yalamov Yu.I., Storozhilova A.I. *Diffusiophoresis of large aerosol particles*. J.Colloid Interface Sci., 1966, Vol.22, p.117-125.
- [6] Schmitt K.H. *Untersuchungen an Schwebstoffteilchen in diffundierenden Wasserdampf*. Z.Naturforschg., 1961, Bd.16a, H.10, S.144-149.

## Gas Condensation by the Porous Layer \*

A.I. Erofeev, O.G. Friedlander, M.N. Kogan  
Central Aerohydrodynamics Institute (TsAGI)  
1, Zhukovsky str., 140160 Zhukovsky, Russia

Heterogeneous reactions play a very important role in many natural and antropogenic processes. For instance, we can mention catalytic reactions in chemical industry, polar stratospheric clouds and ozone holes formation. In the present report a simplest heterogeneous process, namely, condensation in porous media will be considered. The main problem is to define the active surface of the porous body.

Let us consider tubular layer composed of flat or cylindrical parallel channels on the walls of which condensation takes place. Solutions of kinetic Boltzmann equation by DSMC method were obtained. The solutions are defined by five parameters: supersaturation  $(n_\infty - n_s(T_w))/n_\infty$ , walls condensation coefficient  $\alpha_c$ , Knudsen rarefaction parameter  $Kn_d$  ( $d$  is characteristic height of channel), relative channel length  $L/d$  and porosity  $P$ . VHS molecule model corresponding to parameter  $\omega=0.7$  in viscosity/temperature relation  $\mu \propto T^\omega$  is used. Diffuse molecule reflection at the walls is assumed with temperature  $T_w$  and condensation coefficient  $\alpha_c$ . Far from porous layer vapour temperature  $T_\infty=T_w$  and number density  $(n_\infty - n_s(T_w))/n_\infty=0.2$  were selected for calculations. Such small supersaturation provides molecular flow rate/supersaturation linear relation. The other parameters were chosen as follows:  $0.05 \leq \alpha_c \leq 0.5$ ,  $0 \leq Kn_d^{-1} \leq 8$ ,  $2.5 \leq L/d \leq 40$ ,  $0.5 \leq P \leq 1$ . Calculations performed show that there exists such limiting porous layer thickness  $L_c \sim d/\alpha_c^{1/2}$  when condensation flux do not increase at  $L > L_c$ .

Two approximate approaches will be also presented. For small  $\alpha_c$  one dimensional approximation of the flow in a single channel is used. The interaction between channels is modelled using analogy between layer adjacent to the porous body and Knudsen layers near condensing plate (see more details in [1]). Combination of two methods permits to obtain analytical expression for condensing gas flux at arbitrary porosity.

Both approach provide sufficiently good accuracy especially at  $\alpha_c \leq 0.2$ . The error in condensing gas flux does not exceed 5% as compared to numerical results. So the active surface of porous body can be estimated.

## Acknowledgement

The work is carried out at support of International Science and Technology Center (Project 200) and State Program for Leading Research Groups (grant 96-15-96063)

## References

- [1] Erofeev A.I., Friedlander O.G., Kogan M.N., *Rarefied gas flow through porous layer*. Abstract 4941 submitted to the 21st International Symposium on Rarefied Gas Dynamics

\*Abstract 4942 submitted to the 21st International Symposium on Rarefied Gas Dynamics, Marseille, France, July 26-31, 1998



# Condensive Interaction of Porous Particles in Rarefied Gas \*

A.I. Erofeev, O.G. Friedlander, M.N. Kogan  
Central Aerohydrodynamics Institute (TsAGI)  
1, Zhukovsky str., 140160 Zhukovsky, Russia

Catalytic properties of particles in a reacting or condensing gas are defined by their active surface. The dimensions and configuration of particles particularly depends on coagulation process. Any difference in particles velocities can lead to coagulation. An attraction or repulsion between particles enhances or decreases the coagulation rate. In the paper [1] it was shown that condensing particles attract each other in free-molecular flow regime ( $Kn_D \rightarrow \infty$ ). It is obvious that condensation active surface and hence condensation flux on the particle will depend not only on its diameter but also on its porosity. So do the interaction forces.

The aim of the present work is twofold: to define the attractive force at different Knudsen numbers and to estimate the influence of porosity on this force. For porous particles condensation interaction is defined by many parameters. Besides the external parameters there are several internal ones defining porosity and other properties of particle material. Among them are: supersaturation  $n_\infty - n_s(T_w)$ , temperature ratio  $T_\infty/T_w$ , relative distance between particles  $L/D$ , external and internal Knudsen numbers  $Kn_D = \lambda/D$  and  $Kn_d = \lambda/d$  ( $D$  and  $d$  are size of particle and pore width, respectively), porosity  $P$ , condensation coefficient for given particle material  $\alpha_c$ .

The methods developed in work [2] make it possible to divide the problem of condensation inside the particle and the problem of particles interaction caused by condensation. This approximate approach permits to determine the effective condensation coefficient for particles of different form and other parameters necessary to solve external flow problem. The determination of condensive force was carried out by DSMC method for one-component gas and two-component gas mixture for wide range of Knudsen numbers and values of effective condensation coefficient. The problem with one-component gas was solved under strong su-

persaturation conditions. Within the problem of two-component mixture the force generated by the condensed species was studied particularly. The asymptotic value ( $Kn_D \rightarrow 0$ ) was determined.

## Acknowledgement

The work is carried out at support of International Science and Technology Center (Project 200) and State Program for Leading Research Groups (grant 96-15-96063)

## References

- [1] Kogan M.N., Bobrov I.N., Cercignani C., Frezzotti A., *Interaction of evaporating and condensing particles in the free-molecular regime* Phys. Fluids, Vol.7, N7, pp.1775-1781, 1995.
- [2] Erofeev A.I., Friedlander O.G., Kogan M.N., *Gas condensation by porous layer*. Abstract 4942 submitted to the 21st International Symposium on Rarefied Gas Dynamics

\*Abstract 4943 submitted to the 21st International Symposium on Rarefied Gas Dynamics, Marseille, France, July 26-31, 1998

## Two-dimensional problems with temperature gradient along the interphase at the presence of evaporation-condensation \*

A.P.Kryukov, I.N.Shishkova

Department of Low Temperatures, Moscow Power Engineering Institute, Russia  
Inst. High-Performance Comp. and Data Bases, Russia

The two-dimensional problems for evaporation-condensation of a rarefied gas in a rectangular domain with temperature gradient are studied. At this the method of direct numerical solving of the Boltzmann equation [1] is used.

The nonlinear half-space problem has been studied by many authors, the one-dimensional problem for evaporation-condensation (recondensation) between two parallel surfaces has been investigated too. The two- and three-dimensional non-steady problems were less researched.

The statement of the problem is shown in Fig.1. There is vapour in the rectangular domain limited by non-penetrable surfaces with temperature  $T_w = 1$  and interphase with temperature  $T_s(x)$ .  $T_s(x)$  is the lineary function of  $x$ . The vapour density depends on  $x$  lineary or exponentially and is varied from  $n_{s,1}$  to  $n_{s,2}$ . The temperature and density are non-dimensional values related to base parameters. On the limiting non-penetrable surfaces full energy accommodation of molecules is assumed, and velocity distribution function for reflected molecules is half-Maxwellian with zero flow velocity. In zero moment of the time vapour density and temerature in domain are amounted equal to unit.

The example of solution results for steady stage, i.e. large enough time, are presented in Fig.2, 3 for  $n_{s,1} = 1$ ,  $n_{s,2} = 5$ ,  $T_{s,1} = T_w$ ,  $T_{s,2} = 2$  and linear dependence  $n_s(x)$ . Dependences of the mass flux density  $j$  on  $x$  for the various cross-section along  $y$  are shown in Fig.2. In Fig.3 the velocity vectors are presented.  $\lambda$  is mean free path of the vapour at  $n_{s,1}$  and  $T_{s,1}$ .

Formation of the two main ranges of the flow near the interphase is obtained: evaporation part and condensation part. The convective circulation motion is formed. In spite of evaporation along the

all length of the interphase, vapour flows from right side of the surface to the left and is condensed. The maximum flux velocity is  $0.4v^*$ , where  $v^* = \sqrt{RT_w}$ . Therefore this problem is interpreted as the recondensation problem in two-dimensional statement.

The calculations demonstrate, that rise of the  $n_{s,2}$  from 5 to 10 gives the increase of the average density within 30% only.

The investigated problem was studied in another modification also: The interphase is divided in the middle on two parts by non-penetrable surface of different width  $\delta$ . In this case the motion of the vapour is much less. Figures will be presented in 21st International Symposium on RGD. For a example the maximum flux velocity is  $0.12v^*$  for  $\delta = 1.67\lambda$  instead of the value  $0.4v^*$  for the case without non-penetrable middle surface.

This work was supported by the Russian Ministry of Science and Technical Policy and by Russian Foundation for Basic Researches, Grant N 97-03-46003.

## References

- [1] Aristov V.V., Tcheremissine F.G., *The direct numerical solving of the kinetic Boltzmann equation*, Moscow: Computing Center of the Russian Academy of Science. 1992.

\* Abstract 4982 submitted to the 21st International Symposium on Rarefied Gas Dynamics, Marseille, France, July 26-31, 1998

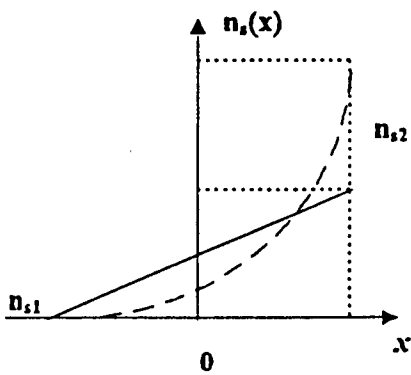
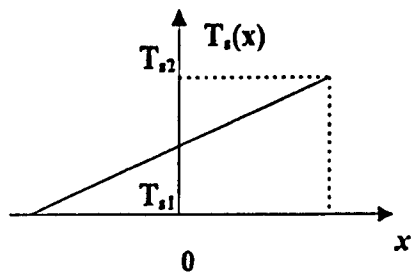
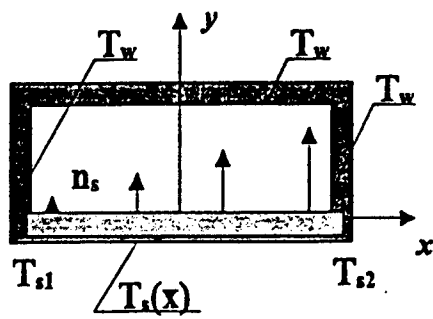


Fig.1

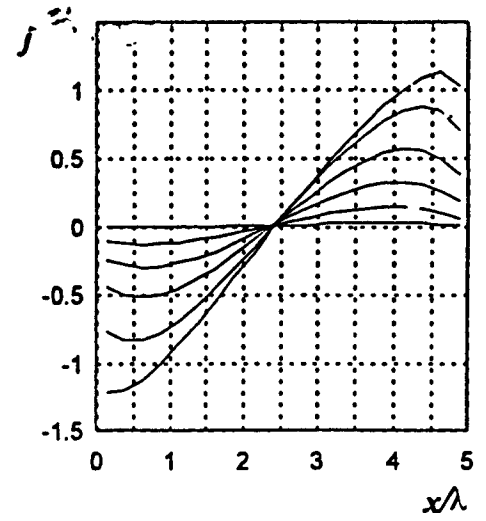


Fig.2

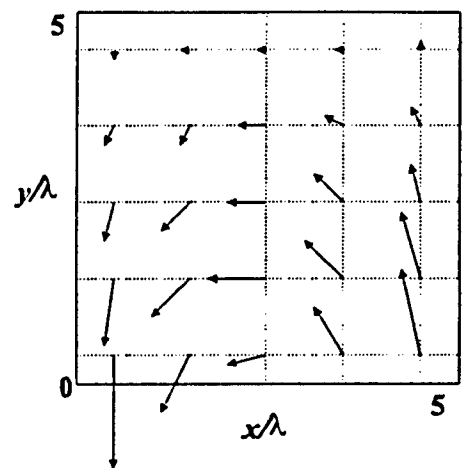


Fig.3

## Small Clusters of Water Vapor in Aircraft Near Wake \*

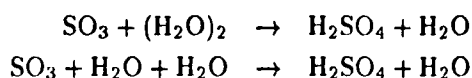
B.V. Egorov, Yu.E. Markachev, E.A. Plekhanov, V.L. Yumashev  
TsAGI, Zhukovski, Russia

Employing gas kinetic model, formation of water vapor dimers, mixed clusters of water vapor with sulfur trioxide and possibility of formation of sulfuric acid in aircraft near wake is studied.

*In-situ* measurements of combustion products emission during flights of *Concorde* in lower stratosphere uncovered high density of aerosols of small size and high degree of conversion of fuel sulfur to sulfuric acid, which did not correspond to numerical simulations based on classical theory of nucleation and assumption about gas phase mechanism of  $H_2SO_4$  formation [1]. Such high degree of conversion of fuel sulfur to  $H_2SO_4$  could be achieved if inside powerplant sulfur would oxidize to sulfur trioxide  $SO_3$  instead of sulfur dioxide  $SO_2$  as current combustion theory predicts [2].

In present study numerical simulations of fuel combustion in SPS-2 powerplant, with nonequilibrium vibrational excitation of molecular hydrogen  $H_2$  taken into account, were performed. Vibrational energy of  $H_2$  is disactivated in nozzle part of engine primarily by vibrational-vibrational  $W'$  exchange with hydroxyl (OH) molecules, mole fraction of which is small. This leads to substantial nonequilibrium of vibrational energy of  $H_2$  and significant increase of speed constant  $K(T, T_{H_2})$  of reaction  $H_2(i) + OH \rightleftharpoons H_2O + H$  in nozzle part and aircraft near wake. Decrease of hydroxyl (OH) level in combustion products because of this effect leads to decrease in production of  $SO_3$  and, in the end, to decrease of level of gaseous sulfuric acid  $H_2SO_4$  in aircraft near wake.

An alternative to gas phase way of  $H_2SO_4$  formation according to (Calwest J.G., Stockwell W.R.) mechanism is cluster one [3]



In present study calculation of numerical density

\*Abstract 5001 submitted to the 21st International Symposium on Rarefied Gas Dynamics, Marseille, France, July 26-31, 1998

of water vapor dimers  $(H_2O)_2$  and  $SO_3 \cdot H_2O$  clusters inside supersonic part of engine and near wake of supersonic and subsonic aircraft was performed. For calculation of numerical density of clusters gas-kinetic model [4] was used. Cluster dissociation constant  $K_{dis}$  was found using monomolecular decay theory, cluster formation constant  $K$  was defined using equilibrium constant  $K_{eq}$ :

$$K_{eq} = \frac{f(\theta_i/T)}{T^4} \exp(E_{dis}/RT), atm^{-1}, \quad (1)$$

where  $E_{dis}$  - dissociation energy,  $\theta_i$  - characteristic vibrational temperatures of the dimer. Values of characteristic intermolecular vibrational temperatures of clusters  $(H_2O)_2$  and  $SO_3 \cdot H_2O$  were found using *ab initio* molecular orbital method. Equation (3) was used to find the standard Gibbs free energy change  $\Delta_{dim}^0 = -RT \log K_{eq}$ , which was compared with existing experimental data.

Numerical simulation of gas dynamic and kinematic parameters of stationary axisymmetrical supersonic flow with mixing, combustion of hydrocarbon fuel and clusterization kinetics taken into account was performed with serial method using parabolized Navier-Stokes equations.

Performed calculations have shown that formation of sulfuric acid  $H_2SO_4$  in aircraft wake occurs primarily in cluster channels (1)-(2). The speed of  $H_2SO_4$  production in these channels is by several orders of magnitude greater than that in common gas phase way, although total quantity of produced sulfuric acid depends only on mole fraction of sulfur trioxide  $SO_3$  at exit from aircraft nozzle.

In conclusion authors express their gratitude to prof. M.N. Kogan for his interest to present work and valuable comments made during its progress.

## References

- [1] Kačher B., Fahey D.W. The role of sulfur emission in volatile particle formation in jet aircraft exhausted plumes // *Geophys. Res. Lett.*, 1997, vol. 24, N 4, pp. 389-392.

- [2] Miale-Lye R.C., M.R. Anderson, R.C. Brown et al. The conversion of  $\text{SO}_2$  to  $\text{SO}_3$  in gas turbine engines //Proceedings of International Colloquium: Impact of Aircraft Emissions upon the atmosphere. Paris Clamant 15-18 October, 1996, vol. I, pp. 125-130.
- [3] C.E. Kolb, J.T. Jayne, D.R. Worshop et al. Gas Phase Reaction of Sulfur Trioxide with Water Vapor //J. Am. Chem. Soc., 1994, v. 116, pp. 10314-10315.
- [4] B.V. Egorov, Yu.E. Markachev. Influence of simplest  $\text{CO}_2$  clusters on hypersonic wind tunnel flows and aerodynamic parameters //Proceedings of the 20th International Symposium RGD, 1997, pp. 906-911.

## One-Dimensional Supersonic Condensation of a Polyatomic Gas \*

I. Kuznetsova, Yu. Yalamov, A. Yushkanov  
Moscow Pedagogical University, Moscow, Russia

The process of supersonic condensation has been investigated in [1-3]. In the paper [1] the surface,  $F(T_s, n_s, T, n, M) = 0$  which determines the relation of gas parameters outside the Knudsen layer: temperature  $T$ , concentration  $n$  and Mach number  $M$  to surface temperature  $T_s$  and saturation vapour concentration  $n_s$ , was obtained. However, authors of [2] have demonstrated, that in the case of supersonic condensation there is a subspace, not surface, of gas parameters in the space  $T, n, M$ . Some sets of gas parameters outside the surface  $F(T_s, n_s, T, n, M) = 0$  have been obtained by numerical method in [2].

In the supersonic condensation regime the shock wave before a condensation surface may exist. The shock wave transforms a supersonic flow into a subsonic. In the case of subsonic condensation such stationary solutions with a shock wave don't exist. The coordinate of the shock wave center is an additional parameter. This parameter brings about the transformation of admissible parameter surface in the case of subsonic condensation into some region of admissible parameters in the case of supersonic condensation.

In present work the problem of a supersonic condensation of a molecular gas in assumption, that with  $M > 1$  the shock-wave type structures near a surface may exist is considered. To describe these structures the Mott-Smith method [4] is used. The analogous approach has been applied in [3].

We take into account internal degrees of freedom of molecules by alteration the value of specific heat of the gas. The influence of internal degrees of freedom on the molecular collision dynamics is not considered. This approach has been developed by Mott-Smith in his work on the structure of a shock waves in molecular gases. Lately this approach was applied to the problem of subsonic condensation of polyatomic gases [5].

In accordance with [4] the volume distribution function of molecules  $f_{vq}$  for one- two- and three-atom

gases (i.e.  $q=1,2,3$ ) has the following form

$$f_{v1}(x, \vec{v}) = \sum_{i=1}^2 a_i(x) \left( \frac{m}{2\pi k T_i} \right)^{3/2} \times \exp \left\{ -\frac{m(\vec{v} - \vec{u}_i)^2}{2k T_i} \right\} \quad (1)$$

$$f_{vq}(x, \vec{v}, w) = \sum_{i=1}^2 a_i(x) h_{qi} \left( \frac{m}{2\pi k T_i} \right)^{3/2} \times \exp \left\{ -\frac{m(\vec{v} - \vec{u}_i)^2 + I w^2}{2k T_i} \right\} \quad (2)$$

$$h_{2i} = \frac{I w}{k T_i}, \quad h_{3i} = \left( \frac{I}{k T_i} \right)^{3/2} \frac{w^2}{\sqrt{2\pi}}$$

Where  $I$  is momentum of inertia,  $w$  is cyclic frequency, subscript  $i = 1$  corresponds to gas parameters outside the Knudsen layer, while subscript  $i = 2$  indicates parameter inside this layer.

Coefficients  $a_1(x)$  and  $a_2(x)$  must satisfy the following conditions at infinity

$$x \rightarrow \infty: \quad a_1(x) = n_1; \quad a_2(x) = 0 \quad (3)$$

The generalised Anisimov [6] boundary condition for distribution function  $f_q^-$  of the molecules moving towards the surface is used

$$f_q^- = \beta f_{vq} + \alpha f_{sq}, \quad v_x < 0 \quad (4)$$

$$f_{s1}(\vec{v}) = n_s \left( \frac{m}{2\pi k T_s} \right)^{3/2} \exp \left\{ -\frac{m v^2}{2k T_s} \right\} \quad (5)$$

$$f_{sq}(\vec{v}, w) = n_s h_{sq} \left( \frac{m}{2\pi k T_s} \right)^{3/2} \times \exp \left\{ -\frac{m v^2 + I w^2}{2k T_s} \right\} \quad (6)$$

$$h_{s2} = \frac{I w}{k T_s}, \quad h_{s3} = \left( \frac{I}{k T_s} \right)^{3/2} \frac{w^2}{\sqrt{2\pi}}$$

Here  $\beta$  and  $\alpha$  are some coefficients, obeying conditions

$$\alpha > 0, \quad \beta > 0 \quad (7)$$

\*Abstract 5006 submitted to the 21st International Symposium on Rarefied Gas Dynamics, Marseille, France, July 26-31, 1998

The introduction of coefficient  $\alpha$  permits to take into account the possibility of evaporated molecules to return to the surface due to collisions.

It is assumed, that the distribution function of evaporated molecules ( $v_x > 0$ ) for one-, two- and three-atom gases has the following form

$$f_q^+ = f_{sq}, \quad v_x > 0 \quad (8)$$

The Boltzmann equation solution for the function  $f_{vq}$  can be obtained in the analogous way as the Mott-Smith solution of the shock wave problem [4]. For Maxwell molecules the corresponding solution has the following form

$$a_1(x) = -\frac{n_1}{1 + A_0 \exp(Lx)} + n_1 \quad (9)$$

$$a_2(x) = \frac{n_2}{1 + A_0 \exp(Lx)} \quad (10)$$

$$L = \frac{16}{15} \left( \frac{2}{\pi} \right)^{1/2} \frac{(3+j)^{3/2} (5+j)^{1/2}}{(2+j)(4+j)} \times \\ \times \frac{[(5+j)M_1^2 - 1](M_1^2 - 1) M_2}{[(5+j)M_1^2 + 3 + j] M_1^2} \lambda^{-1}$$

Here  $A_0$  is integration constant,  $\lambda$  is mean free path outside the Knudsen layer,  $j = 0$  for one-atom gases,  $j = 2, 3$  for two- and three-atom gases,  $A$  and  $K$  - the constants, describing the intermolecular interaction [7].

In the case  $A_0 > 0$  the solution Eq.9, 10 describes the shock wave. This solution exists at all values of variable  $x$ . But in the condensation problem the solution must be obtained in the half-space  $x > 0$  only. So we must require the analytic behavior of Eq.9 and Eq.10 expressions in the half-space  $x > 0$  only. The last condition is less rigid and leads to the additional interval of the admissible integration constant values:  $A_0 < -1$ .

The laws of conservation and relation Eq.7 impose some limitations on distribution function  $f_{vq}$ . We must demand also that the concentration of the molecules approaching the surface is positive. These limitations result in interception of the range of permitted parameters (subspace in the space  $T_1/T_s, n_1/n_s, M_1$ ), in which the solution of Boltzmann equation exists. This range in Fig.1 (for  $M_1 = 1.1$ ) is not shaded.

Solutions of shock-wave type ( $A_0 > 0$ ) are ranged between solid curves 1 for one-atom gases, dashed curve 2 for two-atom gases and dot-and-dash curve 3 for three-atom gases. Solution of quasishock-wave type ( $A_0 < -1$ ) exists in the ranges above and below that of shock-wave type. For one-atom gas this

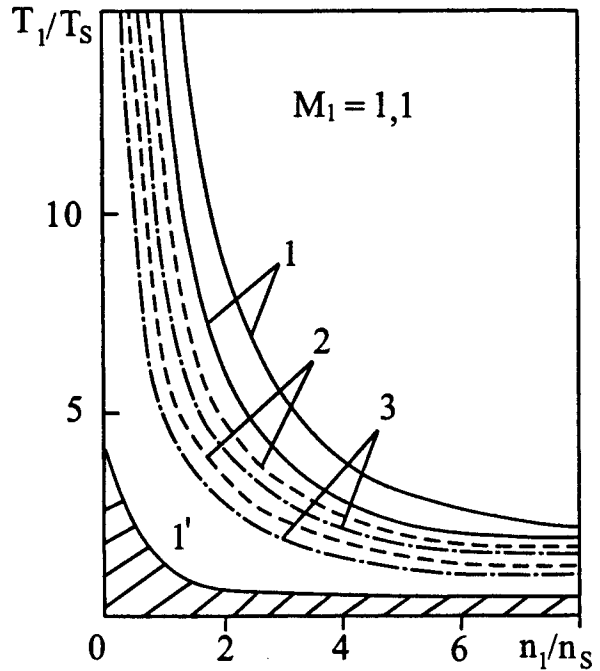


Figure 1:

solution is limited by curve 1'. In the case of molecular gas this curve slightly shifts towards the range of solutions of shock-wave type.

## References

- [1] Oguchi H., Yatakeyama M. *Rarefied Gas Dynamics*. N.Y: AIAA, V.2. pp.321, 1981.
- [2] Abramov A.A., Kogan M.N. *Regime of Supersonic condensation of a Gas*, Dokl. Akad. Nauk SSSR, Vol.278, No.5, pp.1078-1081, 1984.
- [3] Kuznetsova I.A., Yushkanov A.A., Yalamov Yu.I., *Supersonic Condensation of Monoatomic Gas*, High Temperature, Vol.35, No.2, pp.339-343. 1997.
- [4] Mott-Smith H. *The Solution of the Boltzmann Equation for a Shock Wave*, Phus. Rev., Vol.82, No.6, pp.885-892, 1951.
- [5] Kuznetsova I.A., Yushkanov A.A., Yalamov Yu.I. *Intense Condensation of a Polyatomic Gas*, Fluid Dynamics, Vol.32, No.6. 1997.
- [6] Anisimov S.I. *Vaporization of Metal Absorbing Laser Radiation*, Physics JETP, Vol.27, pp.182-183, 1968.
- [7] Kogan M.N. *Rarefied Gas Dynamics, Kinetic Theory*, Plenum Press, N.Y. 1969.

## The Effect of a Phase Transition on the Boundary Conditions for Rarefied Gases \*

S.P. Bakanov, V.I. Roldughin  
Institute of Physical Chemistry, Moscow, Russia

In the majority of cases, when considering flows of rarefied gases, the correction terms in boundary conditions play an important role, for example, in the Navier-Sokes approximation. For flows of rarefied gases, a characteristic feature is the presence, in the region of interface between the phases, of a boundary (Knudsen) layer, inside which the equations of fluid dynamics cannot be used, and it is then necessary to employ the Boltzmann kinetic equation to describe the non-equilibrium state.

When the surface has an arbitrary shape, a kinetic description of gas flows encounters considerable computational difficulties, since the problem is then no longer one-dimensional. Calculations for a slightly curved interface at which phase transition may occur were carried out previously, but only for a model kinetic equation and when there is complete accommodation of the molecules of a single-component gas. However, even when solving flow problems using the Boltzmann equation one cannot always give a clear quantitative description of some phenomena because of the lack of information in the majority of cases regarding the nature of the interaction between the gas and the surfaces over which the flow occurs.

Other methods of constructing the boundary conditions for rarefied gases, which differ from the kinetic method, enable the main features of the non-equilibrium processes at interface to be investigated. The method of non-equilibrium thermodynamics is convenient from this point of view; it enables one to obtain required boundary conditions constructed in this way can, of course, only be calculated by solving the kinetic equation (or obtained from experiment). However, as an analysis shown, the majority of these can be calculated by solving the one-dimensional problem.

In this work we use the methods of non-equilibrium thermodynamics to obtain the boundary conditions

for a binary gas mixture at a surface of a condensed phase, where one of the components may undergo a phase transition.

When a phase transition is taken into account, a number of new effects occur in the boundary conditions. Thus, in addition to the jump in temperature there is a jump in the vapor pressure. Unlike the approximations considered previously, the pressure and temperature jumps are governed not only by the heat and mass fluxes but also by the normal component of the momentum flux and by rate of deformation of the surface of the condensed phase. The motion of the condensed phase also give rise to stresses in the Knudsen layer and a previously unknown form of gas slip on surface of gas transition.

---

\* Abstract 5132 submitted to the 21st International Symposium on Rarefied Gas Dynamics, Marseille, France, July 26-31, 1998



## Numerical Analysis of Radial Flow between Evaporating and Absorbing Co-Axial Cylinders\*

E. M. Shakhov

Moscow State Technical University, Moscow, Russia

The problem on steady radial flow between two co-axial cylinders under boundary conditions of evaporation or condensation at each of the cylinders is solved for the kinetic model equation by finite difference method. The numerical algorithm with taking into account the discontinuities of the distribution function in phase space is constructed. To estimate effect of the discontinuities on accuracy of the solution special investigation was undertaken. The paper is mainly devoted to the flow from inner evaporating cylinder to external absolutely absorbing cylinder. Special attention is paid to development of flow close to evaporating surface. It is of particular importance because in limiting regems of flow (both continuum and free molecular) gradients of flow parameters are equal to infinity at the surface. When the distance between cylinders increases the flow becomes close to the limiting case corresponding to evaporation into vacuum.

The opposite case of flow from external evaporating cylinder to absolutely absorbing inner one is studied as well. In this situation the purpose is to describe the flow of gas from infinity where it is at rest to absolutely absorbing cylindrical sink. The boundary conditions at the external cylinder as well as its position is chosen in an appropriate way.

---

\*Abstract 5171 submitted to the 21st International Symposium on Rarefied Gas Dynamics, Marseille, France, July 26-31, 1998

## Stochastic Simulation of Fluctuation Stage in Cluster Formation \*

G.I. Zmievskaya

Keldysh Institut of Applied Mathematics of RAS, Moscow, Russia

## 1 Introduction

The kinetic approach to model phase transition into solids at their fluctuation stage is discussed as well as the mathematical model of the defect's cluster formation. Computer simulation of gases bubbles (blisters) into solids (or pores of vacancies) are of interest for physical and technical problems. The blisters' development on the dielectrics surfaces can lead to the degradation of optical properties. The blister occurrence into metal, contained in plasma discharge, imposes a limit of the ions solubility into crystal lattice. The blistering investigation presents also an interest as a phase transition at its fluctuational stage in system "the flow of vacancy's or ion's -lattice-cluster" is progressing together with the occurrence of non- stable state of solids.

The model of interacting Brownian particles with alternating variable masses  $m(t)$  (in result of fluctuation changes of physical parameters) is used. The description of Brownian motion /BM/ is made in terms of equations of the mathematical physics (Fokker-Planck-Kolmogorov /FPK/ , Boltzmann, Smolukhovskiy-Kramers /SK/) and equivalent equations of the stochastic analog (the stochastic differential equation Ito) /SDE/. The Ito SDE, which has been earlier used for simulation of non-equilibrium physical-chemical processes in gases and plasmas [1], are formulated now for microdynamics of the clusters. The distribution of clusters according to their sizes is determined. The action of external and self-consistent forces in the system is taken into account.

Of special interest is the study of thermodynamic, kinetic and correlation properties of condensed phase found near the point of phase transition and of the critical state points. The role of the fluctuations could be clarified by stochastic model modification for Smolukhovskii-Kramers equation. Here we have come up against the problem of two-dimensional Markov process realization. Let us formulate 1) the physical model of the fluctuational

stage of clusterization into solids, 2) the kinetic equations of the model, 3) its stochastic analogs -SDE, associated with BM, applied to the dynamic of cluster formation into lattice 4) the results of the both: investigation of the BM as a oscillators behavior with non-linear and distribution with size and instant time of the blister origin into metal, dielectrics or layer structure on the base of solution SDE, responsible to Marcovian processes /MP/ approximation.

## Model of the fluctuation stage of the defect's cluster formation

The initial state of the phase transition in vapor-gas mixture is considered as a collection of different size clusters situated into gas. The chaotic molecules are able to encounter, to stick together and to coagulate to the two- (three- and more) particles aggregates. Simultaneously the reverse process of evaporation occurs. Fluctuations in the number of particles, which compose the cluster, are investigated as a one-dimensional Markov process. In general occasions, as a first step of modelling, if vacancy has been localized into metallic crystalline lattices position ( or into interstitial) and the state of the lattice does not change principally. The analogy between coagulating water vapor and "lattice gas" of vacancies has been used. The defect into lattice is equal to water drop as well as gas molecules are similar to lattice vacancies.  $r_g$  is the radius of a cluster or the spherical BP, consisting of  $g$  particles.

**Kinetic equation** The evolution in time the BP distribution function /DF/ can be described as:

$$\frac{\partial f(v, \vec{r}, t)}{\partial t} + v \frac{\partial f(v, \vec{r}, t)}{\partial r} + \frac{\vec{F}(\vec{r}, t)}{m} \frac{\partial f(v, \vec{r}, t)}{\partial v} = (1) \\ I_r(v, \vec{r}, t) + I_v(v, \vec{r}, t), \\ \vec{F}(\vec{r}, t) = F_0 - n \frac{\partial}{\partial r} \int W(|r - r'|) f(v, \vec{r}, t) dr' dv'$$

Here  $I_r(v, \vec{r}, t)$  and  $I_v(v, \vec{r}, t)$ , both represent the motion of BP in  $v, r$ -phase space,

\* Abstract 5307 submitted to the 21st International Symposium on Rarefied Gas Dynamics, Marseille, France, July 26-31, 1998

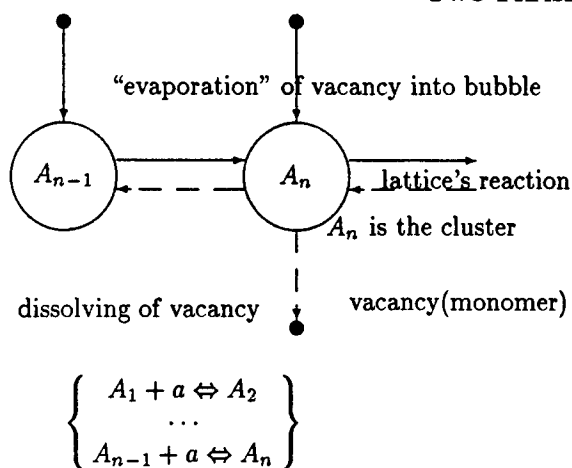


Table 1: The model of the defect's clusterization.

$W(|r-r'| = W_{r,r'})$  and  $\tilde{F}(\vec{r}, t)$  are the potential energy and macroscopic force, respectively. The equation (2) with  $I_v$  (for simplicity, without account  $I_r$  part) is transformed to the FPK equation.

**Stochastic model and FPK equation** A continuous one-dimensional Markov process in  $\{G\}$ -space is:

$$\{g(t), t > 0\}, \quad g \in [2, \{G\}], t \in (0, \infty) \quad (2)$$

$$g(t=0) = g_0 \quad (3)$$

In this process a particle joins the cluster or vaporized from its surface ( $\Delta g = \pm 1$ ). The problem in terms of FPK equation, which is for  $f(g, t)$  the Kolmogorov equation was formulated, related with the Folmer-Zel'dovich problem of the non steady state fluctuation formation description using the following:

$$\frac{\partial f(g, t)}{\partial t} = \frac{\partial}{\partial g} [D(g, t) \frac{\partial f(g, t)}{\partial g}] + \quad (4)$$

$$\frac{1}{kT} \frac{\partial}{\partial g} [D(g, t) f(g, t) \frac{\partial}{\partial g} \{\Delta \Phi(g, t)\}]. \quad (5)$$

Here  $f(g, t)dg$  is the number of clusters in a size interval  $[g, g + \Delta g]$  in a unit volume  $V$ ,  $\Delta \Phi(g, t)$  is the thermodynamic potential or free energy of cluster formation. This function can be approximated by the power series in the cluster size: ( $\Delta \Phi = -(a + c)g + bg^{2/3}$ ),  $D = D(g, t, p, T)$  is a diffusion coefficient  $D(g, t, p, T)$ , it depends on both temperature  $T$  and gas pressure  $p$ , the dependence on cluster size  $g$  is ( $D \sim g^{2/3}$ ) Ito SDE with  $dW$ -Wiener stochastic process have a form:

$$\begin{aligned} dX_t &= H(X(t))dt + \sigma(X(t))dW_t \\ X_{t=0} &= X_0, t \in [t_0, T], \end{aligned} \quad (6)$$

The stochastic simulation method defines concretely the procedure of the stochastic integral calculation and fulfills the requirements of boundedness and smoothness of SDE coefficients. The important points in computer simulation experience are the "standard white noise" approximation and the choice of the time interval needed for the SDE stochastic integral calculations.

The solution of SDE sets (7) for the given initial and boundary conditions is to be interpreted in a mean square sense. At the same time we use the set of random process trajectories ( $i$ ), providing the estimate of the random values mathematical expectation,  $M(g) = \frac{1}{N_L} \sum_i^{N_L} g_i$  and particle size dispersion  $D(g)$ , determined as:  $D(g) = \frac{1}{N_L} \sum_i^{N_L} (g_i - \bar{g})^2$ ,  $\bar{g} \equiv M(g)$  to analyze the one-particle DF.

**Ito-Stratonovich SDE** SDE for Fol'mer-Zel'dovich problem has form[2]:

$$\begin{cases} \frac{\partial g}{\partial t} = -\frac{1}{kT} \frac{\partial \Delta \Phi(g, t)}{\partial g} - \frac{1}{2} \frac{\partial D(g, t)}{\partial g} + \sqrt{D(g, t)} \tilde{\xi}(t), \\ t_0 \leq t \leq T_k, g(t_0) = g_0, t \in [t_0, T_k], g(t) > 2 \end{cases} \quad (7)$$

where  $\tilde{\xi}(t)$  is a standard "white noise" process of unit intensity.

The computer simulation of this model gives the possibility to investigate the fluctuational stage of the first order phase transition. Moments of DF  $f(g, t)$  are as follows:

$$N_L(t) = \int_2^\infty f(g, t) dg, \quad (8)$$

$$q_L(t) = \frac{4}{3} \pi \int_2^\infty g^3 f(g, t) dg, \quad (9)$$

Here  $N_L$  and  $q_L$  are the total cluster number and concentration of the clusters, respectively.

The results of computer simulation devoted to the case of He-ions penetration into Ni-lattice depend of the set of physical parameters.

The work is partly supported by the Russian Foundation for Fundamental Research, grants 97-02-17627 and 96-02-17640.

## References

- [1] Zmievskaya, G.I., Plasma Physics Reports, Vol.23, pp.368-382, 1997.
- [2] Zmievskaya, G.I., in: *Dynamics of Transport in Plasmas and Charged Beams*, Maino, G. and Ottaviani, M., Eds., World Scientific Publishing Co, Singapore-London, 1996, pp.84-98.

# The Homogeneous Nucleation and Vapor Condensation in Presence of the Temperature Pulsations \*

N.M. Kortsenstein, E.W. Samuilow  
Krzhizhanovsky Power Engineering Institute, Moscow, Russia

## 1 Introduction

The homogeneous nucleation is extraordinary sensitive to temperature change. Therefore it is interesting to find out effect of the small temperature pulsations on the processes of homogeneous nucleation and vapor condensation. It is proposed that temperature of the mixture of the supersaturated vapor and the noncondensed gas has the small pulsations relatively to its average mean. It is proposed also that the nucleation rate corresponds to the instant temperature at the any frequency of pulsations. It may be prove that influence of pressure and vapor concentration pulsations may be neglected in by comparison with temperature pulsations at a first approximation.

It was considered large and small supersaturating ratio. It was founded the expression for average nucleation rate by the large supersaturating ratio. In its the pulse part is in proportion to average square of relatively pulse temperature, that is the average nucleation rate is not depended on sign of temperature deviation from its average significance. It was obtained the formula for the nucleation rate with negative deviation of temperature for the small supersaturating ratio. The nucleation rate is zero for positive deviation of temperature for the small supersaturating ratio. It was founded the condition for application of obtained formulas.

It was made numerical estimates on base of obtained results. It was demonstrated, that the nucleation rate may be increase on 50-100% for the large supersaturating ratio with temperature pulse take into account, and that nucleation rate increase considerably, when temperature deviation is negative for the small supersaturating ratio. Thus influence of temperature pulse on the nucleation rate decrease, when the supersaturating ratio increase. Besides that, when nucleation rate increased with small supersaturation, it may be proposed, that the

condensation process with temperature pulse start more early then it take place without temperature pulse. Its corresponds with literature data of other authors (see review [1]) qualitatively.

## 2 Calculations and Results

The algorithm and computer code was realised for solution of the system of gasdynamic and condensation equations with use of the results for nucleation rate with temperature pulse. The test solutions were maked for the condensation process in caesium vapor and argon mixture for flow in wedge-formed nozzle. The temperature of the mixture has the small (amplitude =  $\pm 5\%$ ) random pulsations. The stop parametrs were choosen for the condensation process in supersonic region of nozzle. Results are given on Figures. The dashed lines on all Figures mentioned the results of evaluations without temperature pulse and the solide lines - with temperature pulse. From Figure 1 - Figure 4 it is follow, that calculation with temperature pulse displace condensation region to meet flow. The concentration of the drops ( Figure 2) with temperature pulse is smaller, then without pulse, and average radius ( Figure 3) - is larger. The degree of condensation (percentage ratio of the mass of the drops to the initial mass of vapor, Figure 4) for both variants in condensation region is identical. The distributional function of radius drops (Figure 5) with temperature pulse in flow have a look of the  $\delta$  - function set.

## References

- [1] Zaichik L.I. and Pershukov V.A., Problems of Modeling Gas-Particle Turbulent Flows with Combustion and Phase Transitions. Review, Fluid Dynamics, Vol.31,p.635,1996.

\* Abstract 6667 submitted to the 21st International Symposium on Rarefied Gas Dynamics, Marseille, France, July 26-31, 1998

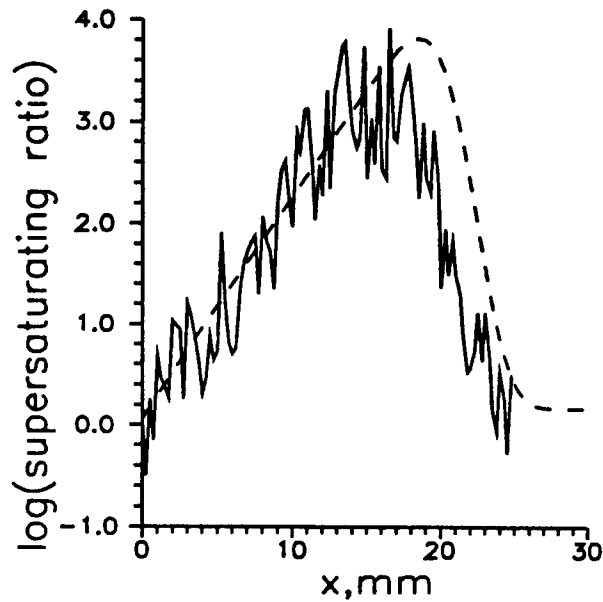


Figure 1:

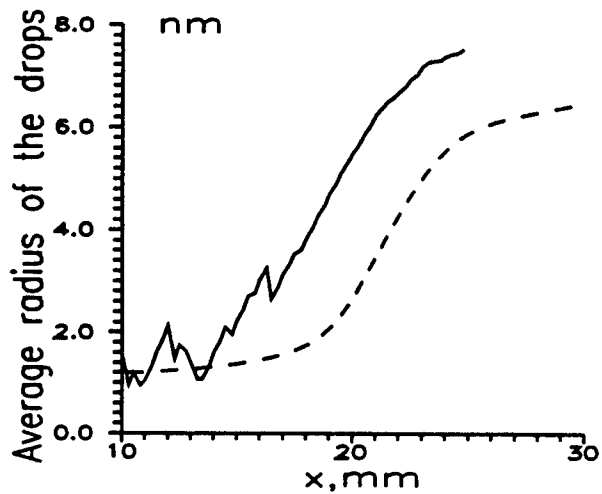


Figure 3:

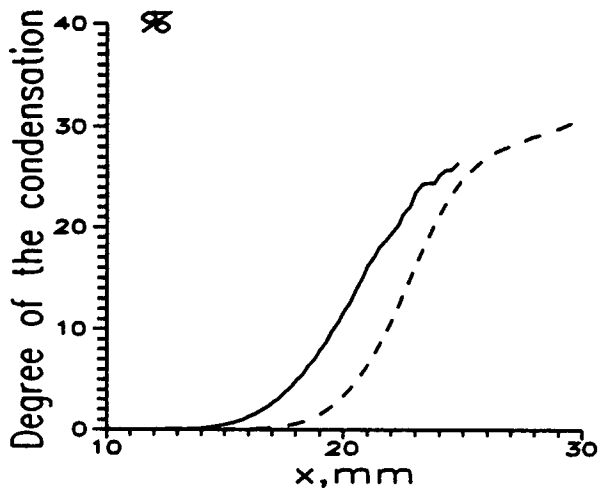


Figure 4:

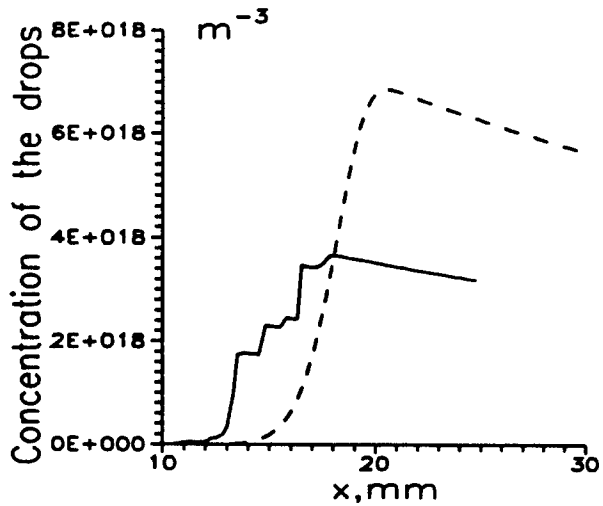


Figure 2:

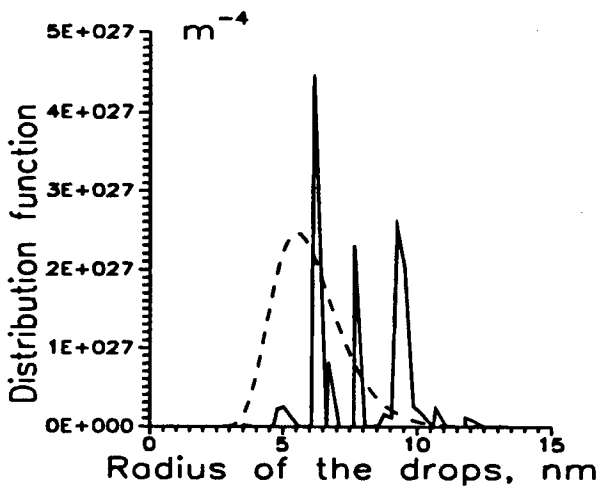


Figure 5:

# On Photophoresis: The Optical Properties of Model Aerosol Particles Measurements \*

F.D.Kovalev, V.A.Runkov, P.E.Suetin

Physics Department, Ural State University, Ekaterinburg, Russia.

## 1 Introduction

The aerosol particle photophoresis phenomenon consists in occurrence of force acting on a particle in an optical radiation field and which is growing out of gas interaction with non-uniform heated particle surface. Photophoresis represents the certain fundamental interest as an object of rarefied gas kinetic theory application. There are many difficulties at the experimental check of existing theories. The majority of experiments leave a significant arbitrariness at comparison with the theory because of number essential parameters uncertainty. Partially these difficulties are eliminated in model experiment: the particle of real size is replaced with macroscopic one, but the measurements carried out at lower gas pressures to ensure the same rarefaction (same Knudsen numbers). Such approach opens wide opportunities to study gas dynamic aspect of photophoresis. All necessary parameters such as thermal conductivity, factor of radiation, factors of light absorption and temperature asymmetry of model particle surface can be obtained with sufficient accuracy. Besides, there always is an opportunity to give a particle the required shape. The particle grounding through suspend string provides absence of non-compensated electric charges capable to influence on gas molecules interaction with particle surface. Macroscopic sizes of a model particle allow using non-monochromatic radiation source. In this case a geometrical optics limit is realized, where the factors of absorption and asymmetry of temperature are not sensitive to change of diffraction parameter (ratio of particle radius to incident radiation wavelength). The represent work is devoted to estimation of model aerosol particles integral optical properties (factors of absorption and asymmetry of temperature of a surface).

## 2 Theory

The solution of kinetic equation with the collision integral in form of S-model for the photophoretic force acting the sphere-shaped particle in parallel light beam (wavelength and polarization are arbitrary) is the following [1]:

$$F = \frac{2\pi}{3} \left( \frac{m}{8kT} \right)^{1/2} I_0 J_1 R_0^2 f(\alpha_i, \Lambda, Kn), \quad (1)$$

here  $m$  - gas molecule mass,  $T$  - equilibrium gas temperature far from particle,  $I_0$  - incident light intensity,  $f$  - some function of accommodation coefficients  $\alpha_i$ ,  $\Lambda$  - ratio of thermal conductivity of particle  $\lambda_p$  and gas  $\lambda_g$ ,  $Kn$  - Knudsen number based on particle radius  $R_0$ . The most difficult is the evaluation of temperature asymmetry factor  $J_1$ :

$$J_1 = 3nk\rho \int_0^1 x^3 dx \int_0^\pi \cos \theta \sin \theta B(x, \theta) d\theta, \quad (2)$$

here  $x = |\mathbf{r}|/R_0$ ,  $\mathbf{r}$  - radius vector with origin in the particle center,  $r$  - diffraction parameter,  $\rho$  and  $k$  - real and imaginary parts of particle complex refraction index,  $\theta$  - azimuth angle. Enough complicated function  $B(x, \theta)$  characterizes the electromagnetic field inside the particle and depends on particle shape and optical properties. In many cases any data on the complex refraction index of the particle is absent.

However, it is possible to obtain the value of  $J_1$  from the temperature distribution measurements on the particle surface. Temperature gradient appeared on the particle surface as a result of light absorption, heat transfer inside particle and gas-surface interaction can be written in series:

$$T_s(\theta) = T + \sum_{l=0}^{\infty} \frac{I_0 J_l P_l(\cos \theta)}{A + 4\sigma\epsilon T^3 + l\lambda_p/R_0} \quad (3)$$

here  $P_l$  - Legendre polynomial,  $\sigma$  - Stephan - Boltzmann constant,  $\epsilon$  - radiation coefficient of the particle, and  $A$  characterizes gas-surface interaction.

\*Abstract 6847 submitted to the 21st International Symposium on Rarefied Gas Dynamics, Marseille, France, July 26-31, 1998

### 3 Experiment

The present research purpose is improvement of the model method offered by Tong [2], and Bogolepov [3] to obtain reliable results for photophoretic force. It is possible to make the following conclusions from analysis of the named works results. It is necessary to refuse from hollow particles, covered with soot. Certainly just on a surface of such particles the greatest temperature gradient can be obtained, so the photophoretic force measurements will be easier. However error brought in by thermal conductivity uncertainty of such particles essential surpasses than force measurement error brought in by torsion balance with electrostatic compensation of photophoretic force. As a result of soot layer degradation in vacuum conditions continuous change of particle thermal and optical properties during experiment take place, therefore results of such experiment are not suitable for comparison with the theory. The particles with thermal conductivity less than 10 Watt/m K and factor of light absorption not less than 0,5 are most preferable. Experimental equipment consists of large vacuum chamber (about 0.5 m<sup>3</sup>). Vacuum system provides wide range of gas pressures (the lower limit 10<sup>-6</sup> torr). Surface temperature measured by means of six thermocouples fixed in different places on the particle surface. Temperature distribution measurements provided with spherical black glass and graphite particles in air in wide range of Knudsen numbers (0.013 ÷ 66) and light intensities (1600 ÷ 3000 W/m<sup>2</sup>). Thermocouples influence was properly accounted. A filament lamp with known emission spectrum and collimator used as a parallel light beam source. To evaluate the light intensity simple but reliable method was developed. A possibility to measure light intensity at any time in vacuum chamber in the place the model particle situated was achieved.

### 4 Results

The following values for absorption factor  $J_0$  and temperature asymmetry factor  $J_1$  were obtained for black glass particle  $J_0 = 0.72 \pm 0.08$ ,  $J_1 = -(0.41 \pm 0.06)$  in free molecular region;  $J_0 = 0.73 \pm 0.07$ ,  $J_1 = -(0.43 \pm 0.04)$  in viscous with sliding region. For graphite particle  $J_0 = 0.7 \pm 0.1$ ,  $J_1 = -(0.48 \pm 0.05)$  in free molecular region and  $J_0 = 0.8 \pm 0.1$ ,  $J_1 = -(0.45 \pm 0.06)$  in viscous with sliding region. The temperature distributions on a glass particle surface and curve designed on (3) in view of the two first items of a series are submitted at figure 1. The obtained values of the factors of absorption

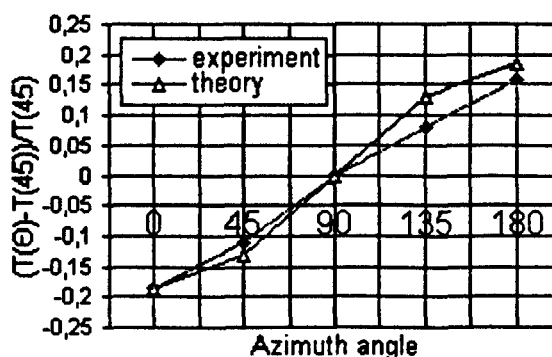


Figure 1: Temperature distribution on black glass particle surface at light intensity 954 W/m<sup>2</sup> and Kn=66 in comparison with theory

and temperature asymmetry are in good accordance with theoretical predictions. Their concurrence within the limits of an error in free molecular and viscous with sliding regions allows to make a conclusion about suitability of the offered technique of model particles optical properties definition. The present results allow to calculate photophoretic force for real aerosols in a geometrical optics limit in a wide range of radiation intensities and Knudsen numbers. The further application of model particles optical properties definition technique in the photophoretic force measurement is planned.

### References

- [1] Beresnev S., Chernyak V., Fomyagin G., *Photophoresis of spherical particle in a rarified gas*, J. of Phys. Fluids A, Vol.5, No.8, pp.2043-2052, 1993.
- [2] Tong N.T., *Experiments on photophoresis and thermophoresis*, J. of Cool Interf. Sci., Vol.51, No.1, pp.143-151, 1975.
- [3] Bogolepov A., Suetin P., Beresnev S., Bystrai G., Chernyak V., *Photophoresis of model aerosole particles*, J. Teplofizika Visokich Temperatur, Vol.34, No.5, pp.751-756, 1996. (in russian)

INSTRUMENTATION AND DIAGNOSTICS - ID P

THURSDAY, JULY 30, 1998

16:00



# Rotational Temperature Measurements in the New DLR-High Vacuum Test Facility STG by Means of REMPI \*

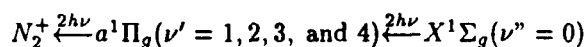
B.K. Nazari<sup>1</sup>, A.E. Beylich<sup>2</sup>, C. Dankert<sup>1</sup>

<sup>1</sup> German Aerospace Center (DLR), Institut for Fluid Mechanics, Göttingen, Germany

<sup>2</sup> Stoßwellenlabor, Rheinisch-Westfälische Technische Hochschule, Aachen, Germany

The new DLR-High Vacuum Test Facility STG enables an experimental investigation of typical thruster plumes as prerequisite to determine disturbance effects of thruster firing like e.g. perturbing forces and moments, excessive heat loads, and contamination). Its main feature, a large liquid helium-driven cryopump allows the undisturbed plume gas expansion into the highly rarefied regime including the backflow. Because of the very low number densities ( $n \leq 10^{13} \text{ cm}^{-3}$ ) in these regions, as an appropriate measurement technique the highly sensitive spectroscopic method REMPI (Resonance Enhanced Multi-Photon Ionization) is applied to obtain multiphoton spectra. This method delivers a precise determination of the most important plume flow characteristics, namely the temperature, the density, and gas velocity.

Since in the experiments thruster nozzles and sonic orifices with various test gases ( $N_2$  and  $H_2$  as two essential components of thruster plumes) instead of real propellants are used, the rotational temperature of nitrogen has been investigated by 2+2 REMPI (Figure 1), Lyman-Birge-Hopfield system :



employing an excimer-pumped pulsed dye laser (13 ns pulses at 283 nm and  $0.2 \text{ cm}^{-1}$  bandwidth). Reliable rotational temperature data are obtained from REMPI spectra using graphical (Boltzmann rotational population distribution) or deconvolution methods. Both methods are applied to plume and to orifice flow with its different flow types (continuum to free molecular flow, isentropic core/boundary layer expansion into the backflow

region). A comparison between experiment and theory along the centerline of the sonic orifice expansion flow presents good agreement. The study opens the possibility of predicting accurately the flow quantities in the off-axis plume flow using this spectroscopic technique.

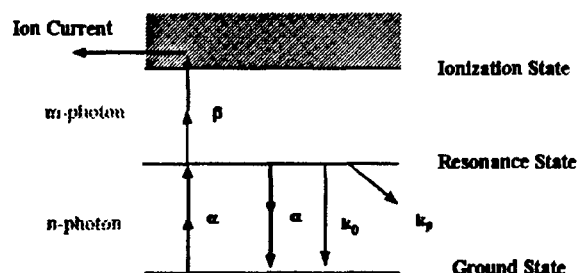


Figure 1: nR+m REMPI

\* Abstract 1660 submitted to the 21st International Symposium on Rarefied Gas Dynamics, Marseille, France, July 26-31, 1998

## Electron Beam Dispersion in Carbon Dioxide\*

R.J. Cattolica, D.R. Farley<sup>a)</sup>, L.H. Clapp

Department of Applied Mechanics & Engineering Sciences

University of California at San Diego, La Jolla, USA

<sup>a)</sup> Present address: Lawrence Livermore National Laboratory

Propagation of medium energy electrons (10 - 20 keV) in carbon dioxide was studied for application to the Electron Beam Fluorescence (EBF) technique<sup>1</sup> with CO<sub>2</sub> as a rarefied gas dynamic diagnostic tool. A collimated (1 mm nominal diameter) electron beam at energies of 10, 15, and 20 keV was injected into a vacuum chamber containing ambient CO<sub>2</sub> maintained at pressures of 50, 100, 200, 400, 600 and 800 mTorr. Through deconvolution of recorded two-dimensional images of the emitted fluorescence, the growth of the root-mean-square (rms) radius of the electron beam was obtained as a function of axial distance. An empirical form of the differential scattering cross-section from Center<sup>2</sup>, which includes the contributions of both elastic and inelastic collisions between fast electrons and CO<sub>2</sub> molecules, was used in single scattering<sup>3</sup>, multiple scattering<sup>4</sup> and scattering envelope<sup>3</sup> models developed for describing the electron distribution along the electron beam. Total scattering cross sections obtained by integrating the differential scattering cross section are presented in Table I for electron beam energies of 10, 15, and 20 keV. The rms radius of the electron beam calculated from imaging of the electron beam fluorescence is presented in Fig.1 for a 20 keV electron beam along with a comparison with single scattering, multiple scattering and scattering envelope models. The rms data for all pressures are presented in terms of the target thickness in units of Torr-cm.

The envelope model under estimates the radius at low target thickness (below 2 Torr-cm) and overestimates the rms radius at higher target thickness. The multiple scattering model also overestimates the rms radius at target thickness above 2 Torr-cm. Although

the single scattering model slightly underestimates the beam rms radius for the 10 and 15 keV data at large target thickness, for the 20 keV data it does well in predicting the rms radius over the range of target thickness. The single scattering model can be used to predict the electron beam disperse in carbon dioxide at a variety of beam energies and CO<sub>2</sub> gas pressures up to a target thickness on the order of 10 Torr-cm. For target thickness on the order of 100 Torr-cm or higher, a multiple scattering model which assumes a Gaussian scattering distribution would be more appropriate. Between the single scattering and multiple scattering limits, a Direct Simulation Monte Carlo (DSMC) simulation of the electron beam propagation is the preferred approach. Such a method has been used previously by Center<sup>4</sup> in his study of differential scattering cross-sections.

### References

- [1] E. P. Muntz, "The electron beam fluorescence technique," *AGARDograph*, **132**, (Von Karman Institute, Rhode-St.-Genese, Belgium, 1965).
- [2] R. E. Center, *Phys. Fluids* **13**, 79 (1970).
- [3] D. R. Farley, "Electron beam fluorescence of carbon dioxide with application to the atmosphere of mars," Ph. D. Dissertation, University of California at San Diego (1996).
- [4] L. H. Clapp, R. G. Twiss, R. J. Cattolica, *Rarefied Gas Dynamics: Proceedings of 17th International Symposium*, edited by A. E. Beylich, (VCH Publishers, New York, 1990) p. 1498.

---

\* Abstract 2426 submitted to the 21st International Symposium on Rarefied Gas Dynamics, Marseille, France, July 26-31, 1998

**Table I.** Total scattering cross-sections for an electron beam propagating through carbon dioxide at energies of 10 keV, 15 keV, and 20 keV.

Beam Energy (keV)	10	15	20
$\sigma(\times 10^{-17} \text{ cm}^2)$	3.7	2.5	1.9

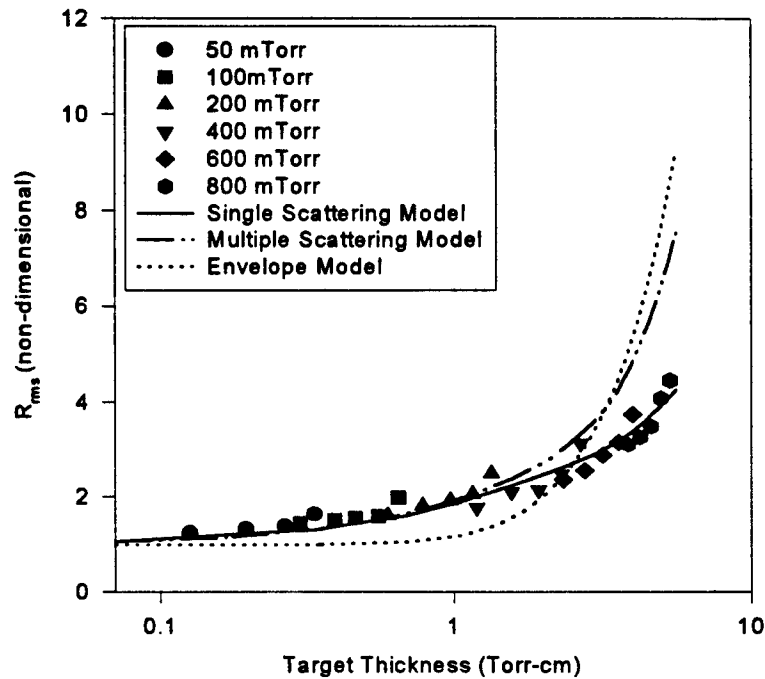


**Figure 1.** Comparison of experimental data and scattering models of the rms radius of an electron beam propagating through carbon dioxide at a beam energy of 20keV.

# On the Use of Actinometry for Dissociation Rate Measurements in Air Plasma-Arc-Jets \*

A. Lebéhot<sup>1</sup>, Z. Szymanski<sup>2</sup>, V. Lago<sup>1</sup>, J. Kurzyna<sup>2</sup>, M. Dudeck<sup>1</sup>

<sup>1</sup>Laboratoire d'Aérodynamique du CNRS, Meudon, France

<sup>2</sup>IPPT-PAN, Warsaw, Poland

## 1. Introduction

Actinometry has proven to be a convenient tool for measuring dissociation rates in oxygen glow discharges [1]. It is expected that this technique could be applied to arc-jet conditions [2]. The principle lies on the analysis of two emission lines, one of atomic oxygen and one of argon, which is introduced as a trace in the gas of interest. The evaluation of the oxygen dissociation rate is then straightforward, provided that a number of assumptions are satisfied. The first assumption is obviously that the small amount of argon does not disturb significantly the properties of the plasma.

## 2. Experimental

The arcjet generator (wind tunnel SR1 [3]) is operated as follows. The arc is produced in the converging part of a convergent-divergent nozzle. The arc current is 100 A under 66 V. The gas used is air with 2 % of argon at a flow rate of 15 l/min. Argon lines are not clearly observed for lower concentrations and it is checked that the intensity of the oxygen lines are not affected by such an amount of argon.

Two different diagnostics are made, as a function of the axial distance: the measurement of the emission line intensities, and the measurement of axial electron temperature and density, thanks to an electrostatic probe. Optical, as well as electrostatic measurements are carried out at distances 2.3, 3.4, 5, 10 cm from the nozzle exit.

## 3. Actinometry procedure

The lines  $^5P \rightarrow ^5S$  at 777 nm for atomic oxygen, and  $2p_1 \rightarrow 1s_2$  at 750 nm for argon, are analysed. The ratio of their intensities can be directly related to the

dissociation rate (with respect to the ground state: O stands for  $O(^3P)$ ) through:

$$\frac{I_{777}}{I_{750}} = \frac{1}{C_{SP}^{2P_1}} \frac{[O]}{[O_2]}$$

provided that the production of the excited state  $O(^5P)$  from a dissociative excitation process can be neglected [1]. The factor:

$$C_{SP}^{2P_1} = \frac{h\nu_{750} A_{kl}^{2P_1} \sum A_{ij}^{5P} + k_Q^{5P} [M_2] k_e^{2P_1} [Ar]}{h\nu_{777} A_{kl}^{5P} \sum A_{ij}^{2P_1} + k_Q^{2P_1} [M_2] k_e^{5P} [O_2]}$$

has to be considered as a constant throughout the experimental measurements. The  $A_{ij}$  are the transition probabilities,  $k_Q$  are the quenching rate constants in the interaction with  $M_2$  molecules ( $O_2$  and  $N_2$ ),  $k_e$  the rate coefficients for the direct electronic excitation process. The quenching rates  $k_Q$  are taken from [1, 2]. The excitation rate constants  $k_e$  are determined from the corresponding cross sections [1], the electron temperature, and the electron energy distribution function  $f(E)$ , as obtained from electrostatic probe measurements:

$$k_e = \left( \frac{2e}{m} \right)^{1/2} \int_{thr}^{\infty} E \sigma(E) f(E) dE$$

One difficulty for applying the actinometry technique for plasma jets is that the absolute local concentrations  $[O_2]$  and  $[Ar]$  are unknown. Nevertheless, as far as the dissociation rate is low enough in the jet, and because the signal viewed by the spectrometer is integrated along a diameter of the plasma jet cross section, the relative concentrations can be assumed as conserved and given by the inlet gas mixture. In the present state of the experiments, the radial intensity profiles have not yet been extracted, and it must be assumed that these profiles

\* Abstract 3209 submitted to the 21st International Symposium on Rarefied Gas Dynamics, Marseille, France, July 26-31, 1998

are the same for argon and atomic oxygen. Then, the ratio  $[Ar]/[O_2]$  on the axis can be considered as equal to 0.02. Also, the absolute local concentration  $[O_2]$  should be known. In a first step, it will be considered as a variable for the determination of  $C_{SP}^{2p1}$ .

#### 4. Results and Conclusion

In Figs. 1 and 2 are reported the measured axial electron temperature and electron density, as a function of the axial distance. The corresponding values of  $C_{SP}^{2p1}$  are shown in Fig. 3, as a function of

$[O_2]$ . It appears that  $C_{SP}^{2p1}$  is constant in a wide range of  $[O_2]$  including the experimental conditions; then, the absolute value of this local concentration is not needed. On the other hand,  $C_{SP}^{2p1}$  is rather sensitive to the electronic temperature, but this one is roughly constant in the range of the measurements. So, it can be concluded that, in the present experimental conditions, the ratio  $[O]/[O_2]$  is given by:

$$\frac{[O]}{[O_2]} = 0.024 \frac{I_{777}}{I_{750}}$$

The results, converted into dissociation rates, are given in Fig. 4. It is noteworthy that the dissociation rates are of the order 12-15%; it may be considered that these values are consistent with the assumption of a weak dissociation, so that the relative error introduced by this assumption on the rate is of its order of magnitude. The slight increase up to an asymptotic value may appear somewhat questionable, within the expected error bars.

#### References

- [1] D. Pagnon, J. Amorim, J. Nahorny, M. Touzeau, and M. Vialle, J. Phys. D Appl. Phys. **28**, 1856 (1995)
- [2] S. Bouillon, Thesis, Université de Limoges (1995)
- [3] V. Lago, M. de Graaf, X. Duten, S. Hulin, and M. Dudeck, 27th AIAA Plasmadynamics and Lasers Conference, June 1996, New Orleans, USA, AIAA paper 96-2302
- [4] P.J. Dagdigian, B.E. Forch, and A.W. Miziolek, Chem. Phys. Lett. **148**, 299 (1988)

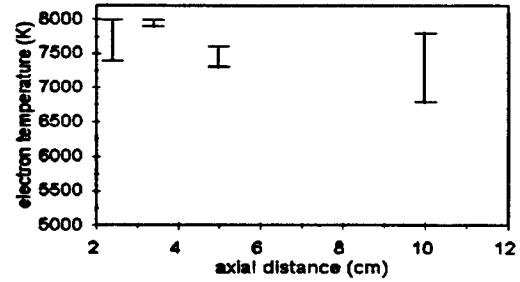


Fig. 1 Measured electron temperature as a function of axial distance

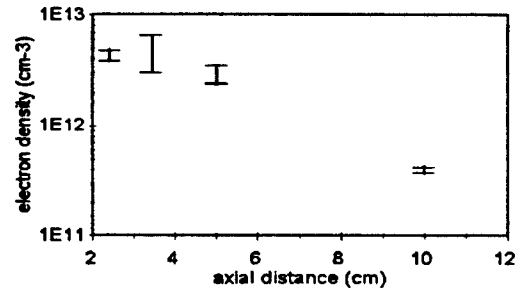


Fig. 2 Measured electron density as a function of axial distance

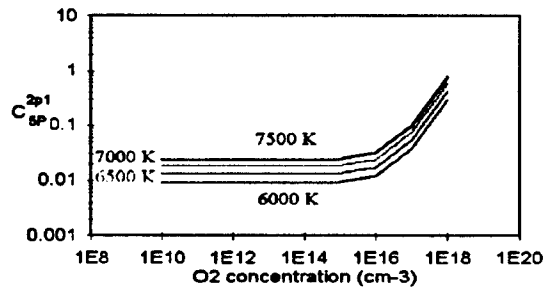


Fig. 3 Values of the constant  $C_{SP}^{2p1}$  as a function of  $[O_2]$  and  $T_e$

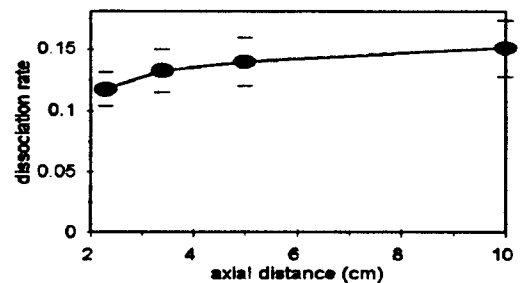


Fig. 4 Dissociation rate  $[O^3P]/[O_2]$  as a function of axial distance

# Fundamental Study of REMPI as a Measurement Technique for Rarefied Gas Flow \*

H. Mori, T. Ishida, S. Hayashi, T. Niimi

Dept. of Electronic-Mechanical Engineering, Nagoya University, Japan

## 1 Introduction

So far, to measure thermodynamic variables in rarefied gas flows, Pitot and Patterson probe have been employed, but it has been pointed out that these probes induce disturbances in the flows and have long response time. On the other hand, the necessity of non-intrusive measurement of the thermodynamic variables has motivated the development of optical techniques, such as electron beam fluorescence (EBF)[1], laser induced fluorescence (LIF)[2], coherent anti-Stokes Raman scattering (CARS)[3]. However, these techniques based on detection of fluorescence or scattering light can not be applied to a highly rarefied regime.

As a candidate of non-intrusive measurement techniques with short response time and high sensitivity, the REMPI (Resonantly Enhanced Multi-Photon Ionization) technique is the most suitable, allowing measurement of thermodynamic variables in the highly rarefied regime. In the REMPI technique, ions excited to the ionization state from the ground state by multiple photons are detected as a signal and its spectra depending on the energy of irradiation are analyzed to measure temperature and density. Because REMPI is a nonlinear optical process and needs  $nR+m$  photons ( $n$ -photon resonance and  $m$ -photon ionization:  $nR+m$  REMPI) from the ground state through the resonance state to the ionization state, an analysis of a REMPI spectrum generally needs somewhat complicated procedures.

As a first step, we employ  $2R+2 N_2$ -REMPI to examine its fundamental properties. In this study, we setup an experimental apparatus for  $2R+2 N_2$ -REMPI and obtain the REMPI spectra for various conditions of pressure and temperature. And the theoretical spectra are also calculated and compared with the experimental ones.

## 2 REMPI Spectra

In the case where the laser power can be assumed to be constant and moderate, the relative strength of rotational lines in a vibrational band is given by[4],

$$I_{J',J''} = Cg(J'')S(J', J'')\exp(-E_{rot}/kT), \quad (1)$$

where  $C$  is a constant independent of the rotational quantum number  $J'$  and  $J''$ , including laser flux, number density, Franck-Condon factor and so on,  $g(J'')$  is the nuclear statistical factor which takes the value of 3 and 6 for odd and even  $J''$  respectively,  $S(J', J'')$  is the rotational strength [two photon Hönl-London factor], and the rest is the Boltzmann factor which originates from the rotational population.  $k$  is the Boltzmann's constant,  $T$  the rotational temperature, and  $E_{rot}$  is the rotational energy. Plotting  $\ln(I/gS)$  versus  $E_{rot}$  according to the above equation, rotational temperatures can be easily determined from its slope  $-1/kT$ .

We select (2,0) band of a  $\leftarrow X$  transition for the two photon excitation from the ground state to the resonance state, because this transition probability is relatively large.

## 3 Experimental Apparatus

Figure 1 shows a schematic diagram of an experimental setup for  $2R+2 N_2$ -REMPI. The laser system consists of a dye laser and a Nd:YAG laser as a pump source. The frequency of the dye laser output, using Fluorescein 27 as a laser dye, is doubled by a BBO crystal and separated from a fundamental beam by a dichroic mirror. Then the UV beam is focused inside a vacuum chamber by a quartz lens (focal length 30 cm). The laser energy is 2 mJ and the minimum linewidth is  $0.4 \text{ cm}^{-1}$ .

A secondary electron multiplier (Murata) is employed as a detector of ions and a Boxcar Integrator as a data logger. A laser pulse detected by a photodiode is transmitted to the Boxcar Integrator as a trigger signal.

\* Abstract 4486 submitted to the 21st International Symposium on Rarefied Gas Dynamics, Marseille, France, July 26-31, 1998

A vacuum chamber is evacuated by a turbo molecular pump and the pressure is kept at from  $10^{-5}$ – $10^{-6}$  Torr, controlled by a leak valve.

## 4 Results

Now, we are carrying out experiments to obtain  $N_2$ -REMPI spectra under the static conditions and to examine the fundamental properties of the spectra. Parallel to the experiments, we calculate the  $N_2$ -REMPI spectra for (2,0) band using eq. (1). Figures 2 and 3 are representative  $N_2$ -REMPI spectra calculated at 20 K and 300 K, respectively. To measure the rotational temperature from the Boltzmann plot, some spectral lines of one branch have to be selected. For low temperature (Fig. 2), it is better to select the S-branch because that is relatively high intensity and easy to extract each rotational line. On the other hand, the REMPI spectrum becomes so crowded in the case of 300 K (Fig. 3) that we can not use the rotational lines near the band head. Therefore, the rotational lines of the O- or P-branch away from the band head, which have large rotational quantum numbers ( $J''$ ), have to be selected to measure the rotational temperature.

## References

- [1] Dankert C., Cattolica R., and Sellers W., *Local Measurement of Temperatures and Concentrations: A review for Hypersonic Flows*, Boutier A. ed., *New Trends in Instrumentation for Hypersonic Research*, pp.563–581, 1994.
- [2] Niimi T., Fujimoto T. and Shimizu N., *Method for Planar Measurement of Temperature in Compressible Flow Using Two-line Laser-Induced Iodine Fluorescence*, *Optics Letters*, Vol.15–16, pp.918–920, 1990.
- [3] Hara Y., Fujimoto T., Niimi T., Fukuda Y., and Oba H., *Measurement of Temperature and Number Density by CARS: Application to Plasma Jets*, RGD 18th International Symposium, AIAA, Vol.160, pp.360–370, 1992.
- [4] Carleton K. L., Welge K. H., and Leone S. R., *Detection of nitrogen rotational distributions by resonant 2+2 multiphoton ionization through the  $a^1\Pi_g$  state*, *Chemical Physics Letters*, Vol.115, No.6, pp.492–495, 1985.

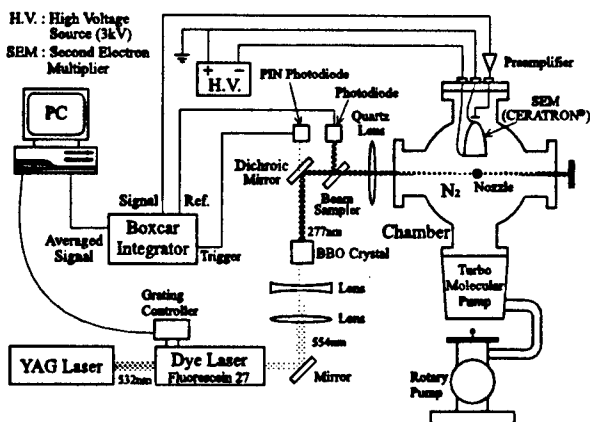


Figure 1: Experimental apparatus

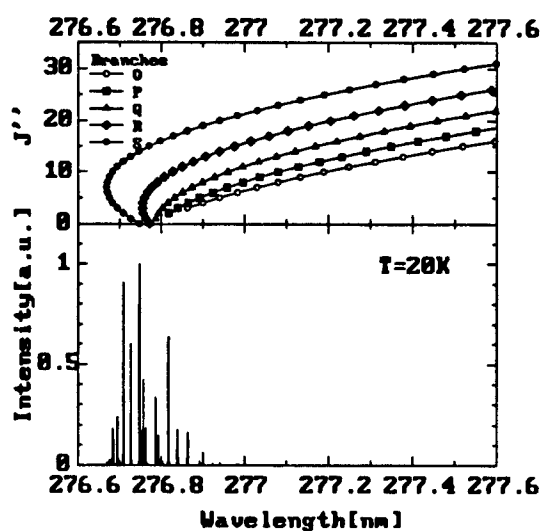


Figure 2: Calculated  $N_2$ -REMPI spectrum at 20K

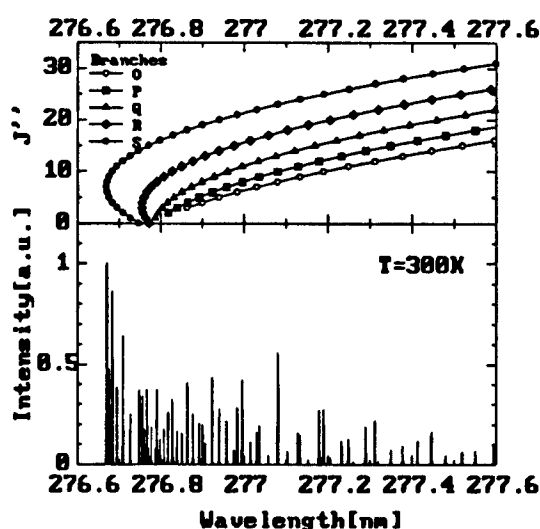


Figure 3: Calculated  $N_2$ -REMPI spectrum at 300K

# Mass-Spectrometry of Dissociative Ionization Products: An Environmental Application \*

A.V.Snegursky

Institute of Electron Physics, Ukrainian Nat.Acad.Sci,  
21 Universitetska str., Uzhgorod 294016, Ukraine

Environmental aspects of human life are now one of the most "hot" items of modern science. Mass-spectrometry is a convenient tool for operative monitoring the products of scientific, industrial and technological activities, especially when we deal with the complex species differing in isotope composition. One of the most effective channels of fragmentation of polyatomic molecule is a production of the ionized fragments due to the process of dissociative ionization (DI) reaction initiated by a low-energy electron impact. Such ionic fragments possess an information on the structure, composition and quantum state(s) of the initial molecule.

We have developed a mass-spectrometric apparatus with crossed electron and molecular beams aimed to investigate the peculiarities of the production of ionized fragments resulted from the dissociative ionization of a wide class of polyatomic molecules. The use of a quadrupole mass-spectrometer (QMS) together with the beam technique allowed the production of the fragment ions in the DI reaction to be studied with the substantial mass ( $\pm 0.05$  a.u.) and energy ( $\pm 0.5$  eV) resolution. We have chosen the organic molecules in order to study the production of the ionized fragments and radicals important in view of the environmental pollution control. For that reason the benzene ( $C_6H_6$ ) molecule appeared to be an attractive object. Our previous data on the appearance of the deuterated DI fragments from the heavy water ( $D_2O$ ) molecule have risen a question of the influence of D atom from the deuterium-containing analog of the benzene molecule on the behaviour of the DI cross-sections. For that reason the  $C_6HD_5$  molecule was chosen as an object of such comparative studies.

Here we report on the new data on the investigation of the electron-impact formation of both hydrogen and deuterium-containing ionic products of the DI reaction for the abovementioned molecular targets.

The milestone of the apparatus is a supersonic nozzle molecular beam source. A QMS was mounted inside a specially designed high-vacuum ( $10^{-7}$  Torr) operating chamber with the oil-free pumping facilities and the axis of the QMS analyzer was oriented normally to the beam intersection plane. The electron beam was produced by a conventional electron gun operating in the electron current stabilization mode and providing the formation of the electron beam of controlled (5-120 eV) energy and 0.1-2 mA electron current at the  $\pm 0.4$  eV energy spread. The channeltron served to detect the ions produced and its output signal was digitally processed to be stored by means of the multichannel pulse analyzer interfaced with the computer. The use of a step voltage generator as an electron energy scanner enabled the energy dependences of the DI cross sections to be measured. The accuracy of the incident electron energy scale calibration was defined almost by the electron beam energy spread and was not worse than  $\pm 0.5$  eV. The electron energy variation step was 1.3 eV when studying the general energy dependences of ion yield and 0.26 eV when measuring the initial areas of the DI curves. The analysis of the near-threshold areas of the DI cross sections vs the incident electron energy allows one to define the energy thresholds of reaction and the appearance potentials for ion fragments. The use of the double differentiation technique had enabled us not only to determine the first appearance potential (i.e. the threshold energy) for each fragment under study but also to evaluate the energies of the production of different groups of ions. In other words, we have observed the onsets of different channels of the initial molecule fragmentation. It was found that the presence of the deuterium atoms in the initial molecule results in the visible reduction of the first appearance thresholds of each ionic radical as well as causes the variation of the appearance energies of ionic groups (in other words, the energy positions of the structure of DI cross sections). These energies show quantitatively the differences

\*Abstract 5766 submitted to the 21st International Symposium on Rarefied Gas Dynamics, Marseille, France, July 26-31, 1998



in the dynamics of production of ionic fragments differing by the isotope composition. As is known, the presence of the additional neutrons in the initial molecule has no noticeable effect on its electronic structure (except the so-called isotopic shift whose energy value is considerably "neglected" by our experimental energy resolution). That is why it seems quite naturally to draw the notion of the collisional kinematics in order to explain the surprising pattern of the threshold shift. Indeed, the production of any fragment results not only from the energy transfer from the bombarding electron to the initial molecule inducing the direct excitation of electronic transitions as well as producing the rotationally and vibrationally excited molecule but also from the complicated mechanism of momentum transfer and branching over all possible collisional products (i.e. the scattered and ejected electron, ionic and neutral fragments which, in turn, may also decay with subsequent production of lower-order fragments). Thus, one should assume that the larger mass of the deuterated target may be responsible for the less probable direct conversion of the incident electron kinetic energy into that of the rotational and vibrational excitation of the target, resulting in the direct electronic transition to the higher excited repulsive molecular states. The decay of these repulsive states causes effectively the production of ion+neutral pair with the simultaneous ejection of electron. Of course, more exact information of that type can be extracted from the precise measurement of the kinetic energy distributions of the ionic fragments and/or the ejected and scattered electrons.

As a conclusion, it should be noted that the production of the deuterated ionized fragments takes place with a distinct (few dozen of meV) shift of the ion appearance energies towards the lower ones. In some cases the energy shift exceeds 3 eV allowing one to separate clearly the production of the ion fragment from the deuterated target. Such surprising pattern gives an evidence for clear "mass and energy" separation of harmful species providing a rapid, reliable and versatile method of monitoring the hazardous species present in the planetary atmosphere.

# Electron-Beam-Excited X-ray Method for Density Measurements of Rarefied Gas Flows Near Models. \*

N.G. Gorchakova<sup>2</sup>, B. Chanetz<sup>1</sup>, L.I. Kuznetsov<sup>2</sup>, D. Pigache<sup>1</sup>

T. Pot<sup>1</sup>, J.P. Taran<sup>1</sup>, V.N. Yarygin<sup>2</sup>

<sup>1</sup> Office National d'Etudes et de Recherches Aéronautiques, France

<sup>2</sup> Institute of Thermophysics, Novosibirsk, Russia

## 1 Introduction

Electron-beam fluorescence is a well-established method for local density measurements of rarefied gas flows. Spectrum excited by a fast electron beam covers the range from the X-ray region to the visible one. For plasma flows and gas flows at higher density and temperature, the use of X-ray radiation (Bremsstrahlung or characteristic one) is preferable because of the absence of quenching processes and spectra transformation. X-ray method of density measurements was proposed in [1] and elaborated in [2]. Nevertheless it is hard to apply this technique for investigation of gas flows around models particularly in the region close to the surface, because of the occurrence of strong X-ray radiation scattered from the surface, which can be higher than that from the gas.

In view of this and in order to avoid the interference of X-ray radiation from the model surface a new method was proposed and realized [3], the E-beam passed through a tube inserted into the model and the density measurements are made below the exit point of the E-beam.

The method described in [3] and improved in the present article applies to axisymmetric flow fields.

## 2 Experimental Procedure and Results

The experiments were carried out in ONERA R5Ch wind tunnel using a contoured nozzle that provides a uniform freestream environment, an electron gun -1- and X-ray measuring systems (fig. 1). The electron beam -2- (having 25 keV, 0.8 mA) crosses the model -4- (which is a hollow

cylinder with a flare) through a thin wall stainless steel tube -3- ( $\phi_{int} = 2.8mm$ ) and continues to the Faraday cup -8-. The X-ray radiation at the point of measurement is selected by the Soller collimator -5-, and detected by the X-ray detectors -6, 7-. One of the detectors -6- is mounted on coordinate mechanical system in order to move the detector and measure the X-ray intensity along the d-e region.

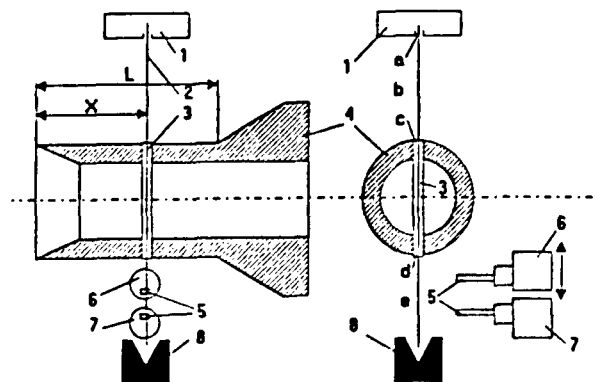


Figure 1: Scheme of normal and axial cuts of an experimental facility

First test measurements [3] were made using only one detecting system -6- and a calibration curve : X-ray intensity vs gas density in static conditions. These measured density values appeared to be lower than the calculated ones. The accuracy of the experiment and the possible reason for the underestimate of the density in the higher density region will be discussed in details in our paper. In order to avoid this difficulty and to improve the accuracy of the density measurements two detectors measure the X-ray radiation intensity in two points : one at a fixed position in the undisturbed flow (detector -7-), one exploring the shock and the boundary layer (detector -6-).

\* Abstract 6311 submitted to the 21st International Symposium on Rarefied Gas Dynamics, Marseille, France, July 26-31, 1998

Fig. 2, as an example, shows the transversal density profile near the model for the cross section  $X/L = 0.3$ . The different curves are the following :

- triangles - represent the results obtained when using just one detector -6- and corresponding calibration curve;
- dark circles - represent the results obtained while measuring by two detectors -6, 7- but using a calibration curve for getting the absolute density values  $\rho$  and  $\rho_0$ ;
- light circles - represent the relative densities measured by two detectors -6, 7- using their intensities ratio (without calibration curves "intensity versus density");
- full line - represent the Navier Stokes calculation results.

Detailed comparison analysis of calculation and experimental results for different model cross sections will be done in a separate report also being presented at this Symposium.

In Fig. 2 one can see that, as it was expected within the region of high densities (about  $10^{16} \text{ cm}^{-3}$ ), a lower relative gas density  $\rho/\rho_0$  is observed when using the absolute density values. However measuring both  $\rho$  and  $\rho_0$  results in more precise data because in this case the difference in E-beam scattering on its "a-e" way in static conditions and in "in-flow" measurements is indirectly taken into account.

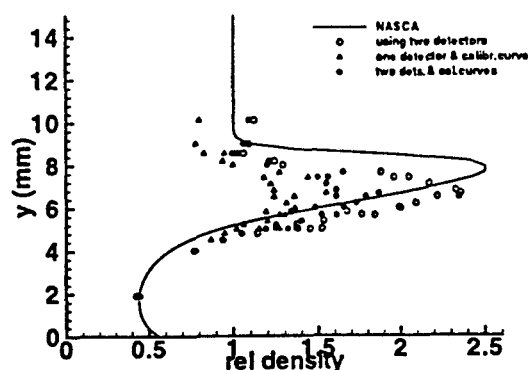


Figure 2: comparison between different methods of measurement

Transversal density profiles have been recorded also at cross sections  $X/L = 0.6$  and  $0.76$ . An attempt

has been made at  $X/L = 1.4$  that is at higher density at the tube extremities and for a longer tube length. In these conditions, the E-beam intensity at the tube exit is too small, making density measurements in the d-e region impracticable. An alternative would be making measurements above the model in the b-c region using the two detectors method. This method has been tested at  $X/L = 0.76$ . The results are practically identical to those obtained previously below the model in the d-e region.

Thus the tube inserted into the model serves to remove the electrons and to prevent their scattering on the model. This method can not be used for measuring the absolute density in the region under research, but accurate relative densities measurements are possible.

### 3 Conclusion

- A method of X-ray electron-beam gas density measurements of the flow around axisymmetrical models is proposed,
- The measurements of transversal gas density distributions of shock and boundary layer around a hollow cylinder with a flare at cross sections  $X/L = 0.3, 0.6, 0.76$  are done.

### References

- [1] Zigler C.A., Bird L.L., Olson K.H. Morreal J.A., *Technique for Determining Density Distribution in Low Pressure, High Temperature Gases*, RSI, Vol. 35, No.4, pp. 450-456, 1964.
- [2] Gorchakova N.G., Kuznetsov L.I., Yarygin V.N., *Electron Beam Diagnostics of High Temperature Rarefied Gas*, Proc. 13th Int. Symposium on RGD, Plenum Press, Vol. 2, pp. 825-832, 1985.
- [3] Bonnet J., Chanetz B., Henry D., Larigaldie S., Lefebvre M., Mohammed A.K., Pigache D., Pot T., Posier B., Taran J.P., Gorchakova N., *Optical Diagnostics for Hypersonic Flows*, Proc. Int. Conf. on Methods of Aerophysical Research, Novosibirsk, Vol. 1, pp. 46-53, 1996.

# The Use of Synthetic Spectra for Temperature Measurements in Different Kinds of Plasmas \*

P. Boubert, B. Van Ootegem, L. Robin, B.G. Chéron, P. Vervisch  
UMR 6614 CNRS / CORIA, Université de Rouen, France

## 1 Introduction

Determination of rotational and vibrational temperatures of a molecular electronic level can be achieved by comparison of an experimental spectrum obtained by emission spectroscopy, with calculated spectra. Indeed, in most of molecular spectra, Boltzmann plot is not applicable because of the overlapping of rotational lines. This fitting technique has been applied in seven main facilities involved in different works, to the spectra of various molecules:

- a low pressure pure nitrogen arc-jet plasma studied as a free stream and under boundary layer conditions ( $N_2^+$  first negative and  $N_2$  second positive systems).
- a low pressure  $CO_2$ - $N_2$  arc-jet plasma involved in Martian entry studies and especially in works on its interaction with C/SiC tiles (CN violet and red systems).
- a low pressure  $CO_2$ - $N_2$  plasma produced in an inductively coupled plasma (ICP) torch used to investigate interaction between turbulence and plasma chemistry (CN violet and  $C_2$  Swan systems).
- a low pressure air plasma produced in the same torch ( $N_2^+$  first negative system).
- an air ICP investigated in Russia during Hermes program ( $N_2^+$  first negative and  $NO\gamma$  systems).
- an air glidarc devoted to air behavior researches (OH near UV bands and  $NO\gamma$  system).
- a silent discharge lamp fed with argon where traces of nitrogen monoxide were introduced; this lamp is designed to become a very convenient VUV absorption source ( $NO\gamma$  system).

For each molecule and each system observed, a synthetic spectrum program has been built and validated by experimental works found in literature. Recent investigations using Fourier transform spectroscopy have determined rotational lines spectral position of the usual systems for a wide range of

diatomic molecules. The lines observed by spectroscopists are often those of low rotational numbers. Indeed, to get a high spectral accuracy, very low temperatures are necessary, which also means a low population rate for high rotational number levels. Thanks to high accuracy hamiltonian matrixes developed since the end of the seventies, which give energy of each rovibronic level involved in a transition, sets of spectroscopic constants are now available for all these systems. Calculations using these constants and the hamiltonian matrix elements to get rovibronic energies, give results in very good agreement with experimental values as far as these values are available. For higher rotational numbers, the only way is to trust in the model. How far? In this study, several examples have been explored to answer this question... Synthetic spectra are then calculated for different rotational and vibrational temperatures as long as a couple gives a good superposition with the experimental spectrum. Rotational temperature is often easier to find first rotational temperature inside lonely bands before finding vibrational temperature by looking at the whole spectrum.

## 2 Results and discussion

$N_2^+$  first negative and  $N_2$  second positive system have been observed in the free stream of a 100Pa pure nitrogen arc-jet plasma. To determine rotational temperature, 0-0 ( $N_2^+$ ) and 2-0 band ( $N_2$ ) are the most interesting in this experimental configuration, since they are not overlapped by any other band and they have thermometric lines i.e. lines whose relative evolution with temperature is very contrasted. To improve accuracy of the method, it is very important to choose these lines quite far from the bandhead. Indeed, although this area is often very sensitive to the temperature, lines density inside is high, then the spectrum is much more sensitive to uncertainties in the calculation. Rotational temperature found with  $N_2^+$  and  $N_2$

\* Abstract 6724 submitted to the 21st International Symposium on Rarefied Gas Dynamics, Marseille, France, July 26-31, 1998

spectra are in good agreement. The uncertainty is less than 200K. In spite of this agreement and because of the pressure conditions, rotational temperature cannot be identified to heavy particles kinetic temperature. A vibrational temperature quite close to electronic one has been obtained for  $C^3\Pi_u$  of  $N_2$  (populated by electronic excitation), but a much higher vibrational temperature has been found for  $B^2\Sigma$  of  $N_2^+$  (populated by nitrogen ion recombination) which cannot be assimilated to electronic temperature.

CN spectra have been recorded at low resolution (0.09nm), in a 100Pa  $CO_2$ - $N_2$  arc-jet plasma. This low resolution did not allow a comparison of thermometric lines intensities with calculations. However, the general evolution of these spectra with temperatures is significant enough to determine these last ones with an uncertainty lower than 300K. The important differences noticed between the numerous temperatures found on CN spectra, point out that one has to be very careful in the interpretation of measured temperatures. Furthermore, CN high temperature violet  $\Delta v=0$  spectrum is a good example of the limits of molecular constants determined at very low temperature. First building of the synthetic spectrum based on recent works gave a very bad simulation of experience: it was clear that the high accuracy constants used were perfect for low rotational numbers but became incorrect for high rotational numbers. Careful modifications of some of these constants allowed to explain intensity "oddities" due, in fact, to 5-5 to 8-8 bands (Fig. 1).

$C_2$  Swan bands have been detected in a  $CO_2$ - $N_2$  ICP.  $C_2$  spectrum is a good illustration of what may happen when a system is very complex and perturbed. In this case, comparison between experience and theory is much more difficult because some constants (especially for high temperature) are totally unknown: no model is able to reproduce the experimental spectrum. Differences between experimental and synthetic spectra are clear for some wavelengths and measurement of temperatures becomes then more doubtful.

NO  $\gamma$  system, intensively studied in many works, has been looked at in two very different sources. First, in a 100W atmospheric air glidarc, three sequences allow quite easy determination of rotational and vibrational temperatures. For  $\gamma$  system, a high accuracy of the model is necessary because of the complexity of the spectra in which satellite branches intensity is far to be negligible.  $T_r$  and  $T_v$  found traduce that an important amount of energy is used to heat the gas in the arc.

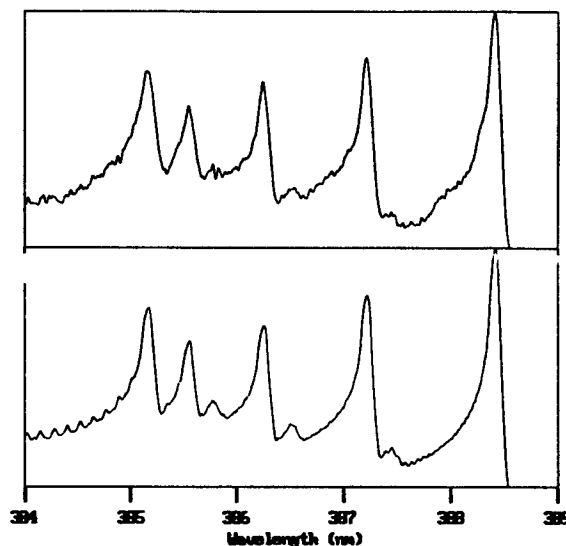


Figure 1: CN violet experimental and synthetic spectra in a  $CO_2$ - $N_2$  arc-jet plasma

The second source is an argon silent discharge lamp producing a cold plasma. Introduction of traces of NO allows observation of  $\gamma$  system at low rotational temperature but high vibrational excitation. The experimental spectra led to a very accurate determination of  $T_r=350\pm 20$ K. Because of vibrational excitation processes, no vibrational temperature was able to simulate the experimental shape of the whole spectrum.

To conclude, application of comparison between synthetic and experimental spectra has been shown to be a good way to determine rotational and vibrational temperature in numerous configurations. It also allowed to suggest two major remarks:

- As far as they exist, various temperatures able to be found in the same plasma on different molecules lead to have a closer look at the experimental conditions and at the complexity of the spectra before conclude about equivalence between excitation and kinetic temperatures.

- Spectra simulation are based on models whose constants are determined at low temperatures. The use of these models at high temperatures can show significant deviations from the experience. Constants have then to be corrected.

A more confident method is to obtain fundamental levels temperatures by absorption or narrow-band LIF spectroscopy. Indeed, synthetic spectra can be built as well for these kinds of spectra.

# Laser-Induced Fluorescence of Carbon Monoxide in a CO<sub>2</sub>-N<sub>2</sub> Low Pressure Plasma \*

P. Boubert, L. Robin, P. Vervisch  
UMR 6614 CNRS / CORIA, Université de Rouen, France

## 1 Introduction

In order to study catalycity of thermal protection materials devoted to Martian atmosphere, a 50%CO<sub>2</sub>-50%N<sub>2</sub> arc-jet plasma is produced by a power of 10kW, under a pressure of 100Pa.

Carbon monoxide being one of the main species in the plasma jet, the knowledge of its behavior near the studied C/SiC tile is essential. Determination of CO densities can be achieved through laser-induced fluorescence techniques. Excitation and fluorescence of products from CO photodissociation by an ArF excimer laser give information about this process and about the local density of CO. Carbon monoxide concentration can be also obtained by fluorescence induced by Raman-shifted laser.

## 2 Results

CO photodissociation scheme by ArF excimer laser is still badly known. In fact, it is surely made up of superposition of two processes having very different efficiencies. They are shown on Fig. 1. The ArF excimer laser used does not emit any radiation at 193.09nm (intracavity absorption). So, fluorescence cannot be observed thanks to the two photons process [1] but only to the three photons process [2]. Nevertheless, carbon monoxide is mainly dissociated through the two photons process whose probability is very high.

Studies carried out on a cell filled with 5000Pa of cold CO, allowed to detect a fluorescence signal one order of magnitude smaller than the one recorded in the 100Pa plasma jet. Temperature effects could not explain this huge difference. In both processes, the more difficult step is the first one because of the metastability of a<sup>3</sup>Π (lifetime 15ns). If this state has already been populated during plasma production, three photons dissociation becomes

\*Abstract 6725 submitted to the 21st International Symposium on Rarefied Gas Dynamics, Marseille, France, July 26-31, 1998

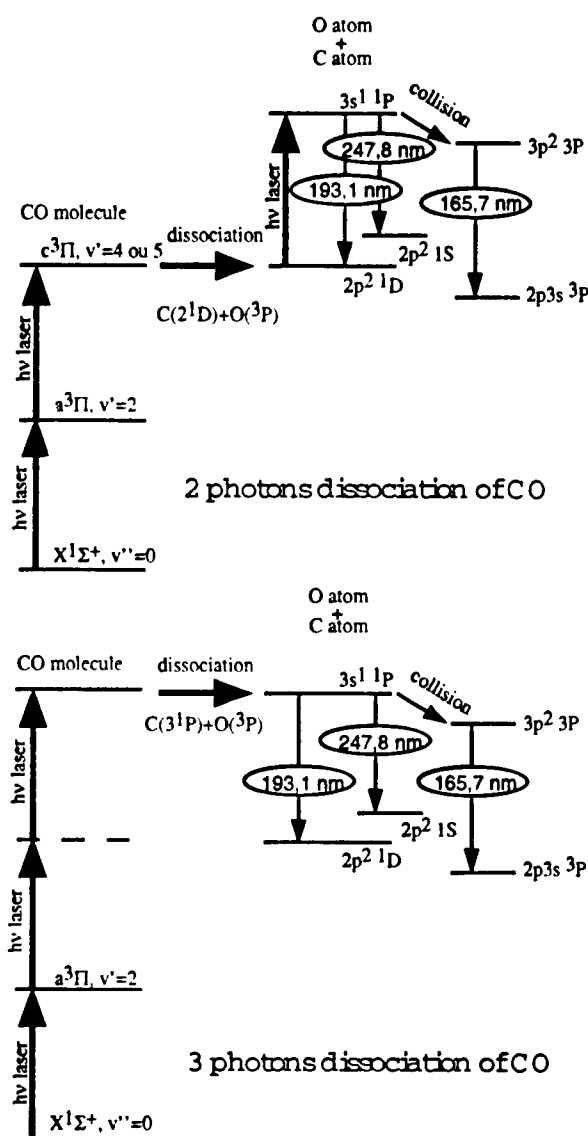


Figure 1: Two photodissociation processes of CO

a two photons dissociation and is able to explain the difference of signal. The hypothesis that a<sup>3</sup>Π state has already existed in the plasma jet, has been confirmed by recording the narrow-band

excitation spectrum. Instead of the lines of the Cameron bands, a featureless spectrum relative to the transition from  $a^3\Pi$  to a high excitation state has been observed.

In fact, the evolution of CO density measured above the C/SiC tile is the evolution of a  $a^3\Pi$  state. No significant evolution is noticed and small variations are explained by temperature evolution in the boundary layer.

Carbon atoms resulting from CO photodissociation can recombine (with CO or another C) in a  $C_2$  molecule. Fluorescence from  $C_2$  comes  $d^3\Pi$  state to  $a^3\Pi$  one (Swan bands) [3]. It has been first observed in a cell filled with 5000Pa of CO with a laser power equal to 150mJ at 193nm and it is visible with the naked eye. Formation of  $C_2$  is a quite slow phenomenon compared to laser pulse duration (20ns), especially at the pressure of this study (100Pa). If this time is long enough, knowing the dimensions of the excitation area, it is conceivable to obtain the jet velocity by measuring the duration of  $C_2$  fluorescence.

For one dissociated molecule of CO, one oxygen atom is produced on its fundamental level. These atoms can be excited thanks to Raman-shifted laser radiation [4]. The sum of the energies of the second and third Stokes photons produced in a deuterium Raman cell pumped by an ArF excimer laser is exactly the energy needed for  $2p^3P \rightarrow 3p^3P$  transition of atomic oxygen. Then, fluorescence can be recorded at 777 and 845nm. This measurement compared to atomic carbon fluorescence is able to give us the probabilities of both photodissociation processes. Nevertheless, it must not be forgotten that formation of  $C_2$  may also yield atomic oxygen during pulse duration which would perturb the measurement of oxygen atoms amount coming from CO photodissociation.

As atomic oxygen, carbon monoxide can also be excited thanks to a Raman-shifted laser [2]. In this case, the ArF excimer laser pumps a Raman cell filled with hydrogen. Two photons of the second Stokes produced are necessary to excite CO from the fundamental state to  $B^1\Sigma$  excited state. Then, fluorescence emission is radiative desexcitation of  $B^1\Sigma(v=0)$  toward  $A^1\Pi(v=0 \text{ to } 3)$  and can be detected in the spectral range 450-600nm. Rotational temperature of CO fundamental state can be measured by recording the excitation spectrum provided by narrow-band mode of the ArF excimer laser. Comparison of this experimental spectrum

with theoretical ones (Fig. 2) is able to give us the searched temperature.

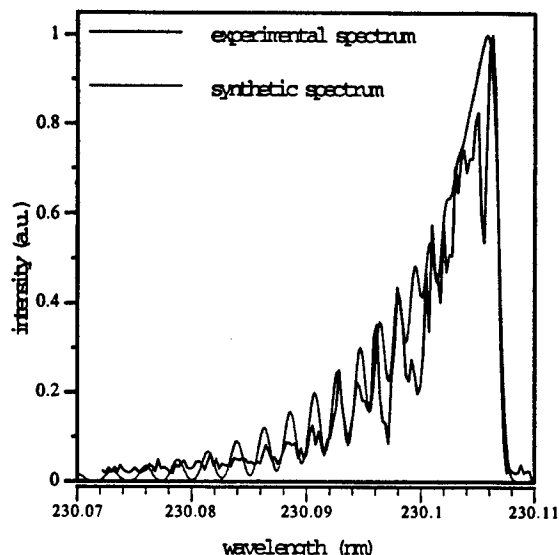


Figure 2: CO experimental and synthetic excitation spectra at 300K

Because of the great number of excitable transitions, fluorescence induced by an ArF excimer laser and/or Raman-shifted laser, proved to be very interesting in our kind of plasma.

Carbon monoxide and atomic oxygen are not the only species able to be investigated by this technique. A comprehensive study on nitrogen monoxide has already been carried out [5] and works about molecular oxygen, atomic nitrogen and silicon monoxide are on way.

This work is supported by SEP/ESTEC.

## References

- [1] Bokor and al., J.Chem.Phys., Vol.72, No.2, pp.965-971, 1980.
- [2] Meijer and al., J.Chem.Phys., Vol.89, No.4, pp.2588-2589, 1988.
- [3] Faust and al., Chem.Phys.Lett., Vol.83, No.2, pp.265-269, 1995.
- [4] Fletcher, Applied Physics B, Vol.B60, No.1, pp.61-65, 1995.
- [5] Honoré, Ph.D. Thesis, Rouen, 1995.

INDUSTRIAL PROCESSES - IP P

THURSDAY, JULY 30, 1998

16:00



## Uniform Deposition of Thin Solid Films on Inner Surface of Cylindrical Channel\*

V.V. Levdansky

Heat and Mass Transfer Institute, Academy of Sciences of Belarus, Minsk, Belarus

The substance deposition from the gas phase is one of the basic methods for production of thin solid films with uniform thickness. The uniform deposition is related to the conformal covering of the different structures (in particular of the inner surface of the channels) [1]. As mentioned in [1], without conformal growth some important steps in current microelectronics fabrication would be impossible. At sufficiently low pressure of the vapor of the substance to be deposited a free-molecular flow regime is created and the thickness of the deposited layer is dependent only on system geometry, the molecular flux incident on the surface and the surface processes.

In the paper the problem of the uniform deposition onto the inner surface of a cylindrical channel is studied on the basis of the molecular-kinetic theory. It should be noted that at the present time external problems have been studied thoroughly. In these cases, the deposition process can be controlled either by changing the position of the material source relatively to the substrate or by changing the geometric parameters of the source itself. Internal deposition problems are more complicated and less studied. Thus, for example, in the case of a thin layer deposition on the inner surface of a channel, where the source of substance to be deposited lies outside the channel, the deposition process can be controlled only by varying the gas pressure at the channel ends and the temperature distribution along the channel. The character of a change in layer thickness along the channel is determined by the resulting molecular flux into the condensate. Let us make some simplifying assumptions. It is assumed that before the beginning of the process the entire inner surface was coated by a layer of condensate (i.e., we will not consider the process of condensate formation on the bare substrate). The condensate is supposed to be solid. We will consider the problem in the quasi-stationary approximation. It is assumed that the growing condensate layer has no effect on the molecule motion

from one surface element to another, i.e. the condensate layer thickness  $h$  during the entire process is assumed to be much less than the channel radius  $R$ . The growth rate of the layer thickness  $h$  is  $\frac{dh}{dt} = n_s^{-1} J$ , where  $J$  is the molecule flux density into the condensate,  $n_s$  is the density of molecules in the condensate. The problem consists in determination of the conditions under which a constant value of  $J = c$  is achieved. For a cylindrical channel the flux  $J$  in the physical deposition (condensation) of gas molecules on the channel walls in a free-molecular flow regime can be written in the form

$$J = \alpha \left[ \int_0^1 (j + I) K_1(|x - x'|) dx' + N_0 K(x) + N_1 K(1 - x) \right] - j, \quad (1)$$

$$I = (1 - \alpha) \left[ \int_0^1 (j + I) K_1(|x - x'|) dx' + N_0 K(x) + N_1 K(1 - x) \right] \quad (2)$$

where  $x$  is a dimensionless coordinate directed along the channel ( $x = \frac{X}{L}$ ,  $L$  is the channel length),  $\alpha$  is the condensation coefficient,  $K$  and  $K_1$  describe the probabilities of molecule motion from one surface element to another,  $N_0$  and  $N_1$  are the flux densities of molecules entering the channel through its ends at  $x = 0$  and  $x = 1$ ,  $I$  is the flux density of reflected molecules,  $j$  is the flux density of the evaporating molecules,

$$j = A \exp \left\{ -\frac{Q}{kT} \right\}. \quad (3)$$

Here  $k$  is the Boltzmann's constant,  $T$  is the temperature,  $Q$  is the heat of evaporation, the preexponential factor  $A$  in Eq. (3) is assumed to be constant.

The term in square brackets of Eqs. (1) and (2) defines the flux density of molecules incident on the element

\* Abstract 2626 submitted to the 21st International Symposium on Rarefied Gas Dynamics, Marseille, France, July 26-31, 1998

of the capillary surface in the vicinity of the point  $x$ . This flux consists of molecules which have arrived from the remaining surface after evaporation or elastic, (but diffuse) reflection and also of molecules which have arrived directly in the given point after entry into the channel from outside. Approximating  $K, K_1$  by exponential expressions we can obtain in the case  $N_0 = N_1$  with account Eqs. (1), (2) and (3) following expression for the temperature distribution along the channel wall which is necessary for uniform deposition

$$T = \frac{Q}{k \ln \left\{ \frac{\alpha}{A} \left[ \frac{N_0}{c} - \frac{l}{2} - \frac{l^2 x(1-x)}{2} \right] - \frac{c}{A} \right\}^{-1}} \quad (4) \quad \text{where} \\ l = \frac{L}{R}.$$

As follows from Eq. (4), to keep the value of  $J$  constant, the temperature must decrease from the ends toward the channel centre. It is seen from Eq. (4) that there is a limitation on the maximum rate of the substance deposition. It depends on the ratio of channel length to its radius.

It should be noted that in the chemical deposition the coefficient  $\alpha$  in Eqs. (1), (2) characterizes the fraction of collisions resulting in reaction. It depends on the temperature. The condition of the uniform deposition for this case is also obtained.

The influence of surface phenomena on trapping of impurity molecules by growing layer of condensate is analysed in the paper. The expression for the concentration of impurity molecules in the deposited layer is obtained. It is shown that resonance (e.g., laser) radiation affecting the surface processes can change this concentration.

## References

- [1] Gates S.M. Chem. Rev. (1996) 96, 1519.

# Monte Carlo Simulation of a Chemical Reaction Transport Flow in a Low Pressure Deposition System \*

S.K.Stefanov<sup>1</sup>, M.Ota<sup>2</sup>

<sup>1</sup> Institute of Mechanics, Bulgarian Academy of Sciences, Sofia, Bulgaria

<sup>2</sup> Tokyo Metropolitan University, Tokyo, Japan

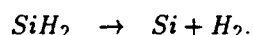
## 1 Introduction

Recently the molecular transport processes in the low pressure chemical vapor deposition (LPCVD) technologies for producing thin epitaxial films with a high uniformity of thickness have been studied using kinetic theory approach with an increasing intensity [1][2][3][4][5]. Generally speaking, the LPCVD process is formed and controlled by the following items: the vacuum conditions, the gas mixture source, the three ( source, wall and substrate ) temperatures  $T_0$ ,  $T_w$ ,  $T_s$ , the reactor geometry and the chemical reaction properties. The present paper is an extension of the previous author's work [6]. Here we investigate the influence of different models of chemical reaction on the growth rate of silicon layer on the substrate. We consider three models of reactive flow with different number of components of the gas mixture which enters the reactor as a binary mixture consisting of reactant gas (silane  $\text{SiH}_4$ ) and carrier gas ( $\text{H}_2$ ):

- silane pyrolysis  $\text{SiH}_4 \rightarrow \text{Si} + 2\text{H}_2$  on the substrate surface (no reactions in the reactor volume and the flow is neutral);
- silane pyrolysis  $\text{SiH}_4 \rightarrow \text{Si} + 2\text{H}_2$  on the substrate surface and a volume irreversible chemical reaction



- silane pyrolysis  $\text{SiH}_4 \rightarrow \text{Si} + 2\text{H}_2$  on the substrate surface and two volume irreversible chemical reactions



We present results obtained for moderate values of the Knudsen number based on the carrier gas mean free path.

\* Abstract 2698 submitted to the 21st International Symposium on Rarefied Gas Dynamics, Marseille, France, July 26-31, 1998

## 2 Particle simulation and results

We consider a typical configuration with idealized geometry ( radius  $R = 50$  mfp and height  $H = 50$  mfp) of a vertical axisymmetric (pancake) reactor with cold walls with temperature  $T_w$ . The mixture of reactant gas and carrier gas having a bulk velocity  $U = 0.5V_{th}$  ( $V_{th} = \sqrt{2R_1T_w}$ ,  $R_1$  is the specific gas constant of the carrier gas) and temperature  $T_0 = 0.5T_w$  enters the reactor through an inflow tube with radius  $r = 5$  mfp ( $x = (0, 5)$ ) attached to the reactor bottom ( Fig. 1 shows the half cross-section of the axisymmetric reactor). The substrate surface is a ring placed also at the bottom with a size  $x = (5, 45)$  and with constant temperature  $T_s = 5T_w$ . All molecules falling into the gap between the substrate and the reactor wall  $x = (45, 50)$  (outlet flux) are removed from further consideration. Diffuse reflection is supposed for all particles of any species hitting the reactor walls. The vertical co-ordinate axis coincides with the reactor axis.

According to the accepted chemical reaction model the simulation employs two( $\text{H}_2, \text{SiH}_4$ )-, three( $\text{H}_2, \text{SiH}_4, \text{Si}$ )- or four( $\text{H}_2, \text{SiH}_4, \text{Si}, \text{SiH}_2$ )-component set of particles. We use simple algorithms for simulation of each chemical reaction whose description will be given in the report. The simulation is carried out in two-dimensional computational domain taking into account the axial symmetry. We include weighting factors in the algorithm in order to equalize the species sample sizes. Part of the obtained results are illustrated in figures 1 and 2. Fig. 1 shows a typical temperature field obtained for the third component  $\text{Si}$  which a product of two chemical reactions.

The third case concerning the model with two chemical reactions (see the introduction) is illustrated with the top graphic in Fig. 2 which shows the distribution of the fluxes falling on the substrate:

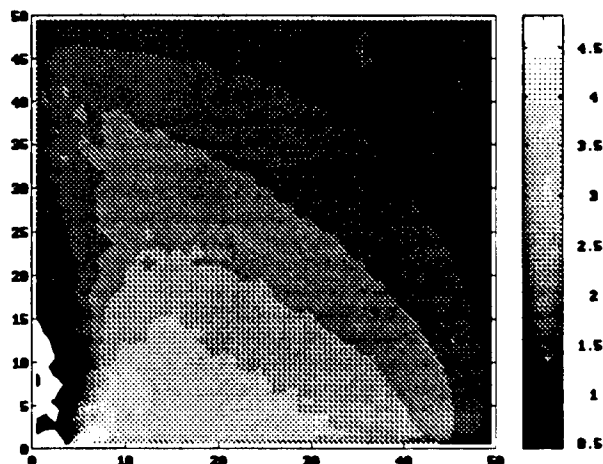


Figure 1: Temperature field obtained for silicon product of two chemical reactions

$\text{SiH}_4$  is noted with 'o', Si with '\*' and  $\text{SiH}_2$  with 'x'.

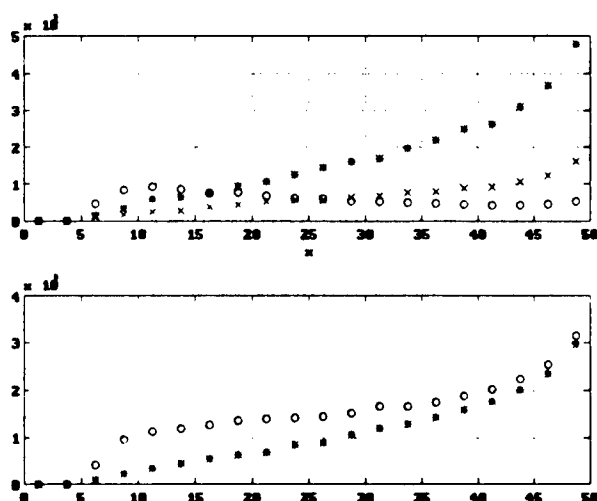


Figure 2: Number fluxes falling on the substrate

The bottom graphic shows the fluxes  $\text{SiH}_4$  and Si in the second case  $\text{SiH}_4 \rightarrow \text{Si} + 2\text{H}_2$ .

A detailed analysis of the obtained results as well as some specific issues of the simulation will be given in the basic report.

## References

- [1] Igarashi S., Nambu K., Mitamira S., Sugawara T., *Growth Rate of Films in Low-Pressure CVD Reactors*, In *Proceedings of RGD17 Symposium*, VCH, Ed. A. Beylich, Aachen, pp.671-678, 1991.

- [2] Coronell D., Jensen J., *Analysis of Transition Regime Flows in Low Pressure Chemical Vapor Deposition Reactors Using the Direct Simulation Monte Carlo Method*, J. Electrochem. Soc., Vol. 139, No. 8, pp. 2264-2273, 1992.
- [3] Stefanov S., *Monte Carlo Simulation of Molecular Beams in a Hot-Wall Epitaxial System*, Vacuum, Pergamon Press, Vol. 45, No.8, pp.857-865, 1994.
- [4] Bartel T., *Low Density Gas Modelling in the Microelectronics Industry*, In *Proceedings of RGD19 Symposium*, J. Harvey and G. Lord eds., Oxford Science Publications, Oxford, Vol. 1, pp.298-304, 1995
- [5] Boyd I., Chen Gang, *Computation of Supersonic Flow for Thin Films Deposition Using Expansion Through a Skimmer*, In *Proceedings of RGD20 Symposium*, Peking University Press, 1997.
- [6] Ota M, Stefanov S., *Monte Carlo Simulation of a Low Pressure Chemical Vapour Deposition Flow*, Peking University Press, pp.624-629, 1997.

# Effect of the Backscattered Vapor Pressure on the Temperature Field of a Metal Heated by an Electron Beam \*

J.L. Fleche<sup>1</sup>, P. Saunois<sup>1</sup>, D. Guilbaud<sup>2</sup>

<sup>1</sup> CEA DCC DPE, Saclay, France

<sup>2</sup> CEA DMT SEMT, Saclay, France

## 1 Introduction

When a metal confined in a water cooled crucible is heated by a focused electron beam, this metal melts to form a pool of liquid metal. The non uniformity of the melt temperature induces convection driven by two forces : a volume force created by the density gradients (buoyancy effect) and a surface force due to the surface tension gradient (Marangoni effect). With this local heating method the melt temperature can reach high values and thereby yield a collisional atomic vapor jet. At high vaporisation rates the liquid-vapor interface is distorted by the effect of escaping vapor and backscattered vapor flow to form a depression. This depression induces strong effects on both liquid and vapor. In the liquid the buoyancy convection in the pool is enhanced which reinforces the heat transfer towards the crucible. As far as vapor is concerned, the backscattered vapor flow is increased because of the depression. The backscattered vapor which is not in equilibrium induces a friction force at the liquid-vapor interface. This force is added to the surface force due to the surface tension gradient and contribute to increase the liquid surface velocity towards the crucible.

In this work we calculate the backscattered vapor pressure (normal and tangential to the liquid-vapor interface) and analyse its effects on the surface depression and the temperature field. For this purpose we use the well known Direct Simulation Monte-Carlo method (DSMC) including atom-atom elastic collisions (No Time Counter method proposed by G.A. BIRD) coupled in an iterative process with the Fluid Mechanics Finite Element Code (TRIO-EF) including the Young-Laplace equation to calculate the liquid-vapor interface.

In addition we model the normal and tangential vapor pressure at the liquid-vapor interface in order

to replace its time consuming DSMC evaluations in the iterative process. We validate this model by some comparisons with the DSMC-TRIO-EF results in the case of the axisymmetric cerium evaporation produced by constant electron beam power (5 kW) and various electron beam diameters (3.4 to 8 mm).

## 2 Vapor model

To model the backscattered normal vapor pressure we assume that in the case of strong evaporation the vapor flow rate is conserved between the surface depression and the plane section at the exit of the depression. The temperature field as a function of radius is the same at the exit section and on the liquid surface. In addition we assume that collisional processes take place to form a Knudsen layer at the exit of the depression. With these assumptions the normal pressure is :

$$P_n(r) = P_{sat}(r) \times (1 - 0.5(1 - \delta_p)g)$$

with

$$g = \frac{\int_0^{r_f} F_{Langmuir}(r) r dr}{\int_0^{r_f} \sqrt{1 + \left(\frac{dy(r)}{dr}\right)^2} F_{Langmuir}(r) r dr}$$

where  $r$  is the radial coordinate,  $y(r)$  the surface depression profile,  $P_{sat}$  the saturation vapor pressure and  $F_{Langmuir}$  the Langmuir vapor flux.  $\delta_p$  represents the backscattered vapor pressure coefficient arising from well-known Knudsen layer treatment. To model the tangential vapor pressure we use the shear stress expression :

$$P_t(r) = -C \lambda \left( \frac{dP_{sat}(r)}{dr} \right) \frac{1 - (1 - \delta_p)g}{\sqrt{1 + \left(\frac{dy(r)}{dr}\right)^2}}$$

where  $\lambda$  is the local mean free path at the spot center and  $C$  a coefficient to be determined.

\* Abstract 2951 submitted to the 21st International Symposium on Rarefied Gas Dynamics, Marseille, France, July 26-31, 1998

### 3 Results

The converged normal and tangential vapor pressures are plotted vs the radial coordinate in Fig.1 and 2 respectively (electron beam diameter = 6 mm). The modelled normal and tangential vapor pressures are also shown in Fig.1 and 2. In Fig.3 and Fig.4 we show respectively the depth of the depression and the temperature at the spot center vs the electron beam diameter. The temperature drop reaches 50 K when we take into account the backscattered vapor pressure. Note the excellent agreement between model and numerical calculations.

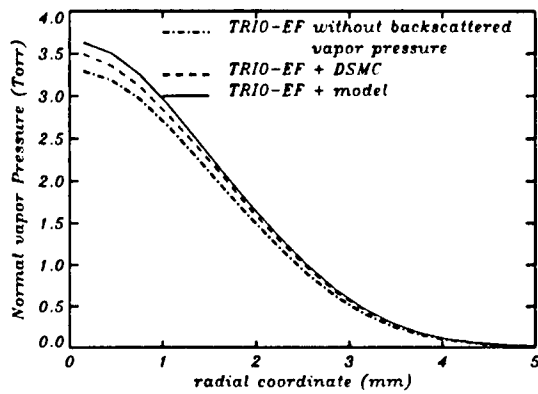


Figure 1: Normal vapor pressure

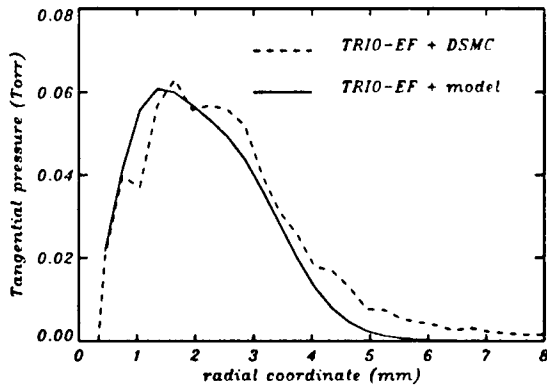


Figure 2: Tangential vapor pressure

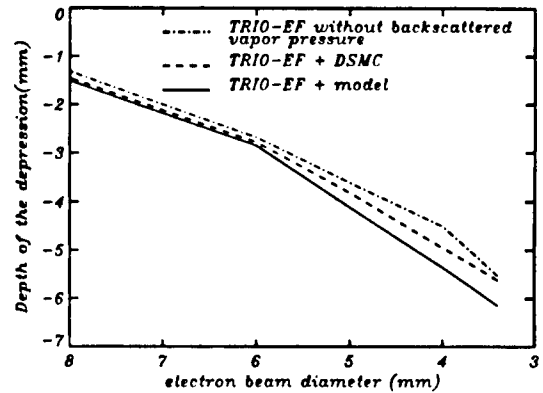


Figure 3: Depth of the depression

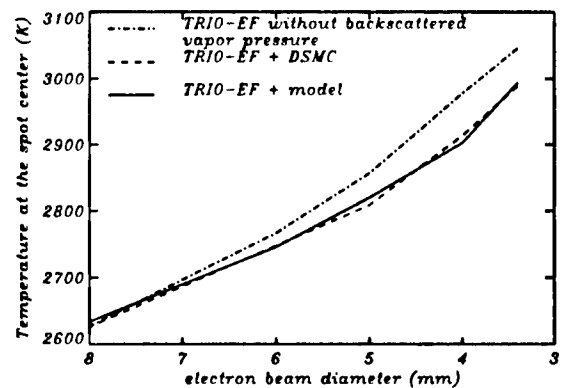


Figure 4: Temperature of the spot center

## DSMC Study of Transition Flow Through Tubes with Sudden Area Change \*

V. Manoj Kumar, Himanshu Agrawal and E. Rathakrishnan  
Department Aerospace Engineering Indian Institute of Technology, Kanpur, India

The present investigation is an application of the DSMC technique for simulation of three-dimensional transitional flows to study the transition flow through circular and rectangular tubes with sudden expansion and sudden contraction. In this study, the diameter ratio of the tubes has been varied from 0.25 to 2.0. The Knudsen number based on the diameter of the first tube has been varied from 0.1 to 1.0. The inlet flow angle of attack has been taken to be zero, *i.e.*, the inlet flow has been assumed to be parallel to the axis of the tube. The speed ratio has been varied from 0 to 10. The length to diameter ratio of both the smaller diameter and the larger diameter tubes has been varied from 0.5 to 5.0. For rectangular tubes the characteristic length has been taken to be quarter of the perimeter instead of the diameter as in the circular tubes. In all the simulations transmission probabilities have been calculated and compared with the Clausing's limit and Rathakrishnan's results. Simulation results for straight constant area tubes are found to be in good agreement with the Clausing's limit. The transmission probabilities for suddenly expanded tubes are found to be matching with the results of Rathakrishnan at low  $l/d$  ratios. At higher  $l/d$  ratios, however, the transmission probabilities are found to be lower than that of Rathakrishnan's results. The observed differences are possibly due the collision model. Some sample results are given in Figs. 1 and 2.

---

\*Abstract 4016 submitted to the 21st International Symposium on Rarefied Gas Dynamics, Marseille, France, July 26-31, 1998

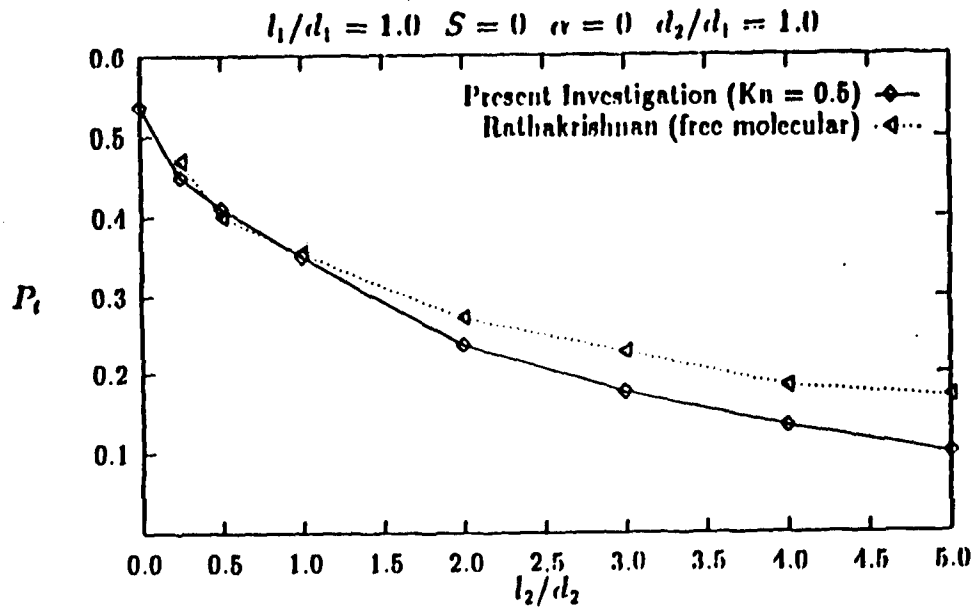


Figure 1: Comparison of total transmission probabilities  $P_t$  for  $l_1/d_1 = 1.0$  and  $d_2/d_1 = 2.0$  at  $S = 0$  with Rathakrishnan's results.

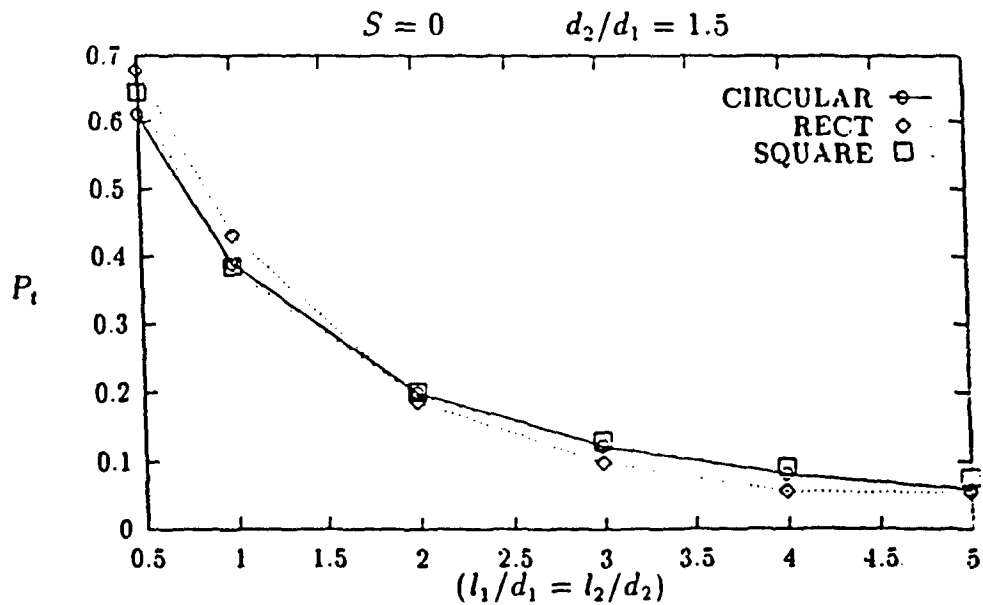


Figure 2: Total transmission probability  $P_t$  for circular ( $d_1 = 2$ ), rectangular ( $3 \times 2$ ), and square ( $2 \times 2$ ) tubes at  $S = 0$ .



## Free Jet Expansion into Vacuum from Long Tubes: A Study of the Correlation between Theory and Experiment \*

A.K. Sreekanth  
India

A series of experiments were performed in which the mass flow of air through short circular tubes of different radii connected in series was measured. The upstream pressures for a given flow geometry were varied in such a way so as to cover the entire flow range from continuum to free molecular. In all the experiments, the downstream pressure was kept at values atleast two to three orders of magnitude lower than the upstream pressure, thereby resulting in choked flow under continuum and near continuum regimes and negligible back flow under free molecular and transitional flow conditions. From the measured mass flow rates the flow conductances were determined.

In free molecular flow, the conductance for a given flow geometry is independent of the pressure and depends only on the temperature of the gas flowing through it. Extending the definition of conductance to a continuum flow of gas, it can be shown that for isentropic flows, the conductance is also independent of the pressure and depends only on the temperature of the gas. However, in viscous continuum flows and also in transition from continuum to free molecular flows, the conductance becomes a function of pressure. It is of interest to know how the conductance varies from its high value in continuum flows to its minimum value in free molecular flows and the nature of this transition. With this as the main objective, the present experiments were conducted.

Figs.1 and 2 show some typical results deduced from the experiments

Discussion of measured results, correlation with relevant theories, determination of transmission probability values using the test particle Monte-Carlo methods are being covered in the full version of the paper.

---

\*Abstract 4027 submitted to the 21st International Symposium on Rarefied Gas Dynamics, Marseille, France, July 26-31, 1998

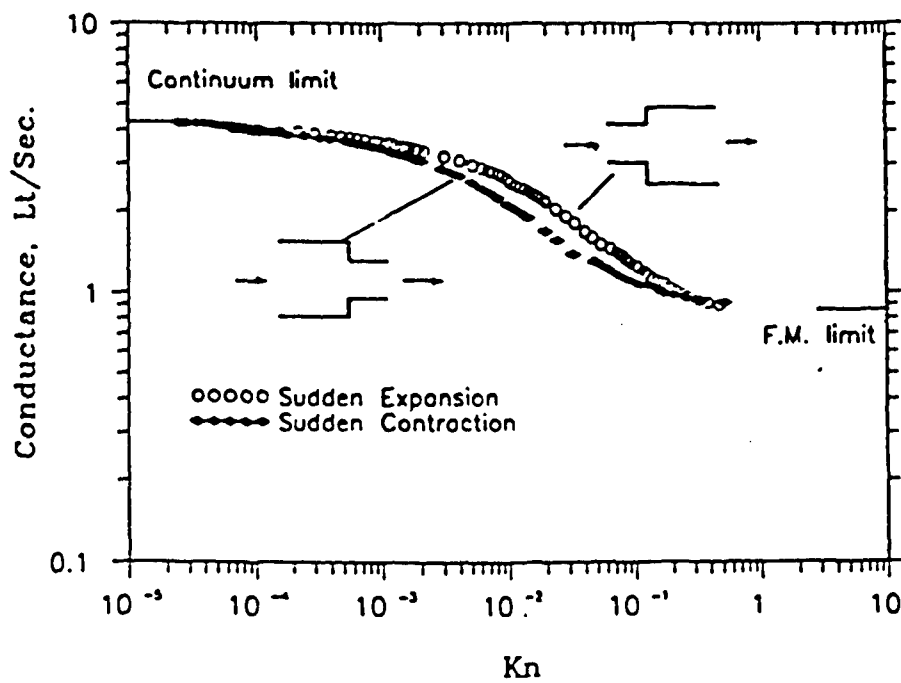


FIG.1 Conductance Vs Kn for Sudden Expansion and Sudden Contraction

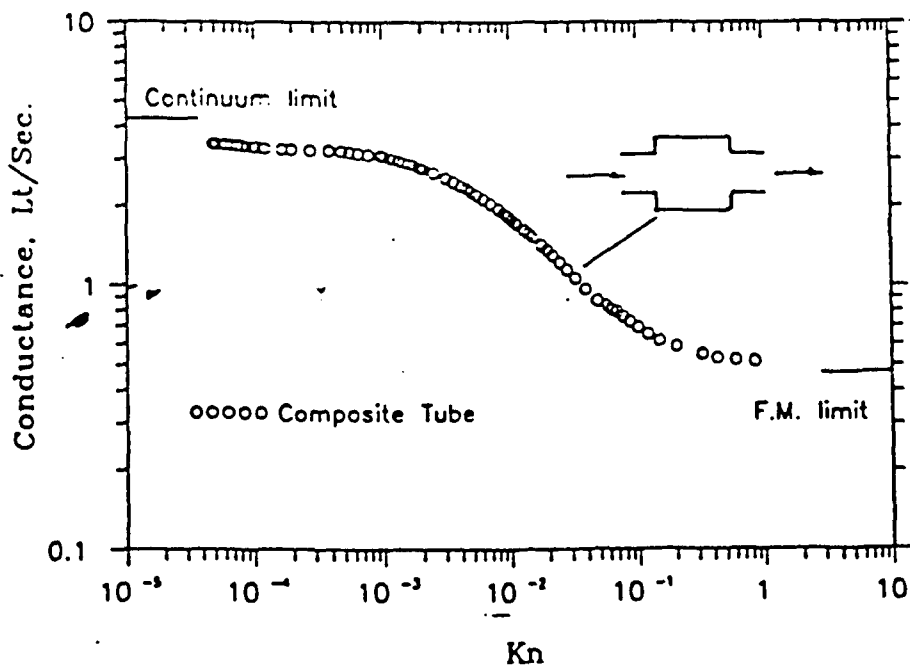


FIG.2 Conductance Vs Kn for Composite Geometry

# Characteristics of Laser Microengine Rotor with low Reflectance Surface by Electrostatic Flocking \*

M. Ota<sup>1</sup>, T. Hayashi<sup>2</sup>, M. Sakamoto<sup>1</sup>

<sup>1</sup>Dept of Mech. Engin., Graduate School of Engin., Tokyo Metropolitan Univ., Japan

<sup>2</sup>Chiba Institute of Technology, Tsudanuma, Japan

In order to realize wireless energy transfer to a micro-machine a small size rotating machine named as rarefied gas dynamics engine, laser microengine or micro mechanical actuator are proposed [1, 2, 3]. With laser beam irradiation on the rotor-blade surface of the microengine the microengine can rotate by a rarefied gas dynamics effect around the rotor. It is said that the effect comes from a thermal force caused by different surface temperatures of the rotor-blade at a rarefied gas condition. For increasing the torque of the rotor, the temperature difference between the forward and backward surface of the rotor should be increased and also the rotor surface must be low reflectance. In this paper the rotor for the microengine with low reflectance surface made by electrostatic flocking method is proposed. The surface temperature difference, light reflectance of the rotor surface and the torsion torque of the laser microengine were measured and discussed on the characteristics of the engines.

Carbon pile (the diameter of the pile is  $10\text{ }\mu\text{m}$  and the length is  $100\text{ }\mu\text{m}$ ) is implanted perpendicularly with respect to the rotor surface, thereby making it possible to form a surface having a very low reflectance owing to the so-called light trap effect, where the laser beam incident to the surface is reflected and attenuated among the fibers. The electrostatic flocking is a technology used to cover a substrate with vertical piles in an electric field. In the electrostatic flocking method a couple of electrodes are fixed in parallel. By the application of high voltage between these electrodes (the distance between the electrodes is 10 cm and the voltage is 20 kV), the piles are attracted by the electric field and start flying to the upper electrodes. If the substrate coated with some adhesive is set on the under surface of the upper electrode, each string of the piles will be placed vertically on the substrate. The surface obtained with this method effectively

absorbs the incident light among the strings and a very low reflectance surface is expected.

The surface temperature difference, laser beam reflectance and the torsion torque of the rotor by the electrostatic flocking were measured. The flocking densities are 4.0, 6.0 and 8.0 mg/cm/cm. The surface temperatures of the rotor irradiated by an argon ion laser beam were measured by infrared thermometer. The torsion torque of the rotor occurred by laser beam irradiation is the greatest at the Knudsen number 0.1 with the flocking density 6.0 mg/cm/cm. The Knudsen number is defined as the ratio of the mean free path length of ambient gas to the blade length. The temperatures are dependent on flocking density. In this study, the temperature difference between the forward surface and the backward surface of the rotors is the greatest at the flocking density, 6.0 mg/cm/cm. The minimum reflectance occurs at the flocking density, 6.0 mg/cm/cm. Therefore, it is concluded that the flocking density of the carbon piles on the micro-engine should be 6.0 mg/cm/cm.

## References

- [1] M. Ota and N. Kawata, *Direct Simulation of Gas flows around Rarefied Gas Dynamics Engines for a Micro-Machine*, Rarefied Gas Dynamics, ed. by J. Harvey and G. Lord, Oxford Univ. Press, 1995, pp.722-728.
- [2] M. Ota, M. Ishiguro and M. Sakamoto, *Blade Edge Effect of Rarefied Gas Dynamics Microengine Rotated by Laser Beam Irradiation*, Rarefied Gas Dynamics, ed. by C. Shen, Peking Univ. Press, 1997, pp.989-994.
- [3] D.C. Wadsworth, E.P. Muntz, G. Pham-Van-Diep and P. Keeley, *Crookes' Radiometer and Micromechanical Actuators*, Rarefied Gas Dynamics, ed. by J. Harvey and G. Lord, Oxford Univ. Press, 1995, pp.708-714.

\*Abstract 4471 submitted to the 21st International Symposium on Rarefied Gas Dynamics, Marseille, France, July 26-31, 1998

# Direct Mass Conversions into Fuel-like Species of (CO<sub>2</sub>) and (CO<sub>2</sub>+H<sub>2</sub>) Molecular Beams Passing through Plasma Fields \*

S. Kato, M. Okuyama, K. Hirose

Department of Mechanical Engineering, Mie University, Japan

## 1 Introduction

In recent CO<sub>2</sub> management technology, plasma assisted direct mass-conversions of CO<sub>2</sub> into fuel-like species have been tried by authors[1, 2], because radical particles produced in plasma fields easily give rise to decompositions of stable species such as CO<sub>2</sub> and to synthesis of desired fuel-like species such as CO, CH<sub>4</sub>, CH<sub>3</sub>OH, etc.

In this paper, experiments are performed on direct mass-conversions of CO<sub>2</sub> pure and (CO<sub>2</sub>+H<sub>2</sub>) mixture molecular beams which are effused into a plasma re-action furnace. Ar molecules are also mixed into the test beams to examine their effect as activating reagents. The mass-converted species and their yields are detected by a combined time-of-flight and mass-spectrometer technique.

## 2 Experimental

Figure 1 shows the experimental apparatus. A plasma reaction furnace consisting of a circular cathode and anode is equipped in an expansion chamber evacuated at  $\sim 0.1$ Pa. The surface heated up to  $\sim 1000$ K emits thermal electrons to keep its glow discharge stable. Both electrodes (30mm in dia.) are mounted parallel at a distance of 30mm. The molecular beams of CO<sub>2</sub> pure and (CO<sub>2</sub>+H<sub>2</sub>) mixture are accumulated once in a source chamber of 7.0kPa and are expanded through a nozzle of 0.15mm in dia. into the expansion chamber. In the plasma reaction furnace, discharged test molecules are attacked by accelerated electrons. The plasma formed is controlled by the voltage between the two electrodes,  $V_{ac}$ , being changed over (100-200)V.

With the aid of plasma, various kinds of chemical species are produced in the furnace and sampled as particle beams through a skimmer (2.0mm in

dia.) passing into a collimation chamber evacuated at  $\sim 0.1$ mPa. A rotating chopper modulates the skimmed particle beam for a time-of-flight measurement. Its gate function has a triangle form. The modulated particle beam enters a detection chamber evacuated at  $\sim 1$  $\mu$ Pa, in which a quadrupole mass-spectrometer is mounted. The existing chemical species are identified from the mass number, tuned and the respective yields are evaluated from the signal outputs.

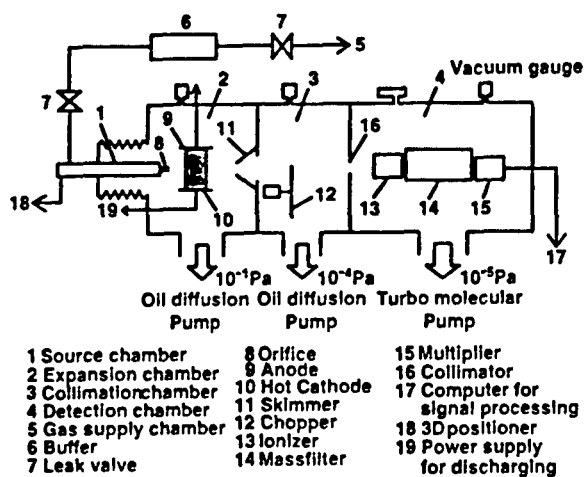


Figure 1: Schematic experimental apparatus.

## 3 Results and Discussion

Figure 2 shows a typical result of the yield of CO decomposed in the plasma furnace from the CO<sub>2</sub> pure molecular beam. Figures 3 and 4 show the respective yields of desired fuel-like species of CH<sub>4</sub> and CH<sub>3</sub>OH synthesized in the furnace from the (CO<sub>2</sub>+ H<sub>2</sub>) and (CO<sub>2</sub>+H<sub>2</sub>+Ar) mixture beams. The yield,  $Y = (V_{out})_i / (V_{out})_{CO_2}$  is defined as the ratio of the detector signal output measured at an arbitrary chemical species at a mass number of  $m=i$ ,  $(V_{out})_i$ , to the CO<sub>2</sub> output before plasma

\* Abstract 4601 submitted to the 21st International Symposium on Rarefied Gas Dynamics, Marseille, France, July 26-31, 1998

discharging, ( $V_{out}$ ) $CO_2$ .

As seen from Figure 2, the signals are detected at  $m=28$  and 44. The former at  $m=28$  is able to be identified as CO which is produced by plasma assisted direct mass-conversion due to thermal decomposition. Its yield reaches  $\sim 63\%$  of which value can be considered higher than that expected under the initial stage conditions. On the other hand, the latter species at  $m=44$  is clearly identified as  $CO_2$  itself. Its yield reduces to  $\sim 21\%$  from 100%. This fact implies that  $CO_2$  molecules are easily mass-converted into CO due to plasma decomposition with a relatively high yield.

Figure 3 shows the yields which are detected at the mass numbers of  $m=16$ , 28, 32 and 44. The first chemical species of  $m=16$  is most probably identified as methane ( $CH_4$ ); the reasons are: (1) since no signal is detected at  $m=16$  before plasma operation, the species is newly mass-converted from the ( $CO_2+H_2$ ) mixture in the plasma furnace, and

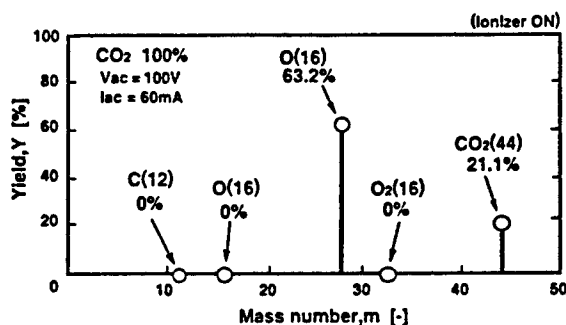


Figure 2: Yields from  $CO_2$  pure molecules.

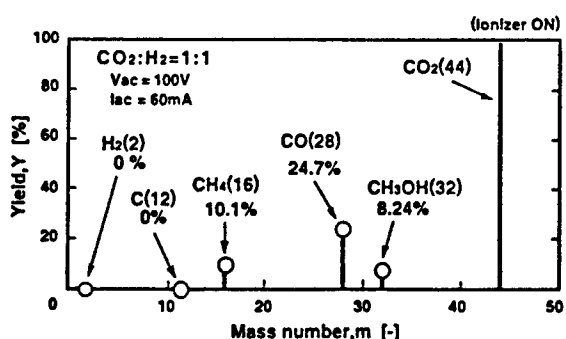


Figure 3: Yields from ( $CO_2+H_2$ ) mixture.

(2) since no oxygen atom having the same mass number is detected, the species is different from O. The  $CH_4$ 's yield reaches  $Y \sim 10\%$ . The second species of  $m=28$  is surely identified as CO, which is produced by thermal plasma decomposition from

$CO_2$ , and its yield reaches  $Y \sim 25\%$ . The third species of  $m=32$  is also most probably identified as methanol ( $CH_3OH$ ); the reasons are: (1) since O<sub>2</sub> having the same mass number is not detected in the experiment using pure  $CO_2$  molecules, the species is different from O<sub>2</sub>, and (2) since  $CH_4$  has been already produced,  $CH_3OH$  is probably synthesized from  $CH_3$  and OH radicals in the plasma field [2]. The yield of  $CH_3OH$  reaches approximately 8% of which value can be considered as fairly good.

The yields of fuel-like species can mentioned above increase significantly with the aid of Ar adding as activating reagents, as seen from Figure 4.

## 4 Conclusion

The experimental results prove that  $CO_2$  pure molecules can be well decomposed into CO with a relatively high yield, and ( $CO_2+H_2$ ) mixture molecules can also synthesize well  $CH_4$  and  $CH_3OH$  with fairly good yields, especially in the case of Ar adding as activating reagents.

## References

- [1] Kato S. and Lee S.J. , *Microscale Thermophysical Engineering*, Vol.1, No.3. pp.245-251, 1997.
- [2] Kato S., Yamamoto Y. and Okuyama M. , *Proc. of 1997 Int. Joint Power Generation Conf.*, Vol.1, pp.497-502, 1997.

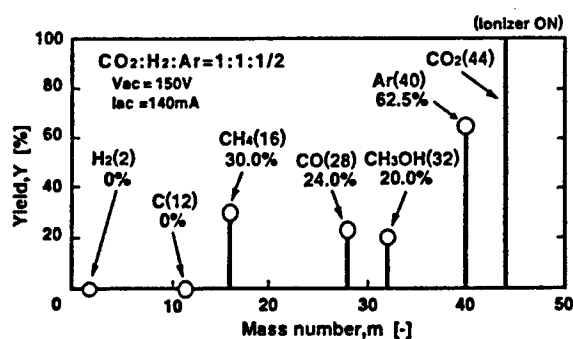


Figure 4: Yields for Ar adding.

# The Direct Simulation Monte Carlo of the Laser Ablation Products Expansion in Vacuum \*

N.Y. Bykov, G.A. Lukianov

Institute for High Performance Computing and Data Bases  
St. Petersburg, Russia

## 1 Introduction

Laser ablation is an important process for films deposition technology. Ablation process results gas or plasma flow from a target surface toward a substrate. The film thickness distribution depends on gas parameters distribution in a flow field. Understanding of a whole flow picture is very important here. In general case it is possible to distinguish particular stages and regions in the flow. General gasdynamic model for description of ablation products expansion is considered in this work.

Non-stationary laser ablation process modelling are enough difficult for computing and requires development of high-performance algorithms for efficient calculations. We concern solution of this problem in this paper.

## 2 Method

Laser jets have been simulated by the DSMC method under following setting. 2D axisymmetrical expansion in vacuum of laser ablation products from a round one-component solid target is considered. Laser ablation process is described as process of atoms thermal emission under given parameters of atoms velocity distribution function at the target surface  $f_w$ . During ablation process (ablation duration  $t_s$ ) parameters at the surface remain constant. Under this setting products of ablation are atoms. Inelastic processes (ionization, condensation etc) are not considered. NTC-scheme is used for description of atoms collisions and elastic collisions mechanics corresponds to VHS-model [1].

For the direct simulation of non-stationary flow high-efficient parallel algorithm was employed. This

algorithms provides execution of particular statistical independent calculations for statistical average in particular processors and gives possibility to achieve near maximum speedup and efficiency. Computing was fulfilled with the use of parallel system Parsytec CC/16.

In terms of molecular gasdynamic method dimensionless parameters of considered flow (in this setting) are determined by the type of function  $f_w$ , particles collision model, Knudsen number  $Kn = \lambda_w/d$  ( $\lambda_w$  - free length path near the target surface,  $d$  - target diameter) and by two dimensionless parameters (Struhal numbers):  $\tau_s = t_s u_w/d$  and  $\tau = t u_w/d$  ( $u_w$  - center-of-mass velocity near the target surface). Two models for  $f_w$  were considered: (1) Maxwell distribution function with  $u_w = 0$ , that corresponds to classical atoms thermal emission from a surface, (2) Maxwell distribution function with  $u_w = a$ , that corresponds to outflow gasdynamic model under Mach number  $M = 1$  ( $a$  - sound velocity).

## 3 Results

flow evolution includes two stages. First one (ablation stage) corresponds to the time interval  $t \leq t_s$ , second one (stage of "flying away") corresponds to  $t > t_s$ , when there is no surface ablation. Flow picture for both stages depends strongly on the value of  $\tau_s$ . It is possible to distinguish three basic flow regimes: regimes of short ( $\tau_s \ll 1$ ), middle ( $\tau_s \approx 1$ ) and long ( $\tau_s \gg 1$ ) impulses. Under  $\tau_s \ll 1$  gas motion in the stage of outflow ( $\tau < \tau_s$ ) is practically one-dimension and corresponds to a flow in a plate rarefaction wave. Under  $\tau_s > 1$  the flow has 2D and more difficult structure. Investigation had been fulfilled for  $\tau_s = 0.1 - 10$ ,  $Kn = 10^{-1} - 10^{-4}$  and  $\tau \gg \tau_s$ .

For long impulse regimes under  $\tau \geq 1$  steady flow field are formed near target. With elevation of  $\tau$  size

\* Abstract 4843 submitted to the 21st International Symposium on Rarefied Gas Dynamics, Marseille, France, July 26-31, 1998

of this field is rising. Steady flow formation speed in central and side domains is different. In central domain this formation proceeds more quickly and practically does not depend on Kn number. In non-stationary flow area character of expansion corresponds approximately to a spherical rarefaction wave. Peculiarities of translation relaxation in stationary and non-stationary flow areas are considered. Data about distribution functions is given.

Under  $\tau > \tau_s$  jet outflow is transforming to the space flying away of outflowed gas, density curve at the axes becomes non-monotonous. Density maximum value decreases rapidly under increase of a distance from a target. End of ablation process results rebuilding of density curves. Under  $\tau > \tau_s$  velocity value near target surface is equal to zero. Value of velocity is rising monotonously with increase of a distance from a target. With the lapse of time axial density curve becomes linear. Peculiarities of space products ablation flying away were investigated. Under  $Kn < 0.1$  general picture of expansion depends weakly on Kn number. Decrease of  $\tau_s$  ( $0.1 \leq \tau_s \leq 10$ ) leads to narrowing of solid angle, within which main part of gas is flying away.

Simulations data corresponds well to the experimental data [2] and gives possibility to explain the effect of forward peaked angular distribution under short durations of laser pulse.

## References

- [1] Bird G.A., *Molecular gasdynamics and the direct simulation of gas flows*, Clarenton Press, Oxford, 1994.
- [2] Pietch W., J. of Appl. Phys., 1996, 79, pp. 1250-1257.

## Thin Film Growth Dynamics on Solids with Defects \*

Yu. G. Markoff

Inst. for Mathematics and Mechanics, St-Petersburg State Univ., Russia

The growth dynamics of multilayer adsorbed films is one of the actual and actively studied problems in microelectronics, material researches, device design, vacuum technologies. It contains the most difficult questions of synergetics (nonlinear transfer, phase transitions, instabilities). In the present report the problem of detailed growth kinetics of multilayer films on the solids with defects is investigated in the frame of so called generalized kinetic BET - model (GKBET - model) [1,2]. According to assumptions of GKBET - model the thin film growth is described by the equation

$$\partial_t \theta(\alpha, t) = \sum_{\alpha} M(\alpha, \alpha|\theta) [B^D(\alpha|\theta') - B^D(\alpha|\theta)] + A(\alpha|\theta) [\exp(\mu^c) - B^a(\alpha|\theta)] \quad (1)$$

$$B^{D,a}(\alpha|\theta) = \exp[\mu^{D,a}(\alpha|\theta)],$$

$$\mu^{D,a}(\alpha|\theta) = -\epsilon^{D,a}(\alpha) - \phi\theta(\alpha) + \ln \frac{\theta(\alpha)}{q(\theta)};$$

$$M(\alpha, \alpha|\theta) = \nu_s \omega^s(\alpha, \alpha|\theta) q(\theta) q(\theta'),$$

$$A(\alpha|\theta) = \nu_1 a(\alpha|\theta) q(\theta), \quad s = 1, 2;$$

$$\sum_{\alpha} \omega^s(\alpha, \alpha|\theta) = 1; \omega(\alpha, \alpha|\theta) = \omega(\alpha, \alpha|\theta),$$

$$\mu^c = \ln \frac{j\sigma}{\nu_1};$$

$$q(\theta) = \begin{cases} 1 - \theta(\alpha), & l = 1 \quad \alpha = (l, \vec{R}) \\ \{1 - \theta(\alpha)\} \theta(\alpha_-), & l \geq 2 \\ & \alpha_- = (l-1, \vec{R}) \\ & q(\theta') = q(\theta(\alpha)) \end{cases}$$

In this equation  $\epsilon^{D,a}$  are the diffusion and adsorption potentials, respectively;  $\theta(\alpha, t)$  is the coverage;  $\nu_{1,2}$  are the frequencies of adatom vibrations in the normal and tangential directions, respectively;  $\omega^s(\alpha, \alpha)$  are the average probabilities of diffusion jumps;  $a(\alpha|\theta)$  is the adsorption probability;  $j$  is the

density flux of gaseous atoms;  $\sigma$  is the area of a cell;  $\phi = \beta z \epsilon_{nn}$ ,  $\beta = (kT)^{-1}$ ,  $T$  is the temperature;  $z$  is the coordination number of adsorbate,  $\epsilon_{nn}$  is the energy of lateral interactions of adatoms;  $\alpha = (l, \vec{R})$ ,  $l$  is the number of thin film layer,  $\vec{R}$  is the two-dimensional radius vector. Using  $\theta(\alpha, t)$  one can calculate various parameters of growing films, such as the mean local height  $h(\vec{R}, t)$ , its mean dispersion  $\Delta(\vec{R}, t)$  according to the relations (given in one layer height units)

$$h(\vec{R}, t) = \frac{N_1(\vec{R}, t)}{N_0(\vec{R}, t)},$$

$$\Delta(\vec{R}, t) = \frac{N_2(\vec{R}, t) - h^2}{N_0(\vec{R}, t)},$$

$$N_0(\vec{R}, t) = 1 + \sum_{l \leq 2} \theta(\alpha, t),$$

$$N_1(\vec{R}, t) = 1 + \sum_{l \leq 2} l \theta(\alpha, t),$$

$$N_2(\vec{R}, t) = 1 + \sum_{l \leq 2} l^2 \theta(\alpha, t).$$

The dependence of thin film growth dynamics on the solids defects are investigated in the frame of appropriate initial boundary value problems for Eq.(1).

In the report I consider also the case when the deposited particles are created in the gas phase due to chemical reactions. In this case it is necessarily to find the flow  $j(\vec{r}, t)$  as the solution of the following problem

$$\frac{\partial \vec{j}(\vec{r}, t)}{\partial t} = D_g \Delta \vec{j}(\vec{r}, t) + Q(\vec{j}(\vec{r}, t)), \quad (2)$$

$$\vec{j}(\vec{r}, t)|_{h(\vec{R}, t)} = a(\alpha, \theta) \vec{n} \nabla \vec{j}(\vec{r}, t)|_{h(\vec{R}, t)},$$

where  $\vec{n}$  is the unit normal vector to thin film surface;  $D_g$  is the matrix of the diffusion in the gas phase; the operator  $Q$  describes the chemical reactions;  $\vec{r}$  is three-dimensional radius vector;  $h(\vec{R}, t)$  is the profile of thin film.

In the report the above mentioned parameters of thin film growth are obtained. The comparison of

\* Abstract 5047 submitted to the 21st International Symposium on Rarefied Gas Dynamics, Marseille, France, July 26-31, 1998



these results obtained in the frame of GKBET - model with experimental data and the results of other authors are carried out using the singular spectrum analysis.

## References

- [1] Dubrovskiy G.V. (1994), *Realistic kinetic boundary conditions on surfaces*, Proceedings of RGD18 Symposium, **158**, 554 - 561. Vancouver, Canada.
- [2] Dubrovskiy G.V., Kuzmenko A.V., Markoff Yu.G. (1995), *A three - dimensional lattice gas approximation for multilayer adsorption*, Theoretical and Mathematical Physics, **105**, 1291 - 1306.

# DSMC Study of the Expansion of Laser-Evaporated Material into Vacuum \*

M.Yu. Plotnikov, N.M. Bulgakova, A.K. Rebrov  
Institute of Thermophysics, Novosibirsk, Russia

The objective of this work is to study the generation and expansion of a cloud of laser-evaporated material from a target into vacuum in a wide range of the Knudsen number up to continuum region formation with the Knudsen layer near the evaporated surface, using unsteady Direct Simulation Monte Carlo method (DSMC) [1]. Special attention is paid to the investigation of translational nonequilibrium and Knudsen layer formation near evaporation surface.

Evaporation is assumed to take place from a round spot of a radius  $R$  in a time interval  $\tau_1$ , according to diffusive law with the particle energy corresponding to the surface temperature  $T_s$ . The particle flux  $\Psi$  is constant during time  $\tau_1$  and equal to  $n_0 v_T / 4$  where  $v_T = \sqrt{8kT_s / (\pi m)}$ . Here  $m$  is the molecular mass and  $k$  is the Boltzmann constant. All the molecules, which reach the target surface when moving back to the target, are condensed. Expansion occurs during a given time  $t$  in an axially symmetric volume of radius  $R_1$  whose walls are fully absorbing. At a distance  $h$  from the target, a substrate is located where the particle absorption takes place as well. Considered evaporation corresponds to rather small laser fluences when the ionization processes may be neglected.

Gas-dynamic analysis, from the standpoint of the theory of similarity and dimensions, allows to recognize the governing criteria of the problem - characteristic Knudsen numbers:

- 1)  $Kn_1 = l/R$  where  $l$  is mean free path which is determined by the molecule density  $n_0$ ;
- 2)  $Kn_2 = l/(v_T \tau_1)$  where  $v_T \tau_1$  is the distance which is passed by a molecule with mean velocity in time  $\tau_1$ .

To characterize nonequilibrium degree in the expanding cloud, a concept of a local Knudsen number  $Kn_l = \frac{\lambda}{n} \frac{dn}{dx}$  is used where  $n$  is the density and  $\lambda$  is

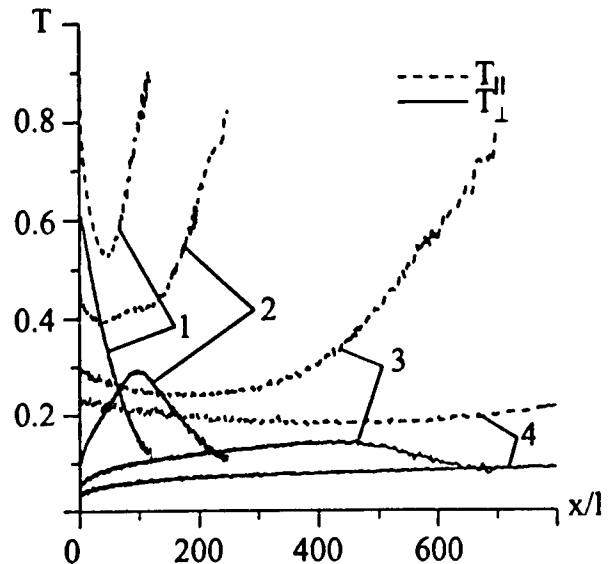


Figure 1: The distribution of the temperatures along the different directions for the time  $t/\tau_1 = 1; 2; 5; 10$  (line 1,2,3,4 correspondingly).  $Kn_2 = 0.0177$ .

the local mean free path. In the numerical experiments, the temporal and spatial evolution of the flow parameters has been investigated.

The data on the angle distribution of the deposit along a substrate placed in parallel with the target for Knudsen number  $Kn_1 = 10^{-2}$  have been obtained as well.

A wide series of calculation has been carried out for the case of expansion from a flat infinite surface (one-dimensional case). Planar expansion of a gas is of interest for understanding of the nonequilibrium processes in the immediate vicinity of the evaporated surface. Let's consider in details the peculiarities of the planar cloud expansion into vacuum by the example of  $Kn_2 = 0.0177$ . Degree of nonequilibrium is characterized by the comparison of the temperatures (the energies of the chaotic motion) along the different directions (fig.1). The difference between the temperatures  $T_{\perp}$  and  $T_{\parallel}$  (per-

\* Abstract 5101 submitted to the 21st International Symposium on Rarefied Gas Dynamics, Marseille, France, July 26-31, 1998

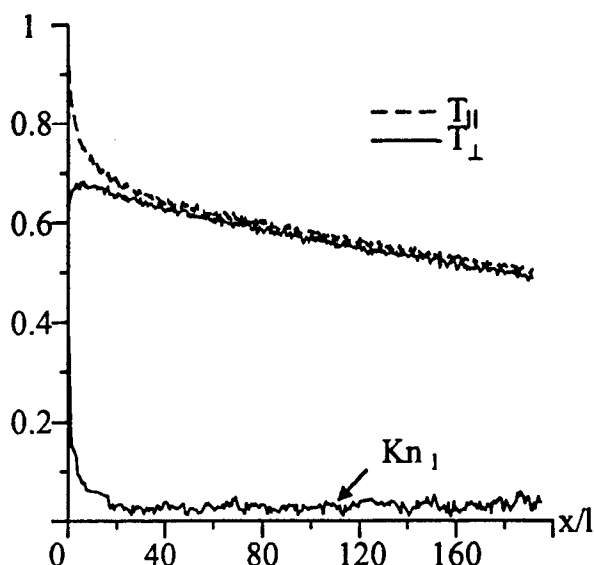


Figure 2: The distribution of the temperatures along the different directions and Knudsen number  $Kn_1$  for a time  $t = \tau_1$ .  $Kn_2 = 0.002$ .

pendicular and parallel to the target surface, respectively) thorough the time everywhere in the expanding cloud point to the essential nonequilibrium in the cloud under given conditions. A distinctive feature of a considered flow is that to the time  $t = 2\tau_1$  the temperature  $T_\perp$  acquires a maximum in the cloud "core" which persists during succeeding expansion. The temperature  $T_\parallel$  always exceeds  $T_\perp$ . Increasing of  $T_\parallel$  with the distance from the surface can be explained by earlier arrival to this region of high-energy molecules which have undergone lesser collisions and keep "the memory" about the energy after previous collisions or start from the surface. When  $Kn_2$  decreases, a region with translational equilibrium arises in the flow for a period of time (the region with  $Kn_1 < 0.01$ ). Formation of the flow region with the conditions close to equilibrium is associated both with the density increase near the surface and with the decrease of the parameter gradients during filling the space by gas (vapor).

To answer the question, under what conditions, namely, for what minimum values of  $Kn_2$ , a continuum region with  $Kn_1 < 0.01$  begins to be formed, the calculations of parameter distributions were carried out for  $Kn_2$  in the range  $2 \times 10^{-3} - 2 \times 10^{-4}$ . Figure 2 presents the distributions of the temperatures  $T_\perp$  and  $T_\parallel$  and Knudsen number  $Kn_1$  with the distance from the evaporated surface. The value of local Knudsen number decreases sharply near the surface and takes a stable value of about 0.02 in the region where the difference between  $T_\perp$  and  $T_\parallel$

become small. Farther from the evaporated surface  $Kn_1$  increases, and the flow becomes nonequilibrium again. When  $Kn_2$  is an order lower (for  $Kn_2 = 2 \times 10^{-4}$ ), the value  $Kn_1$  is stabilized at a level of about 0.005. In both cases equilibrium approached in subsonic region. These results allow to conclude that a continuum region in the plume occurs under  $Kn_2 < 2 \times 10^{-3}$ .

## Acknowledgements

This work was supported by the Russian Foundation for Basic Research.

## References

- [1] Bird G.A., *Molecular gas dynamics and the direct simulation of gas flows*, Oxford, Clarendon Press, 1994.

# The Optimization of Internal Gas Flow in a Centrifuge \*

O.E. Aleksandrov, B.T. Porodnov, V.D. Seleznev

Department of molecular physics

Urals state technical university

Ekaterinsburg, Russia

The efficiency improvement of gas centrifuges requires the prediction of the maximum theoretical separation coefficient. The purpose of this paper is to work out the theory of the centrifuge separation coefficient and to obtain the analytical expression for the maximum separation coefficient as a function of centrifuge parameters.

The centrifuge type known as Zippers' centrifuge, widely used in the uranium enrichment industry, is considered. This work is based on the method, developed by Cohen [1]. The main difference from the former investigations is that we find the maximum separation coefficient for a fixed feed stream.

First of all we modify the derivation of Cohens' diffusion equation to remove the restriction of uniform circulation gas flow along the centrifuge axis. The suggested modification consists of the separation of the internal gas flow onto two parts: the vortex flow and the potential flow. Using this method we can prove that the modified Cohens' method is applicable in the case of strongly non uniform gas flow along the centrifuge axis. The obtained analog of Cohens' diffusion equation has some differences from the original one and permits us to better understand the role of the internal gas flow in centrifuge performance.

In the next step we suggest the more general method of linearization for the nonlinear Cohens' diffusion equation and obtain the equation solution. On the basis of this solution, the perfect centrifuge problem is formulated. The similarities and peculiarities of the perfect centrifuge related to the perfect cascade are discussed also.

Finally the perfect centrifuge separation coefficient and the optimal axial intensity profile of the internal gas flow are obtained. The perfect centrifuge separation coefficient is significantly higher than in the case of uniform axial gas flow. However, the perfect centrifuge axial flow profile differs from the

circulation intensity profile in a perfect cascade. A centrifuge may be represented as a cascade with the cascade unit separation coefficient dependent on the circulation intensity.

The reported research gives us a way to optimize the internal flow in the centrifuge. It also shows the upper limits of the centrifuge efficiency. For instance, we can confirm that the short centrifuge is more efficient than a long centrifuge in the case of perfect internal flow.

## References

- [1] Cohen K., *The theory of isotope separation as applied to the large-scale production of  $^{235}\text{U}$* , McGraw-Hill Book, 1951.

\*Abstract 6526 submitted to the 21st International Symposium on Rarefied Gas Dynamics, Marseille, France, July 26-31, 1998

# The Role of the Transition to Free Molecular Flight in Pulsed Laser Ablation \*

T. E. Itina<sup>1</sup>,  
W. Marine<sup>2</sup>, M. Autric<sup>3</sup>

<sup>1</sup> Central Scientific Research Institute of Machine Building (TSNIIMASH),  
Moscow Region, Russia

<sup>2</sup> Laboratoire Interdisciplinaire Ablation Laser et Applications, CNRS, France

<sup>3</sup> IRPHE- LP3, UMR, CNRS, Marseilles, France

Pulsed laser ablation has attracted a great attention over past few years as an efficient method for depositing thin films. The theoretical studies of this phenomenon [1-3] show that when the yield of material is sufficiently high, gas-phase interactions occur leading to the formation of a Knudsen layer (KL) that evolves into unsteady adiabatic expansion (UAE). In the Knudsen layer, the initially non-equilibrium velocity distribution transfers into Maxwell-Boltzmann distribution with flow velocity. Then, during UAE the flow is in equilibrium and analytical solution can be obtained using gas-dynamic equations that are valid until the transition of the flow to free-flight [3].

However, both in Monte Carlo simulations and in experiments there was an indication that the results were better fitted using an elliptical Boltzmann distribution with two temperatures: a temperature  $T_z$  parallel to the flow velocity and an oblique temperature  $T_{xy}$ . In the present study we note that this distribution can result from the disturbance of equilibrium distribution during the transition of the flow to free molecular flight, that gives rise to the deviation of the parallel temperature  $T_z$  from the perpendicular one ( $T_{xy}$ ) [4]. The temperature parallel to the flow velocity tends to be frozen as a result of free-expansion, while the kinetic temperature in perpendicular direction decreases with the increase of the distance from the surface. This result is in agreement with our previous Monte Carlo simulation.

Here, with the aid of both Monte Carlo simulation and momentum method we relate the parameters of the resulting velocity distribution function with the characteristics of the flow before the transition to free flight. Using KL-UAE solution the resulting parameters can be connected with initial conditions.

It should be noted, that for more rigorous analysis, the condensation of vapor must be considered, resulting from the supersaturation in the vicinity of the irradiated surface. The investigation of these phenomena is also under way.

[1] R. Kelly and R. W. Dreyfus, Nucl. Instrum. Methods B 32, 314 (1988)

[2] R. Kelly and R. W. Dreyfus, Surface Science 198, 263 (1988)

[3] R. Kelly, J. Chem. Phys. 92(8), 5047 (1990)

[4] B.B.Hamel, D.R. Whillis, Phys.Fluids, 9, 829 (1966)

---

\* Abstract 6812 submitted to the 21st International Symposium on Rarefied Gas Dynamics, Marseille, France, July 26-31, 1998

## The application of Local Estimators to the Simulation of the Transport of laser-Ablated Atoms in a Dilute Gas\*

T.E. Itina, A.A. Katasonov, A.N. Ruminsky

Central Scientific and Research Institute of Machine Building (TsNIIMASh), Russia

The transport of laser-ablated atoms in a diluted gas is described by linear Boltzmann equation. The most elaborated (from mathematical standpoint) approach to the solution of such equations by Monte Carlo method is the following one:

1. the equation in question is written in integral form;
2. all values to be calculated are expressed through functional dependencies (integrals) of the integral equation solution;
3. the evaluation of the functional dependencies over Markov's chain is applied in order to obtain numerical results.

Such approach to numerical simulation is rather well elaborated for transport of neutrons and infra-red radiation. The list of its main advantages includes:

- the possibility of developing numerical methods for "true" local characteristics of the process in question and not for ones averaged over some regions;
- sophisticated formal mathematical methods for the study of corresponding equations and convergence of numerical Monte Carlo procedures;
- easy calculation of results accuracy.

In this paper we represent the results of construction of functional dependencies of integral equation solution for the calculation of ablated atoms flux in an arbitrary point. Such formal mathematical approach allows to investigate the behavior of physical parameters near axis of symmetry. We also investigate the possibility of creating similar mathematical methods for time-dependent Boltzmann equation and obtaining time-dependent characteristics of process of transport of ablated atoms.

---

\* Abstract 6813 submitted to the 21st International Symposium on Rarefied Gas Dynamics, Marseille, France, July 26-31, 1998

## Free Molecular Internal Flows in Complex Axisymmetrical Structures \*

Paklin B.L.

Novosibirsk State Technical University, Russia

This paper deals with a new approach of Monte Carlo simulation algorithm of Clausing coefficient calculation for molecular fluxes through complex axisymmetrical structures. This parameter means the molecule probability to overcome a channel with arbitrary geometrical configuration.

Two limits exist while considering internal flows in transition regime - free molecular and continuous ones. Free molecular simulation can easily provide the main effect and due to its simplicity allows to desolve practically important problems [1, 2]. It is obviously clear theoretical and any numerical results should be tested by free molecular limit. For this reason it is necessary to apply simple and reliable algorithm that can permit to fulfil this goal.

A new algorithm suggested in this paper allows for a short time to elaborate and test program practically excluding errors. So simplicity and reliability are the main features and advantages. As in any Monte Carlo technique we should simulate a number of molecular histories. Considering molecular path as a direct line the intersection with control parallel planes is defined. This approach means the solution of the first order equation. If molecule has passed the control surface it is followed by in another section. In negative case the interaction with axisymmetrical surfaces of internal walls is considered. Only in last case it is necessary to solve the second order equation. The fastest calculation is obvious advantage. Logical scheme of such algorithm is very simple and possible for any axisymmetrical structures of internal flows.

There is some analogy with light rays. It is clear light rays or photons can not overcome converging channels even for specular walls and absolutely black body or black hole can be mentioned as a result of this consideration. It looks like a trap. For diverging channels light pass straight fully. The integral effect of any pair of surfaces can be estimated.

From this point of view it is possible to analyze the productivity of vacuum devices and make molecular flux estimations as upper limit for any kind of industrial apparatus.

Some interesting fundamental results will be presented in full paper.

### References

- [1] Paklin.B.L., Rebrov A.K., Sadykov K.S., Figuurov S.A., *Direct Statistical Simulation of Molecular Flux Interaction with a Free Jet*, RGD XVII-th Int. Symp. Proc., Aachen 1990, pp.1561-1567.
- [2] Saksaganskii G.L., *Molecular Fluxes through Complex Vacuum Structures*, Moscow, 1980 (in Russian).

\*Abstract 6901 submitted to the 21st International Symposium on Rarefied Gas Dynamics, Marseille, France, July 26-31, 1998

## Radial Transition Flow Between Parallel Disks: Comparison of Computations and Experiments \*

L. A. Gochberg<sup>1</sup>, R. G. Wilmoth<sup>2</sup>, A. Krishnan<sup>3</sup>

<sup>1</sup> Novellus Systems, Inc., San Jose, California, USA

<sup>2</sup> NASA Langley Research Center, Hampton, Virginia, USA

<sup>3</sup> CFD Research Corporation, Huntsville, Alabama, USA

Computations using a continuum Navier-Stokes (CFD) and direct simulation Monte Carlo (DSMC) were performed in 2D, and compared to experimental data and an analytical solution for radial flow between parallel disks. The flow conditions spanned the regime between the limits of continuum and free molecular flow. The data and analytical solution used in the comparisons were presented previously [1], and investigated helium, nitrogen and argon gases in the experimental parallel disk flows.

The DSMC code [2] was modified to correctly handle boundary conditions in subsonic flow [3] in a manner as similar to the boundary conditions used in CFD as was possible. The CFD software [4] incorporated slip boundary conditions [5] to extend its application into the transition flow regime. Results showed that the analytical solution, DSMC, and experimental data matched extremely well. DSMC results were obtained for Knudsen numbers of 0.1, 1, and 100. The CFD results showed the expected good comparison for continuum flow conditions, and also slightly into the into the near continuum portion of the transition regime. However, CFD with slip boundary conditions showed a surprising ability to capture the trends seen in the data out to Knudsen numbers as large as 5, though the absolute errors were expectedly large. Applicability of CFD in these flows is typically quoted as being limited to Knudsen numbers less than 0.05 - 0.1.

This result has an industrial application in the design of electrostatic chucks in chemical vapor deposition (CVD) semiconductor equipment. In between the wafer and the surface of the electrostatic chuck, a gas flow of helium is used to provide some controlled cooling of the wafer in the CVD reactor. The gap between the wafer and the chuck is small enough such that much of the flow there is well into the transition regime. In some thin film processing

applications, the cooling of the wafer needs to be controlled. If the flow and heat transfer is in the transition regime, a change in gas pressure can be used to vary the heat transfer between the wafer and chuck, and thus control the wafer temperature as different processes are performed.

However, the chuck geometry also includes portions of the flow that are almost continuum in nature. DSMC is a logical computational approach to try for this transition flow problem. However, DSMC codes will be very slow to run in this problem due to: 1) the very slow gas flow velocities (~1 m/s), 2) the large dimension in the flow direction (100-150 mm). These factors result in extremely long run time requirements to get statistically significant molecular sampling for an accurate solution. The time requirement estimates show that DSMC is not currently capable of providing solutions in an industrial time scale (several days of CPU time).

The 2D radial flow problem examined here has a very similar geometry to the wafer/chuck geometry. If the success of the 2D CFD models with slip boundary conditions can be extended to the geometrically complex 3D wafer/chuck problem, some limiting, worst case flow conditions can be estimated. Successful computations like this would allow for some degree of optimization in the design of the flow channels on the chuck. Additionally, this type of model might also be extended to compute the conjugate heat transfer through the silicon wafer to the cooled chuck. Such a model might suggest design changes to optimize process control of the thin film deposition and/or increase the thermal uniformity on the wafer to improve thin film quality.

---

\* Abstract 6916 submitted to the 21st International Symposium on Rarefied Gas Dynamics, Marseille, France, July 26-31, 1998



## References

- [1] Browne, V. d'A and John, J. E. A., "Vacuum Radial Flow From the Viscous Through the Free Molecule Regime", *Vacuum*, Vol. 20, No. 12, p. 525, 1970.
- [2] Bird, G. A., Molecular Gas Dynamics and the Direct Simulation of Gas Flows, Clarendon Press, Oxford, England, UK, 1994.
- [3] Nance, R. P., Hash, D. B., and Hassan, H. A., "Role of Boundary Conditions in Monte Carlo Simulation of MEMS Devices", AIAA Paper 97-0375, 1997.
- [4] CFD-ACE Version 2.0, CFD Research Corporation, Huntsville, AL, 1997.
- [5] Kersch, A. and Morokoff, W. J.), Transport Simulation in Microelectronics, *Progress in Numerical Simulation for Microelectronics*, Vol. 3, edited by K. Merten and A. Gilg, Birkhäuser Verlag, Basel, Switzerland, p. 101-113, 1995.

**IONIZATION AND RADIATION - IR P**

**THURSDAY, JULY 30, 1998**

**16:00**

# Ionizing Shock Flow Pattern at Intensive Plasma Energy Release \*

A. S. Baryshnikov

A.F. Ioffe Physico-Technical Institute, St. Petersburg, Russia

In previous papers [1] the mechanism of flow pattern reconstruction (FPR) behind shock wave (SW) was proposed. A new pattern is distinguished by high gradients of physical quantities as well as by intensive radiation ("flashes" of radiation) behind the wave front. However there was no confirmation in kinetics. In this work such confirmation is intended to get due to new ideas suggested. So, the principle idea of previous proposal was the cubic dependence of radiation intensity on the components concentrations. Now there is an opinion that in atoms and ions of some gases (Ar, Xe) distribution of metastable and resonance excitation levels is suitable for cubic radiation model. Besides that, high mobility of charged particles in plasma make up to take into account the effects of ambipolar diffusion. In accordance with classic principles of synergetics it is the balance between third order nonlinearity and diffusion leads to arising of dissipative structures. Computations of plasma flow behind ionizing shock wave in Ar carried out in accordance with suggested model indeed show the abrupt but adiabatic jump of gas density by 3-4 times as it should be in additional shock wave, the pressure rises by about 20% possibility of control of external and internal reacting gas flow at high Mach number with use of effect investigated.

## References

- [1] Baryshnikov A.S., *Intensive plasma energy release behind shock wave and a flow pattern*, In: Rarefied gas dynamics, Ed. by Beylich A.E., Proc. 17th Int. Symp. on Rarefied Gas Dynamics, VCH, Weinheim - N.Y. - Basel - Cambridge: 263-270, 1991

---

\* Abstract 1971 submitted to the 21st International Symposium on Rarefied Gas Dynamics, Marseille, France, July 26-31, 1998

# The Non-Local Kinetic Equations for Polarizable Plasmas \*

V.V. Belyi<sup>1</sup>, Yu.A. Kukhareno<sup>2</sup>, J. Wallenborn<sup>3</sup>

<sup>1</sup> IZMIRAN, Troitsk, Moscow regoin, 142092, Russia

<sup>2</sup> UITPRAN, Moscow, Russia

<sup>3</sup> Physique Statistique, Plasma et Optique non lineaire, Univ. Libre de Bruxelles, Belgium

In many problems, non-locality in space must be considered as well as non-Markovian character (or non-locality in time). Therefore, we have extended our previous work [1] to the study a non-uniform weakly non-ideal multicomponent plasma.

We made a double expansion of the resolvent for the BBGKY hierarchy in the plasma approximation, both in the non-Markovianity and non-uniform parameters (respectively, the inverse product of the plasma frequency times the relaxation time and the ratio of the Debye length to the mean free path). We have obtained in this way the pair correlation function which determines the non-dissipative properties of the non-ideal system as well as the dissipative contributions to the collision integral. Therefore a non-linear kinetic equation, which is non-local in space and time in a consistent approximation, has been deduced. This equation is a generalization of the Balescu-Lenard equation for the inhomogeneous a non ideal multicomponent plasma.

We have shown that this equation describes correctly the local conservation laws for the particle density, momentum and total energy in an approximation which, at equilibrium, is equivalent to the Debye- Hückel one. This equation is then the basis for deriving the nonlinear hydrodynamics of non-ideal plasmas.

## References

- [1] V.V. Belyi, Yu.A. Kukhareno, J. Wallenborn, Phys. Rev. Letters, vol. 76, p. 3554 (1996)

---

\*Abstract 1986 submitted to the 21st International Symposium on Rarefied Gas Dynamics, Marseille, France, July 26-31, 1998

# On the Theory of Light-Induced Drift of Rarefied Gases in Capillaries \*

V.G. Chernyak, E.A. Vilisova

Physics Dept., Ural State University, Ekaterinburg, Russia

The phenomenon of the drift of a binary gas mixture induced by a resonant optical radiation has been studied theoretically at intermediate Knudsen numbers ( $Kn$ ).

A kinetic theory of the light-induced drift (LID) of a gaseous mixture was developed in Ref.[1] at arbitrary  $Kn$ . However, the results obtained there are limited by the assumption that the radiative decay rate  $\Gamma_m$  of an excited level is small compared to the intermolecular collision rate  $\gamma_n$ , i.e.  $\Gamma_{mn} = \Gamma_m/\gamma_n \ll 1$ . Such approximation can be realized for molecules, but it is difficult to execute for one-atomic gas. For this reason the theory [1] does not describe experiments [2] on LID of sodium vapour in inert gases.

In this work the theory of LID for a binary gas mixture has been studied at arbitrary values of parameter  $\Gamma_{mn}$  and  $Kn$  number. It is assumed that the radiation intensity is uniform along the cross section of the capillary. The change in intensity along the capillary is small. It is considered the case in which the concentration of absorbing species is low. The two-level approximation for absorbing particles is used. A traveling light wave is absorbed by molecules in the electronic or vibrational-rotational transition from the ground state  $n$  to an excited state  $m$ . The velocity distribution functions for excited, ground-state and buffer gas molecules satisfy the system of three kinetic equations. Specular-diffuse reflection model is used as boundary condition. It is assumed that the collisions of gas particles with the capillary wall and with each other are elastic. The accommodation coefficients of excited ( $\varepsilon_m$ ) and ground-state ( $\varepsilon_n$ ) particles are different, and the effective diameters  $d_m$  and  $d_n$  are different too.

The surface (accommodation) and bulk (buffer) mechanisms of the effect which are inspired respectively by the difference in the accommodation coefficients and the collision cross sections for excited

and ground-state particles have been analyzed.

In assumption of small difference between the effective diameters of the excited and ground-state particles and at nearly diffuse scattering of particles on the capillary surface, for the flow of absorbing gas  $J_1$  (LID) and the flow of buffer gas  $J_2$ , averaged over the cross-section of the capillary, the following expressions have been obtained:

$$J_i = n_1 r A \left( G_i^{(1)} \Delta \varepsilon + G_i^{(2)} \frac{\Delta d}{d_{n2}} \right), \quad i = 1, 2,$$

$$\Delta \varepsilon = \varepsilon_n - \varepsilon_m \ll 1,$$

$$\frac{\Delta d}{d_{n2}} \ll 1, \quad \Delta d = d_{m2} - d_{n2}, \quad d_{j2} = \frac{1}{2}(d_j + d_2).$$

Here  $n_1$  is the number density of absorbing species,  $r$  is the radius of the capillary,  $A$  is the quantity determined by the radiation-gas interaction characteristics,  $d_2$  is the effective diameter of buffer gas particles,  $G_i^{(1)}$  and  $G_i^{(2)}$  are the dimensionless kinetic coefficient, characterizing respectively the surface and buffer mechanisms of LID ( $i = 1$ ) and buffer gas flow ( $i = 2$ ).

The analytic expressions for  $G_i^{(1)}$  and  $G_i^{(2)}$  have been obtained only for large and small values of the Knudsen number. The dependences of  $G_i^{(1)}$  and  $G_i^{(2)}$  on  $Kn$  and on rate parameter  $\Gamma_{mn}$  have been calculated numerically at intermediate Knudsen number. It has been shown that at transition from the free-molecule to the slip-flow regime the values of surface LID decrease monotonically. The dependences of magnitudes of  $G_1^{(2)}$ ,  $G_2^{(1)}$  and  $G_2^{(2)}$  on  $Kn$  have a maximum at  $Kn \sim 1$  and decrease to zero in the slip-flow ( $Kn \rightarrow 0$ ) and in the free-molecule ( $Kn \rightarrow \infty$ ) regimes. The dependences of  $G_i^{(1)}$  and  $G_i^{(2)}$  on  $Kn$  are equidistant at any rate parameter  $\Gamma_{mn}$  values.

It has been shown that the surface and bulk components of LID decrease at fixed  $Kn$  if the rate parameter  $\Gamma_{mn}$  increases.

The kinetic coefficients which characterize the LID depend weakly on molecular mass ratio  $m_1/m_2$ .

\* Abstract 2041 submitted to the 21st International Symposium on Rarefied Gas Dynamics, Marseille, France, July 26-31, 1998

The kinetic coefficients which characterize the buffer gas flow depend strongly on the  $m_1/m_2$  and on effective diameter ratio  $d_n/d_2$ .

The theory is compared with the experiments on the LID of natrium vapour in inert gases [2]. Under experimental conditions, the rate parameter  $\Gamma_{mn}$  increases from  $\sim 0.3$  at high pressures of buffer gas to  $\sim 150$  at low pressures. Besides, the product  $\Gamma_{mn}p$  does not deped on the pressure  $p$ :  $\Gamma_{mn}p \sim 3.1kPa$  at any  $p$ . As a result of comparison of the theory with experiment for the mixture  $Na - He$  it has been obtained:

$$\Delta d/d_{n2} = -4.05 \cdot 10^{-3}, \quad \Delta \varepsilon = -3.07 \cdot 10^{-3}.$$

The same comparison of the theory with the experiments on light-induced drift of natrium vapour in argon and xenon has been conducted. As a result it has been obtained:

for the mixture  $Na - Ar$

$$\Delta d/d_{n2} = -1.36 \cdot 10^{-2}, \quad \Delta \varepsilon = -7.33 \cdot 10^{-2},$$

for the mixture  $Na - Xe$

$$\Delta d/d_{n2} = -1.48 \cdot 10^{-2}, \quad \Delta \varepsilon = -1.79 \cdot 10^{-2}.$$

The sign "—" in numeral meanings of thees parameters is explained by that the flow of natrium vapour is opposite to the radiation direction. The theory describes experimental date over the whole range of pressure satisfactory.

## References

- [1] Chernyak V.G., Vilisova E.A., *Theory of light-induced drift of a binary gas mixture in a capillary*, Zh. Eksp. Teor. Fiz., Vol.107, pp.125-139, 1995.
- [2] Atutov S.N., Ermolaev I.M., Shalagin A.M., *Investigation of the light-induced drift of Na vapour*. Zh. Eksp. Teor. Fiz. Vol.92, pp.1215-1227, 1987.

## Optimal Design of HF Impedance Probes \*

J. de Boer and R. Godard

Department of Physics and Mathematics Royal Military College of Canada

The ambient ionospheric electron density is a basic plasma parameter in Space Physics. The electron density can be obtained from:

1. The electrostatic (Langmuir) probes.
2. A Receiver for Exciter (REX). The electron density is obtained from the detection of the characteristic frequencies of the plasma, the local plasma frequency, the local cyclotron frequency, and the cutoff of the X mode of propagation.
3. The quadripolar probe (mutual impedance probes).
4. The resonance impedance probe.
5. The HF impedance probe (Sayer's probe).

In this study, we present a new 2-D, quasistatic, collisionless fluid model of the HF impedance probe, the numerical simulation of the signal and, an optimal design of the electrodes. This new geometry reduces edge effects for the plasma capacitor. With respect to previous capacitor models which are a 1-D simulation, we include the transparency of the grids in the boundary conditions, we consider the edge effects, and we add the time-averaged repelling force on electrons due to a nonlinear effect of the HF near field. Finally we do parametric studies of the working frequency, of the geometry of the electrodes.

### A. Basic theory for Sayer's probes

The electrodes consist of two discs in the form of transparent grids, approximately 10 cm dia. and spaced 10 cm apart, mounted on a boom emerging from the spacecraft. The electron density probe measures the impedance between the electrodes at a working frequency  $\omega$  of 39 Mhz. If the working frequency is high enough, the permittivity is given by the Appleton-Hartree equation:

$$K = 1 - (\omega_{pe}/\omega)^2, \quad \omega_{pe} = (N_e e^2 / m \epsilon_0)^{1/2} \quad (1)$$

where  $N_e$ ,  $e$ ,  $m$  are the electron density, charge and, mass respectively. The measurement of the capacitance at the plasma potential enables a direct estimation of the average electron density. Because the floating potential of the spacecraft is negative, it is necessary to detect the plasma potential by a DC sweep in potential from -6V to +6V. However, it is important to simulate numerically the variation of the average electron density between the electrodes as a function of the applied DC potential.

### B. The mathematical model

We consider a two-fluid (electrons and ions) model of the plasma. The plasma obeys to continuity and momentum equations for electrons and ions, and the electrostatic potential is described by Poisson's equation. The fluid model was preferred to a kinetic model because of the high transparency of the electrodes. We consider a quasi-steady state model:

\* Abstract 2706 submitted to the 21st International Symposium on Rarefied Gas Dynamics, Marseille, France, July 26-31, 1998

$$\nabla \cdot (N_e V_e) = \nabla \cdot (N_i V_i) = 0$$

(2)

$$N_e m_e (V_e \cdot \nabla) V_e + k_B T_e \nabla N_e + N_e e (E_{dc} + E_{pon}) = 0 \quad (3)$$

$$N_i m_i (V_i \cdot \nabla) V_i + k_B T_i \nabla N_i - N_i e E_{dc} = 0 \quad (4)$$

$$\nabla \cdot E_{dc} = e / \epsilon_0 (N_i - N_e) \quad (5)$$

$$E_{dc} = -\nabla V_{dc} \quad (6)$$

$$V_{pon} = (-e / 4 m_e \omega^2) A^2 \quad (7)$$

where A is the amplitude of HF electric field

### C. The boundary conditions

Our model is based on the following hypotheses:

we assume a full transparency of the electrodes. There is no wall effect.

The boundary conditions for the electric potential are:

$$V_{dc}(z=0) = V_{elec} ; \text{ (at the electrode surface) } \quad (8)$$

$$\partial V_{dc} / \partial z(a) = 0 ; \text{ (Neuman's condition at the plane of symmetry) } \quad (9)$$

The boundary conditions for the electron density are:

$$\text{We assume a periodic capacitor.} \quad (10)$$

$$\partial N_e / \partial z(z=a) = 0 ; \text{ (Neuman's condition at the plane of symmetry) } \quad (11)$$

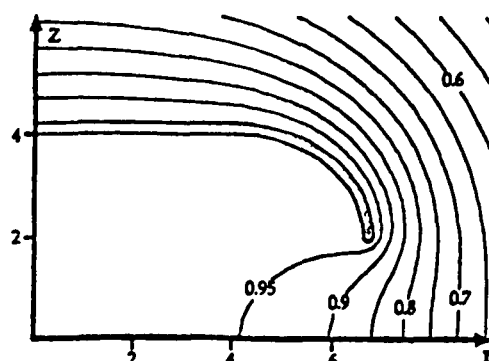
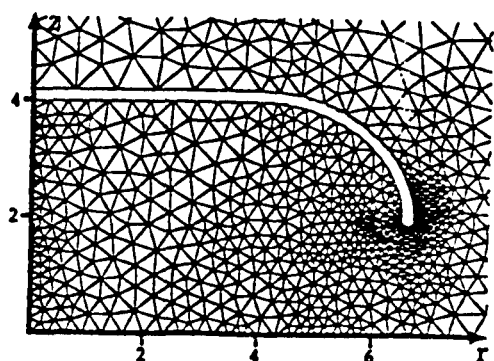
At the outer computational boundary, we have:

$$N_e(P \rightarrow \infty) = N_i(P \rightarrow \infty) = N_\infty ; P \text{ is the current point.} \quad (12)$$

$$V_{dc}(P \rightarrow \infty) = 0 \quad (13)$$

### D. Optimal design of the electrodes

A major problem of the plasma capacitor is edge effects. We present an optimal design of the electrodes. The constraints are a uniform electric field between the two discs. We have found optimal geometries for guard rings around the electrodes, where the electric field is trapped. The next figures represent the finite element computational domain, and one optimal geometry of the plasma capacitor:





# Calculation of Nonequilibrium Radiation in the Low-density Regime with Direct Simulation Monte Carlo (DSMC) \*

Chuanping He, Ching Shen  
Institute of Mechanics, CAS, 100080, Beijing, China

## 1 Introduction

The DSMC (Direct Simulation Monte Carlo) method is widely used to simulate all kinds of complicated phenomena in the flows of low-density regimes. Because of its complexity and importance, nonequilibrium radiation has become an interesting subject and a considerable number of papers have been devoted to it.

In this paper, the Direct Simulation Monte Carlo method, incorporated with a real air model with thermal radiation, is applied to nonequilibrium flows in the transition regimes. Aside from the basic models used by Bird(1), some state-of-the-art models are introduced in dealing with chemical reactions, plasma effects, thermal radiation and absorption process respectively. In the simulation of thermal radiation, a group of collisional excitation numbers suggested by Bird(1) are used, then a method proposed by A.B. Carlson et al.(2) is involved which bases the determination of these numbers on the available rate data for electronic excitation and values of radiative state lifetimes. While dealing with absorption process, both the constant absorption cross section(1) and the method advanced by H.A.Hassan et al.(3) are used. The calculation and the comparisons with the experimental data and numerical results show the advantages and disadvantages of these models.

With the introduction of electrons and ions generated from the related chemical reactions, it is necessary to calculate the corresponding electric field and the movement of the electrons and ions in this self-induced field. It seems natural to obtain the electric field by solving the Poisson equation according to the charge distribution, but Bird mentioned(1), in the DSMC method, the fluctuations in the charge field lead to electric fields far stronger

than the real fields. In the recent works of direct simulation of reentry flows with ionization(e.g.(5)), the concept of ambipolar diffusion is introduced to determine the self-induced electric field and the motion of the charged particles. While it is successful in calculating the electric field, the field is obtained indirectly and not verified by the solution of the Poisson equation. An attempt is made to test the validity of the ambipolar diffusion method of determination of the electric field by applying it to an example case in which the direct solution of the Poisson equation(6) is available.

## References

- [1] G.A.Bird, AIAA paper 87-1543(1987)
- [2] Ann B.Carlson,H.A.Hassan, AIAA paper 91-1409(1991)
- [3] A.K.Berghausen,J.C.Taylor,H.A.Hassan, AIAA paper 95-2051(1995)
- [4] G.A.Bird,,AIAA paper 86-1310(1986)
- [5] J.C.Taylor,Ann B.Carlson,H.A.Hassan, AIAA paper 92-0493(1992)
- [6] R.W.Hockney,J.W.Eastwood, *Computer Simulation Using Particles*

\*Abstract 2848 submitted to the 21st International Symposium on Rarefied Gas Dynamics, Marseille, France, July 26-31, 1998

# Particle Density and Temperature Distribution in Short Pulse Laser-Plasma Interaction \*

V.G. Molinari, M. Sumini

Dipartimento di Ingegneria Energetica, Nucleare e del Controllo Ambientale - DIENCA  
Laboratorio di Ingegneria Nucleare di Montecuccolino, Bologna, Italy

## 1 The physical problem

The object of the work is to predict the electronic density and the self consistent electric field as a function of space and time, generated by a jump in both temperature and density, as happens for instance in laser-plasma interaction.

The model problem is represented by two semi-infinite media kept at two different temperatures  $T_{00}$  and  $T_{01}$ , with  $T_{01} > T_{00}$ , and two different densities,  $N_{00}$  and  $N_{01}$ , with  $N_{01} > N_{00}$ , that are suddenly generated at time  $t = 0$ .

The problem is approached starting from the Boltzmann-Vlasov equation [1], [2], written in its integral form to treat explicitly and more easily the above discontinuity:

$$\begin{aligned} f(\mathbf{r}, \mathbf{v}, t) = & f(\mathbf{R}_0, \mathbf{V}_0, t=0) \exp \left[ - \int_0^t v du' \right] + \\ & + \int_0^t du \left\{ \exp \left[ - \int_u^t v du' \right] \times \right. \\ & \times \int_{\mathbb{R}_3} K[\mathbf{R}(u), \mathbf{v}' \rightarrow \mathbf{V}(u)] \times \\ & \times f(\mathbf{R}(u), \mathbf{v}', u) d\mathbf{v}' \left. \right\}, \end{aligned} \quad (1)$$

where  $\mathbf{R}(u)$  and  $\mathbf{V}(u)$  are the solution of the motion equations:

$$\frac{\partial \mathbf{R}(u)}{\partial u} = \mathbf{V}(u), \quad (2)$$

$$\frac{\partial \mathbf{V}(u)}{\partial u} = -\frac{e}{m_e} \mathbf{E}(\mathbf{R}(u), u), \quad (3)$$

with the conditions  $\mathbf{R}(u=t) = \mathbf{r}$  and  $\mathbf{V}(u=t) = \mathbf{v}$ , respectively.

The electron density for the collisionless case can be approximated as:

$$n^{(0)}(x, t) = \int_{\mathbb{R}_3} f^{(0)}(x, \mathbf{v}', t) d\mathbf{v} =$$

$$\begin{aligned} = & \frac{1}{2} \exp[-\nu t] \times [N_{01} + N_{00} - \\ & - N_{01} \operatorname{erf} \left( \sqrt{\frac{m_e}{2T_{01}}} V_{x1}(x, t; E(x, t)) \right) + \\ & + N_{00} \operatorname{erf} \left( \sqrt{\frac{m_e}{2T_{00}}} V_{x1}(x, t; E(x, t)) \right) ], \end{aligned} \quad (4)$$

where  $V_{x1}(x, t; E(x, t))$  is the initial velocity along the  $x$  axis of a particle in  $\mathbf{X}(u=0) = 0$  at time  $t = 0$  and  $E(x, t)$  the self-consistent electric field. The limit initial velocity, calculated from the motion equations, is found to be:

$$V_{x1}(x, t; E(x, t)) = \frac{x}{t} + \frac{e}{m_e t} \int_0^t du \int_0^u E(x, u') du'. \quad (5)$$

The self-consistent electric field can be obtained from the Gauss equation for the density  $n^{(0)}$ . Obviously the problem is non-linear, insofar as  $n^{(0)}$  depends from  $E(x, t)$  through  $V_{x1}(x, t; E(x, t))$  and an iterative (but rapidly converging) procedure must be defined [3]. Moreover, with a little effort is possible to enhance the picture evaluating the first order collision density. We also point out that, at least for the zero collision term, an approximated analytical expression for the density (Vlasov equation solution) can be obtained and, consequently, the velocity of the shock wave can be studied.

## 2 Conclusions

From the density (up to the first order in collisions) and the electric field, the distribution function can be written, and from this latter the particle current and the heat flow.

## References

- [1] Molinari V. G., Peerani P., *Electron Oscillations in a Plasma: Effect of Collisions on Lan-*

\*Abstract 4136 submitted to the 21st International Symposium on Rarefied Gas Dynamics, Marseille, France, July 26-31, 1998

*dau Damping* Il Nuovo Cimento 5D, pp 527-538, 1985.

- [2] Molinari V. G. , Sumini M., Ganapol B. D., *Electron oscillations, Landau and collisional damping in a partially ionized plasma*, 16th Int. Symp. Rarefied Gas Dynamics, Pasadena, 1988, Progress in Astronautic and Aeronautics, A.I.A.A., vol. 116, 102 1989
- [3] Molinari V.G., Mostacci D., Sumini M., *Particle Density and Temperature Distribution in the Early Stage of Laser-Plasma Interaction*, 1995 APS Topical Conf. on Shock Compression and Condensed Matter, AIP Press, Schmidt S. C., Tao W. C., ed.s, pp 1251-1254, 1996.

# Charge Distribution Function of Laboratory Plasma Dust Particles \*

B.F. Gordiets<sup>†</sup>, C. M. Ferreira

Centro de Física de Plasmas, Instituto Superior Tecnico, Lisboa, Portugal

<sup>†</sup> - On leave from Lebedev Physical Institute of the Russian Acad. of Sciences, Moscow

## 1 Introduction

It is known that plasma dust particles usually acquire negative charge [1-4]. A classic approximation for electron and ion fluxes on spherical grain with radius  $R$  and potential  $\varphi$  is usually used to calculate the average particle charge  $\langle Z \rangle$  [1,2]. However, this approximation can have a poor accuracy in the case of small particles with  $\langle Z \rangle \sim 1$  and does not allow to calculate the charge distribution function (CDF), which is necessary for the investigation of particle coagulation [2]. A discrete CDF has been obtained for grains in the interstellar clouds in [3], where a Maxwellian energy distribution for electrons was used and secondary electron emission from grains was not taken into account.

The aim of the present work is to obtain the analytical discrete CDF of dust particles for non Maxwellian electron energy distribution function (EEDF) which exists in the laboratory plasma, and to take into consideration the process of secondary electron emission and dependence on particle radius of the absorption coefficient  $\alpha$  for the interaction of electron with grain.

## 2 Equations and probabilities

The CDF can be obtained from the balance master equations for densities  $N_0$  and  $N_Z$  of neutral and charged monodispersed (with radius  $R$ ) dust particles with  $Z$  discrete elementary negative charges:

$$\begin{aligned} \frac{dN_0}{dt} &\approx (Q_0 N_0 - L_1 N_1) \quad \text{for } Z = 0; \\ \frac{dN_Z}{dt} &\approx (Q_{Z-1} N_{Z-1} - L_Z N_Z) - \\ &-(Q_Z N_Z - L_{Z+1} N_{Z+1}) \quad \text{for } Z \geq 1. \end{aligned} \quad (1)$$

\*Abstract 4785 submitted to the 21st International Symposium on Rarefied Gas Dynamics, Marseille, France, July 26-31, 1998

The probabilities  $Q_Z$  and  $L_Z$  (in  $\text{sec}^{-1}$ ) describe the change of density due to acquisition or loss of unit elementary negative charge. The increase of charge for negative charged grains is due to the process of electron attachment, and the losses are due to electron detachment (secondary electron emission) and ion recombination. The probabilities  $Q_Z^{\text{att}}$ ,  $L_Z^{\text{rec}}$  were derived in this work and are given by:

$$Q_Z^{\text{att}} \approx \alpha \bar{v}_e \pi R^2 N_e \exp \left\{ - \left( \frac{r_e a_0}{R b_m} Z \right)^m \right\} \frac{a_e}{c_m} \quad (2)$$

$$L_Z^{\text{rec}} \approx \beta \bar{v}_i \pi R^2 N_i \left( 1 + \frac{r_i}{R} Z \right) a_i, \quad (3)$$

where  $N_e$ ,  $\bar{v}_e$ ,  $N_i$ ,  $\bar{v}_i$  are the electron and ion densities and average velocities respectively;  $r_e = \frac{e^2}{4\pi\epsilon_0 k T_e}$ ;  $r_i = \frac{e^2}{4\pi\epsilon_0 k T_i}$  ( $e$  is the electron charge,  $\epsilon_0$  is the vacuum permittivity);  $b_m = \frac{3}{2} \Gamma(\frac{3}{2m}) / \Gamma(\frac{5}{2m})$ ;  $c_m \approx 1$  for  $y \equiv \Gamma(\frac{2}{m}) \times \left[ \frac{r_e a_0}{R b_m} Z \right]^{2-m} \leq 1$  and any  $Z$ , and  $c_m \approx y$  for  $y > 1$  and  $Z > 0$ ;  $\Gamma$  is the Gamma function. The parameters  $a_0$ ,  $a_e$ ,  $a_i$  describe the influence of polarization interaction of grain with plasma electron or ion. Without such interaction  $a_0 = a_e = a_i = 1$ .

The arbitrary EEDF  $f_e(\epsilon) \sim \exp\{-\epsilon^m/B\}$  ( $\epsilon$  is electron energy) and a Maxwellian distribution for the ions (with "temperatures"  $T_e$  and  $T_i$  respectively) are used to obtain (2), (3).

The multipliers  $\alpha$  and  $\beta$  in (2), (3) are the parts of electron and ion fluxes on grain, which are really absorbed by particle. We have assumed  $\beta \approx 1$  and used for  $\alpha$  the simple dependence

$$\alpha \approx [1 - \exp(-R/L)], \quad (4)$$

where  $L(T_e)$  is the characteristic length for absorption of electrons by grain. To obtain (4) the one dimensional model for the transmission of the electrons through the thin plate have been used assuming small electron energy losses over the length  $L$ . The value of  $L$  is determined by the molecular density in grain and the cross sections for electron scattering and attachment.

The probability  $L_Z^{det}$  for loss of charge due to detachment (secondary electron emission) is:

$$L_Z^{det} \approx Q_Z^{att} g_{ion} \exp \left\{ - \left( \frac{E^{det}}{b_m k T_e} \right)^m \right\}, \quad (5)$$

where  $E^{det} = E^{ion} + E^{des}$ ;  $g_{ion} = \delta_{ion}(1 - \alpha)/\alpha$  and

$$\delta_{ion} \approx [L/(2L_{ion}) + R/L_{ion} \exp(-R/L)] \quad (6)$$

$L_{ion}(T_e)$  is the characteristic length for ionization of molecules in grain by electron,  $E^{ion}$  is the energy threshold for this ionization and  $E^{des}$  is the activation energy for desorption of electrons from the grain surface. For macroscopic particles the value  $E^{ion} + E^{des}$  is a work function. The same assumption as for (4) have been used to obtain (6).

### 3 Charge Distribution Function and some calculation results

The CDF can be obtained from (1). For quasi stationary conditions

$$N_Z = N_0 \prod_{z'=1}^Z \frac{Q_{Z'-1}^{-att}}{L_{Z'}^{-rec} + L_{Z'}^{-det}}; \quad Z \geq 1 \quad (7)$$

The neutral particle density  $N_0$  can be obtained from the condition  $N_\Sigma = N_0 + \sum_{Z \geq 1} N_Z$ , where  $N_\Sigma$  is the total density of particles with radius  $R$ . An example of CDFs is presented on Fig. 1 for typical plasma conditions. The CDFs are calculated using Maxwellian ( $m = 1$ ) and Druvesteyn ( $m = 2$ ) EEDF. We can see from Fig. 1 that the value of the adsorption coefficient  $\alpha$  and EEDF can strongly influence the CDF.

To investigate particle coagulation it is necessary to know the relative concentration  $f_0$  of neutral grains, which is presented on Fig. 2 as a function of particle radius  $R$  for typical plasma and particle parameters. The calculated particle average charge  $\langle Z \rangle$  is also given on Fig. 2. This figure also shows the strong influence of both the EEDF and the characteristic length  $L$ .

#### Acknowledgments

This work have been supported by a contract with the Portuguese Ministry of Science and Technology under the Program PRAXIS XXI, partly funded by the EU Program FEDER.

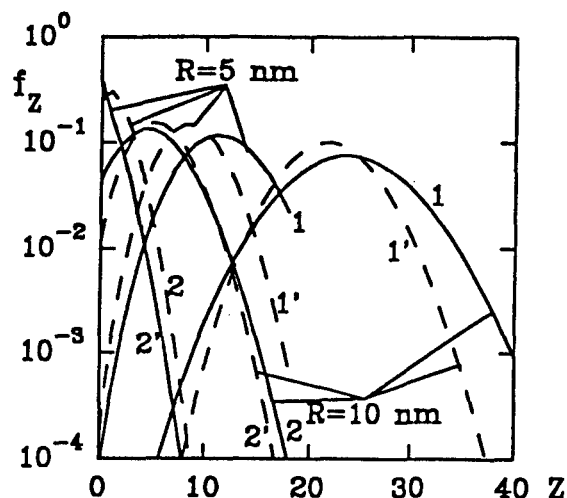


Fig.1 The normalized charge distribution function  $f_Z$  for dust particles of different radius  $R$  calculated with Druvesteyn (full lines) and Maxwellian (broken lines) EEDF. The calculations are carried out with parameters  $N_e/N_i = 5 \times 10^{-2}$ ;  $T_e = 6$  eV;  $T_i = 500$  K;  $E^{det} = 5$  eV;  $L_{ion} = 10 \times L$  and for  $L = 5 \times 10^{-7}$  cm (1,1') and  $5 \times 10^{-6}$  cm (2,2').

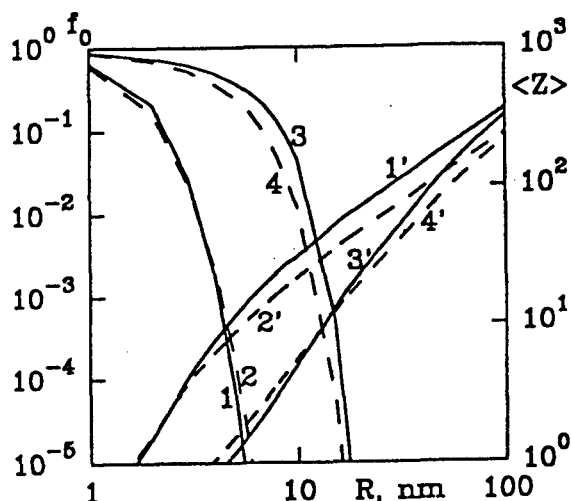


Fig.2 The relative concentration  $f_0$  of neutral dust particles (1-4) and their average negative charge  $\langle Z \rangle$  (1'-4') as a function of particle radius  $R$ , calculated with Druvesteyn (full lines) and Maxwellian (broken lines) EEDF and for  $L = 5 \times 10^{-7}$  cm (1,2,1',2') and  $5 \times 10^{-6}$  cm (3,4,3',4'). The calculation conditions are the same as in the caption to Fig.1.

### 4 References

- [1] J.P. Boeuf - Phys. Rev. A., 1992, 46, 7910.
- [2] C. Courteille, Ch. Hollenstein, J.-L. Drier, P. Gay, W. Schwarzenbach, et al - J. Appl. Phys., 1996, 80, 2069.
- [3] B.T. Draine and B. Sutin - Astrphys. J., 1987, 320, 803.

# Numerical Modeling of Nonequilibrium Ionization and Radiation Behind Shock Wave in Martian Atmosphere \*

A.Yu.Kireev<sup>1</sup>, S.V.Shilenkov<sup>2</sup>

<sup>1</sup>Central Aerohydrodynamic Institute, Zhukovsky-3, Moscow Region, Russia

<sup>2</sup>Moscow Institute of Physics and Technology, Moscow, Russia

The goal of this investigation is the elaboration of numerical model to estimate nonequilibrium ionization parameters and radiation intensity during vehicle's entry into Martian atmosphere. Martian gas mixture in shock layer was simulated by species: CO<sub>2</sub>, CO, N<sub>2</sub>, CN, C<sub>2</sub>, O<sub>2</sub>, O, N, NO, NCO, C, C<sup>+</sup>, O<sup>+</sup>, N<sup>+</sup>, N<sub>2</sub><sup>+</sup>, CO<sup>+</sup>, O<sub>2</sub><sup>+</sup> and e.

Under conditions of a vehicle's entry into Martian atmosphere physical-chemical processes in the shock layer are of nonequilibrium nature, that is, the relaxation of the inner degrees of freedom of the mixture species occurs in times comparable with gasdynamical processes. Of a nonequilibrium character are: vibrational relaxation of CO<sub>2</sub>, CO, N<sub>2</sub>, CN, C<sub>2</sub>, O<sub>2</sub>, NO molecules; dissociation and exchange reactions; ionization and the processes of charge exchange. The electron temperature  $T_e$  differs, in general case, from the translational  $T$  and vibrational temperatures of the molecules and is defined from the equation of the electron-gas energy balance. It is assumed that molecule rotational degrees of freedom are assumed in an equilibrium state with the translational ones.

Carbon dioxide constitutes the main mass fraction (97%) vibrational degrees of freedom of a CO<sub>2</sub> and diatomic molecules CO, N<sub>2</sub>, CN, C<sub>2</sub>, O<sub>2</sub> are highly energy-intensive, its impact on the gas thermodynamics of nonequilibrium flow is great. For describing the time of VT-relaxation for molecules, two approaches were used: computation of the relaxation time from Millican-White formula [1] and computation of the relaxation time by the formulae allocated by the data base of the AVOGADRO [2]. CO<sub>2</sub> vibration relaxation is described by Camac's model [3]. Non-physical description of the vibrational relaxation at high temperatures with using the above formulae was adjusted by introducing Park's correction [4].

The computational model makes use of data on dis-

sociation and exchange reactions, recommended by [2]. The vibrational-dissociative coupling and its impact on the characteristics of flow in the shock layer are taken into consideration with using three models: Park's model, CVDV model and model recommended by the AVOGADRO [2]. The computational model includes a number of ionization reactions and processes of charge exchange between neutral and positively charged components of the mixture. Electrons and ions appear behind the wave front in the course of the associative ionization.

The processes involving the electrons are defined by the reactions rate constants, which depends on the temperature of electrons  $T_e$ . The temperature of free electrons  $T_e$  is derived from the master equation for electron-gas energy balance. The electrons gain (lost) their energy during the reactions of the associative ionization, elastic collisions with heavy mixture species and nonelastic collisions with exciting rotational, vibrational and metastable electronic states of molecules, dissociation and ionization of molecules with electron impact, excitation of lower electronic states of atoms N, C, O by electron impact.

Several molecular band system emission is studied numerically. Diatomic molecules CO, NO and CN emission is considered, namely: CO(4+), NO( $\gamma$ ), CN(violet), CN(red). To estimate radiation intensity in these molecular band systems, the step-by-step model of electronic-vibrational molecular states excitation is elaborated. This model includes the following processes: direct and step-by-step excitation of the states by heavy particles and electrons; resonant energy exchange reactions; radiative population and destruction of the states; dissociation of the excited states and their formation in recombination reactions.

The results of test computations, can be divided into two groups. The first group includes the data obtained when selecting kinetical model and data base of kinetics, which defines the vibrational relax-

\* Abstract 4926 submitted to the 21st International Symposium on Rarefied Gas Dynamics, Marseille, France, July 26-31, 1998

ation and rate constants of reactions. This stage, the calculations of ionization and radiation parameters are compared with measured ones, carried out in Arc-Driven Shock Tube (ADST) [5], to correct numerical model and estimatively known reactions rate constants. Using this approach, the numerical and kinetical model of ionization and emission, verified by measured data, is elaborated for shock wave propagation in  $\text{CO}_2\text{-N}_2$  mixture at velocity range  $V_S = 4\text{-}9$  km/s.

The second group includes the results proper for nonequilibrium flow parameters calculations behind the wave in Martian atmosphere. This group also includes the influence of the choice some or other kinetical model on the parameters of the flow in the region of relaxation. For example, in the zone behind the shock wave the choice of the vibrational-dissociative coupling (VDC) model can strongly influence the gas temperature and molecule vibrational degrees of freedom. A similar effect has a choice of the VDC model on the profiles of the distribution of some mixture species concentrations, such as CO, for example.

This work has been supported by International Science and Technology Center (ISTC) through Project N036.

## References

- [1] Milliken R.C., White D.R. *Systematics of Vibrational Relaxation*, J. of Chem. Phys., No.12, 1963.
- [2] Losev S.A. et al., *Thermochemical Nonequilibrium Kinetics Models in Strong Shock Waves in Air*, AIAA Paper 94-1990, 1994.
- [3] Camac M., *CO<sub>2</sub> Relaxation Processes in Shock Waves*, in *Fundamental Phenomena in Hypersonic Flow*, ed. by Hall J.G., Cornell Univ. Press, Ithaca, NY, 1966.
- [4] Park C., Howe I.T., Jaffe R.L. and Candler G.V., *Review of Chemical-Kinetic Problems of Future NASA Missions, II- Mars Entries*, J. of Thermophysics and Heat Transfer, Vol.8, No. 1, Jan.-March 1994.
- [5] Gorelov V.A., Gladyshev M.K., Kireev A.Y., Yegorov I.V., Plastinin Y.A. and Karabadzha G.F., *Nonequilibrium Shock Layer Radiation in the Systems of Molecular Bands NO and N<sub>2</sub><sup>+</sup>(1-): Experimental Study and Numerical Simulation*, AIAA Paper 96-1900, June 1996.

# Density Distribution behind a Planar Shock Wave Propagating through a Discharge Plasma \*

F.V. Shugaev, G.I. Singayevskaya  
Moscow State University, Department of Physics, Moscow, Russia

Shock wave structure in a low-temperature weakly ionized plasma of a transverse rf discharge has been investigated both theoretically and experimentally. Experiments have been carried out in a single-diaphragm shock tube of rectangular cross-section of  $40 \times 60 \text{ mm}^2$  area. The test section has optical windows of 60 mm diameter. Two metal plates were mounted on the upper and lower walls of the test section. A transverse rf discharge was generated between the plates ( $f = 13.6 \text{ MHz}$ ). The density of the current was equal to  $40 \text{ mA/cm}^2$  while the length of the discharge zone was 80 mm. Ar,  $\text{CO}_2$ ,  $\text{N}_2$  were used as the test gases. The initial pressure was 5–10 Torr. The Mach numbers were equal to 2–4. The density behind the shock was measured by a laser-schlieren technique (Kiefer et al. 1980, [2]). We used a He-Ne laser with a beam diameter of 1 mm. The shock velocity was measured with pressure transducers beyond the discharge zone and from schlieren signals within the discharge zone. The initial density was measured with the aid of a Fabry-Perot interferometer. The initial translational temperature was equal to 1100 K. The degree of ionization temperature was  $10^{-7}$  ahead of the shock wave.

The value of the schlieren signal  $V$  is as follows (Ivanov et al. 1997 [1])

$$\begin{aligned} V(x) = & \frac{2kk_{GD}l}{\sqrt{\pi}} \frac{\sqrt{(a+b)^2+p^2}}{a^2+p^2} \\ & \times \frac{dV}{d\eta} \int_{-\infty}^{+\infty} \Delta\rho(s)L(x-s)ds \\ L(t) = & \text{Im}\{\exp(-t^2)(A+A^*) \\ & \times \text{cerf}(-tv_s(A_1^*-B_1)/A_1^*B_1)\}, \\ x = & v_s t, \quad A = -ik/(2(a-ip)), \\ B = & -ik/2b, \quad A_1 = 1/A, \\ B_1 = & 1/B, \quad p = kw_0^2, \quad k = 2\pi/\lambda, \end{aligned} \quad (1)$$

where  $a$  is the distance between the laser and the test section,  $b$  is the distance between the test section and the detector,  $k_{GD}$  is the Gladstone-Dale

coefficient,  $l$  is the width of the test section,  $dV/d\eta$  is the calibration constant,  $\eta$  is the displacement of the detector,  $w_0$  is the diameter of the beam,  $\rho$  is the density,  $\text{cerf}$  is the error function of a complex argument, asterisk means complex conjugate. Eq. (1) was solved numerically by the method proposed by Tikhonov.

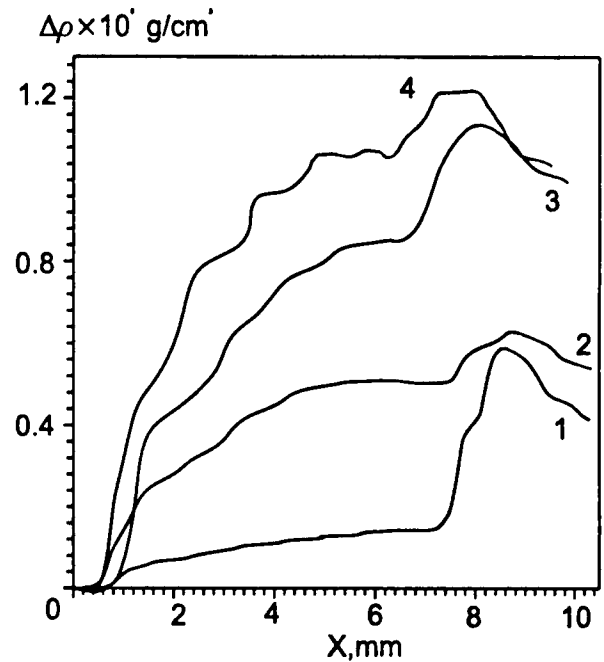


Figure 1: Density distribution in the neighbourhood of the shock front (Ar). 1 —  $M = 2.42$ ; 2 —  $M = 3$ ; 3 —  $M = 3.25$ ; 4 —  $M = 3.4$ .

Fig. 1 shows the density distribution in the neighbourhood of the shock front in a low-temperature weakly ionized plasma (Ar as the test gas). One can see that the shock front displays a two-step structure. The shock thickness is greater in plasma than in gas. The measured values of density behind the shock wave agree well with the calculated ones. The measured values of density behind the shock wave in molecular gases ( $\text{CO}_2$ ,  $\text{N}_2$ ) are two times less than the calculated ones (without taking into account the

\* Abstract 5196 submitted to the 21st International Symposium on Rarefied Gas Dynamics, Marseille, France, July 26–31, 1998



energy release behind the shock front). It is due to the fact that the vibrational temperature is higher than the translational one ahead of the shock wave. An additional energy release takes place behind the shock wave.

We numerically analyzed the propagation of a shock wave through a weakly ionized plasma. The flow was assumed to be one-dimensional and unsteady. The problem is as follows. The shock wave which primarily propagates through a gas meets with the surface of discontinuity which separates the gas and the weakly ionized plasma. The plasma is a mixture of atoms, electrons and ions. There is an energy release behind the shock wave due to electric current. The equations of continuity, of momentum and of energy for  $j$ -species are as follows (Jaffrin, 1965, [3])

$$\begin{aligned} \frac{\partial \rho_j}{\partial t} + \frac{\partial \rho_j v_j}{\partial x} &= S_j, \\ \frac{\partial(\rho_j v_j)}{\partial t} + \frac{\partial}{\partial x}(\rho_j v_j^2) &= \frac{4}{3} \frac{\partial}{\partial x} \left( \mu_j \frac{\partial V_j}{\partial x} \right) + \rho_j e E + P_{ja} + P_{je}, \\ \frac{\partial}{\partial t} \left( \rho_j \left( e_j + \frac{v_j^2}{2} \right) \right) + \frac{\partial}{\partial x} (v_j (\rho_j (e_j + v_j^2/2) + p_j)) &= \frac{2}{3} \frac{\partial}{\partial x} \left( k_j \frac{\partial e_j}{\partial x} \right) + \frac{4}{3} \frac{\partial}{\partial x} \left( \mu_i V_i \frac{\partial V_i}{\partial x} \right) + w_{ji} + w_{je}, \end{aligned}$$

where  $S_j$  is the net source of particles for  $j$ -species. The quantities  $P_{ja}$  and  $P_{je}$  characterize the momentum scattering. The quantities  $w_{ji}$  and  $w_{je}$  give the energy loss due to inelastic collisions. Subscripts  $e, i$  relate to electrons and ions, respectively. The longitudinal electric field depends on the distribution of the charge through Poisson's equation for the potential. The numerical results are in good accordance with the experimental ones.

## References

- [1] Ivanov V.I., Singayevskaya G.I., Fomenko E.N., Shugaev F.V., *Density reconstruction in the neighbourhood of a plane shock wave from the shape of schlieren signal*, Moscow University Bull. Vol. 3, 30, 1997.
- [2] Kiefer J.N., Hayduk J.C., *Rate measurements in shock waves with the laser-schlieren technique*, In: Lifshitz A., Rom J. (eds) Proc. 12th Intl. Symp. on Shock Tubes and Waves, Magnes Press, Jerusalem, pp. 97-110, 1980.
- [3] Jaffrin N.Y., *Shock structure in a partially ionized gas*, Phys. Fl. 8: 606, 1965.

# Electrical Current Density in a Dilute Gas under Shear Flow \*

C. Marín<sup>1</sup>, V. Garzó<sup>2</sup>

<sup>1</sup> Departamento de Matemáticas, Universidad de Extremadura, Badajoz, Spain

<sup>2</sup> Departamento de Física, Universidad de Extremadura, Badajoz, Spain

## 1 Introduction

A problem of practical and physical interest is the analysis of transport properties of charged test particles immersed in a rarefied gas of neutral particles and subjected to a constant electric field  $\mathbf{E}$ . The system can be seen as a dilute binary mixture in which the concentration of the charged particles (labeled with the index 1) is much smaller than that of the neutral gas (labeled with the index 2). This implies that one can neglect the effect of collisions among the charged particles themselves on the state of the charged species. In addition, the state of the neutral gas is not disturbed by the presence of the charged particles. In these conditions (*tracer limit*), the interactions of type charged-neutral and neutral-neutral are the dominant ones in the mixture. This assumption simplifies enormously the problem since the Coulomb interaction does not need to be considered in our description.

When the neutral gas is at equilibrium and the external field is weak, the electrical current density  $\mathbf{j}_1$  obeys the Ohm law  $\mathbf{j}_1 = \sigma_0 \mathbf{E}$ , where  $\sigma_0$  is the electrical conductivity coefficient whose expression can be obtained, for instance, from the Chapman-Enskog method [1]. This situation has been studied in the past few years in different contexts [2]. Nevertheless, much less is known when the rarefied neutral gas is far from equilibrium. This is due basically to the scarcity of exact solutions to the Boltzmann equation in inhomogeneous situations. One of the few exact solutions of the Boltzmann equation corresponds to the so-called uniform shear flow, namely, a state macroscopically characterized by a linear velocity field and uniform temperature and density. In the case of Maxwell molecules (repulsive potential of the form  $\kappa_{rs} r^{-4}$ ), almost forty years ago Ikenberry and Truesdell [3] derived explicit expressions for the rheological properties of the gas (non-newtonian shear viscosity and viscometric effects) as functions of the (arbitrary) shear

rate. Here, our aim is to get the current density induced by the action of a weak electric field when the background neutral gas is under uniform shear flow.

## 2 Description of the problem

Let us consider a binary mixture in the low-density regime. According to the assumptions established in the tracer limit, the kinetic equations describing the mixture reduce to a (closed) Boltzmann equation for the velocity distribution function of neutral particles  $f_2(\mathbf{r}, \mathbf{v}; t)$  and a Boltzmann-Lorentz equation for the velocity distribution function  $f_1(\mathbf{r}, \mathbf{v}; t)$  of the charged species. We also assume that the neutral gas is under uniform shear flow (USF) so that the number density  $n_2$  and the partial temperature  $T_2$  are uniform and the only nonzero gradient is  $\partial u_{2,x}/\partial y = a \equiv \text{const.}$ ,  $\mathbf{u}_2$  being the flow velocity of species 2. In order to maintain a steady state an external force of the form  $\mathbf{F}_s = -m_s \alpha \mathbf{V}$  must be applied to particles of each species. Here,  $m_s$  is the mass of a particle of species  $s$ ,  $\mathbf{V}_i = \mathbf{v}_i - a_{ij} \mathbf{r}_j$  is the peculiar velocity,  $a_{ij} = a \delta_{ix} \delta_{jy}$ , and  $\alpha$  (which plays the role of a thermostat parameter) is a nonlinear function of the shear rate. In the steady shear flow state, the velocity distribution function becomes homogeneous under the change of variable  $\mathbf{v} \rightarrow \mathbf{V}$ , i.e.,  $f_s(\mathbf{r}, \mathbf{v}) \rightarrow f_s(\mathbf{V})$ . Recently this problem has been exactly solved for the particular case of Maxwell molecules [4].

Since the state of the neutral gas is well characterized, our purpose now is to solve the Boltzmann-Lorentz equation corresponding to the charged species. According to the geometry of the shear flow state and in the steady state, the kinetic equation of  $f_1(\mathbf{V})$  becomes

$$-\frac{\partial}{\partial V_i} (a_{ij} V_j + \alpha V_i) f_1 + \frac{q\mathbf{E}}{m_1} \cdot \frac{\partial}{\partial \mathbf{V}} f_1 = J_{12}[f_1, f_2], \quad (1)$$

where  $q$  is the charge, and  $J_{12}$  is the Boltzmann collision operator. We are interested in analyzing the influence of the shear flow on the electrical current

\*Abstract 5341 submitted to the 21st International Symposium on Rarefied Gas Dynamics, Marseille, France, July 26-31, 1998

density. To this end, we shall solve Eq. (1) by means of a perturbative expansion in powers of the electric field. The main feature of the expansion is that the zeroth-order approximation (reference state) is a nonequilibrium state (USF) with an arbitrarily large velocity gradient. As a consequence, the corresponding transport coefficients will be nonlinear functions of the shear rate and the parameters of the system (mass and force constant ratios). Thus, we look for solutions of the form  $f_1 = f_1^{(0)} + f_1^{(1)} + \dots$ , where  $f_1^{(k)}$  is of order  $k$  in  $\mathbf{E}$  but retains all the nonlinear dependence on  $a$ . Here, we will restrict ourselves to the first order in the external field.

### 3 Electrical conductivity

In the first order of the expansion, one gets the kinetic equation

$$-\frac{\partial}{\partial V_i} (a_{ij} V_j + \alpha V_i) f_1^{(1)} + \frac{q\mathbf{E}}{m_1} \cdot \frac{\partial}{\partial \mathbf{V}} f_1^{(0)} = J_{12}[f_1^{(1)}, f_2]. \quad (2)$$

We are interested in evaluating the electrical current density  $\mathbf{j}_1^{(1)}$ . At this order it is defined as

$$\mathbf{j}_1^{(1)} = q \int d\mathbf{v} \mathbf{V} f_1^{(1)}. \quad (3)$$

The current density can be obtained from the Boltzmann-Lorentz equation (2) after multiplying it by  $q\mathbf{V}$  and integrating over the velocity space. Thus, one finds that

$$a_{ik} j_{1,k}^{(1)} + \alpha j_{1,i}^{(1)} - \frac{n_1 q^2}{m_1} E_i = -\frac{\lambda_{12} n_2}{m_1} j_{1,i}^{(1)}, \quad (4)$$

where  $\lambda_{12} = 1.69\pi(\kappa_{12} m_1 m_2 / (m_1 + m_2))^{1/2}$ . The solution to Eq. (4) can be recast into the form of a generalized Ohm law, i.e.,  $j_{1,i} = \sigma_{ij} E_j$ , with the electrical conductivity tensor given by

$$\sigma_{ij} = \frac{n_1 q^2}{m_1} \frac{1}{\alpha + \tau} \left( \delta_{ij} - \frac{a_{ij}}{\alpha + \tau} \right), \quad (5)$$

where  $\tau \equiv \lambda_{12} n_2 / m_1$ . When  $a = 0$ ,  $\sigma_{ij} = \sigma_0 \delta_{ij}$ ,  $\sigma_0 = n_1 q^2 / m_1 \tau$ , and one recovers the usual Ohm law. Furthermore, according to Eq. (5), the only nonzero elements of  $\sigma_{ij}$  are  $\sigma_{ii} = \sigma_0 \tau / (\alpha + \tau)$  and  $\sigma_{xy} = -\sigma_0 a \tau / (\tau + \alpha)^2$ . In general, the diagonal elements decrease as the shear rate increases so that the presence of shear flow inhibits the diffusion of charge particles. The off-diagonal element measures cross effects induced by the shear flow in the current density. The dependence of  $\sigma_{ii}$  and  $\sigma_{xy}$  with the shear rate will be illustrated for several values of the parameters of the mixture.

In summary, in this paper we investigate the influence of shear flow on the current density induced by the action of a weak electric field. We consider a dilute binary mixture of Maxwell molecules with a tracer concentration of the charged particles. The system is in a steady uniform shear flow state with an arbitrarily large velocity gradient. Under these conditions, the current density is a linear function of the electric field although a shear-rate dependent electrical conductivity tensor rather than a scalar can be defined. This tensor happens to be a nonlinear function of the shear rate and the parameters of the system, namely, the mass ratio and the force constant ratio.

### References

- [1] S. Chapman and T.G. Cowling, *The Mathematical Theory of Nonuniform Gases* (Cambridge University Press, Cambridge, 1970).
- [2] L. C. Woods, *An Introduction to the Kinetic Theory of Gases and Magnetoplasmas* (Oxford University Press, Oxford, 1993).
- [3] E. Ikenberry and C. Truesdell, *J. Rat. Mech. Anal.* **5**, 55 (1956).
- [4] C. Marín, V. Garzó and A. Santos, *Phys. Rev. E* **52**, 3812 (1995).

# Modeling the Coupling between Ion Recombination and Turbulence in an Argon Plasma using Probability Density Function Approach. \*

T. Benazzouz, P. Domingo  
LMFN, CORIA, Université de Rouen, France

Most studies related to turbulence in plasma neglect the coupling between chemistry and turbulence. In these approaches, the mean chemical source terms in the averaged conservation equations for species are assumed to be functions of the averaged temperatures and species densities which is probably a too restrictive hypothesis (see for instance Chang and Ranshaw [1]).

In this study, an approach of the modeling of the coupling between chemistry and turbulence in a plasma based on the probability density models is proposed. Argon has been retained. Indeed, the properties of this gas are well-known and the ionization and recombining process can be described by a single reaction ( $Ar + e^- \leftrightarrow Ar^+ + 2e^-$ ).

When evaluating chemical source terms in a turbulent plasma, one must account for fluctuations of chemical species and temperatures. In addition, the physical situation is complicated by the need of including thermal non-equilibrium effects together with their coupling with turbulence. In term of modeling, a parallel can be drawn between this problem and turbulent combustion where the one-point probability density function (pdf) approach has proved to be an effective tool. Using pdf, source terms defined in one-point can be dealt within a closed and exact form [2, 3, 4]. Nevertheless, all terms involving two-points information (fluxes) need to be modeled (diffusion of species, thermal conduction, ...). Therefore with pdfs, the effects of fluctuations on chemical source terms are directly included, whereas turbulent micro-mixing (small scale diffusion) mechanisms needs a closure. A previous study based on direct numerical simulation (DNS) [5] has proposed a closure for micro-mixing based on the linear relaxation model of Dopazo and O'Brien [4]. In the case of a recombining argon plasma, comparison between pdf

modeling and DNS has been found to be satisfactory (situation of homogeneous freely decaying turbulence).

Our purpose here is to apply this approach to the modeling of an high velocity turbulent argon plasma jet. The Favre averaged Navier-Stokes equations closed with a  $k-\epsilon$  model are solved coupled with the resolution of the joined pdf for heavy translational temperature, electron temperature and ion density. Monte-Carlo simulation is used for the resolution of the pdf transport equation.

The study is performed in close conjunction with an experiment studied by Leborgne et al [6]. Validation and discussion of the results obtained in this situation will be presented.

## References

- [1] C. H. Chang, J. D. Ramshaw, *Numerical simulations of argon plasma jets flowing into cold air*, Plasma Chemistry and Plasma Processing 1993, vol. 13
- [2] S. B. Pope, *Pdf method for turbulent reacting flows*, Prog. Energy Combust. Sci., 1985, vol. 11
- [3] W. Kollmann, *The pdf approach to turbulent flow*, Theor. and Comp. Fluid Dynamics, 1990, vol. 1
- [4] C. Dopazo, *Recent developments in pdf methods*, publisher Academic Press London, pages 375-474
- [5] P. Domingo, T. Benazzouz, L. Vervisch, *Studying turbulent plasma using direct numerical simulation and probability density function*, AIAA paper, AIAA 98-0982
- [6] L. Leborgne, B. Van Ootegem, P. Vervisch, *Investigation of a low pressure supersonic turbulent argon plasma jet with electrostatic probes*

\*Abstract 6826 submitted to the 21st International Symposium on Rarefied Gas Dynamics, Marseille, France, July 26-31, 1998

NON-EQUILIBRIUM FLOWS - NE P

THURSDAY, JULY 30, 1998

16:00

## Two-Temperature Thermochemical Relaxation Model Based on a Treanor Distribution \*

S. Génieys<sup>1</sup>, A. Chikhaoui<sup>2</sup>

<sup>1</sup> Université Paul Sabatier, Lab. MIP, Toulouse, France

<sup>2</sup> IUSTI/MHEQ, Marseille, France

The two-temperature thermochemical relaxation models are suited to describe the reacting gas mixtures for which rotational and translational modes can be assumed equilibrated and can be described by a single temperature, but for which the vibrational relaxation is longer, involves a distinct temperature and has to be coupled with the chemical relaxation. In particular, these models are used to describe the environment around hypersonic vehicles during their entry flights, [4, 6, 8, 10]. Most of these models assume that the vibration of the molecules is harmonic, which yields to a Boltzmann distribution in the vibrational mode.

The Treanor distribution, [12], generalizes the Boltzmann distribution to the case of anharmonic oscillators. It is obtained considering rapid phenomena which conserve the density of each species, the impulsion and the total energy of the mixture and the number of vibrational quanta of each vibrating species (but not their vibrational energy). It is usual to express the Treanor distribution as a function of the total temperature (temperature associated with the total energy) and the temperature of first vibrational level.

A thermochemical relaxation model based on a Treanor distribution has been derived from the Boltzmann equation in [1], under the assumption that the rapid phenomena are the exchanges of translational energy, the exchanges of rotational energy and the exchanges of vibrational quanta between molecules of the same chemical species. This model will be described in the present talk. It consists of three equations for the density, momentum and total energy, supplemented with an equation for the variations in the density of each species and with an equation for the variations in the number of vibrational quanta of each vibrating species. The densities and numbers of vibrational quanta evolve due

to the slow phenomena.

One particular feature of this model is that the vibrational energy does not depend on a single temperature. It depends on the total temperature and on the temperature of first vibrational level. This leads to particular thermodynamic relations between the conservative variables and the temperatures, which are described in [1, 2] and will be presented in the talk.

One important question for thermochemical relaxation models is the taking into account of slow phenomena. Translational-vibrational exchanges and vibrational exchanges between different species are usually modeled by relaxation time operators, [9]. The chemical production terms and vibrational production terms due to chemical-vibrational exchanges are related to each other and have to be modeled under the same assumptions. There exists numerous models (chemistry-vibration-chemistry coupling models) for these terms, see [5], most of them assuming harmonic oscillations. In [2] is presented a new anharmonic coupling model based on Treanor distributions. This model will be detailed in the talk. It uses the same assumptions as the Treanor-Marrone model [8] for dissociation of harmonic oscillators, and its extension to exchange reactions between harmonic oscillators given in [11]. In particular this model takes into account that dissociation can occur preferentially from the higher vibrational levels. To this aim is introduced an additional parameter with dimensions of a temperature describing the distribution of the dissociation probability over the vibrational levels. Unfortunately, the correct value of this preferentialisation parameter is not accurately known.

In [3] the sensibility of these three models on their preferentialisation parameter is investigated in the test case of the air heated by a plane shock-wave. Also are studied Knab's model [6] (which involves the same preferentialisation parameter) and Park's and Macheret's models, [10, 7]. The results ob-

\* Abstract 1401 submitted to the 21st International Symposium on Rarefied Gas Dynamics, Marseille, France, July 26-31, 1998

tained with these five models are compared with shock tube experimental data in infrared radiations of nitric-oxide taken from [13]. The study of the sensibility on the free parameter and the comparison with the experimental data will be shown in the talk.

## References

- [1] A. Chikhaoui, J. P. Dudon, E. V. Kustova, E. A. Nagnibeda. Transport properties in reacting mixture of polyatomic gases, *Physica A*, accepted for publication.
- [2] A. Chikhaoui, J. P. Dudon, S. Génieys, E. V. Kustova, E. A. Nagnibeda. Multi-temperature model of heat transfer in a reacting gas mixture, *Phys. fluids* submitted.
- [3] S. Génieys, A. Chikhaoui. Comparative study of several two-temperature thermochemical relaxation models, in preparation.
- [4] P. Hammerling, J. D. Teare, B. Kivel. Theory of Radiation from Luminous Shock Waves in Nitrogen, *Phys. Fluids*, 2 (4):422-426, 1959.
- [5] E. A. Kovach, S. A. Losev, A. L. Sergievskaya. Two-temperature kinetic models for dissociation of molecules in strong shock waves, *Lomonosov Moscow State University*, preprint, 1995.
- [6] O. Knab, H. H. Frühauf, E. W. Messerschmid. Theory and Validation of the Physically consistent Coupled Vibration-Chemistry-Vibration Model, *Journ. of Therm. and Heat Tans.*, 9 (2):219-226, 1995.
- [7] S. O. Macheret, A. A. Fridmann, I. V. Adamovich, J. W. Rich, C. E. Treanor. Mechanisms of Nonequilibrium Dissociation of Diatomic Molecules, *AIAA*, 94-1984, 1994.
- [8] P. V. Marrone, C. E. Treanor. Chemical Relaxation with Preferential Dissociation from Excited Vibrational Levels, *Phys. Fluids*, 6 (9):1215-1221, 1963.
- [9] R. C. Millikan, D. R. White. Systematics of Vibrational Relaxation, *Journ. of Chem. Phys.*, 39 (12):3209-3213, 1963.
- [10] C. Park. Assessment of Two-Temperature Kinetic Model for Ionizing Air, *AIAA*, 87-1574, 1987.
- [11] S. Seror, M. C. Druguet, E. Schall, D. Zeitoun. A new vibration-exchange reaction coupling model for hypersonic air flows, *AIAA*, 97-2556, 1997.
- [12] C. E. Treanor, I. W. Rich, R. G. Rehm. Vibrational relaxation of anharmonic oscillators with exchange dominated collisions, *Journ. of Chem. Phys.*, 48:1798, 1968.
- [13] C. E. Treanor, M. J. Williams. Kinetic of Nitric Oxide Formation Behind 3 to 4 km/s Shock Waves, U. S. Army Research Office Final Rept., Contract DAAL03-92K-0003, Calspan Univ. of Buffalo Research Center, Buffalo, New-York, 1993.

# Inversion in Vibrational Population of CN behind a Strong Shock Wave in N<sub>2</sub>/CH<sub>4</sub>/Ar Mixture \*

D. Ramjaun, M.-P. Dumitrescu, R. Brun  
IUSTI/MHEQ, Marseille, France

## 1 Introduction

Time-resolved spectroscopy of the  $B^2\Sigma^+ \leftrightarrow X^2\Sigma^+$  electronic band of CN has been studied behind a strong shock wave in 92%N<sub>2</sub>, 3%CH<sub>4</sub>, 5%Ar mixture, simulated atmosphere of Titan (Nelson et al. [1]) at different Mach numbers (15.8 and 14.6) and initial test gas pressures in the TCM2 Hypersonic facility. Fitting of calculated spectra assuming a Boltzmann distribution for vibrational population with experimental spectra shows some deviation at low initial test gas pressure and a very marked one at high initial test gas pressure. An iterative method has been used to deduce the real vibrational population distribution and the corresponding mean vibrational temperature.

## 2 The experimental setup

The TCM2 hypersonic facility is a free-piston facility (Brun et al. [2]). For the emission experiments (Table 1), its shock tube was specially equipped with an experimental chamber, fitted with BK7 windows and gauge mounting ports. Light emitted from the shock is collected by a vertical slit, 500  $\mu\text{m}$  wide and is directed into a Jobin-Yvon 640 monochromator, equipped with interchangeable holographic gratings giving spectral ranges from 85 to 570  $\text{\AA}$  at the wavelengths observed and a maximum spectral resolution of 1  $\text{\AA}$ , see Fig. 1. The streak camera system (Hamamatsu Photonics), fixed at the output of the monochromator, had its time scale fixed at approximately 16  $\mu\text{s}$  for the series of shots observed. The two-dimension data (spectrum versus time) is recorded on a CCD camera at the end of the streak unit.

\*Abstract 1551 submitted to the 21st International Symposium on Rarefied Gas Dynamics, Marseille, France, July 26-31, 1998

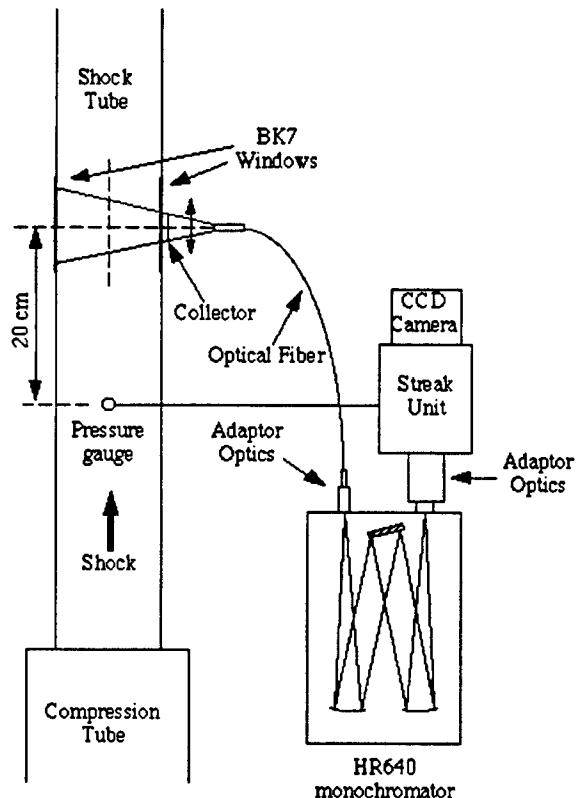


Figure 1: Streak system optical setup.

Table 1: Characteristic shots.

Shot	P1 (mb)	P2 (bar)	U (m/s)
Titan 1	2.2	0.7	5560
Titan 2	11.0	3.4	5130

## 3 Results and discussion

A preliminary analysis of the spectra shows that in the shots done at lower initial pressure, vibrational population inversion occurs briefly at the shock layer (for a maximum of 2  $\mu\text{s}$  after) and for a very long time in the shots at higher initial pressure (for



8  $\mu$ s of spectra recorded). Fig. 2 shows the  $\Delta v = 0$  band of  $CN$  as recorded by the streak camera taken from the two series of shot with normalised spectrum intensities. The ratios of the (1,1), (2,2) and (3,3) bands to the (0,0) band can be seen to be unexpectedly high for the spectrum at higher initial test gas pressure. Assuming a Boltzmann distribution in vibrational population, a least-square fit of a simulated spectrum to the experimental one at lower test gas pressure, taken as far as possible from the shock layer (more than 5  $\mu$ s), can be done and yields a rotational and vibrational temperature of 8000 and 7500 [3]. For the spectrum at higher pressure, we have to proceed differently: an iterative method is used to deduce the vibrational population distribution from a calculated spectrum and thus, a mean vibrational temperature can be derived. Fig. 3 shows such a vibrational population distribution; it can be noticed that a maximum deviation from a Boltzmann plot occurs at  $v = 4$ .

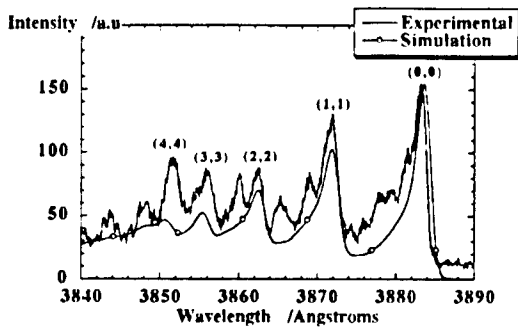


Figure 2:  $\Delta v = 0$  band of  $CN$  at 2 mb and 11 mb initial test gas pressure.

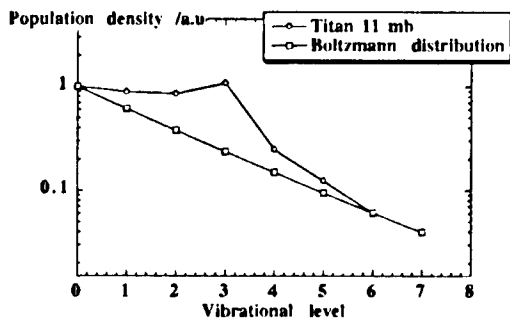


Figure 3: Calculated vibrational population distribution of  $CN$  at 11 mb initial pressure.

## 4 Conclusion

Non-Boltzmann distribution of vibrational population of  $CN$  in titan mixture has been observed at the TCM2 hypersonic facility, the phenomenon being more pronounced at higher initial test gas pressure. Vibrational population distribution evolution behind the shock is being calculated and will be presented for both series of shots. The corresponding vibrational and rotational temperatures will be deduced and also presented in the full paper.

## References

- [1] Nelson H.F., Park C., Whiting E.E., *Titan Atmospheric Composition by Hypervelocity Shock Layer Analysis*. AIAA 24th Thermophysics Conference, Buffalo, New York, 1989.
- [2] Brun R., Burtschell Y., Chaix A., Druguet M.-Cl., Dumitrescu L.-Z., Dumitrescu M.-P., Martin R., and Zeitoun D., *Flow in the TCM2-Marseille hypersonic Facility: some new experimental results*, Proc. 20th Shock Waves Symposium in Pasadena, Vol.1, pp.227-232, 1995.
- [3] Labracherie L., *Détermination des températures rotationnelles et vibrationnelles de CN à l'aval d'un choc droit se propageant dans une atmosphère de Titan reconstituée*, Ph.D Thesis, Marseille, France, 1994.

## Study of Curved Flow Stability of Reacting Gases \*

A. S. Baryshnikov

A.F. Ioffe Physico-Technical Institute, St. Petersburg, Russia

Instability of exothermally reacting gas flow is well known [6]. Today interesting is paid to instability of flow with endothermal reactions. For instance, instability of bow shock and bow layer behind it in polyatomic reacting gases with low specific heats ratio [1]. Disturbances is found to appear at regimes of chemical dissociation. The mean energy of disturbances is shown to coincide with energy of chemical transfer [2]. Experiments show that dimensions and form of flying body have significant influence on the appearance and amplitude of the disturbances [1, 5]. Of course the low specific heats ratio  $k$  also leads to instability [3].

In this work the longitudinal two-dimensional flow of compressible reacting gas is considered. The chemical reasons for layer instability are found. Effects of shear viscosity is considered to be negligible as compared with the effects of inner chemical processes. The energy of chemical transfer is considered in this work as volume power of energy release -  $Q$ . Its derivations by temperature and gas density are taken into account. Geometry is accounted through gradient of gas velocity across the layer -  $U'$ . The direction of coordinate across the layer is chosen along the direction of pressure disturbances spreading. So the convex layer corresponds to  $U' > 0$  and concave layer corresponds to  $U' < 0$ . As usually basic equations are reduced to single differential equation of second order [4]. The solution of equation is found in the form:  $p = \text{Amp}(p) \exp(i b y)$ ,  $\text{Im} b = 0$ . It's easy to show that problem reduces to solving the algebraic equation with independent variable  $Z = -ia(U - c)/(fs)$ . The equation depends on 4 parameters  $k$ ,  $a$ ,  $d = (dQ/dT)/(fs)$ ,  $g = 2abrU'/(fs)$ , ( $a$  and  $b$  are wave numbers along and across the layer,  $s = Pr/M$ ,  $f = \sqrt{a^2 + b^2}$ ,  $P$  - pressure,  $r$  - density,  $M$  - Mach number,  $c$  - sound speed). It's accepted that  $|g| < 0.1$ . It means that wave length of disturbances  $l = 1/a$  is about by 20 times less than length of gasdynamical influences of different

parts of flow one to other. Such conditions enables us to investigate local stability of longitudinal two-dimensional layer.

For endothermal chemical processes (dissociation) with normal thermal and pressure dependencies  $2 > k > 0$  and  $1 > d > 0$ . The computation of equation is held for these regimes. Two complex and two real solutions are obtained. One of the later is great than zero for any  $k$ ,  $g$ ,  $d$  ("gradient" solution). This solution at  $g < 0$  is unstable and at  $g > 0$  is stable. The case of more interest is  $g > 0$ , because it corresponds to convex flow. In this case "gradient" solution is stable, but "wave" solution at some parameters can be unstable. The results of calculations give that there is mean value region on  $k$  at which flow is stable ( $\text{Re } Z < 0$ ). For lower and higher values flow is unstable. The width of this region depends on  $k$ ,  $d$ ,  $g$  and  $a$ . Increasing  $k$  and  $d$  (at constant  $g$ ) leads to spreading of stability region (especially for low  $d$ ). Thus with increasing  $k$  from 1.2 (for polyatomic gases) up to 1.4 (for air) at  $d < 0.1$  the stability region spreads by two times. At  $d = 0.4$  the dependence on  $g$  is linear. It's ought to be mentioned that at  $d = 0$  for  $k = 1.2$  the stability region is absent, as the flow for  $k = 1.4$  at  $d = 0$  is stable at region  $0.1 < a < 0.65$ . Since inverse wave number  $a$  is proportional to wave length  $l$ , instability takes place as for very short wave and for very long wave disturbances. The experimental study of disturbances of such wave length needs the tools of very high accuracy. Contraction of stability region at low  $k$  enables us to find instability for polyatomic using usual tools [1, 2, 5]. Thus for polyatomic gases with very low specific heats ratio the flow instability can be observed and for endothermal processes.

## References

- [1] Baryshnikov A.S., Bedin A.P., Maslennikov V.G., Mishin G.I., *About instability of bow shock wave*, Pis'ma v Zh.Tekh.Fiz. Vol.5, No.5, pp.281-284, 1979.

\*Abstract 1972 submitted to the 21st International Symposium on Rarefied Gas Dynamics, Marseille, France, July 26-31, 1998

- [2] Baryshnikov A.S., Bedin A.P., Derevjanko V.G., Rumjantsev A.A., *Statistical characteristics of flow fluctuations and shock wave instability mechanism in relaxing gases*, Paper, Physical-Technical Institute, N 816, 1983.
- [3] Gurevich L.Ye., Rumjantsev A.A. *Shock wave spreading in decreasing density media*, Zh.Tekh.Fiz., Vol.58, No.3, pp.1395-1399, 1980.
- [4] Gaponov S.A., Maslov A.A. *Disturbances evolution in compressed flows*, Novosibirsk, Nauka, 1980.
- [5] Mishin G.I., Bedin A.P., Juschenkova N.I., Skvortsov G.E., Rjazin A.I. *Anomalous relaxation and shock wave instability in gases*, Zh.Tekh.Fiz. Vol.51, No.4, pp.2315-2324, 1981.
- [6] Zeldovich Ja.B., Barenblat G.I., Librovich V.B., Mahviladze G.I. *Mathematical theory of combustion and explosion*, Moscow, Nauka, 1980.

# On Peculiarities of High Threshold Physical-Chemical Transformation within a Translational Non-Equilibrium Region in a Shock Wave Front\*

V.Yu.Velikodny and V.A.Bityurin

Institute of High Temperatures of the Russian Academy of Sciences, Moscow, Russia

## 1. Introduction

The original idea on an exceptional role of translational non-equilibrium region for physical-chemical reactions in a shock wave front was formulated in 1979 by Ya.B.Zeldovitch with co-workers in the paper [1]. It was shown that high threshold physical chemical processes can occur in this region.

The first reason for this feature is that in this region the relative number of collisions with translational energy higher than activation energy can be higher by several order of magnitude as compared with those in equilibrium behind the shock wave front (see [2]).

The second reason is that the inelastic collision process can follow the non-adiabatic mechanism of Landau-Zinner resulting in significant growth of non-elastic collision cross-section up to gas-kinetics one.

It was shown theoretically in [2] and confirmed later experimentally [3] that these two reasons are responsible for significant yield of a physical-chemical transformation with a high threshold activation energy in the translational non-equilibrium region much higher than in the equilibrium region behind the shock wave front in spite of the small size of such a translational non-equilibrium region.

This effect can find applications and can be useful for

- the definition of the cross-sections of excitation and quenching of electron levels on Landau-Zinner mechanism in shock tunnel experiments;
- the production of primary activated centres in avalanche and chain type processes (chain reactions, discharges);
- the radio wave propagation through super ionized region behind a shock wave ;

- the reformation of the internal structure (including de-structure) of super heavy particles (molecules, fullerenes, clusters, viruses).

## 2. Results

In this paper the analysis of the shock wave structure in chemically reacting gas mixtures with very different particles mass is carried out on the base of Boltzmann' equation solved with the modified Mott-Smith' method [4] taking into account non-elastic collisions. The influence of particles mass ratio, relative concentration, cross-section values, flow Mach number, the chemical composition of gas mixture on kinetics of high threshold physical-chemical transformation are studied.

The structure of shock waves in a two-components mixture of a light inert carrier and a heavy non-elastic interacting admixture (simulating an electron excitation, for example) is considered. The characteristics parameters are  $n_l \gg n_h$  and  $\rho_h/\rho_l \approx 1$ ,  $E/kT_\infty = 150 - 300$  for mach number  $M = 3 - 5$ , where  $n_l, n_h, \rho_l, \rho_h$  are concentrations and density for light and heavy components correspondingly,  $E$  is activation energy,  $k$  — is Boltzmann' constant,  $T_\infty$  is the temperature of incoming flow. The analysis based on the calculation of shock wave structure in two cases of particular two-components mixtures: (1)  $H_2$  - 99%,  $I_2$  - 1% and (2)  $He$  - 99%,  $I_2$  - 1% for Mach numbers  $M=3-5$  for  $I_2$  electron excitation process with  $E \approx 6\text{eV}$  has shown that the ratio of the non-elastic process rate constant at the maximum is  $k_{neq}/k_{\infty} > 10^8$  where  $k_{neq}$  is the maximum rate constant in the translational relaxation region and  $k_{\infty}$  is the same value in the equilibrium region

\* Abstract 1976 submitted to the 21st International Symposium on Rarefied Gas Dynamics, Marseille, France, July 26-31, 1998

behind the shock wave. The comparison of the experimental data [3] with the calculations based on the adiabatic Messy mechanism or on Landau-Zinner mechanism has shown that the process passes through a quasi-particle formation, i.e. follows the Landau-Zinner mechanism. It should be noted a significant discrepancy between the numerical data for two-component mixture obtained in this paper and the data calculated in paper [5] with Monte-Carlo method. As in this paper  $k_{neq}/k_{+\infty} > 10^4 - 10^8$  in the good accordance with experimental data the Monte-Carlo' calculations result in  $k_{neq}/k_{+\infty} \approx 10$  for the same mixture and flow parameters. This discrepancy can be explained by the fact that the approach developed in this paper takes into account properly the high energy tails of the distribution function.

1. A shock wave structure in the three-component mixture of a light inert carrier and two heavy reacting admixtures (case of electron excitation and dissociation) with the following parameters:  $n_e \gg n_h$ ,  $\rho_h/\rho_e \leq 1$ ,  $m_{h2} \geq m_{h1} \gg m_e$ ,  $E/kT_{-\infty} = 150-300$ , where and  $m_{h1}$ ,  $m_{h2}$  mass of two heavy components, for Mach number range  $M=3-5$ . The analysis has shown that the rate constants of high threshold reaction of heavy particles  $h_1$  and  $h_2$  in the translational non-equilibrium region are significantly higher than for those under equilibrium conditions behind the shock wave front:  $k_{neq}/k_{+\infty} > 10^4 \div 10^8$  and even higher. Furthermore  $k_{h2,h2} > k_{h1,h2} > k_{h1,h1}$ . The latter differs significantly from results obtained with Monte-Carlo technique in paper [6], where  $k_{h1,h2} \gg (k_{h2,h2}, k_{h1,h1})$ . The increase of  $k_{h1,h2}$  as compared with  $k_{+\infty}$  found in this paper can be explained with the corresponding shift of the heavy particle distribution function core, and the increase of  $k_{h2,h2}$ ,  $k_{h1,h1}$  is caused by a thickening of high energy tail of the distribution function.

## References

- [1] Zel'dovich Ya.B., Genich A.P., Manelis G.B., Dokl. Acad. Nauk USSR, 1979, vol.248, No.2, p.349-351 (Russian)
- [2] Velikodny V.Yu., Bityurin V.A., High Temperature, 1997, vol.35, No.2, pp.346-349.
- [3] Bazhenova J.V., Emelianov A.V., Eremin A.V., Velikodnyi V.Yu., Proc. 21 th Int. Symp. Shock Waves. Australia. 1997, p.31.
- [4] Bashlykov A.M., Velikodny V.Yu., Zh.Tekhn.Fiz., 1991, vol.61, No.8, fl.32-42.
- [5] Genich A.P. et.al. *Translation Relaxation in Shock Waves in Gases*. Preprint of Joint Inst.Chem.Physics. Chernogolovka. 1991, 68p.
- [6] Kulikov S.V., *Shock Waves* 1997, vol.7, No.1, pp.25-28.

# Classical Dynamics of Two Coupled Rotors. Excitation of Diatomic Molecules \*

R.E. Kolesnick

Department of Physics, The University of Newcastle upon Tyne, UK

In practice studying molecular dynamics quite often one needs to introduce angle-action variables to express the Hamiltonian, particularly the PES (potential energy surface). Very often the PES depends on geometrical angles, which should be connected with the action-angle variables directly. A direct geometrical attack is not very elegant and is still unsuccessful, because of the very complex geometry of the problem. Even for small molecules it is quite difficult to develop accurate classical models of collisions in action-angle variables.

The conception of classical canonical transformations given by Miller<sup>1</sup> was defined in terms of the  $F_4$  generating function, which is defined in the space of classical actions and it is still difficult to implement, because the PES depends on both angle and action variables.

Nevertheless, we propose a complementary way to get angle-action variables. It provides the possibility to cover all the angles together in a single framework. In the present report we develop the classical theory of transformations for canonical angles, by associating the canonical angles with rotation matrices directly. The geometrical angles were included conveniently via canonical actions, which are specifying the position of interatomic vectors. The multiplication of one rotation matrix,  $M$  by another is equivalent to carrying the frame of reference from one position to another. So, the Cartesian coordinates and canonical variables should be connected directly in the framework of our method. Thus, the  $M$ -matrix approach is the corresponding matrix formulation to the  $F_4$  classical canonical transformation, which has been derived in terms of classical actions<sup>2</sup>. This approach provides the possibility to find connections between uncoupled and canonical coupled variables quite easily. It is easier to implement in molecular dynamics problems elaborate accurate models, especially for small molecules.

As applications, we consider the rotational dynamics of a rotor-rotor system. Because scattering occurs at large impact parameters, the calculations must include large total angular momentum  $J$  values. Collinear approximations or calculations at  $J = 0$  are totally inappropriate<sup>3</sup>. By using such a matrix approach the classical theory of scattering of two rotors has been studied in detail. Various possible cases of reduction to particular cases are considered for classical rotor-rotor collisions. Thus, some of the simplified geometrical configurations of two coupled rotors were distinguished. They are: the fixed configuration<sup>4</sup> of  $J$  and the plane configuration of it against an arbitrary configuration. It is found that our model agrees with the previous one.

Angle-action variables are employed to describe the three angular momenta of interest: the two internal

rotational angular momenta of the rotors,  $j_1$  and  $j_2$  and the orbital angular momentum of the relative motion,  $l$ . For rotor-rotor collisions three angular momentum coupling schemes may be employed: a fully uncoupled scheme,  $j_1, j_2, l, m_1, m_2, m_l$ , where  $m_l$  is the projection of the corresponding  $j_l$  on the  $OZ$  axis, or a partially coupled scheme  $j_1, j_2, j_{12}, l, m_{12}, m_l$ , where  $j_{12} = j_1 + j_2$ , or a fully coupled scheme involving  $J = j_{12} + l$ . The three possible choices for the intermediate angular momentum ( $j_1 + j_2, j_2 + l, l + j_1$ ) are equivalent in any exact formulation.

In general the PES depends on the separation of the centres of mass of the rotors and on three angles. Expressing these angles in terms of the action-angle variables can be complex<sup>4</sup>. We have found that expressing these angles in terms of the rotation matrices for the transformation defined by Euler angles such as  $(Q_M, \beta_J, Q_J)$ , and similarly for the other angular momenta, allows some simplification in the presentation of the results. Here the angles  $Q_M$  and  $Q_J$  are conjugate to  $M$  and  $J$ , respectively and  $\cos \beta_J = M/J$ . Such expressions were found for all the geometrical configurations and corresponding coupling schemes of two rotors.

A new concept of two coupled rotors was developed. The partially coupled set and the fully coupled one are considered separately. Thus, we found an approach to the problem. The accurate description of coupling of two rotors to introduce angle-action variables has been given. A detailed analysis of the different types of coupling has been carried out. We have classified and developed some theoretical models of coupling and introduced action-angle variables for rotors. The principal result is an analytical prescription how to write the Hamiltonian for two rotors in the case when the total angular momentum is orientated arbitrarily, given  $J$ , that facilitates solving the equations of motion of diatomic molecules in classical trajectory calculations. The necessary analytical expressions will be reported at the meeting.

## ACKNOWLEDGMENTS

This work is supported by the Royal Society- NATO Postdoctoral Fellowship Programme.

<sup>1</sup> A.S. Dickinson, W.-K. Liu J. Phys. Chem. 90, 3612, 1986

<sup>2</sup> W.H. Miller Adv. Chem. Phys. 25, 69, 1974

<sup>3</sup> R.J. Cross J. Chem. Phys. 95, 1900, 1991

<sup>4</sup> Turfa, A.F., Fitz, D.E. and Marcus, R.A. J. Chem. Phys. 67, 4463, 1977

\* Abstract 2906 submitted to the 21st International Symposium on Rarefied Gas Dynamics, Marseille, France, July 26-31, 1998

# Computation of Flows in Vibration-Dissociation Nonequilibrium \*

N. Belouaggadia, R. Brun  
IUSTI/MHEQ, Marseille, France

Considering dissociating flow of diatomic gases in vibrational nonequilibrium, the Boltzmann equation for the molecules  $p$  on the quantum level  $i$ , including a rotational and a vibrational level, may be written under the following nondimensional form:

$$\frac{df_{ip}}{dt} = \frac{1}{\epsilon_{tr}} J_{tr} + \frac{1}{\epsilon_v} J_v + \frac{1}{\epsilon_c} J_c \quad (1)$$

Where  $f_{ip}$  is the distribution function of the considered molecules,  $J_{tr}$ ,  $J_v$  and  $J_c$  are their corresponding collisional balances respectively due to translation-rotation, vibration and chemical exchanges.  $\epsilon_{tr}$ ,  $\epsilon_v$  and  $\epsilon_c$  respectively represent the ratio of the corresponding characteristic times  $\tau_{tr}$ ,  $\tau_v$ ,  $\tau_c$  to a reference flow time  $\theta$ .

Multiplying (1) by various collisional invariants, summing and integrating, one obtains macroscopic conservation equations for the atom-molecule mixture including species conservation equations and vibrational energy equation for molecules  $p$ . Thus, the source terms of these equations respectively  $\dot{w}_p$  and  $\dot{e}_p$  are given by the following expressions :

$$\dot{w}_p = K_D n_p^2 \quad (2)$$

$$\dot{e}_p = \dot{e}_p^0 - (E_{vd} - E_v) K_D n_p \quad (3)$$

where  $K_D$  is the dissociation rate constant influenced by vibrational relaxation,  $E_v$  is the mean vibrational energy of molecules  $p$  and  $E_{vd}$  the part of this energy lost per dissociation.  $n_p$  is the molecular density and  $\dot{e}_p^0$  the usual source term coming from vibrational exchanges. The second term of (3) represent the influence of dissociation on vibrational energy  $E_v$ .

In order to close the conservation equation system, expressions of transport terms - not presented here - but also of  $K_D$  and  $E_{vd}$  terms must be found as functions of translation-rotation temperature  $T$  and vibrational temperature  $T_v$ .

With this aim in view, Chapman-Enskog methods may be used, but, because of the presence of different time scales  $\tau_{tr}$ ,  $\tau_v$ ,  $\tau_c$ , and  $\theta$ , each one only covers specific situations: Thus, expressions for  $K_D$  and  $E_{vd}$  have been proposed for weak vibrational nonequilibrium (WNE)<sub>v</sub> and strong chemical nonequilibrium (SNE)<sub>c</sub> situations, that is for  $\tau_v \ll \tau_c \sim \theta$  [1] then this case has been extended to quasi equilibrium situations for chemistry by constructing a generalized Chapman-Enskog method [2]. Finally considering all practical nonequilibrium regimes excluding only strong gradient regions, it is possible to obtain closing relations for  $K_D$  and  $E_{vd}$ , i.e:

$$K_D(T, T_v) = \bar{K}_D \left[ 1 - \left( \frac{\bar{E}_{vd} - \bar{E}_v}{kT} \right) \left( \frac{E_v - \bar{E}_v}{C_v T} \right) \right] \quad (4)$$

$$E_{vd}(T, T_v) = \bar{E}_{vd} \frac{\bar{K}_D}{K_D(T, T_v)} \times \\ \times \left[ 1 + \frac{E_v - \bar{E}_v}{C_v T} \left( \frac{2N - 1}{3} \frac{\theta_v}{T} - \frac{\bar{E}_v}{kT} \right) \right] \quad (5)$$

where  $\bar{K}_D$ ,  $\bar{E}_{vd}$  and  $\bar{E}_v$  are equilibrium expressions of the corresponding quantities,  $k$ ,  $C_v$  and  $N$  being respectively the Boltzman constant, the vibrational specific heat and the number of levels.  $\theta_v$  is the vibrational characteristic temperature. The expression (5) written for harmonic oscillator may be easily generalized to anharmonic model. The extension to flows in which recombination is non negligible is also straightforward.

Complete computation of relatively simple nonequilibrium flows are operated including flows behind strong shock waves, steady expansions in nozzles and boundary layer flows, generalizing examples presented in [1] and [2]. Thus, non-Arrhenius behavior of dissociation rate constants is found in the boundary layer arising at the end wall of a shock tube after the reflection of the incident shock: the rate constant is increasing close to the wall where the translational temperature is decreasing but where a freezing zone is created.

\* Abstract 3292 submitted to the 21st International Symposium on Rarefied Gas Dynamics, Marseille, France, July 26-31, 1998

## References

- [1] R. Brun and M. Llorca: *Vibration-Dissociation Coupling Revisited by Chapman-Enskog Procedure*, Rarefied Gas Dynamics, Ed. V. Harvey and G. Lord Oxford Univ. Press. P.427. 1995.
- [2] N. Belouaggadia and R. Brun: *Chemical Rate Constants in Nonequilibrium Flows*, 32nd Thermophysics Conf. Atlanta. AIAA Paper 97-2555, 1997.



# Dynamic Molecular Collision (DMC) Model of Diatomic Molecules for DSMC Calculation \*

T. Tokumasu and Y. Matsumoto

Department of Mechanical Engineering, University of Tokyo, Japan

## 1. INTRODUCTION

The Direct Simulation Monte Carlo (DSMC) method is widely used to simulate rarefied gas flows. Many calculation techniques [1,2] for molecular collision and molecular models in which inelastic effects, internal degree of freedom, chemical reactions, electronic excitation and radiation, are taken into account have been developed [3,4]. In this paper, the Dynamical Molecular Collision (DMC) Model of diatomic molecules for DSMC calculation is constructed based on the Molecular Dynamics (MD) simulation of binary collision of  $N_2$  molecules. To make sure of its validity, the translational and rotational energy distributions at the equilibrium condition and the structure of the normal shock wave is simulated and the results are compared with theoretical or experimental ones.

## 2. MD SIMULATIONS OF THE COLLISION OF DIATOMIC MOLECULES

In this simulation both collision molecules are nitrogen and assumed as rigid rotors. This means the vibrational degree of freedom is neglected. The rotational energy has continuous values. The force and moment which acts on the collision molecules are calculated by the sum of the potential force which act on the two atoms of collision molecules. As the interaction potential, the Lennard-Jones (12-6) potential is used. The parameters are determined as  $\sigma_a = 3.17 \times 10^{-10}[\text{m}]$ ,  $\epsilon_a = 6.52 \times 10^{-22}[\text{J}]$ . The diagram of MD simulation are shown in Fig.1.

Figure 2 shows the calculated results of translational and rotational energy distribution after the collision, where  $T_{tr} = 400[\text{K}]$ ,  $T_{r1} = 400[\text{K}]$  and  $T_{r2} = 600[\text{K}]$ . The figure shows that the energy distribution after the collision has a peak near the initial energy and due to the varying initial phase, direction of rotational vector or impact parameter, it distributes over a wide range.

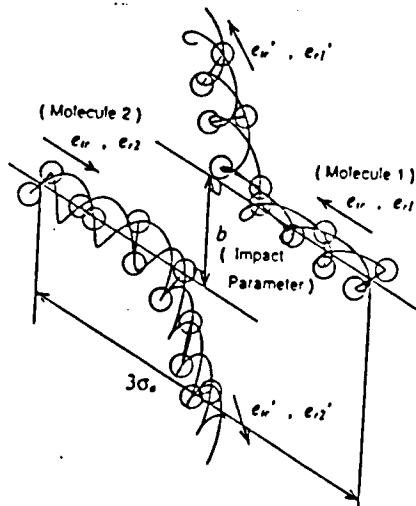


Fig.1 : Diagram of MD simulation.

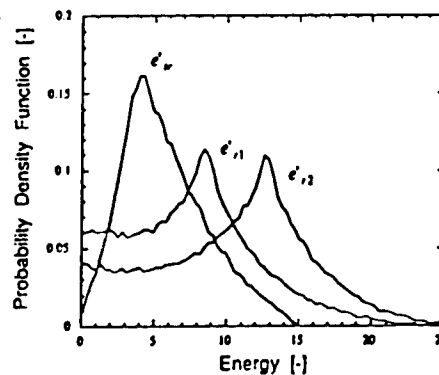


Fig.2 : Energy distribution after the collision.

## 3. CONSTRUCTION OF COLLISION MODEL

In all simulated data, only the data that the two molecules collide with each other within the collision cross section is considered. The collision model of diatomic molecules is constructed by approximating this distribution to particular functions. Consequently, the collision model of diatomic molecules is constructed as follows,

$$f(e') = \begin{cases} A_l \exp \{-B_l(e_l - e)\} & \text{:left side} \\ A_r \exp \{-B_r(e - e_l)\} & \text{:right side} \end{cases}$$

\*Abstract 4646 submitted to the 21st International Symposium on Rarefied Gas Dynamics, Marseille, France, July 26-31, 1998

where,  $e_i$  is the initial energy.  $A_i, B_i, A_r, B_r$  are determined so that the probability and deviation of left and right side of this function agree with those of MD results.

In the DSMC method, the energy after collision is determined so that the total energy is conserved. For this reason, two of the three energies  $e'_{tr}, e'_{r1}, e'_{r2}$ , which are chosen randomly, is determined by the method mentioned above. Finally, the rest is determined by subtracting these two energies from  $e_{total}$ .

## 4. THE VALIDITY OF THE PRESENT MODEL

In order to verify the validity of the present model, the calculated translational and rotational energy distributions at the equilibrium condition are compared with theoretical values. The typical results are shown in Fig.3 ( $T=300[K]$ ). As shown in this figure, the calculated results are in good agreement with Maxwell-Boltzmann distribution.

Next, the normal shock wave of  $N_2$ , in which the nonequilibrium condition between the translational and the rotational energies exists, is calculated. These results are compared with the experimental ones by Robben and Talbot [5] to make sure of its validity.

The typical result is shown in Fig.4 ( $M_{in} = 12.9$ ). As shown in this figure, the translational energy parallel with the movement of shock front increases first, the translational energy vertical with the movement of shock front follows it and at last the rotational energy increases. It can be seen that this calculation result is in good agreement with experimental results of Robben and Talbot. For this reason, we can say that this model can calculate nonequilibrium flows like high Mach number shock waves very well.

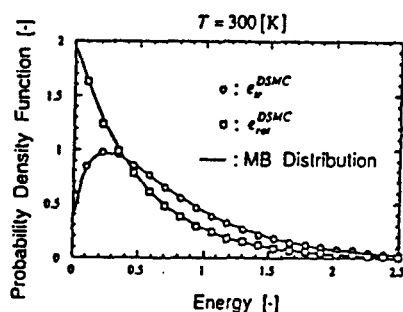


Fig.3 : Energy distribution at equilibrium condition ( $T = 300[K]$ ).

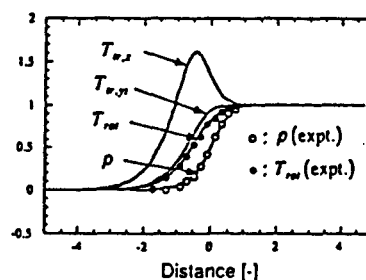


Fig.4 : Normal shock wave ( $M_{in} = 12.9$ ).

## 5. CONCLUDING REMARKS

The inelastic collision of diatomic molecule is simulated by the MD method and the Dynamical Molecular Collision (DMC) model is constructed based on these MD results. The validity of the model is verified by calculating the translational and rotational energy distributions at the equilibrium condition and the normal shock wave in the DSMC method using this model. These results show that the collision of diatomic molecules can be calculated very well by using this model even though some assumptions exist in the simulation.

## REFERENCES

- [1] Bird, G.A., Molecular Gas Dynamics, (1976), Clarendon Press, Oxford.
- [2] Nanbu, K., Direct simulation scheme derived from the Boltzmann equation. I. Monocomponent gases, J. Phys. Soc. Jpn., Vol. 49 (1980), p. 2042.
- [3] Koura, K., Null collision technique in the direct simulation Monte Carlo Method, Phys. Fluids, Vol. 29 (1986), p. 3509.
- [4] Borgnakke, C. and Larsen, P.S., Statistical collision model for Monte Carlo Simulation of polyatomic gas mixture, J. Comput. Phys., Vol. 18 (1975), p. 405.
- [5] Robben, F. and Talbot, L., Experimental study of the rotational distribution function of nitrogen in a shock wave, Phys. Fluids, Vol. 9 (1966), p. 653-662.

## Nonequilibrium Kinetics of Diatomic Molecule Dissociation \*

O.G. Buzykin, N.K. Makashev, V.I. Nosik

Dep. of Fundamental Research, Central Aerohydrodynamic Institute, Zhukovsky, Russia

The rates of chemical reactions between the vibrationally excited particles depend on the particle distribution over vibrational levels. Because these distributions are generally different in various kinds of gas flow, the fact is not surprising that the difference between theoretically predicted and experimental rates or between the experiments carried out in different flows is usually significant. The description of such a situation becomes simpler when the time of vibrational relaxation  $\tau_v$  is much less than the flow time  $\Theta$ .

$$\tau_v \ll \Theta \quad (1)$$

In this case the rate constants are usually considered to be functions of the local gas temperature. Nevertheless, in certain situations the validity of condition (1) is not sufficient for this simple relationship. Specifically, this situation takes place in presence of considerable temperature gradient for reactions with high energy thresholds (e.g. dissociation), because for such reactions the vibrationally excited particles are responsible for the main contribution in the reaction rate. The reason is that the high-energy tails of vibrational distribution function in non-uniform gas may significantly differ from ones in a uniform gas due to convective or diffusional transfer of molecules in non-uniform field of gas temperature. The theory of these phenomena is developed in [1] - [8] along with appropriate asymptotic methods for the solution of master equations of vibrational level kinetics. There was proved that under the conditions (1) and

$$\nabla \ln F_i \ll \nabla \ln Y_i^0, Y_i = F_i Y_i^0 \quad (2)$$

a strong non-equilibrium and still local solution can be obtained for the vibrational distribution function  $Y_i$  (superscript 0 denotes the local equilibrium distribution). As a result the dissociation rate constant was found to be in exponential dependency not only on the local gas temperature but also on the local temperature gradient [1] - [4].

It should be noted that in strong non-equilibrium a number of two-temperature models of dissociation kinetics are usually used (Marrone-Treanor, Losev, Park, Macheret-Rich-Fridman, Brun and others). However, these models can not correctly describe the non-equilibrium phenomena, when the influence of diffusional transfer of highly excited molecules on the rate of dissociation is considerable. For example, this may be essential in boundary or viscous shock layers.

Recently authors have obtained some new results in the theory of high energy tails of distribution functions and of the rates of high threshold reactions. It was shown that the presence of reactions between the molecules on the low vibrational levels (e.g. exchange reaction in air) reduces the effect of the gas temperature gradient on the dissociation rate. But in this case the effect under consideration can be also significant [5]. The dependence of diffusion coefficient on the vibration level number, which is due to the cross-section varies along with the molecule excitation, weakly influences on the our non-equilibrium correction for dissociation rate [6]. The vibrational unharmonism of real molecule slightly reduces the value of the correction [4]. VV-exchanges weakly influences on the non-equilibrium correction because of reduction of the exchange probability for upper levels due to molecular unharmonism [7]. The expression for the dissociation rate of unharmonic oscillator in two-temperature boundary layer depending on the gradients of vibrational and translational temperatures was obtained [8].

The importance of non-equilibrium corrections in the boundary layer flow was investigated in [1], [9]. For the small admixture of dissociating nitrogen in argon the effect was found to be maximum for the catalytic surface [1]. For the dissociation of pure nitrogen this effect is considerable for non-catalytic surface [9]. However, it should be noted that this conclusions were made by use of the local non-equilibrium solutions of vibrational level kinetic equations which are not valid in boundary layer near the surface, where the conditions (1) and

\* Abstract 5088 submitted to the 21st International Symposium on Rarefied Gas Dynamics, Marseille, France, July 26-31, 1998

(2) are not satisfied due to low surface temperature and high temperature gradient. More exact result can be obtained by solving of master level equation in coupling with boundary layer equations. The existing solutions of master vibrational level equations in boundary layer (Doroshenko at al., Capitelli at al.) ignore backward influence of non-equilibrium vibrational energy distribution on macroscopic rate constant.

The models were offered to take such interaction into account [10]. It was supposed that level dissociation probability is proportional to  $C(T) \exp(E_i/kU(T))$ . Constants  $C(T)$  and  $U(T)$  were selected to ensure a best fit to the experimental data for dissociation of nitrogen behind the shock wave.

The gasdynamic parameters of boundary layer in nitrogen flow were calculated by means of this models [11]. It was shown that the internal energy distribution is strongly nonequilibrium and differs from Boltzman or Treenor ones. Various variants of level models give close results. In the same time various two-temperature models give a different vibration temperature and heat flux on non-catalytic for vibration relaxation surface. Heat flux on the surface in level kinetics approach is 10-15% higher than in two-temperature approach.

Taking into account for the effect of non-equilibrium vibration energy distribution on the dissociation rate by use of vibrational level kinetic approach weakly influences upon the distributions of velocity, translation temperature, density and degree of dissociation over the boundary layer thickness. Though both dissociation and the recombination rates in such approach greatly differ from that given by macroscopic models, the total reaction rate was found out to be rather indifferent. The heat flux on catalytic for vibrational relaxations surface is 15-20% more then one on non-catalytic for vibration relaxation surface.

Two-temperature models giving acceptable results when the gas temperature drops down, poorly work under the temperature rise. So only the level vibration kinetic approach is capable to describe correctly the flows where are both the decrease and the increase of gas temperature.

This work was supported by the Russian Foundation for Basic Research (Grant No. 95-01-00236 and State Program for Leading Research Group Grant No.96-15-9603).

## References

- [1] Makashev N.K., Provotorov V.P., *Nonequilibrium Dissociation of Diatomic Molecules in Boundary Layer*, Fluid Dynamics, Vol.20, No.1, 1985.
- [2] Makashev N.K., *The Kinetic Theory of the High Threshold Reactions and Dissociation in Gas Flow*, RGD. Proc. of The 19th Int. Symp. 1995, Oxford University Press, V1, pp.3-12.
- [3] Makashev N.K., *Nonequilibrium Dissociation of Diatomic Molecules in Flows with Convective and Diffusion Transfer of Particles*, Fluid Dynamics, Vol.20, No.6, 1985.
- [4] Makashev N.K., Strakhov L.B., *Thermal dissociation of unharmonic oscillator in boundary layer*. Fluid Dynamics, Vol.22, No.5, 1987.
- [5] Nosik V.I., Rastigeev E.A., *Thermal dissociation of diatomic molecules in non-isothermic boundary layer with exchange reactions*, Fluid Dynamics, Vol.30, No.1, pp.133-141, 1995.
- [6] Galkin V.S., Makashev N.K., Rastigeev E.A., *Estimation of the effect of molecular vibrational excitation on their diffusional transfer and dissociation rate in moving gas*. Fluid Dynamics, Vol.31, No.1, pp.144-155, 1996.
- [7] Nosik V.I., *Non-equilibrium thermal dissociation of diatomic molecules with account of VV, VT and VT<sup>1</sup> exchange reactions*. Fluid Dynamics, Vol.29, No.1, pp.133-139, 1994.
- [8] Nosik V.I., *Thermal dissociation of diatomic molecules in a nonisothermal two-temperature boundary layer*. Fluid Dynamics, Vol.31, No.2, pp.325-333, 1996.
- [9] Nosik V.I., *The Effect of Nonequilibrium Dissociation on Boundary Layer Flow*, Fluid Dynamics, Vol.30, No.4, pp.629-637, 1995.
- [10] Buzykin O.G., Nosik V.I., *Simulation of Vibration-Dissociation Interaction*, Fluid Dynamics, Vol.31, No.6, pp.920-927, 1996.
- [11] Buzykin O.G., Nosik V.I., *The Effect of Nonequilibrium Vibration on Dissociation and Boundary Layer Flow*, Fluid Dynamics, 1998, in press.

# Translational and Rotational Energy Relaxation in Free Jet Expansion of Polyatomic Gas \*

A.V. Lazarev<sup>1</sup>, V.M. Zhdanov<sup>2</sup>, N.N. Zastenker<sup>1</sup>, D.N. Trubnikov<sup>1</sup>

<sup>1</sup>Moscow State University, Moscow, Russia

<sup>2</sup>Moscow Engineering Physics Institute, Moscow, Russia

In the present work consequent asymptotic analysis of moment equations for polyatomic gases, following from Wan Chang-Uhlenbeck kinetic equation, is developed on the assumption of weakly nonequilibrium jets. This allows to obtain sufficiently simple analytical expressions for parameters on the centerline of an axisymmetric free jet. In particular, dependencies of parallel  $T_{||}$ , perpendicular  $T_{\perp}$  and rotational  $T_r$  temperatures on conditions in source and rotational collision number  $Z$  have the form

$$\frac{T_i(r)}{T_0} = (1.046 \cdot 10^4)^{-\frac{12}{5j+11}} \Phi_i(r; j, Z) \times \left( \frac{\epsilon}{kT_0} \sigma^6 \right)^{-\frac{4}{5j+11}} \left( \frac{p_0 D}{T_0} \right)^{-\frac{12}{5j+11}},$$

where  $i = ||, \perp$  or  $r$ ;  $T_0$  (K),  $p_0$  (torr) are temperature and pressure in source;  $D$  (cm) is the nozzle orifice diameter;  $j$  is the number of rotational degrees of freedom;  $k$  is Boltzmann constant;  $\epsilon$  (erg) and  $\sigma$  (Å) are Lennard-Jones potential parameters;  $\Phi_i(r; j, Z)$  are functions of  $r$  and  $Z$  independent of source conditions and universal for any gas with given  $j$ , which form is given in [1].

The concrete calculations are performed for  $N_2$  ( $j = 2$ ;  $\epsilon/k = 91.5$  K;  $\sigma = 3.681$  Å). Fig.1 shows comparison of calculated and experimental dependencies of terminal rotational temperature  $T_r(\infty)$  on  $n_0 D$  ( $n_0$  is number density in source) with use of the results of works [2] and [3]. Curve 1 was calculated in [2] on the base of linear equation of rotational energy relaxation for  $Z_r = 3$ . Calculation by our formula with  $Z=9$  gives curve 2. The distinction in determination  $Z_r$  in [2,3] and  $Z$  of the present work should be noted.  $Z_r$  is defined in [2] and [3], as well as in many other papers, by relation

$$Z_r = \tau_r \cdot \nu_{rs},$$

where  $\tau_r$  is rotational relaxation time,  $\nu_{rs} \sim T^{-1/6}$  is the collision frequency for rigid sphere potential. This relation does not take into account real behavior of  $\nu_{rs}$  at low temperatures, which for Lennard-Jones potential is  $\nu_{L-D} \sim T^{1/6}$ . Such difference in determination of frequencies leads to lowered values of rotational collision number, defined experimentally in jets. A reason of divergence of theory and experiment at small  $p_0 D$  is apparently nonequilibrium both at translational and rotational degrees of freedom which increases with decreasing  $p_0 D$ .

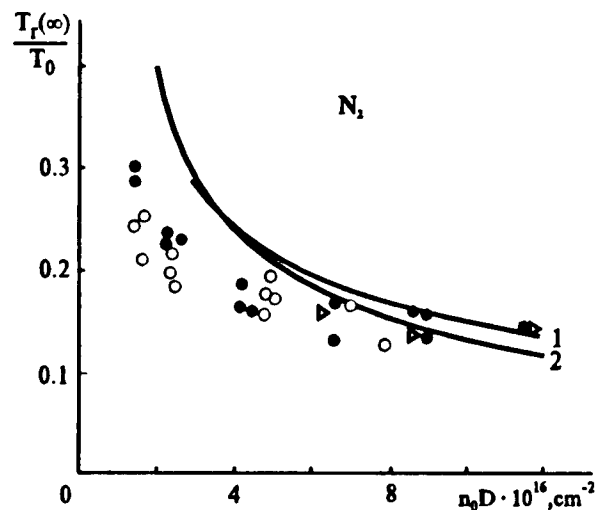


Figure 1: Dependence  $T_r(\infty)/T_0$  on  $n_0 D$ :  
• - experiment [2] ( $T=300$  K); ○ - experiment [2] ( $T=600$  K); 1 - theory [2]; 2 - the present work for  $Z=9$ ; ▴ - calculation [3] for data [2].

\* Abstract 5135 submitted to the 21st International Symposium on Rarefied Gas Dynamics, Marseille, France, July 26-31, 1998

## References

- [1] Lazarev A.V, Zhdanov V.M., Zastenker N.N. Trubnikov D.N., *Relaxation of rotational energy in supersonic gasdynamical jet expanding into vacuum*, J. of Applied Mechanics and Technical Physics, Vol.38, No.5, pp.65-72, 1997. - in Russian
- [2] Poulsen P., Miller D.R., *The energy balance and free jet expansions of polyatomics*, Proc. 10th Int. Symp. on Rarefied Gas Dynamics, J.L. Potter, ed., AIAA, New York, 1977, Part 2, pp.899-911.
- [3] Lang H., *Rotational and translational relaxation in free jet expansions*, Proc. 11th Int. Symp. on Rarefied Gas Dynamics, R. Camparque, ed., Paris, 1979, Vol. 2, pp.823-832.

## Kinetic Models of Diatomic and Inert Gas Mixtures \*

M.A. Rydalevskaya  
St.-Petersburg University, Russia

The investigation of quazi-stationary nonequilibrium states of vibrationally relaxing diatomic and inert gas mixtures is very important in connection with the problems of chemical technology, laser physics, high-velocity and high-temperature gasdynamics.

This problem is investigated by application of the kinetic equations. Different molar correlations of the diatomic gas with rotational and vibrational degrees of freedom and inert gas mixture are considered.

The kinetic equations for the distribution functions are written in the following dimensionless form

$$Df_1 = \frac{1}{\varepsilon_1} J_1^I + J_1^{II},$$

$$Df_{2vr} = \frac{1}{\varepsilon_2} J_{2vr}^I + J_{2vr}^{II}.$$

Here  $f_1(\mathbf{r}, \mathbf{u}, t)$  is distribution function of atoms;  $f_{2vr}(\mathbf{r}, \mathbf{u}, t)$  is distribution function of molecules,  $v$  is a level number of molecular vibrational energy  $\varepsilon_{2v}$  (the anharmonic oscillator model is used),  $r$  is a level number of rotational energy  $\varepsilon_{2r}^{(v)}$ ;  $J^I$  are the most frequent collision operators;  $\varepsilon = \tau^I/\theta$ , where  $\tau^I$  are the characteristic times between collisions  $I$ ,  $\theta$  is the flow time (it has been assumed that  $\tau^I \ll \theta$ );  $J^{II}$  are the infrequent collision operators.

As it was assumed in paper [1], the following stages of relaxation may be defined:

1. The collisions  $I$  include only  $TT$  (elastic) and  $TR$  (translation-rotation) exchanges;
2. The collisions  $I$  also include  $TV$  (translation-vibration) exchanges if relative defect of vibrational energy resonance  $\alpha \leq 1/8$ ;
3. The collisions  $I$  also include  $TV$  exchanges if relative defect of resonance  $\alpha \leq 1/4$ ;
4. The collision  $I$  include also  $TV$  exchanges if relative defect of resonance  $\alpha \leq 1/2$ ;

5. The collision  $I$  include all exchanges.

The additive invariants of the collisions  $I$  at the stages of relaxation 2 – 4 are determined. The solutions of suitable equations

$$J_1^I = 0,$$

$$J_{2vr}^I = 0$$

are obtained. It is shown that these solutions depend on ratio  $n_2/n_1$  ( $n_1$  ( $n_2$ ) is the number of atoms (molecules) in the unit of volume). The influence of the value  $n_2/n_1$  on nonequilibrium quazi-stationary vibrational distribution functions of diatomic gas is investigated.

If  $n_2 \sim n_1$  or  $n_2/n_1 > 1$ , the nonequilibrium relative populations of vibrational levels coincide with ones from [1] (in that paper nonequilibrium stages 2 – 4 of vibrational relaxation in chemically homogeneous gas of anharmonic oscillators were considered).

If  $n_2/n_1 \ll 1$ , the nonequilibrium vibrational distribution functions at the stages 2 – 4 of relaxation differ from appropriate distributions in chemically homogeneous gas. In this report new nonequilibrium distribution functions of vibrational levels populations at the different values  $n_2/n_1$  are obtained.

The concrete examples of nonequilibrium distributions in gas mixtures are presented. The closed systems of gasdynamic equations at different stages of vibrational relaxation and different values  $n_2/n_1$  are derived and investigated.

## References

- [1] Rydalevskaya M.A., *Relaxing Gas of Anharmonic Oscillators. Kinetics and Gasdynamics*, Rarefied Gas Dynamics 19. Oxford, New York, Tokyo: Oxford University Press, 1995. P. 578-582.

\*Abstract 5146 submitted to the 21st International Symposium on Rarefied Gas Dynamics, Marseille, France, July 26-31, 1998

# Transport Processes at Different Stages of Vibrational Relaxation Gases \*

M.A. Rydalevskaya, T.V. Ryabikova  
St.-Petersburg University, Russia

Transfer processes in vibrationally relaxing pure diatomic gas are considered on the basis of the kinetic equations for the distribution functions.

We have used the kinetic equations for the distribution functions  $f_{vr}(\mathbf{r}, \mathbf{u}, t)$

$$Df_{vr} = \frac{1}{\varepsilon} J_{vr}^I + J_{vr}^{II}.$$

Here  $v$  is a level number of vibrational energy (we used the anharmonic oscillator model);  $Df_{vr}$  is a differential operator;  $J_{vr}^I$  is the most frequent collision operator (it corresponds to the rapid stage of the process);  $\varepsilon = \tau_I/\theta$  ( $\tau_I$  is characteristic time between collisions  $I$ ,  $\theta$  is flow time,  $\tau_I \ll \theta$ );  $J_{vr}^{II}$  is the infrequent collision operator (it corresponds to slow stage of process).

By rapid collisions we mean  $TT$ ,  $TR$ ,  $RR$  - exchanges of translational and rotational energy. Besides as well as in [1] there are  $VV$  and  $VT$  - exchanges if the relative defect of vibrational energy resonance is less than some parameter  $\alpha$  ( $0 < \alpha < 1$ ). We consider the following nonequilibrium conditions: the collisions  $I$  include the exchanges of vibration energies if  $\alpha = 1/8$ ,  $\alpha = 1/4$  and  $\alpha = 1/2$ . In the previous paper [1] the additive invariants connected with rapid energy exchanges were determined. In the same paper the system of gasdynamic equations for the minimal number of macroscopic variables, enabling describe gasdynamics and vibrational relaxation of a flow in a closed form, was obtained.

In this report we get the distribution functions in the zero and first approximations of the generalized Chapman - Enskog method. In the first approximation the pressure tensor, the heat flux vector and the flux vector of a complementary additive invariant  $\psi_\alpha(v)$  are obtained. (The invariant  $\psi_\alpha(v)$  was presented in [1]). The both flux vectors must be expressed in the terms of intensive parameters adjoint to extensive gasdynamic parameters. It al-

lows to define the coefficients of heat conductivity at the different nonequilibrium stages of vibrational relaxation of anharmonic oscillators better. In the report all transport coefficients are determined by the corresponding integral brackets. They depend on the cross - sections of the most frequent collisions  $I$  only. It is shown that Onsager symmetry of transport coefficients is valid at each nonequilibrium stage of vibrational relaxation. This fact follows from the symmetry of the integral brackets, connected with additive invariants of collisions.

For example, the coefficients of heat conductivity in  $N_2$  at different stages of vibrational relaxation are calculated in a wide range of temperature changing. In the report the figures depicted the coefficients of heat conductivity in  $N_2$  are presented.

## References

- [1] Rydalevskaya M.A., *Relaxing Gas of Anharmonic Oscillators. Kinetics and Gasdynamics*, Rarefied Gas Dynamics 19. Oxford, New York, Tokyo: Oxford University Press, 1995. P. 578-582.

\*Abstract 5147 submitted to the 21st International Symposium on Rarefied Gas Dynamics, Marseille, France, July 26-31, 1998



## The Modeling of Thermal Non- Equilibrium Chemical Reactions in Gas Dynamics \*

A. L. Sergievskaya, S. A. Losev, E. A. Kovach  
Moscow State University, Russia

The description problem of chemical reacting system without thermal equilibrium between vibrational and translational degrees of freedom of reacting molecules is considered. This lead to concept of multi-temperature chemical kinetics of gases in thermal non-equilibrium.

The scientific research KINTVT system is dedicated to ensure the information, logical and computer support for mathematical modeling in thermal non-equilibrium kinetics. The basis of this system concept is the integration of information fund (databases), base of models being investigated and research software component being used for computer experiment.

The level of modeling represent microscopic, kinetics and macroscopic description of gas. The vibrational temperature  $T_v$  concept for real conditions in non-equilibrium gas is justified using results of collisional dynamics numerical solutions. This concept provides the possibility of macroscopic description of thermal non-equilibrium gas.

Non-equilibrium factor  $Z(T, T_v) = k(T, T_v) / k^*(T)$  provides a relative measure of non-equilibrium rate constants  $k(T, T_v)$  of processes in investigated gases. The summary information on non-equilibrium factor modeling is presented including description of diatomic molecules dissociation, bimolecular reactions of chemical exchange, decay of polyatomic molecules.

There are many semi-empirical and theoretical based models for description of two-temperature rate constant. This models are based on different assumptions. Early non-equilibrium dissociation models of Hammerling, Losev, Treanor and Marrone, Park are constructed on base of the most general representation about role of vibrational excitation in dissociation. In these models the simple empirical dependencies and parameters, enabling to receive the simple analytical expressions for  $Z(T, T_v)$ , participate.

The more exact models are built with account anharmonic properties of excited molecules and on the basis of analysis of VT- and VV-exchanges (for example, Kuznetsov model and Gordiets model). Macheret-Fridman model considerate the direct dissociation from the bottom of the potential well which is important for high temperature.

At the modeling of non-equilibrium factor in research KINTVT system on level of condition of applicability the hierarchy of information support of mathematical models is formulated. Some models can be realized at minimum information support about vibrational-excited particles, other models require more detailed information about particles and about appropriate thermal reactions. The most advanced models require data for structure and properties of all components of gas, in which the non-equilibrium reaction occurs.

---

\* Abstract 5166 submitted to the 21st International Symposium on Rarefied Gas Dynamics, Marseille, France, July 26-31, 1998

The different theoretical justification of these models is discussed. The simplest and sufficiently adequate models of non-equilibrium factor are recommended.

Flows behind shock waves front and in supersonic cooling are the examples of two-temperature media. The results of the two-temperature models implementation for molecular vibrational excitation, dissociation and chemical exchange in thermal non-equilibrium flows are used in application gasdynamics problems.

The expert training of the above mentioned analytical and numerical models makes possible to extrapolate chemical rate constants and vibrational relaxation times for air components to very high temperature (up to 90000 K). By this means the mechanism of thermochemical non-equilibrium kinetics in strong shock waves on air and flows characteristics behind shock wave front have been obtained. Using chemical sensitivity analysis methods we can form the minimum synergetic description of non-equilibrium gas medium for user goal function. It is important for solution of complex problems in hypersonic aerothermodynamics.

The results of non-equilibrium kinetics investigation in high-temperature (up to 40000 K)  $\text{CO}_2 / \text{N}_2$  mixture behind strong shock waves modeling vehicle flight in Martian atmosphere are presented.

# Stochastic Simulation Method and Nonequilibrium Phenomena in Collisional Media \*

G.I. Zmievskaya

Keldysh Institute of Applied Mathematics of RAS, Moscow, Russia

## 1 Introduction

In many technology problems require numerical analysis of fast collisional processes. The stochastic simulation method (SSM) is based on the strict results of the probability analysis of mathematical physics equations, the kinetic theory of plasmas and rarefied gases, and the theory and practice of the numerical experiment in the nonlinear discrete plasma simulations. SSM makes it possible to study the particle velocity distribution functions (DF) in laser, space and thermonuclear non-equilibrium plasmas. Inelastic collisions in partially ionized gases can be modelled by jump like and diffusion Markovian processes (MP). The processes, which are responsible for the variation in the population of the energy levels of molecular or multicharged ions, are described by equations of the Boltzmann (BE) [1] type, while characteristic plasma collisions are described by the Fokker-Planck-Landau (FPL) equation [2]. The evolution of the MP is determined by numerical solution of set of the Itô stochastic differential equation (SDE):  $\frac{dX}{dt} = \mathcal{A}(t, X) + \mathcal{B}(t, X)dW(t)$ ,  $X|_{t=0} = X_0$ ,  $t \geq 0$ , where  $\mathcal{A}(t, X)$ ,  $\mathcal{B}(t, X)$  are the given nonlinear functions, and  $W(t)$  is the random function with a pointwise and continuous measures (see ref.9-13, 21-26 in[1]),  $W(t)$  process has no mean-square derivative, and  $dW$  is not a differential in any standard sense. The author has developed kinetic models of collisions with the Markovian properties, has proved the applicability of the Itô and Itô-Stratonovich SDE as a stochastic analog of the modeled processes in specific applications. The efficient stable algorithms for solving the sets of SDE have been modified to code PLASCOL and code NICOL, so that these could be used for solving the applied problems.

## 2 Mathematical model

Many of the physical phenomena, which exhibit the probability nature, can be described by models based on the kinetic equation

$$\frac{\partial f}{\partial t} = \mathcal{L}(f), \quad (1)$$

where  $\mathcal{L}$  is the nonlinear integro-differential operator. In the kinetic theory, the subject of study is the one-particle DF  $f(x, v, t)$ , which is function of the phase coordinates  $\{x, v\}$ , where  $v$  is the velocity and time  $t$ . The operator  $\mathcal{L}$  is able to be presented as a sum of linear  $\mathcal{L}^0$ ,  $\mathcal{L}^j$  and non-linear (BE) parts:  $\mathcal{L}(f) = \mathcal{L}^0(f) + \mathcal{L}^j(f) + \mathcal{L}^B(f)$ , where

$$\mathcal{L}^0(f) = - \sum_{k=1}^N \frac{\partial}{\partial x_k} a_k(x, t) \quad (2)$$

and

$$\mathcal{L}^j(f) = \frac{1}{2} \sum_{k=1}^N \sum_{j=1}^N \frac{\partial^2}{\partial x_k \partial x_j} b_{kj}(x, t) \quad (3)$$

The state of the discrete medium changes  $\{\vec{X}\} \rightarrow \{\vec{X}'\}$  as a result of jumps (collisions) or (and) fluctuation stochastic processes in the phase space  $\{\mathcal{R}^N\}$  during the time interval  $\Delta t$

We write down the 1D Itô SDE for the variable velocity (here we use the scalar quantity  $\xi$  instead of  $\vec{V}$  in order to simplify the equations of the stochastic analog) and out of spatial coordinate  $r$ ; both quantities depend on time  $t$ . On the basis of definition of the stochastic Itô integral we have

$$\xi_t = p + \int_{t_0}^t \mathcal{A}_\tau d\tau + \int_{t_0}^t \mathcal{B}_\tau dw_\tau + \int_{t_0}^t \int_{\mathcal{R}} \mathcal{C}(t, x) \Delta \mathcal{P}^0(t, dx) \quad (4)$$

with the initial condition  $\xi(t = 0) = p$  and  $t > t_0$ . Here  $\mathcal{A}_t = \mathcal{A}(t, X(t))$ ,  $\mathcal{B}_t = \mathcal{B}(t, X(t))$ ,  $\mathcal{C}_t = \mathcal{C}(t, X(t))$  are the given nonlinear functions,  $w_t$  is a one-dimensional Wiener process in phase space

\*Abstract 5306 submitted to the 21st International Symposium on Rarefied Gas Dynamics, Marseille, France, July 26-31, 1998

$\mathcal{R}$ , and  $\Delta\mathcal{P}^0(t, dx)$  is the change in the centered pointwise Poisson process  $\mathcal{P}^0(t, dx)$  in the space  $\mathcal{R}$ . The bounds of the range of definition of the MP  $X(t)$ ,  $t \geq 0$  are determined by conservation of energy and momentum of colliding particles. It is seen in (4) that functional coefficients of the SDE depend on the mathematical expectation of the stochastic process  $\{X(t)\}$ .

Two-dimensional Itô-Stratonovich SDE for plasma particles of the  $\alpha$  species  $\vec{V}_\alpha$  are :

$$\begin{aligned} d\vec{V}_\alpha(t) &= \vec{A}_\alpha(\vec{V}(t), t)dt + \mathcal{B}_\alpha(\vec{V}(t), t)dW(t), \quad (5) \\ \vec{V}_\alpha(t)|_{t=0} &= \vec{V}_\alpha^0(t), \quad t \in [t_0, T], \\ \vec{V}_\alpha(t) &= \{V_x^\alpha(t), V_y^\alpha(t)\}^T; \quad \alpha = e, i \end{aligned}$$

where  $\vec{A}(t, \vec{V}(t))$  is the column-vector of the drift function,  $\mathcal{B}(t, \vec{V}(t))$  - is the  $2 \times 2$  diffusion matrix, and  $W(t)$  is the Wiener stochastic process. The relation between coefficients of the FPK equation ( $a_i^\alpha, b_{ij}^\alpha$ ) and coefficients  $\mathcal{A}$  and  $\mathcal{B}$  of the SDE (5) is follows:

$$\vec{A}_i^\alpha(t, \vec{V}(t)) = a_i^{\alpha T}(t, \vec{V}(t)) - \frac{1}{4} \sum_{j=1}^2 \frac{\partial b_{ij}^\alpha(t, \vec{V}(t))}{\partial V_j}, \quad (6)$$

$$\mathcal{B}_{ij}^\alpha \mathcal{B}_{ji}^\alpha = b_{ij}^\alpha(t, \vec{V}(t)) \quad (7)$$

Matrix equation (6) shows that the Stratonovich form is used to find this relation (see ref.14, 26-27 in [1]).

Such representation of the SDE coefficients is very important, since, in this case, the algorithm is stable. In addition, it is necessary to determine, whether the sign of the quadratic form of the diffusion matrix  $a_{ij}$  is positive, and define more exactly the boundaries of the region of existence of the solution corresponding to the MP.

The numerical method for solving the nonlinear SDE is based on the expansion of the exact solution in the stochastic Taylor series with respect to two components of the vector variable  $\vec{V}(t + \Delta t)$ .

Modern stable algorithms for solving SDE with the functional coefficients (namely : "weight" scheme for BE as well the optimal "filtering" of diffusion processes for FPK and FPL, Stratonovich form of Itô integral et all.) make it possible to study the nonlinear mechanisms of collisional processes in nonequilibrium media.

### 3 Results

Computer experiments confirmed some features of the nonequilibrium processes in gases and plasmas, which were previously deduced from the analysis of one-particle DF in velocity:

- rapid thermalization of the neutral gas in a hot plasma through the resonant charge exchange;
- freezing of the nonequilibrium electron DF in the uniformly expanding partially ionized gas;
- appreciable deviation of the velocity DF of the molecular hydrogen in the electron- excited state from the equilibrium distribution, when the excitation of the noble gas in the discharge is quenched by the two-atomic molecule.

We have studied the parameters of the discharge, in which the vibrational states of gas molecule can be excited, which is the necessary condition for the efficient dissociative attachment of the low-energy electrons to a molecule.

In analyzing the multicharged ions, which are promising for creation of a UV laser, an effect was discovered of

- inverse population of the "working" levels of the hydrogen-like carbon ions in the colliding flows of the laser plasma;
- in the multicharged ion plasma confirmed the role of cooling the plasma electrons as necessary condition for the lasing effect, as it is follows from the results of laboratory experiments;
- the results of computer experiments take into account the resonance charge exchange;
- the results depend on the degree of phase space intermixing by collisions.

The numerical model based on the diffusion MP is developed for the fluctuation stage of the condensation of the water vapor. The nonstationary size distributions of clusters are obtained, which characterizes the mechanism of phase transition.

### 4 Conclusion

SSM was used for simulation of the kinetic phenomena in the plasma of the multicharged carbon ions (see ref.37-39 in [1]) for studies of the efficiency of the dissociative decay of the gas molecules (see ref.9,13,53 in [1]), for modeling the fluctuation stage

of the phase transition of the first kind in the supersaturated water vapor (see ref.12.14.67 in [1]) as well the initial stage of cavitation, and for modeling the clusterization of defects of the crystal lattice (see ref.66.73 in [1]). Areas of applicability of SSM using the kinetic codes NICOL and PLASCOL are large enough.

The work is partly supported by the Russian Foundation for Fundamental Research, grant 97-02-17627.

## References

- [1] Zmievskaya G.I., Plasma Physics Reports, Vol.23, pp.368-382, 1997.
- [2] Zmievskaya G.I., in: *Discrete Modelling of Plasma*, Sigov, Yu.S., Ed., Moscow: Keldysh Inst.Appl.Math., 1990.

## An Heuristic Model for Interatomic Potential \*

V. Sankovitch

Dept. Fisica Fundamental, UNED, Madrid, Spain

The formal examination of the elementary interaction between atoms (or molecules) is usually carried out by means of an interaction potential, fictive function of the distance between the interacting atoms. Often, however, this function is not sufficient to allow the understanding of the observed phenomenon. So, for example, in the case of heterogeneous catalysis, we have a "complex" interaction and observe a whole set of such phenomena: reagents adsorption on the metal surface, their activation, chemical reaction, and finally the desorption of the reagents and the reaction products. These last ones abandon the surface, as experiments show, in a strongly excited state and with a high velocity, much superior to the thermal velocity corresponding to the metal temperature. All these phenomena depend on the metal temperature and on the energy of the reagent molecules falling onto the surface. It is not possible to understand all this set by the "realistic" potential curve without the introduction of complementary ad hoc hypothesis for each of this phenomena.

practice and therefore they are not a special interest. The author looks upon this attempt only as a "ballon d'essai", allowing to judge the possibility of such superposition, which would facilitate the understanding of all above-mentioned phenomena.

The author proposes to displace slightly the accent of the problem and to examine the interaction issue with regard to the wave structure of the atom field, which, contrarily to a potential, really exists. This approach seems, to the author's mind, justified also because, strictly speaking, the concept of potential is not applicable to the atom : its electromagnetic field is not potential. A "realistic" potential obtained on the base of various experimental data, undoubtedly contains in itself the information about the actual field of the interacting atoms. Therefore, as a first approximation to this issue, it was used as true energy profile for an hypothetical atom field. The well-known potential curves for inert gases were presented, with quite a good precision, as the superposition of two waves of the type  $(a/r^3) \sin(b/r^3)$  or  $(a/r^4) \sin(b/r^2)$ . The formulas are not in themselves any better, nor worse, than all other approximations used in the nowadays

---

\* Abstract 5366 submitted to the 21st International Symposium on Rarefied Gas Dynamics, Marseille, France, July 26-31, 1998

# Further Evaluation of a Model of Collisional Dissociation \*

R.G. Lord<sup>†</sup>

Department of Engineering Science  
Oxford University, England

## 1 Introduction

A model of dissociation of diatomic molecules in intermolecular collisions, for use in Direct Simulation Monte Carlo calculations, has been proposed by Lord [1]. This model is a development of the exact available energy or vibrationally-linked chemistry model of Bird [2], which models dissociation via Borgnakke-Larsen type energy redistribution between translation and internal modes, dissociation being assumed to occur whenever the vibrational energy of a molecule exceeds its dissociation energy.

However, Bird assumes the existence of discrete energy levels above the dissociation limit, which is unrealistic; furthermore, the dissociation probability is found to depend on the (arbitrary) spacing assumed for these levels [3], [4]. In fact, the discrete vibrational levels all lie below the dissociation energy and a continuous spectrum of dissociated levels lies above it. Unfortunately, Bird's method cannot be used without modification with this more realistic energy level scheme because the existence of an infinite density of dissociated states leads to the prediction of dissociation in every collision in which sufficient energy is available.

Lord's model overcomes this problem by introducing the constraint that only the kinetic part of the energy of vibration is exchanged in collisions. This model, when used in conjunction with the energy level scheme of a Morse oscillator, has been shown to yield equilibrium dissociation rate constants for N<sub>2</sub> which are in excellent agreement with published values and to exhibit vibrational favouring of dissociation [1]. However, as pointed out by Wadsworth and Wyson [5], the predicted rate constant is dominated by the collision selection algorithm and is thus a rather poor measure of the validity of a model.

The aim of the paper is to present the results of

more stringent tests on the model, and to make more detailed comparisons with other dissociation models. Particular attention will be paid to the phenomenon of vibrational favouring of dissociation, as evidenced by the variation of the rate constant with vibrational temperature at constant transrotational temperature, the dissociation probabilities from different vibrational energy levels for a given collision energy and the pre-collision energy distributions of molecules which become dissociated.

Consideration will also be given to oxygen and hydrogen molecules in addition to nitrogen, and to the sensitivity of the predictions to the precise shape of the assumed interatomic potential.

## 2 Preliminary results

Figure 1 shows dissociation probabilities predicted by the model for a nitrogen molecule in collision with a second molecule at various total collision energies (transrotational and vibrational) greater than the dissociation energy. The procedure used here is the serial procedure, in which the vibrational energy of the second molecule does not contribute to the exchange, but complete exchange is allowed between the kinetic energy of vibration of the first molecule and the transrotational energy of the collision. The probability of dissociation is plotted against the vibrational energy of the molecule before collision and can be seen to approach unity in each case as this energy approaches the dissociation energy.

Figure 2 shows the pre-collision vibrational distribution of nitrogen molecules which become dissociated in a gas in equilibrium at 10000K, compared with the equilibrium vibrational distribution of all molecules at this temperature. The quantity plotted is the normalized frequency of each vibrational level. In this case the colliding molecules were considered together and the vibrational kinetic energies of both molecules contributed to the exchange. The graph clearly demonstrates the vibrational favour-

\* Abstract 5622 submitted to the 21st International Symposium on Rarefied Gas Dynamics, Marseille, France, July 26-31, 1998

ing which is inherent in the model.

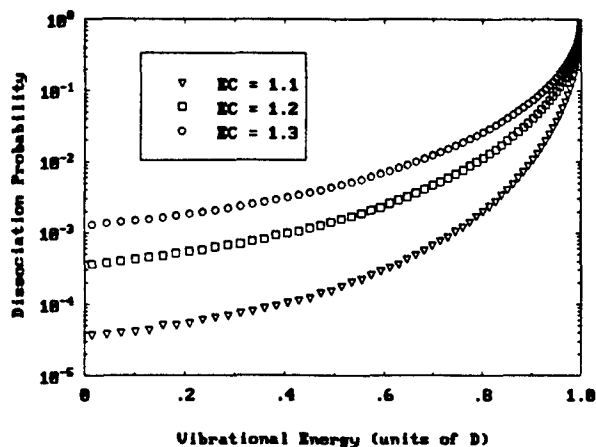


Figure 1: Dissociation probabilities of nitrogen

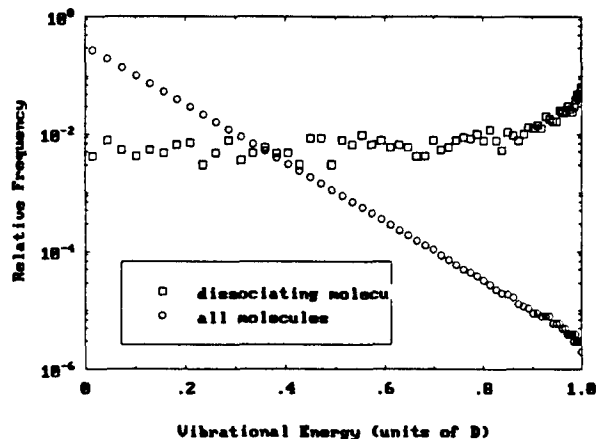


Figure 2: Pre-collision vibrational energy distributions of nitrogen molecules at 10000K

## References

- [1] Lord R.G., *Modelling dissociation of diatomic molecules using the Morse Potential*, in *Rarefied Gas Dynamics 20*, ed Ching Shen, Peking University Press, Beijing, 1997, pp.180-185.
- [2] Bird G.A., *Molecular Gas Dynamics and the Direct Simulation of Gas Flows*, Oxford University Press, 1997, pp.2451-251.
- [3] Carlson A.B. and Bird G.A., *Implementation of a Vibrationally Linked Chemical Reaction Model*, in *Rarefied Gas Dynamics 19*, ed J.K. Harvey and R.G. Lord, Clarendon, Oxford, 1995, pp.434-440.

- [4] Wadsworth D.C. and Wysong I.J., *Examination of DSMC Chemistry Models: Role of Vibrational Favoring*, in *Rarefied Gas Dynamics 20*, ed Ching Shen, Peking University Press, Beijing, 1997, pp.174-179.
- [5] Wadsworth D.C. and Wysong I.J., *Vibrational Favoring Effect in DSMC Dissociation Models*, *Physics of Fluids* (to appear).



# Dissociation Rate Constants of $O_2$ , $N_2$ , $NO$ , $CO$ , $CN$ , $C_2$ and $CO_2$ -Molecules in Thermally Equilibrium Conditions at Temperatures 300 – 40000K \*

L.B. Ibraguimova, G.D. Smekhov, O.P. Shatalov  
Institute of Mechanics, Moscow State University, Moscow, Russia

The dissociation processes of molecules dictate the structure of relaxation region behind the strong shock waves, for instance, behind the bow shock during hypersonic flow streaming around the bodies moving through the atmospheres. The conditions in chemical relaxation region behind the shock wave may be local-equilibrium or non-equilibrium ones. This is defined by the relation between gas flow parameters behind the surface of discontinuity and dissociation rates of molecules. Dissociation rate constants  $k_0(T)$  are presented as one-temperature function at local-equilibrium conditions because in this case the distribution of molecules over the translational and internal degrees of freedom is defined by single temperature  $T$  named as gas or translational temperature. However a situation often arises when the local-equilibrium conditions don't take place behind the shock wave front. In shock-tube experiments it has been shown the difference exists between the vibrational  $T_v$  and translational  $T$  temperatures at some conditions in gas. It also has been established that vibrational non-equilibrium was the important factor in diatomic molecules dissociation. In these cases the dissociation rate constants of molecules  $k_d$  are controlled by both temperatures,  $T$  and  $T_v$ . The necessity of treatment of molecular dissociation at these conditions caused a great quantity of theoretical models to be created where many-temperature dissociation rate constants were considered. These models were systematized in some reviews (for instance [1]) where  $k_d$  was often presented as:

$$k_d(T, T_v) = k_0 \cdot Z(T, T_v)$$

Here  $Z(T, T_v)$  is non-equilibrium factor which defines the deviation of distribution over molecular internal degrees of freedom from equilibrium one;  $k_0(T)$  is the equilibrium value of dissociation rate

constant corresponding to thermally equilibrium conditions, i.e.  $k_0 = k_d$  and  $Z = 1$  at  $T_v = T$ .

The aim of the present work was the determination of equilibrium dissociation rate constants  $k_0$  with the reasonable degree of reliability at the wide temperature range.

There are no many of the theoretical models making possible to calculate the absolute values of equilibrium rate constants  $k_0$ . So if there was a necessity to obtain such values the scientist usually would use the experimental data. In doing so he should have the assurance that gas flow conditions in the experiments would correspond to thermal equilibrium process of dissociation. However the extrapolation of these values  $k_0$  to other than measured temperature ranges may come to great errors. This is true for very high temperatures 20000 – 50000K typical for strong shock waves, and also for low temperatures that are marked in cooling gas flows or boundary layers.

To obtain the reliable values of equilibrium dissociation rate constants  $k_0$  at wide temperature range is possible only if we rely on the theoretical models and the experimental data as well. The theoretical models give justified temperature dependence of rate constants and the experimental data make possible to normalize these calculated values of  $k_0$ . This is precisely the method used in the present work. The models of [2] and [3] were used for calculation of  $k_0$ -values. The quantities for normalizing of calculated  $k_0$ -values were taken from data [4,5]. In these works the experiments on dissociation of  $O_2$ ,  $N_2$ ,  $NO$ ,  $CO$ ,  $CN$ ,  $C_2$  and  $CO_2$ -molecules were analysed and the recommended dissociation rate constants were obtained at the temperature range that was not higher than 10000 – 15000K and not lower than 2000 – 3000K. The available data on recombination rate constants at low temperatures were also taken into account. As the result the values of  $k_0$  were recommended for these molecules at temperature range  $T = 300 - 40000K$  and were pre-

\*Abstract 6396 submitted to the 21st International Symposium on Rarefied Gas Dynamics, Marseille, France, July 26-31, 1998

sented as:

$$k_0 = A \cdot T^n \cdot (1 - \exp(-\Theta/T)) \cdot \exp(-D/T)$$

Here  $\Theta$  and  $D$  are the characteristic vibrational temperature and dissociation energy of molecule accordingly,  $A$  and  $n$  are the parameters obtained. The analysis of uncertainties of rate constants  $k_0$  was also performed at temperature range in question.

The work was supported by Grant INTAS-RFBR No 95-510.

## References

- [1] Kovach E.A., Losev S.A., Serguievskaya A.L. Chem.Phys.Reports. 1995. Vol.14. No 9. P.1353.
- [2] Kuznetsov N.M. *Kinetics of monomolecular reactions*. Moscow. Nauka. 1982. 221 p.
- [3] Smehkov G.D., Yalovik M.S. Chem.Phys.Reports. 1996. Vol.15. No 4. P.483.
- [4] Ibraguimova L.B. *Recommended values of gas-phase chemical reactions rate constants in the atomic system N-C-O*. Preprints No 29-97; No 30-97. The Institute of Mechanics. Moscow State University. 1997.
- [5] Krivonosova O.E., Losev S.A., Nalivaiko V.P. et al. *Recommended data on the rate constants for chemical reactions between molecules consisting of N and O atoms*. Plazma Chemistry. No 14. Moscow: Energoatomizdat. 1987. P.3.

# Assessment of New Theoretical Information on Rotational Collision Number of Nitrogen at High Temperatures and its Possible Effect on Modeling of Reacting Shocks \*

I.J. Wysong, D.C. Wadsworth  
Hughes STX, Air Force Research Laboratory,  
Propulsion Sciences Division, Edwards Air Force Base, California USA

Rotational relaxation of a bulk gas is usually quantified in terms of a characteristic rotation time ( $\tau_R$ ) or rotational collision number  $Z_R$ .  $Z_R$  is approximately equal to  $1/n$  where  $n$  is the number of collisions required to reach equilibrium. Many studies have produced predictions of  $Z_R$  and its variation with temperature, with nitrogen the molecule most commonly examined. A study by Parker [1] used a simplified (2D) classical model of rotation to derive predictions for the value of  $Z_R$  and its dependence on temperature for diatomic molecules for the case of no initial rotation. The resulting expressions for the rotational energy gained per collision and  $Z_R(T)$  depend on several poorly-known parameters representing the intermolecular potential and are generally used with an empirically adjusted value. Lordi and Mates [2] have extended Parker's analysis to obtain  $Z_R(T)$  for initially rotating nitrogen molecules.

Lordi and Mates, and others, have shown that, when a gas departs significantly from equilibrium,  $Z_R$  is not well-defined and the apparent rotational relaxation time may vary depending on the type and degree of nonequilibrium. In particular, for a shock case where the initial rotational temperature is very low, the effective value of  $Z_R$  is significantly reduced over the corresponding near-equilibrium value for that translational temperature.

Most direct simulation Monte Carlo (DSMC) simulations use the approximation of classical (continuous) rotational energy characterized by some value of  $Z_R$ . A reasonable estimation of the temperature dependence of  $Z_R$  is a desired part of a simplified model of rotational relaxation in a flowfield. Several authors have presented DSMC rotation models based on Parker's energy gain function where the probability of rotational relaxation decreases with

increasing collision energy with an adjustable parameter to match the value of  $Z_R$  at some given temperature. Basing a DSMC variable relaxation probability model on the Parker energy gain correlation is certainly problematic, since its stated applicability is only to cases where the initial rotational energy is zero. On the other hand, it does produce the correct trend in  $Z_R$  versus  $T$ , and no other simple analytical expression has been produced.

Although the best information on the temperature dependence of  $Z_R$  for  $N_2$  with an emphasis on the lower (below room temperature) range has been summarized recently by Belikov [3, 4], some information regarding the higher temperature range has become available in the past few years. Values of  $Z_R$  have been obtained from two state-to-state rate constant models. The quasiclassical energy-corrected sudden (qECSE) model has been presented by Strekalov [5, 6], and the statistical power-exponential gap (SPEG) model is a semi-empirical fitting law used in correlating Raman line widths to state-to-state rate constants [7]. In addition, recent high-level theoretical calculations [8] on the best  $N_2$ - $N_2$  potential surface have provided predictions for the bulk viscosity and rotational relaxation cross sections for  $77 < T < 2000$  K. These results are compared with the predictions of Parker and of Lordi and Mates.

In spite of the large scatter, the newer results indicate that the value of  $Z_R$  levels off above 1000 K and thus the Parker correlation predicts too high a value of  $Z_R$  at high temperatures, by about a factor of two. This will be further exacerbated in the case of a high-temperature shock, where the initial low rotational temperature will produce an even lower effective value of  $Z_R$ . DSMC calculations of a simplified bow shock flowfield have been undertaken to show the effect of changing the estimated value of rotational collision number. The implications for

\* Abstract 6506 submitted to the 21st International Symposium on Rarefied Gas Dynamics, Marseille, France, July 26-31, 1998

flowfield simulations are discussed.

## References

- [1] J.G. Parker, *Rotational and vibrational relaxation in diatomic gases*, Phys. Fluids **2**, 449 1959.
- [2] J.A. Lordi and R.E. Mates, *Rotational relaxation in nonpolar diatomic gases*, Phys. Fluids **13**, 291 1970.
- [3] A.E. Belikov, R.G. Sharafutdinov, and M.L. Strekalov, *Temperature dependence of the rotational relaxation time in nitrogen*, Chem. Phys. Lett. **231**, 444 1994.
- [4] R.G. Sharafutdinov, A.E. Belikov, M.L. Strekalov, and A.V. Storozhev, *State-to-state rate constants and rotational relaxation time in nitrogen*, Chem. Phys. **207**, 193 1996.
- [5] M.L. Strekalov, *Rotational relaxation and collisional energy transfer calculations based on a new fitting law*, Mol. Phys. **86**, 39 1996.
- [6] M.L. Strekalov, *Temperature dependence of rotationally inelastic rate constants and fitting laws*, Mol. Phys. **90**, 475 1997.
- [7] S. Temkin, J.M. Thuet, L. Bonamy, and D. Robert, *Angular momentum and rotational energy relaxation in  $N_2$ - $N_2$  collisions calculated from coherent and stimulated Raman spectroscopy data*, Chem. Phys. **158**, 89 1991.
- [8] E.L. Heck and A.S. Dickinson, *Transport and relaxation properties of  $N_2$* , Mol. Phys. **81**, 1325 1994.

# Experimental Study of Nonequilibrium Processes within Shock Wave Front in Gaseous Mixtures \*

A.V. Emelianov, A.V. Eremin, V.Yu. Velicodny

Lab. of Nonequilibrium Processes HEDR Center, RAS, Moscow, Russia

## 1 Introduction

It is well known that velocity of gaseous flow behind incident shock wave can be essentially higher than mean heat velocities of the molecules within this flow. Therefore one can consider the zone of velocity distribution transformation in the front of shock wave as a region of fast molecular beam interaction with immovable gaseous media. Such an approach makes clear that the mean energies of collisions within the front are mainly determined by shock wave velocity instead of sound velocity behind the wave and can exceed considerably the mean energies of collisions in the equilibrium zone.

However to observe any nonequilibrium inelastic threshold processes induced by these collisions, an inordinately large energy transfer in a single encounter i.e. so-called non-adiabatic "supercollisions" has to proceed. The mechanism and efficiencies of supercollisions are determined by the interaction potential of colliding molecules [1], but are not finally studied yet.

Thus, the goal of this study is not only the experimental observation of nonequilibrium effects within the shock wave front, but the attempt to extract the supercollision probabilities for concrete molecular transition.

According to [2] the influence of high-energy collisions within shock wave front on the rates of high threshold processes must be the most essential when shock wave is propagating in the light "carrier" gas with the small admixture of heavy reactive molecules. Based on this inference the measurements of short-lived nonequilibrium radiation from  $I_2$  band ( $D^3\Sigma \rightarrow B^3\Pi$ ) ( $\lambda = 320-345$  nm) at the front of shock waves in  $He$ ,  $Ne$ ,  $Ar$  and  $H_2$  with the small admixture of iodine molecules were performed.

The upper state of this transition  $D^3\Sigma$  has the bot-

tom energy about 4.8 eV that is much above the dissociation threshold of  $I_2$  ( $D=1.54$  eV) and therefore can not be excited by the weak collisions and the only reason for nonequilibrium radiation at 340 nm within shock wave front appearance would be the non-adiabatic supercollisions.

## 2 Experimental

During experiments the intensive peaks of nonequilibrium radiation within shock wave front in  $He$ ,  $Ne$ ,  $Ar$  and  $H_2$  with 0.1 ÷ 3 % admixture of iodine molecules were registered. In Fig. 1 Boltzmann plot of equilibrium intensities  $J_{eq}$  measured from quasy-stationary traces and maximum intensity values  $J^*$  in the peaks are given. The measured intensities  $J_{eq}$ ,  $J^*$  are normalized by the intensity  $J_0$  of reference source (tungsten lamp) at the brightness temperature 1600 K.

The slope of the experimental dependence

$$\ln(J_{eq}/J_0 \cdot n) \sim 1/kT_2$$

must reflect the effective excitation energy  $E$  of radiative state  $I_2(D^3\Sigma)$ . The equilibrium data obtained at high temperatures fit the straight line with the slope  $E = 5.45$  eV, which is in a good agreement with iodine molecule geometry. At the lower temperatures, when the equilibrium radiation intensities become lower the sensitivity limit, only the peak intensities  $J^*$  were registered. These data display the essential overpopulation of  $I_2(D^3\Sigma)$  state and apparent decrease of effective excitation energy caused by high-energy collisions within shock wave front.

## 3 Discussion

The experimental data analysis revealed that peak intensities in the different gases containing about 1%  $I_2$  admixture don't depend on  $H_2$  and  $He$  concentrations and increase proportionally to  $Ne$  and

\*Abstract 6621 submitted to the 21st International Symposium on Rarefied Gas Dynamics, Marseille, France, July 26-31, 1998

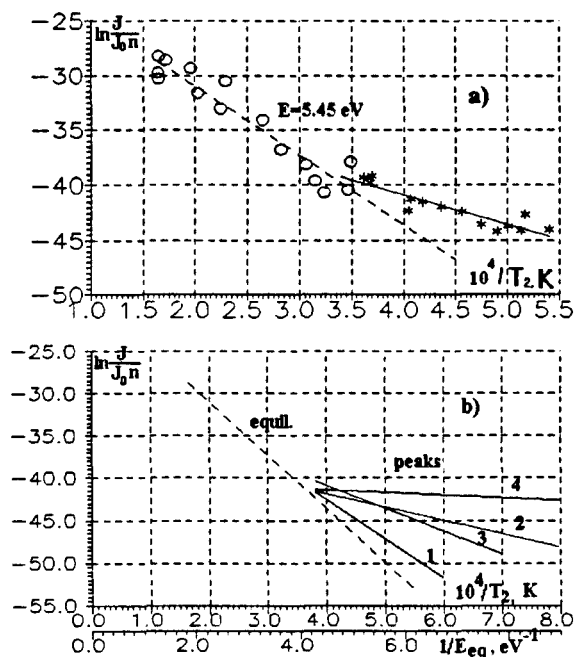


Figure 1: Boltzman plot of emission data versus equilibrium temperature behind shock wave. /a/ - experimental data for  $I_2 + He$  mixture. o - equilibrium intensities; \* - maximum intensity in the peaks. /b/ - summarized plot of all experimental dependences obtained in various  $I_2 + R$  mixtures. /1/ -  $R = Ar$ , /2/ -  $R = Ne$ , /3/ -  $R = He$ , /4/ -  $R = H_2$ .

$Ar$  concentrations. Based on this fact it was concluded that in the light gases ( $H_2$  and  $He$ ) inelastic collisions  $I_2 + I_2$  predominate, while in more heavy gases ( $Ne$  and  $Ar$ ) collisions  $I_2 + Ne$  and  $I_2 + Ar$  prevail.

In Fig. 2 experimental data  $\ln(n^*/n)$  (measured in  $H_2$  and  $He$ ) dependence on the reversal effective energy of collision are given. Besides the values of  $E^*$  (b), calculated on the basis of Boltzmann equation solution by the modified Tamm-Mott-Smith method [2] the estimation of  $E_l = mV^2/2$  (a) and  $E_h = MV^2/4$  (c), made in assumption of molecular beam of light or heavy molecules, moving with shock wave velocity  $V$  are shown. It is clearly seen that only  $E^*$  values fit the experimental measurements: a good coincidence between data in  $H_2$  and  $He$  exists and the slope of the dependence is close to the excitation energy of  $I_2(D^3\Sigma)$  state, while  $E_l$  and  $E_h$  values are not capable of describing the experiments. Thus, the important conclusion can be made that mean energies  $E^*$  of collisions within shock wave front attain factor of 10 more than equilibrium ones  $kT_2$  behind shock wave.

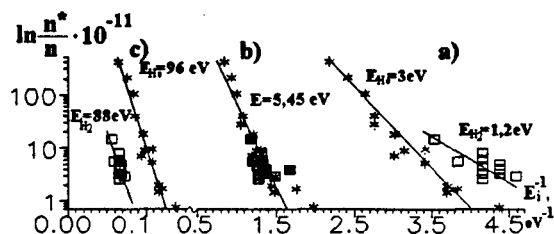


Figure 2: Nonequilibrium populations of  $I_2(D^3\Sigma)$  state in dependence on the effective energy of collisions  $E_i$  (see text).

The last part of experimental data treatment was aimed to estimate the absolute value of non-adiabatic supercollisions probabilities  $P_{na}$  and compare it with the numerical calculations of effective adiabatic transition probability.

To obtain the apparent values of  $P_{na}$ , the experimental data of  $J^*$  were related to corresponding equilibrium radiation intensities  $J_{eq}$ , extrapolated from high-temperature dependence of Fig 1. Then it was assumed that:

$$\frac{J^*}{J_{eq}} \cong \frac{n^*}{n_{eq}} = \frac{P_{na} \exp(-E/E^*)}{\exp(-E/kT_2)}.$$

The transition probabilities  $I_2(^1\Sigma_g^+ \rightarrow D^3\Sigma)$  extracted from experimental data by means of this relation exceeded the calculated ones in the frames of adiabatical approach by the factors of  $10^{15} \div 10^{20}$ . Thus, exciting collisions  $I_2 + I_2$  certainly have a strong non-adiabatic nature and, most likely represent some kind of complex-forming supercollisions.

**Acknowledgement.** The present research was supported by the grant 96-02-19694a of Russian Fundamental Research Foundation.

## References

- [1] Bernshtein V., Oref I., Lendvay G. *Energy transfer rate coefficients from trajectory calculations and contributions of supercollisions to reactive rate coefficients.*, J. Phys. Chem., Vol.100, pp.9738-9744, 1996.
- [2] Velikodny V., Biturin V., *Influence of translational nonequilibrium effects on kinetics of physico-chemical transformations in shock wave front.*, Pis'ma v Zh. T. F. Vol.22, No.4, pp.39-45, 1996 (in Russian).

# Non-Equilibrium Flow behind Medium Hypersonic Shock Waves \*

Y. Watanabe<sup>1</sup>, A. K. Hayashi<sup>2</sup>, H. Iwagami<sup>2</sup>, T. Tokunaga<sup>2</sup>, M. Hiraoka<sup>2</sup>

<sup>1</sup> National Aerospace Laboratory, Tokyo, Japan

<sup>2</sup> Aoyama Gakuin University, Tokyo, Japan

## 1 Introduction

For the development of a space vehicle, severe conditions such as the reentry problem should be overcome. Highly non-equilibrium flow behind the strong shock wave has been investigated by many researchers and the radiation from atomic species has been well established. However, sufficient data have not been obtained in the wide Mach number range by experimental studies, and details of the radiation from molecules are still unknown. In this study, our aims are to obtain detail data focused on the medium hypersonic region such as the Mach number is in the neighborhood of 10. A free-piston shock tube was newly constructed and used as a experimental apparatus. The performance of the free-piston shock tube and primary results on the non-equilibrium flow behind a shock wave were reported in this abstract.

## 2 Experimental setup

Figure 1 shows the schematic diagram of the free-piston shock tube. The quick opening valve was installed in the high pressure chamber. The free piston, having the mass of 2.3 kilogram, was set upstream end of the compression tube. The aluminum diaphragm incised crucially in advance was set at the end of compression tube. Three pressure taps were installed at the position denoted by a symbol # as shown in fig.1. In addition, a photo diode was located at the opposite side of the pressure tap #3 to measure the duration of radiation. The radiation behind a strong shock wave was observed by using the image converter camera.

The used gas and the initial condition of each sections are shown in tab.1. The gas was charged into each sections after making highly vacuum condition. In order to avoid an exudation of impurities from the material inside the tube under the high

vacuum condition, the low pressure section, test section and dump tank were made of aluminum.

The compression process of the helium by the piston was nearly isentropically and the maximum pressure was well predicted by solving a simple equation of motion. After the pressure of helium has reached nearly maximum pressure, the aluminum diaphragm was broken, and then, the strong shock wave was generated and propagated downstream in the low pressure section.

## 3 Experimental results

Figure 2 shows the diagram of the Mach number of the shock wave versus the initial pressure in the high pressure chamber. Experimental results were shown in the diagram as well as the theoretical analysis, which was not taken into account the real gas effects. However the experimental results were considerably lower than theoretical prediction, the shock wave of Mach number is 10, which is our primary aim, were achieved.

Figure 3 shows the radiation behind the shock wave observed by using the image converter camera. The shock wave propagates from left to right. The change in intensity of the radiation behind the shock wave was shown in fig.4. From figs. 3, 4, there was no radiation immediately behind the shock wave. The intensity of the radiation increased and then decreased as reduce in the distance from the shock wave. In the boundary layer, the radiation of very high intensity was observed.

The comparison of the experimental results and the numerical calculation, which is taken into account the real gas effects, will be shown in the symposium.

## 4 Conclusion

The free-piston shock tube was newly constructed. The primary data of the radiation behind the shock wave was observed.

\* Abstract 6690 submitted to the 21st International Symposium on Rarefied Gas Dynamics, Marseille, France, July 26-31, 1998

# NON-EQUILIBRIUM FLOWS - NE P

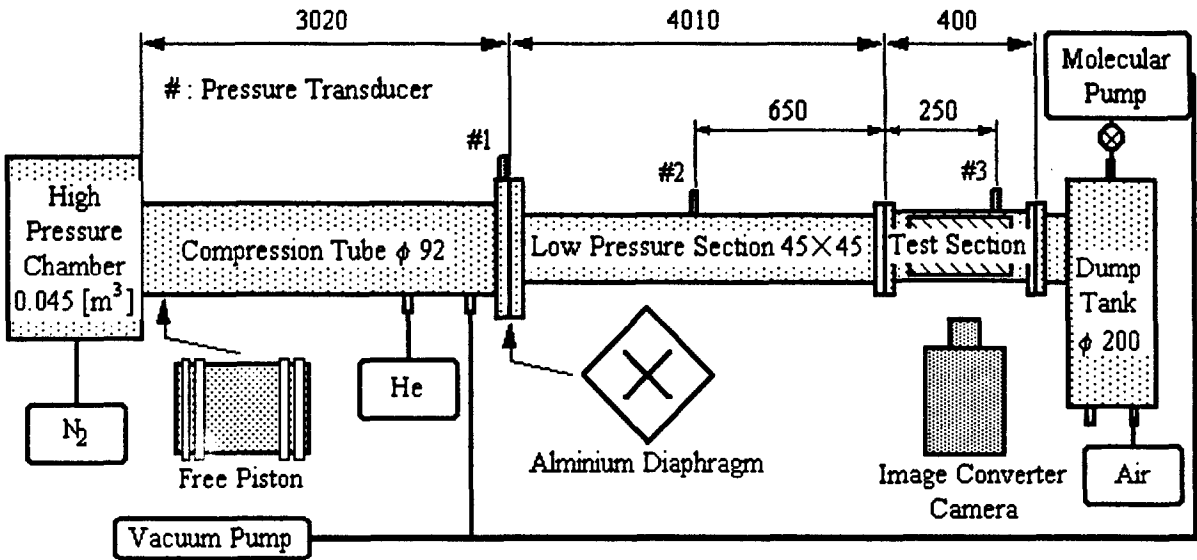


Figure 1: Schematic diagram of experimental apparatus (Unit : mm)

	High pressure chamber	Compression tube	Low pressure section
Used gas	Nitrogen	Helium	Pure air
Initial pressure	0.2~2.0 [MPa]	100.0 [kPa]	300 [Pa]

Table 1: Experimental condition

## References

- [1] Park C., *Assessment of Two-Temperature Kinetic Model for Ionizing Air*, AIAA 87-1574, 1987.
- [2] Page W. A. and Arnold J. O., *Shock-Layer Radiation of Blunt Bodies at Reentry Velocities*, NASA TR R-193, 1964.

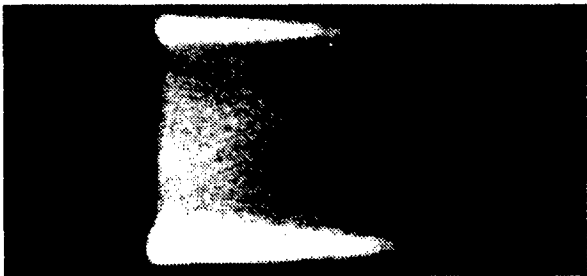


Figure 3: Radiation behind shock wave

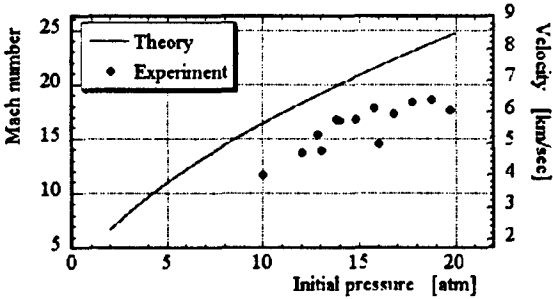


Figure 2: Mach number of shock wave

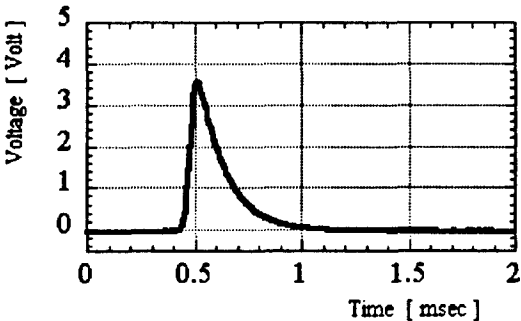


Figure 4: Duration of radiation behind shock wave



## Hypersonic Reactive Flows in a Nozzle \*

A. Nebbache<sup>1</sup>, A. Chikhaoui<sup>2</sup><sup>1</sup>LMFN-CORIA, INSA, St-Etienne-du-Rouvray, France<sup>2</sup>IUSTI - Technopôle de Chateau Gombert, Marseille, France

The aim of this paper is a numerical simulation of compressible high enthalpy air flows in a hypersonic nozzle. In such conditions air is considered as a five component mixture  $N_2$ ,  $O_2$ , NO, N and O. In the expanding nozzle the temperature associated to the translation-rotational and vibrational modes decrease along the axis and the chemical composition and the vibrational temperature of the molecules  $N_2$  and  $O_2$  are frozen near the exit of the nozzle and are different from their equilibrium values.

The molecules  $N_2$  and  $O_2$  are considered in vibrational non-equilibrium while NO is assumed in vibrational equilibrium due to its small vibrational relaxation time in comparison to the characteristic time scale of the flow. The vibrational relaxation of  $O_2$  and  $N_2$  is considered to occur via the Vibrational-Translational (T-V) energy exchanges in addition of the Vibration-Chemistry exchanges. The order of magnitude of the relaxation time of the vibrational process and the chemical reaction being similar, there results a strong coupling between these non-equilibrium phenomena.

Different models of coupling between vibrational and chemical reactions have been developed during the last years [1], [2], [3], [4], [5] and most of them are based on various coupling parameters which are poorly known. More recently, a kinetic model [6] based on a scaling of characteristic times of elementary collisional processes including translational-rotational-vibrational exchanges and chemical transformations is performed by solving the Boltzmann equation. In this study, five models are considered for the computation of the flow in hypersonic nozzle and the results obtained by using the different models of coupling are compared between them and with the ones obtained by using the model derived from the kinetic theory [6]. The test case is a high enthalpy air mixture flow expanding in TCM2 wind tunnel nozzle where the total pres-

sure and temperature are respectively 220 bars and 6340K.

The compressible reactive Navier-Stokes equations are solved by using a fully implicit finite volume predictor-corrector MacCormack's scheme [7]. This numerical method, unconditionally stable, is second order accurate in space and time. It is based upon the second order flux difference splitting procedure.

## References

- [1] Marrone P.V., Treanor C.E., *Chemical relaxation with preferential dissociation from excited vibrational levels*, Phys. Fluids, 6 (9) 1215-1221, 1963
- [2] Macheret S.O., Fridmann A.A., Adamovich I.V., Rich J.W., Treanor C.E., *Mechanisms of nonequilibrium dissociation of diatomic molecules*, AIAA paper, No 94-1984, 1984.
- [3] Knab O., Fruhauf H.H., Messerschmid E.W., *Theory of validation of the physically consistent coupled vibrations-chemistry-vibration model*, Journ. of Therm. and Heat Trans., 9(2), pp 219-226, 1995.
- [4] Park C., *Assessment of two-temperature kinetic model for ionising air*, AIAA paper, No 87-1574, 1987.
- [5] Serror S., Druguet M.C., Schall E., Zeitoun D., *A new vibration-exchange reaction coupling model of hypersonic air flows*, AIAA paper, No 97-2556, 1997.
- [6] Belouaggadia N., Brun R., *Chemical rate constants in nonequilibrium flows*, AIAA paper, No 97-2555, 1997.
- [7] MacCormack R.W., *Current status of numerical solutions of the Navier-Stokes equations*, AIAA paper, No 85-0032, 1985.

\* Abstract 6752 submitted to the 21st International Symposium on Rarefied Gas Dynamics, Marseille, France, July 26-31, 1998

# Mass Transport in Rarefied Gases; a Comparison of Linear and Nonlinear Treatments \*

C.J. Kloimböck, U.M. Titulaer  
Institute for Theoretical Physics,  
Johannes Kepler University, Linz, Austria

## 1 Introduction

Transport problems in rarefied gases in one-dimensional geometries can be solved by various numerical methods when the linearized Boltzmann equation may be applied; solution methods for the nonlinear Boltzmann equation are known mainly for the BGK model and some generalizations [1]. An early study by Willis [2] showed that the effects of the nonlinearities are surprisingly small for the heat transport problem. In the work reported here we therefore studied the influence of the nonlinearity for another transport problem, the mass transport between two walls at different chemical potentials. The main application is a vapor between two walls at different temperatures covered by liquid films. In such a case both heat and mass are transported. However, in the results reported here explicitly, we confine ourselves to the pure mass transport.

## 2 Solution Methods used

The most convenient method for linear problems in the given geometry is the moment method, a systematic generalization of Grad's 13-moment method. We used the version developed in an earlier paper from our group [3], where references to earlier work can be found. For operators of BGK-type, the nonlinear problem can be solved either by a reduction to a set of coupled integral equations [2] or by a direct solution, by discretization in space and longitudinal velocity, of the set of coupled differential equations for the relevant moments of the transverse velocity, which is a finite set for operators of this type.

## 3 Typical Results

We present the results for a given chemical potential or pressure difference  $\Delta p$ ; in Fig. 1 we present the resulting particle current in the BGK-model as a function of the plate distance (in units of the mean free path) for various linear and nonlinear treatments. The moment method and the other methods agree for the linearized case to within the accuracy shown. They interpolate between the free flow result at low  $d$  and the small Knudsen number expansion by Sone et al. [4] at large  $d$ . The discrepancy between linear and nonlinear treatment is appreciable only for large  $d$ ; it amounts to approximately 4% for  $\Delta p = 1$ ; it may be reduced to 0.6% when we linearize around a drifting Maxwellian with the right current (via an iterative procedure). Hence, qualitatively we obtain the same result as Willis: the nonlinear effects are small for our problem as well.

In Table 1 we present numerical results, both for the BGK model and for various modifications that yield the correct Prandtl number. In the linear case one has the freedom to choose the relaxation times for the higher moments of the momentum distribution function either equal to that of the viscous mode (model I) or to that of the heat conductivity mode (model II). The differences both with the pure BGK model and between the corrected models are about 1.6% for model I and about 0.3% for model II. For the nonlinear case one has more freedom; we considered the elliptic model [5] and Shakov's model [6]. Here the effects are quite small and quite similar for the two models and also similar in magnitude to those for the linear model I.

## 4 Further Results

In the full paper we also present results obtained for gas mixtures and for the coupled mass and heat transport problem. In the latter case we calculate

\*Abstract 6766 submitted to the 21st International Symposium on Rarefied Gas Dynamics, Marseille, France, July 26-31, 1998

# NON-EQUILIBRIUM FLOWS - NE P

$\Delta p$	BGK(nonlinear)	Shakov	ellip.	BGK(lin.)	lin I	lin II
0.002	-0.3336	-0.3346	-0.3353	-0.3336	-0.3392	-0.3346
0.2	-0.3352	-0.3358	-0.3370	-"	-"	-"
0.5	-0.3394	-0.3396	-0.3410	-"	-"	-"
1.0	-0.3448	-0.3457	-0.3459	-"	-"	-"

Table 1: The  $\Delta p$  dependence of the normalized particle current in the hydrodynamic limit for different models; the first three columns are the nonlinear cases, where the first column has a Prandtl number equal to 1 in contrast to the following two. The situation for the linearized versions is similar. lin I,II denote two different variants of the linearized BGK model with a corrected Prandtl number.

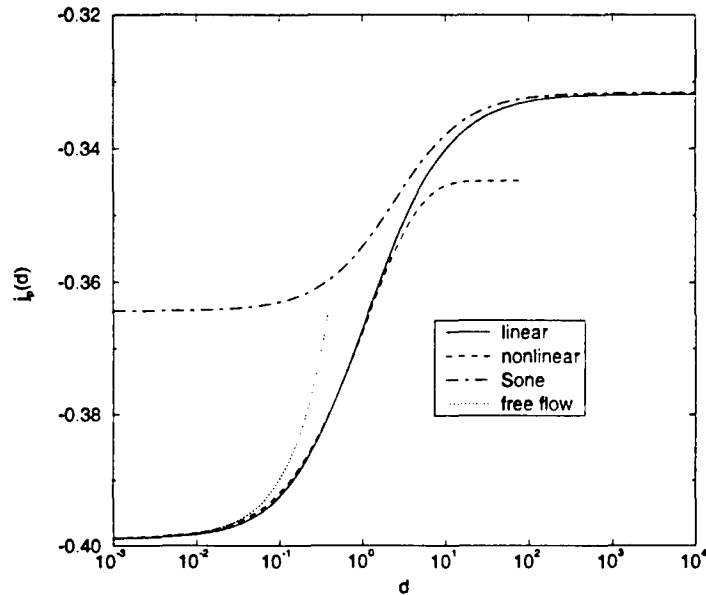


Figure 1: The particle current plotted against the plate distance in reduced units in the linearized and the nonlinear case. Sone's hydrodynamic approach is in good agreement with our results.

heat and mass current as functions of the applied temperature and pressure (chemical potential) differences. They are connected by a coefficient matrix of Onsager type, which reduces to the Onsager matrix in the linearized case. The dependence of the coefficients on the plate distance is calculated. The negative temperature gradient effect first described in [7] is also found and discussed.

## References

- [1] Cercignani C., *Theory and Application of the Boltzmann Equation*, Cambridge University Press, Cambridge, third edition, 1970.
- [2] Willis D.R., *Heat Transfer in Rarefied Gases*, Rarefied Gas Dynamics (ed. Laurmann), Academic Press, New York, pp.208-225, 1963.
- [3] Widder M.E. and Titulaer, U.M., *The moment method for boundary layer problems in brownian motion theory*, J.Stat.Phys, Vol.56, pp.471, 1989.
- [4] Sone Y. and Onishi, Y., *Kinetic theory of evaporation and condensation.*, J.Phys.Soc.Japan, Vol.44, No.6, pp.1981-1994, 1978.
- [5] Holway L.H., *New statistical models for kinetic theory: Methods of construction*, Phys.Fluids, Vol.9, No.9, pp.1658-1673, 1966.
- [6] Shakov E.M., *Generalization of the Krook relaxation equation*, Fluid Dynamics, Vol.3, No.5, pp.95-96, 1968.
- [7] Pao Y.-P., *Appliation of Kinetic Theory to the problem of Evaporation and Condensation*, Phys.Fluids, Vol.14, pp.306-312, 1971.

# Transport Properties in Gases and Plasma Mixtures of Gasdynamic Rarefied Flows \*

Irina A. Sokolova

Institute for Mathematical Modeling RAS, Moscow, RUSSIA

The recent advances in computer industry makes it possible to develop efficient algorithms and numerical schemes while solving complex thermophysical and gasdynamic problems. However the progress in the computing simulating can be reached if chemical-physical processes are taking into account. And to get full use of the benefits gained from computer modelling efficient chemical-physical models are needed. That is the hydrodynamic equations and corresponding coefficients in the molecular fluxes have to be consistent with the global requirement of the accuracy.

As well known, experimental investigation in the field of high temperature transport properties measurements are not available because of technical difficulties of treatment. Some experiments with partially ionised gases are not justified. From the other hand advanced theory, comprehensive analysis of particle interactions and computer simulation may be foundation for reliable transport properties much more than direct experiments.

The main goal of the report is to investigate the different approaches to transport coefficients and to collision integrals of species which are the coefficients in the rarefied gasdynamic flows equations. Models of transport coefficients bounded with the molecular fluxes are regarded both for thermochemical equilibrium and nonequilibrium states.

Generalisation of kinetic theory of rarefied gas on the mixtures of gases and the Chapmen-Enskog method with procedure of Sonine's polynomial expansion provides description of the molecular transport properties starting at microscopic level, effective cross sections and collision integrals and as result, to the molecular flux and transport coefficients.

The new transport equations and coefficients based on the Chapmen-Enskog method have been derived, which are simpler in compare with the ordinary used of the Hirschfelder, Cirtiss, Bird ones.

In particular, the number of elements of matrix in the ration of determinants ( $N \times n$ ) is reduced on the  $N$ , where  $N$  is the number of particles in mixtures and  $n$  is the number of Sonine polynomial; the laborious procedure of reverse matrix transformation is excluded, and so on. These advantages of the new expressions make it possible wide numerical calculations of all transport coefficients for various gas mixtures and to work out simple improved formulas needed in practice.

The convergence of Sonine's polynomial expansions for partially ionised mixtures in thermal conductivity, viscosity, diffusion coefficients are examined. The best level of kinetic theory simulation is compared with the simplified Devoto formula, separating the kinetic expression on two part: the hard particles thermal conductivity and the electron one. The errors of Devoto formula in the area of the competitive contribution of hard particles and electron part are found for different gas mixtures.

The models of different description levels for transport properties, viscosity, thermal conductivity, diffusion [1] for multicomponent partially dissociated and partially ionised gas mixtures are analysed and hierarchy of models and validation limits are established. The new algebraic formulas without determinant ratio but closed to high level kinetic theory numerical results are derived.

The second problem is that the reliable data of transport properties depend on information about particles interactions. In partially ionised gas excitations and exchanges processes may be important. The molecules, atoms, ions may be occurred in different exited states. One of the most important process is the resonant charge exchanges, reducing the thermal conductivity of chemical equilibrium mixture of order. The different approaches of charge resonant exchanges cross sections and corresponding collision integrals of ion and identical name atom are examined. Manifestation of varying in such properties as viscosity, thermal conductivity, diffusion coefficients owing to charge exchanged processes is shown by computing partially ionised

\* Abstract 6791 submitted to the 21st International Symposium on Rarefied Gas Dynamics, Marseille, France, July 26-31, 1998

mixtures of chemical equilibrium and nonequilibrium atmosphere gases.

Scattering process of neutral particles is accompanied by vibration, rotation, electronic levels excitation. The most important one is vibration-vibration resonant internal energy interchanges. Kinetic theory formalism for excited gas mixtures is not completed for implementation of formal deductions because of difficulties of collision integrals calculations for non-spherical symmetric potentials and deficiency of required information. So the inelastic scattering processes may be accounted with the help of effective cross sections and effective potential functions, which adequately describe the transport property under real conditions, using the kinetic theory foundation for spherical-symmetric molecules.

Library of the effective potential functions of atoms, molecules, ions is gathered and analysed for typical important atmosphere gases and its pollution. The combined potential models with 'splines' are derived. Their comparison with simple two-parameters potential models usually used for transport properties calculations shows that simple models hold within their limits of temperatures. So, the Lennard - Jones potential brings error of 30-50% correspondingly, if temperature increases over 2000-3000K. The Born-Mayer potential brings errors of 20-30

The data base of effective potentials, cross sections, collision integrals and transport properties for mixtures of neutral molecules, atoms, ions and electrons is included into Computerised Library [2]. The information completeness of the Computerised Library about transport properties and data of potentials, cross sections and collision integrals is superior the well-known data bases, either over the ranges of temperature and pressure, or over the set of mixtures, and in some cases by the level of modelling.

The work was supported by RFBR, grant N 97-01-00005

#### References

- 1.I. A. Sokolova. Molecular Transfer in Heat Transfer and Gasdynamic Problems /Reviews of Thermophysical Properties of Matters (Rus.). - Moscow. Institute of High Temperature RAS. N2 (94), 1992, p.1-100.
- 2.I.A. Sokolova. Computerised Library of Transport Properties of Gases and Plasma Mixtures. /15-th International CODATA Conference. Japan, 29 Sep.-3 Oct. 1996.

**AEROSPACE APPLICATIONS - AA P**

**THURSDAY, JULY 30, 1998**

**16:00**

# Impingement of Low-Density Jets on Inclined Flat Plates \*

J. Kurian, R. Babu, S.P.

Department of Aerospace Engineering, Indian Institute of Technology Madras, India

Low density freejets are found in numerous aerospace applications and are predominantly used as thrust generators. Impingement of such jets on surfaces of various shapes and orientations is consequential in many such applications. Undesirable forces / torques, heat loads and contamination result on the surfaces due to impingement of jets from, for example, rocket nozzle or a thruster nozzle. Evaluation of such undesirable effects is important for the performance estimation of many an aerospace vehicles. Considering the significance of the impingement effects, studies have been reported earlier by various research groups [1-5]. In the present paper, results of an experimental study of impingement effects on inclined flat plates subjected to low density freejets are presented.

The experiments were conducted on the Rarefied Gas Dynamics Laboratory of Indian Institute of Technology Madras [6]. Studies undertaken were on freejets emanating from conical nozzles of Mach numbers 2.5, 3.5, 4.5 and 6.2. The range of Knudsen numbers covered in the experiments were from 0.0018 to 4.22 encompassing continuum and free molecular regimes. The pressure ratios covered in the experiments were from 100 to 27000 spanning a Reynolds number range from 2 to 2000. Before the study of impingement effects was carried out, flow field of the freejets was studied using Sankowich type impact pressure probe mounted on externally controlled precision three axes traversing mechanism. Surface pressures on the plates were measured using calibrated matched pairs of thermistors (Fenwal Electronics, USA). All the pressure measurements were done with capacitance type (MKS Baratron, model 220A and 220B) pressure transducers of appropriate ranges. For measurement of upstream pressures, analog pressure manometer of Wallace and Tiernan make (Model 62A-3P) was also employed. Visualisation of the freejet and impingement flow fields was done by glow discharge technique.

Plume impingement studies were performed by arranging the flat plate parallel to the plume axis at a

distance  $Z_0$  from the axis. Plume studies were also done with the plate kept at inclination angles of  $6^\circ$ ,  $9^\circ$  and  $12^\circ$  to the axis. Results of plume studies in underexpanded jets show the following trends:

1. At the lower Reynolds numbers, calculated values of the Freezing Parameter show that the flow is frozen. At higher Reynolds numbers, impact pressure surveys show the presence of shocks which is evidently not found in frozen flows. In higher Reynolds number regime the axial impact pressure profiles fall rapidly and at a downstream location show an upward trend. This upward trend shows the location of the shock as corroborated from the glow discharge pictures.
2. For the impingement studies, the plate was kept at different angles. With the plates in position, pressure surveys were done in X, Y and Z directions. From the pressure profiles, the influence of the plate on the flowfield at various Knudsen numbers was understood. The asymmetry brought about by the plate and the difference between the lower and higher Reynolds number flows were discernible.
3. From the pressure measurements on the surface of the plates and the resultant isobars, normal forces acting on the plates were calculated. The normal force calculation was done by summing the products of average pressure between two isobars and the corresponding area. The normal force which is a function of the plate dimensions was found to overshoot the thrust levels of the nozzle used.
4. The glow discharge pictures depicts the freejet structure and the impingement shock system.

Detailed results will be presented in the final paper.

## References

- [1] Lengrand J.C., Allègre J. and Raffin M. (1982) AIAA Journal, Vol.20, No1. pp.27-28.
- [2] Allègre J. and Raffin M. (1985) 13th RGD Symp., pp.965-974

\* Abstract 4013 submitted to the 21st International Symposium on Rarefied Gas Dynamics, Marseille, France, July 26-31, 1998

# AEROSPACE APPLICATIONS - AA P

- [3] Legge H. and Boettcher R.D. (1982), TR, DLR  
Inst. for Fluid Mechanics, Gottingen, Germany
- [4] Legge H. (1986) 15th RGD Symp. pp.955-962
- [5] Detteleff G. (1991) Prog. in Aerospace Sci. Vol28,  
pp.1-71
- [6] Deependran B., Sujith R.I., Job Kurian (1996)  
AIAA Journal, vol.35, 9, pp.1536-1542



## Measurement of Heat Transfer to Blunt Bodies in Low Density Flows \*

M. Kamalakkannan, T.M. Muruganandam, R.I. Sujith, J. Kurian  
Department Aerospace Engineering Indian Institute of Technology, Madras, India

Aerospace missions involve design and deployment of vehicles that encounter continuum atmosphere, transitional and the free molecular regimes during their flight path. The physics of flight in the free-molecular and in the continuum regimes has been reasonably well understood, whereas that in the transitional zone is still subjected to considerable study and research. One of the aspects of flight in the transitional zone that remains to be understood is the heat transfer to the bodies flying at high speeds. The aerodynamic heating is proportional to the density of the operating environment. Hence at lower altitudes the aerodynamic heating is extremely high and the payload (say, satellite in the case of a satellite launch vehicle) that is being carried can therefore be subjected to very high thermal loads. Therefore, a thermal protection shielding is provided for safeguarding the payload. The thermal protection shielding must be sufficient to withstand the aero-thermodynamic loads imposed upon it. As the density falls rapidly with altitude, aerodynamic heating also reduces. At some point in flight, an altitude is reached where the aerodynamic heating is low enough that the satellite does not need any thermal protection. When such an altitude is reached, the heat shield is jettisoned. Due to scarcity of heat transfer data under low density transitional regime, the criterion for the jettisoning of the heat shield is conservative. It may be possible that heat shield could be jettisoned at a lower altitude, if the heat transfer rates at that altitude are not high enough to cause any kind of damage to the satellite. If that is accomplished, corresponding increase in the payload could be achieved.

A detailed experimental investigation of heat transfer to a bluff body under low density hypersonic conditions has been carried out. The Rarefied Gas Dynamics Facility of Indian Institute of Technology Madras with a stagnation heating arrangement was used for the purpose. Details of this facility, having a vacuum capability down to  $10^{-5}$  Torr are in Ref. [1-2]. The desired flow field was obtained by a conical nozzle of area ratio 190. The nozzle flow field has been calibrated for various pressure ratios across the nozzle using a Sankowich type impact pressure probe [3] mounted on a three axes traverse mechanism which requires no viscous corrections on its readings. The probe was connected to a capacitance type pressure transducer. (MKS Baratron make, Type 390)

---

\* Abstract 4015 submitted to the 21st International Symposium on Rarefied Gas Dynamics, Marseille, France, July 26-31, 1998

Experiments were performed with a flat faced cylinder and a cylinder with a hemispherical head, both 10 mm in diameter. The heat transfer rates were measured using platinum resistance gauges, etched on the model surface. Experiments were conducted for the stagnation temperatures ranging from 500 to 1000K in the free stream Mach number range from 4.35 to 7.66. Experiments were performed in Knudsen number ranges spanning continuum, transition and free molecular regimes.

The heat transfer data has been calculated in terms of heat flux, dimensional heat transfer coefficient and Stanton number. The dependence of the recovery factor on the speed ratio has been demonstrated. A comparison of the results from the completed experiments which are representative of the three low density flow regimes with the scarcely available earlier studies shows comparable trends. The features of low density transition flow were observed. Glow discharge visualization of the flow field in the presence of the model gave a better insight into the related fluid dynamics. Glow discharge images confirmed the flow to be more rarefied than that indicated by the free stream Knudsen numbers. Bridging relations for predicting the heat transfer in the transition regime based on the values in the continuum and free molecular regimes will be obtained on completion of the full range of experiments.

## References

- [1] Sreekanth, A. K., Anil Prasad and Dilip Prasad (1990) 'Numerical and Experimental Investigations of Rarefied Gas Flows through Nozzles and Composite Systems.' Beylich, A. E., editor, *Rarefied Gas Dynamics*, pp. 987-994, Aachen, Germany, VCH Publishers.
- [2] Raju, C. and Job Kurian (1994) 'Experimental Investigation of Rarefied Gas Flow through Rectangular Slits and Nozzles'. *Experiments in Fluids*, 17(4), pp. 220-224.
- [3] Raju, C., Sreekanth, A. K. and Kurian, J. (1994) 'Impact Measurements in High Speed Rarefied Flow' *Mechanics Research Communications*, 21(2), pp. 131-138.

# Three Dimensional Separation in Hypersonic Rarefied Flow \*

S. Igarashi

Department of Mechanical Engineering, Iwaki Meisei University,  
Iino Chuohdai, Iwaki 970, JAPAN

## 1 Introduction

Three-dimensional hypersonic rarefied flow around an obstacle is one of the most important problems in connection with flow separation for flight control of reentry vehicles. For reentry, three main types of flows are encountered : free molecular, transitional and continuum. In the past, many investigations have been performed in connection with shock wave-boundary layer interaction from continuum flow [1]. Delery and Coet[2] made an experimental study on 2D and 3D wedge at high Reynolds numbers and pointed out that there appears a sudden change in heat transfer near the separation point. Rarefaction effect was studied by Chun[3] and Chun et. al[4] experimentally and theoretically. But the results are qualitative and the flows are not fully three-dimensional, that is, a flat plate flow followed by a wedge. The present author made a 3D flow simulation on a swept wedge[5].

In this paper, a fully 3D flow is modeled by a double cone. Effect of cone angle on the flow characteristics is investigated by use of the Monte Carlo direct simulation method[6]. To clarify the three-dimensional interaction, a comparison is made of the distributions on the wall as well as the flow characteristics near the compression corner.

## 2 Numerical Simulation

Figure 1 shows the body configuration. The length of the whole cone is  $\ell$  and that of the forward cone is  $\ell_1 = 0.85\ell$ . The Knudsen number is defined by  $Kn = \lambda_\infty/\ell$ , where  $\lambda_\infty$  is the mean free path in the freestream. The flow is simulated by use of the Monte Carlo direct simulation method. Molecular model is Maxwell molecule with the internal degree of rotation and the variable hard sphere (VHS) model is adopted to simplify the scattering law. Collision is assumed to be fully inelastic and is sim-

ulated by the phenomenological Larsen-Borgnakke model.

## 3 Results and Discussion

Practical calculation was performed for the freestream Mach number of  $M_\infty = 10$ , the Knudsen number of  $Kn = 0.01$  and the wall to freestream temperature ratio of  $T_w/T_\infty = 6$ . The forward cone half angle is  $\beta = 10^\circ, 20^\circ$  and  $30^\circ$  with the second one  $\sigma = 45^\circ$  fixed.

Figure 2 compares the wall pressure distributions ( $c_p = 2(p - p_\infty)/\rho_\infty U^2$ ) for three cone angles. For larger angles of  $\beta$ , sudden increase and decrease near leading edge is followed by a little bit oscillating pressure distribution. For  $\beta = 10^\circ$ , on the other hand, pressure rise is small. As the connecting region is approached, pressure gradually increases as is expected from continuum flow.

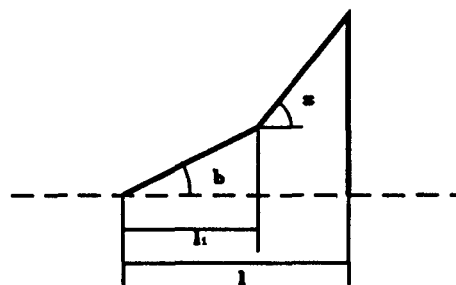


Figure 1: Body configuration

Next, we consider the heat transfer to the wall. Figure 3 shows the distributions ( $c_h = 2\dot{q}/\rho_\infty U^3$ , [ $\dot{q}$  is heat flux to the wall]). We can see a large change near leading edge for larger cone angles just like the pressure distributions. After this initial change, the distribution decreases and increases gradually as the connecting region is approached.

Figure 4 shows the skin-friction ( $c_f = 2\tau_w/\rho_\infty U^2$ ). For all cone angles, the distributions near the leading edge have the same tendency as those of the pressure and heat transfer. Toward

\*Abstract 4321 submitted to the 21st International Symposium on Rarefied Gas Dynamics, Marseille, France, July 26-31, 1998

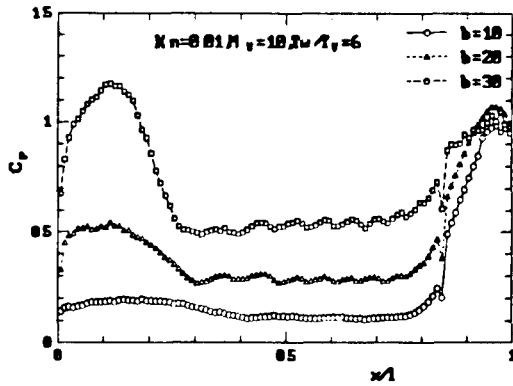


Figure 2: Pressure distributions

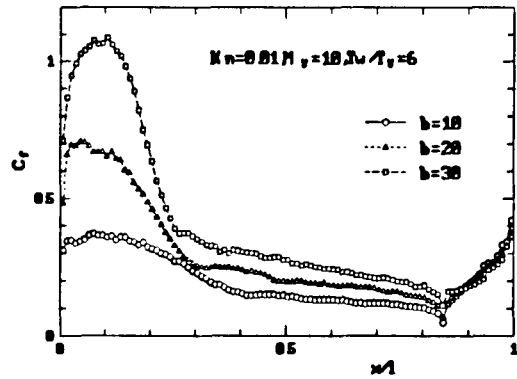


Figure 4: Skin friction distributions

the downstream region, they decrease gradually and take the minimum near the connecting region. The minimum value is the smallest for  $\beta = 10^\circ$  but is positive. That is, separation does not occur.

In these flows, the equivalent wedge angle  $\beta_e$  for the double cone is considered to be  $\sigma - \beta$ . In 2D compression corner flow, the incipient separation angle  $\beta_i$  is expressed by  $\beta_i = 80\sqrt{\bar{V}}$ , where  $\bar{V} = M_\infty \sqrt{C/Re}$  is the hypersonic interaction parameter. This suggests that the three dimensional separation might occur for smaller Mach number and cone angle  $\beta$  when the parameters  $Kn = 0.01$  and  $\sigma = 45^\circ$  are fixed [7].

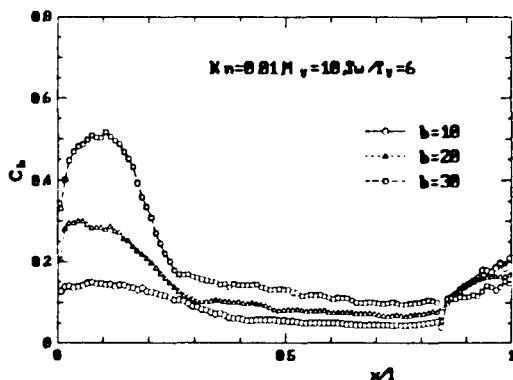


Figure 3: Heat transfer distributions

## References

- [1] Hayes, W.D. and Probstein, R.F., *Hypersonic Flow Theory*, 1959. Academic Press, New York and London.
- [2] Delery J. and Coet M.- C., *Hypersonic Flows for Reentry Problems*, edited by J.A. Désidéri, R. Glowinski and J. Périaux, Vol. II, Springer-Verlag, Berlin, 1991, 97-128.
- [3] Chun, Ch.-H., *Rarefied Gas Dynamics*, ed. by Baylich, VCH, Weinheim, 562-569, 1992.
- [4] Moss, J.N., Price, J.M and Chun, Ch.-H., AIAA 91-1313, 1994.
- [5] Igarashi, S., *Rarefied Gas Dynamics*, ed. by J. Harvey and G. Lord, Vol.2, Oxford Univ. Press, Oxford, 1270-1276, 1995.
- [6] Bird, G. A., *Molecular Gas Dynamics and the Direct Simulation of Gas Flows*, Clarendon Press, Oxford, 1994.
- [7] Igarashi, S., *Compu. Fluid Dyn.*, 2(1993), 219-226.

# Numerical Simulation of Interaction between Shock Waves and Boundary Layer in Hypersonic Rarefied Flow \*

N. Tsuboi and Y. Matsumoto

Department of Mechanical Engineering, University of Tokyo, Japan

## 1 Introduction

Interaction between shock waves and boundary layer over a flat plate with and without compression corner in hypersonic rarefied flow has been studied by many researchers with respect to the nonequilibrium characteristics around space vehicles. In rarefied regime, mean free path of molecular is so large that nonequilibrium between translational and rotational temperature appears near the leading edge and compression corner of the plate. Therefore, the interaction between them in rarefied regime needs to be researched in detail.

In numerical simulation of the interaction between them in rarefied regime, DSMC(Direct Simulation of Monte Carlo) is valid due to the treatment of particles directly<sup>[1, 2]</sup>. Matsumoto and Tokumasu have constructed the model which is able to capture the nonequilibrium characteristics in rarefied flow<sup>[3]</sup>. The model(Dynamic Molecular Collision(DMC) model) is based on the cross sections and energy distributions obtained by Molecular Dynamics for diatomic molecules. This research is to conduct the numerical simulation over the plate in hypersonic rarefied flow using the DSMC with the DMC model and to obtain knowledge on the nonequilibrium characteristics.

## 2 Numerical Method

The DMC model of diatomic molecules is based on the cross sections and energy distributions after molecular collisions which are obtained by the MD simulation. The procedure of the DMC model is related as follows. Two-body collision of diatomic molecules with various translational/rotational energy are conducted using the MD simulation. Then, probability density functions which represent energy distributions after collisions and collision cross sections are constructed, and the data tables of those are established. Furthermore, in the DSMC simulation, energy distributions after collisions in each cell are calculated from those before collisions using the data tables. The detail of the procedure is shown in reference 3. The null-collision technique<sup>[4]</sup> is adopted in collision-frequency technique, and the diffuse reflection is imposed on the wall boundary. The Navier-Stokes calculation using the second-order modified Harten-Yee TVD method<sup>[5]</sup> is conducted to compare with the DSMC calculation.

## 3 Results

Inflow conditions are as follows:  $M_\infty = 20.2$ ,  $Re_\infty = 566$ (based on a half length of the plate),  $Kn_\infty = 0.047$ ,  $T_{wall} = 290K$ ,  $T_0 = 1,100K$  <sup>[6, 7]</sup>. In DSMC simulation, the plate has a angle of the leading edge of 30 degrees.

Figure 1 shows the computed gas density contours over the plate in the DSMC and NS results. The results between the DSMC and NS simulations is quite different with respect to the width of shock wave. Figure 2 shows the density profiles over the plate at  $X/L = 1.5$ ( $L$  means a half length of the plate). The NS results have disagreement with the experimental results, but the DSMC results have agreement with those. Furthermore, it is shown that the leading edge effect in the DSMC results is large with respect to the location of the maximum density. Figures 3

\* Abstract 4432 submitted to the 21st International Symposium on Rarefied Gas Dynamics, Marseille, France, July 26-31, 1998

and 4 show the heat transfer rate and temperature profiles on the plate. It is shown that the DSMC results have agreement with the experimental results and that the effects of the leading edge on the heat transfer rate and wall temperature are as large as those on the density profiles.

#### References

- [1] Bird, G. A. , *Molecular Gas Dynamics*, Clarendon Press, Oxford, 1976.
- [2] Nanbu, K., J. Phys. Soc. Jpn. , Vol. 49, p. 2042-2049, 1980.
- [3] Tokumasu, T. and Matsumoto, Y., Proc. of the 20th Int. Symp. on Rarefied Gas Dynamics, p. 737-742, 1996.
- [4] Koura, K., Phys. Fluids, Vol. 29, p. 3509-3511, 1986.
- [5] Yee, H. C. , NASA TM-89464, 1987.
- [6] Chpoun, A. , Lengrand, J. C. and Heffner, K. S. , AIAA Paper 92-2900, 1992.
- [7] Lengrand, J. et al. , 18th Int. Symp. on Rarefied Gas Dynamics(Columbia), p. 276-284, 1992.

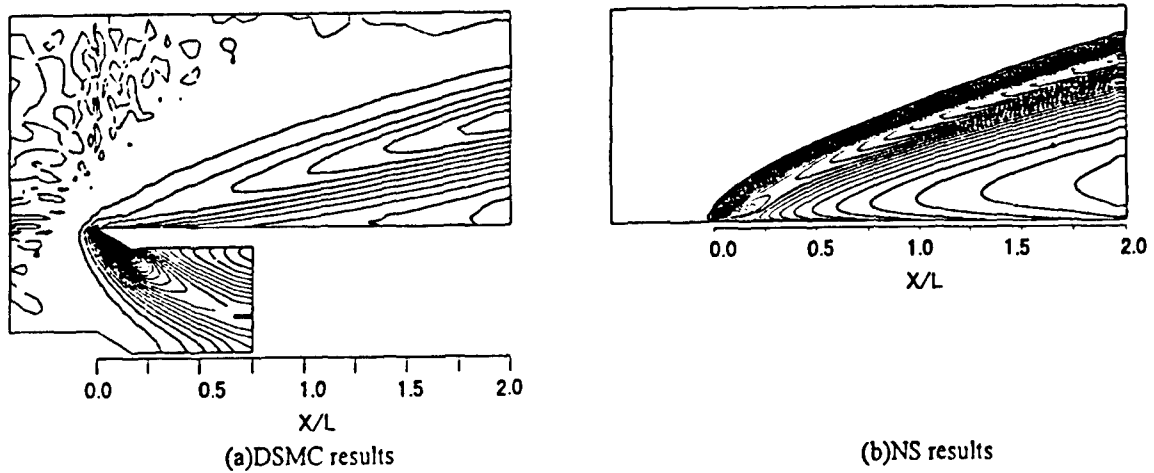


Fig.1 Density contours over the flat plate

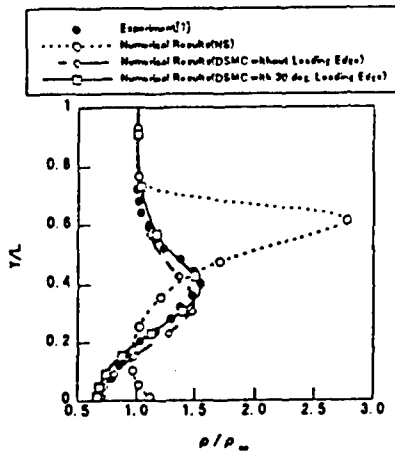


Fig.2 Density profiles over the flat plate at  $X/L=1.5$

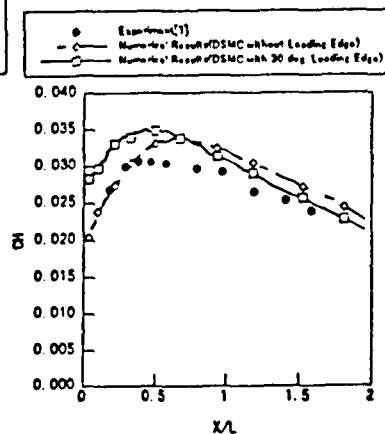


Fig.3 Heat transfer rate distributions on the flat plate

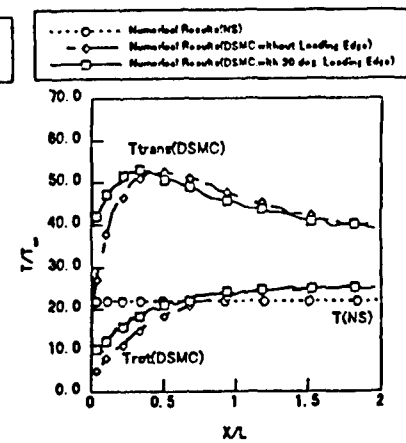


Fig.4 Temperature distributions on the flat plate

# On Self-Excited Oscillations in Supersonic Rarefied Impact Jets \*

G.F. Gorshkov, V.N. Uskov

Baltic State Technical University, St.-Petersburg, Russia

## 1 Introduction

This paper is devoted to experimental investigation of influence of ambient atmosphere rarefaction on supersonic impact jets (under-expanded jets interacting with normal limited flat obstacles).

## 2 Experimental apparatus and procedures

Experiments were carried out on the vacuum test bench GURS-1 that contains vacuum chamber of 10 m<sup>3</sup>, two vacuum pumps BN-6, booster-pump BN-15000. The chamber contains remotely operated device that carries an obstacle. A cylinder with flat butt-end (diameter  $d_{ob} = 16$  mm) with the IS-2156 detector of pressure in the center was used as the obstacle.

Jets were produced by Laval's nozzle (geometrical Mach number  $M_a = 2$ , critical diameter  $d_* = 4$  mm, half-clearance angle  $15^\circ$ ). Stagnation pressure  $p_0$  and static pressure  $p$  were measured both in receiver and at the obstacle, along with pressure in the vacuum chamber  $p_\infty$ , and pulsations of pressure on the obstacle.

Variation of critical Reynolds number  $Re_* = (\rho U d / \mu)_*$  was being implemented by variation of  $p_0$ , while constant  $p_\infty$  was ensured by air supplies through the vacuum-pumps with constant flow rate.

Pressure  $p_\infty$  was being gauged by DMI sensor in reference to some basic pressure  $p_b$ . The constant value of  $p_b = 10$  Pa in one of the gauge's pockets was maintained by vacuum-pump NBZ-20 and was being measured by PMT-2 thermo-pair and vacuum-meter VT-2, the later was calibrated by Mc-Leod manometer.

The equipment and data evaluation methods described in [1] were used for data retrieval of ampli-

tude and frequency response of self-sustained oscillations.

The research was carried out with following parameters ranges:  $T_0 = 293$  K;  $\gamma = 1.4$ ;  $p_0 = (0.86 - 6.5) \cdot 10^3$  Pa;  $n = p_a/p_\infty = 2 - 13.5$ ;  $Re_* = (0.59 - 3.84) \cdot 10^3$ ;  $Re_L = Re_*(p_0/p_\infty)^{-0.5} = 114 - 371$ ; distance from the nozzle exit section to the obstacle  $h = l/r_a = 2 - 30$ . Vacuum rate estimation revealed that Knudsen number variation  $(0.67 - 5.1) \cdot 10^{-3}$  is such that the flow near the obstacle is continuous, while viscosity and rarefaction effects took place in the boundary layer.

## 3 Experimental results and discussion

Two types of flow over the obstacle were determined for rarefied impact jets: one occurs in case both first (1) and second (2) regimes of self-excited oscillations take place simultaneously; another happens when only (1) mode exists as in case of dense jets. Realization of one of these flow types depends on combination of parameters:  $M_a, H = h/[d_* M_a (\gamma n)^{0.5}]$  and  $Re_L$ .

Thus the first regime is marked by multiple discrete components presence in the frequency spectrum, powerful oscillations of shock-wave picture (SWP) and of pressure at the obstacle. Oscillations have clearly defined regular structure. Sections of increasing of integral level of pressure pulsations  $\Delta L^0$  at the obstacle have clearly defined borders. The end of the second (2) regime is always matched by appearance of the first non-disturbed "cell". This fact has been proved by both pressure measurement results and the SWP visualization.

The second regime has significantly lower  $\Delta L^0$  level and shorter  $H$  range ( $H$  range was 3 times shorter than for the first (1) mode). The second regime is marked by single discrete component of frequency spectrum and by moderate pulsations level at the obstacle. This regime is sensitive to variation of

\*Abstract 4810 submitted to the 21st International Symposium on Rarefied Gas Dynamics, Marseille, France, July 26-31, 1998

rarefaction parameter  $Re_L$ . Under the experiments conditions the end of the (2) regime always comes before the radial spreading of the flow with non-disturbed first "cell" takes place. Because of hysteresis of average pressure at the obstacle, the start of unsteady regime coincides with the "destruction" moment of the flow with the non-disturbed first "cell".

Arising of the single self-excited oscillations regime takes place at such  $n$  values, when the central shock wave (CSW) diameter is essentially smaller than obstacle diameter, or when they are roughly equivalent but  $Re_L$  value is small enough to influence the second regime ("gobbles it up"): ( $n = 6.6$ ;  $Re_L = 147$ ); (4.8; 172); (3.5; 189); (3.3; 189); (2.6; 163).

Arising of self-excited oscillations in both flow regimes may be coupled by both relatively smooth  $\Delta L^0$  level increase and by a sudden change of it. The transfer from the second regime to the flow with the non-disturbed first "cell" takes place with abrupt changes.

Increasing of  $H$  inside boundaries of existence of each regime brings to the monotonous decrease of basic pulse frequency  $f_r$  at the obstacle, but when the transfer from the first to the second regime takes place, it brings to the sudden change of the  $f_r$ . The "saw"-like changes of  $f_r$  parameter correspond to  $f_r$  behavior in dense under-expanded jets [2].

Experiments showed that for the fixed initial parameters  $M_a$ ,  $\gamma$ ,  $n$  and  $Re_L$  of rarefied impact jets the hysteresis in  $\Delta L^0$  level (in contrast to the pressure at the obstacle) does not exist for any type of obstacle flow [3].

Rarefaction influence on self-excited oscillations is found as follows: at high values of  $Re_L$ , boundaries of existence of self-excited oscillations are independent of  $Re_L$  and may be determined by the same complexes as in [2].

The decrease of  $Re_L < 371$  (rarefaction increase) might bring to vanishing of the second regime and after that of the first regimes. This fact is associated with both transfer to X-like structure of shock waves and with the "wash-out" of first jet "cell" [4].

Decreasing density in a free ambient jet with  $M_a = 2$  (in contrast to  $M_a = 1$ ) and  $n = \text{const}$  leads to decreasing of Mach-disk diameter, moving it farther from the nozzle and finally to organization of regular shock-wave structure [4].

When  $Re_L$  becomes  $Re_L < 172$  ( $n = 6.6 - 2.6$ ), then the only self-excited oscillations regime exists — the first one, while for  $Re_L < 121$  no self-excited

oscillations have been found. Vanishing of the second regime is caused by decrease of impact layer thickness during the transfer to regular shock-wave structure.

Frequency characteristics of self-excited oscillations  $f_r$  in both regimes were summarized by all-purpose empirical function :

$$Sh_r^{-1} = a_0 / (f_r d_a n^{0.5}) = A_1 \Delta / (d_a n^{0.5}) + B_1,$$

where  $A_1 = 4.3$ ;  $B_1 = 1.2$  — 1-st regime;  $A_2 = 1.3$ ;  $B_2 = 1.4$  — 2-nd regime;  $a_0$  — sound velocity;  $\Delta$  — distance of CSW from the obstacle (average value of distance of  $\Delta$  was taken from [5]).

## References

- [1] Favorsky V.S., Savin A.V., Shatalov I.V., Sokolov E.I., *Rarefaction Effect Non-Stationary Interaction of Supersonic Underexpanded Jets with the Normal Infinite Flat Plate*, Rarefied Gas Dynamics, Proc. of the 17-th Int. Symp. on RGD, VCH Verlagsgesellschaft mbH, pp. 979-986, 1991.
- [2] Gorshkov G.F., Uskov V.N., Favorsky V.S., *On Peculiarity of Non-Stationary Impingement of a Supersonic Underexpanded Jet into an Infinite Obstacle*, Zhurnal Prikladnoi Mekhaniki i Technicheskoi Fiziki, No. 4, pp. 58-65, 1993, (in Russian).
- [3] Gorshkov G.F., Uskov V.N., *On Self-sustained Oscillations in Supersonic Impact Jets*, Fundamental Research in Aerospace Science, Book Abstracts Int. Conf. (Sep. 22-24, 1994), Zhukovsky, Russia: TsAGI, Section 3, pp. 65-67, 1994.
- [4] Lukyanov G.A., Shatalov I.V., Sokolov E.I., *Impingement of a Supersonic Underexpanded Rarefied Jet Upon a Flat Plate*, Rarefied Gas Dynamics, Proc. of the 13-th Int. Symp. on RGD, Plenum Press., N.-Y., Vol. 2, pp. 993-1000, 1985.
- [5] Golubkov A.G., Koz'menko B.K., Ostapenko V.A., Solotchin A.A., *On the Interaction of an Underexpanded Supersonic Jet with a Finite Flat Baffle*, Fluid Mech. Sov. Res., Vol. 3, pp. 96-102, 1974.



# The Peculiarities of Rarefied Separated Flow on a Flat Plate with Barrier \*

A.I. Erofeev, V.N. Gusev, V.P. Provotorov  
Central Aerohydrodynamic Institute (TsAGI)  
1, Zhukovsky str., 140160 Zhukovsky, Russia

The separated laminar flows on a flat plate with barrier is well investigated at large Reynolds numbers. With a decreasing of a Reynolds number the flow in separation region will vary as a result of increasing of a boundary layer thickness and structure of a shock induced by the barrier. The given work studies of peculiarities of the separation flows at small Reynolds numbers.

The hypersonic rarefied flows about the flat plate of length  $L$  with the flat barrier of height  $H$  was studied by the DSMC method at Reynolds number  $Re_\infty = \rho_\infty U_\infty L / \mu_\infty \leq 1.5 \cdot 10^4$ . Here  $\rho_\infty$ ,  $U_\infty$ ,  $\mu_\infty$  - density, velocity and viscous coefficient of undisturbed flow. The data describing the flow peculiarities in pre-separated and separated zones are obtained as function of the Mach number  $M_\infty = 10$  and 23, the temperature factor values  $t_w = T_w / T_0 = 0.05 \div 1$  ( $T_w$  - wall temperature,  $T_0$  - stagnation temperature), ratio  $h^* = H/L = 0.08, 0.16$  and 0.24 and a specific heat ratio  $\gamma$ .

It was shown, that at  $h^* \geq 0.16$  and  $Re_\infty \geq 10^4$  the distribution of pressure coefficient  $C_p = 2P / \rho_\infty U_\infty^2$  on a plate surface, as well as in case of a continuous flow, have characteristic isobaric area with explicitly expressed plateau of pressure, i.e. the developed separation takes place. At smaller Reynolds numbers, namely up to  $Re_\infty \approx 0.25 \cdot 10^4$ , the area of back current is still present, though there is no plateau in pressure profile (Fig.1,  $M_\infty = 23$ ,  $Re_\infty = 10^4$ ,  $t_w = 0.081$ ,  $\gamma = 5/3$ ). In Fig.1 marker "blank circle" and the inscription "Flat Plate" shows result for a flat plate without barrier. The effect of increasing of a heat flux to a surface in pre-separated zone, where maximum value position is near to a separation point up on a stream, turned out to differ essentially from data, available in the literature for large numbers  $Re_\infty$  ( $Re_\infty \geq 10^5$ ). This effect is illustrated in Fig.2, where the distribution of a heat

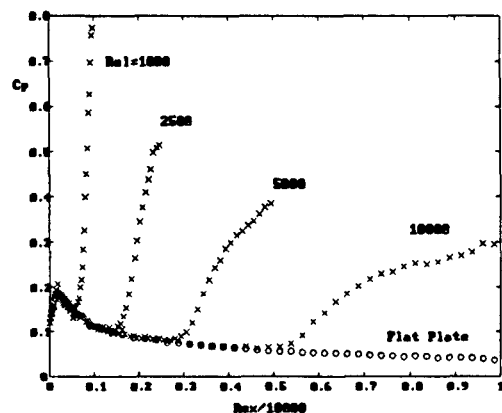


Figure 1: Pressure distribution on plate

flux coefficient  $Ch = 2Q / \rho_\infty U_\infty^3$  ( $M_\infty = 23$ ,  $Re_\infty = 10^4$ ,  $t_w = 0.081$ ,  $\gamma = 5/3$ ,  $h^* = 0.16$ ) at different numbers  $Re_\infty$  is given. As follows from Fig.2, with the Reynolds number increasing the magnitude of a maxima of a heat flux decreases.

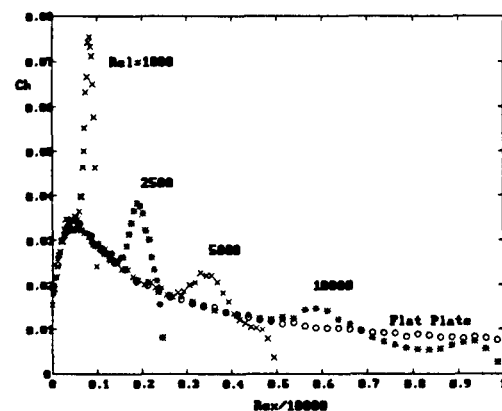


Figure 2: Heat flux distribution on plate

\*Abstract 4874 submitted to the 21st International Symposium on Rarefied Gas Dynamics, Marseille, France, July 26-31, 1998

It is known, that for a solution of the boundary

layer equations for viscous interaction regime the group transformation (see, for example, [1]) is applied which at the same time determines the similarity criteria. As it appeared, that criteria, defined for a continuous condition, remain correct in rarefied gas flow practically down to numbers  $Re_\infty = 10^3$ , as it takes place at a flow about unconcave bodies [2]. As an example,

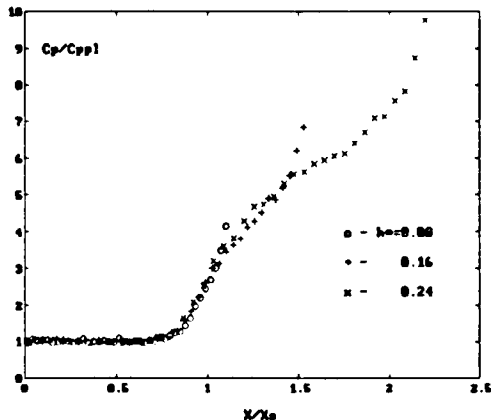


Figure 3: Dimensionless pressure distribution on plate

Fig.3 shows the dependence  $C_p/C_{ppl}$  against  $X/X_s$ , where  $C_{ppl}$  - pressure coefficient for a flat plate without a barrier, and  $X_s$ -coordinate of a separation point. It can be seen that such functional dependence permit to correlate data in preseparation zone at various Reynolds numbers. The similar dependences take place for friction and heat flux.

## Acknowledgement

The work was carried out at support of the Russian Foundation for Basic Research (Grant 97-01-00577) and State Program for Leading Research Groups Support (Grant 96-15-96063)

## References

- [1] Neiland V.Ya., *Asymptotic theory of the separation and boundary layer supersonic gas flow interaction*, Advances in Mechanics, Vol.4, No2, pp.3-62, 1981 (in Russian).
- [2] Gusev V.N., Erofeev A.I., Provotorov V.P., Yegorov I.V., *Numerical modelling and experiment in rarefied gas dynamics*, Proc. 20th RGD Intern. Symp, Peking Univ. Press, Beijing, China, pp.441-446, 1997.

# Influence of Vibrational Excitation of Molecules on Kinetic Processes During Modeling of Supersonic Combustion in Hypersonic Wind Tunnel With MHD Accelerator \*

V.I. Alfeyorov, L.M. Dmitriev, B.V. Egorov, V.A. Mokhov, Yu.E. Markachev  
TsAGI, Zhukovskiy, Russia

Study [1] has shown that only wind tunnels with MHD accelerators can recreate conditions in combustor of scramjet in SSTO vehicle moving with speed of  $M > 10$ . Special attention in [1] was directed on influence of seed on kinetic processes during hydrogen combustion in partially dissociated air with atomic oxygen, nitrogen oxide, etc.

Present study analyzes influence of vibrational excitation of molecular hydrogen on ignition time of mixture at entry into combustor of scramjet, and composition of combustion products. Special attention is directed on level of components critical to ecological consequences of flights of SSTO vehicle with scramjet and their dependence on vibrational excitation of molecular hydrogen.

Presented data reflect work of wind tunnel with MHD accelerator in wide range of initial conditions in precombustion chamber of engine and its electromagnetic parameters ( $P_0 = 2 \dots 200$  atm,  $T_0 = 3000 \dots 5000$  K,  $\alpha_{Na} = 0.25 \dots 2\%$ ,  $B = 2.4 \dots 7$  T,  $j = 20 \dots 200$  A/cm<sup>2</sup>,  $\beta = 0 \dots 1.5$  deg, where  $P_0, T_0$  - pressure and temperature of deceleration in precombustor of engine,  $\alpha_{Na}$  - mole fraction of seed in form of Na,  $B, j$  - induction and current density in accelerator,  $\beta$  - opening angle of accelerator).

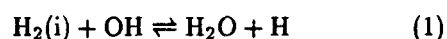
In process model used during simulation of vibrational and chemically nonequilibrium flow inside MHD accelerator channel, electron energy was not only transferred to vibrational degrees of freedom of gas, but also excited resonance conditions of atoms of seed alkalic metals that were used to create gas conductivity. Subsequently electron excitation energy of seed had transferred to translatory degrees of freedom of gas during collisions with molecules of nitrogen  $N_2$ . Besides, fast VT relaxation of  $N_2$  was taken into account via resonance conditions of

seed atoms, which turned out to be essential along all length of MHD accelerator channel.

Dependencies of speed constants on vibrational temperatures for reactions in high-temperature air were taken into account for determination of chemical composition of gas in MHD accelerator channel.

Kinetic scheme of combustion of molecular hydrogen  $H_2$  in air contained 43 equations for 15 components ( $H_2, O_2, N_2, NO, NO_2, HNO_2, HNO, HNO_3, H, OH, HO_2, H_2O_2, H_2O, O_3$ ). Besides this, reactions of combustion products with seed atoms of form Na, leading to formation of NaOH,  $NaO_2$ , NaO, were considered.

As performed calculations have shown, amount of vibrational excitation has most influence on composition of combustion products and induction time of hydrogen in air. Reaction:



Speed constant of (1) in forward direction,  $K(T, T_{H_2})$  heavily depends on vibrational excitation of  $H_2$  [2]. Vibrational relaxation of  $H_2$  in combustor is determined by VV' processes with hydroxyl OH molecules, which appear in mixture during initial phase of combustion. Amount of hydroxyl OH in flux itself depends on level of vibrational excitation of molecular hydrogen  $H_2$ .

Large values of vibrational excitation of  $H_2$  cause speed of reaction (1) in forward direction to increase and mole fraction of OH in mixture to rapidly decrease. Low amount of OH, causes decrease of amount of  $HNO_3$  and  $H_2SO_4$  in combustion products, which is an important issue for aerosol formation in SSTO near wake [3, 4].

Low values of vibrational excitation of  $H_2$  shift reaction (1) to the left side, which leads to increase in amount of OH in combustion products, and also has

\* Abstract 5002 submitted to the 21st International Symposium on Rarefied Gas Dynamics, Marseille, France, July 26-31, 1998

significant influence on ignition time of hydrogen in air [3].

## References

- [1] V.I. Alfeyorov, L.M. Dmitriev, B.V. Egorov, Yu.E. Markachev, A.P. Rudakov. On Possibility of Reproducing Flight Condition for Vehicles Hypersonic MHD-Gas Acceleration Wind Tunnels //In book: Twelfth International Conference on Magnetohydrodynamic Electrical Power Generation. The Yokohama Symposia, 15-18 October, Japan, 1996, vol. 1, pp. 435-444.
- [2] Combustion Chemistry //Edited by W.C. Cordiner Jr. Springer-Verlag, New York Inc., 1984, Chapter 3.
- [3] B.V. Egorov, Yu.E. Markachev. Influence of nonequilibrium vibrational energy exchange on induction time in supersonic combustion of hydrogen in air (in Russian) //In compilation: Theory and construction of aircraft engines. Moscow, Phasis, 1994. pp. 33-35.
- [4] B.V. Egorov, V.A. Mokhov, Yu.E. Markachev. Numeric simulation of nonequilibrium flows in nozzle and jet of SSTO scramjet //same.

# Aerodynamical Hysteresis at Hypersonic Viscous Flow Around SOYUZ Landing Vehicle. Flight Data \*

A.G. Reshetin

Rocket Space Corporation Energia, Korolev, Russia

The Hysteresis of main aerodynamical coefficients of longitudinal  $C_A(\alpha)$  and normal  $C_N(\alpha)$  forces and moment  $C_m(\alpha)$  were founded in wide range of  $\alpha = -110^\circ \div +18^\circ$  at flight tests of SOYUZ lander during reentry in viscous interaction mode (altitude  $H=82 \div 86$  km,  $M \sim 28$ ). This phenomenon, well known in aerodynamics, for the first time was determined at special test flights of two landers having special purpose of aerodynamical characteristics estimation. Before and later at wind tunnel tests with fixed angles of attack we have not seen this effect. Unfortunately, we also do not know methods of calculation, that can indicate such phenomena. Nevertheless, the obtained information validity was thoroughly tested and is beyond any doubt.

The scheme of experiment follows. Lander, using jets system, was oriented at large angle of attack  $\alpha \approx -110^\circ$ . After that, control system was turned out and vehicle performed free oscillations with damping amplitude during 30 seconds. Using movement parameters measurements the main aerodynamical coefficients  $C_A(\alpha)$ ,  $C_N(\alpha)$ ,  $C_m(\alpha)$  were determined. The significant deviation of these coefficients values at  $\alpha = \text{Const}$  and at angle of attack increasing and diminishing was obtained. In range  $\alpha = 0 \div -90^\circ$  this deviation is for coefficient  $C_A(\alpha)$  about 20% and for coefficient  $C_N(\alpha)$  about 17% of their maximum values at  $\alpha = 0^\circ$  and  $\alpha = -90^\circ$  correspondingly. The distinctive feature is that absolute differences in  $C_A(\alpha)$  and in  $C_N(\alpha)$  practically doesn't depend on angle of attack in range  $\alpha = 0 \div -90^\circ$  at landing vehicle angular rates  $\omega_z = 0.5^\circ \div 20^\circ/\text{sec}$ .

Significant difference was observed in lift to drag ratio  $k(\alpha) = C_L(\alpha)/C_D(\alpha)$ .  $k_{\max}$  values for case of growing angles of attack is threefold greater than values for diminishing  $\alpha$ .

Maximum differences in coefficient of moment  $C_m(\alpha)$  is observed at angles of attack range  $\alpha = -35^\circ \div -110^\circ$ . In case of angle of attack decreasing at oscillations relatively mass center  $C_m(\alpha)$  values (at  $\alpha = \text{Const}$ ) are significantly greater than in case of increasing  $\alpha$ . At lesser angle of attack values  $\alpha = -35^\circ \div 0^\circ$  the hysteresis is insignificant.

At landing vehicle flight in more dense atmosphere  $H=66 \div 60$  km,  $M=23 \div 22$ , values of coefficients  $C_A(\alpha)$ ,  $C_N(\alpha)$ ,  $C_m(\alpha)$  practically do not depend on sign of  $\alpha$  time derivative in range of  $\alpha = -45^\circ \div -10^\circ$ . Hysteresis is practically absent.

Flight test results allowed to refine aerodynamical characteristics (including moment ones), update landing vehicle balancing and to increase payload weight more than 100 kg.

\* Abstract 5126 submitted to the 21st International Symposium on Rarefied Gas Dynamics, Marseille, France, July 26-31, 1998

## Expansion of Supersonic Gas Flow around a Corner \*

E.M. Shakhov, V.A. Titarev  
 Moscow State Technical University, Moscow, Russia

The paper is devoted to numerical analysis of two-dimensional steady supersonic rarefied gas flow of type Prandtl-Meyer expansion around a corner between two half-planes. The flow is studied within the framework of the kinetic model equation by finite difference method. Undisturbed uniform stream of monoatomic rarefied gas flows along half-plane  $y = 0, x < 0$  under boundary condition of specular reflection of molecules. At the origin of cartesian co-ordinate system the angle point of the bounding surface is located. Downstream of the angle point, at the half-plane  $y = x \operatorname{tg} \varphi, x > 0$  specular-diffuse boundary condition for surface-molecule interaction is assigned. Main attention is paid to the limiting cases: 1) specular reflection of oncoming molecules and 2) absolute absorption of oncoming molecules with no reflection from the surface. In the first case effect of rarefaction induced by deflection of the flow near the angle point is only studied. In the second case the effect of absorbing surface (modeling cryogenic panel) is investigated in addition. The numerical solution is performed for different values of the deflection angle  $\varphi$ . Characteristic Mach number  $M=3$ . Special attention is paid to the flow under deflection angle  $\varphi_{\max}$  corresponding to the maximum angle in gasdynamical Prandtl-Meyer expansion into vacuum. For this angle in continuum regime mass flow to the absorbing plane is equal to zero. But in the kinetic theory of gases the mass flux is non-zero. The main purpose of this work is to estimate the value of this flux.

The numerical results will be presented at the conference.

---

\*Abstract 5173 submitted to the 21st International Symposium on Rarefied Gas Dynamics, Marseille, France, July 26-31, 1998

# Impingement of Extended Supersonic Jets onto Flat Surface \*

S.B.Svirschevsky, E.L.Tarhov, S.A.Popov

Moscow State Aviation Institute-Technical University, Moscow, Russia

The underexpanded plumes from rocket engines and other nozzle sources may impinge on surfaces of planets, spacecrafts, criopanel and etc. causing pressure load, surface heating, and contamination. At this moment the studies of plume impingement become important for practical goals [1-3]. However few works were done about interaction of plumes with surfaces at the big distance from nozzle sources and with nonparallel jets.

In this paper the results of experimental studies of the interaction of single plume and multi-plume with a flat plate normal to the axis of jet source are presented. It is known that the impingement of an high density plume upon a surface produces a number of regimes. The regime type depends on the next gasdynamic parameters: the exit Mach number  $M_j$ , the expansion ratio  $n$  ( $n = P_j/P_\infty$ ;  $P_j$ ,  $P_\infty$  are the exit and background pressure), the Reynolds number  $Re_*$  ( $Re_*$  is calculated with throat flow parameters), the geometric parameter  $H_*$  ( $H_* = H/d_j$ ;  $H$  is the distance between surface and nozzle;  $d_j$  is the nozzle throat diameter) and so on.

The aim of the present experiments is to classify the types of interactions of extended jets with surface and to investigate some phenomena of such flow field. The experiments have been made in the low-pressure chamber of the sub-supersonic closed layout wind tunnel T2 MAI. The experiments included the visualization of the jet flow by means of optical system TE-21 and detailed pressure measurements on the flat surface. The investigations were conducted under the following range of parameters;  $M_j = 2.46 - 4.4$ ,  $n = 1.1 - 75$ ,  $H_* = 20 - 172$ ,  $f_j = 1 - 19$  ( $f_j$  is the number of the nozzles),  $d_j = 0.805 - 2.012$  mm,  $P_\infty = 5800 - 6860$  Pa. The outer surface of nozzle source was spherical with radius  $R = 27.5$  mm. The air at the stagnation temperature  $T_0 = 288$  K was used. It were found the pressure ratio  $P_* = (P - P_\infty / P_\infty)_{max}$  as the function of  $M_j$ ,  $n$ ,  $f_j$ ,  $x_*$  ( $x_* = x/d_j$ ,  $x$  is the distance from axis of nozzle source), the characteristic length of the interaction

area  $x_{max}$ . The experimental results for single jet is shown in fig 1. The dots on this figure correspond to the next parameters: 1 -  $M_j=2.46$ ,  $n=75$ ; 2 -  $M_j=2.46$ ,  $n=40$ ; 3 -  $M_j=3.04$ ,  $n=1.7$ ; 4 -  $M_j=2.46$ ,  $n=10.3$ ; 5 -  $M_j=4.06$ ,  $n=1.1$ ; 6 -  $M_j=3.04$ ,  $n=8.4$ ; 7 -  $M_j=2.46$ ,  $n=2.2$ . It is seen that in the case 1 and 2 for  $n \gg 1$  the pressure ratio strongly depends on the structure of plume. The different phenomena jet flows are discussed in the paper.

## References

- [1] Lukyanov G.A., Sokolov E.I., Shatalov I.V. *Impingement of a Supersonic Underexpanded Rarefied Jets Upon a Flat Plate. Rarefied Gas Dynamics*. Plenum Press, New-York, V. 2, pp. 993-1000, 1985.
- [2] Lengrand J.C. *Plume Impingement Upon Spacecraft Surfaces. Rarefied Gas Dynamics*, Tokyo University Press, Tokyo, V.1, pp.217-228, 1984.
- [3] Deependran B., Sujith R.L., Kurian J. *Impingement of Low Density Freejets On a Flat Plate. Rarefied Gas Dynamics*, Peking University Press, Beijing, pp. 465-466, 1997.

\*Abstract 5187 submitted to the 21st International Symposium on Rarefied Gas Dynamics, Marseille, France, July 26-31, 1998

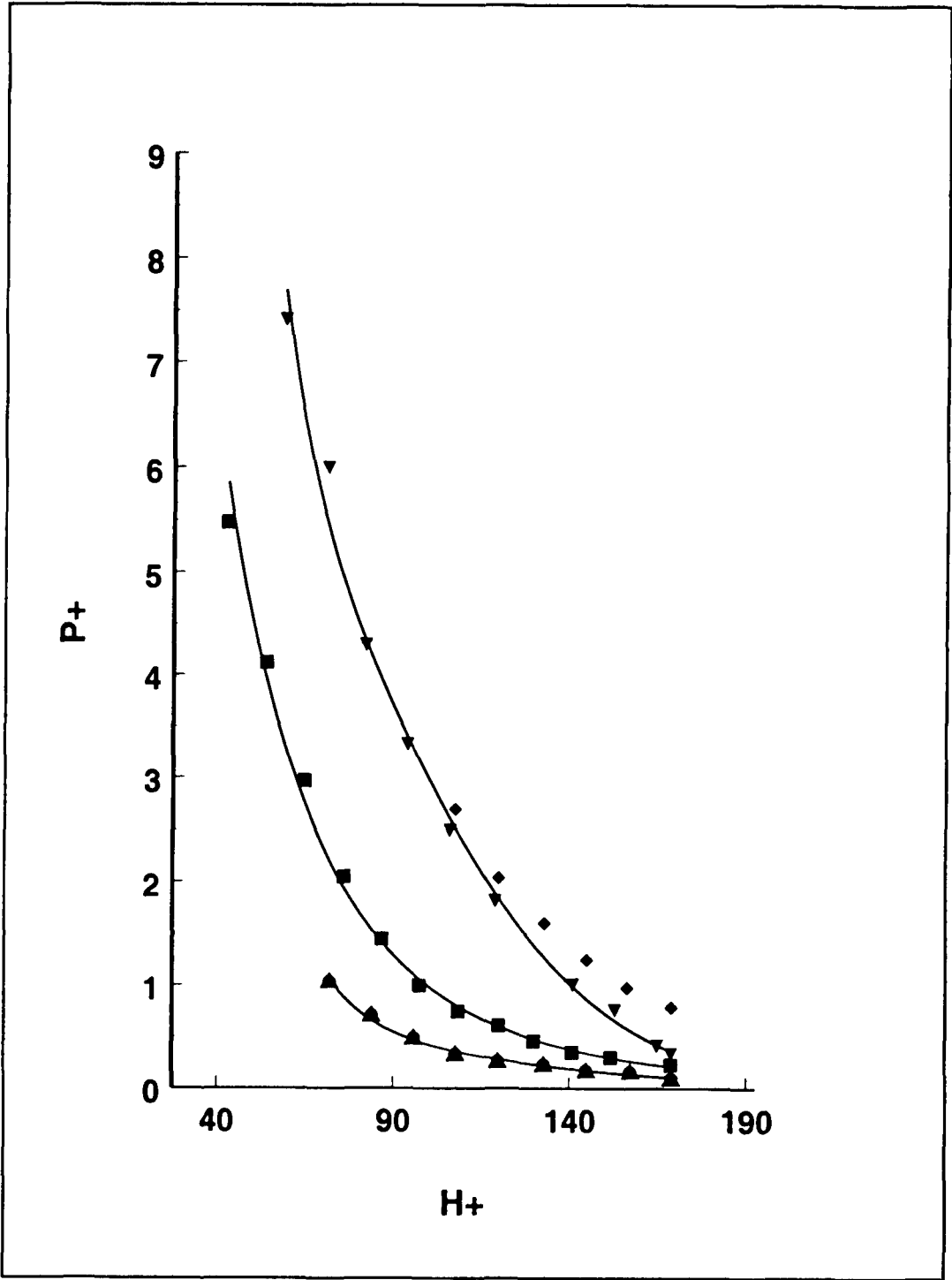


Figure 1: Pressure ratio distribution of jets impinging on a plate



# Comparison of Exact and Approximate Models of Near-Field of a Plume Issuing into Vacuum \*

E.I. Sokolov<sup>1</sup>, A.A. Ignatiev<sup>1</sup>,  
J.F. Vodovozova<sup>1</sup>, G.A. Markelov<sup>2</sup>, M.S. Ivanov<sup>2</sup>

<sup>1</sup> Institute for High Performance Computing and Data Bases, Saint - Petersburg, Russia

<sup>2</sup> Institute of Theoretical and Applied Mechanics, Novosibirsk, Russia

Prediction of power/heat loads and contamination effects due to firings of various thrusters of space vehicles is, up today, an important problem of rarefied gasdynamics. Both DSMC and continuous media equations (Euler and Navier-Stokes) are used for jet/plume calculations as well as numerous approximate methods. Last ones, however, are usually developed for far field of a plume. This paper presents the results of verification of some approximate methods in near field of a plume. Main idea is the verification of possibilities of these approaches in the case of non - zero thickness of nozzle lip and their further modification in order to make them more exact and real.

Numerical simulation of plumes under the study was made by Euler, Navier - Stokes (N-S) equations in the case of continuous media; brand new algorithm was developed particularly for N-S calculations of plumes of extremely large expansion ratios (up to  $10^{10}$ ). These results were compared with DSMC calculations. Jets of perfect argon and nitrogen were analyzed. Both no - slip and kinetic conditions were used along inner and outer walls of nozzle unit in N-S and DSMC calculations.

Two approximate models were taken for further analysis: widely used Simons model [1] and its few modifications and model presented in [2] based on quite different from [1] ideas. First one can take into account nozzle boundary layer with appropriate chosen constants in exponential law for outer plume region; second one can do it in the way of description of profiles of gasdynamic parameters of nozzle boundary layer at the exit cross section. Modification of approximate model [2] for the case of slip and temperature jump conditions as far as for the case of presence of non - zero nozzle lip is presented.

Possibilities of combination of full or parabolized

N-S equations for calculation of gas flow inside a nozzle and vicinity of its exit and Euler equations for more far plume regions are analyzed. In this case, coordinates connected with streamlines are used. It is known such coordinates allow to take into account some physical effects inside the plume ( e.g., condensation) in most simple way [3]. In the frames of local approach [2], an analysis of possible affect of mentioned physical processes on normal and shear stresses distributed along flat plate placed inside peripheral region of a plume is presented.

## References

- [1] Simons G.A., *Effect of Nozzle Boundary Layers on Rocket Exhaust Plumes*, AIAA Journal, V.10, No.11, pp. 1534-1535, 1972.
- [2] Sokolov E.I., Suslov V.P., Bykov F.B. *Supersonic Jet - Surface Interaction in Free - Molecular and Transitional Flow Modes*, Proceedings of the 17-th Int. Symposium on Rarefied Gas Dynamics. Aachen, pp. 979-986, 1990.
- [3] Skovorodko P.A., Lengrand J.-C., *Computation of plume flow exhausting into a vacuum, including the corresponding viscous flow in the nozzle*, Report 90-9, Laboratoire d'Aérothermique de CNRS. December 1990.

\*Abstract 5232 submitted to the 21st International Symposium on Rarefied Gas Dynamics, Marseille, France, July 26-31, 1998

# Continuum Models for the Problems of Hypersonic Flow of Rarefied Gas over Blunt Body \*

G.A. Tirskiy Institute of Mechanics, Moscow State University, Russia

We derive all existing continuum models for steady 2D super- and hypersonic flows past smooth blunted bodies from the Navier-Stokes equations. A unified asymptotic approach is used to obtain the models covering the full range of Reynolds numbers  $Re$ , i.e., from small  $Re$  (free-molecular and transient regimes) to large  $Re$  (boundary layer regime). In particular new gas-dynamic model is discovered for  $Re \rightarrow 0$  and  $k \rightarrow 0$  under the condition  $(k/Re)^{1/2} \rightarrow 0$ , where  $k$  is the ratio of the free-stream density to the density just behind the shock. This model differs from boundary layer, viscous shock layer, and parabolized Navier-Stokes models derived in the past for large, moderate, and small  $Re$  numbers, respectively. The model is reduced to the approximate "local" Stokes equations with vanishing inertia and pressure forces, with boundary conditions imposed on the unknown free boundary (shock wave). The solution for supersonic flow within the model yields free-molecular limit for the friction, pressure, and heat-transfer coefficients. So, the Newton limit for the wave drag is obtained strictly from the Navier-Stokes equations. In doing so, the Knudsen number, defined by using the vanishing (within the model) thickness of the shock layer, tends to zero. Thus, the condition for continuum approach is satisfied.

The equations for all models are written out in the Dorodnitsyn-Lees variables known from the boundary layer theory. This enables one to estimate approximately the second-order effects of the boundary layer theory depending on the Reynolds number  $Re$  and parameter  $k$  (measure of the compression in the shock layer), and to present all aerodynamic and heat characteristics using a unified dependence on the Reynolds number in the whole range of its values, i.e., from zero to infinity.

Earlier, the author together with collaborators developed an effective numerical method of global iterations for integrating the viscous shock layer equa-

tions. The method can be applied to super- and hypersonic flows over the windward part of a blunt body within the unified model for all Reynolds numbers. The only necessary correction consists in specifying  $(k/Re)^{1/2} \rightarrow 0$  as  $Re \rightarrow 0$ . This means that instead of calculation of aerodynamic and thermodynamic characteristics by using different models corresponding to different ranges of  $Re$  (different flow regimes), one can carry out calculations within a unified model along the whole (re)entry trajectory of a space vehicle or a natural space object (meteoroid).

Further, on the base of extensive numerical solutions of supersonic viscous perfect gas flow over the sphere when Mach number  $M_\infty = 2 - 10$  and  $Re_\infty = 100 - 10000$  the comparison of solutions for three gas dynamic models have done. The first one get out in the framework of Navier-Stokes equations (NS), the second one used the parabolized Navier-Stokes equations (PNSE) and the third one obtain in the framework of viscous shock layer (VSL).

When  $Re_\infty \geq 500$  over the whole range of Mach numbers, and when  $Re_\infty \approx 100$  and if  $M_\infty$  is small, the solution obtained by all those models are similar to each other. When  $Re_\infty \approx 100$  and when  $M_\infty$  is large the distinction became appreciable. Over the whole range of  $Re_\infty$  and  $Me_\infty$  under the consideration the heat transfer flux and skin friction coefficient at the sphere are weekly depend on gas-dynamic model. When  $k \rightarrow 0$  and  $Re \rightarrow 0$  PNSE solutions gives us the free-molecular limit for the drag coefficient, skin friction coefficient and heat transfer.

\*Abstract 5251 submitted to the 21st International Symposium on Rarefied Gas Dynamics, Marseille, France, July 26-31, 1998

## Hypersonic Separated Flows at Low Reynolds Number Conditions \*

J. N. Moss<sup>1</sup>, B. R. Hollis<sup>1</sup>, B. Chanetz<sup>2</sup>, T. Pot<sup>2</sup>

<sup>1</sup> NASA Langley Research Center, Hampton, VA, USA

<sup>2</sup> ONERA, Chalais-Meudon, France

### Abstract

Results of numerical simulations of Mach 10 air flow about a hollow cylinder-flare and spherically blunted cone configurations are presented. The simulations are achieved using the direct simulation Monte Carlo (DSMC) method of Bird [1] for low Reynolds number conditions that ensure laminar separation and laminar reattachment. Particular emphases are placed on the sensitivity of the computed results to grid resolution as well as the run time simulation to ensure converged results. Both factors are critical for generating credible results for viscous interacting flows, particularly those that include separation.

Hypersonic flows involving separation have been and continue to be a challenge for accurate numerical simulation. The two problems for which computations are made in the present study are those that have been investigated as part of an AGARD Working Group 18 activity [2]: shock wave/boundary layer interactions for a hollow cylinder with a 30-deg flare and the flow separation and reattachment resulting from the flow about 70-deg spherically blunted cones with extended afterbodies. The experiments for the hollow cylinder flare have been completed using the ONERA R5Ch wind tunnel. Tests are being organized in R5Ch using 5.08 cm diameter blunted cone models for 1998. Consequently, calculations will be made for both model configurations using the flow conditions produced in the R5Ch tunnel. The nominal test conditions are: Mach 9.91 air, freestream unit Reynolds number of 178,900 per meter, stagnation temperature of 1050 K, and a wall temperature of 293 K.

Details of the experiments for the hollow cylinder flare are presented by Chanetz [3] and a recent summary of both experimental and computational contributions is presented by Chanetz et al [4].

\* Abstract 6211 submitted to the 21st International Symposium on Rarefied Gas Dynamics, Marseille, France, July 26-31, 1998

The present computations address grid refinement and its impact on flowfield structure and surface results. Also, a time evolution of the DSMC results will be presented to indicate the nature of the convergence and to ensure that steady state conditions are achieved prior to the generation of the final time-averaged results. Comparisons with the measurements of Chanetz will be made concerning surface heating and pressure along with locations for flow separation and reattachment as inferred from oil flow measurements.

The blunt body/wake flow experiments being organized for 1998 are a continuation of the AGARD WG18 activity. The objective is to obtain fully laminar wake data for code validation where tests will be made in two low density wind tunnels at low enthalpy conditions. Model configurations that will be used in this test program are the AGARD WG18 configuration and a Mars Pathfinder model. Common to both models is a 70-deg spherically blunted cone forebody where the nose radius is 50 percent of the base radius. The WG18 model has a flat afterbody while the Mars Pathfinder derived model has a conical frustum afterbody. Both models are supported with a sting attached to the base. These models will be extensively instrumented with thin-film heat transfer gages (up to 70 gages) along both the model and the sting.

The blunt body calculations will emphasize the effect of grid resolution and time evolution of the wake flow to ensure accurate time-averaged results. If results are available from the experimental test program, comparisons of calculated and measured heating distributions will be made.

### References

- [1] Bird, G. A., *The G2/A3 Program Users Manual*, G.A.B. Consulting Pty Ltd, Killara, N.S.W., Australia, March 1992.

- [2] Anon, *Hypersonic Experimental and Computational Capabilities: Improvement and Validation*, AGARD AR-319, Vol. 2, To be published, 1998.
- [3] Chanetz, B., *Study of Axisymmetric Shock Wave/Boundary Layer Interaction in Hypersonic Laminar Flow*, ONERA Technical Report n RT 42/4623 AN, Feb.1995.
- [4] Chanetz, B., Benay, R., Bousquet, J. -M., Bur, R., Pot, T., Grasso, F., and Moss, J., *Experimental and Numerical Study of the Laminar Separation in Hypersonic Flow*, To be published in Aerospace Science and Technology, 1997.

# Rarefied Aerothermodynamic Predictions for Mars Global Surveyor \*

R. G. Wilmoth<sup>1</sup>, D. F. G. Rault<sup>1</sup>, R. W. Shane<sup>2</sup>, R. H. Tolson<sup>2</sup>

<sup>1</sup> NASA Langley Research Center, Hampton, VA, USA

<sup>2</sup> George Washington University, Hampton, VA, USA

## Abstract

Mars Global Surveyor (MGS) is the first planetary mission designed to use aerobraking as a primary means of customizing its orbit in order to achieve its mission objectives [1]. The aerobraking requirements together with post-launch anomalies [2] have presented a unique challenge to provide accurate predictions of the aerothermodynamic environment of the spacecraft in the rarefied transitional flow regime. A variety of three-dimensional Direct Simulation Monte Carlo (DSMC) and free-molecular techniques have been used to satisfy the prediction requirements, and this is the first major planetary mission in which rarefied-flow predictions have played such a critical role all the way through the design, mission planning, and operational phases. The purpose of this paper is to discuss these requirements, describe the particular three-dimensional DSMC and free-molecular tools used, and present selected results from the computational studies.

The studies performed include pre-launch aerodynamic and heating predictions that were used (1) in the design of the solar panel arrays which are the principal drag-producing components, (2) in the mission planning for selecting specific aerobraking parameters, e.g., altitude, attitude limits, and panel sweep angles and (3) to investigate specific issues such as aerodynamic interactions caused by reaction control jet firings [3]. Incomplete deployment of one of the solar arrays shortly after launch produced additional analysis requirements: (1) to devise an alternate aerobraking configuration and confirm its aerodynamic characteristics, (2) to investigate specific aerodynamic heating issues arising for this modified configuration, and (3) to re-define the aerodynamic databases needed for atmospheric density reconstruction from on-board ac-

celerometer measurements. Finally, anomalous deflections of the partially-deployed solar panel that occurred in the early drag passes required extensive analyses to determine the aerodynamic stability of alternate configurations that might reduce these deflections[4].

The analyses were carried out using three-dimensional DSMC and free-molecular codes that have been developed in recent years for analyzing complex geometries. The NASA LaRC 3D DSMC code (denoted DSMC1 herein) uses an unstructured grid where each computational cell is composed of one or more elements from an underlying uniform Cartesian mesh which may be made finer near the body[5]. The body geometry is described as a discrete set of small Cartesian elements but the code retains information on local surface normals from a more exact geometry definition and allows the inclusion of a body-fitted grid region near the wall to capture Knudsen layers. The DAC (DSMC Analysis Code) code (denoted DSMC2 herein) uses a two-level Cartesian grid, where the first level is a uniform structured mesh and the second level consists of a locally refined Cartesian mesh within each first-level cell[6]. The body geometry is described as an unstructured triangular grid which clips the local Cartesian grid. Each code has certain unique advantages but both codes use similar DSMC procedures and physical models and both are capable of handling the complex geometry of the MGS spacecraft. The DSMC codes are complemented by several 3D free-molecular codes each of which uses analytical free-molecular analysis and line-of-sight shadowing techniques to model the flow about complex geometries.

Analysis of MGS aerodynamics and heating was performed primarily using DSMC1 in the design phase and in the early post-launch, pre-aerobraking phase[7], while DSMC2 was used primarily in the later post-launch, pre-aerobraking phase and in the early operational phase of aerobraking. Calculations were performed for a variety of solar panel po-

\* Abstract 6466 submitted to the 21st International Symposium on Rarefied Gas Dynamics, Marseille, France, July 26-31, 1998

## AEROSPACE APPLICATIONS - AA P

sitions and spacecraft attitudes and for atmospheric densities ranging from free-molecular to transitional flow (Knudsen numbers less than 0.1). A typical geometry model used in computations with DSMC1 is shown in Fig. 1. This model was constructed from a highly detailed thermal analysis model and contains considerable details of the spacecraft bus assembly. A somewhat simplified model (not shown) was used by DSMC2. The simplified model has a similar definition of the solar panels but a simpler description of the spacecraft bus constructed from a free-molecular geometry model used for much of the mission analysis. Results obtained with each model and code demonstrate that both approaches give quite similar aerodynamic predictions in the free-molecular and transitional flow regimes. A sample comparison of drag coefficients computed for various geometry models is shown in Fig. 2 as a function of atmospheric density. The final paper will include selected results that illustrate the computational capabilities in providing the needed predictions, comparisons of the aerodynamic predictions between the various DSMC and free-molecular codes, and results that demonstrate the significant transitional flow effects on both the heating and aerodynamic behavior of MGS. Emphasis will be given to more recent results that address specific post-launch rarefied aerothermodynamic issues.

- [6] Wilmoth, R. G., LeBeau, G. J.; and Carlson, A. B., *DSMC Grid Methodologies for Computing Low-Density, Hypersonic Flows About Reusable Launch Vehicles*, AIAA Paper 96-1812, June 1996.
- [7] Shane, R. W., Rault, D. F. G., and Tolson, R. H., *Mars Global Surveyor Aerodynamics for Maneuvers in Martian Atmosphere*, AIAA Paper 97-2509, June 1997.

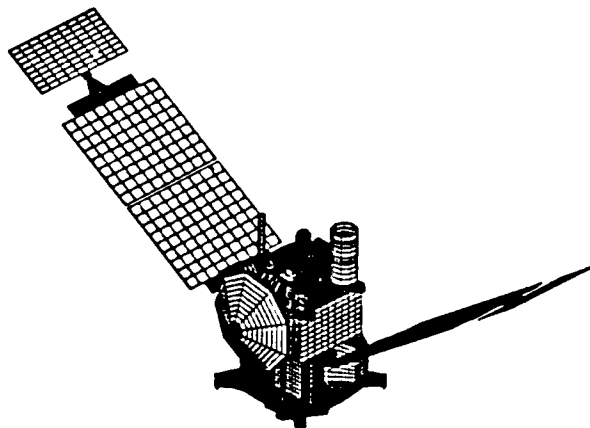


Figure 1: Detailed Pre-Launch MGS Geometry Model. (Actual surface resolution used was higher for some elements. Resolution reduced for illustration purposes only.)

## References

- [1] Dallas, S. Sam, *Mars Global Surveyor Mission*, Proceedings of IEEE Aerospace Conference, Vol. 4, Snowmass at Aspen, CO, Feb. 1-8, 1997, pp. 173-189.
- [2] Lyons, Daniel T., *Mars Global Surveyor: Aerobraking with a Broken Wing*, AAS Paper 97-618.
- [3] Rault, D. F. G., *RCS Plume Effect on Spacecraft Aerodynamics*, 20th Rarefied Gas Dynamics Symposium, Beijing, China, August, 1996.
- [4] Wilmoth, R. G., Cheatwood, F. M., Engelund, W. C., Qualls, G. D., and Shane, R. W., *Rarefied Aerodynamics of Mars Global Surveyor Aerobraking Configurations*, Submitted to Journal of Spacecraft and Rockets.
- [5] Rault, D. F. G., *Towards an Efficient Three-Dimensional DSMC code for Complex Geometry Problems*, 18th Rarefied Gas Dynamics Symposium, Vancouver, British Columbia, July 1992

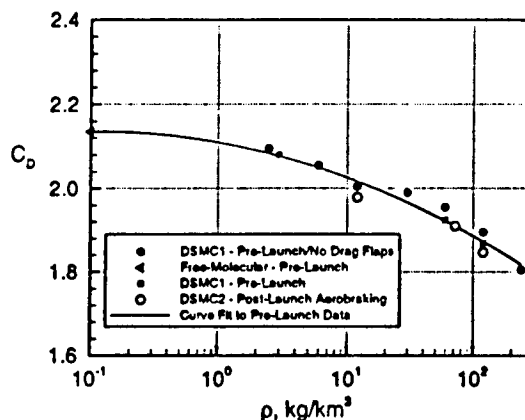


Figure 2: Comparison of Drag Predictions for Various Geometry Models and DSMC Codes.

# CDF/DSMC Simulation of Cold Gas Thruster Nozzle and Plume Flow and Comparisons with Space Flight Data \*

N. A. Gatsonis<sup>1</sup>, R. Nanson<sup>1</sup>, G. J. Lebeau<sup>2</sup>

<sup>1</sup> Computational Gas & Plasma Dynamics Laboratory  
Mechanical Engineering Department, Worcester

<sup>2</sup> JSC, NASA, Houston

The study of plumes from small attitude control thrusters is very important for contamination purposes, as well as for determining plume impingement forces. There have been numerous ground-based experimental investigations of small thruster plumes. Numerical simulation studies of plumes have been carried out with Navier-Stokes codes. The major shortcomings of the continuous description of the expanding plume are related to the breakdown and non-equilibrium due to the rarefaction effects and have been addressed with the Direct Simulation Monte Carlo (DSMC) method. Recent studies combine the two methods by following the flow via a Navier-Stokes approach until breakdown is established, then continue with the DSMC approach. In cases of plumes from low-density nozzles the flow may be followed using the DSMC method in its entirety.

Data analyses from space-based experiments with thrusters have been limited and mostly related to the Space Shuttle. Since the early Shuttle flights ample evidence has been provided to demonstrate the effects of thruster firings on the induced environment. Many subsequent investigations have addressed the plasma, neutral, and electromagnetic environment during thruster firings. However, the complexity of the Shuttle operations, its geometry, and its induced environment make the interpretation of neutral environment parameters very difficult. Recently, data from rocket experiments have also demonstrated the effects of thruster firings on the neutral pressure environment.

This study presents a combined CFD/DSMC study of the nozzle and plume flow of attitude control thrusters. The simulations are performed in order to compare with pressure measurements taken onboard the Environmental Monitor Package (EMP) suborbital spacecraft. The data were obtained during thruster firings of the N<sub>2</sub> cold-gas attitude control system.

## Experiment Description

An experiment to characterize the induced environment around a suborbital spacecraft was conducted by the Applied Physics Laboratory. The spacecraft, called the Environmental Monitor Package (EMP), contained instruments designed to measure the total gas pressure, water vapor concentration, neutral and ion gas concentration, and flux of dust particles. Pressure measurements taken onboard the spacecraft exhibited non-periodic pulses during attitude control thruster firings. The attitude control system located at the bottom of the conical EMP spacecraft included eight thrusters for pitch, yaw and roll control. The pitch and yaw thrusters delivered 1.245 N thrust while the roll thrusters delivered 3.278 N with impulses that lasted up to 0.03 s with multiple pulses per firing. The pressure sensor was housed inside the spacecraft and was connected to the outside with a 0.1-m long, 0.022-m diameter tube. Pressure pulses appeared instantaneously with the firings even for thrusters without a direct line-of-sight with the sensor entrance. Pressure data are superimposed on a background pressure that can be attributed to internal outgassing. Plumes from thrusters with the same level of thrust resulted in large differences in pressure depending on their orientation with respect to the pressure sensor. Data analysis demonstrated plume wrap-around and free surface/plume interaction phenomena.

---

\* Abstract 6601 submitted to the 21st International Symposium on Rarefied Gas Dynamics, Marseille, France, July 26-31, 1998

#### **Nozzle and Plume Flow Simulations**

A combined CFD/DSMC analysis was performed for the EMP thrusters. In order to obtain estimates of the plume rarefaction effects, simulations of the nozzle and plume flows were performed using Rampant, a finite-volume Navier-Stokes solver. The computational domain used in these continuous simulations is three-dimensional and includes the nozzle and the EMP surface. A large computational domain was used in order to study the expansion process of the plume. The density and Mach number profiles show the development of the boundary layer in the small EMP nozzles and the rapid expansion near the lip region. The breakdown parameter defined by Bird as the approximate condition for rarefaction is obtained and used to define the breakdown surface. These continuous results indicated that the plumes become rarefied at length scales that are smaller than the diameter of the EMP bottom surface.

In order to capture the rarefied part of the plume flow DSMC simulations were performed using that DAC code. The DSMC simulation domain includes the EMP spacecraft. Inputs to the DSMC are obtained from flow conditions defined at the breakdown surface. The DSMC simulations showed plume-surface interactions and rarefaction effects. Roll, yaw and pitch thrusters were simulated and the predicted surface pressure at the sensor location was compared with the flight data.



## Rarefied Flow Computations around Cylindrical Bodies. \*

A.A.Frolova

Computing center of RAS, Moscow, Russia

## 1 Introduction

Boltzmann equation approach of calculating of rarefied flow encounters great computational difficulties. Being multidimensional and nonlinear the equation requires to develop new effective methods for solving the problem. New conservative method of discrete ordinates [1] is used to study the flow around cylindrical bodies of different cross-sections. Combination of conservative evaluation of Boltzmann integral by projection method and different schemes of calculating of free molecular flow allows to compute complex configurations of circulation.

## 2 Statement of the problem

Consider the stationary flow of rarefied gas of hard spherical molecules around cylindrical body. The nonlinear Boltzmann equation for this flow has the form (in common notation):

$$\frac{\partial f}{\partial t} + \xi \frac{\partial f}{\partial \mathbf{x}} = \frac{1}{Kn} I(f, f)$$

It is assumed that axis of the cylinder is directed along  $z$ -axis and vector of velocity of undisturbed flow of gas directed along  $x$ -axis. So attack angle equals to zero. The distribution function  $f$  at  $\infty$  and distribution function of molecules reflected from surface of the cylinder are supposed to be Maxwell ones. The Maxwell distribution of reflected molecules is characterized by a given temperature  $T_w$  and density  $n$  calculated so that normal flux at surface is equal to zero. On the  $x$ -axis the condition of symmetry is satisfied.

## 3 The solution method

Consider a sphere in velocity space with center at

$$\frac{\xi_{x,max} + \xi_{x,min}}{2}, \quad \xi_y = 0, \quad \xi_z = 0,$$

\*Abstract 6626 submitted to the 21st International Symposium on Rarefied Gas Dynamics, Marseille, France, July 26-31, 1998

and radius

$$R = \frac{\xi_{x,max} - \xi_{x,min}}{2}$$

The velocity field is defined in nodes of uniform three-dimensional grid bounded of chosen sphere. Boltzmann equation is approximated by the system of the transfer equations with nonlinear source. At the first stage of calculations we make operator (time) splitting of the system of equations. The transfer equation is approximated with first-order upwind scheme. In order to treat geometry of the body we use curvilinear coordinates  $\rho(x, y)$ ,  $\varphi(x, y)$  on  $x, y$  plane. The functions  $\rho, \varphi$  depend on the shape of cross-section and can be changed according to the gradients of the dynamic parameters. To integrate the system of equations both divergent and nondivergent forms are used. It is well known that momentum equations obtained from upwind approximation of Boltzmann equation have an additional first-order error not equal to zero at uniform flow. A scheme of such type is not self-consistent. This can distort a behavior of macroscopic momenta. It can be especially dangerous when gradients of momenta are near to zero. To decrease both errors of not self-consistency and viscosity of scheme the second-order approximation is used. To compare different methods and choose more effective one we used the coordinate splitting scheme with one-dimensional corrections [2] and the W-modification of Godunov's method [3]. The W-modification is based on two-dimensional equation without splitting and uses two-dimensional corrections. The different flux limiters were tested also. To evaluate the collision integral a special projective method is used. The method guarantees strict preservation of mass, momentum, and energy on uniform velocity grid.

## 4 Calculations results.

The calculations were carried out for cylinder with elliptic cross-sections. The Mach number was about 2.0 and Knudsen number was varied from 0.01 to 0.001. The calculations showed that the scheme of

the first-order approximation used on adaptive grid gave good results. But in the shadow of the body the scheme of the second-order approximation allowed to obtain more correct and detailed structure of the flow. The calculations allowed to discover some thin effects (vorticity) behind the cylinder.

## References

- [1] F.G.Tcheremissine, *Conservative Discrete Ordinates Method for Solving Boltzmann Kinetic Equation*//Comp.Cent.of the Rus.Ac.of Scien.,Moscow,1996.
- [2] A.Harten, *High resolution schemes for hiperbolic conservation laws*//J.Comput.Phys.1983.V.49.P.357-393
- [3] E.I.Vasil'ev, *W-modification of Godunov's method and its application for 2-d non-stationary flows of dusty gas*// Comput.Maths.Math.Phys.V.36, N.1, 1996, p.122-136

# Mathematic Modeling of Processes Underlying the Glow above Spacecraft in a Free-Molecular Flow \*

N.M. Kortsenstein<sup>1</sup>, Yu.A. Plastinin<sup>2</sup>, E.W. Samuilow<sup>1</sup>

<sup>1</sup> Krzhizhanovsky Power Engineering Institute, Moscow, Russia

<sup>2</sup> TsNIIMash, Korolev, Russia

## 1 Introduction

Substantial attention is paid to the research of the orange glow above spacecraft (S/C) surfaces nowadays. Several reviews are known to discuss this problem ([1] and some others). In particular, various mechanistic interpretations proposed by several research teams are reviewed there. Some laboratory experiments were also published [1],[2], in which the researchers tried to reproduce an in-flight environment. For example, Slanger [3] insists that  $OII^*$  molecules (the asterisk denotes molecules in the electron-excited state) are responsible for the glow above a satellite surface. Besides, glow mechanism, in which  $NO$  and then  $NO_2^*$  molecules are formed is investigated to explain the orange glow above ram surfaces of satellites and reusable S/C,  $NO_2^*$  being responsible for the  $NO$  luminescence. Torr et al.[4] proposed that atoms of  $N$  and  $O$  are recombining upon a satellite surface to form  $NO$ . Later this mechanism was developed in other papers (see review [5]). In the process of investigating the orange glow some interesting peculiarities were revealed, amongst them a linear dependence of the glow brightness versus atomic oxygen concentration at altitudes higher than 160 km both for satellites and, as it was described in review [5], the Shuttle Orbiter. To further clarify the role of various collisional and surface-bound processes, a mathematical model should be built implying available experimental data.

## 2 Model definition

A mathematical model is proposed in this paper to describe the mechanism of the orange glow through the formation of  $NO_2^*$  molecules. The following method of solution is proposed: (a) a

set of kinetic equations is written down for possible chemical reactions; (b) through its resolution time-dependent concentrations of various chemical components above and on the S/C surface are defined; (c) steady-state concentrations are derived from them; (d) these results will help to define the intensity of  $NO_2^*$  radiation as well as the transient-to-steady-state interval. The core of the model is the concept of active centers on the S/C surface which play host to adsorption-desorption processes, and chemical transformations. The surface can be covered with not more than one layer of atoms or molecules. In the proposed model the authors have taken into consideration the following chemical components involved in the processes on the surface and above it:  $O$ ,  $NO_2$ ,  $NO$ ,  $N_2$ ,  $NO_2^*$ ,  $NO^*$ . The following processes have been included into the model: scattering; adsorption of molecules on the surface; thermal desorption; collisional desorption; chemical transformations and excitation of molecules in the collision of the ram with the adsorbed components (Eley-Rideal model); chemical transformations between components on the surface (Langmuir-Hinshelwood model); chemical transformations in the vicinity of the surface proceeding through singular collisions between components on the ram and components bounced or desorbed from the surface.

The method of computing incident flows on to the S/C surface is following. As it is known, for a free-molecular flow the density of molecules above S/C surface is higher than that of the surrounding environment due to the backscattering of molecules of the ram from the S/C surface. At high altitudes the molecules of the surrounding environment practically do not collide with the molecules in the above mentioned region of increased density because the absolute value of this density is very low and the free path of molecules is substantially greater than the S/C dimensions. At that altitudes the incident flows computed with help of the free path method. As the altitude decreases, the atmospheric density

\*Abstract 6666 submitted to the 21st International Symposium on Rarefied Gas Dynamics, Marseille, France, July 26-31, 1998

increases; firstly singular collisions of the environmental molecules with the denser region molecules become possible, then two-fold, etc. In particular, Caledonia et al.[1] proposed to consider the  $NO$  flow to the S/C surface because of singular collisions of  $N_2$  and  $O$  with  $O$  and  $N_2$  backscattered by the S/C surface. Therefore at the altitude below 160 km it was considered the process of singular collisions in expression for incident flow.

### 3 Computation of processes

The set of kinetic equations was numerically resolved by the Kutta-Merson method. Steady-state solutions of the kinetic equations were used to find outgoing flow of  $NO_2^*$  molecules per unit time from unit area ( $G_{NO_2^*}$ ). Using these data one can compute the intensity of photon flows for any given range, provided that life time of exited  $NO_2^*$  molecules and the total photon flow from the unit area are known. Computational research of the  $G_{NO_2^*}$  carried out as applied to altitudes 140 to 280 km. Five computational variants were fulfilled to reveal roles of various processes in the glow (see Figure 1). On Figure 1 Rgraf is reformed experimental results from [5],  $n(O)$  is the density of the atmospheric oxygen atoms,  $cm^{-3}$ . It was found that computations with proposed model give quantitative matching with experimental results at 280 km 160 km and qualitative matching below 160 km (see Figure 1, var1, var5), where var1 and var5 are correspond to two different methods of calculation  $NO$  flow to S/C in result of singular collisional of  $N_2$  and  $O$  with  $O$  and  $N_2$  backscattered by S/C surface. It was noticed that the processes involving atomic atmospheric nitrogen (see Figure 1, var4) and molecular atmospheric nitrogen (see Figure 1, var2), which not accounted for in the radiation model proposed in [6], play an important role within the full range of altitudes (140 to 280 km) used in computations. Correct estimation of  $NO$  and  $N$  formation in the gas above the S/C surface is also very important for reproduction of available experimental results of the brightness curve below 160 km (see Figure 1, var3). No substantial influence of the processes on the surface, which proceed according to the Langmuir-Hinshelwood model, at chosen values of the rate constants was found.

### References

- [1] Caledonia G.E., Holetzclaw K.W., Krech R.H. and Sonnenfroth D.M., Leone A., Blumberg W.A., *Mechanistic Investigation of Shuttle Glow*, J.Geophys.Res., Vol.98, No A3, 1993.
- [2] Sonnenfroth D.M. and Caledonia G.E., *Collision Desorption of NO by Fast O Atoms*, J. Geophys.Res., Vol.98, No A12, 1993.
- [3] Slanger T.G., *Conjectures on the Origin of the Surface Glow of the Space Vehicles*, Geophys.Res.Lett., Vol.10, p.130, 1983.
- [4] Torr M.R., Hays P.P., B.C.Kennedy B.C. and Walker J.C.G., *Intercalibration of Airglow observation with the Atmospheric Explorer Satellite*, Planetary and Space Sci., Vol.25, p.173, 1977.
- [5] Garrett H.B., Chatjan A., Gabriel S.B., *Glow above Spacecraft Surface and its Effects on On-board Equipment Operation*, J.Spacecraft and Rockets, No5, p.321, 1988.
- [6] Caledonia G.E. and Krech R.H., *An Investigation of the Mechanism for the Visible Shuttle glow*, Missile signature and Aerothermochemistry Meeting, Logan UT, 8 april 1994.

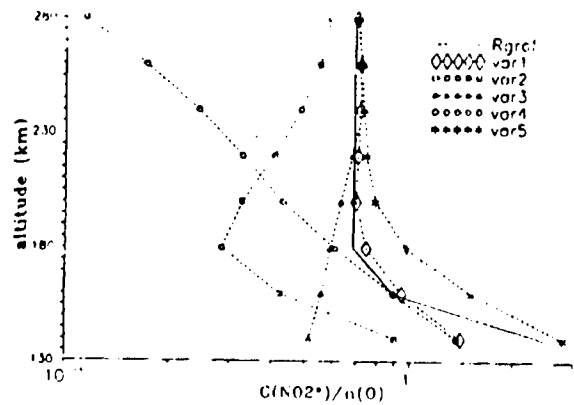


Figure 1:

# Direct Monte Carlo Simulation of Shock-wave/Boundary-layer Interaction \*

T. Soga<sup>1</sup>, Y. Iwayama<sup>1,a</sup>, B.G. Kim<sup>1,b</sup>, N. Hirose<sup>2</sup>, M. Yasuhara<sup>3</sup>

<sup>1</sup> Department of Aerospace Engineering, Nagoya University, Chikusa-ku, Nagoya, Japan

<sup>2</sup> National Aerospace Laboratory, Chofu, Tokyo, Japan

<sup>3</sup> Department of Mechanical Engineering, Nagoya Institute of Technology  
Yakusa-cho, Toyota, Japan

<sup>a</sup> Present address: Toshiba Co. Ltd, Kawasaki, Japan

<sup>b</sup> Present address: Hyndai Electronics Co. Ltd, Seoul, Korea

## 1 Objectives

This paper is concerned with the problem of shock-wave/boundary-layer interactions. Since the studies of Liepmann[1], Lees and Reeves[2], and Henderson[3], the phenomena of impingement of the oblique shock wave on the laminar boundary layer on the flat plate was intensively studied from the view point of continuum flow. Recent numerical studies by Zhong[4], and Kao et. al[5] demonstrated that continuum flow theory can well reproduce the experimental results of pressure distribution and shear force on the plate in the vicinity of the shock-wave/boundary-layer interaction. Recent development of the DSMC method make it tractable to treat the more complex shock-wave/shock-wave/boundary-layer interaction like the Edney's IV type interaction(Bird[6]).

However, the detailed studies of the present problem from the view point kinetic theory, especially impingement of shock-wave on the sonic line in the boundary-layer remain to be carried out till now. As is well known, present problem includes two length-scales, one is  $1/Re$  which is pertinent to the shock-wave and the other is the  $x/\sqrt{Re}$  which is pertinent to the boundary layer. CFD technique overcomes this disparate difference of the scales by introducing fine-multi-grids where the boundary layer is divided into over 20 or thirty grids; the TVD and other technique catch the shock-wave in a few or several meshes. In spite of such success in CFD, the shock-broadening in the vicinity of the sonic line and the dispersion of the shock wave in the subsonic region of the boundary-layer can be pre-

cisely studied from the aspect of molecular motions. Studies based upon the DSMC method can visualize the separation of the boundary layer flow and its re-attachment due to the impingement of shock-wave on the boundary-layer in the scale of mean free path.

## 2 Results

Oblique shock-wave was generated by the wedge with the half-aps angle of about  $22^\circ$  in the uniform supersonic flow of Mach number 5 impinges on the boundary-layer on the flat plate of length of 325 mean free path in the same supersonic flow. Two-dimensional flow field was divided into about 40,000 cells; most cells had a size,  $1\lambda_\infty \times 1\lambda_\infty$  where  $\lambda_\infty$  is the mean free path in the uniform flow. The height of cells adjacent to the plate wall was set to  $0.2\lambda_\infty$  so as to observe the velocity-slip adjacent to the wall.

Ten molecules, as a mean, were distributed in each cell at the beginning of the simulation. The total number of molecules was about 830,000 after the quasi-steady state is established. The average number of sampled molecules in each cell was about 18,000. Results of the present simulation were as follows:

(1) It is observed that the subsonic region in the boundary-layer swelled out in the vicinity of the shock-wave-impingement. The boundary of this region, i.e., iso-Mach line for  $M = 1$  had a peak and the both sides of this peak showed concaved contours. Many compression waves emerged from this concaved surface and they intersected the incident shock-wave forming a shock-wave; these compression waves seemed to be a dispersion of the incident

\* Abstract 6866 submitted to the 21st International Symposium on Rarefied Gas Dynamics, Marseille, France, July 26-31, 1998

shock-wave.

(2)The thickness of the boundary layer at  $x = 150\lambda$  (from the leading edge and outside of the interaction region) was about  $15\lambda_\infty$  and the location of the sonic line was about  $3\lambda$  from the wall, while at  $x = 225\lambda_\infty$  the location of the sonic line becomes about  $20\lambda$  from the wall, i.e., the subsonic region became 7 times thicker than the uninteracted case.

(3)The incident shock-wave reflected on the sonic line as an expansion wave; the actual reflection of the shock-wave took place in the supersonic region of the boundary layer from  $M = 1.5$  to  $M = 1$ . This expansion wave accelerated the flow toward the wall and there the reflected shock-wave merged on the concaved sonic line. Dispersion of the shock-wave(compression wave) was observed clearly. The location of the sonic line just downstream the reflected shock-wave was about  $6\lambda_\infty$  from the wall. This height controls the magnitude of the maximum heat flux on the wall in the shock-wave impingement on the boundary-layer.

(4)the distance between the separation point and the reattachment point was  $64\lambda_\infty$ . Negative shear stress was observed in this region.

(5)Obtained velocity profiles in the separation bable showed a good agreement with the theoretical prediction of Stewartson[2]. But it is worth noting that the separation-bable was on a stream-wise slip flow.

[4] X. Zhong, AIAA J. 32, p. 1606(1994).

[5] K-H. Kao, M-S. Liou, and C-Y Chow, AIAA J. 32, p.942(1994).

[6] G.A.Bird, in Rarefied Gas Dynamics, ed. by J. Harvey and G. Lord(Oxford University Press, 1995), Vol. Two, p.754.

### 3 Prospect

Present simulation suggested that the most important phenomena included in the shock-wave/boundary-layer interaction is the reflection of the incident and reflected shock-wave on the sonic line. So, how to predict the sonic line in the boundary-layer must be the most significant task in this problem. For the case of turbulence boundary-layer, sonic line must be always swaying in the scale of the thickness of shock-wave. Pressure distribution along the wall must be swaying about the mean values. Thus, unsteady shock-wave/boundary-layer interaction may be next target of this simulation.

### References

- [1] H. W. Liepmann, J. Aeronaut. Sci. 13, p. 623(1946).
- [2] L. Lees and B. L. Reeves, AIAA J. 2, p. 1907(1964).
- [3] L. F. Henderson, J. Fluif Mech., 30, p. 699(1967).

ASTROPHYSICS AND ENVIRONMENT - AE P

THURSDAY, JULY 30, 1998

16:00

# Aerophysical and Aeronomical Experiments Aboard of Space Orbital Research Module \*

V.P. Bass, V.I. Brazinsky

Institute of Technical Mechanics of Ukrainian National Academy of Science  
and Ukrainian National Space Agency, Dnepropetrovsk, Ukraine

## 1 Introduction

The proposals on realization of some aerophysical and aeronomical experiments which are to be carried out aboard of space low-orbital module with the aid of mass-spectrometric (MS) and spectrophotometric (SP) measuring equipment are considered.

Among the main experiments the following ones have to be mentioned:

- the study of effective cross-sections of scattering (CSS) for atoms and molecules of various gases in their interaction with multicomponent free stream in upper Earth atmosphere;
- investigation of gas flow mechanism in the vicinity of spacecraft (SC) surface and its influence on the onboard equipment;
- investigation of molecular composition variations in the upper Earth atmosphere during the period of high Solar activity;
- investigation of the gas dynamic processes, determining the formation of ambient atmosphere in the vicinity of SC.

The importance of numerical simulation and laboratory tests in treatment of data obtained during the space experiments, is emphasized.

## 2 Problem statement

The short-distant forces in the molecular interaction are rather thoroughly studied nowadays with the use of theoretical and experimental means. The main results, related to CSS measurement, have been obtained basically with the aid of particle accelerator, which is able to generate high energy

beams (up to  $E \sim \text{KeV}$ ). The range of moderate energies, corresponding to free stream interaction with satellite surface ( $E \sim 1\text{eV}$ ), is still poorly investigated. At the same time the solution of many theoretical and practical problems, related to rarefied gas kinetics, require more accurate data about the potentials of molecular interaction within this range of energies.

Collision processes to much extent are responsible for Earth atmosphere luminosity and for glow effects in the vicinity of satellite surface at the shadowed parts of the orbit. The glow phenomenon has negative effect on optical sensors and other onboard instruments, accustomed to function at low altitude orbits ( $\sim 300\div 400$  km above the Earth surface). The only first steps have been made lately toward the numerical analysis of satellite glow phenomenon and its effect on the onboard equipment.

The first onboard experiments supposed to be performed during the period of high Solar activity (in 2001÷2002), when considerable variations of atmosphere parameters on the altitudes 300÷400 km are expected.

The Solar effects on Earth atmosphere are still poorly investigated and presented in aeronomy. It seems to be the unique opportunity to learn these effects by launching the satellite during the high Solar activity. The appropriate collection of onboard equipment enables one to perform series of experiments to measure pressure variation of residual gases inside of different nonhermetic space modules.

## 3 The ways of realization and expected results

It is supposed to arrange the experiment in the following order:

\*Abstract 2281 submitted to the 21st International Symposium on Rarefied Gas Dynamics, Marseille, France, July 26-31, 1998



- the controlled source of selected gas composition with known flow parameters is installed aboard of orbital module;
- only those gases have to be selected, which are absent in upper atmosphere and their molecular weight sufficiently differ from atmosphere components, for example, Ne, Kr, Xe and others;
- the highly sensitive MS, installed aboard of space module, is destined to register separate atmosphere components flux at a given altitude and return flux of injected gases interacting with multicomponent free stream;
- SP is also installed on aboard space module in order to register light flux from ambient gas layer;
- the selected model of molecular interaction makes it possible to determine the cross-section of scattering and corresponding photometric parameters on the basis of measured data and numerical simulation of a given experiment.

Experiment is based on measuring of the flux of different classes of particles:

- all free stream components in the upper Earth atmosphere;
- return flux of particles from outgasing surfaces, which are scattered interacting with free stream in the unit volume;

It is also based on SP measuring of spectral and integral characteristics of object ambient layer glow.

This experiment is logical extension of research works performed in the Institute of Technical Mechanics of National Academy of Science (Ukraine) with the aid of Vacuum Aerodynamic Tube (VAT-2M) [1].

The treatment of obtained experimental data and their interpretation is supposed to perform with the aid of corresponding software [2]. It is supposed to use the onboard measuring equipment designed at the Physical and Technical Institute of Low Temperatures of National Academy of Science (Ukraine). The test and calibration of this equipment will be carried out at VAT-2M.

It is expected that in the framework of experiment the coordinated data, related to density variation of Earth atmosphere at the low altitudes (200÷400 km), spectral and integral characteristics of satellite structures radiation and effective CSS of various atoms and molecules will be obtained.

## References

- [1] Abramovskaja M.G., Bass V.P., Petrov O.V., Tokovoj S.V., *The measurement of full cross-section scattering of inert gases within the range of reciprocal energies 7-17 eV*, Journal of applied mechanics and Technical Physics, No.4, pp.28-32, 1988. (In Russian)
- [2] Bass V.P., Brazinsky V.I., *Numerical procedure to calculate mass-transfers in highly rarefied gases*, Journal of computational mathematics and mathematical physics. Vol.28, No.7, pp.1078-1098, 1988. (In Russian)

## Experimental Study of a Laboratory Stationary Plasma Thruster in the PIVOINE French Test Facility\*

C. Pérot, N. Gascon, A. Hauser, S. Béchu, P. Lasgorceix, M. Dudeck  
Laboratoire d'Aérodynamique du CNRS, Orléans, France

Considering the important international competition in the field of satellites, it is fundamental to extend the lifetime and increase the payload mass/structural mass ratio of spacecraft in order to reduce the launch and operation costs. These requirements have led several space organizations to study and develop electric propulsion systems, which are more interesting than the chemical ones for ensuring orbit maintenance and attitude control of geostationary satellites.

In France, CNES (Centre National d'Etudes Spatiales) has initiated research and development studies on a particular type of electric propulsion system: the Stationary Plasma Thruster (SPT), also called Hall thruster, or plasma thruster with closed electron drift. These studies support the works of the French spacecraft engines manufacturer SEP (Société Européenne de Propulsion).

The SPT, which was first developed in Russia in the 1960s, has several advantages: for a typical SPT100 (100mm diameter discharge chamber), an efficiency of 45-50%, a specific impulse (thrust/propellant flow) of 1400-1500s, a thrust of 70-80mN, a long lifetime (up to 5000h) and a large number of on/off cycles (up to 4000).

A SPT produces an ion beam within an annular discharge chamber (channel). The discharge is sustained between an external hollow cathode and an internal ring-shaped anode. Electromagnets are used to generate within the channel a radial magnetic field, which reduces the electron conductivity and permits the plasma to sustain a high axial electric field, which in turn accelerates the thrust-producing ions.

Though the functioning principle of a SPT is simple, a lot of the physical processes that occur in the thruster are not yet fully understood. Thereby, the optimization of a SPT is a very complex task. For these studies, the French Research Group "Plasma Propulsion for Orbital Systems" has been created,

joining teams of CNRS (Centre National de la Recherche Scientifique), ONERA (Office National d'Etudes et de Recherches Aéronautiques) and SEP. The research program includes theoretical, computational and experimental studies, which aim at better understanding the physical and operational characteristics of the SPT, in order to improve the performances.

The experimental studies of the program need special facilities to simulate the space environment where the SPT work. The quality of the environment simulation is important to obtain reliable ground data on thruster performances in space. A clean vacuum is required, with a pressure of less than  $2 \times 10^{-5}$  mbar (for a flow rate of xenon propellant of 5 mg/s. In the beginning of the research program, CNES decided to build a completely new test facility which would fulfill the requirements of experimental plasma propulsion research. The designing, building and operational managing responsibility was given to the Laboratoire d'Aérodynamique.

The test facility, located in Orléans, France, and named PIVOINE (Propulsion Ionique pour les Vols Orbitaux - Interprétation et Nouvelles Expériences), was presented during its building phase at the last RGD Conference in 1996. It is now operational.

The test facility design is based on the SPT100 characteristics (xenon mass flow rate, thrust, plume divergence...). The vacuum chamber has been tested and its expected performances (e.g. pumping speeds) have been reached. In the first part of this paper, we present these performances.

The validation tests with a functioning thruster were conducted with the A53, an SPT100-type engine manufactured by SEP. The main tests deal with:

- pressures within the vacuum chamber,
- thrust,

\* Abstract 3208 submitted to the 21st International Symposium on Rarefied Gas Dynamics, Marseille, France, July 26-31, 1998

- analysis of the discharge current fluctuations,
- analysis of the plasma characteristics (density, electron energy distribution function, ion current density, potential) in the exhaust plume at 50 cm from the channel outlet, with an electrostatic probe.

The research program experiments use the SPT100-ML, a thruster specially designed and built for the PIVOINE test facility. As a preliminary phase of the program, we investigate the working characteristics of the thruster by varying the following parameters:

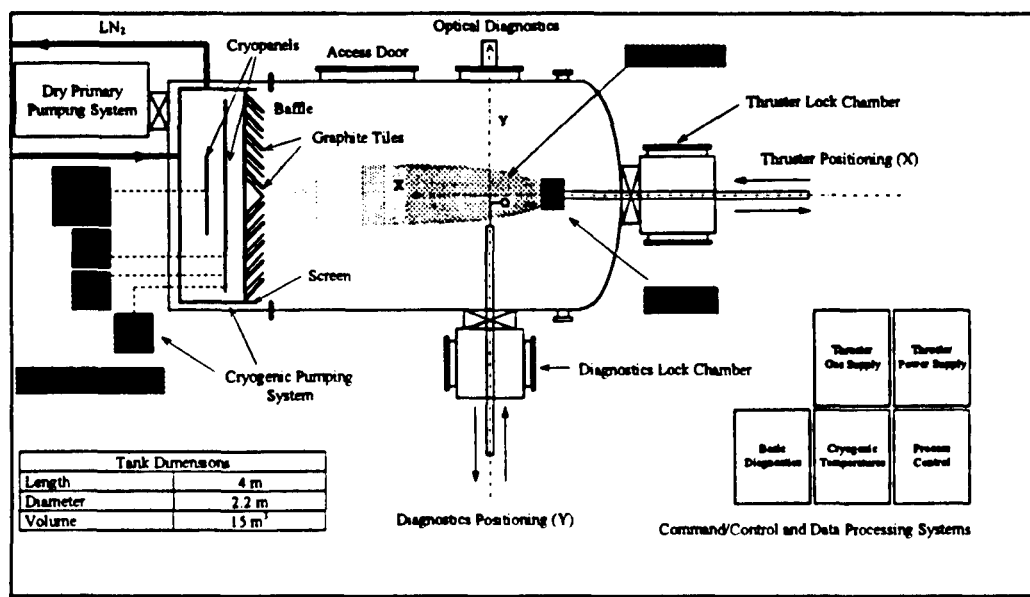
- discharge voltage,
- xenon mass flow rate at the cathode and the anode,
- magnetic field configuration and intensity,
- channel length.

These parameters determine the operating points of the thruster. The measurements and analysis made are the same as for the A53 tests. In the second part of this paper, we present and discuss the results of this investigation.

At the end of this preliminary phase, we've got a large data bank concerning the operational characteristics of the SPT100-ML, using the PIVOINE facility. Some of the operating points will be chosen, then most of the next experiments in the program will be made with the SPT100-ML working at these points. Many kinds of diagnostics will be used to characterize the plasma properties: Langmuir probes, ion probes, optical probes, a high-speed camera, etc.

## References

- [1] P.Lasgorceix, M.Raffin, C.Pérot, J.-C.Lengrand, M.Dudeck, T.Beltan, A.Cadiou, "PIVOINE, a facility for the investigation of rarefied xenon plasma jet", 20th Symposium on Rarefied Gas Dynamics, Beijing, China, August 1996.
- [2] P.Lasgorceix, C.Pérot, M.Dudeck, "PIVOINE Ground test facility for ion thruster testing", 2nd European Spacecraft Propulsion Conference, Noordwijk, The Netherlands, May 1997.



*Schematic of the PIVOINE test facility*

# Analysis of density gradients in the high atmosphere and satellite aerodynamics \*

G. Koppenwallner, B. Fritsche

HTG -Hypersonic Technology Göttingen, Katlenburg Lindau, Germany

## 1. Introduction

Due to the high requirements for precise orbit and position prediction of high altitude satellites also accurate prediction of the aerodynamic forces and moments acting on these satellites is necessary. For earth observation satellites like ERS, with orbital height between 600 and 700 km detailed aerodynamic analysis have been performed. Also for the GPS class of satellites with orbital heights above 1000 km aerodynamic and radiation pressure forces have to be considered for precise position analysis.

## 2. The high atmosphere and its special features [1],[2],[3].

Special features of the high atmosphere are not only the low density but also the dramatic change of molecular composition and its high temperature of about 1500 K.

Another special phenomena of the high atmosphere can be found when comparing the density decrease with altitude and the mean free path, which are shown in Fig. 1 [1]. We can see that at 600 km the mean free path has a value of  $\lambda = 100$  km. On the other side we have in an altitude span of 100 km a density change by a factor of 3. This means that we observe in the high atmosphere within one mean free path extreme large density gradients. In order to demonstrate this more clearly we show in Fig. 2 the following gradients :

Norm. density gradient per mean free path:  $(dn/dz)(\lambda/n)$

Norm. density and kin. temperaturer gradient per km:  $(dn/dz)(1/n); (dT/dx)(1/T), \text{ km}^{-1}$

At 600 km we obtain with an altitude change of  $\pm \lambda$  a density ratio of  $n(600 \pm \lambda)/n(600) = 1/e^{\pm 1}$

It therefore seems questionable if the atmosphere above 300 km is in a thermodynamic equilibrium state. In the following we investigate the possible error in aerodynamic analysis, which is performed on the basis of a homogeneous equilibrium free stream.

## 3. Simple analysis of density gradient influence on aerodynamics.

In analogy to the classical simple derivation of transport coefficients in a nonuniform velocity or temperature field [4], [5] we estimate the influence of the atmospheric density gradients on aerodynamic forces acting on a flat plate in parallel flow. We neglect in a first step the graviational forces.

As the high atmosphere  $z > 300$  km is almost isothermal we have only to consider the number density gradient  $dn/dz$ .

We assume the particles impinging on the lower or upper side of the plate have their origin in an atmospheric layer with a distance of one mean free path below or above of the plate.

For the net normal momentum flux impinging on both sides of the plate we then obtain:

$$p_{12} - p_{21} = -\frac{1}{2} m \cdot n \cdot c^2 \frac{\lambda}{n} \frac{dn}{dz}$$

We define the gradient induced lift coefficient  $C_{L,g}$ :

$$C_{L,g} = \frac{(p_{12} - p_{21})}{0.5 \cdot m \cdot n \cdot V^2} = -\frac{1}{S_{\infty}^2} \frac{\lambda}{n} \frac{dn}{dz}$$

In Fig 3 we compare this gradient induced lift with the lift coefficient of a flat plate in uniform flow. It is evident that density gradients introduce lift forces, which can not be neglected.

\* Abstract 3801 submitted to the 21st International Symposium on Rarefied Gas Dynamics, Marseille, France, July 26-31, 1998

Due to the neglect of gravitational forces there will be no balance of the molecular particle flux between the different atmosphere layers.

We obtain for the unbalanced molecular flux by simple analysis:

$$\frac{n_{up} - n_{down}}{n \cdot c} = -0.5 \frac{\lambda}{n} \frac{dn}{dz},$$

This contradicts thus the assumption of a stationary atmosphere.

#### 4. Analysis with density gradient and gravity field.

Due to the gravity field the upwards moving molecules are decelerated and the downward moving molecules accelerated. The loss or gain of kinetic energy must be equal to the gain or loss of potential energy, i.e:

$$\pm g \Delta z = \mp \frac{1}{2} \Delta c^2$$

Thus another important quantity is the ratio between potential energy gain over one vertical mean free path and the mean thermal energy of a particle.

$$\frac{e_{pot}}{e_{therm}} = \frac{g\lambda}{(1/2)c^2} = \frac{g\lambda}{(3/2)RT},$$

At an altitude of  $z = 600$  km we have  $\lambda = 10^5$  m,  $T = 1500$  K which gives:

$$\frac{g\lambda}{(3/2)RT} \approx 1$$

Particles with  $(3/2)RT < g\lambda$  should not be able pass an altitude step of  $\lambda$ .

If we perform a momentum flux analysis with consideration of gravitational ac- and deceleration we obtain the following simple expression for the lift acting on a flat plate:

$$C_{L,g} = -\frac{1}{S_\infty^2} \left( \frac{\lambda}{n} \frac{dn}{dz} + \frac{2g\lambda}{c^2} \right)$$

As  $dn/dz$  is negative the gravity term acts against the density gradient.

If we request zero normal momentum transport through a horizontal plane, which in principle means zero lift force, we obtain an expression, which is the basis for the isothermal barometric altitude law.

$$\frac{1}{n} \frac{dn}{dz} = -\frac{2g}{c^2} = -\frac{g}{RT}$$

Bird [ 6] analysed with DSMC method the adiabatic atmosphere. He found that for  $(\lambda/n) dn/dz > 0.003$  the temperature departs from the adiabatic continuum value, however the pressure follows the barometric continuum law also in the rarefied regime.

#### 5. Conclusion.

Based on a simple analysis approach we obtain contradictory results concerning the influence of gravity induced density gradients on aerodynamic analysis. We therefore will analyse in more detail the basis of high atmospheric models and the resulting implications concerning free molecular aerodynamic analysis.

Questions to be answered are: Can we use the present approach of a uniform Maxwellian freestream or do we have to consider also gradients and the gravity forces acting on the molecules between two successive collisions.

#### References

- [1] Anonym. : *U.S. Standard atmosphere* 1962
- [2] D. Rees: *Cospar International Reference Atmosphere: 1986*, Advances in Space Research, Vol. 8, Number 5-6. 1988
- [3] J.K. Hargreaves, *The Upper Atmosphere and Solar Terrestrial Relations*, Van Nostrand, 1979
- [4] Vincenti w.G., Kruger H.Ch., *Introduction to Physical Gasdynamics*, John Wiley, 1967
- [5] J.H. Jeans, *Dynamische Theorie der Gase*, Vieweg, Braunschweig 1926
- [6] G. A. Bird, *Molecular Gas Dynamics and the Direct Simulation of Gas Flows*, Clarendon Press, Oxford 1994

# ASTROPHYSICS AND ENVIRONMENT - AE P

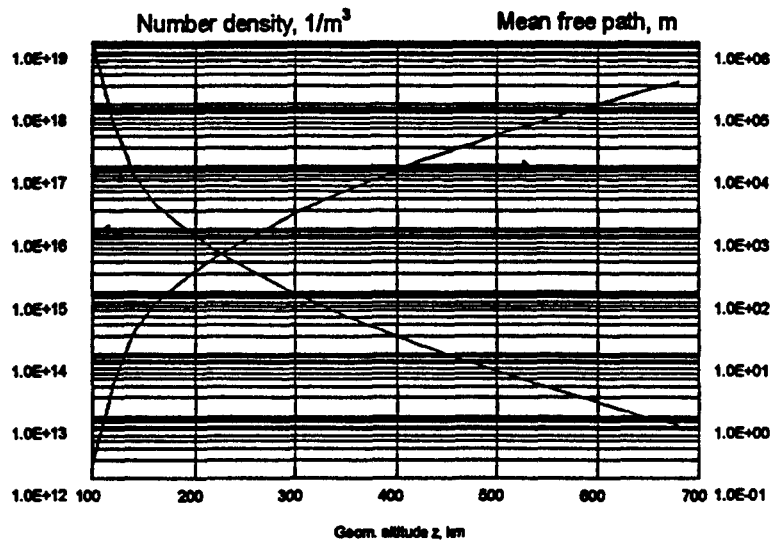


Fig.1 Mean free path and number density as function of geometric altitude  
US Standard Atmosphere 1962

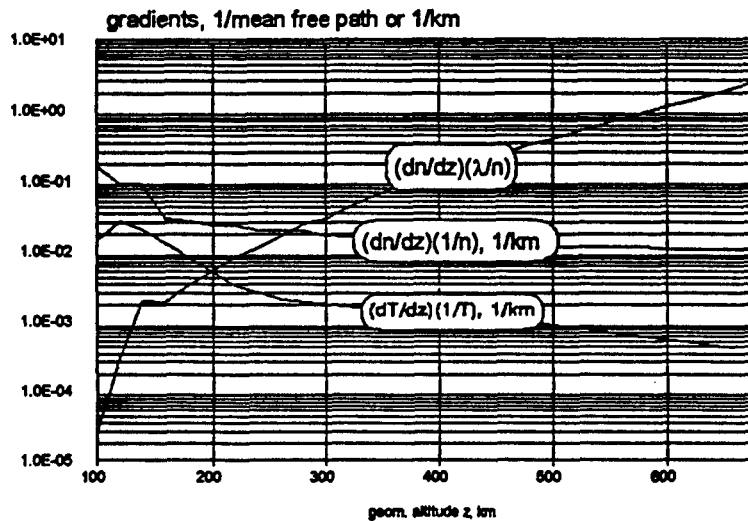


Fig.2 Normalized atmospheric gradients as function of geometric altitude  
US Standard Atmosphere 1962

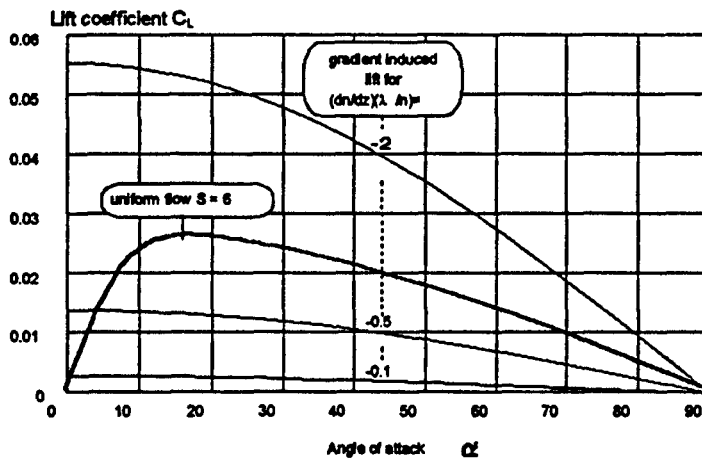


Fig. 3 Flat plate lift coefficient in uniform flow, speed ratio  $S = 6$  and gradient induced lift, isothermal atmosphere, no gravity forces.

# The Direct Simulation of 2D and 3D Jet Flows in a Dusty Gas Atmosphere of a Comet \*

A.V. Bogdanov, N.Y. Bykov, Yu.E. Gorbachev,  
V.V. Zakharov, G.A. Lukianov, G.O. Khanlarov  
Institute for High Performance Computing and Data Bases,  
St.Petersburg, Russia

## 1 Introduction

Observations of Halley Comet revealed that internal atmosphere (coma) has non-uniform and asymmetric structure. Comet images demonstrate jet structures - coma regions, which have high brightness (density of radiative and dispersed environment)[1]. Majority of existing atmosphere gasdynamic models assume spherical shape of comet nucleus. Under spherical nucleus shape jet flows formation is possible under highly non-uniform surface activity (gas production)[2]. Real comet nucleus is not sphere and jet formations may be result of both non-uniform activity and nucleus surface shape.

This work investigates the influence of shape and non-uniform nucleus quasi-spherical surface activity on comet gas and dust parameters. Plate parts, bumps and hollows were employed as basic objects of comet structure.

The investigations were fulfilled for two-phase flow: one-component ( $H_2O$  molecules) gas phase and heavy dust phase. Linear approach was used. There was no influence of heavy dust phase on gas flow; collisions between heavy particles were neglected; heavy particles motion was determined by gas phase parameters.

## 2 Method

The direct simulation Monte Carlo method (NTC-scheme) was employed for gas flow modelling. Mechanics of particles collision corresponds to VHS-model. It is assumed, that vibration levels of  $H_2O$  molecules are not excited. For description of energy exchange between translation and rotation degrees of freedom two models were em-

ployed: Borgnakke-Larsen model and quaziclassical RT transition model. Decomposition method (sharing domain on parts) was used for effective computing. Computation area was chosen to be approximately 100 radii of the surface. The whole computation area was divided into two regions. Different parameters of the scheme were used in each region. The time step in the far field was chosen to be 30-100 times larger than in inner region. This approach gives possibility to decrease computation time 5-10 times in comparison with the scheme where time step is the same for all regions. Simulations fulfilled for the range of Knudsen numbers  $Kn = 10^{-1} - 10^{-4}$  ( $Kn = \lambda/R_w$ ,  $\lambda$  - minimal free length path near surface,  $R_w$  - nucleus radius). At the comet nucleus surface velocity distribution function was Maxwell

$$f_w = \frac{n_w}{(2\pi RT_w)^{3/2}} \exp\left[-\frac{(v_x - u)^2 + v_y^2 + v_z^2}{2RT_w}\right].$$

Here  $v_x, v_y, v_z$  - components of velocity,  $x$  - perpendicular to the nucleus surface coordinate,  $n_w, T_w$  and  $u$  - numerical density, temperature and center-of-mass velocity of  $H_2O$  molecules at the surface. Two types of initial conditions were considered: (1) a subliming source (Mach number  $M = u/a_w = 0$ ,  $a_w$  - sound velocity), (2) source with sound velocity of outflow ( $M = 1$ ). The surface nucleus temperature was constant and equal to 200K. Initial values of  $H_2O$  molecules translation and rotation temperatures were equal. Dust particles had spherical shape (diameter  $d = 0.1 - 10\mu m$ ). Particle motion equation was following:

$$\frac{d\vec{v}_p}{dt} = \frac{3\rho}{4d\rho_p} C_D |\vec{v} - \vec{v}_p| (\vec{v} - \vec{v}_p).$$

Here  $\rho, \rho_p$  - gas and dust particles density,  $C_D$  - drag coefficient. For description of gas-particles interactions free molecular outflowed regime approach was used (diffusive reflection, complete thermal ac-

\*Abstract 4842 submitted to the 21st International Symposium on Rarefied Gas Dynamics, Marseille, France, July 26-31, 1998

comodation). Dust particles temperature was determined by the balance between absorbed sun radiation energy and energy of particle radiation.

### 3 Results

Results of simulations show strong influence of the shape on flow picture in coma. Changing of surface curvature leads to jet-like gas and dust flows formation. Character of surface relief that is under sun radiation in a given time moment is most important. Dependence of jet formation longitudinal size and cross size vs size of non-spherical surface elements was considered. Dust flow picture depends on size distribution of dust particles. Coma non-uniformity is increased under certain combination of geometric factors and non-uniform activity of surface nucleus.

The work demonstrates gas and dust parameters and also computer analogies of coma images (under some assumption about coma luminance mechanisms) which correspond to observations of rotating comet from flyby spacecraft. Problem of such images identification is discussed.

### References

- [1] Crifo J.F., *Comets as a large dirty snowballs sublimating in interplanetary space: a review of gasdynamic models*, In: Boffi V. and Cercignani C. Ed. *Rarefied Gas Dynamics* 15. 229-250, Stuttgart: BG Teubner, 1986.
- [2] Crifo J.F., Itkin A.L., Rodionov A.V. *The near-nucleus coma formed by interacting dusty gas jets effusing from a cometary nucleus: I*, ICARUS.1995, 116, pp.77-112.
- [3] Bird G.A. *Molecular gas dynamics and the direct simulations of gas flows*, Clarenton Press, Oxford, 1994.



## Experimental Simulation of Nonequilibrium Ionization and Radiation Behind Shock Wave in Martian Atmosphere \*

V.A. Gorelov, M.K. Gladyshev, V.G. Tchebureev

Central Aerohydrodynamic Institute, Zhukovsky-3, Moscow Region, Russia

The results of experimental investigation of nonequilibrium processes, when a strong shock wave propagates in gas mixture simulating Martian atmosphere, are presented. The goal of experiments is getting of measured data to verify nonequilibrium physical - chemical models for numerical simulation of flow around vehicles during Martian atmosphere entry.

Experimental investigations have been carried out in Arc-Driven Shock Tube (ADST) where studies on physical-chemical processes behind strong shock waves with propagation velocities of 4 - 15 km have been performing for the last years [1,2]. ADST discharge driver had ceramic walls and molibden electrodes. Driver gas was helium heated by a powerful electric discharge. A low pressure driven channel represented a glass sections structure with the length about 5m and diameter of 57mm assembled by means of metallic flanges. The structure's sections had a sealed lead-in for probe devices and windows for the optical recording. The simulation of Martian mixture was carried out by using the mixture of CO<sub>2</sub> and air. A certified carbon dioxide (99.9 %) used. It was delivered into the ADST channel evacuated up to the pressure at which the channel was filled with the mixture containing CO<sub>2</sub> (96 %Martian atmosphere is in the increased concentration of O<sub>2</sub>. However, the calculations of the gas species behind the shock wave front specially carried out have shown that the change in the content of O<sub>2</sub> before the shock wave within 0-3% of the experiments was carried out at the pressure in the channel  $P_1 = 0.2 (\pm 1\%)$  torr and within the range of shock wave velocities 4.5-9.5 km/s.

In the studies on the measurements of ionization parameters there were used probe techniques of diagnostics with required characteristics of the resolution and range of measuring the ionization properties. To define ion and electron concentration

the electric probes of different type were used. Single probes with cylindrical electrodes were installed parallel and normal to the gas flow under study. They operated in the regimes of gathering the ion and electron current. The diameters of electrodes changed from 0.1 to 0.01mm. All probes were expendable. When processing the results of probe measurements there were used the data of detailed studies on the peculiarities of the operation of cylindrical probes under conditions of the supersonic flow behind the shock wave in the transitional Knudsen regime [1]:  $0.1 < Kn < 10$  ( $Kn = \lambda_{i,e}/r_p$ ,  $\lambda_{i,e}$  is the length of free path of ions and electrons,  $r_p$  is probe radius).

The measurement of electron temperature  $T_e$  when a shock wave is propagating along the ADST channel is required not only for defining  $n_{e,i}$  from probe measurements, but is of a special interest because  $T_e$  is an important parameter in determining radiation properties of gas. Besides,  $T_e$  can be used to verify numerical models of nonequilibrium processes related to the propagation of strong shock waves in gas medium under consideration. The method of a triple probe [3] and the experience gained in applying this method during experiments in the ADST [1] were used to measure  $T_e$ . A spatial resolution of the measuring system along the flow velocity vector is about 0.5mm, a time resolution of the measuring system  $\tau$  is about 0.1mks.

Simultaneously with the measurements of  $n_{i,e}$  and  $T_e$  a nonequilibrium radiation in the band systems of several molecules (CN, C<sub>2</sub>, NO) was recorded. In studies on the ionization processes peculiarities the recording of the radiation was aimed at determining the time and spatial correlations between the nonequilibrium processes of  $n_{e,i}$  - formation, change in  $T_e$  and generation of the radiation. To register an emission, routine method of spectral measurements [2] was used. The optical system ensured the spatial resolution on the ADST channel axis about 0.1mm. Spectral diapason of the system is  $\lambda = 200 - 1000$  nm.

\* Abstract 4851 submitted to the 21st International Symposium on Rarefied Gas Dynamics, Marseille, France, July 26-31, 1998

In experiments the peak value of electron temperature  $T_{em}$  in a shock wave front was established for wide diapason of wave velocities. This peak value correlates with radiation intensity  $I_m$ , ion and electron concentrations  $n_{e,im}$  peak values. The dependencies of peak values  $T_{em}$ ,  $I_m$ ,  $n_{e,im}$ , quasistationary values  $T_{eqs}$ ,  $I_{qs}$ ,  $n_{eqs}$  and temporary characteristics of  $n_e$ ,  $T_e$  and  $I_\lambda$  nonequilibrium distributions behind shock wave are obtained. Temporary characteristics includes  $\tau_{peak}$ - time of the  $n_e$ ,  $T_e$  and  $I_\lambda$  - increase in nonequilibrium peak and  $\tau_{qs}$ - time of the quasistationary  $T_{eqs}$ ,  $I_{qs}$ ,  $n_{eqs}$  values achievement behind shock wave.

In experiments a strong precursor photoionization effect was detected. It is our opinion, that the effect of the photoionization defining the values  $n_{e,i}$  and  $T_e$  ahead of the shock wave manifests itself in the gas mixture under study much stronger than in air. For example, in a number of cases the value of  $T_e$  ahead of the front is comparable or exceeds the maximum value of  $T_e$  behind the shock front in the gas mixture, which was not observed in air experiments. The ratio of the concentration of charged particles ahead of the front to the quasi-steady value of  $n_{eqs}$  behind the wave front in the mixture exceeds the corresponding ratio for air by more than an order. This calls for additional investigations which are assumed to complete to the date of Paper preparation.

This work has been supported by International Science and Technology Center (ISTC) through Project N 036.

## References

- [1] Gorelov V.A., Kildushova L.A. and Kireev A.Y., *Ionization Particularities Behind Intensive Shock Waves in Air at Velocities of 8-15 km/s*, AIAA Paper 94-2015, June 1994.
- [2] Gorelov V.A., Gladyshev M.K., Kireev A.Y., Fedotov I.V., Plastinin Y.A. and Karabadzhak G.F., *Nonequilibrium Shock Layer Radiation in the Systems of Molecular Bands NO and  $N_2^+(1-)$ : Experimental Study and Numerical Simulation*, AIAA Paper 96-1900, June 1996.
- [3] Chen S.L. and Sekiguchi, *Instantaneous Direct-Display System of Plasma Parameters by Means of Triple Probe*, Journal of Applied Physics, Vol.36, No.8, pp. 2363-2375, 1965.

# Kinetic Modeling of the Hot Neutral Planetary Coronas \*

V.I. Shematovich

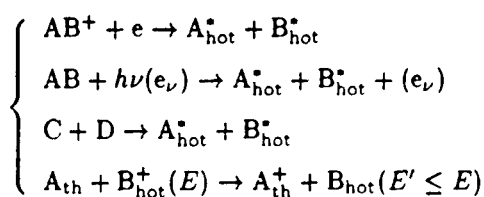
Institute of Astronomy of the Russian Academy of Sciences, Moscow, Russia

## 1 Introduction

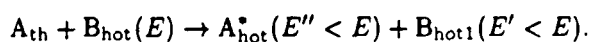
The present understanding of planetary coronas (the top very rarefied atmospheric layers) is determined by satellite and ground based observations of coronal emissions [1]. In particular, it was found that usually the planetary corona for both light and heavier species (H, He, C, N, O, etc.) may be presented by two populations - thermal (characterized by the Maxwellian distribution) and nonthermal (characterized by the nonequilibrium distribution for superthermal energies) ones [1],[2].

## 2 Kinetic model

The main source of superthermal (or hot) particles in the planetary corona is connected with their transport from the transition region between dense collision-dominated atmosphere and collisionless exosphere. The superthermal particles are produced in various nonthermal processes by dissociative recombination, photo- and impact dissociation, exothermic chemically reactive, inelastic, or charge exchange collisions,



their products having translational energies of a few eV. The superthermal particles loose translational energy in elastic and inelastic collisions



In the case when superthermal particles are chemically homogeneous with the ambient atmospheric gas ( $A = B$ ), the collisional processes become completely nonlinear, because the particles of secondary origin (with  $E' \gg kT$ ) are nonthermal, and their

subsequent collisions with the ambient gas lead to cascade formation of new nonthermal particles.

For different celestial bodies the relative input of the considered sources of superthermal particles are different and specific sets of these processes must be considered [1]. If these hot particles are injected in the tail of the Maxwellian thermal distribution and are not thermalized quickly enough, a large fraction of them may disturb an initially Maxwellian distribution in the planetary corona. It results in significant amount of superthermal particles in this region, which define the parameters of the planetary corona. This was in particularly revealed by the analysis of experimental data for planetary coronas [1].

The nonequilibrium properties of the particles formed with an excess of kinetic and internal energy make it necessary to study these processes at the microscopic kinetic level. For a rigorous self-consistent consideration of nonthermal particles and the role they play in the hot neutral corona formation, the system of nonlinear Boltzmann type kinetic equations [3]

$$\left\{ \begin{array}{l} \frac{\partial}{\partial t} F_{nth} + c \frac{\partial}{\partial r} F_{nth} + S \frac{\partial}{\partial c} F_{nth} = Q_{nth} + \\ + J_{el}(F_{nth}, F_{th}) + J_{in}(F_{th}, F_{nth}) \\ \frac{\partial}{\partial t} F_{th} + c \frac{\partial}{\partial r} F_{th} + S \frac{\partial}{\partial c} F_{th} = J_{el}(F_{th}, F_{nth}) + \\ + J_{in}(F_{th}, F_{nth}) \end{array} \right.$$

must be solved. Here  $F_{th}$  and  $F_{nth}$  are the velocity distribution functions for thermal and nonthermal populations of the planetary corona. The left-side of these equations describes the particle movement in the planetary gravitational field, and the right-side one includes the terms corresponding to the formation of superthermal particles ( $Q_{nth}$ ) and their collisional relaxation in elastic and inelastic processes. This system of kinetic equations was solved using the modification [3] of the Direct Simulation Monte Carlo method.

## 3 Results

The described above kinetic model was applied to the investigation of the hot oxygen corona forma-

\* Abstract 5186 submitted to the 21st International Symposium on Rarefied Gas Dynamics, Marseille, France, July 26-31, 1998

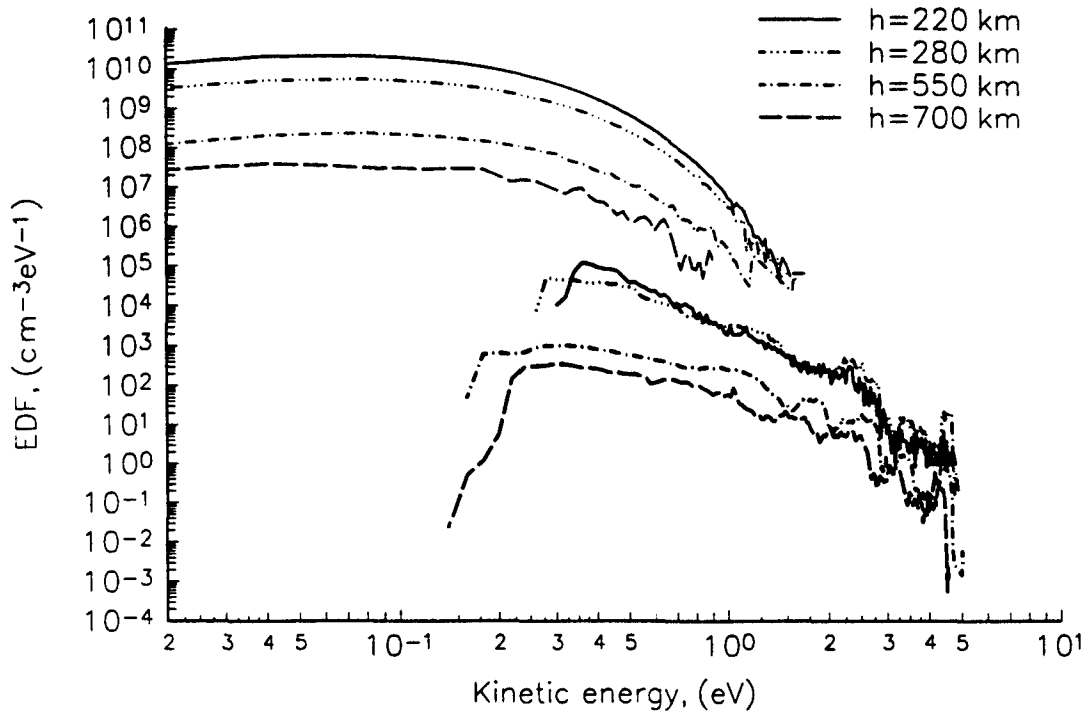


Figure 1: Energy distribution functions for thermal (thin lines) and nonthermal (thick lines) populations of the hot atomic oxygen geocorona at different atmospheric heights

tion in the Earth's upper atmosphere and the hot nitrogen corona formation in the Kronian satellite Titan atmosphere. For hot oxygen geocorona the main source of superthermal oxygen atoms are the reaction of dissociative recombination of ion  $O_2^+$  and the set of exothermic chemical reactions. The formed superthermal oxygen atoms share their excess (up to a few eV) kinetic energy in the collisions with the ambient thermal atmospheric oxygen atoms causing the cascade formation of secondary suprathermal population of hot nonthermal particles. In the fig.1 the calculated energy distribution functions (EDF) of thermal and nonthermal population of atomic oxygen in the Earth's upper atmosphere are shown. Thus, both disturbed thermal atoms from the tail of Maxwellian distribution and superthermal atoms are the source of the hot oxygen geocorona formation.

## References

- [1] Chamberlain J.W., and Hunten D.M. *Theory of planetary atmospheres. An introduction to their physics and chemistry*, Academic Press, New York, 1987.
- [2] Shizgal B.D., and Arkos G.G. *Nonthermal escape of the atmospheres of Venus, Earth, and Mars*, Reviews of Geophysics, V.34, No. 4, pp. 483-505, 1995.
- [3] Shematovich, V.I., Bisikalo, D.V., and Gerard, J.-C. *A kinetic model of the formation of the hot oxygen geocorona. I. Quiet geomagnetic conditions*, J. Geophys. Res., V. 99, pp. 217-227, 1994.

## Resonant Interaction between Magnetoacoustic Waves \*

R. Ciurea- Borgia, M. Ignat  
Al. I. Cuza University, Faculty of Physics, Romania

This paper deals with resonant interactions between three magnetoacoustic waves propagating through an ideal magnetohydrodynamic plasma. Thus, we get the interaction equations between the fundamental mode and its first harmonic component. These equations were numerically solved and the time dependencies of the magnetic energy densities  $|b_1(\omega)|^2$ ,  $|b_2(2\omega)|^2$  were plotted.

As we can observe from fig.1, the presence of the harmonic component favours the amplification of the fundamental wave. Instead, after few damped oscillations, the density energy for the magnetoacoustic wave with  $2\omega$  frequency stabilises to a value less than the initial one (a part of its energy is transferred to the fundamental mode, to determine its development).

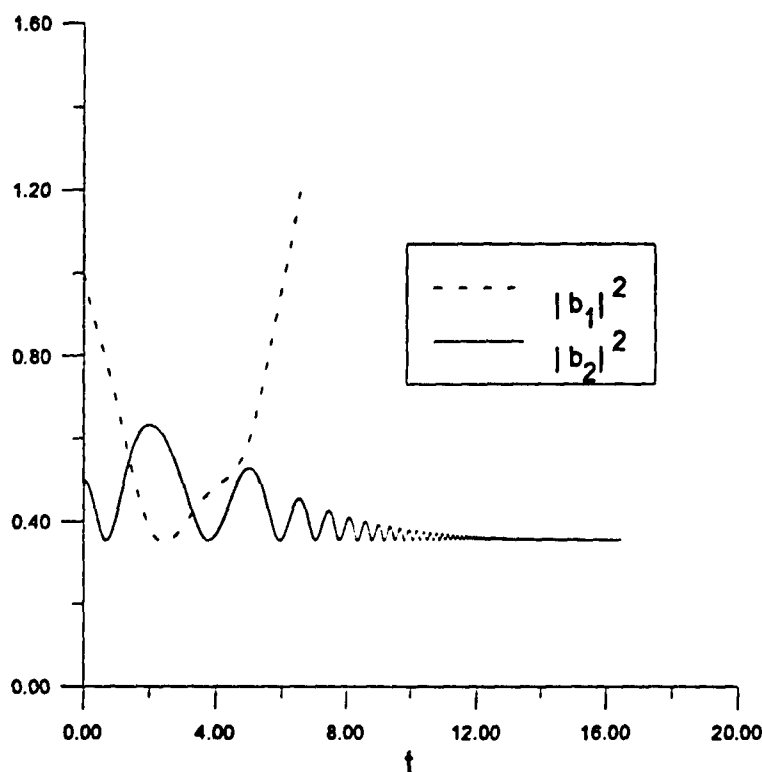


Figure 1

This result is of interest in Earth's ionosphere and magnetosphere: These regions abound of magnetoacoustic waves with large amplitude [1]. One of the mechanisms responsible of their appearance may be the resonant interaction described above.

[1]. Goldsten, R.J., Rutherford, P.H.: "Introduction in Plasma Physics", Inst. Of Physic Publication, Bristol 1995, p. 10

\* Abstract 6882 submitted to the 21st International Symposium on Rarefied Gas Dynamics, Marseille, France, July 26-31, 1998

# Inner Shock in the Solar Wind Interaction with Comet Exosphere: Was it Detected by Giotto \*

V.I. Nikolova, M.D. Kartalev  
Institute of Mechanics, BAS, Sofia, Bulgaria

## Introduction

One of the most challenging experimental results obtained during the intensive spacecraft investigations of the comets ten years ago was the detection of the magnetic field - free cavity near the comet Halley. The magnetic cavity boundary (CS) was crossed by Giotto at a cometocentric distance about 4470 km inbound and 4155 km outbound. The magnetic field magnitude drops suddenly from about 60 nT to zero at this boundary.

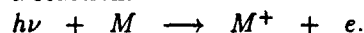
The predicted from the "pre- encounter" models picture of the solar wind interaction with the comet ionosphere includes outer and inner shock waves and a contact surface. The latter is supposed to separate the inward solar wind flow from the outward flow of the ionized gas with cometary origin. The classic MHD picture predicts inward penetration of the interplanetary magnetic field till the contact surface only. The region between the inner shock and the contact surface is supposed to be magnetic field - free in the frame of the MHD approach. That is why the penetration of the interplanetary magnetic field to the CS was widely accepted as a proof that this is rather a contact surface.

Here, analyzing some results of their earlier works ([7], [6], [2]), as well solving numerically the problem of magnetic field distribution (magnetic convection approach), the authors are trying to demonstrate evidences in favour of the interpretation of the diamagnetic cavity boundary as an inner shock.

## Some features of the used models

The problem of the solar wind-comet exosphere interaction is modeled numerically in the frame of the single fluid gas dynamic approach, including the main known mass - loading and sink reactions:

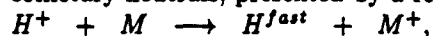
**Photoionization** by solar extreme ultraviolet radiation. If  $M$  denotes cometary neutral species such as  $H_2O$ ,  $CO$ ,  $O$ , or  $H$ , this source is illustrated by a reaction:



The photoionization rate at 1 AU is  $\sigma \sim 5 \times 10^{-7} s^{-1}$  for solar minimum solar conditions (a value of

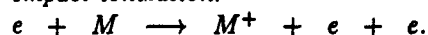
$\sigma = 10^{-6} s^{-1}$  is used for the calculations).

**Charge transfer** of solar wind protons with cometary neutrals, presented by a reaction:

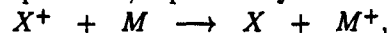


where  $H^+$  represents solar wind protons

**Impact ionization:**



**Charge transfer** between ion species  $X^+$  and neutral species  $M$ , expressed by:



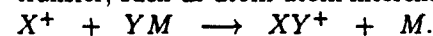
where  $X^+$  can represent any cometary ion such as  $O^+$ ,  $H_2O^+$ , or cometary  $H^+$ . The corresponding reaction rate coefficient could be represented [2] as:

$$k_{ch} = q_{ch} V_{eff} \text{ cm}^3 s^{-1};$$

$$V_{eff} = \left[ (w - v)^2 + \frac{128k(T+T_n)}{9\pi m_c} \right]^{1/2} \text{ cm s}^{-1},$$

where  $v$  and  $T$  are the ion's gas mean velocity and temperature,  $w$  and  $T_n$  are the velocity and the temperature of the neutrals ( $T_n$  is taken to be zero here),  $k$  is the Boltzmann constant and  $m_c$  is the mass of the cometary neutrals. The effective charge-exchange cross-section between  $H_2O$  neutral molecules and  $H_2O^+$  ions is supposed to be between  $q_{ch} = 10^{-14} \text{ cm}^2$  and  $q_{ch} = 10^{-15} \text{ cm}^2$ .

**Ion-neutral chemical reactions**, other than charge-transfer, such as atom-atom interchange:



Such an example is the reaction with  $X = H_2O$ ,  $Y = H$  and  $M = OH$  with a reaction rate coefficient  $k_{in} = 1.1 \times 10^{-9} \text{ cm}^3 s^{-1}$ .

**Dissociative recombination:**



The reaction rate coefficient is

$$\alpha = 5 \times 10^{-7} (300/T_e)^{1/2} \text{ cm}^3 s^{-1}. \text{ Here } T_e \text{ is the electron temperature.}$$

It is worthy to note the special form of the used magnetic induction equation, derived in [5]:

$$\frac{\partial \mathbf{B}}{\partial t} = \text{rot} \left[ (\mathbf{u} \times \mathbf{B}) - \frac{N_f}{n} (\mathbf{w} \times \mathbf{B}) \right],$$

where  $\mathbf{w}$  is the neutral outflow velocity vector. The density of the non picked - up new ions ("fresh ions")  $N_f$  is adopted to be  $\tau_f I_i n_n$ , denoting by  $\tau_f$  the characteristic ions' life-time in the "fresh ion stage". Here  $I_i$  is the new ions' production rate and  $n_n$

\*Abstract 6892 submitted to the 21st International Symposium on Rarefied Gas Dynamics, Marseille, France, July 26-31, 1998

is the number density of the background cometary neutrals.

### Some results

The probable conclusion that the magnetic cavity boundary is an inner shock follows from the parallel analyses of the results from different approaches, modelling the inner coma. We are showing also quite impressive supports of such a conclusion by a comparison with Giotto experiments.

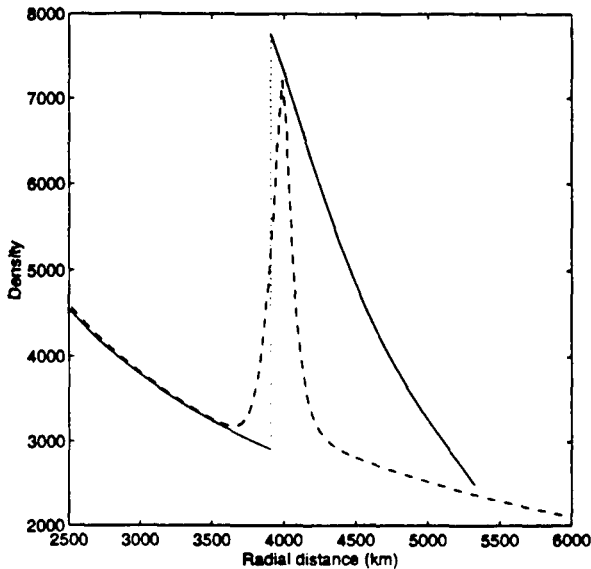


Figure 1: A comparison between the density distributions, obtained as follows: *Dashed line*- Cravens', 1989 [3] one dimensional consideration (see also [5]); *Solid line*- numerical result (in axially symmetrical approach) of Nikolova and Kartalev, 1998 [7], taken approximately along Giotto trajectory.

**Acknowledgements** - This research was supported by the Bulgarian National Foundation "Scientific Research" under grant NZ 522.

### References

- [1] Balsiger, H. et al. Ion composition and dynamics at comet Halley, *Nature*, **321**, 330, 1986.
- [2] Baranov V.B. and M.G. Lebedev, The interaction between the solar wind and the comet P/Halley atmosphere: observations versus theoretical predictions. *Astron. Astrophys.*, **273**, 695, 1993.
- [3] Cravens, T.E. A magnetohydrodynamical model of the inner coma of comet Halley, *J. Geophys. Res.*, **94**, 15025, 1989.
- [4] Flammer, K. The cometary diamagnetic cavity and inner shock. in: *Plasma Environments of Non-Magnetic Planets*, COSPAR Colloq., vol. 4, 1993.
- [5] Kartalev M.D. On the single fluid modeling of mass-loaded plasma. in press *Geophys. and Astrophys. Fluid Dynamics*, 1998.

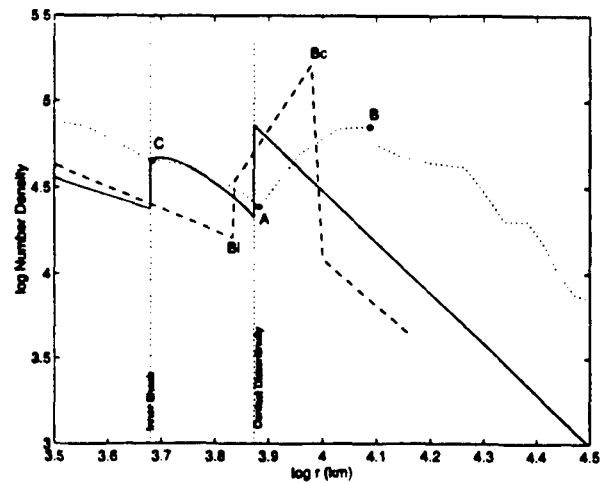


Figure 2: Density distribution for a segment of the inner coma region. The dotted line is the measured density variation along the Giotto trajectory (from [1]). The dashed line presents the computed in [2] density variation along the radius at  $90^\circ$  from the comet-solar line. The solid line is the density distribution along the radius at  $108^\circ$  from [7]).

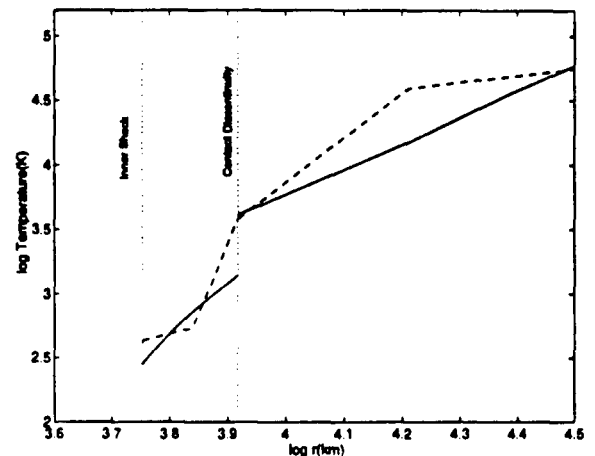


Figure 3: The dashed line presents the temperature distribution, used usually as *given* in the semi-empirical interpretations of the experimental data (see for instance [4]).

- [6] Kartalev M.D. and Nikolova V.I. On the magnetic field diffusion in MHD modeling of the inner coma of comet Halley, *subm. to Geophys. and Astrophys. Fluid Dynamics*.
- [7] Nikolova V.I. and Kartalev M.D., Numerical grid-characteristic gasdynamic modeling of the solar wind flow around comet, in press, in: *Finite difference methods - theory and applications*. (ed. A.A. Samarskii et al.), Nuova Science, USA, 1998.

# Index

Author	Paper	Vol	Session	Author	Paper	Vol	Session
Abe T.	1817	I	IR1	Beresnev S.A.	4902	II	TP-P
Abe T.	1816	I	MCM3	Beskok A.	6021	I	RF3
Abramov A.A.	5039	II	NS-P	Beylich A.E.	1627	II	GS-P
Abramovskaja M.G.	2282	I	RF3	Beylich A.E.	1660	II	ID-P
Abramovsky E.R.	2282	I	RF3	Beylich A.E.	1628	I	Invited
Adamovich I.V.	2286	I	NE2	Beylich A.E.	1626	II	NS-P
Agrawal H.	4016	II	IP-P	Billing G.D.	1771	I	GS2
Aksyutenko A.N.	2069	II	GS-P	Bird G.A.	1006	I	MCM1
Alder B.J.	5821	I	NS1	Biturin V.A.	1976	II	NE-P
Aleksandrov O.E.	6526	II	IP-P	Blanchard R.	2351	I	Invited
Alexandrychev I.P.	6527	II	GS-P	Blanchard R.C.	6467	I	AA2
Alexandrychev I.P.	6528	II	GS-P	Blömer J.	1627	II	GS-P
Alexeev B.V.	1918	II	KTM-P	Bobylev A.V.	1871	I	Invited
Alfyorov V.I.	5002	II	AA-P	Bobylev A.V.	4111	I	KTM4
Ambroso A.	6776	II	KTM-P	Boeuf J.P.	1226	I	Invited
Amouroux J.	1106	II	GS-P	Bogdanov A.V.	4842	II	AE-P
Anolik M.V.	1921	II	GS-P	Bogdanov A.V.	5235	I	GS3
Anolik M.V.	1922	II	NS-P	Borisov S.F.	6736	II	GS-P
Aoki K.	4361	I	NS1	Borisov S.F.	6737	II	GS-P
Aoki K.	4586	I	RF3	Boubert P.	6724	II	ID-P
Aoki K.	4621	I	TP1	Boubert P.	6725	II	ID-P
Aristov V.V.	1931	I	MCM3	Bouchardy P.	6314	I	AA2
Aristov V.V.	1932	II	NS-P	Bourdon A.	6721	I	NE1
Arkhipov Yu.Y.	4286	I	KTM4	Bowden R.L.	5866	II	KTM-P
Armenise M.	1946	I	NE1	Boyd I.D.	2369	I	IP2
Arnal D.	6515	I	AA3	Boyd I.D.	2367	I	MCM2
Asadzadeh M.	2100	I	NS2	Boyd I.D.	2366	I	NE2
Asano K.	1831	I	KTM1	Boyd I.D.	2368	I	RF4
Aspect A.	7106	I	Invited	Brazinsky V.I.	2281	II	AE-P
Aufrère L.	3291	I	GS2	Brun R.	1551	II	NE-P
Austin J.V.	6327	I	AE1	Brun R.	3292	II	NE-P
Autric M.	6811	I	IP2	Buet C.	1466	I	IR2
Autric M.	6812	II	IP-P	Buet C.	1431	I	KTM4
Azarova O.A.	5276	I	MCM2	Bulgakova N.M.	5101	II	IP-P
Babu R.S.P.	4013	II	AA-P	Bur R.	6312	I	AA2
Badie J.M.	1141	I	GS4	Buzykin O.G.	5087	II	KTM-P
Bakanov S.P.	5132	II	TP-P	Buzykin O.G.	5088	II	NE-P
Bakker P.	5456	I	MPT	Bykov N.Y.	4842	II	AE-P
Balakrishnan J.	2369	I	IP2	Bykov N.Y.	4843	II	IP-P
Balat M.	1141	I	GS4	Cabannes H.	1301	I	KTM2
Barantsev R.G.	1922	II	NS-P	Cacciatore M.	1771	I	GS2
Bartel T.	2336	I	IP1	Cacciatore M.	1946	I	NE1
Bartel T.	5966	I	IP1	Cai C.-P.	2368	I	RF4
Bartel T.	2337	I	MCM4	Capitelli M.	1776	I	Invited
Baryshnikov A.S.	1971	II	IR-P	Capitelli M.	1801	I	NE1
Baryshnikov A.S.	1972	II	NE-P	Capitelli M.	1946	I	NE1
Bass V.P.	2281	II	AE-P	Carabadgk G.F.	5096	I	AA4
Bass V.P.	2069	II	GS-P	Cattolica R.	2426	II	ID-P
Bass V.P.	2282	I	RF3	Cavadias S.	1106	II	GS-P
Béchu S.	3208	II	AE-P	Celenligil M.C.	2171	I	IP2
Bell J.B.	5821	I	NS1	Cercignani C.	4111	I	KTM4
Belouaggadia N.	3292	II	NE-P	Cercignani C.	4112	I	MCM3
Belyi V.V.	1986	II	IR-P	Cercignani C.	2697	I	RF3
Benazzouz T.	6826	II	IR-P	Chanetz B.	6312	I	AA2
Beresnev S.	4901	II	TP-P	Chanetz B.	6314	I	AA2



<i>Author</i>	<i>Paper</i>	<i>Vol</i>	<i>Session</i>	<i>Author</i>	<i>Paper</i>	<i>Vol</i>	<i>Session</i>
Chanetz B.	6211	II	AA-P	Elizarova T.G.	3237	II	KTM-P
Chanetz B.	6313	II	AA-P	El-Shall M.S.	2622	II	TP-P
Chanetz B.	6311	II	ID-P	Emelianov A.V.	6621	II	NE-P
Chapovsky P.L.	5456	I	MPT	Ender A.Ya.	6837	I	KTM3
Charrier P.	1521	I	KTM3	Ender I.A.	6837	I	KTM3
Charrier P.	3301	I	KTM4	Eremin A.V.	6623	I	NE1
Chen J.	5866	II	KTM-P	Eremin A.V.	6621	II	NE-P
Chernyak V.G.	2041	II	IR-P	Erofeev A.I.	4874	II	AA-P
Chernyak V.G.	4902	II	TP-P	Erofeev A.I.	2068	I	KTM6
Cheron B.G.	6724	II	ID-P	Erofeev A.I.	4941	I	RF2
Chikhaoui A.	1536	II	KTM-P	Erofeev A.I.	4942	II	TP-P
Chikhaoui A.	6752	II	NE-P	Erofeev A.I.	4943	II	TP-P
Chikhaoui A.	1401	II	NE-P	Esposito F.	1776	I	Invited
Ching Shen	2846	II	NS-P	Fan J.	2847	I	NS2
Chirokov I.A.	2056	II	KTM-P	Farley D.R.	2426	II	ID-P
Choquet I.	1406	I	GS3	Fateeva E.I.	5156	I	NE1
Ciurea-Borcia R.	6882	II	AE-P	Ferreira C.M.	4785	II	IR-P
Clapp L.H.	2426	II	ID-P	Feugeas J.L.	1521	I	KTM3
Collins R.J.	6121	I	AE2	Fisenko S.P.	2621	II	TP-P
Colonna G.	1801	I	NE1	Fisenko S.P.	2622	II	TP-P
Cook S.	5876	II	GS-P	Flèche J.L.	2951	II	IP-P
Cook S.R.	2471	I	GS1	Frezzotti A.	4081	I	MCM4
Cordier S.	1431	I	KTM4	Friedlander O.G.	5096	I	AA4
Crutchfield Wm.Y.	5821	I	NS1	Friedlander O.G.	2069	II	GS-P
Cumin L.M.G.	2676	II	NS-P	Friedlander O.G.	2068	I	KTM6
Dam N.J.	2156	I	RF4	Friedlander O.G.	4941	I	RF2
Danckert A.	1640	I	GS1	Friedlander O.G.	4942	II	TP-P
Dankert C.	1656	I	GS1	Friedlander O.G.	4943	II	TP-P
Dankert C.	1660	II	ID-P	Fritsche B.	3801	II	AE-P
de Boer J.	2706	II	IR-P	Frolova A.	6626	II	AA-P
de Socio L.M.	1766	II	NS-P	Fujita K.	1817	I	IR1
Dellacherie S.	1466	I	IR2	Funabiki K.	1816	I	MCM3
Desvillettes L.	4532	I	KTM1	Furukawa T.	4266	II	TP-P
Dettleff G.	1666	I	RF4	Gai S.L.	2541	I	AA2
Dmitriev L.M.	5002	II	AA-P	Galkin V.S.	5087	II	KTM-P
Dogra V.K.	6121	I	AE2	Gallis M.A.	5711	I	IR2
Doi T.	4541	II	TP-P	Gallis M.A.	5712	I	MCM3
Domingo P.	6826	II	IR-P	Garcia A.L.	5821	I	NS1
Domingo P.	6721	I	NE1	Garrigues L.	1226	I	Invited
Dubroca B.	1521	I	KTM3	Garzó V.	5341	II	IR-P
Dubroca B.	3301	I	KTM4	Garzo V.	5376	I	MPT
Dudeck M.	3208	II	AE-P	Gascon N.	3207	I	AA4
Dudeck M.	3209	II	ID-P	Gascon N.	3208	II	AE-P
Dudeck M.	3166	I	IP2	Gatignol R.	3001	II	KTM-P
Dudeck M.	3167	I	IR1	Gatignol R.	3002	I	KTM5
Dudeck M.	1536	II	KTM-P	Gatsonis N.	6021	I	RF3
Dudeck M.	3207	I	AA4	Gatsonis N.A.	6601	II	AA-P
Dudon J.P.	1536	II	KTM-P	Gatsonis N.A.	6602	I	IR2
Dumitrescu M.-P.	1551	II	NE-P	Genieys S.	1401	II	NE-P
Duruissseau P.	3001	II	KTM-P	George M.A.	5876	II	GS-P
Ebinuma Y.	1817	I	IR1	Gevorkyan A.S.	5235	I	GS3
Economou D.	2336	I	IP1	Gillet D.	3041	I	Invited
Egorov B.V.	5002	II	AA-P	Gimelshain S.F.	5039	II	NS-P
Egorov B.V.	5001	II	TP-P	Gimelshein S.F.	4831	I	AA3
Elizarova T.G.	2057	I	KTM2	Gimelshein S.F.	4832	I	IR2
Elizarova T.G.	2056	II	KTM-P	Gimelshein S.F.	4890	I	NS1

<i>Author</i>	<i>Paper</i>	<i>Vol</i>	<i>Session</i>	<i>Author</i>	<i>Paper</i>	<i>Vol</i>	<i>Session</i>
Gimelshein S.F.	5041	I	RF3	Honda T.	4361	I	NS1
Giordano D.	1801	I	NE1	Honma H.	5581	I	IR1
Giuriin M.C.	2697	I	RF3	Hubert D.	3211	I	AE2
Glass C.E.	6741	I	RF1	Hudson M.	2336	I	IP1
Gochberg L.A.	6916	II	IP-P	Hudson M.	5966	I	IP1
Godard R.	2706	II	IR-P	Hudson M.	2337	I	MCM4
Goldstein D.	6326	I	NS1	Hyakutake T.	4496	I	AA1
Goldstein D.B.	6327	I	AE1	Ianiro N.	1766	II	NS-P
Golse F.	4532	I	KTM1	Ibraguimova L.B.	6396	II	NE-P
Gopinath A.	6056	I	RF4	Igarashi S.	4321	II	AA-P
Gorbachev Yu.	6921	I	NE2	Ignat M.	6882	II	AE-P
Gorbachev Yu.E	4842	II	AE-P	Ignatiev A.A.	5232	II	AA-P
Gorchakova N.G.	6312	I	AA2	Ishida T.	4486	II	ID-P
Gorchakova N.G.	6311	II	ID-P	IshikawaH.	3830	I	KTM4
Gordiets B.F.	4785	II	IR-P	Itina T.E.	6811	I	IP2
Gordillo-Vasquez F.J.	6651	I	MPT	Itina T.E.	6812	II	IP-P
Gorelov S.L.	5293	I	NE3	Itina T.E.	6813	II	IP-P
Gorelov V.A.	4851	II	AE-P	Itkin A.I.	4883	I	AE1
Gorse C.	1776	I	Invited	Itkin A.I.	4881	II	TP-P
Gorshkov G.F.	4810	II	AA-P	Ivanov A.G	6529	II	NS-P
Grachyov I.A.	6737	II	GS-P	Ivanov M.S.	4831	I	AA3
Grasso F.	6313	II	AA-P	Ivanov M.S.	5232	II	AA-P
Graur I.A.	2057	I	KTM2	Ivanov M.S.	4832	I	IR2
Greber I.	5861	I	NS2	Ivanov M.S.	6921	I	NE2
Greenberg W.	5866	II	KTM-P	Ivanov M.S.	4890	I	NS1
Gregory J.C.	5876	II	GS-P	Ivanov M.S.	5039	II	NS-P
Grigoryan A.G.	5235	I	GS3	Ivanov M.S.	5041	I	RF3
Grigoryev Yu.N.	6631	II	KTM-P	Iwagami H.	6690	II	NE-P
Grmela M.	2651	II	KTM-P	Iwayama Y.	6866	II	AA-P
Gromov V.G.	5156	I	NE1	Jing Fan	2846	II	NS-P
Guarrigues L.	1226	I	Invited	Johannes J.	2336	I	IP1
Guerra V.	4781	I	IR1	Kaltz T.L.	6146	I	TP2
Guilbaud D.	2951	II	IP-P	Kandemir I.	5861	I	NS2
Gundlach G.	1656	I	GS1	Kane D.B.	2622	II	TP-P
Gusev V.N.	4871	I	AA3	Karniadakis G.E.	6021	I	RF3
Gusev V.N.	4874	II	AA-P	Karsten V.M.	5216	I	RF3
Gusev V.N.	4873	II	NS-P	Kartalev M.D.	6891	I	AE2
Hadjadj A.	6856	II	NS-P	Kartalev M.D.	6892	II	AE-P
Hanser F.	2601	I	KTM6	Katasonov A.A.	6811	I	IP2
Harvey J.K	5711	I	IR2	Katasonov A.A.	6813	II	IP-P
Harvey J.K	5712	I	MCM3	Kato S.	4601	II	IP-P
Harvey J.K.	5713	I	IP2	Kawamoto S.	4576	I	NS2
Hash D.B.	5921	I	IP1	Kawashima S.	6911	I	Invited
Hatakeyama M.	3830	I	KTM4	Kazmierczak B.	4756	I	TP2
Hauser A.	3208	II	AE-P	Ketsdever A.D.	6031	I	AA1
Hayashi A.K.	6690	II	NE-P	Khabalov V.D.	1921	II	GS-P
Hayashi S.	4486	II	ID-P	Khalidov I.A.	1921	II	GS-P
He C.	2848	II	IR-P	Khanlarov G.O.	4842	II	AE-P
Heinrich S.	7111	I	MCM4	Khisamutdinov A.I.	4916	I	MCM2
Hermans L.J.F.	5456	I	MPT	Khisamutdinov A.I.	4917	II	NS-P
Hiraoka M.	6690	II	NE-P	Khlopkov Yu.I	5292	II	NS-P
Hirose K.	4601	II	IP-P	Khlopkov Yu.I.	5294	II	NS-P
Hirose N.	6866	II	AA-P	Kim B.G.	6866	II	AA-P
Hoffbauer M.A.	2471	I	GS1	Kireev A.Yu.	4926	II	IR-P
Hoffbauer M.A.	5876	II	GS-P	Kloimboeck C.J.	6766	II	NE-P
Hollis B.R.	6211	II	AA-P	Koch D.L.	6056	I	RF4

<i>Author</i>	<i>Paper</i>	<i>Vol</i>	<i>Session</i>	<i>Author</i>	<i>Paper</i>	<i>Vol</i>	<i>Session</i>
Kogan M.N.	4941	I	RF2	Lengrand J.C.	2056	II	KTM-P
Kogan M.N.	4942	II	TP-P	Lengrand J.C.	3237	II	KTM-P
Kogan M.N.	4943	II	TP-P	Leroux A.	6721	I	NE1
Kolesnick R.E.	2906	II	NE-P	Levdansky V.V.	2626	II	IP-P
Koppenwallner G.	3801	II	AE-P	Levin D.A.	6121	I	AE2
Kortsenstein N.M.	6666	I	AA4	Liming Chen	2846	II	NS-P
Kortsenstein N.M.	6667	II	TP-P	Lions P.L.	3246	I	Invited
Kotake S.	4392	I	GS3	Liu F.	6021	I	RF3
Koulidiati J.	3167	I	IR1	Long L.N.	6146	I	TP2
Koulikov S.V.	4956	I	NE2	Longo S.	2367	I	MCM2
Koura K.	4396	I	MCM1	Longo S.	1802	II	NS-P
Kovach E.A.	5166	II	NE-P	Lord G.	5621	I	Invited
Kovalev F.D.	6847	II	TP-P	Lord R.G.	5622	II	NE-P
Kovalev V.L.	4966	I	GS4	Losev S.A.	5166	II	NE-P
Kovalev V.L.	4967	I	GS4	Loureiro J.	4781	I	IR1
Kowalczyk P.	4741	II	NS-P	Lucquin-Desreux B.	3256	I	KTM6
Krasnolutsii S.	5138	II	KTM-P	Lucquin-Desreux B.	3257	II	KTM-P
Kremer G.M.	2677	I	NE3	Lukianov G.A.	4842	II	AE-P
Kremer G.M.	2676	II	NS-P	Lukianov G.A.	4843	II	IP-P
Krishnan A.	6916	II	IP-P	Lukshin A.V.	1931	I	MCM3
Krupnov A.A.	4966	I	GS4	M.K.Gladyshev	4851	II	AE-P
Kryukov A.P.	4981	I	TP2	Maeno K.	5581	I	IR1
Kryukov A.P.	4982	II	TP-P	Makashev N.K.	5088	II	NE-P
Kudryavtsev A.N.	5041	I	RF3	Makashev N.K.	5039	II	NS-P
Kukhareenko Yu.A.	1986	II	IR-P	Makihara Y.	4531	I	TP1
Kunc J.A.	6651	I	MPT	Makowski K.	3207	I	AA4
Kurian J.	4013	II	AA-P	Mallinger F.	6921	I	NE2
Kurian J.	4015	II	AA-P	Manoj Kumar V.	4016	II	IP-P
Kurzyrna J.	3209	II	ID-P	Marconi M.L.	4466	I	AE1
Kustova E.	4996	I	MPT	Mariage E.	1141	I	GS4
Kustova E.	1946	I	NE1	Marín C.	5341	II	IR-P
Kustova E.	6921	I	NE2	Marine W.	6811	I	IP2
Kustova E.	4997	I	NE3	Marine W.	6812	II	IP-P
Kuznetsov L.I.	6311	II	ID-P	Marino L.	1766	II	NS-P
Kuznetsova I.	5006	II	TP-P	Markachev Yu.E.	5002	II	AA-P
Kuzyakin D.V.	5294	II	NS-P	Markachev Yu.E.	5001	II	TP-P
Lago V.	3209	II	ID-P	Markelov G.A.	5232	II	AA-P
Lago V.	3166	I	IP2	Markelov G.N.	4890	I	NS1
Lago V.	3167	I	IR1	Markelov G.N.	5041	I	RF3
Lampis M.	4112	I	MCM3	Markoff Yu.G.	5046	II	GS-P
Larina I.N.	5016	II	NS-P	Markoff Yu.G.	5047	II	IP-P
Lasgorceix P.	3207	I	AA4	Marriott P.	5631	I	AE2
Lasgorceix P.	3208	II	AE-P	Matsui J.	3861	II	GS-P
Lazarev A.V.	5135	II	NE-P	Matsumoto Y.	4432	II	AA-P
Lebeau G.J.	6601	II	AA-P	Matsumoto Y.	3861	II	GS-P
Lebéhot A.	3209	II	ID-P	Matsumoto Y.	4431	II	GS-P
Leblanc F.	3211	I	AE2	Matsumoto Y.	4646	II	NE-P
Lebon G.	2651	II	KTM-P	McDaniel J.C.	6686	I	RF1
Leborgne L.	6723	I	IR1	Méhats F.	6776	II	KTM-P
Lécot C.	2381	II	NS-P	Memnonov V.P.	5057	I	NS1
Lee D.D.	4706	I	NE2	Méolans J.G.	3291	I	GS2
Lefebvre M.	6314	I	AA2	Meyyappan M.	5921	I	IP1
Legge H.	1640	I	GS1	Micci M.M.	6146	I	TP2
Lemou M.	6926	II	NS-P	Mieussens L.	3301	I	KTM4
Lengrand J.C.	3238	II	GS-P	Mikhailov V.V.	1918	II	KTM-P
Lengrand J.C.	2057	I	KTM2	Milthorpe J.F.	2541	I	AA2

<i>Author</i>	<i>Paper</i>	<i>Vol</i>	<i>Session</i>	<i>Author</i>	<i>Paper</i>	<i>Vol</i>	<i>Session</i>
Miroshin R.N.	5062	II	KTM-P	Park H.K.	4706	I	NE2
Mohamed A.	1656	I	GS1	Parsons T.L.	5712	I	MCM3
Moiseev M.M.	5292	II	NS-P	Pellerin S.	3167	I	IR1
Mokhov V.A.	5002	II	AA-P	Peradzynski Z.	3207	I	AA4
Molinari V.G.	4136	II	IR-P	Perminov V.D.	5096	I	AA4
Monaco R.	2601	I	KTM6	Pérot C.	3208	II	AE-P
Montanero J.M.	5377	I	MPT	Perraud J.	6515	I	AA3
Mori H.	4486	II	ID-P	Petrova V.N.	5062	II	KTM-P
Morimoto T.	4476	I	MCM2	Pettersson R.	5386	I	KTM1
Morioka T.	5581	I	IR1	Piechor K.	4756	I	TP2
Morozov A.A.	5066	I	AA3	Pigache D.	6312	I	AA2
Morozov A.A.	5067	II	NS-P	Pigache D.	6311	II	ID-P
Morozov A.A.	5102	II	NS-P	Plähn K.	1657	I	RF2
Moss J.N.	6312	I	AA2	Plähn K.	1666	I	RF4
Moss J.N.	6467	I	AA2	Plastinin U.A.	5096	I	AA4
Moss J.N.	6211	II	AA-P	Plastinin Yu.A.	6666	I	AA4
Muntz E.P.	6031	I	AA1	Platkowski T.	4741	II	NS-P
Muntz E.P.	6216	I	Invited	Plekhanov E.A.	5001	II	TP-P
Muntz E.P.	6032	I	IP1	Plotnikov M.Yu.	5066	I	AA3
Murakami M.	4266	II	TP-P	Plotnikov M.Yu.	5101	II	IP-P
Nagata K.	4501	I	KTM5	Plotnikov M.Yu.	5067	II	NS-P
Nagels B.	5456	I	MPT	Plotnikov M.Yu.	5102	II	NS-P
Nagnibeda E.	4996	I	MPT	Plotnikov M.Yu.	5121	I	TP1
Nagnibeda E.	1946	I	NE1	Polycarpov Ph.J.	6737	II	GS-P
Nagnibeda E.	4997	I	NE3	Polycarpov Ph.J.	6736	II	GS-P
Nakakita M.	3861	II	GS-P	Popken L.	7101	II	KTM-P
Nanbu K.	4476	I	MCM2	Popov S.A.	5187	II	AA-P
Nanbu K.	4576	I	NS2	Popov S.P.	5246	I	RF2
Nanson R.	6601	II	AA-P	Popov V.V.	5292	II	NS-P
Napier D.G.	2776	I	KTM2	Porodnov B.T.	6526	II	IP-P
Nazarenko A.I.	2069	II	GS-P	Porodnov B.T.	6529	II	NS-P
Nazari B.K.	1660	II	ID-P	Pot T.	6312	I	AA2
Nebbache A.	6752	II	NE-P	Pot T.	6314	I	AA2
Nicodin I.	3001	II	KTM-P	Pot T.	6211	II	AA-P
Niimi T.	4486	II	ID-P	Pot T.	1656	I	GS1
Nikiforov A.P.	2069	II	GS-P	Pot T.	6311	II	ID-P
Nikolova V.I.	6891	I	AE2	Powell A.	2171	I	IP2
Nikolova V.I.	6892	II	AE-P	Prettyman T.	5876	II	GS-P
Nishida M.	4496	I	AA1	Provotorov V.P.	4874	II	AA-P
Nishide T.	4673	II	NS-P	Purpura C.	6313	II	AA-P
Nishigori T.	4501	I	KTM5	Pyarnpuu A.A.	5111	I	GS4
Nosik V.I.	5087	II	KTM-P	Qian Y.H.	3002	I	KTM5
Nosik V.I.	5088	II	NE-P	Raines A.A.	5116	I	NS2
Novopashin S.	1656	I	GS1	Ramjaun D.	1551	II	NE-P
Nyeland C.	2916	I	GS2	Rathakrishnan E.	4016	II	IP-P
Ogawa S.	6961	I	MCM4	Rault D.F.G.	6466	II	AA-P
Oguchi H.	4516	I	KTM5	Raviart P.A.	6776	II	KTM-P
Ohwada T.	4531	I	TP1	Rebrov A.K.	5066	I	AA3
Okuyama M.	4601	II	IP-P	Rebrov A.K.	5101	II	IP-P
Onishi Y.	4541	II	TP-P	Rebrov A.K.	5218	II	NS-P
Ooshida T.	4541	II	TP-P	Rebrov A.K.	5121	I	TP1
Ota M.	2698	II	IP-P	Reitshammer C.	2602	I	IR2
Ota M.	4471	II	IP-P	Reshetin A.G.	5126	II	AA-P
Oualid S.	3238	II	GS-P	Rich J.W.	2286	I	NE2
Paklin B.L.	6901	II	IP-P	Rjasanow S.	3971	I	MCM1
Pandolfi Bianchi M.	4146	II	KTM-P	Robin L.	6724	II	ID-P

<i>Author</i>	<i>Paper</i>	<i>Vol</i>	<i>Session</i>	<i>Author</i>	<i>Paper</i>	<i>Vol</i>	<i>Session</i>
Robin L.	6725	II	ID-P	Serikov V.V.	4576	I	NS2
Robinson C.D.	5713	I	IP2	Shakhmistov V.M.	2069	II	GS-P
Röck W.	3166	I	IP2	Shakhov E.M.	5173	II	AA-P
Röck W.	3167	I	IR1	Shakhov E.M.	5172	II	GS-P
Rodulghin V.I.	5132	II	TP-P	Shakhov E.M.	5171	II	TP-P
Roldughin V.I.	5131	I	KTM3	Shane R.W.	6466	II	AA-P
Rosenhauer M.	1657	I	RF2	Sharafutdinov R.G.	5216	I	RF3
Rossani A.	2602	I	IR2	Sharipov F.M.	2686	II	KTM-P
Rossani F.	2601	I	KTM6	Sharipov F.M.	2676	II	NS-P
Rouminsky A.N.	6811	I	IP2	Sharipov F.M.	2687	II	NS-P
Rousseau P.	1106	II	GS-P	Shatalov I.V.	5176	I	AA1
Roussinov V.	2697	I	RF3	Shatalov O.P.	6396	II	NE-P
Roveda R.	6326	I	NS1	Shematovich V.I.	5186	II	AE-P
Rudyak V.	5136	I	KTM6	Shematovich V.I.	5111	I	GS4
Rudyak V.	5138	II	KTM-P	Shen C.	2848	II	IR-P
Ruminsky A.N.	6813	II	IP-P	Shen C.	2847	I	NS2
Runkov V.A.	6847	II	TP-P	Shilenkov S.V.	4926	II	IR-P
Rusakov S.V.	5293	I	NE3	Shiliu Peng	2846	II	NS-P
Rutigliano M.	1771	I	GS2	Shiota T.	4702	I	GS3
Rutigliano M.	1946	I	NE1	Shishkova I.N.	4981	I	TP2
Ryabichova T.V.	5147	II	NE-P	Shishkova I.N.	4982	II	TP-P
Rydalevskaya M.A.	5146	II	NE-P	Shizgal B.D.	2776	I	KTM2
Rydalevskaya M.A.	5147	II	NE-P	Shkarupa E.V.	5191	II	NS-P
Rykov V.A.	5016	II	NS-P	Shugaev F.V.	5196	II	IR-P
Rymarchuk A.V.	5111	I	GS4	Shumova V.V.	6623	I	NE1
Sabelfeld K.K.	2511	I	MCM4	Shvedov F.	6529	II	NS-P
Saito T.	4551	II	NS-P	Sidorenko L.L.	4917	II	NS-P
Sakai K.	4476	I	MCM2	Sijtsema N.M.	2156	I	RF4
Sakamoto M.	4471	II	IP-P	Simonin O.	3003	II	KTM-P
Sakharov V.I.	5156	I	NE1	Singayevskaya G.I.	5196	II	IR-P
Sakiz M.	3003	II	KTM-P	Skovorodko P.A.	5217	II	NS-P
Sakurai A.	4561	I	RF4	Skovorodko P.A.	5218	II	NS-P
Sakurai N.	5581	I	IR1	Skovorodko P.A.	5216	I	RF3
Samuilow E.W.	6666	I	AA4	Skrynnikov A.V.	5216	I	RF3
Samuilow E.W.	6667	II	TP-P	Smekhov G.D.	6396	II	NE-P
Sankovitch V.	5367	I	GS4	Smith A.	1141	I	GS4
Sankovitch V.	5366	II	NE-P	Smyth W.H.	4466	I	AE1
Santos A.	5377	I	MPT	Snegursky A.V.	5766	II	ID-P
Santos A.	5376	I	MPT	Soares A.J.	4146	II	KTM-P
Sato S.	1817	I	IR1	Söderholm L.H.	5396	I	KTM3
Saunois P.	2951	II	IP-P	Soga T.	6866	II	AA-P
Saveliev V.L.	6761	II	KTM-P	Soga T.	4520	I	KTM5
Savin A.V.	5231	I	RF1	Sokolov E.I.	5176	I	AA1
Sazhin O.V.	6737	II	GS-P	Sokolov E.I.	5232	II	AA-P
Schneider J.	6801	II	KTM-P	Sokolov E.I.	5231	I	RF1
Schram D.C.	6906	I	Invited	Sokolova I.A.	6791	II	NE-P
Schuerrer F.	2602	I	IR2	Sone Y.	4361	I	NS1
Schuerrer F.	2601	I	KTM6	Sone Y.	4586	I	RF3
Schulte D.	6312	I	AA2	Sone Y.	4531	I	TP1
Schweigert V.A.	4832	I	IR2	Sreekanth A.K.	4026	II	IP-P
Seleznev V.D.	6527	II	GS-P	Starikov S.A.	4902	II	TP-P
Seleznev V.D.	6528	II	GS-P	Starinov A.	4901	II	TP-P
Seleznev V.D.	6526	II	IP-P	Stark J.	5731	II	KTM-P
Seleznev V.D.	6529	II	NS-P	Stefanov S.	2698	II	IP-P
Sentis R.	1466	I	IR2	Stefanov S.	2697	I	RF3
Sergievskaya A.L.	5166	II	NE-P	Stefanov S.K.	2368	I	RF4

<i>Author</i>	<i>Paper</i>	<i>Vol</i>	<i>Session</i>	<i>Author</i>	<i>Paper</i>	<i>Vol</i>	<i>Session</i>
Struckmeier J.	4112	I	MCM3	Vervisch P.	6724	II	ID-P
Struckmeier J.	2697	I	RF3	Vervisch P.	6725	II	ID-P
Suetin P.	4901	II	TP-P	Vervisch P.	6723	I	IR1
Suetin P.E.	6847	II	TP-P	Vervisch P.	6721	I	NE1
Sugimoto H.	4586	I	RF3	Vijayakumar P.	2366	I	NE2
Sumini M.	4136	II	IR-P	Vilisova E.A.	2041	II	IR-P
Suslov O.N.	4967	I	GS4	Vizcaino A.	3166	I	IP2
Svirschevsky S.B.	5187	II	AA-P	Vlasov V.I.	4873	II	NS-P
Szymanski Z.	3209	II	ID-P	Vodovozova J.F.	5232	II	AA-P
T. Hayashi T.	4471	II	IP-P	Voronich I.V.	5292	II	NS-P
Takaada A.	3830	I	KTM4	Wadsworth D.C.	6031	I	AA1
Takata S.	4621	I	TP1	Wadsworth D.C.	6506	II	NE-P
Takayama F.	4561	I	RF4	Wagner W.	3971	I	MCM1
Takayama K.	4551	II	NS-P	Walenta Z.A.	4771	I	RF2
Taran J.P.	6311	II	ID-P	Wallenborn J.	1986	II	IR-P
Tarhov E.L.	5187	II	AA-P	WalusW.	4741	II	NS-P
Taylor J.C.	6406	II	NS-P	Watanabe Y.	6690	II	NE-P
Tchebureev V.G.	4851	II	AE-P	Wilmoth R.	2351	I	Invited
Tcheremissine F.G.	5247	II	NS-P	Wilmoth R.G.	6467	I	AA2
Tcheremissine F.G.	5246	I	RF2	Wilmoth R.G.	6466	II	AA-P
ter Meulen J.J.	2156	I	RF4	Wilmoth R.G.	6916	II	IP-P
Teshima K.	4641	I	AA1	Wong M.C.	4466	I	AE1
Teshima K.	4672	I	AA1	Woo M.	5861	I	NS2
Tessarotto M.	4241	II	NS-P	Wysong I.	6507	I	Invited
Thivet F.	6515	I	AA3	Wysong I.J.	6506	II	NE-P
Tij M.	5376	I	MPT	Yalamov Yu.	5006	II	TP-P
Tirskiy G.A.	5251	II	AA-P	Yamamoto K.	4701	I	GS2
Titarev V.A.	5173	II	AA-P	Yamamoto K.	4702	I	GS3
Titarev V.A.	5172	II	GS-P	Yamanishi N.	4431	II	GS-P
Titulaer U.M.	6766	II	NE-P	Yanitskii V.E.	5276	I	MCM2
Toennies J.P.	2916	I	GS2	Yarygin V.N.	6311	II	ID-P
Tokmantsev V.I.	6529	II	NS-P	Yasuhara M.	6866	II	AA-P
Tokumasu T.	4646	II	NE-P	Yigiter O.	2171	I	IP2
Tokunaga T.	6690	II	NE-P	Yin X.	6602	I	IR2
Tolboom R.A.L.	2156	I	RF4	Yonemura S.	4476	I	MCM2
Tolson R.H.	6466	II	AA-P	Yoshida N.	5396	I	KTM3
Tomoeda M.	4656	II	NS-P	Yoshimoto M.	4361	I	NS1
Trapaga G.	2171	I	IP2	Ytrehus T.	4731	I	TP1
Trubnikov D.N.	5135	II	NE-P	Yumashev V.L.	5001	II	TP-P
Tsuboi N.	4432	II	AA-P	Yurasov V.S.	2069	II	GS-P
Tuttafesta M.	1801	I	NE1	Yushkanov A.	5006	II	TP-P
Usami M.	4672	I	AA1	Zabelok S.A.	1931	I	MCM3
Usami M.	4673	II	NS-P	Zakharov V.V.	4842	II	AE-P
Uskov V.N.	4810	II	AA-P	Zastenker N.N.	5135	II	NE-P
Van Ootegem B.	6724	II	ID-P	Zhdanov V.M.	5131	I	KTM3
Van Ootegem B.	6723	I	IR1	Zhdanov V.M.	5296	I	NE2
Vandromme D.	6856	II	NS-P	Zhdanov V.M.	5135	II	NE-P
Varghese P.	6326	I	NS1	Zmievskaia G.I.	5306	II	NE-P
Vargo S.E.	6031	I	AA1	Zmievskaia G.I.	5307	II	TP-P
Vargo S.E.	6032	I	IP1	Zolotoukhina T.N.	4392	I	GS3
Velicodny V.Yu.	6621	II	NE-P	Zorat R.	4241	II	NS-P
Velikodny V. Yu.	1976	II	NE-P				